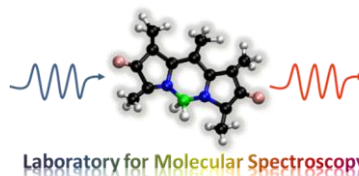


Caracterización fotofísica y simulación estructural de nuevos colorantes BODIPY para aplicaciones fotónicas

TESIS DOCTORAL

Ixone Esnal Martinez

Bajo la dirección de: Jorge Bañuelos Prieto e Iñigo López Arbeloa



Leioa, 2015

RESUMEN

La presente memoria se centra en el análisis de la influencia de la estructura molecular en las propiedades fotofísicas de los cromóforos conocidos como BODIPYs. Se pretende, de esta forma, relacionar las propiedades espectroscópicas con el comportamiento de los colorantes como medios activos de láseres sintonizables principalmente, y también como sondas moleculares para monitorizar las propiedades fisicoquímicas del medio que les rodea. Para ello se han registrado las propiedades fotofísicas y electroquímicas de un amplio abanico de nuevos fluoróforos BODIPY mediante técnicas espectroscópicas de absorción UV/Vis y fluorescencia (tanto en estado estacionario como resuelta en el tiempo) y la voltametría cíclica, respectivamente. Dicho estudio experimental se ha completado con la simulación mecanocuántica de las estructuras mediante métodos computacionales avanzados (*ab initio* y teoría del funcional de densidad).

El patrón de sustitución del BODIPY ha permitido modular y optimizar sus propiedades espectroscópicas. De hecho, tanto la posición cromofórica en la que se incorpore el sustituyente como su carácter dador/aceptor de electrones determina la respuesta fluorescente del colorante. El conocimiento acumulado como resultado de esta tesis doctoral posibilita sentar las bases de las modificaciones estructurales óptimas para el diseño de nuevos fluoróforos a la carta con propiedades específicas.

Así, la modificación controlada de la estructura molecular básica del BODIPY ha permitido no sólo optimizar la eficiencia fluorescente en la región verde/amarilla del visible (funcionalización del puente de boro), sino también extenderla de forma modulable hacia el extremo azul (heteroátomos en *meso*) o alternativamente a la región roja/NIR (extensión del sistema π deslocalizado). Como resultado se han desarrollado nuevos colorantes láser BODIPY cubriendo toda la región espectral visible y con prestaciones fotofísicas y láser mejoradas respecto a los colorantes comerciales existentes.

Además, la funcionalización selectiva ha facilitado también promover la activación de nuevos procesos fotofísicos. La inducción de procesos de transferencia de carga por medio de la aminación o la nitración, permite emplear esos fluoróforos como sondas fluorescentes de polaridad. Por otra parte, los procesos de transferencia de energía que tienen lugar en sistemas multicromofóricos basados en estructuras de BODIPYs y cumarinas unidas covalentemente, posibilita mejorar la absorción de luz y obtener la brillante emisión del BODIPY tanto bajo excitación visible como ultravioleta.

El estudio realizado a lo largo de esta tesis demuestra la importancia del conocimiento de las propiedades fotofísicas de los colorantes para evaluar y explicar su comportamiento láser y testar sus posibles aplicaciones como sondas o sensores fluorescentes.

LABURPENA

Memoria honetan, BODIPY izenaz ezagunak diren kromoforoen egitura molekularrak propietate fotofisikoen gainean duen eragina aztertzen da. Horrela, propietate espektroskopikoak eta koloratzaileen jokabidea elkarren artean erlazionatzen dira, gehienbat laser sintonizagarrien ingurune-aktibo modura, eta baita zunda molekularretan ere, beraien ingurunearen propietate fisikokimikoak monitorizatzeko. Horretarako, BODIPY fluoroforo berrien propietate fotofisikoak eta elektrokimikoak erregistratu dira, alde batetik, ultramore-ikuskorreko absortzioaren eta fluoreszentziaren (egoera geldikorrean zein denborarekin korrelazioan) teknika espektroskopikoak erabiliz, eta bestetik, boltametri ziklikoa, hurrenez hurren. Ikerketa esperimental hori osatzeko, egituren simulazio mekanokuantikoa egin da metodo konputazional aurreratuak erabiliz (*ab initio* eta dentsitate funtzionalaren teoria).

BODIPYaren ordezkapen patroia kontuan hartuz, propietate espektroskopikoak modulatu eta optimizatu daitezke. Horrela, koloratzailearen fluoreszentziaren erantzuna zehazten da, kromoforoaren gaineko funtzionalizazio posizioa zein den kontuan hartuta bai eta ordezkatzailearen elektroien izaera emailea/hartzailea zein den. Doktoretza-tesi honetan lortutako ezagutza dela medio, propietate espezifikoak fluoroforo berrien egituraren aldaketa ezin hobeak proposatzeko oinarriak finkatzen dira.

Horrela, BODIPYaren oinarritzko egitura molekularren aldakuntza zuzenak, zera eragiten du, ikuskorraren eremu berde/horian ahalmen fluoreszentea optimizatzea (boro zubiaren funtzionalizazioa), eta banda espektralak desplazatzea, bai eremu urdinera (heteroatomoak *meso* posizioan), bai NIR edo gorri eremura (π sistema deslokalizatuaren hedapena). Ondorioz, koloratzaile komertzialekin konparatuz gero, ikuskorraren eremu espektral osoa betetzen duten BODIPY koloratzaile berriak garatu dira, ezaugarri fotofisiko eta laser hobeez.

Funtzionalizazio selektiboak prozesu fotofisiko berrien aktibazioa eragin dezake. Aminazioaren edo nitrazioaren bidezko karga-transferentziako prozesuen indukzioaren ondorioz, fluoreszentziaren polaritate zunda modura izan daitezke erabilgarriak fluoroforo horiek. Bestalde, sistema multikromoforikoetan (BODIPY eta kumarina egituren arteko lotura kobalentean oinarrituta) gertatzen diren energia-transferentziako prozesuek argiaren absortzioa hobetzeaz gain, BODIPYaren emisio distiratsua lortzea ahalbidetzen du, kitzikapena ikuskorrean zein ultramorean posiblea izanik.

Tesi honetan egindako ikerketaren ondorioz, koloratzaileen propietate fotofisikoen ezagueraren garrantzia egiaztatzen da; horrela, laser jokabidea ebaluatu eta azaldu daiteke, baita zunda edo sentsore-fluoreszenteen aplikazio posibleak frogatu ere.

ABSTRACT

The herein presented thesis deals with the impact of the molecular structure on the photophysical properties of the chromophores known as BODIPYs. The final goal is to correlate them with the behavior of these fluorophores mainly as active media of tunable dye lasers, and also as molecular sensors to monitor the physicochemical properties of the surrounding environment. To this aim, the photophysical and electrochemical signatures of a wide library of novel BODIPY dyes have been recorded by means of spectroscopic techniques (such as, UV/Vis absorption and fluorescence, both steady-state and time-resolved) and cyclic voltammetry, respectively. Such experimental study has been complemented by the quantum mechanical simulation of the molecular structures using advanced computational methods (*ab initio* and density functional theory).

The imposed substitution pattern on the BODIPY core allows the fine modulation and optimization of its spectroscopic characteristics. Thus, the chromophoric position in which the substituent is anchored, as well as its electronic donor/acceptor ability, rules the fluorescence response of the dye. In this regard, the accumulated background as result of this thesis provides the most recommended structural guidelines to design tailor-made luminophores with specific properties.

Therefore, the controlled modification of the BODIPY core has promoted not only the optimization of the fluorescence signal in the green/yellow region of the visible (by the functionalization at the boron bridge), but also the tunable shift of the spectral bands towards the blue-edge (heteroatoms at *meso* position) as well as to the red/NIR-edge (extension of the delocalized π -system). As result, new BODIPY laser dyes have been developed spanning the whole visible spectral region and with improved photophysical and laser performance with regard to the commercially available laser dyes.

Such selective functionalization leads also to the activation of new photophysical pathways. The induction of charge transfer (i.e., by amino or nitro groups) enables the use of these fluorophores as polarity fluorescent sensors. Alternatively, multichromophoric assemblies (BODIPYs and coumarin covalently linked) undergoing energy transfer processes provide a most efficient light harvesting and lead to the bright emission from the BODIPY under visible or ultraviolet excitation.

The results derived from this thesis highlight the key role of the knowledge of the photophysical properties of the dyes to explain their laser behavior and evaluate their viability as fluorescent sensor or probes.

INDICE

INTRODUCCIÓN	1
Objetivos.....	9
Estructura de la memoria.....	10
Bibliografía.....	11
MÉTODOS Y TÉCNICAS EXPERIMENTALES	13
I. Colorantes y preparación de muestras.....	13
II. Técnicas experimentales.....	14
Espectroscopía de absorción ultravioleta-visible.....	15
Espectroscopía de fluorescencia.....	15
Contador cuántico de fotones correlacionado con el tiempo.....	17
Electroquímica.....	19
III. Métodos Computacionales.....	21
Bibliografía.....	24
Capítulo 1: ESTRUCTURA Y FOTOFÍSICA DE PIRROMETENOS	25
1.1. Estructura de BODIPYs.....	26
1.2. Fotofísica general de BODIPYs.....	29
Bibliografía.....	34
Capítulo 2: BODIPYs EN LA REGIÓN VERDE-AMARILLA DEL VISIBLE	35
2.1. <i>F</i> -BODIPYs comerciales.....	36
2.2. <i>E</i> - y <i>C</i> -BODIPYs.....	40
2.3. <i>O</i> -BODIPYs.....	44
Bibliografía.....	48
Capítulo 3: BODIPYs EN LA REGIÓN ROJA DEL ESPECTRO VISIBLE	49
3.1. BODIPYs con conformación restringida.....	52
3.2. BODIPYs por extensión periférica de la deslocalización.....	55
Bibliografía.....	61

Capítulo 4: BODIPYs EN LA REGIÓN AZUL DEL ESPECTRO VISIBLE.....	63
4.1. 8-Amino BODIPYs.....	65
4.1.1. BODIPY sustituido por amina primaria en <i>meso</i>	65
4.1.2. BODIPYs sustituidos por aminas secundarias en <i>meso</i>	68
4.1.3. BODIPYs sustituidos por aminas terciarias en <i>meso</i>	74
4.2. 8-Alcoxi y 8-Ariloxi BODIPYs.....	77
4.2.1. 8-Alcoxi BODIPYs.....	78
4.2.2. 8-Ariloxi BODIPYs.....	80
4.3. 8-Sulfo BODIPYs.....	82
4.4. Metilación de las posiciones α en los 8-heteroBODIPYs.....	84
Bibliografía.....	89
Capítulo 5: BODIPYs SENSIBLES A LA POLARIDAD DEL MEDIO.....	91
5.1. Transferencia de carga en BODIPYs.....	94
5.1.1. Sustitución directa en las posiciones α o β	94
5.1.1.1. Funcionalización con amino.....	95
5.1.1.2. Funcionalización con nitro.....	97
5.1.2. Sustitución en posición <i>meso</i> con espaciador metileno.....	99
5.2. Sonda de polaridad colorimétrica.....	104
Bibliografía.....	109
Capítulo 6: MULTICROMÓFOROS BODIPY-CUMARINA.....	111
6.1. Diada BODIPY-cumarina.....	115
6.2. Híbridos BODIPY-cumarina.....	117
6.2.1. Híbridos mono-sustituidos.....	118
6.2.2. Híbridos di-sustituidos.....	121
Bibliografía.....	125
CONCLUSIONES GENERALES.....	127
PERSPECTIVAS FUTURAS.....	129
ANEXOS.....	133

INTRODUCCIÓN

Los colorantes son moléculas orgánicas con sistemas π extendidos que posibilitan la absorción eficiente de la radiación electromagnética en la región visible. A consecuencia de su cromaticidad se han empleado, a lo largo de la historia, en estética o en la industria textil, principalmente como pigmentos. Muchos de estos cromóforos se caracterizan también por ser altamente fluorescentes. Los avances en síntesis orgánica y en las técnicas espectroscópicas de alta resolución, así como las peculiares propiedades fotofísicas de alguno de estos fluoróforos, han impulsado su uso en otros campos tecnológicos y comerciales, tales como la electrónica (para almacenamiento de datos), la medicina (con fines terapéuticos), la fotografía o las impresoras, por nombrar solo algunas de las aplicaciones más significativas^[1].

El auge de estos luminóforos orgánicos ha suscitado un creciente interés en el desarrollo de nuevos colorantes fluorescentes con propiedades fotofísicas mejoradas, bien sea mediante la modificación estructural de moléculas ya existentes, bien diseñando nuevas familias de colorantes. A modo de ejemplo, y debido al avance tecnológico de las técnicas relacionadas con la imagen fluorescente (Figura 1), los colorantes son ampliamente empleados como marcadores fluorescentes para monitorizar *in situ* y de una forma barata y directa, procesos de interés bioquímico y biofísico^[2-3], así como para determinar la morfología de las células o los tejidos^[4]. En la actualidad existe un amplio catálogo comercial de estructuras moleculares susceptibles de ser empleadas como sondas fluorescentes específicas para la detección a nivel molecular^[5-7].

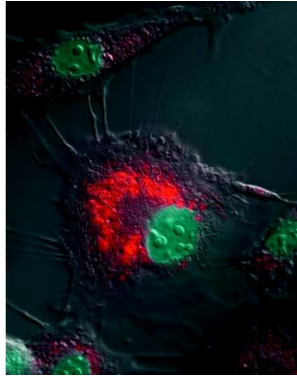


Figura 1. Células bovinas, marcadas con LysoTracker® Red DND-99 (un derivado BODIPY) y Hoechst 33342. Imagen realizada por microscopía DIC (Differential Interference Contrast).

Paralelamente, en los últimos años, uno de los campos donde los colorantes han sido empleados con más asiduidad y con gran éxito, son los láseres sintonizables. Hoy en día, la radiación LASER (acrónimo de *Light Amplification by Stimulated Emission of Radiation*) es una herramienta imprescindible en diversas áreas de la ciencia, la ingeniería, la industria o la medicina entre otras, así como en el desarrollo de técnicas espectroscópicas avanzadas de alta resolución. La emisión láser consiste en la concentración de luz en un haz estrecho en una dirección, que además conserva su energía a largas distancias de propagación (Figura 2.a). La radiación láser es una emisión coherente (tanto espacial como temporal), monocromática y capaz de alcanzar potencias extremadamente altas.

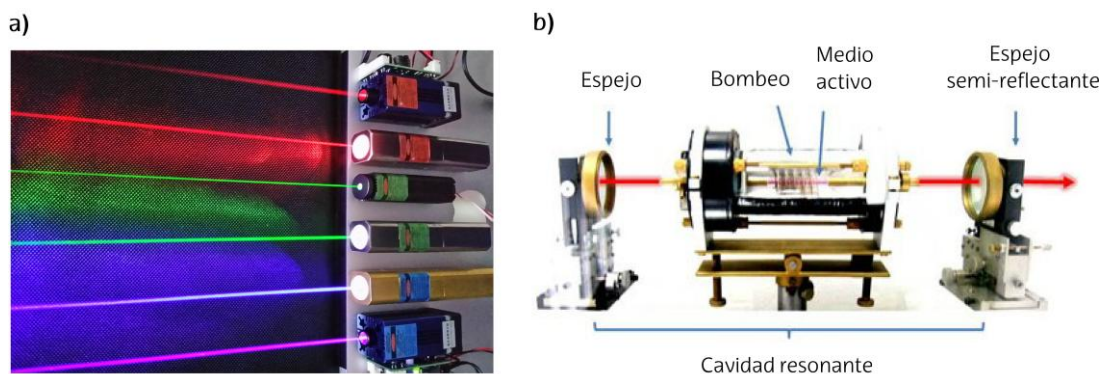


Figura 2. a) Emisión de varios láseres en estado sólido. b) Esquema general de los láseres.

De forma general, el dispositivo para generar emisión láser consta de una fuente de excitación o bombeo externa, un medio activo y una cavidad resonante (Figura 2.b). La obtención de la emisión se basa en la excitación de las especies que forman el medio activo empleando la fuente de bombeo. Como consecuencia de un bombeo intenso se provoca la

inversión de población, es decir, la población de átomos, moléculas o iones con un electrón en el estado excitado es superior a las del estado fundamental (Figura 3). Dicho electrón puede decaer espontáneamente al estado fundamental emitiendo un fotón, que a su vez puede provocar la emisión estimulada de un segundo fotón desde otro estado excitado. Los fotones emitidos están en fase (coherencia) y emiten la misma longitud de onda.

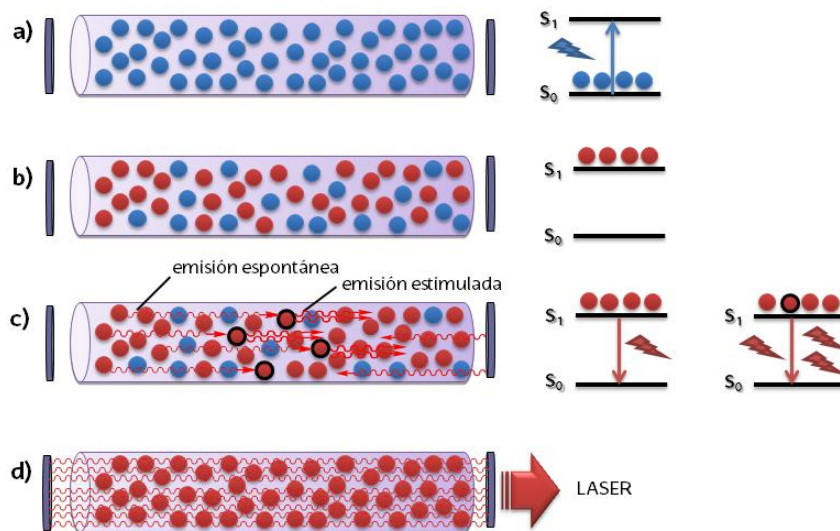


Figura 3. Esquema del proceso láser en el medio activo: **a)** moléculas en estado fundamental; **b)** inversión de población; **c)** emisión espontánea y emisión estimulada; **d)** amplificación de la emisión y emisión láser.

Por otro lado, el medio activo se dispone en la cavidad resonante compuesta por dos espejos paralelos entre sí, uno a cada extremo del material activo, siendo uno de ellos parcialmente reflectante (Figura 2.b). Dicha disposición permite amplificar el número de fotones emitidos, ya que el haz de radiación se refleja en los espejos y atraviesa sucesivamente el medio activo (retroalimentación) donde se ha provocado la inversión de población, con lo que se aumenta la emisión estimulada de fotones. Una vez que la amplificación de la radiación supera las pérdidas de luz en la cavidad resonante, un haz láser monocromático, coherente y amplificado sale de la cavidad a través del espejo semireflectante (Figura 3.d).

Los láseres se pueden clasificar en función de la naturaleza del medio activo empleado^[8]: de fase gaseosa (como los láseres de Ar, de He-Ne o de CO_2), de fase líquida (láser de colorante o Quantum Dots) o de estado sólido (por ejemplo el láser de Nd:YAG). Una de las principales ventajas de los láseres de colorante (Figura 4.a), es que su banda de emisión es más ancha que en el resto de los láseres anteriormente citados (Figura 4.b), lo que posibilita un amplio rango de sintonizabilidad de la longitud de onda de emisión láser y la posibilidad de

generar pulsos ultra cortos (femtosegundos)^[8-9]. El primer láser de colorante orgánico en disolución fue desarrollado en 1966, por un lado por Sorokin y Lankard^[10] y por otro por Schäfer, Schmidt y Volze^[11], para lo que utilizaron un colorante orgánico de ftalocianina y diversos colorantes de cianina, respectivamente. El medio activo de estos láseres de estado líquido consta de una disolución concentrada de colorante que fluye continuamente para evitar procesos de degradación. Sin embargo, este dispositivo requiere de grandes volúmenes de disolución y de disolventes que suelen ser tóxicos e inflamables^[8]. Por tanto, aunque muchos medios activos líquidos muestran excelentes prestaciones láser en términos de modulación de la longitud de onda de emisión, eficiencia láser (energía obtenida respecto a la empleada en el bombeo) y fotoestabilidad (resistencia ante la degradación provocada por el bombeo láser), se requiere eliminar el uso de esos disolventes, principalmente con vistas a extender su uso y comercialización. Como consecuencia existe una importante actividad investigadora en el desarrollo de láseres de colorante en estado sólido (por ejemplo embebiendo el colorante en matrices poliméricas^[12] o materiales sol-gel^[13-14]) lo que permite miniaturizar y compactar el dispositivo que a su vez es más seguro y menos contaminante^[15].

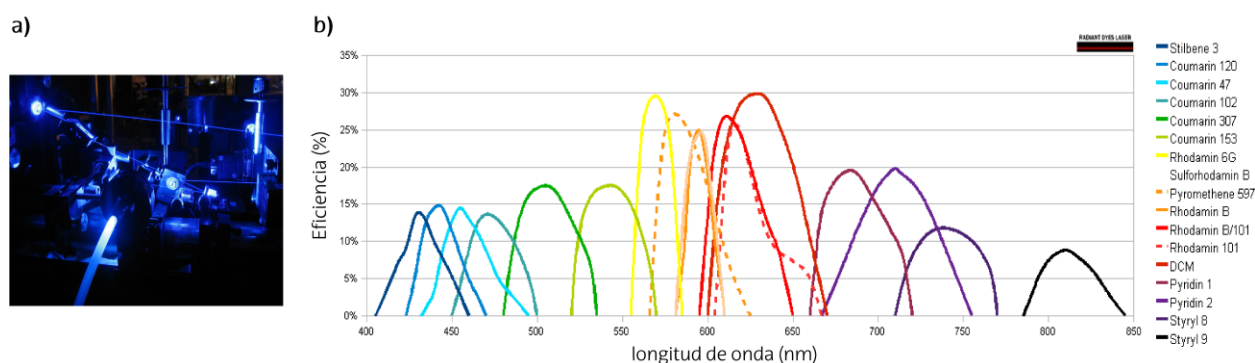


Figura 4. a) Láser de colorante de estilbeno. b) Espectros de emisión de diversos colorantes láser^[16]

Desde el punto de vista fotofísico, una molécula orgánica tiene que cumplir una serie de requisitos para ser considerada un colorante de láser:

- Fuertes bandas de absorción y fluorescencia que faciliten la inversión de población inducida por el bombeo y aumenten la probabilidad de emisión estimulada y con ello las ganancias en la cavidad resonante.
- Baja probabilidad de desactivación no-radiante para reducir las pérdidas en la cavidad resonante. Sobre todo se debe evitar, en la medida de lo posible, el cruce

intersistema puesto que los estado tripletes se caracterizan por tiempos de vida largos y la absorción triplete-triplete solapa con la banda de emisión láser^[17].

- Baja tendencia a agregarse, ya que los agregados desactivan eficientemente la emisión radiante de los monómeros^[18].
- Es conveniente mantener alto el desplazamiento de Stokes. Es decir, bajo solapamiento de la banda de absorción y fluorescencia para reducir la probabilidad de los procesos de reabsorción/reemisión que cobran importancia en medios de alta densidad óptica como los requeridos para la emisión láser^[19].
- Es beneficioso tener alta estabilidad química, termoestabilidad y fotoestabilidad para que el medio activo sea duradero y disponga de un largo tiempo operativo.

En la actualidad existe un amplio abanico de moléculas orgánicas susceptibles de ser empleadas como medios activos de láseres de colorante sintonizables y con emisión a lo largo de toda la región ultravioleta-visible (UV-Vis). Entre las diversas familias de colorantes láser disponibles comercialmente^[20-22] (Figura 5), hay que destacar las cumarinas en la región azul, los derivados del xanteno (rodaminas o fluoresceína) en la región verde-amarilla y las oxacinas (azul de nilo o violeta de cresilo) en la región roja del visible.

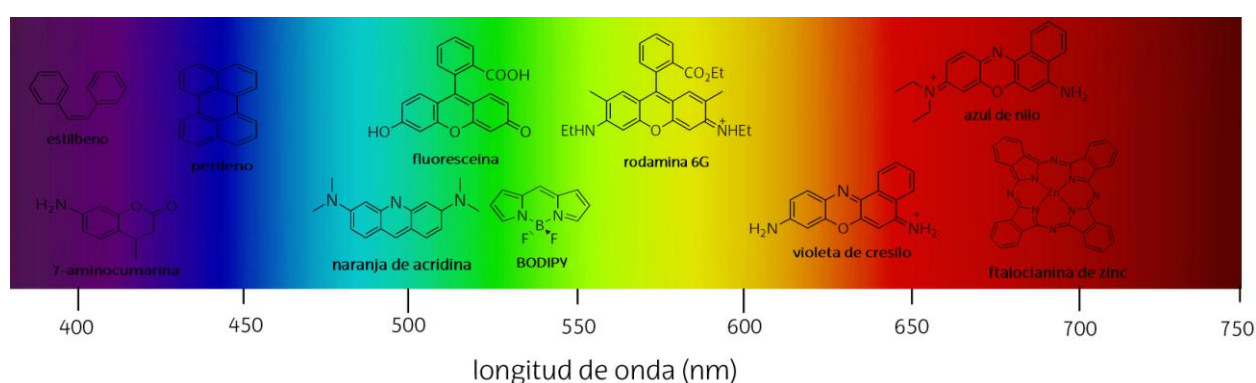


Figura 5. Estructuras de diversos colorantes láser.

La búsqueda continua de nuevos cromóforos con prestaciones fotofísicas y láser desembocó en una nueva familia de colorantes conocidos como boro-dipirrometeno (BODIPY

o 4,4-difluoro-4-bora-3a,4a-diaza-s-indaceno, Figura 5). Aunque fueron sintetizados en los años 60^[23], no fue hasta los 90 cuando ganaron reputación entre la comunidad científica como colorantes láser^[24-25]. De hecho, hoy en día son probablemente los medios activos más empleados en láseres sintonizables y están considerados como los sistemas de referencia por su óptimo comportamiento láser^[26-27]. La fotofísica de los BODIPYs cumple la mayoría de los requisitos mencionados anteriormente para colorantes láser. Así, su robusto cromóforo es soluble en la mayoría de los disolventes orgánicos, proporciona intensas bandas de absorción (absorción molar cercana a 100 000 M⁻¹cm⁻¹), y emisión, tanto fluorescente (rendimientos cuánticos de fluorescencia próximos al 100%)^[4,28], como láser (eficiencias superiores al 50%) en la región verde-amarilla del visible como consecuencia de su sistema π cuasi-aromático que recuerda a las cianinas cíclicas o polimetinos^[29-30]; además este fluoróforo resiste prolongados e intensos bombeos^[31-32]. Todo ello es, en buena parte, debido a la prácticamente nula población del estado triplete^[33-35], y su baja tendencia a agregarse^[36].

Una de las mayores ventajas que ofrecen los BODIPYs es la versatilidad química de su núcleo cromofórico. Así, la estructura del boro diaza-indaceno es susceptible de ser exhaustivamente derivatizada mediante un amplio abanico de rutas sintéticas y de forma selectiva en cualquiera de las posiciones del núcleo BODIPY^[28,37-40] (Figura 6). No en vano algunos autores han denominado a los BODIPYs como "El Dorado" para la química orgánica sintética^[41]. Esta reactividad química permite incorporar numerosos y variados grupos funcionales al cromóforo y de esta manera modular las propiedades espectroscópicas del colorante (por ejemplo desplazar las bandas espectrales a voluntad) o inducir nuevos procesos fotofísicos (tales como transferencia electrónica o de energía) que permiten expandir sus campos de aplicación^[42-43]. Dicho de otra manera, los BODIPYs muestran un carácter camaleónico que les permite adaptarse a diferentes requerimientos tras un diseño molecular racional.

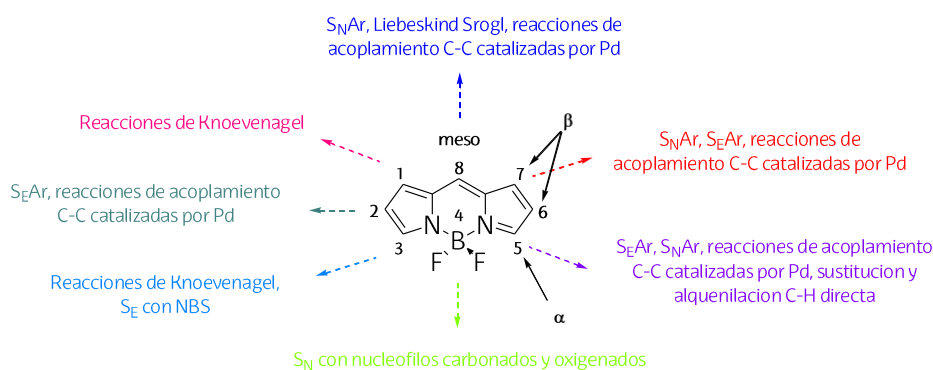


Figura 6. Reactividad del núcleo BODIPY.

El número de publicaciones que tienen por objeto los BODIPYs ha crecido exponencialmente en los últimos años (Figura 7), puesto que estos fluoróforos se han empleado exitosamente en diversos campos de la fotónica, biofotónica y biomedicina. Así, los BODIPYs han encontrado cabida de forma exitosa en numerosos campos científicos, entre los que cabe destacar los mencionados a continuación:

- Como medios activos de láseres sintonizables^[44-45]
- Como recolectores de luz^[46-47], mediante la inducción de procesos de transferencia de energía de excitación (EET)^[48]
- Como marcadores biomoleculares^[49-51], debido a la posibilidad de funcionalizar el cromóforo con grupos que permitan el anclaje covalente a biomoléculas^[52-54]
- Como sondas^[55] o "interruptores" fluorescentes de polaridad, acidez o iones, mediante la inducción de procesos de transferencia de carga (CT) o transferencia electrónica fotoinducida (PET)^[56-57]
- En dispositivos electroluminiscentes^[58-59]
- En células solares como captadores de luz e inyectores de electrones^[60-62]
- Como generadores de oxígeno singlete en terapia fotodinámica para el tratamiento del cáncer^[63-64]

En otras palabras, se podría concluir que los BODIPYs son la elección acertada para prácticamente cualquier aplicación científica que requiera de un fluoróforo, siempre y cuando el diseño molecular sea el adecuado.

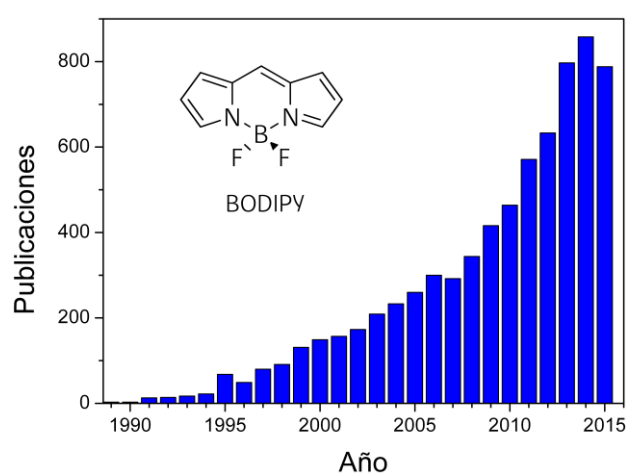


Figura 7. Publicaciones relacionadas con BODIPYs (Fuente: SciFinder; Periodo de búsqueda: hasta octubre de 2015).

La presente memoria de Tesis Doctoral se centra en la caracterización fotofísica así como en la simulación mecanocuántica de nuevas estructuras orgánicas basadas en BODIPYs con vistas a optimizar su comportamiento láser y extender su rango espectral de aplicación. En algunos casos, la modificación estructural ha dado lugar a la aparición de nuevos procesos fofotísificos sensibles a las condiciones ambientales que rodean al colorante, y por tanto esos fluoróforos son susceptibles de ser empleados como sensores moleculares.

Algunos de los colorantes estudiados a lo largo de esta tesis, especialmente aquellos con intensa y brillante emisión dentro de la ventana biológica ($\lambda_{fl} > 650$ nm), son potenciales candidatos como sondas moleculares para bioimagen. De esta forma, y debido a su alta eficiencia fluorescente, se mejora la sensibilidad en el proceso de detección mediante la microscopía confocal de fluorescencia, y su alta fotoestabilidad, posibilita largos periodos de irradiación. Los nuevos avances en la resolución de las técnicas microscópicas, avaladas por la reciente concesión del Premio Nobel de Química de 2014 a E. Betzig^[65], W. E. Moerner^[66] y S. W. Hell^[67], como consecuencia del desarrollo de la nanoscopía donde es viable la detección a nivel molecular (Figura 8), ha impulsado la búsqueda de nuevas estructuras moleculares con propiedades optimizadas para monitorizar mediante la emisión fluorescente procesos de interés bioquímico y biológico^[68].

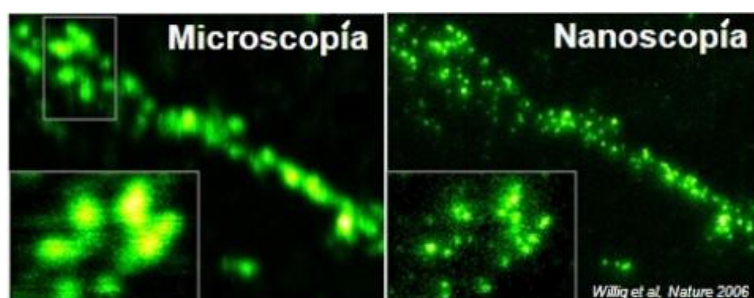


Figura 8. Comparación de la resolución en una imagen realizada por microscopía confocal (izda) y microscopía STED (Stimulated Emission Depletion, dcha)^[69]

Objetivos

El trabajo realizado para la consecución de la presente tesis doctoral ha consistido en la caracterización fotofísica y electroquímica, así como la simulación mecanocuántica de nuevos BODIPYs con vistas a sus aplicaciones como láseres de colorantes, sensores moleculares y eventualmente como sondas fluorescentes en el futuro. Es por ello, que para lograr los objetivos planteados a continuación, se ha modificado de forma controlada la estructura molecular:

- Modular la posición de las bandas espectrales desde la región verde-amarilla, donde normalmente se sitúan los BODIPYs, tanto hacia el extremo azul como el rojo del visible. Con ello se pretende disponer de colorantes láser altamente fluorescentes y estables a lo largo de toda la región visible.
- Optimizar las propiedades fotofísicas de los BODIPYs. Para ello se va a analizar en detalle el efecto estérico y electrónico de una amplia gama de sustituyentes en posiciones específicas del núcleo cromofórico. Con ello se pretende recopilar información de la influencia del patrón de funcionalización para poder diseñar estructuras con propiedades específicas y dirigidas.
- Correlacionar las características fotofísicas con las propiedades láser. El conocimiento y entendimiento de la fotofísica es fundamental no sólo para explicar el comportamiento láser, sino también para orientar el diseño molecular de nuevas estructuras mejoradas para su aplicación láser.
- Caracterizar los procesos de transferencia de carga y determinar su probabilidad según la naturaleza dadora/aceptora del sustituyente, la posición cromofórica en la que se incorpore y las características fisicoquímicas del medio. Se pretende así, desarrollar fluoróforos que funcionen como sensores de polaridad donde dicha propiedad se pueda monitorizar fácilmente por el cambio del color emitido (sensores colorimétricos) o de la eficiencia de fluorescencia (interruptores on/off).
- Dado que los BODIPYs se caracterizan por bajos desplazamientos de Stokes, se pretende alejar la región de excitación de la de emisión, mediante su incorporación en sistemas multicromofóricos susceptibles de dar lugar a procesos de transferencia de energía. Se determinará el mecanismo de dicho proceso en base a la probabilidad de acoplamiento electrónico entre los cromóforos de la diada.

Estructura de la memoria

La presente tesis doctoral se ha realizado en forma de compendio de publicaciones científicas, por lo que los diferentes apartados sirven para organizar y resumir los resultados obtenidos a lo largo del trabajo de investigación realizado, y facilitar así la lectura y comprensión de la memoria. A continuación de esta introducción general se especifican los métodos y técnicas experimentales empleados. Posteriormente la discusión de los resultados se divide en 6 capítulos generales. Cada capítulo consta de una introducción específica con los correspondientes objetivos perseguidos, una discusión de los resultados más significativos de los artículos publicados, y unas conclusiones específicas del capítulo.

- Capítulo 1; se exponen los detalles generales de la estructura y la caracterización fotofísica del cromóforo BODIPY más simple.
- Capítulo 2; se estudian las propiedades fotofísicas de BODIPYs disponibles comercialmente en la región espectral verde-amarilla, pero modificados en el boro, con el fin de mejorar sus prestaciones láser.
- Capítulo 3; se analizan las propiedades espectroscópicas de BODIPYs con deslocalización π extendida, con el fin de obtener colorantes láser en la región espectral roja.
- Capítulo 4; se caracterizan los cambios inducidos por heteroátomos en la posición *meso* sobre la distribución electrónica de BODIPYs, que conlleva un desplazamiento espectral hacia la región azul.
- Capítulo 5; se considera la activación de procesos de transferencia de carga en función del tipo de sustituyente y posición cromofórica de anclaje con la intención de diseñar nuevos fluoróforos BODIPY como sensores de polaridad del medio.
- Capítulo 6; se estudia una nueva serie de multicromóforos basados en estructuras híbridas BODIPY-cumarina, con el fin de mejorar las prestaciones láser de los BODIPY por la inducción de procesos de transferencia de energía.

Finalmente, se presentan las conclusiones generales y las perspectivas futuras en cuanto a otros BODIPYs también estudiados durante la tesis doctoral, y se anexan los artículos publicados.

Bibliografía

- [1] Mustroph, H.; Ernst, S.; Senns, B.; Towns, A. D.; *Color. Technol.*, **2015**, *131*, 9. Mustroph, H.; Ernst, S.; Senns, B.; Towns, A. D.; *Color. Technol.*, **2015**, *131*, 9.
- [2] Weissleder, R.; Pittet, M. J.; *Nature*, **2008**, *452*, 580.
- [3] Wennmalm, S.; Simon, S. M.; *Annu. Rev. Biochem.*, **2007**, *76*, 419.
- [4] Ni, Y.; Wu, J.; *Org. Biomol. Chem.*, **2014**, *12*, 3774.
- [5] Johnson, I.; Spence, M.; Eds.; *The Molecular Probes Handbook. A Guide to Fluorescent Probes and Labelling Technologies*, 11th ed.; Life Technologies: Eugene, OR, **2010**.
- [6] Haugland, R. P.; *Handbook of Fluorescent Probes and Research Chemicals*, 6th ed.; Molecular Probes: Eugene, OR, **1996**.
- [7] <https://probes.invitrogen.com>
- [8] Schäfer, F. P.; *Dye Lasers*, Springer-Verlag, Berlin, Germany, **1990**.
- [9] Duarte, F. J.; Hillman, L. W.; Eds.; *Dye Laser Principles*, (Ed.: Duarte, F. J.), Academic Press, New York, **1990**.
- [10] Sorokin, P. P.; Lankard, J. R.; *IBM J. Res. Dev.*, **1966**, *10*, 162.
- [11] Schäfer, F. P.; Schmidt, W.; Volze, J.; *Appl. Phys. Lett.*, **1966**, *9*, 306.
- [12] Costela, A.; García-Moreno, I.; Sastre, R.; *Phys. Chem. Chem. Phys.*, **2003**, *5*, 4745.
- [13] Reisfeld, R.; *Opt. Mater.*, **2001**, *16*, 1.
- [14] García, O.; Garrido, L.; Sastre, R.; Costela, A.; García-Moreno, I.; *Adv. Funct. Mater.*, **2008**, *18*, 2017.
- [15] Chénais, S.; Forget, S.; *Polym. Int.*, **2012**, *61*, 390.
- [16] <http://www.radiant-dyes.com/index.php/products/laser-dyes/list-of-laser-dyes>
- [17] Pavlopoulos, T. G.; *Prog. Quantum Elec.*, **2002**, *26*, 193.
- [18] López Arbeloa, F.; Ruiz Ojeda, P.; López Arbeloa, I.; *J. Photochem. Photobiol.*, **1988**, *45*, 313.
- [19] Demas, J. N.; Crosby, G. A.; *J. Phys. Chem.*, **1971**, *75*, 991.
- [20] Maeda, M.; *Laser Dyes*; Academic Press, Tokio, **1984**.
- [21] Shankarling, G. S.; Jarag, K. J.; *Resonance*, **2010**, 804.
- [22] Lavis, L. D.; Raines, R. T.; *ACS Chem. Biol.*, **2008**, *3*, 142.
- [23] Treibs, A.; Kreuzer, F.-H.; *Justus Liebigs Ann. Chem.*, **1968**, *718*, 208.
- [24] Shah, M.; Thangaraj, K.; Soong, M.-L.; Wolford, L. T.; Boyer, J. H.; Politzer, I. R.; Pavlopoulos, T. G.; *Heteroatom Chemistry*, **1990**, *1*, 389.
- [25] Boyer, J. H.; Haag, A. M.; Sathyamoorthi, G.; Soong, M.-L.; Thangaraj, K.; Pavlopoulos, T. G.; *Heteroatom Chemistry*, **1993**, *4*, 39.
- [26] Costela, A.; García-Moreno, I.; *Ciencia y Sociedad: Aplicaciones recientes de la luz en medicina, medioambiente y nuevos materiales*, (Eds.: Armesto, D, Sastre, R.), Editorial Complutense, **2010**, Cap.4, p. 81.
- [27] López Arbeloa, F.; López Arbeloa, T.; López Arbeloa, I.; *Handbook of Advanced Electronic and Photonic Materials and Devices*, (Ed.: Nalwa, H. S.), Academic Press, **2001**, Vol. 7, Cap. 5, p. 209.
- [28] Loudet, A.; Burgess, K.; *Chem. Rev.*, **2007**, *107*, 4891.
- [29] Fabian, J.; Hartmann, H.; *Light Absorption of Organic Colorants*, Springer-Verlag, Berlin, **1980**.
- [30] Zollinger, H.; *Color Chemistry*, Verlag Helvetica Chimica Acta, Switzerland, **2003**.
- [31] Mackey, M. S.; Sisk, W. D.; *Dyes and Pigments*, **2001**, *51*, 79.
- [32] Ahmad, M.; King, T. A.; Ko, D.-Y.; Cha, B. H.; Lee, J.; *Opt. Comm.*, **2002**, *203*, 327.
- [33] Pavlopoulos, T. G.; *Appl. Opt.*, **1997**, *36*, 4969.
- [34] Lam, S. Y.; Damzen, M. J.; *Opt. Comm.*, **2003**, *218*, 365.
- [35] Gorman, A. A.; Hamnlett, I.; King, T. A.; Rahn, M. D.; *J. Photochem. Photobiol.*, **2000**, *130*, 127.
- [36] López Arbeloa, F.; López Arbeloa, T.; López Arbeloa, I.; *J. Photochem. Photobiol., A.*, **1999**, *121*, 177.
- [37] Bessette, A.; Hanan, G. S.; *Chem. Soc. Rev.*, **2014**, *43*, 3342.
- [38] Boens, N.; Verbelen, B.; Dehaen, W.; *Eur. J. Org. Chem.*, **2015**, 6577.
- [39] Benstead, M.; Mehl, G. H.; Boyle, R. W.; *Tetrahedron*, **2011**, *67*, 3573.
- [40] Ulrich, G.; Ziesel, R.; Harriman, A.; *Angew. Chem. Int. Ed.*, **2008**, *47*, 1184.

- [41] Ziesel, R.; Ulrich, G.; Harriman, A.; *New J. Chem.*, **2007**, *31*, 496.
- [42] Boens, N.; Leen, V.; Dehaen, W.; *Chem. Soc. Rev.*, **2012**, *41*, 1130.
- [43] Lu, H.; Mack, J.; Yang, Y.; Shen, Z.; *Chem. Soc. Rev.*, **2014**, *43*, 4778.
- [44] Gartzia-Rivero, L.; Yu, H.; Bañuelos, J.; López-Arbeloa, I.; Costela, A.; García-Moreno, I.; Xiao, Y.; *Chem. Asian J.*, **2013**, *8*, 3133.
- [45] Zhang, D.; Martín, V.; García-Moreno, I.; Costela, A.; Pérez-Ojeda, M. E.; Xiao, Y.; *Phys. Chem. Chem. Phys.*, **2011**, *13*, 13026.
- [46] Awuah, S. G.; You, Y.; *RSC Adv.*, **2012**, *2*, 11169.
- [47] Turan, I. S.; Cakmak, F. P.; Yildirim, D. C.; Cetin-Atalay, R.; Akkaya, E. U.; *Chem. Eur. J.*, **2014**, *20*, 16088.
- [48] Kostereli, Z.; Ozdemir, T.; Buyukcakil, O.; Akkaya, E. U.; *Org. Lett.*, **2012**, *14*, 3636.
- [49] Sameiro, M.; Goncalves, T.; *Chem. Rev.*, **2009**, *109*, 190.
- [50] Rezende, L. C. D.; Emery, F. S.; *Orbital Elec. J. Chem.*, **2013**, *5*, 62.
- [51] Fan, G.; Yang, L.; Chen, Z.; *Front. Chem. Sci. Eng.*, **2014**, *8*, 405.
- [52] Umezawa, K.; Citterio, D.; Suzuki, K.; *Anal. Sci.*, **2014**, *30*, 327.
- [53] Yuan, L.; Lin, W.; Zheng, K.; He, L.; Huang, W.; *Chem. Soc. Rev.*, **2013**, *42*, 622.
- [54] Qian, X.; Xiao, Y.; Xu, Y.; Guo, X.; Qian, J.; Zhu, W.; *Chem. Commun.*, **2010**, *46*, 6418.
- [55] Ueno, T.; Urano, Y.; Kojima, H.; Nagano, T.; *J. Am. Chem. Soc.*, **2006**, *128*, 10640.
- [56] Son, H.; Lee, H. Y.; Lim, J. M.; Kang, D.; Han, W. S.; Lee, S. S.; Jung, J. H.; *Chem. Eur. J.*, **2010**, *16*, 11549.
- [57] Song, H.; Rajendiran, S.; Kim, N.; Jeong, S. K.; Koo, E.; Park, G.; Thangadurai, T. D.; Yoon, S.; *Tetrahedron Lett.*, **2012**, *53*, 4913.
- [58] Rong, Y.; Wu, C.; Yu, J.; Zhang, X.; Ye, F.; Zeigler, M.; Gallina, M. E.; Wu, I. C.; Zhang, Y.; Chan, Y.-H.; Sun, W.; Uvdal, K.; Chiu, D. T.; *ACS Nano*, **2013**, *7*, 376.
- [59] Liu, C.-L.; Chen, Y.; Shelar, D. P.; Li, C.; Cheng, G.; Fu, W.-F.; *J. Mater. Chem. C.*, **2014**, *2*, 5471.
- [60] Kolemen, S.; Cakmak, Y.; Erten-Ela, S.; Altay, Y.; Brendel, J.; Thelakkat, M.; Akkaya, E. U.; *Org. Lett.*, **2010**, *12*, 3812.
- [61] Mao, M.; Zhang, X.-L.; Fang, X.-Q.; Wu, G.-H.; Ding, Y.; Liu, X.-L.; Dai, S.-Y.; Song, Q.-H.; *Organic Electronics*, **2014**, *15*, 2079.
- [62] Singh, S. P.; Gayathri, T.; *Eur. J. Org. Chem.*, **2014**, 4689.
- [63] Kamkaew, A.; Lim, S. H.; Lee, H. B.; Kiew, L. V.; Chung, L. Y.; Burgess, K.; *Chem. Soc. Rev.*, **2013**, *42*, 77.
- [64] Awuah, S. G.; You, Y.; *RSC Adv.*, **2012**, 211169.
- [65] Betzig, E.; *Angew. Chem. Int. Ed.*, **2015**, *54*, 8034.
- [66] Moerner, W. E.; *Angew. Chem. Int. Ed.*, **2015**, *54*, 8067.
- [67] Hell, S. W.; *Angew. Chem. Int. Ed.*, **2015**, *54*, 8054.
- [68] Kowada, T.; Maeda, H.; Kikuchi, K.; *Chem. Soc. Rev.*, **2015**, *44*, 4953.
- [69] Willig, K. I.; Rizzoli, S. O.; Westphal, V.; Jahn, R.; Hell, S. W.; *Nature*, **2006**, *440*, 935.

MÉTODOS Y TÉCNICAS EXPERIMENTALES

En esta sección se detalla la metodología de preparación de las muestras de los colorantes BODIPY utilizados en la presente memoria y las técnicas empleadas para su caracterización fotofísica y electroquímica. Posteriormente, se indican los métodos mecanocuánticos aplicados en la simulación teórica de las geometrías, cargas, orbitales moleculares y transiciones electrónicas de los colorantes.

Reseñar que este trabajo de tesis doctoral ha sido fruto del trabajo coordinado con grupos especializados en síntesis orgánica y en caracterización láser, tal y como se refleja en esta sección y en las publicaciones resultantes.

I. COLORANTES Y PREPARACIÓN DE MUESTRAS

Los BODIPYs comerciales fueron suministrados por Exciton (grado láser). El resto de colorantes empleados en el presente trabajo fueron proporcionados por los grupos de investigación de síntesis orgánica del Prof. Eduardo Peña de la Universidad de Guanajuato en México y de la Prof. M^a Jose Ortiz y el Dr. Santiago de la Moya de la Universidad Complutense de Madrid. A lo largo de la memoria se especifican las estructuras de todos los BODIPYs estudiados y se aportan las referencias donde se detallan los pormenores del proceso sintético de cada uno de ellos.

Las propiedades fotofísicas se registraron en disoluciones diluidas (alrededor de $2 \cdot 10^{-6}$ M) para evitar los procesos de filtros internos o reabsorción/reemisión y posibles fenómenos de agregación^[1-3]. Las disoluciones fueron preparadas a partir de una disolución concentrada (10^{-3} M) de partida del correspondiente colorante en acetona a la que, tras evaporación al vacío de la acetona, se añadía la cantidad adecuada del disolvente requerido hasta conseguir la concentración de colorante final deseada. Los disolventes empleados fueron de grado espectroscópico (Merck, Fluka o Aldrich) y utilizados sin ninguna purificación.

Las medidas electroquímicas se realizaron en disoluciones concentradas (0.5-1mM) de acetonitrilo a las que se añadió un exceso (hasta 0.1M) de tetrabutil amonio hexafluorofosfato (TBAPF₆, electroquímicamente inerte). La presencia de este electrolito en exceso en el disolvente polar aumenta la fuerza iónica del medio y asegura una alta constante dieléctrica que posibilita el flujo de la corriente. Además, asegura que el transporte de las especies hacia el electrodo sea únicamente por difusión, a la vez que evita la migración de los iones electroquímicamente activos entre el electrodo de trabajo y auxiliar (ver sección de electroquímica). Las disoluciones se purgaron con argón y las medidas se realizaron bajo esta atmosfera inerte.

II. TÉCNICAS EXPERIMENTALES

La caracterización de los colorantes considerados en los diversos medios se realizó mediante técnicas espectroscópicas y electroquímicas. En el primer caso se usaron espectrofotómetros de absorción y emisión fluorescente (en modo estacionario y correlacionado en el tiempo) de luz ultravioleta-visible para registrar los espectros correspondientes de disoluciones diluidas ($2 \mu\text{M}$) en cubetas de cuarzo de 1 cm de camino óptico y termostalizadas a una temperatura de 20 °C. Las medidas fueron realizadas en muestras aireadas, ya que previamente se comprobó que la eliminación del oxígeno disuelto en el disolvente (mediante burbujeo de argón durante 10 min) no afectaba a los resultados. En el segundo caso, la caracterización electroquímica se realizó empleando la técnica de voltametría cíclica en atmosfera inerte usando un sistema de 3 electrodos.

La caracterización de las propiedades láser fue realizada por el grupo de investigación formado por la Prof. Inmaculada García Moreno, el Prof. Angel Costela y el Dr. Luís Cerdán del Instituto de Química-Física "Rocasolano" del CSIC, Madrid.

Espectroscopía de absorción ultravioleta-visible

La absorción de radiación se obtuvo registrando la pérdida de intensidad de la luz transmitida una vez atravesada la muestra con respecto a la radiación incidente. Los espectros de absorción se realizaron en un espectrofotómetro UV-Vis de doble haz Varian (modelo Cary 4E) en modo de absorbancia. El espectrofotómetro consta de una lámpara halógena (región Vis) y otra de deuterio (región UV), automáticamente intercambiables en la zona de 350 nm, un monocromador doble con una red de difracción 1200 líneas/mm con una resolución de $\pm 0,5$ nm, y un fotomultiplicador Hamamatsu R928 como detector (Figura 9). Las medidas se realizaron con una resolución espectral de 0,5 nm y con un tiempo de integración de 0,1 s, lo que dio lugar a una velocidad de barrido de 300 nm/min. Previamente a la obtención del espectro de absorción se registró una línea base con el correspondiente disolvente sin colorante.

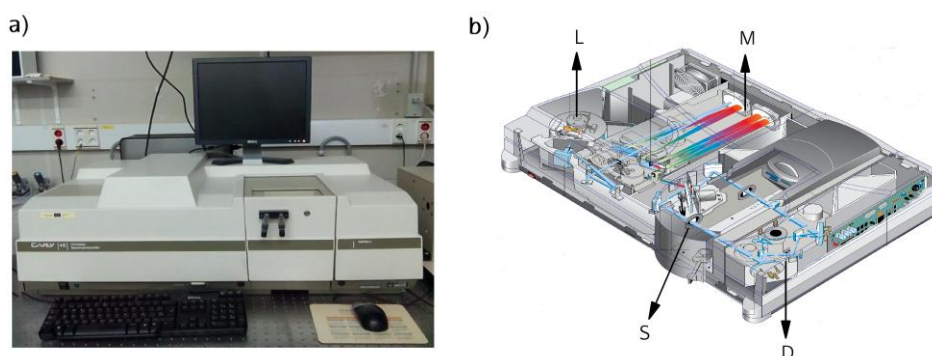


Figura 9. a) Espectrofotómetro de doble haz UV/Vis Varian Cary 4E. b) Sistema óptico del espectrofotómetro de absorción; L: fuente de excitación, M: doble monocromador, S: compartimento de la muestra, D: detector (PM Hamamatsu R928).

Espectroscopía de fluorescencia

La fluorescencia se obtuvo a partir de la intensidad emitida por la muestra previamente excitada en configuración de ángulo recto. Los espectros de fluorescencia y excitación se registraron en un fluorímetro SPEX modelo Fluorolog 3-22 o en un espectrofluorímetro Edinburgh Instruments modelo FLSP920. Este último espectrofluorímetro se usó especialmente en el caso de los colorantes con la emisión localizada en la parte menos energética (roja) del visible (ventana espectral > 600 nm) debido a la mayor sensibilidad del detector en dicha región espectral. Ambos fluorímetros constan de una lámpara Xe (450 W), dobles-monocromadores, para mejorar la resolución de la longitud de onda tanto en excitación como emisión, y un fotomultiplicador Hamamatsu R928-P como detector, especialmente

sensible a altas longitudes de onda y refrigerado electrónicamente por un peltier que reduce el ruido de fondo y mejora la relación señal/ruido (Figura 10). Los espectros de emisión fueron registrados con una velocidad de barrido de 300 nm/min y una resolución de $\pm 0,5$ nm. Los espectros de fluorescencia fueron corregidos respecto a la dependencia de la sensibilidad del aparato con la longitud de onda. Las medidas a bajas temperaturas (hasta 77K) se realizaron utilizando un criostato (Oxford) refrigerado con nitrógeno líquido y un controlador de temperatura electrónico externo.

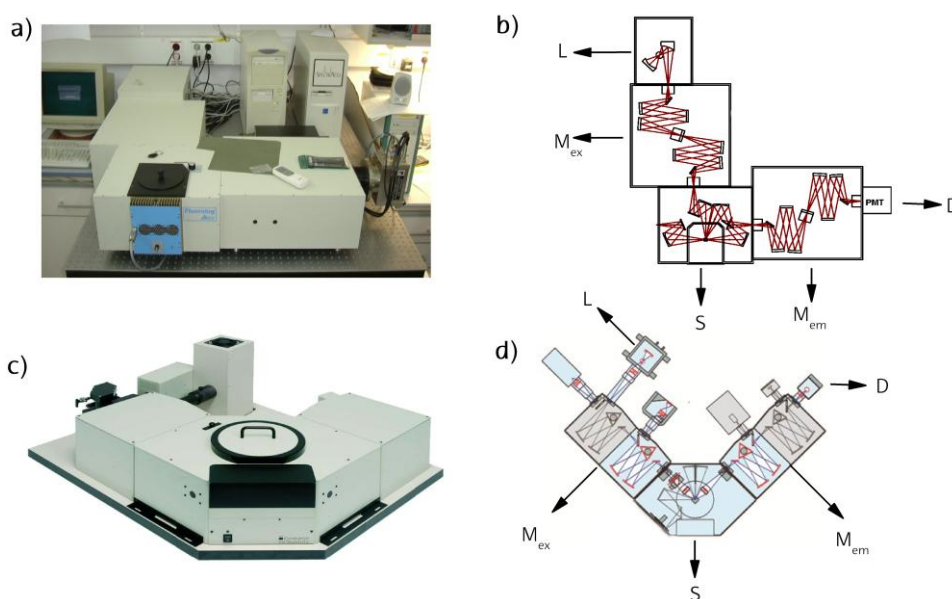


Figura 10. a) Espectrofluorímetro SPEX Fluorolog 3-22. b) Sistema óptico del espectrofluorímetro SPEX; L: fuente de excitación, M_{ex} : doble monocromador de excitación, S: compartimento de la muestra, M_{em} : doble monocromador de emisión, D: detector (PM Hamamatsu R928-P). c) Espectrofluorímetro Edinburgh Instruments FLSP920. d) Sistema óptico del espectrofluorímetro Edinburgh Instruments.

Los rendimientos cuánticos de fluorescencia (ϕ) se obtuvieron a partir de los espectros de fluorescencia corregidos (considerando la transmitancia del monocromador de emisión y la sensibilidad del fotomultiplicador a cada longitud de onda) y usando un colorante comercial adecuado como referencia (para información particular de cada caso, ver la sección experimental de los artículos adjuntos al final de la memoria). El espectro de fluorescencia de la referencia se registró en las mismas condiciones que el de la muestra. La determinación de ϕ se llevó a cabo a partir del área bajo la curva del espectro de emisión (A_{ri}) y de la intensidad de luz absorbida a la longitud de onda de excitación (I_{ab}) tanto de la muestra como de la referencia (superíndice r) y teniendo en cuenta el efecto del índice de refracción (n) del disolvente mediante la ecuación 1^[1]:

$$\phi = \phi^r \frac{n^2}{(n^r)^2} \frac{I_{ab}^r(\lambda_{exc}) A_{fl}}{I_{ab}(\lambda_{exc}) A_{fl}^r} \quad (1)$$

Contador cuántico de fotones correlacionado con el tiempo

El tiempo de vida (τ) del estado excitado se determinó a partir de la pérdida de intensidad de emisión con el tiempo tras la excitación. Las curvas de desactivación fluorescente fueron registradas mediante un contador cuántico de fotones correlacionado con el tiempo (TC-SPC, *Time-Correlated Single Photon Counting*) Edinburgh Instruments modelo FL920, con resolución temporal de unos 30 ps (Figura 11). La excitación se llevó a cabo usando láseres pulsados de diodo (PicoQuant; modelos LDH370, LDH 410, LDH440, LDH470 y LDH530, donde el número indica la longitud de onda de trabajo) en el que la energía y frecuencia del pulso se controlaba externamente (PicoQuant, modelo PDL800-B). En todos los casos se trabajó a una frecuencia de pulso de 20 MHz con una potencia fija, previamente optimizada para cada cabezal. La anchura de pulso conseguida (FWHM, *Full width at half maximum*) fue de 120 ps. La emisión se monitorizó en todos los máximos observados en los espectros de fluorescencia usando para ello un doble monocromador, en modo sustractivo, y un detector fotomultiplicador *microchannel plate* (Hamamatsu, modelo MCP-HFAC) refrigerado con un dispositivo Peltier (Hamamatsu, modelo C4878).

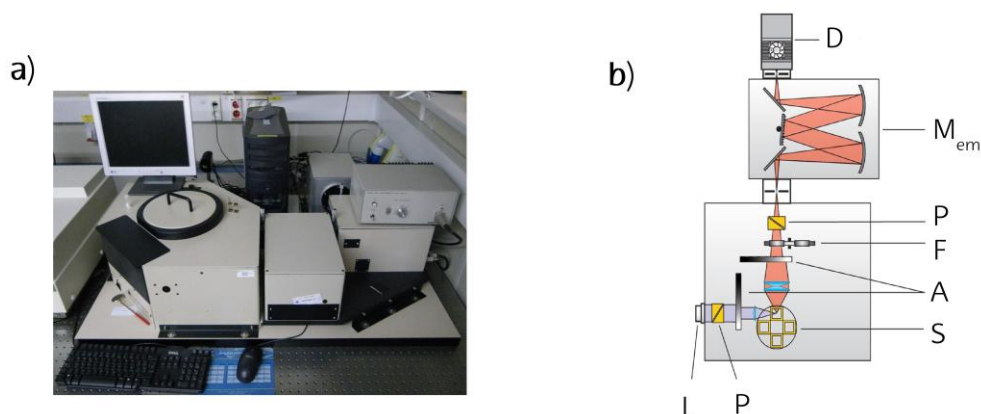


Figura 11. a) Contador cuántico de fotones Edinburgh Instruments FLS920 correlacionado en el tiempo (TC-SPC). b) Esquema de la técnica TC-SPC; L: láser de diodo, P: polarizadores, S: compartimento de la muestra, A: atenuadores de señal, F: filtros, M_{em} : doble monocromador de emisión, D: detector (Hamamatsu MCP-HFAC).

El contador de fotones determina el tiempo de vida a partir del registro del tiempo transcurrido desde la excitación de la muestra mediante un pulso de luz del láser (señal de *start*)

hasta la detección del primer fotón emitido que llega al detector (señal de *stop*). La medida temporal se realiza midiendo el voltaje generado por la acción del convertidor tiempo/amplitud (CTA) desde la señal *start* (por medio de un fotodiodo) hasta que el detector manda la señal de *stop*. Posteriormente, la amplitud de dicho voltaje queda almacenado como una cuenta en un canal. El uso del detector multicanal permite almacenar fotones (o cuentas) en función del tiempo, ya que cada canal corresponde a una amplitud de voltaje. La repetición de este proceso da lugar a un histograma del número de cuentas (proporcional al número de fotones detectados) en función de los canales (proporcional al voltaje generado, es decir, al tiempo transcurrido entre la señal *start* y *stop*)^[4-5]. La curva de decaimiento obtenida es el resultado del 2% de las cuentas registradas por pulso de excitación, para evitar la acumulación de cuentas ya registradas.

Las curvas de desactivación fluorescente se registraron hasta obtener 10000 cuentas en el máximo. Con el fin de eliminar la contribución de la fuente de excitación, se registró su radiación mediante un difusor (una suspensión coloidal de Ludox) que permite detectar la luz de excitación a 90°. Los tiempos de vida se obtuvieron en base a un ajuste exponencial de la curva de decaimiento, previamente deconvolucionada mediante el algoritmo de Marquardt para eliminar la anteriormente citada señal del láser, y a partir de la pendiente de cada recta. El método de la deconvolución considera que la descripción óptima de los datos experimentales es aquella que minimiza la suma promediada de los cuadrados de las desviaciones de los datos experimentales respecto a los propuestos por la función de ajuste calculada, que se define mediante la ecuación 2:

$$I_{fl}(t) = A_1 \exp(-t/\tau_1) + A_2 \exp(-t/\tau_2) + \dots \quad (2)$$

donde A_i es el factor preexponencial que controla el peso estadístico de cada exponencial y τ_i es el tiempo de vida correspondiente a cada decaimiento exponencial.

La bondad del ajuste (bien sea monoexponencial o de orden superior) se determinó en base al parámetro estadístico chi-square (límite considerado $\chi^2 < 1.2$) y la distribución del análisis de los residuos que indica la desviación del ajuste exponencial considerado respecto a las cuentas experimentales, lo cual se puede hacer visualmente o mediante el parámetro de Durbin-Watson^[6-8].

Las constantes de velocidad de desactivación radiante (k_{fl}) y no-radiante (k_{nr}) se calcularon a partir del rendimiento cuántico de fluorescencia y el tiempo de vida, $k_{fl} = \phi/\tau$ y $k_{nr} = (1-\phi)/\tau$, respectivamente.

Electroquímica

El análisis electroquímico se realizó mediante la técnica de la voltametría cíclica. Esta técnica consiste en la medida de la intensidad eléctrica al aplicar diversos potenciales con un potenciostato de manera cíclica^[9]. Partiendo de un potencial inicial, se hace un barrido entre dos potenciales extremos prefijados, llamados potenciales de cambio (Figura 12). Es decir, se aumenta el potencial hasta un máximo dado y luego se invierte completamente el potencial hasta un potencial mínimo para finalmente volver al punto inicial. Este proceso se puede iniciar aumentando el potencial (barrido positivo) o disminuyéndolo (barrido negativo).

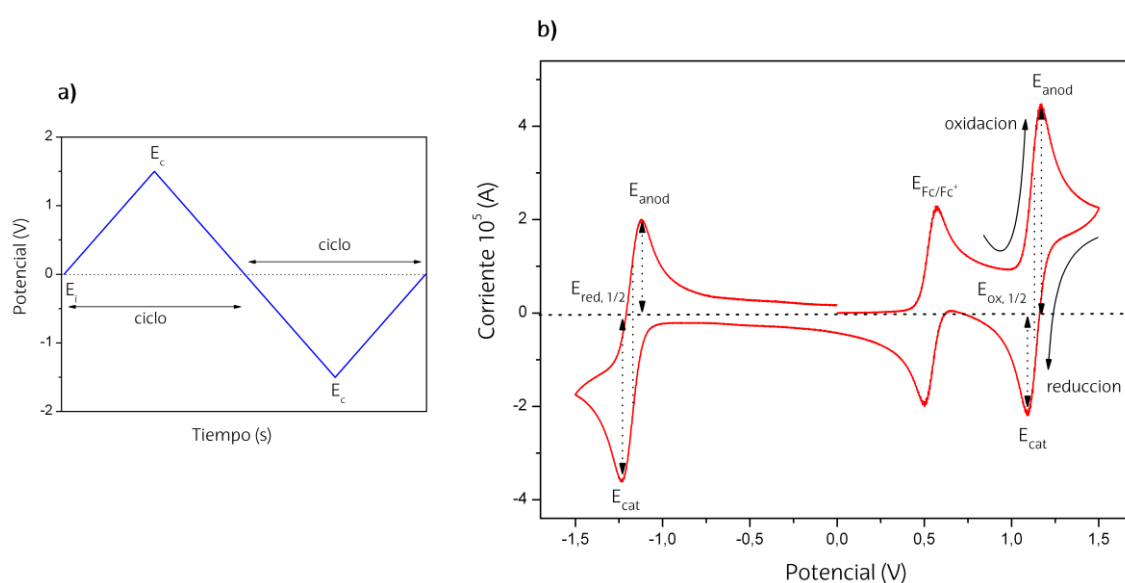


Figura 12. a) Barrido de onda triangular entre el potencial inicial (E_i) y el de intercambio (E_c) máximo y mínimo. b) Voltamograma cíclico; E_{anod} : potencial anódico, E_{cat} : potencial catódico, $E_{1/2}$: potencia de onda medio para el proceso de reducción y oxidación; E_{Fc/Fc^+} : potencial del ferroceno. La dirección del barrido (en este caso positivo) se indica con las flechas.

Por lo tanto, un aumento del potencial (barrido positivo) hasta sobrepasar el potencial de oxidación del analito de interés provoca su oxidación en las inmediaciones del electrodo ($A \rightarrow A^+ + e^-$) y la generación de una corriente anódica (intensidad eléctrica positiva) que aumenta hasta llegar a un valor máximo, correspondiente al momento en que se agota la especie electroquímicamente activa, por lo que la intensidad comienza a descender (Figura 12). Cuando se llega al potencial máximo de inversión se invierte el potencial y se empieza a disminuir. Si dicho proceso de oxidación es reversible ($A \leftarrow A^+ + e^-$) se observará una corriente catódica (intensidad electrónica negativa) simétrica, en cambio si es irreversible no se detectara corriente alguna. De forma análoga a los procesos de oxidación, si se alcanzan potenciales menores que el potencial de reducción del analito, se produce la reducción del mismo

($A + e^- \rightarrow A^-$) y en consecuencia se detecta una corriente catódica. Una vez alcanzado el potencial mínimo de intercambio se vuelve al potencial de inicio, y de nuevo, si el proceso de reducción es reversible ($A + e^- \leftarrow A^-$) se observará la correspondiente banda anódica simétrica al aumentar el potencial. De forma que del máximo de las ondas anódicas o catódicas en los procesos irreversibles o del punto intermedio en los procesos reversibles se puede determinar el potencial de oxidación o reducción respectivamente (Figura 12).

Los voltagramas cíclicos se registraron en un Metrohm Autolab usando una celda electroquímica de tres electrodos (Figura 13): el electrodo de trabajo (WE), el electrodo de referencia (RE) y el contra-electrodo (CE). La presencia de este último electrodo auxiliar (hilo de platino) es transportar la corriente eléctrica que pasa a través del electrodo de trabajo (por eso también es conocido como electrodo contador) y en su superficie no tienen lugar los procesos electroquímicos. Como electrodo de trabajo se utilizó un disco (3 mm de diámetro) o placa de platino (superficie 8 mm x 7,5 mm) y como electrodo de referencia un hilo de Ag/AgCl con el electrolito como soporte. En el registro del voltagrama, el voltaje se controló entre los electrodos WE y RE y el flujo de la corriente entre los electrodos WE y CE. Las medidas se realizaron con una velocidad de barrido de $0,2 \text{ Vs}^{-1}$ fijando los potenciales de cambio en -2 y +2 V (o en su defecto -1,5 y +1,5 V). Para que los datos de potenciales de reducción y oxidación sean comparables con los existentes en la bibliografía, fueron corregidos respecto al potencial del ferroceno en agua (0.424 V vs SCE, es decir, usando como referencia el electrodo de calomelanos), que se usó como patrón interno ($c = 0.40 \text{ mM}$).



Figura 13. a) Voltámetro Metrohm Autolab. b) Celda electroquímica; WE: electrodo de trabajo, RE: electrodo de referencia, CE: contra-electrodo.

III. MÉTODOS COMPUTACIONALES

La química computacional se basa en simulaciones matemáticas del comportamiento de los átomos y moléculas a nivel microscópico. En el presente trabajo se emplean los métodos de la mecánica cuántica como base para la computación, que describen las moléculas en términos de interacciones entre núcleos y electrones, y la geometría molecular sobre la base de la disposición nuclear de mínima energía. En concreto, los cálculos teóricos se han centrado en la optimización de las geometrías, tanto en estado fundamental como en estado excitado, la simulación de la distribución de cargas y los mapas de densidad electrónica de los orbitales moleculares y la predicción de los tránsitos electrónicos de absorción y emisión, considerando en todos ellos el efecto del disolvente.

De forma general los cálculos teóricos se clasifican en semiempíricos y *ab initio*. Los métodos semiempíricos resuelven el hamiltoniano simplificado despreciando algunas integrales y/o asignando un valor basándose en datos experimentales, proceso al que se denomina parametrización. Por el contrario, el cálculo *ab initio* resuelve el hamiltoniano electrónico verdadero y no utiliza datos empíricos que simplifiquen su resolución, por lo que calculan soluciones a la ecuación de Schrödinger usando aproximaciones matemáticas. Por tanto, los cálculos semiempíricos son relativamente sencillos y rápidos computacionalmente hablando, mientras que los *ab initio* son mucho más costosos, pero más exactos. Como consecuencia la aplicación de estos últimos se limita a pequeños sistemas de decenas de átomos. Para moléculas mayores, como el caso que nos ocupa de los colorantes BODIPY, una alternativa interesante es la de los métodos basados en la teoría funcional de la densidad (DFT, *Density Functional Theory*)^[10]. En este caso, para solucionar la ecuación de Schrödinger, se determina la energía electrónica a partir de la densidad electrónica sin necesidad de calcular la función de onda. Además, a diferencia de los métodos *ab initio* basados en Hartree-Fock, el método DFT incluye intrínsecamente la energía de correlación electrónica. Esto hace que el método sea computacionalmente más eficiente y permite acometer el estudio teórico de moléculas grandes de forma satisfactoria en un tiempo razonable y con una capacidad computacional accesible^[11-13].

Por tanto, en el presente trabajo los cálculos teóricos se realizaron principalmente con el método DFT. Concretamente la optimización de geometría del estado fundamental se llevó a cabo usando el funcional B3LYP (método híbrido de Becke de 3 parámetros^[14] que usa el funcional de correlación de Lee, Yang y Parr^[15]) que ha demostrado ser uno de los funcionales más adecuados dentro de los DFT, ya que presenta un buen compromiso entre exactitud y

coste computacional. Con el fin de acelerar el cálculo DFT las geometrías fueron optimizadas previamente con el método semiempírico AM1 (*Austin Model 1*)^[16], implementado en el MOPAC 2000^[17] del Chem3D Ultra 7.0). Esta geometría minimizada se tomó como punto de partida para la optimización posterior con B3LYP. Por otra parte, la optimización del primer estado excitado se realizó a partir de la geometría del estado fundamental proporcionada por B3LYP, minimizando la energía mediante el método *ab initio* CIS (*Configuration Interaction Singles*)^[18]. En este método se consideran configuraciones excitadas consecuencia únicamente de excitaciones simples.

En la optimización de ambos estados se utilizó el sistema de bases de doble valencia 6-31G, que emplea funciones de base gaussianas para definir las funciones de onda de cada átomo (definido por una combinación lineal de seis gaussianas para describir los orbitales atómicos internos y una combinación de tres y una gaussianas para describir los orbitales de valencia interno y exterior, respectivamente). Previamente se determinó que la adición de funciones de polarización (*) y difusas (+) a la base 6-31G en el cálculo DFT no mejoraba ostensiblemente la exactitud del cálculo y por el contrario aumentaba considerablemente el tiempo de cálculo. Esto sugiere la validez del nivel de cálculo B3LYP/6-31G para la simulación de los BODIPYs. La optimización de la geometría se hizo sin ninguna restricción geométrica y se consideró que la geometría obtenida después de alcanzar la condición de autoconsistencia de campo (establecida por los límites de convergencia) se correspondía como un mínimo de energía cuando el correspondiente análisis de las frecuencias no arrojaba ninguna frecuencia negativa.

Una vez optimizadas las geometrías, bien sea en estado fundamental o excitado, se procedió a determinar la distribución de cargas (método CHelpg), la orientación y valor del momento dipolar, y los mapas de orbitales moleculares (HOMO, *Highest Occupied Molecular Orbital* y LUMO, *Lowest Unoccupied Molecular Orbital*) y potencial electrostático.

El espectro de absorción se calculó como una transición vertical (Franck-Condon) desde el estado fundamental (S_0) a los estados excitados (S_1 , S_2 , ...) a partir de la geometría optimizada en el estado fundamental (B3LYP/6-31G), mientras que el de fluorescencia se predijo de forma similar pero siendo el tránsito desde el nivel excitado S_1 al nivel S_0 y tomando como referencia la geometría optimizada en S_1 (CIS/6-31G). En la predicción de ambos tránsitos electrónicos se empleó el método *Time Dependent*^[19-20] (TD-B3LYP)^[21] con la misma base (6-31G).

También se consideró en todos los cálculos anteriores, bien fuesen puntuales o de optimización de geometría, el efecto de disolvente para una mejor comparación con los resultados fotofísicos experimentales en disolución. La solvatación se evaluó teóricamente usando el método del campo autoconsistente de reacción (SCRF, *Self Consistent Reaction Field*). El entorno del disolvente se considera como un medio homogéneo que responde a la carga del colorante inmerso en el disolvente por medio del modelo del continuo polarizado (PCM, *Polarizable Continuum Model*)^[22-23] que define la cavidad como una serie de esferas superpuestas y centradas en los átomos. Es decir, el método sólo tiene en cuentas las interacciones universales soluto-disolvente introduciendo una distribución de carga en la superficie de la cavidad según la constante dieléctrica del disolvente.

Todos los cálculos *ab initio* y DFT se realizaron en el programa GAUSSIAN 09^[24] usando el cluster informático "ARINA" (Figura 14) bajo entorno LINUX que dispone el servicio SGIker de la UPV/EHU.

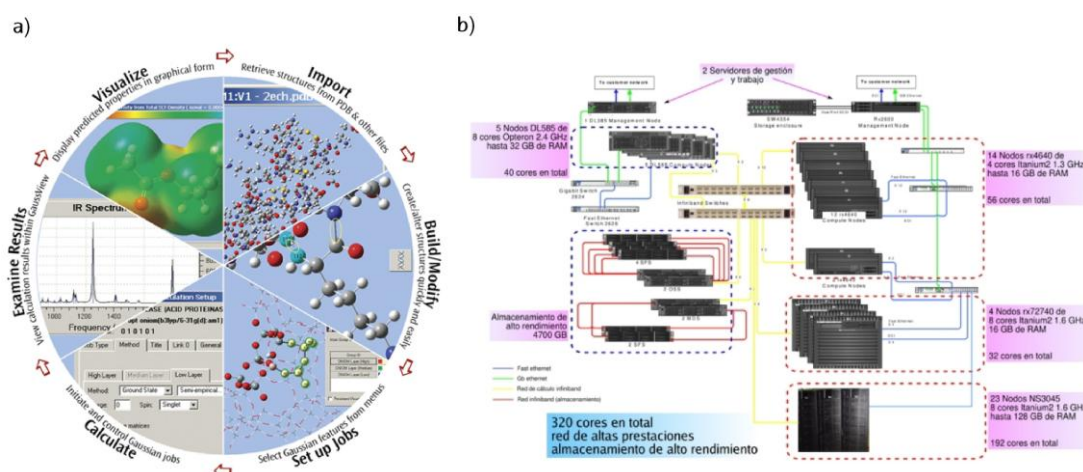


Figura 14. a) Esquema de las posibilidades de cálculo que ofrece Gaussian 09. b) El cluster informático "ARINA" donde se han realizado los cálculos de Gaussian en entorno linux.

Bibliografía

- [1] Demas, J.N.; Crosby, G.A. *J. Phys. Chem.* **1971**, 75, 991.
- [2] López Arbeloa, I. *J. Photochem.* **1980**, 14, 97.
- [3] Parker, C.A. *Photoluminescence of Solutions*; Elsevier: Amsterdam, **1968**.
- [4] Demas, J.N. *Excited State Lifetime Measurements*; Academic Press: New York, **1983**.
- [5] O'Connor, D.V.; Phillips, D. *Time-Correlated Single Photon Counting*; Academic Press: London, **1984**.
- [6] Boens, N.; van de Zegel, M.; De Schryver, F.C. *Chem. Phys. Lett.* **1984**, 111, 340.
- [7] Boens N.; van de Zegel, M.; De Schryver, F.C. ; Desie, G. *Photochem. Photobiol. Supp.* **1987**, 93.
- [8] Van de Zegel, M.; Boens, N. ; Daems, D. ; De Schryver, F.C. *Chem. Phys.* **1986**, 101, 311.
- [9] Brett, C.H.A.; Brett, A.M.O. *Electrochemistry: Principles, Methods and Applications*, Oxford University Press, Oxford, **1993**.
- [10] Kohn, W.; Becke, A.D.; Parr, R.G. *J. Phys. Chem.* **1996**, 100, 12974.
- [11] Bertrán Rusca, J.; Branchadell Gallo, V.; Moreno Ferrer, M.; Sodupe Roure, M. *Química Cuántica; Síntesis*: Madrid, **2002**.
- [12] Szabo, A.; Ostlund, N.S. *Modern Quantum Chemistry: Introduction to Advanced Electronic Structure Theory*; Dover Publications, Inc: New York, **1996**.
- [13] Foresman, J.B.; Frisch, H. *Exploring Chemistry with Electronic Structure Methods*; Gaussian, Inc: Pittsburgh, PA, **1996**.
- [14] Becke, A. D. *J. Chem. Phys.* **1996**, 104, 1040.
- [15] Lee, C.; Yang, W.; Parr, R. G. *Phys. Rev. B* **1988**, 37, 785.
- [16] Dewar, M.J.S.; Zoebisch, E.G.; Helay, E.F.; Stewart, J.J.P. *J. Am. Chem. Soc.* **1985**, 107, 3902.
- [17] Stewart, J.J.P. *Mopac 2000V1.3*; Fujitsu Limited: Tokyo, 2000.
- [18] Foresman, J.B.; Head-Gordon, M.; Pople, J.A.; Frisch, M.J. *J. Phys. Chem.* **1992**, 96, 135.
- [19] Wiberg, K.B.; Stratmann, R.E.; Frisch, M.J. *Chem. Phys.* **1998**, 297, 60.
- [20] Hirata, S.; Lee, T.J.; Head-Gordon, M.J. *J. Chem. Phys.* **1999**, 111, 8904.
- [21] Bauernschmitt, R.; Ahlrichs, R. *Chem. Phys. Lett.* **1996**, 256, 454.
- [22] Tomasi, J.; Persico, M. *Chem. Rev.* **1994**, 94, 2027.
- [23] Miertus, S.; Scrocco, E.; Tomasi, J. *Chem. Phys.* **1981**, 55, 117.
- [24] Frisch, M.J.; Trucks G.W.; Schlegel H.B.; Scuseria G.E.; Robb M.A.; Cheeseman J.R.; Scalmani G.; Barone V.; Mennucci B.; Petersson G.A.; Nakatsuji H.; Caricato M.; Li X.; Hratchian H.P.; Izmaylov A.F.; Bloino J.; Zheng G.; Sonnenberg J.L.; Hada M.; Ehara M.; Toyota K.; Fukuda R.; Hasegawa J.; Ishida M.; Nakajima T.; Honda Y.; Kitao O.; Nakai H.; Vreven T.; Montgomery J.A.; Peralta Jr., J.E.; Ogliaro F.; Bearpark M.; Heyd J.J.; Brothers E.; Kudin R.N.; Staroverov V.N.; Kobayashi R.; Normand J.; Raghavachari K.; Rendell A.; Burant J.C.; Iyengar S.S.; Tomasi J.; Cossi M.; Rega N.; Millam J.M.; Klene M.; Knox J.E.; Cross J.B.; Bakken V.; Adamo C.; Jaramillo J.; Gomperts R.; Stratmann R.E.; Yazyev O.; Austin A.J.; Cammi R.; Pomelli C.; Ochterski J.W.; Martin R.L.; Morokuma K.; Zakrzewski V.G.; Voth G.A.; Salvador P.; Dannenberg J.J.; Dapprich S.; Daniels A.D.; Farkas Ö.; Foresman J.B.; Ortiz J.V.; Cioslowski J.; Fox D.J. *Gaussian-09*; Gaussian, Inc., Wallingford CT, **2009**.

CAPÍTULO 1

ESTRUCTURA Y FOTOFÍSICA DE PIRROMETENOS

Antes de entrar en detalle en la discusión de la influencia en las propiedades espectroscópicas de los diversos derivados del 4,4-difluoro-4-bora-3a,4a-diaza-s-indaceno (o más comúnmente conocidos como boro-dipirrometenos o BODIPYs^[1]), es conveniente reseñar brevemente los aspectos fotofísicos y estructurales más destacados de la estructura básica de estos colorantes. Para ello tomamos como referencia el cromóforo BODIPY más simple, con su esqueleto de indaceno hidrogenado, sin sustitución (también llamado BDP). Curiosamente, aunque los primeros estudios de BODIPYs datan de 1968^[2], y desde entonces se ha modificado su estructura exhaustivamente^[3-4], el cromóforo simple no ha sido obtenido hasta hace pocos años (2009), debido a la inestabilidad del dipirrometeno^[5].

Por tanto, en éste capítulo introductorio se presentan las características fotofísicas generales del BDP (Figura 1.1), que servirá como punto de partida o referencia para la discusión del resto de colorantes descritos a lo largo de la tesis. Los resultados experimentales se complementan con cálculos mecanocuánticos que modelan las estructuras y propiedades, tanto electrónicas como espectroscópicas, de estos colorantes.

1.1. ESTRUCTURA DE BODIPYS

El núcleo de BODIPY consta de dos pirroles unidos por un grupo metileno, que permite la deslocalización de la densidad electrónica π entre ambos anillos, y por un puente de unión BF_2 , que no participa en la deslocalización pero le confiere rigidez a la estructura molecular (Figura 1.1). La numeración de las posiciones del cromóforo BODIPY según el sistema IUPAC es el empleado para el carbociclo análogo indaceno, mientras que los términos α -, β - y *meso*- indican las mismas posiciones que en el núcleo del dipirrometeno.

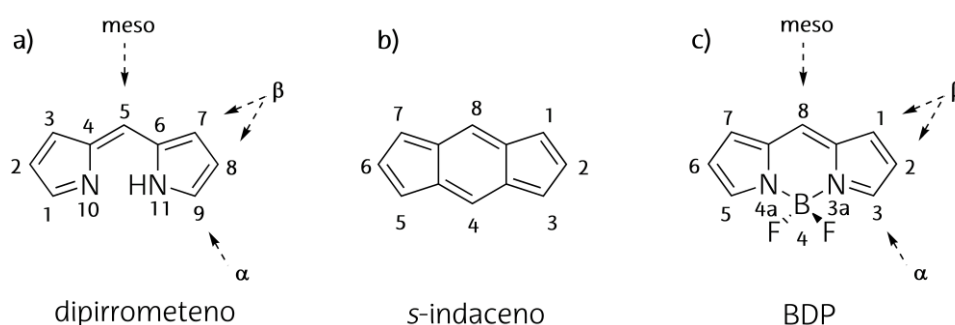


Figura 1.1. Estructuras generales de los núcleos del a) dipirrometeno b) indaceno y c) BODIPY.

La simulación mecanocuántica (B3LYP/6-31G) propone una estructura plana para el cromóforo BDP (Figura 1.2), asignándole un grupo de simetría C_{2v} . De hecho, los parámetros geométricos son simétricos en torno al eje molecular menor (transversal) y la desviación de la planaridad, marcada por los ángulos diedros, es de apenas $0,1^\circ$ y localizada principalmente en la zona del boro, debido a su hibridación tetraédrica. La excitación (CIS/6-31G) conlleva pequeñas variaciones en la geometría molecular, tal y como era de esperar en una estructura rígida.

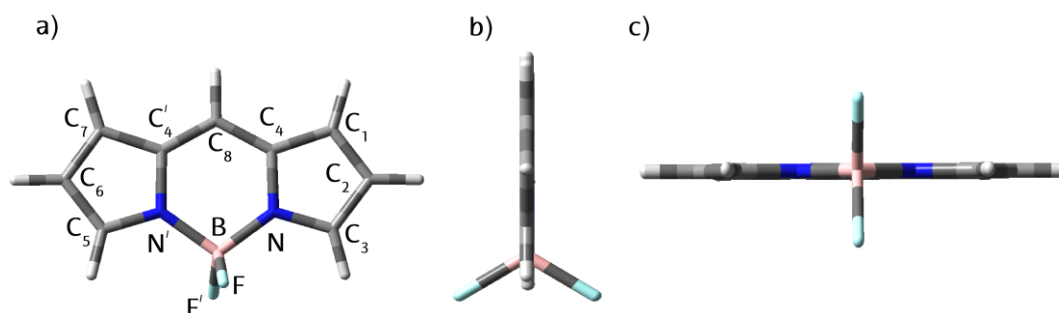


Figura 1.2. Geometría optimizada del BDP, junto con la numeración de los átomos del cromóforo y las respectivas perspectivas desde los ejes a) x, b) y, c) z.

La validez de los métodos de los cálculos teóricos realizados se confirma mediante la comparación con la técnica de difracción de rayos X^[5] (Tabla 1.1). Se constata que las distancias de enlace teóricas no difieren en más de 0.03 Å (la mayor desviación se observa en el enlace B-F) respecto a los datos de rayos X (Tabla 1.1), lo que indica la idoneidad de los métodos de cálculo empleados. Hay que mencionar que los datos experimentales de rayos X se han obtenido en muestras sólidas cristalinas mientras que los cálculos teóricos se realizan en fase gas o disolución.

Tabla 1.1. Tabla de las distancias de enlace del BDP obtenidas por rayos-X y simulación teórica de los estados S_0 y S_1 . La numeración de los átomos se indica en la Figura 1.2.

Enlace	Distancias de enlace (± 0.001 Å)		
	Rayos X ^[5]	Teóricas (S_0)	Teóricas (S_1)
C ₄ -C ₈	1.383	1.392	1.396
C ₁ -C ₄	1.410	1.424	1.418
C ₁ -C ₂	1.370	1.394	1.383
C ₂ -C ₃	1.400	1.416	1.412
C ₃ -N	1.339	1.352	1.334
C ₄ -N	1.391	1.408	1.409
N-B	1.545	1.557	1.538
B-F'	1.387	1.425	1.423
B-F	1.396	1.425	1.423

Los BODIPYs son moléculas neutras con una estructura zwitteriónica caracterizada por tener una carga negativa en el átomo de boro (tetracoordinado) y una carga positiva en principio localizada en un átomo de nitrógeno. Sin embargo, esta carga positiva es susceptible de deslocalizarse a través del sistema π electrónico del cromóforo, dejando a los átomos de nitrógeno el par de electrones libres sin compartir (Figura 1.3). Teniendo en cuenta las formas resonantes del BODIPY, se pueden considerar dos estructuras extremas: la estructura "a" con un átomo de nitrógeno cargado positivamente y la estructura "d" donde la carga positiva se localiza en la posición *meso* del cromóforo, lo que proporciona mayor separación de cargas a lo largo del eje molecular más corto.

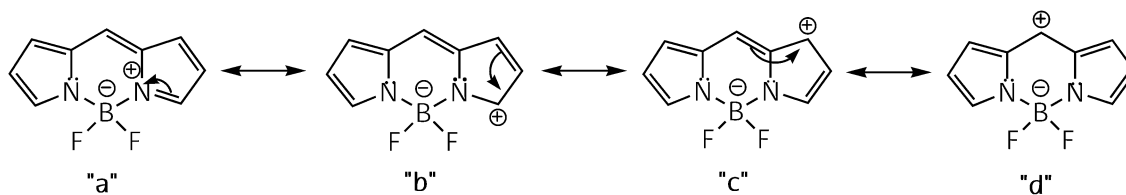


Figura 1.3. Estructuras resonantes del BODIPY (las correspondientes formas simétricas no se han incluido).

No obstante, la simulación de la distribución de cargas (CHelpg) predice una alta carga positiva localizada en el átomo de boro, mientras que la carga negativa se distribuye principalmente entre los átomos de nitrógeno y flúor debido a su mayor electronegatividad (Figura 1.4.a). De hecho, el mapa del potencial electrostático localiza gran densidad electrónica negativa en los átomos de flúor (color rojo) y, en menor medida en los nitrógenos (amarillo, Figura 1.4.b). Todas estas tendencias, inducen a pensar que los enlaces en los que está involucrado el átomo de boro no son todos covalentes, si no que los enlaces con los átomos de flúor adquieren cierto carácter iónico, de ahí su mayor distancia de enlace^[6] (Tabla 1.1).

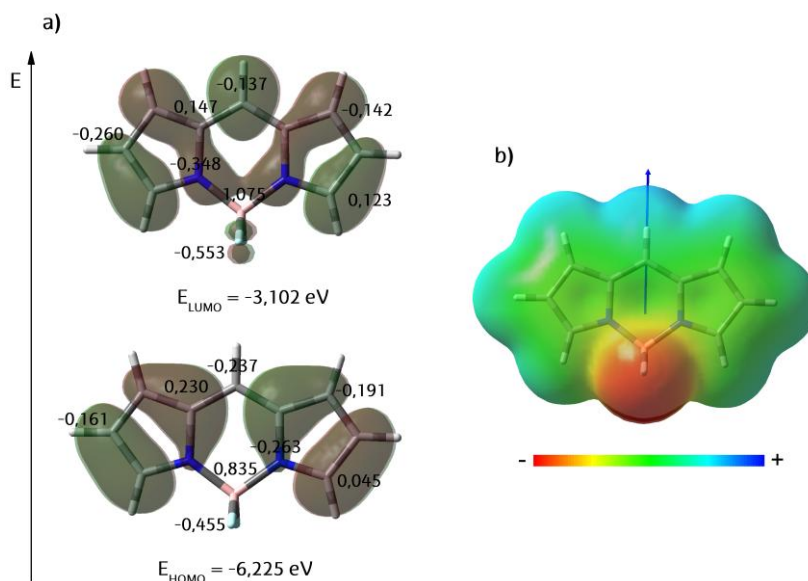


Figura 1.4. a) Mapas de densidad electrónica de los orbitales moleculares frontera (HOMO y LUMO), junto con las cargas parciales CHelpg del BDP (no se incluyen las cargas de los correspondientes átomos simétricos). b) Mapa del potencial electrostático sobre la densidad electrónica (rojo indica carga negativa y azul positiva), junto con el vector del momento dipolar.

La distribución de cargas predice una alternancia en las cargas puntuales de los átomos de carbono (positiva y negativa) a través del sistema π conjugado, por lo que los pirrometenos se pueden definir como estructuras tipo cianina o polimetino^[7-8]. La aromaticidad de dicho

sistema deslocalizado se puede cuantificar cualitativamente a través del parámetro BLA (*Bond Length Alternation*)^[9], que se define por la ecuación $BLA = \bar{L}_{C-C} - \bar{L}_{C=C}$, siendo \bar{L}_{C-C} y $\bar{L}_{C=C}$, respectivamente, el promedio de la longitud de los enlaces simples y dobles alternativamente distribuidos en el sistema π conjugado y obtenidos a partir de los datos teóricos (Tabla 1.1). Cuando dicho parámetro es cero es indicativo de que las distancias de enlace simple C-C y doble C=C se igualan e implica una total deslocalización de los electrones π en todo el sistema conjugado. Para el caso del BDP el parámetro BLA toma valores pequeños ($\sim 0.03 \text{ \AA}$), lo que sugiere una alta aromaticidad.

Como consecuencia de la simetría C_{2v} del BDP, la distribución de densidad de carga es totalmente simétrica en ambos pirroles (Figura 1.4). Por lo tanto, la separación de cargas tiene lugar en eje transversal y el momento dipolar eléctrico de BDP está orientado a lo largo del eje molecular más corto de la molécula, tal y como muestra claramente el mapa de potencial con la carga negativa (rojo) en la zona del puente de difluoroboro y la carga positiva (azul) alrededor de la posición *meso* (Figura 1.4), y en concordancia con las formas resonantes (estructura "d", Figura 1.3). El valor del momento dipolar obtenido para los pirrometenos es relativamente bajo (en torno a 5.1 D)^[10], de ahí su carácter hidrófobo y su baja solubilidad en agua. Probablemente ésta sea una de las mayores limitaciones de estos colorantes, aunque salvable debido a su versatilidad sintética, que permite la inserción de grupos amonio o polieteres^[11], entre otros.

Tal y como se detalla en el siguiente subapartado 1.2, la transición electrónica $S_0 \rightarrow S_1$ es el resultado de la promoción de un electrón del orbital HOMO al LUMO del cromóforo. Así, la densidad electrónica del nivel HOMO se localiza principalmente en los pirroles, detectándose un nodo en el eje transversal, mientras que en el estado LUMO se localiza una alta densidad electrónica en el anillo central, especialmente alrededor de la posición *meso* (Figura 1.4).

1.2. FOTOFÍSICA GENERAL DE BODIPYS

Las propiedades fotofísicas de los BODIPYs se han obtenido a partir de los espectros de absorción y emisión, así como de las curvas de desactivación fluorescente.

Debido a la deslocalización tipo cianina^[12], estos colorantes muestran fuertes bandas de absorción y emisión en la región media del espectro visible (Figura 1.5). El espectro de absorción del BDP consta de una banda principal en torno a 500 nm asignada a la transición $S_0 \rightarrow S_1$ y caracterizada por su alta intensidad ($\epsilon_{\text{max}} \sim 7 \cdot 10^4 \text{ M}^{-1} \text{ cm}^{-1}$). Dicha banda presenta un hombro

vibrónico a mayores energías que el máximo (a unos 1100 cm^{-1}), que se atribuye a vibraciones fuera del plano de los enlaces C-H del sistema aromático^[13-14]. En la región UV cercano aparecen una serie de bandas más débiles y anchas, resultado de transiciones desde el estado fundamental S_0 a los diferentes estados electrónicos excitados singletes S_1 más energéticos.

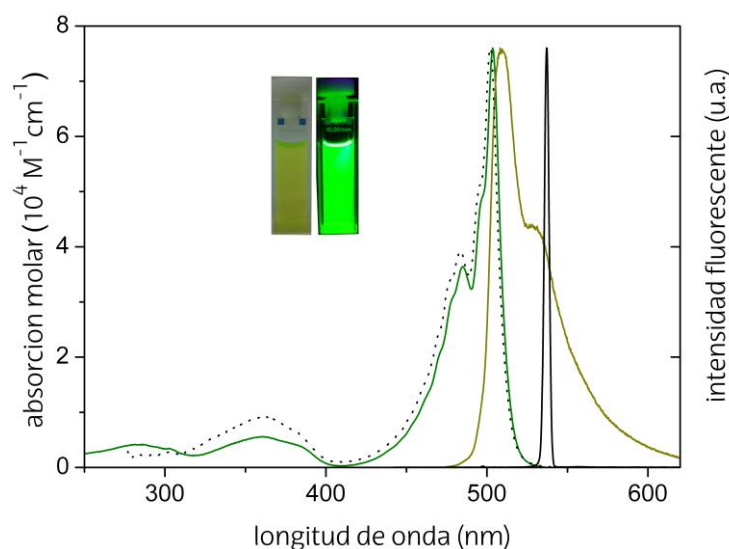


Figura 1.5. Espectros de absorción UV/Vis (línea verde continua), fluorescencia ($\lambda_{exc} = 470\text{ nm}$, línea verde-oliva continua), excitación (línea punteada) y láser (línea negra continua) normalizados del BDP ($2 \cdot 10^{-6}\text{ M}$) en ciclohexano. Se insertan fotografías bajo luz ambiente y luz UV.

La simulación del tránsito electrónico (TD B3LYP/6-31G considerando hasta 30 estados en el espacio activo) asigna dicha absorción al salto de un electrón del HOMO al LUMO y localiza el momento de la transición electrónica en el eje longitudinal del cromóforo^[6]. El cálculo predice una alta probabilidad de absorción, tal y como lo atestiguan el valor de la fuerza del oscilador ($f \approx 0.5$, calculado a partir del área del espectro de absorción) y el elevado momento de transición (que tiene en cuenta el solapamiento de los mapas de contorno de los niveles involucrados^[15]), en concordancia con el alto valor del coeficiente de absorción molar determinado experimentalmente. Señalar que el paso del HOMO al LUMO supone un trasvase de densidad electrónica desde los pirroles al anillo central. Seguramente esta es la razón por la que la posición *meso* se postula como la más sensible al efecto del sustituyente, ya que pasa de una densidad electrónica prácticamente nula en el HOMO, a tener localizada mucha en el LUMO^[12]. El cálculo sobreestima el salto energético ($\sim 0.5\text{ eV}$)^[16], pero a pesar de que el valor cuantitativo no sea muy exacto, sí que predice bien el efecto del sustituyente en la posición de la banda (Figura 1.6).

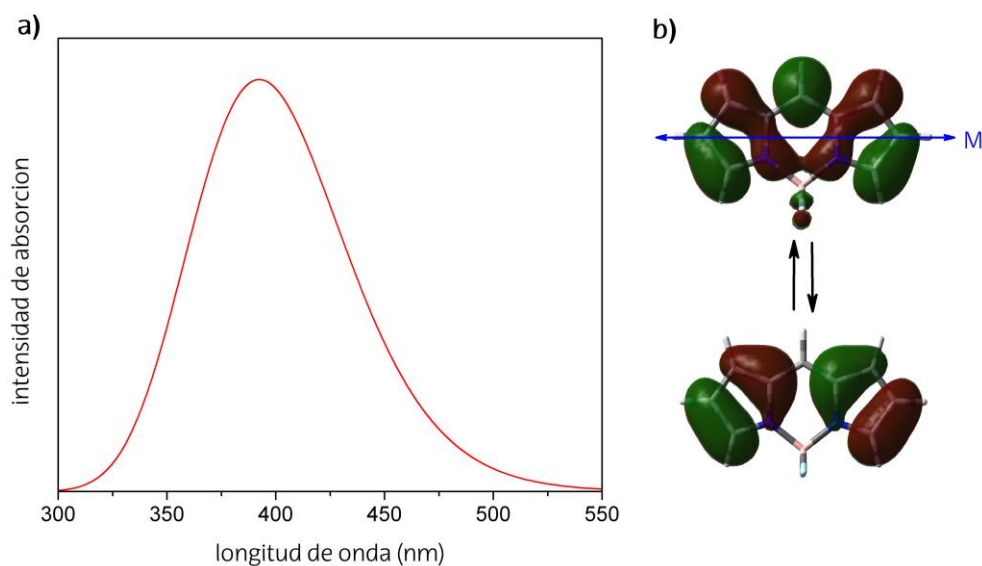


Figura 1.6. a) Simulación del espectro de absorción ($TD=1state$). b) Mapas de densidad electrónica de los orbitales moleculares, indicando el vector del momento de transición (M).

Por su parte, la banda fluorescente se localiza en torno a 510 nm, por lo que el BDP se caracteriza por pequeños desplazamientos de Stokes (en torno a 300 cm^{-1}). Esto concuerda con la baja reorganización geométrica tras la excitación predicha teóricamente, consecuencia de la rigidez estructural (sección 1.1). La forma del espectro de fluorescencia tiende a ser prácticamente una imagen especular de la banda de absorción (Figura 1.5), lo que sugiere que la geometría y los niveles vibracionales de los estados fundamental (S_0) y excitado (S_1) son similares entre sí^[17]. Además, dicho espectro no depende de la longitud de onda de excitación, indicando que la emisión fluorescente ocurre desde el nivel vibracional más bajo del estado excitado S_1 , independientemente del nivel poblado por excitación. De hecho, el espectro de excitación coincide plenamente con el de absorción (Figura 1.5). Lo más destacable de estos colorantes es su alta capacidad fluorescente, que puede llegar hasta el 100% en medios apolares. De hecho, el rendimiento cuántico de fluorescencia del BDP en *c*-hexano llega a ser de 0.96 ^[18].

La alta eficiencia fluorescente de los BODIPYs puede explicarse en base a su estructura molecular que asegura una baja probabilidad de las desactivaciones no-radiantes. Por un lado, la rigidez estructural otorgada por el puente de unión BF_2 reduce los procesos de conversión interna que están relacionados principalmente con la flexibilidad estructural^[13,19]. Por otro lado, los BODIPYs se clasifican como colorantes cuasi-aromáticos^[20], ya que al no participar el puente BF_2 en la deslocalización, ésta no es cíclica, disminuyendo así el acoplamiento spin-orbita y con ello la probabilidad de cruce intersistema. Esta característica supone una ventaja a destacar en

los pirrometenos con respecto a otros colorantes láser, ya que una de las mayores pérdidas en la cavidad resonante durante la generación láser es la población de los estados tripletes^[21].

La curva de decaimiento fluorescente del BDP se describe satisfactoriamente como monoexponencial (Figura 1.7), siendo el tiempo de vida en c-hexano de 6.47 ns^[18]. Se constató que las curvas de desactivación fluorescente también son independientes de la longitud de onda de excitación y emisión, confirmando de nuevo que la emisión sucede desde el nivel vibracional cero del estado S_1 .

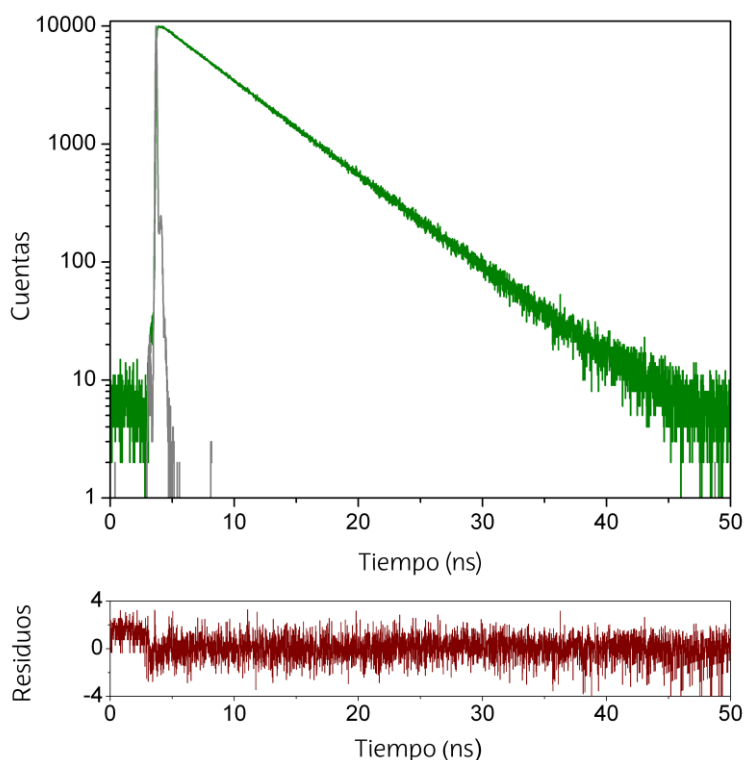


Figura 1.7. Curva de desactivación fluorescente del BDP ($2 \cdot 10^{-6}$ M) en c-hexano junto con el pulso de excitación y la correspondiente distribución de los residuos del ajuste.

En cuanto al efecto del disolvente, los BODIPYs en general son poco sensibles a las propiedades del medio^[22-23] y las evoluciones observadas se deben principalmente a interacciones generales (tipo polaridad/polarizabilidad) con el disolvente^[24]. Sin embargo, la presencia de sustituyentes adecuados induce nuevos procesos fotofísicos que pueden ser sensibles a la polaridad del medio. Generalmente, las bandas espectrales se desplazan a mayores energías, debido a que el estado excitado es menos polar que el fundamental ($\Delta\mu \approx -1$ D), mientras que el rendimiento cuántico disminuye ligeramente, a la vez que el tiempo de vida de fluorescencia aumenta, al incrementar la polaridad/proticidad del medio.

En general, se puede decir que los BODIPYs presentan fuertes bandas de absorción ($\epsilon_{\text{max}} \sim 10^5 \text{ M}^{-1}\text{cm}^{-1}$) normalmente en la región verde (490-530 nm) del espectro visible, mientras que la correspondiente emisión fluorescente tiene lugar en la región verde-amarilla (510-550 nm) con un alto rendimiento cuántico (0.7-0.9) y un tiempo de vida fluorescente en torno a 5-6 ns. Como consecuencia estos colorantes presentan fuertes bandas de emisión láser en la zona del espectro de fluorescencia que no solapa con el espectro de absorción, de ahí que su popularidad haya aumentado exponencialmente al ser empleados como medios activos de láseres sintonizables^[25-27]. Destacar la buena correlación entre las propiedades fotofísicas del BDP y sus características láser^[28], en lo que se refiere a posición de la banda fluorescente vs láser, y rendimiento cuántico de fluorescencia (especialmente con la constante de desactivación no-radiante, k_{nr}) vs eficiencia láser.

Las propiedades fotofísicas y resultados de la modelización mecanocuántica descritas para el BDP se tomarán como referencia a lo largo de la presente memoria para analizar los BODIPYs que se presentan a continuación.

Bibliografía

- [1] Haugland, R.P.; *The Handbook. A Guide to Fluorescent Probes and Labeling Technologies, Molecular Probes*, Invitrogen, Carlsbad, CA, 10th edn, **2005**.
- [2] Treibs, A.; Kreuzer, F.-H.; *Justus Liebigs Ann. Chem.*, **1968**, 718, 208.
- [3] Loudet, A.; Burgess, K.; *Chem. Rev.*, **2007**, 107, 4891.
- [4] Ulrich, G.; Ziessel, R.; Harriman, A.; *Angew. Chem., Int. Ed.*, **2008**, 47, 1184.
- [5] Arroyo, I.J.; Hu, R.; Merino, G.; Tang, B.Z.; Peña-Cabrera, E.; *J. Org. Chem.*, **2009**, 74, 5719.
- [6] Bañuelos Prieto, J.; López Arbeloa, F.; Martínez Martínez, V.; López Arbeloa, I.; *Chem. Phys.*, **2004**, 296, 13.
- [7] Tyulyulkov, N.; Fabian, J.; Mehlhorn, A.; Dietz, F.; Tadjer, A.; *Polymethine Dyes*, University Press, **1991**.
- [8] Fabian, J.; Hartmann, H.; *Light Absorption of Organic Colorants*, Springer-Verlag, Berlin, **1980**.
- [9] Bourhill, G.; Brédas, J.-L.; Cheng, L.-T.; Marder, S.R.; Meyers, F.; Perry, J.W.; Tiemann, B.G.; *J. Am. Chem. Soc.*, **1994**, 116, 2619.
- [10] Bergström, F.; Mykhalyov, I.; Hägglof, P.; Wortmann, R.; Ny, T.; Johansson, L.B.A.; *J. Am. Chem. Soc.*, **2002**, 124, 196.
- [11] Romieu, A.; Massif, C.; Rihn, S.; Ulrich, G.; Ziessel, R.; Renard, P.-Y.; *New J. Chem.*, **2013**, 37, 1016.
- [12] López Arbeloa, F.; Bañuelos, J.; Martínez, V.; Arbeloa, T.; López Arbeloa, I.; *Int. Rev. Phys. Chem.*, **2005**, 24, 339.
- [13] Drexhage, K.H.; *Dye Lasers*, edited by F. P. Schäfer, Springer-Verlag, Berlin Heidelberg, **1990**.
- [14] Birks, J. B.; *Photophysics of Aromatic Molecules*; Wiley-Interscience: London, **1970**.
- [15] Michl, J.; Thulstrup, E.W.; *Spectroscopy with Polarized Light*; VCH: New York, **1986**.
- [16] Fabian, J.; *Dyes and Pigments*, **2010**, 84, 36.
- [17] Lakowicz, J. R.; *Principles of Fluorescence Spectroscopy*; Kluwer Academic, Plenum Press: New York, **1999**.
- [18] Bañuelos, J.; Martín, V.; Gómez-Durán, C. F. A.; Arroyo Córdoba, I. J.; Peña-Cabrera, E.; García-Moreno, I.; Costela, A.; Pérez-Ojeda, M. E.; Arbeloa, T.; López Arbeloa, I.; *Chem. Eur. J.*, **2011**, 17, 7261.
- [19] Bañuelos, J.; López Arbeloa, F.; Martínez, V.; Arbeloa López, T.; Amat-Guerri, F.; Liras, M.; López Arbeloa, I.; *Chem. Phys. Lett.*, **2004**, 385, 29.
- [20] Pavlopoulos, T. G.; *Prog. Quantum Elec.*, **2002**, 26, 193.
- [21] Gorman, A. A.; Hamblett, I.; King, T. A.; Rahn, M. D.; *J. Photochem. Photobiol. A: Chem.*, **2000**, 130, 127.
- [22] López Arbeloa, F.; López Arbeloa, I.; López Arbeloa, T.; *Handbook of Advanced Electronic and Photonic Materials and Devices*, edited by H.S. Nalwa (Academic Press, San Diego, **2001**), Vol. 7, p. 209.
- [23] López Arbeloa, F.; López Arbeloa, T.; López Arbeloa, I.; *Recent Res. Devel. Photochem. Photobiol.*, **1999**, 3, 35.
- [24] Bañuelos, J.; López Arbeloa, F.; Martínez, V.; Liras, M.; Costela, A.; García-Moreno, I.; López Arbeloa, I.; *Phys. Chem. Chem. Phys.*, **2011**, 13, 3437.
- [25] Costela, A.; García-Moreno, I.; Sastre, R.; *Phys. Chem. Chem. Phys.*, **2003**, 5, 4745.
- [26] Yang, Y.; Wang, M.; Qian, G.; Wang, Z.; Fan, X.; *Opt. Mat.*, **2004**, 24, 621.
- [27] Ahmad, M.; King, T. A.; Ko, D.-K.; Cha, B. H.; Lee, J.; *J. Phys. D: Appl. Phys.*, **2002**, 35, 1473.
- [28] Esnal, I.; Valois-Escamilla, I.; Gómez-Durán, C. F. A.; Urías Benavides, A.; Betancourt-Mendiola, M. L.; López-Arbeloa, I.; Bañuelos, J.; García-Moreno, I.; Costela, A.; Peña-Cabrera, E.; *ChemPhysChem*, **2013**, 14, 4134.

CAPÍTULO 2

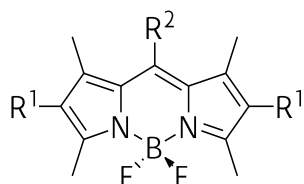
BODIPYs EN LA REGIÓN VERDE-AMARILLA DEL ESPECTRO VISIBLE

En el presente capítulo se analizan las propiedades fotofísicas de una serie de BODIPYs disponibles comercialmente con emisión típica en la región verde-amarilla del espectro visible, en los que se realizan modificaciones estructurales en el boro con el fin de mejorar, más aún si cabe, las prestaciones fotofísicas y láser de estos colorantes. La estrategia sintética ha consistido en la sustitución de los átomos de flúor (*F*-BODIPYs) por derivados alquilo o arilos (*C*-BODIPYs)^[1-3], grupos etinilos (*E*-BODIPYs)^[4-6] y derivados alcoxi o ariloxi (*O*-BODIPYs)^[7-9].

Todos los colorantes analizados en este capítulo (excepto los obtenidos comercialmente, Exciton) han sido sintetizados por la Prof. M^a Jose Ortiz de la UCM. A continuación se presenta una breve descripción de las características espectroscópicas más significativas de los BODIPYs de grado láser disponibles comercialmente para posteriormente pasar a discutir los resultados más relevantes de la caracterización fotofísica y mecanocuántica de los correspondientes derivados obtenidos al reemplazar los átomos de flúor del boro por grupos funcionales de diversa índole y con diferente comportamiento electrónico (p.ej., dadores y aceptores de electrones). Los detalles sintéticos así como los pormenores de la simulación mecanocuántica o la caracterización fotofísica y láser de estos derivados se analiza en los artículos del Anexo I adjuntos al final de la memoria.

2.1. F-BODIPYS COMERCIALES

Los BODIPYs comerciales de grado láser analizados, presentan su núcleo cromofórico metilado al menos en las posiciones 1, 3, 5 y 7, y difieren en la sustitución de las posiciones 2 y 6, y 8 (Figura 2.1).



Colorante	R ¹	R ²
PM 546	H	CH ₃
PM 567	CH ₂ CH ₃	CH ₃
PM 580	(CH ₂) ₃ CH ₃	CH ₃
PM 597	C(CH ₃) ₃	CH ₃
PM 597-8C9	C(CH ₃) ₃	(CH ₂) ₈ CH ₃
PM 605	CH ₂ CH ₃	CH ₂ OCOCH ₃
PM 650	CH ₃	CN

Figura 2.1. Estructuras moleculares de pirrometenos comerciales.

Así el colorante más simple es el PM546 (metilo en posición *meso*, Figura 2.1). La alquilación en las posiciones 1, 3, 5, 7 y 8 del cromóforo prácticamente no altera la posición de las bandas espectrales del PM546^[10] (Figura 2.2) respecto al cromóforo sin alquilar de referencia (BDP en capítulo 1). Sin embargo, la adición de cadenas alifáticas lineales en las posiciones simétricas 2 y 6 del PM546 (etilo en PM567^[11] y butilo en PM580, Figura 2.1) alarga el desplazamiento batocrómico (aproximadamente 25 nm y 30 nm, respectivamente respecto al PM546, Figura 2.2) por el efecto inductivo dador de electrones de los grupos alquilo. De forma general, todos estos F-BODIPYs alquilados presentan propiedades fotofísicas similares al BDP con excelentes rendimientos cuánticos (Tabla 2.1).

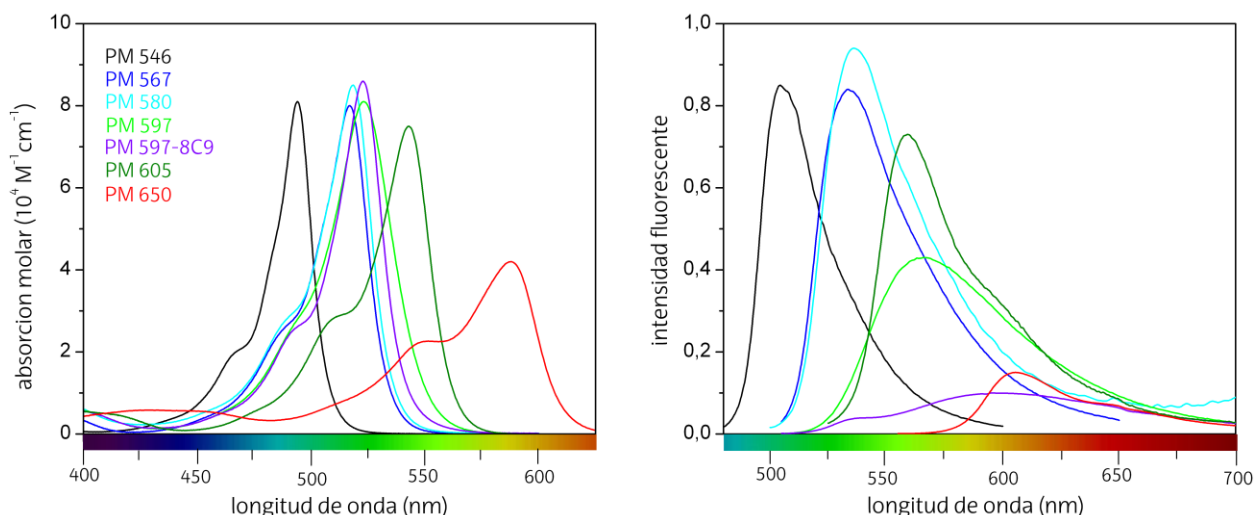


Figura 2.2. Espectros de absorción y fluorescencia (normalizados) de los F-BODIPYs comerciales en acetato de etilo.

Tabla 2.1. Propiedades fotofísicas de los F-BODIPYs comerciales en acetato de etilo (λ_{ab} : longitud de onda máxima de absorción; ϵ_{max} : coeficiente de absorción molar máximo; λ_{fl} : longitud de onda máxima de fluorescencia; $\Delta\nu_{St}$: desplazamiento de Stokes; ϕ : rendimiento cuántico de fluorescencia; τ : tiempo de vida; k_{fl} : constante de velocidad de desactivación radiante; k_{nr} : constante de velocidad de desactivación no-radiante).

Colorante	λ_{ab} (nm)	ϵ_{max} ($10^4 \text{ M}^{-1} \text{ cm}^{-1}$)	λ_{fl} (nm)	$\Delta\nu_{St}$ (cm^{-1})	ϕ	τ (ns)	k_{fl} (10^8 s^{-1})	k_{nr} (10^8 s^{-1})
PM 546	494.0	8.1	506.5	500	0.85	5.58	1.52	0.27
PM 567	517.0	7.6	533.0	580	0.84	5.78	1.45	0.28
PM 580	518.5	8.5	536.5	650	0.94	5.93	1.6	0.10
PM 597	523.5	7.7	565.0	1405	0.47	4.31	1.09	1.23
PM 597-8C9	523.0	8.6	595.5	2330	0.10	1.14	0.88	7.9
PM 605	543.0	7.3	558.5	510	0.73	6.64	1.10	0.40
PM 650	588.0	4.2	603.0	425	0.15	2.37	0.63	3.59

Por el contrario, la presencia de alquilo ramificados, como el *tert*-butilo, en las posiciones 2 y 6 (PM597^[12] y PM597-8C9 con nonilo en posición 8, Figura 2.1) implica cambios importantes en la fotofísica del BODIPY. La banda de absorción del PM597 se desplaza 10 nm hacia menores energías respecto al PM567 (Figura 2.2) como consecuencia del mayor efecto inductivo por la ramificación (especialmente evidente al comparar PM580, *n*-butilo, con PM597, *t*-butilo, Tabla 2.1). Dicho desplazamiento batocrómico es mucho más fuerte en la banda fluorescente (hasta 40 nm, Figura 2.2), lo que provoca un importante aumento del desplazamiento de Stokes (de $\sim 600 \text{ cm}^{-1}$ a 1600 cm^{-1}). Además tanto el rendimiento cuántico

de fluorescencia como el tiempo de vida disminuyen considerablemente (alrededor de un 50%, Tabla 2.1). La optimización de las geometrías muestra que el impedimento estérico inducido por los voluminosos grupos *tert*-butilo provoca una pérdida de planaridad del cromóforo sobre el eje transversal especialmente en el estado excitado (12° en el PM597, Figura 2.3.a). Curiosamente dicha mayor distorsión de la planaridad con la excitación implica una disminución de la energía de resonancia (efecto Brunings-Corwin^[13] o *loose-bolt effect*^[14]) que desemboca en una banda fluorescente muy desplazada respecto a la banda de absorción, es decir, en un alto desplazamiento de Stokes como consecuencia de una fuerte reorganización geométrica tras la excitación^[12]. Además, la pérdida de planaridad se traduce en un aumento de los procesos de conversión interna, lo que explica la mencionada disminución de la capacidad fluorescente^[15]. Todas estas tendencias son más pronunciadas en el PM597-8C9. De hecho, la simulación teórica predice una pérdida de planaridad aún mayor (25° en el estado S_1 , Figura 2.3.b) posiblemente debido a que la geometría está más congestionada por la presencia adicional de la cadena alifática en *meso*.

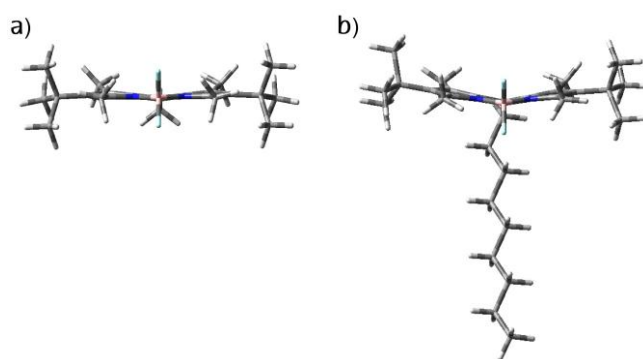


Figura 2.3. Vista desde la perspectiva del eje *z* de las geometrías optimizadas en el estado excitado del **a)** PM 597 y **b)** PM 597-8C9.

Por otro lado, la posición *meso* es muy sensible al efecto del sustituyente probablemente debido al fuerte cambio de densidad electrónica que tiene lugar al pasar del HOMO al LUMO como consecuencia de la transición electrónica (Figura 1.4 en capítulo 1). Así la presencia de un grupo metilacetoxi (PM605^[16], Figura 2.1) da lugar a un desplazamiento batocrómico (unos 25 nm respecto a su análogo PM567, Figura 2.2) por su efecto atractor de electrones, a pesar de que el grupo acetoxi no está unido directamente al cromóforo (separado por un metileno), ya que provoca una estabilización preferencial del orbital LUMO (caracterizado por una alta densidad electrónica π en posición *meso*) respecto al HOMO (nodo en dicha posición). Como consecuencia de dicho carácter atractor de electrones la capacidad fluorescente se resiente ligeramente (disminución del 15-30%, Tabla 2.1).

Estas tendencias se acentúan por la inserción de un grupo ciano (PM650, Figura 2.1)^[17], fuertemente aceptor de electrones, directamente unido en la posición *meso*. Así este colorante es el *F*-BODIPY con la emisión más desplaza a menores energías de todos (la banda de fluorescencia se centra en torno a 600 nm, Figura 2.2) debido a una fuerte estabilización del LUMO. Sin embargo, su capacidad fluorescente disminuye fuertemente, a la vez que el tiempo de vida se hace mucho más corto, especialmente en medios polares ($\phi < 10\%$ y $\tau \approx 1$ ns) como consecuencia de un fuerte aumento de los procesos no-radiantes (Tabla 2.1). Dicha sensibilidad del rendimiento cuántico con el disolvente, junto con el fuerte carácter atractor de electrones del ciano induce a pensar en la formación de un estado de transferencia de carga intramolecular (ICT, *Intramolecular Charge Transfer*)^[18-19] no-fluorescente en el estado excitado, que desactiva eficientemente la fluorescencia del estado localmente excitado del colorante (LE, *Locally Excited*). La alta polaridad de dicho estado debido a la separación de cargas generada, supone que el ICT se establezca fuertemente en medios polares, por lo que se puebla en mayor medida desde el LE y como resultado su efecto desactivador es más notorio^[20-23](Figura 2.4).

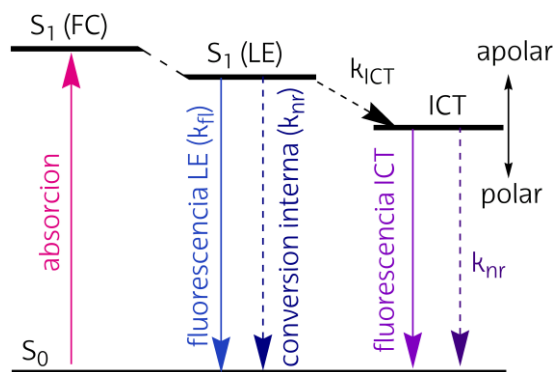


Figura 2.4. Diagrama de energía de los procesos de desactivación desde el estado excitado S_1 para el PM 650; LE: estado localmente excitado; FC: estado de Franck-Condon; ICT: estado de transferencia de carga intramolecular. Las líneas continuas y discontinuas representan los procesos radiantes y no-radiantes, respectivamente.

Por último, recalcar de nuevo tal y como se hizo previamente en el capítulo 1, la satisfactoria correlación entre las propiedades fotofísicas de los *F*-BODIPYs comerciales y las características láser^[24-27]. Así los derivados alquilados con grupos alifáticos lineales (PM546, PM567 y PM580) presentan altas eficiencias láser, mientras que PM605 y PM650 presentan una señal láser desplazada progresivamente a menores energías pero con una menor eficiencia, especialmente en el último caso por el ya citado estado ICT. Señalar que el PM597 presenta un óptimo comportamiento láser a pesar de su menor capacidad fluorescente. Dicha limitación es compensada por el alto desplazamiento de Stokes que disminuye las pérdidas por los

fenómenos de reabsorción/reemisión en la cavidad láser. Estos procesos no están presentes en las medidas fotofísicas por la baja concentración empleada pero sí en el registro láser ya que requiere una alta densidad óptica y su influencia es fundamental.

2.2. E- y C-BODIPYs

En vista de las excelentes propiedades fotofísicas que ofrecen los pirrometenos comerciales, se ha obtenido una nueva serie de E- y C-BODIPYs con diferentes grupos funcionales (alquinilo, ciano, vinilo, arilo, y alquilo) conectados directamente al átomo de boro y reemplazando a los átomos de flúor (Figura 2.5). El objetivo es mejorar más si cabe las prestaciones fluorescentes y por ende láser de los anteriores F-BODIPYs comerciales en su misma región espectral de trabajo, procurando un incremento en la estabilidad de los mismos. En la publicación *Chem. Eur. J* 2014 adjunto al Anexo I al final de la memoria se analizan los pormenores de los resultados de la presente serie de E- y C-BODIPYs.

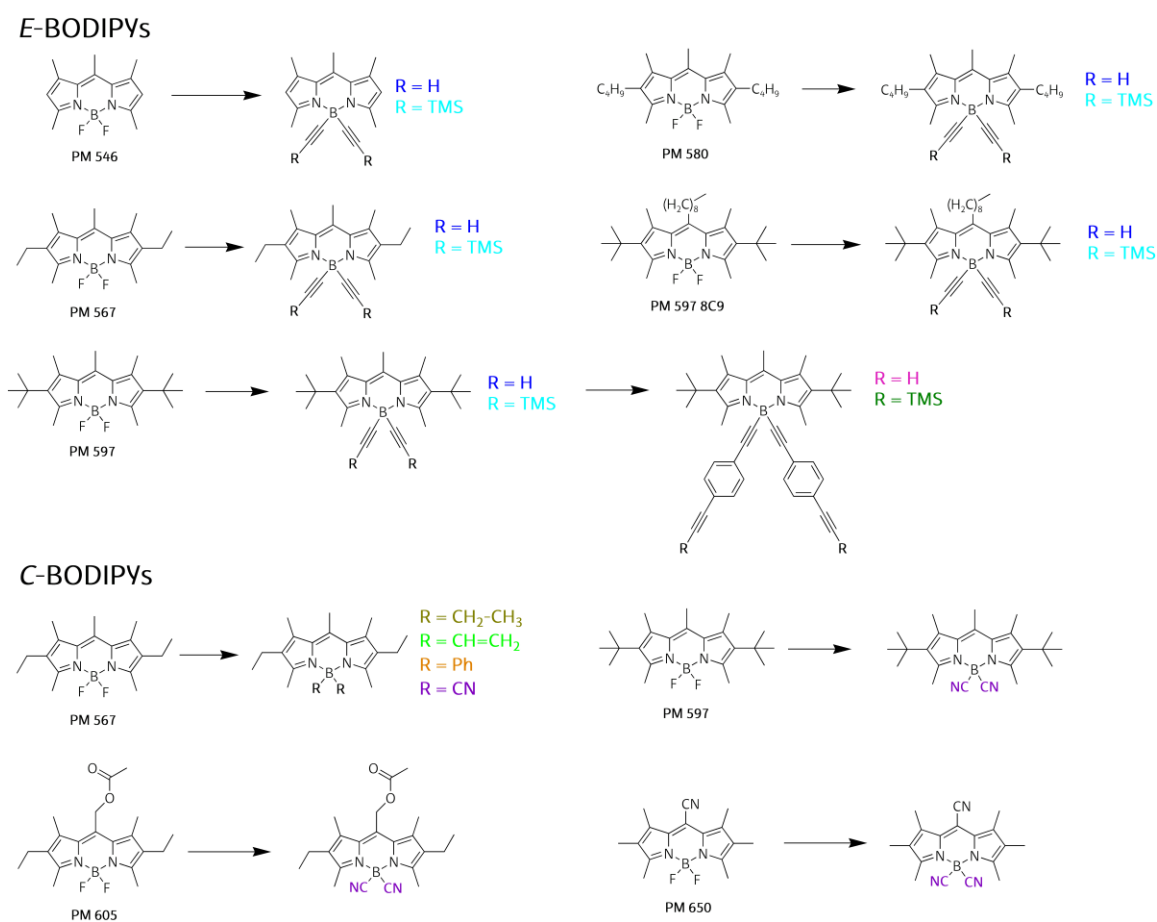


Figura 2.5. Estructuras de los E- y C-BODIPYs estudiados; TMS: trimetilsililo y Ph: fenilo.

La posición de las bandas espectrales de los nuevos *E*- y *C*-BODIPYs son prácticamente las mismas que las de sus respectivos *F*-BODIPYs. Este hecho era de esperar teniendo en cuenta que el puente BF_2 no participa en la deslocalización del sistema π cromofórico, si no que únicamente actúa como puente de unión para mantener la planaridad y rigidez del cromóforo. De hecho, la distribución de densidad electrónica de los orbitales HOMO y LUMO permanece inalterada y se localiza exclusivamente en el indaceno. En general las propiedades fotofísicas son parecidas respecto a las registradas en los comerciales pero si que se observan diferencias en la capacidad fluorescente según la naturaleza electrónica del sustituyente (dador o aceptor de electrones) incorporado en el boro.

La sustitución de flúor por acetileno, independientemente de la funcionalización de este último (por TMS o fenilo adicional, ver serie del PM597 en Figura 2.5) supone por norma una ligera mejora en la capacidad fluorescente del BODIPY (en torno al 10%), obteniéndose valores mayores del 90% por ejemplo para el PM546 (Figura 2.6).

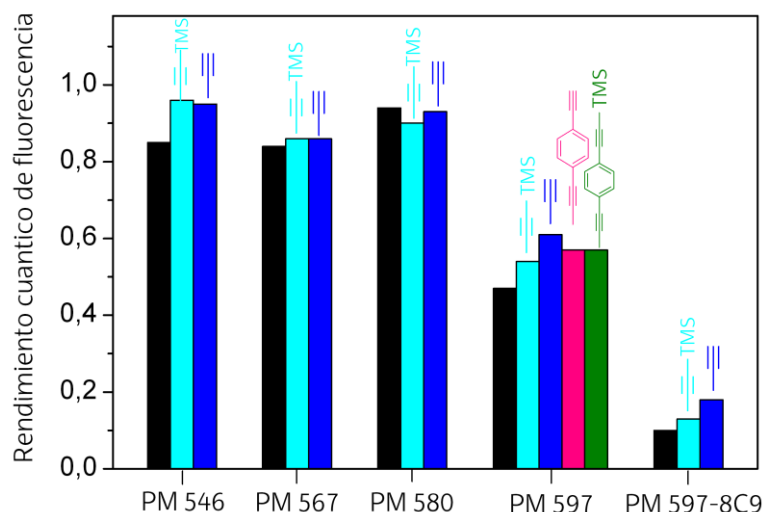


Figura 2.6. Rendimientos cuánticos de fluorescencia de los *F*-BODIPYs comerciales (negro) y los correspondientes *E*-BODIPYs en acetato de etilo (los colores de la gráfica corresponden a los derivados que se muestran en la Figura 2.5; se adjuntan los fragmentos correspondientes a cada derivado).

Aunque la sustitución del boro no participe en el sistema π deslocalizado, si que puede alterar la distribución de cargas de la cianina. De hecho, en el mapa de potencial electrostático (Figura 1.4.b en capítulo 1) se localiza densidad electrónica negativa en los flúor, por lo que su reemplazo debe condicionar la distribución de cargas global del cromóforo. Para analizar con más detalle este aspecto vamos discutir los BODIPYs más representativos donde se insertan sustituyentes con diferente carácter aceptor/dador de electrones.

La variación de la insaturación del alquilo insertado en el boro, o la presencia de fenilos o cianos en el boro (ver especialmente serie del PM567, Figura 2.5) produce variaciones del rendimiento cuántico más notorias que en el caso de los *E*-BODIPYs (Figura 2.7). Además, no todas las modificaciones estructurales en los *C*-BODIPYs se traducen en mejoras de la capacidad fluorescente sino que en algunos casos se empeora.

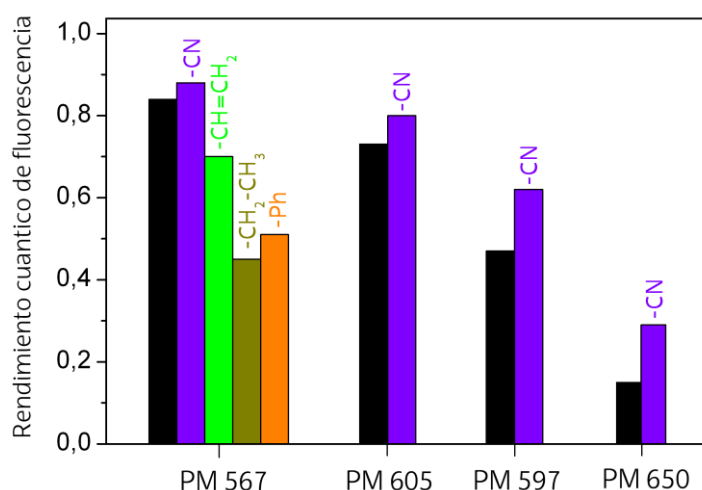


Figura 2.7. Rendimientos cuánticos de fluorescencia de los *F*-BODIPYs comerciales (negro) y los correspondientes *C*-BODIPYs en acetato de etilo (los colores de la gráfica corresponden a los derivados que se muestran en la Figura 2.5; se adjuntan los fragmentos correspondientes a cada derivado).

El grupo acetileno de los *E*-BODIPYs se caracteriza por su leve carácter aceptor de electrones (parámetro Hammett, $\sigma_p^+ = 0.18$)^[28] y su presencia implica un ligero aumento de la eficiencia fluorescente (Figura 2.6). Un aumento de la capacidad atractora de electrones en los *C*-BODIPYs por la inserción del grupo ciano ($\sigma_p^+ = 0.66$)^[28], da lugar a un notable incremento de la capacidad fluorescente, especialmente en el PM650 (aumento de hasta el 50%, Figura 2.7). Es posible que en este último derivado, los grupos ciano posicionados a ambos lados del eje longitudinal más corto del cromóforo dificulten la población del estado ICT que limitaba las prestaciones fluorescentes del PM650 (sección 2.1). Por el contrario, la presencia de grupos dadores como el fenilo ($\sigma_p^+ = -0.18$)^[28] provoca una disminución significativa de la capacidad fluorescente (descenso del 40%, Figura 2.7). Además, el impedimento estérico que proporcionan dichos grupos voluminosos también contribuye a aumentar la desactivación no-radiante ya que los cálculos predicen una pérdida de planaridad en el cromóforo (hasta 25° en S_1). La gran influencia de la capacidad dadora/aceptora de electrones en la eficiencia fluorescente queda claramente reflejada al analizar los derivados del PM567 con diferente grado de insaturación. Así el cambio de acetileno a vinilo y de aquí a etilo supone una

progresiva disminución de la capacidad fluorescente del colorante (ϕ pasa del 86% en Figura 2.6, al 70% y 45% en Figura 2.7, respectivamente), en perfecta correlación con un progresivo aumento del carácter dador ($\sigma_p^+ = 0.18$, $\sigma_p^+ = -0.16$ y $\sigma_p^+ = -0.30$, respectivamente)^[28].

En vista de que la naturaleza electrónica del grupo incorporado en el boro controla la capacidad fluorescente del colorante, a continuación se analiza la distribución de carga en el cromóforo y la aromaticidad del mismo a través de la alternancia de las distancias de enlace (parámetro BLA, definido en capítulo 1). A modo representativo se muestran los C-BODIPYs del PM567 con el grupo más aceptor (ciano) y más dador (etilo) (Figura 2.8), mientras que la distribución y aromaticidad de otros derivados se representan en el artículo *Chem. Eur. J* 2014 adjunto al Anexo I al final de la memoria.

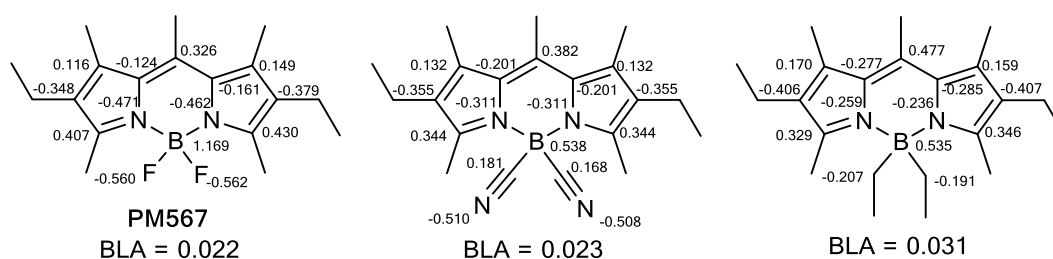


Figura 2.8. Cargas parciales $CHelpg$ de los derivados más representativos del PM 567.

La presencia de un grupo fuertemente aceptor (ciano), implica una considerable reorganización en la distribución de carga cromofórica. Así, la carga positiva del boro disminuye considerablemente y los nitrógenos pirrólicos localizan también menos carga negativa (Figura 2.8). En consecuencia el par de electrones libres está menos localizado en el nitrógeno y más deslocalizado a través del sistema π . Todo ello da lugar a un colorante con alta aromaticidad (BLA similar al PM567 de referencia, Figura 2.8). De hecho, el derivado con ciano es el que promueve mayores eficiencias, y el que presenta el menor BLA de todos los BODIPYs considerados en este apartado. Por otro lado, un incremento en la capacidad dadora del sustituyente (etilo) provoca una importante reducción en la aromaticidad del sistema (aumento del parámetro BLA, Figura 2.8), de acuerdo con la pérdida de emisión fluorescente observada experimentalmente (Figura 2.7).

En resumen, el reemplazamiento de flúor por grupos atradores de electrones es una estrategia adecuada para incrementar la capacidad fluorescente de los BODIPYs comerciales. Dicha mejora en las características fluorescentes se refleja en las propiedades láser ya que se registra un importante aumento de la eficiencia láser de hasta el 52% en el PM546 sustituido

por acetilenos respecto al correspondiente *F*-BODIPY, siendo en este último del 23%. Asimismo, en dicho derivado se mantiene la fotoestabilidad en un 92% después de 100000 pulsos, respecto al 60% registrado para el comercial. En concordancia con los resultados fotofísicos obtenidos, los derivados ciano sustituidos presentan un aumento en la eficiencia láser de aproximadamente el 40% (especialmente en los derivados del PM567 y PM597) y fotoestabilidades del 100% (tras 100000 pulsos).

2.3. *O*-BODIPYs

En vista de los resultados obtenidos en la sección anterior, otra de las propuestas para incrementar la capacidad fluorescente de los BODIPYs comerciales sin alterar la región de emisión, ha sido conectar directamente al átomo de boro dos grupos carboxilo (acetoxi o trifluoroacetoxi) para dar lugar a los correspondientes *O*-BODIPYs. Con intención de profundizar en la influencia del carácter electrónico del sustituyente en la emisión fluorescente, se ha considerado una batería de derivados con diversos grupos funcionales (acrililoiloxi, propioloiloxi, metoxi o nitrofenoxi) (Figura 2.9). En el Anexo I al final de la memoria se adjunta la publicación *Adv. Funct. Mater.* 2013 que ha dado lugar este trabajo.

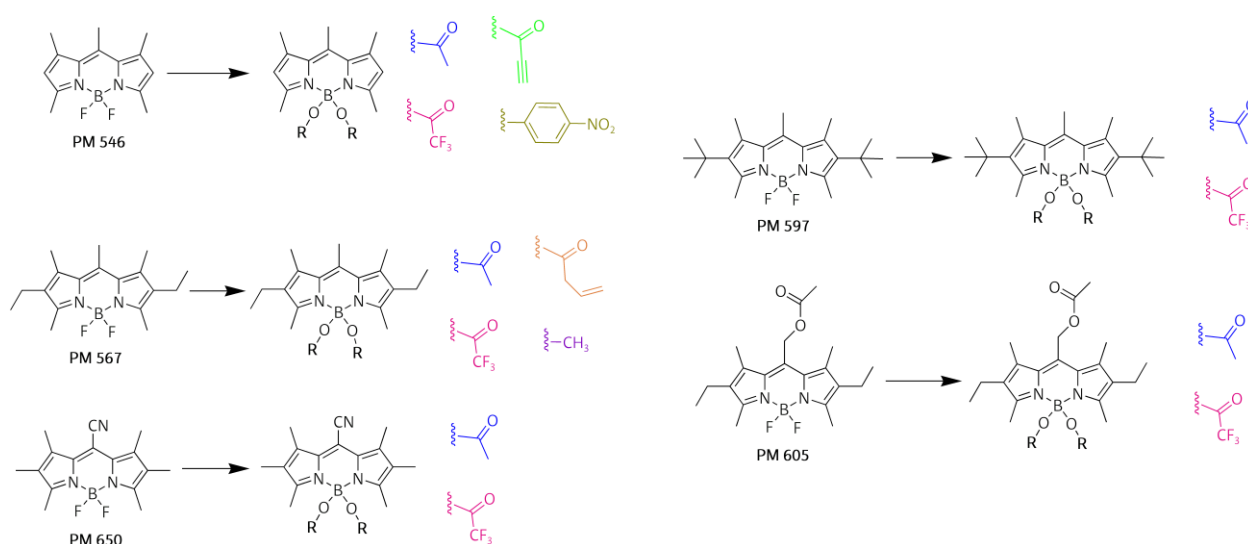


Figura 2.9. Estructuras de los *O*-BODIPYs estudiados.

Las propiedades fotofísicas de los *O*-BODIPYs siguen tendencias parecidas a los *E*- y *C*-BODIPYs (sección 2.2). Así, en todos los casos un aumento progresivo del carácter aceptor de electrones del sustituyente incorporado (de acetato a trifluoroacetoxi o la adición de dobles y

triples enlaces en el acetato) permite un incremento gradual de la capacidad fluorescente (de hasta un 10%, Figura 2.10). Esta tendencia es más pronunciada en los derivados del PM597 (ϕ pasa de 45% a 80%) cuyas propiedades fotofísicas están gobernadas por los impedimentos estéricos de los grupos *tert*-butilo. Por el contrario, la sustitución por el grupo metoxi dador de electrones ($\sigma_p^+ = -0.27$)^[28] provoca el efecto contrario.

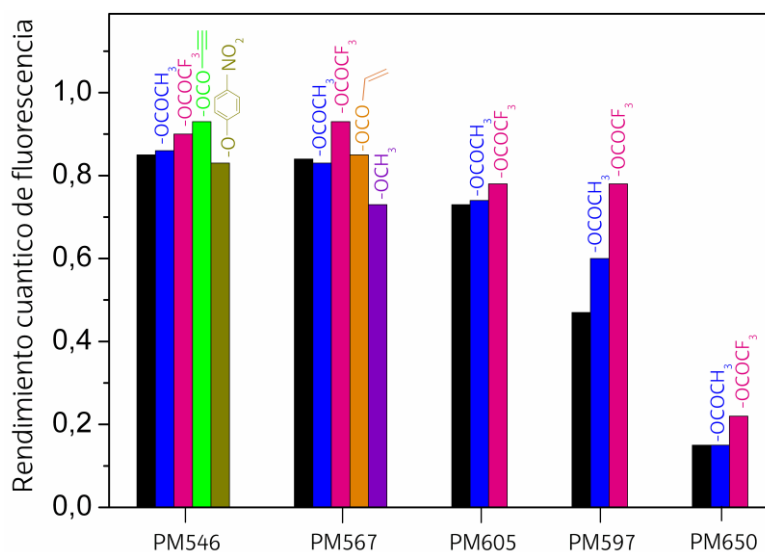


Figura 2.10. Rendimientos cuánticos de fluorescencia de los F-BODIPYs comerciales (negro) y los correspondientes O-BODIPYs en acetato de etilo (los colores de la gráfica corresponden a los derivados de la Figura 2.9; se adjuntan los fragmentos correspondientes a cada derivado).

En esta ocasión, la presencia de los alcoxidos en el boro también condiciona la distribución de carga y la aromaticidad del colorante. Así, los grupos atractores (por ejemplo, trifluoroacetoxi, $\sigma_p^+ = 0.46$)^[28] aumentan la carga positiva del boro y disminuyen la de los átomos de nitrógeno pirrólicos, lo que sugiere que el par de electrones libres estén más deslocalizados a través del sistema π . Por lo tanto, los grupos atractores inducen mayor deslocalización (menor parámetro BLA) que el colorante de referencia (Figura 2.11). Señalar que en los E- y C-BODIPYs la mejora de la capacidad fluorescente era menor que en los O-BODIPYs lo que concuerda con una mayor aromaticidad de estos últimos derivados (menores valores de BLA). Por el contrario, la presencia del grupo metoxi dador de electrones ($\sigma_p^+ = -0.27$)^[28], proporciona el comportamiento contrario (aumento del parámetro BLA y menor aromaticidad), en concordancia con la disminución de la eficiencia fluorescente.

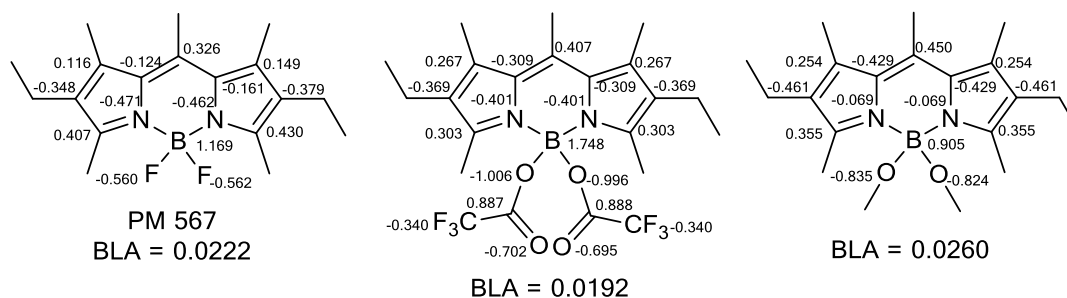


Figura 2.11. Cargas parciales $CHelpg$ de los derivados más representativos del PM 567.

Sin embargo, un grupo excesivamente atractor puede provocar el efecto contrario al deseado, tal y como es el caso del derivado de PM546 con grupos nitro ($\sigma_p^+ = 0.78$)^[28]. A pesar de que en acetato de etilo muestra una capacidad fluorescente razonadamente alta (con ϕ del 83%), un aumento de la polaridad supone una importante reducción de la capacidad fluorescente (hasta el 33% en metanol o el 5% en F_3 -etanol). De hecho, las curvas de desactivación fluorescente se vuelven biexponenciales en medios polares y están caracterizadas por tiempos de vida cortos (pasa de 5,94 ns en ciclohexano, a 2,65 y 0,18 ns en metanol y F_3 -etanol, respectivamente, Figura 2.12). Dicha sensibilidad con la polaridad del medio es indicativa de un proceso extra de desactivación no-radiante que se atribuye a un proceso de ICT desde dicho grupo nitro al BODIPY), especialmente estable en medios polares (Figura 2.4 en la sección 2.1).

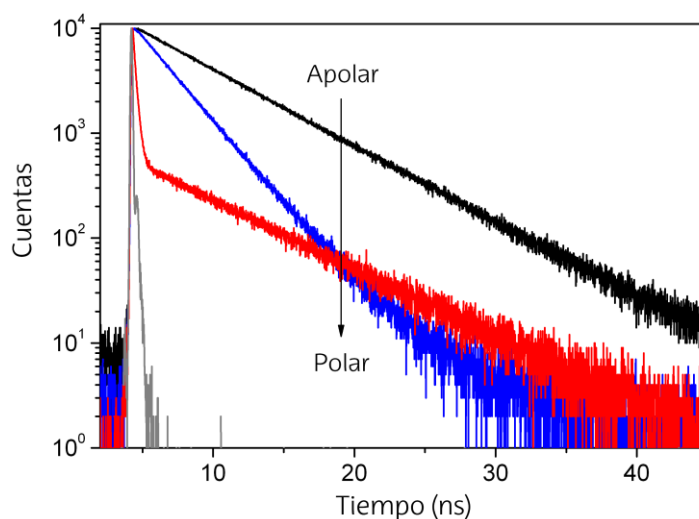


Figura 2.12. Influencia de la polaridad (ciclohexano en negro, metanol en azul y F_3 -etanol en rojo) en los tiempos de vida fluorescentes del PM 546 p-nitro-fenil sustituido.

En analogía a las propiedades fotofísicas y exceptuando los derivados con grupos dadores o los que favorecen procesos ICT, los presentes *O*-BODIPYs exhiben mejoras en las eficiencias láser (llegando a ser de hasta el 68% en los derivados con grupos trifluoroacetoxi) respecto a los correspondientes *F*-BODIPYs de partida analizados, que oscilan entre el 23-55%. Generalmente, dichos *O*-BODIPYs mantienen fotoestabilidades de hasta el 100% tras el bombeo de 100000 pulsos, superando en todos los casos las estabilidades de los respectivos comerciales (excepto en los *O*-BODIPYs que activan los procesos ICT).

En resumen, la sustitución de los átomos de flúor por grupos atractores de electrones supone una estrategia simple y eficiente para mejorar el comportamiento fluorescente y la acción láser de los BODIPYs, dando lugar a cromóforos más aromáticos con eficiencias fluorescentes mejoradas y más estables.

El presente capítulo ha dado lugar a dos publicaciones en *Chemistry - A European Journal* (2014) y *Advanced Functional Materials* (2013), que se adjuntan en el Anexo I al final de la memoria y donde se puede encontrar información más detallada de la caracterización fotofísica y láser de los *E*- y *C*-BODIPYs, y *O*-BODIPYs, respectivamente.

Bibliografía

- [1] Goze, C.; Ulrich, G.; Mallon, L. J.; Allen, B. D.; Harriman, A.; Ziesse, R.; *J. Am. Chem. Soc.*, **2006**, *128*, 10231.
- [2] Ziesse, R.; Ulrich, G.; Harriman, A.; *New J. Chem.*, **2007**, *31*, 496.
- [3] Loudet, A.; Burguess, K.; *Chem. Rev.*, **2007**, *107*, 4891.
- [4] Goze, C.; Ulrich, G.; Ziesse, R.; *J. Org. Chem.*, **2007**, *72*, 313.
- [5] Goze, C.; Ulrich, G.; Ziesse, R.; *Org. Lett.*, **2006**, *8*, 4445.
- [6] Ulrich, G.; Goeb, S.; De Nicola, A.; Retailleau, P.; Ziesse, R.; *J. Org. Chem.*, **2011**, *76*, 4489.
- [7] Crawford, S. M.; Thompson, A.; *Org. Lett.*; **2010**, *12*, 1424.
- [8] Yang, L.; Simionescu, R.; Lough, A.; Van, H.; *Dyes and Pigments*, **2011**, *91*, 264.
- [9] Lundrigan, T.; Crawford, S. M.; Cameron, T. S.; Thompson, A.; *Chem. Commun.*, **2012**, *48*, 1003.
- [10] López Arbeloa, F.; López Arbeloa, T.; López Arbeloa, I.; *J. Photochem. Photobiol. A: Chemistry*, **1999**, *121*, 177.
- [11] López Arbeloa, F.; López Arbeloa, T.; López Arbeloa, I.; García-Moreno, I.; Costela, A.; Sastre, R.; Amat-Guerri, F.; *Chem. Phys.*, **1998**, *236*, 331.
- [12] Bañuelos Prieto, J.; López Arbeloa, F.; Martínez Martínez, V.; Arbeloa López, T.; López Arbeloa, I.; *J. Phys. Chem. A*, **2004**, *108*, 5503.
- [13] Hofer, J. E.; Grabenstetter, R. J.; Wiig, E. O.; *J. Am. Chem. Soc.*, **1950**, *72*, 203.
- [14] Turro, N. J.; *Modern Molecular Photochemistry*, **1978**, Benjamin/Cummings, Menlo Parck, CA, Chap. 5.
- [15] Boyer, J. H.; Haag, A. M.; Sathyamoorthi, G.; Soong, M.-L.; Thangaraj, K.; Pavlopoulos, T. G.; *Heteroatom Chem.*, **1993**, *4*, 39.
- [16] Costela, A.; García-Moreno, I.; Gomez, C.; Sastre, R.; Amat-Guerri, F.; Liras, M.; López Arbeloa, F.; Bañuelos, Prieto, J.; López Arbeloa, I.; *J. Phys. Chem. A*, **2002**, *106*, 7736.
- [17] López Arbeloa, F.; Bañuelos Prieto, J.; Martínez Martínez, V.; Arbeloa López, T.; López Arbeloa, I.; *ChemPhysChem*, **2004**, *5*, 1762.
- [18] Kollmannsberger, M.; Rurack, K.; Resch-Genger, U.; Rettig, W.; Daub, J.; *Chem. Phys. Lett.*, **2000**, *329*, 363.
- [19] Chattopadhyay, N.; Serpa, C.; Pereira, M. M.; Seixas de Melo, J.; Arnaut, L. G.; Formosinho, S. J.; *J. Phys. Chem. A*, **2001**, *105*, 10025.
- [20] Kollmannsberger, M.; Rurack, K.; Resch-Genger, U.; Daub, J.; *J. Phys. Chem. A*, **1998**, *102*, 10211.
- [21] Parusel, A. B. L.; Rettig, W.; Rotkiewicz, K.; *J. Phys. Chem. A*, **2002**, *106*, 2293.
- [22] Onkelinx, A.; De Schryver, F. C.; Viaene, L.; Van der Auweraer, M.; Iwai, K.; Yamamoto, M.; Ichikawa, M.; Masuhara, H.; Maus, M.; Rettig, W.; *J. Am. Chem. Soc.*, **1996**, *118*, 2892.
- [23] Zilberg, S.; Haas, Y.; *J. Phys. Chem. A*, **2002**, *106*, 1.
- [24] López Arbeloa, T.; López Arbeloa, F.; López Arbeloa, I.; García-Moreno, I.; Costela, A.; Sastre, R.; Amat-Guerri, F.; *Chem. Phys. Lett.*, **1999**, *299*, 315.
- [25] Costela, A.; García-Moreno, I.; Figuera, J. M.; Amat-Guerri, F.; Sastre, R.; *Laser Chem.*, **1998**, *18*, 63.
- [26] Costela, A.; García-Moreno, I.; Sastre, R.; in *Handbook of Advanced Electronic and Photonic Materials and Devices*, edited by H.S. Nalwa (Academic Press, San Diego 2001), Vol. 7, p. 161.
- [27] Costela, A.; García-Moreno, I.; Sastre, R.; *Phys. Chem. Chem. Phys.*, **2003**, *5*, 4745.
- [28] Hansch, C.; Leo, A.; Taft, R. W.; *Chem. Rev.*, **1991**, *91*, 165.

CAPÍTULO 3

BODIPYs EN LA REGIÓN ROJA DEL ESPECTRO VISIBLE

En los últimos años se está prestando especial interés al desarrollo de fluoróforos que emitan en la región espectral del infrarrojo cercano (NIR) (> 650 nm), por sus diversas y útiles aplicaciones^[1], especialmente en biomedicina y/o biofotónica^[2-3]. Estos colorantes son ampliamente empleados en campos tan relevantes como el de la energía fotovoltaica y optoelectrónica avanzada^[4-5], terapia fotodinámica (PDT, *Photodynamic Therapy*)^[6-9] o en bioimagen no-invasiva^[10]. La radiación NIR destaca por una alta capacidad de penetrabilidad en los tejidos (Figura 3.1)^[11-12] y además permite mayor resolución y sensibilidad en los procesos de monitorización de marcadores fluorescentes^[13-14] ya que a altas longitudes de onda no hay interferencias con la emisión fluorescente de las biomoléculas presentes en el medio.

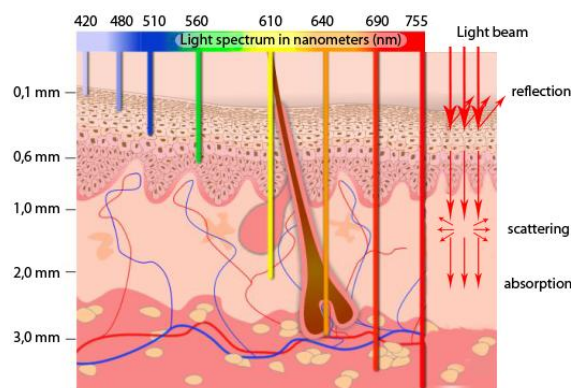


Figura 3.1. Penetrabilidad de las diferentes longitudes de onda de la luz en los tejidos.^[15]

A pesar de la variedad y disponibilidad comercial de colorantes NIR (Figura 3.2)^[16-17], las prestaciones de la mayoría de ellos están limitadas principalmente por el pequeño salto energético entre los orbitales HOMO y LUMO, necesario para conseguir el incremento de la longitud de onda de emisión. La proximidad entre dichos niveles electrónicos provoca que el acoplamiento vibracional sea más eficiente, se aumente la conversión interna y, por lo tanto, la desactivación del estado excitado sea muy rápida y de lugar a bajos rendimientos cuánticos de fluorescencia y poca fotoestabilidad^[18-19]. Además, los colorantes NIR necesitan de sistemas conjugados muy extendidos y por tanto suelen ser estructuras voluminosas que presentan baja solubilidad en medios polares (especialmente en agua). Por eso, y en vista de las excelentes propiedades que ofrecen los BODIPYs^[20], tal y como se ha destacado en los capítulos anteriores, en los últimos años se ha suscitado un creciente interés en el diseño y desarrollo de BODIPYs con emisión en la región roja del espectro visible e incluso NIR^[21-22], con especial hincapié en la región entre 800-900 nm, como alternativa a las familias de colorantes disponibles comercialmente en esa ventana espectral.

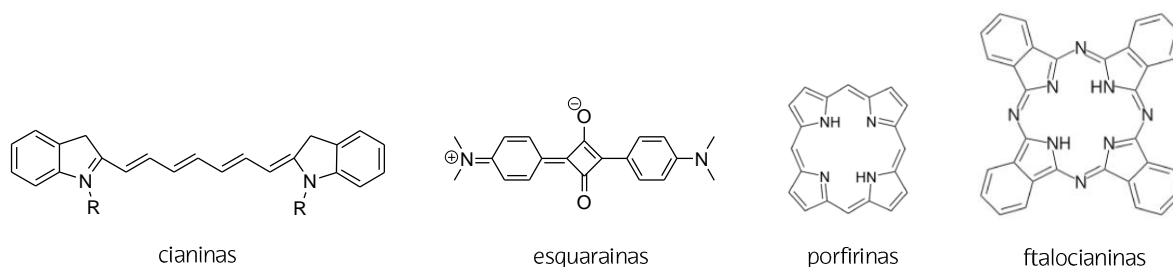


Figura 3.2. Estructuras generales de diversos colorantes NIR fluorescentes.

En base a la versatilidad sintética que ofrece el cromóforo BODIPY, existen diversos métodos y estrategias de modificación estructural para el desplazamiento de sus bandas espectrales hacia la región menos energética del visible (Figura 3.3)^[5,23-25]. Entre ellas destacan: (1) la sustitución del átomo de carbono en posición *meso* por un átomo de nitrógeno (aza-BODIPYs)^[26-28]; (2) la extensión de la conjugación π del sistema por la sustitución periférica del núcleo BDP^[29-31]; (3) la fusión de anillos aromáticos a los pirroles del cromóforo BDP^[32-34]; (4) la inducción de procesos “*push-pull*”^[35-37] o transferencia de carga ICT^[38-39]; o (5) la combinación de varias estrategias en una única estructura molecular^[40-42].

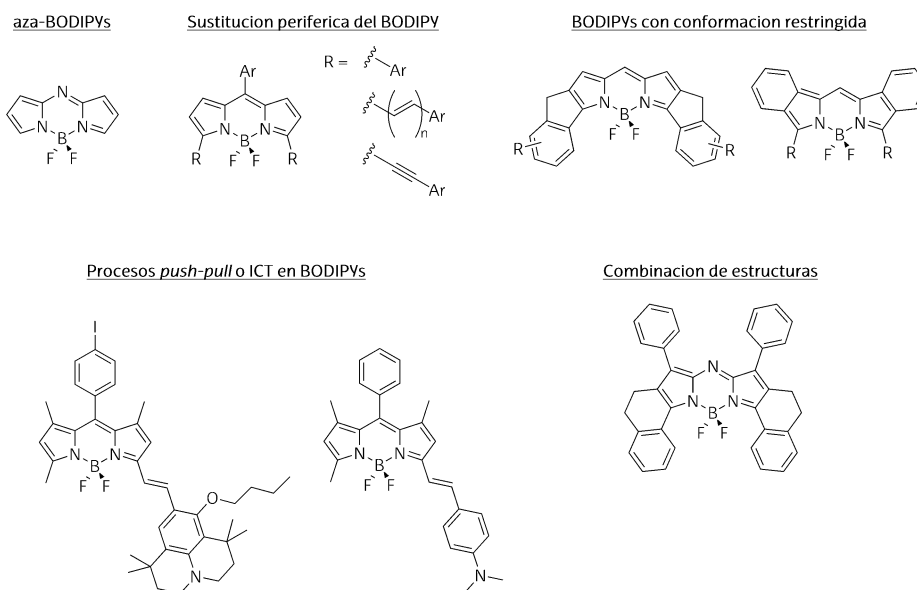


Figura 3.3. Clasificación general de las estructuras NIR-BODIPYs.

Por todo ello, es crítico disponer de una ruta sintética versátil pero robusta para alcanzar la funcionalización deseable de los análogos NIR BODIPY. Así, en el presente capítulo se analizan una serie de derivados, funcionalizados exhaustivamente y procedentes del 8-tiometil-BODIPY, sintetizados por el Prof. Eduardo Peña de la Universidad de Guanajuato (México) mediante reactividad ortogonal. Esta novedosa metodología no solo permite introducir un amplio abanico de grupos funcionales en el cromóforo de BODIPY, sino que también permite hacerlo selectivamente. Es decir, es posible funcionalizar las posiciones 8 (mediante acoplamientos de Liebeskind-Srogl - LSCC, *Liebeskind-Srogl cross-coupling* - o sustituciones nucleófilas, S_NAr), 2 y 6 (reacciones catalizadas por metales como Suzuki, Sonogashira o Stille), y 3 y 5 (Knoevenagel) sin alterar el resto, lo que permite diseñar nuevos colorantes a la carta con diferentes patrones de sustitución en posiciones ortogonales (Figura 3.4).

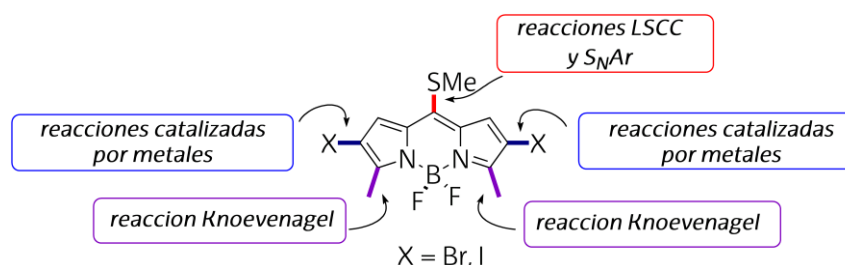


Figura 3.4. Diferentes puntos de reacción del BODIPY.

Por lo tanto, en el presente capítulo se tienen en cuenta algunas de las estrategias detalladas anteriormente en la Figura 3.3 para desarrollar BODIPYs con emisión en la región roja del espectro visible mediante la ruta sintética de la reactividad ortogonal. Concretamente se analizan derivados con conformación restringida mediante la fusión de anillos aromáticos al núcleo BDP (apartado 3.1) y derivados con sistemas conjugados extendidos por un aumento de la deslocalización a través de las posiciones α (3 y 5) y β (2 y 6) (apartado 3.2). También se considera la influencia de grupos dadores y aceptores en la misma estructura (BODIPYs *push-pull*). En el capítulo solo se tienen en cuenta las conclusiones más significativas de los BODIPYs rojos analizados, mientras que los detalles tanto sintéticos de la metodología de la reactividad ortogonal (en general y concretamente para los BODIPYs del apartado 3.2) como de las características fotofísicas, mecanocuánticas y láser se encuentran en el artículo adjunto al Anexo II al final de la memoria.

3.1. BODIPYs CON CONFORMACIÓN RESTRINGIDA

En esta aproximación para desplazar la emisión de los BODIPYs hacia la parte roja del espectro visible, se analiza la extensión de la deslocalización del sistema π cromofórico por la fusión de anillos aromáticos al núcleo BDP^[43-44]. Así, la fusión de anillos 3,5-dioxi-benzofurano en el enlace β (situado entre las posiciones α y β) del BDP permite obtener colorantes rígidos con conformación restringida. Los nuevos colorantes difieren en la sustitución de la posición 8 cromofórica (Figura 3.5), donde se han considerado anillos con libre giro (fenilo y *para*-tolilo), con giro restringido por impedimento estérico (*orto*-tolilo) y con grupos dadores de electrones (*para*-metoxifenilo).

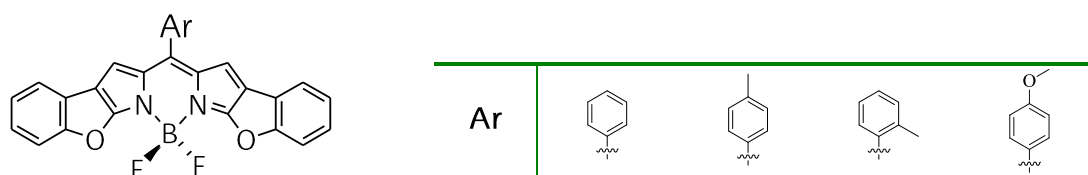


Figura 3.5. Estructuras moleculares de los BODIPYs con conformación restringida.

La fusión de anillos provoca fuertes desplazamientos batocrómicos de las bandas espectrales (del orden de 85 nm con respecto al BDP de referencia, Figura 3.6).

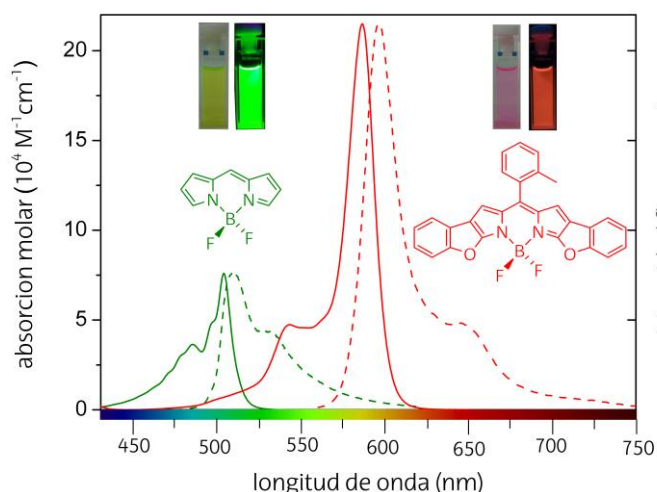


Figura 3.6. Espectros de absorción y fluorescencia (normalizados) en ciclohexano del 8-*o*-tolilBODIPY con conformación restringida (en rojo) vs BDP (en verde, capítulo 1). Se insertan fotografías bajo luz ambiente y luz UV.

Mediante la simulación mecanocuántica también se predice una disminución del salto energético entre los orbitales moleculares ($\Delta E \sim 2.7$ eV respecto al BDP con $\Delta E \sim 3.1$ eV). De hecho, tanto en el HOMO como en el LUMO el sistema π se extiende hacia los anillos benzofurano fusionados al indaceno (Figura 3.7.a). Dicho aumento de la deslocalización se refleja también en las elevadas probabilidades de absorción del hasta $21 \cdot 10^4 \text{ M}^{-1} \text{ cm}^{-1}$. Señalar que el arilo en 8 apenas participa en el sistema conjugado cromofórico al estar girado 90° por la sustitución en *orto*.

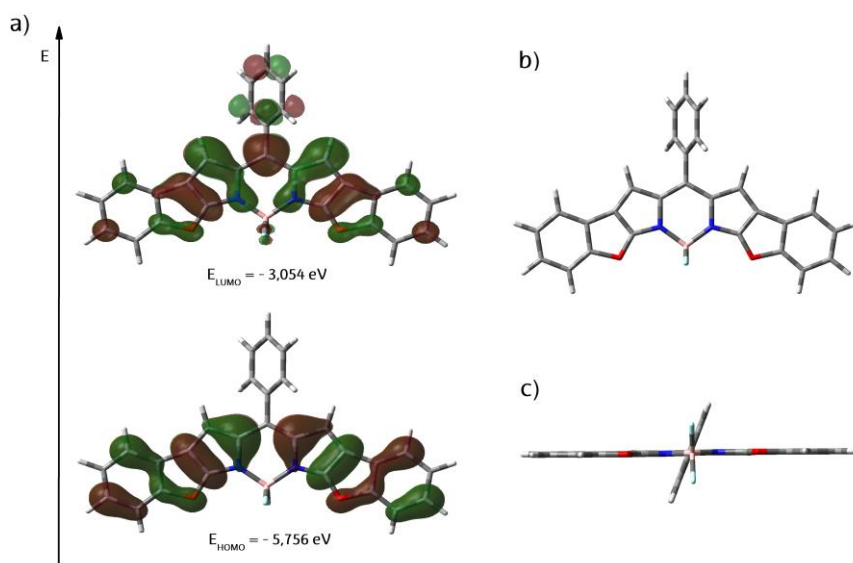
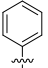
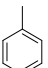
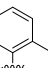
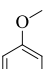


Figura 3.7. a) Mapas de densidad electrónica de los orbitales moleculares (HOMO y LUMO) del BODIPY con conformación restringida más representativo. b) Vista de las geometrías optimizadas en el estado excitado desde la perspectiva del eje x, y/c) eje z.

En general, las características fotofísicas de todos los derivados son muy similares e independientes del medio (Tabla 3.1) y, lo que es más sorprendente, de la funcionalización en la posición *meso*, calificada como la más sensible al carácter del sustituyente incorporado (capítulo 1). Ni tan siquiera la presencia de metoxi en para del fenilo (grupo dador de electrones y susceptible de promover la formación de estados ICT) origina cambios en las propiedades fotofísicas. Normalmente la presencia de arilos con libertad de giro provoca una fuerte disminución de la señal fluorescente porque facilitan acoplamiento vibracional que desembocan en un significativo aumento de la conversión interna^[45], mientras que la restricción de su libertad conformacional por impedimentos estéricos permite recuperar la alta capacidad fluorescente al evitar dichos procesos de relajación no-radiantes. Sin embargo, en el caso que nos ocupa, independientemente del impedimento estérico del 8-arilo, controlado por la sustitución en *orto*, las eficiencias fluorescentes se mantienen altas (superiores al 80%), con tiempos de vida del orden de 4 ns, en todos los derivados (Tabla 3.1). La simulación mecanocuántica indica que el aumento de la deslocalización hacia los anillos benzofurano retira parte de la densidad electrónica de la posición 8, debilitando así la influencia del libre giro de los arilos en dicha posición, cuyo efecto negativo en la capacidad fluorescente es evidente en los BODIPYs más simples, con la densidad electrónica más concentrada en el indaceno^[46-47].

Tabla 3.1. Propiedades fotofísicas de los BODIPYs con conformación restringida en función de la polaridad del disolvente (*c-hex*: ciclohexano, *EtOAc*: acetato de etilo, *MetOH*: metanol). El sustituyente *Ar* corresponde a la estructura base de la Figura 3.5.

Ar	Disolvente	λ_{ab} (nm)	ϵ_{max} ($10^4 \text{ M}^{-1}\text{cm}^{-1}$)	λ_{fl} (nm)	$\Delta\nu_{St}$ (cm^{-1})	ϕ	τ (ns)	k_{fl} (10^8 s^{-1})	k_{nr} (10^8 s^{-1})
	<i>c-hex</i>	586.0	15.6	597.5	330	0.84	3.99	2.10	0.40
	<i>EtOAc</i>	581.0	12.4	596.5	445	0.82	4.10	2.00	0.44
	<i>MetOH</i>	579.0	12.0	596.5	505	0.76	4.02	1.89	0.60
	<i>c-hex</i>	584.5	21.5	596.5	345	0.88	4.09	2.15	0.29
	<i>EtOAc</i>	579.5	17.0	594.5	435	0.86	4.18	2.06	0.33
	<i>MetOH</i>	578.0	16.4	594.5	480	0.79	4.08	1.94	0.51
	<i>c-hex</i>	586.5	21.5	595.5	260	0.88	4.21	2.09	0.29
	<i>EtOAc</i>	582.0	16.9	595.0	375	0.93	4.41	2.11	0.16
	<i>MetOH</i>	580.5	16.4	595.0	420	0.88	4.44	1.98	0.27
	<i>c-hex</i>	583.5	20.0	593.5	290	0.88	4.10	2.15	0.29
	<i>EtOAc</i>	578.0	15.7	594.0	465	0.83	4.22	1.97	0.40
	<i>MetOH</i>	576.5	15.2	592.0	455	0.79	4.14	1.91	0.51

Reseñar también que a pesar de la tensión geométrica que implica la fusión de los benzofuranos, el cromóforo destaca por su geometría planar (desviaciones de tan solo 2° en estado excitado, Figura 3.7.c). Dicha rigidez estructural implica que haya muy poca reorganización geométrica tras la excitación lo que explica el bajo desplazamiento de Stokes (apenas 350 cm^{-1}). Además, facilita la deslocalización, de ahí que se obtengan derivados con alta aromaticidad (parámetro BLA ~ 0.02), tal y como se refleja en la alta probabilidad de absorción ($\epsilon_{\text{max}} > 10^5\text{ M}^{-1}\text{ cm}^{-1}$) y emisión ($k_{\text{fl}} > 2 \cdot 10^8\text{ s}^{-1}$), y lo que es más significativo evitándose en gran medida procesos de conversión interna a pesar de la cercanía de los estados fundamental y excitado.

Por lo tanto, la fusión de anillos al cromóforo BDP para dar lugar a colorantes rígidos con conformación restringida es una alternativa excelente para desplazar las bandas espectrales a menores energías (absorción hasta 585 nm y fluorescencia hasta 595 nm), mejorando la capacidad de absorción y manteniendo las elevadas eficiencias fluorescentes ($\phi > 80\%$) tan características de los BODIPYs.

3.2. BODIPYs POR EXTENSIÓN PERIFÉRICA DE LA DESLOCALIZACIÓN

En el apartado anterior, se han obtenido BODIPYs eficientes con emisión próxima a 600 nm . Con vistas a llevar dicha emisión a menores energías para llegar al NIR se consideró otra estrategia complementaria que se basa en la extensión de la deslocalización del sistema π por la inclusión de cadenas aromáticas en la periferia del núcleo BDP (principalmente a través de las posiciones α ^[48]). De forma adicional también se insertaron grupos dadores y aceptores de electrones para favorecer en mayor medida el desplazamiento batocrómico.

Los derivados obtenidos por extensión periférica de la deslocalización que se analizan a continuación (Figura 3.8) constan de cadenas aromáticas con grupos aceptores (*p*-CF₃-estirilo) en las posiciones α del núcleo BDP y difieren bien sea en la sustitución en la posición *meso* con grupos neutros (*o*-metilfenilo), aceptores (*p*-CF₃-fenilo) o dadores (*p*-metoxifenilo), o bien en las posiciones β , donde se han considerado grupos dadores (*p*-metoxifenilo) o aceptores (*p*-formilfenilo).

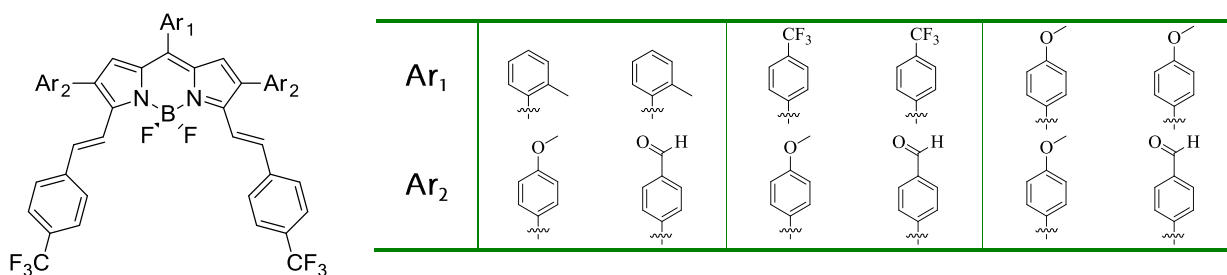


Figura 3.8. Estructura de los BODIPYs por extensión periférica de la deslocalización.

La funcionalización completa del cromóforo BDP implica un fuerte desplazamiento espectral a menores energías (en torno a 150 nm con respecto al BDP de referencia, Figura 3.9.a), aún mayor que el registrado para los BODIPYs fusionados (Figura 3.6, sección 3.1). Dicho significativo aumento del desplazamiento batocrómico es consecuencia de un sistema π que se extiende prácticamente en toda la molécula a través de las posiciones α y β (Figura 3.9.b). Además, la simulación mecanocuántica también estima un salto energético todavía menor ($\Delta E \sim 2.1$ eV respecto al BDP con $\Delta E \sim 3.1$ eV) que el calculado en los BODIPYs con conformación restringida ($\Delta E \sim 2.7$ eV, sección 3.1). Este aumento de la deslocalización se refleja de nuevo en un incremento de la probabilidad de absorción ($\sim 10^5$ M⁻¹cm⁻¹, Figura 3.9). Señalar que la extensión del sistema conjugado es más eficiente a través de las posiciones 3 y 5, que por las 2 y 6. Es más, la excitación del cromóforo supone un trasvase de la densidad electrónica de estos últimos sustituyentes al cromóforo^[49]. Por otro lado, la interacción de las cadenas aromáticas con el cromóforo, preferentemente de los estirilos en 3 y 5, provoca un importante incremento de la intensidad de absorción en la región UV (en torno a 350 nm, Figura 3.9.a). Esta fuerte banda de absorción supone una importante ventaja de estos nuevos BODIPYs con vistas a su aplicación láser. El bombeo de los colorantes existentes comercialmente en la región roja del visible no es trivial debido a su baja absorción de luz a 532 y 355 nm, longitudes de onda típicas de bombeo por Nd-YAG en láseres de colorante, que implica la necesidad de altas concentraciones. Sin embargo, en estos BODIPYs la fuerte absorción a 355 nm facilita su bombeo y posibilita obtener señal láser en medios activos de menor densidad óptica.

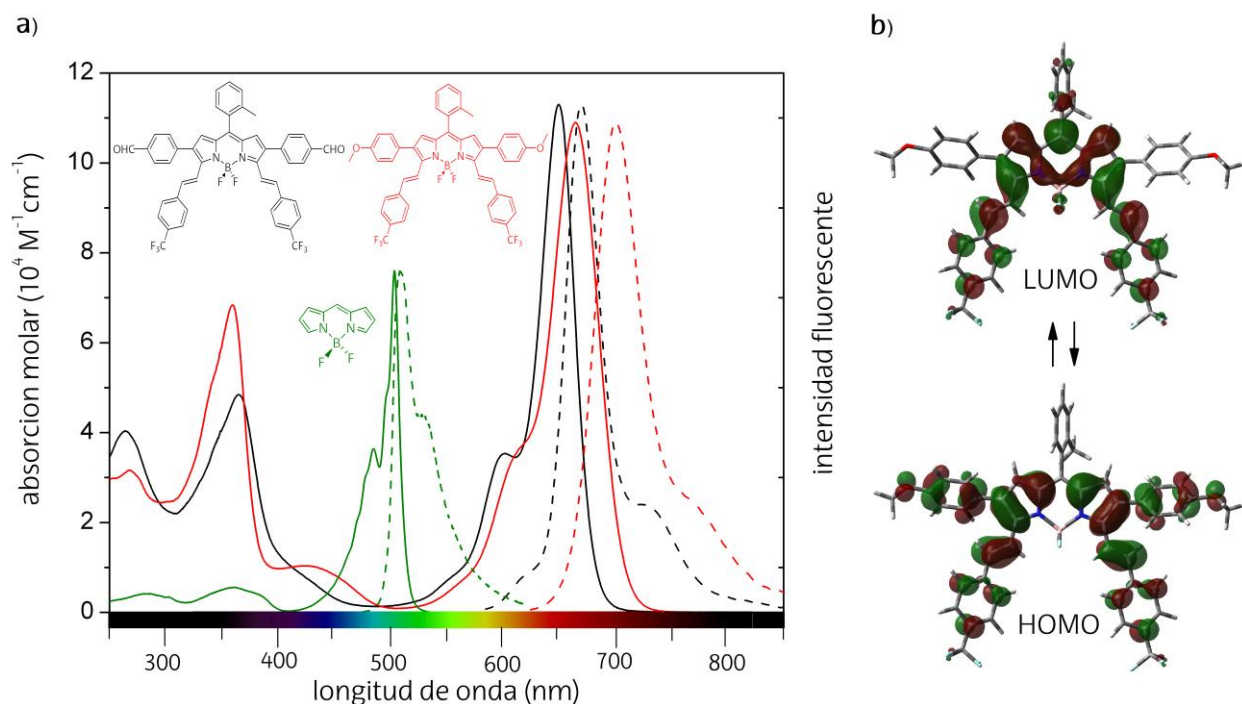
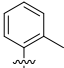
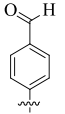
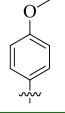
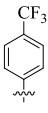
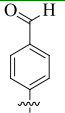
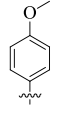
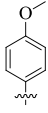
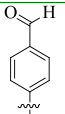
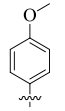


Figura 3.9. a) Espectros de absorción UV-Vis y fluorescencia normalizados en ciclohexano de los BODIPYs con extensión periférica de la deslocalización más representativos vs BDP (capítulo 1). b) Mapas de densidad electrónica de los orbitales moleculares (HOMO y LUMO).

De nuevo, y en concordancia con lo observado en la sección 3.1, el libre giro de los arilos en la posición *meso* (sustituyentes Ar_1) no parece afectar negativamente a la capacidad fluorescente por el ya señalado aumento de conversión interna^[45], y se registran rendimientos cuánticos fluorescentes altos (mayores al 50% en medios apolares como el ciclohexano en la Tabla 3.2), bien sea con giro libre del fenilo en 8 (*p*-trifluorometilolilo o *p*-metoxifenilo) o restringido por impedimento estérico (*o*-tolilo). Recordar que la presencia de 8-*p*-tolilo en el BDP simple daba lugar a una casi nula señal fluorescente^[50]. Por lo tanto, se confirma que la extensión de la deslocalización minimiza el efecto desactivador de la libre rotación de los arilos en *meso*. Sin embargo, es cierto que el derivado más fluorescente es aquel con el giro del fenilo restringido (hasta 87% con 8-*o*-metilfenilo, que se dispone girado unos 72° en el estado S_0), aunque la razón de esta mejora no es estérica sino más bien electrónica, tal y como se describe a continuación en los derivados con libertad de giro en 8. De hecho, en esta tanda de derivados, a parte de los que presentan 8-*o*-tolilo, se contemplan otros con 8-*p*-metoxifenilo o 8-*p*-trifluorometilfenilo (Figura 3.8), es decir, grupos con fuerte carácter dador y aceptor de electrones, respectivamente. Si a esto se le añade que en la misma estructura coexisten grupos aceptores (tales como trifluorometilo en 3 y 5) y eventualmente dadores (metoxi en 2 y 6), no es de extrañar que haya procesos de ICT. En otras palabras, algunos de estos colorantes tienen un

marcado carácter *push-pull*, ya que en la misma estructura hay una parte claramente dadora de electrones (*push*) y otra aceptora (*pull*), lo cual determinará las propiedades fluorescentes de los BODIPYs, tal y como se analiza a continuación.

Tabla 3.2. Propiedades fotofísicas de los BODIPYs por extensión periférica de la deslocalización en función de la polaridad del disolvente (*c-hex*: ciclohexano, *MetOH*: metanol). Los sustituyentes Ar_1 y Ar_2 corresponden a la estructura base de la Figura 3.8.

Ar_1	Ar_2	Disolvente	λ_{ab} (nm)	ϵ_{max} ($10^4 M^{-1}cm^{-1}$)	λ_{fl} (nm)	$\Delta\nu_{St}$ (cm^{-1})	ϕ	τ (ns)	k_{fl} ($10^8 s^{-1}$)	k_{nr} ($10^8 s^{-1}$)
		<i>c-hex</i>	650.0	11.3	670.0	460	0.87	4.61	1.90	0.28
		<i>MetOH</i>	644.0	10.4	668.0	560	0.73	4.36	1.67	0.62
		<i>c-hex</i>	665.0	10.9	701.0	770	0.61	4.25	1.43	0.92
		<i>MetOH</i>	657.5	8.9	708.0	1090	0.13	1.20	1.09	7.25
		<i>c-hex</i>	666.5	11.3	699.0	700	0.67	4.60	1.45	0.72
		<i>MetOH</i>	659.0	10.3	699.0	870	0.39	3.18	1.22	1.92
		<i>c-hex</i>	672.5	9.3	715.0	885	0.47	3.70	1.27	1.43
		<i>MetOH</i>	664.5	8.7	726.0	1275	0.06	0.73*	-	-
		<i>c-hex</i>	645.0	5.9	662.5	410	0.58	4.51	1.28	0.93
		<i>MetOH</i>	638.0	5.6	661.0	545	0.49	4.40	1.11	1.16
		<i>c-hex</i>	661.0	8.5	696.0	760	0.47	4.46	1.05	1.20
		<i>MetOH</i>	653.0	6.8	703.0	1090	0.11	1.50*	-	-

*Decaimiento biexponencial, se muestra el tiempo de vida mayoritario.

Así, las bandas espectrales de los derivados 8-*o*-tolilo con grupos débilmente aceptores (formaldehído) en 2 y 6 siguen la tendencia típica de los BODIPYs con la polaridad del medio (sección 1.2 del capítulo 1), mostrando ligeros desplazamientos hipsocrómicos y leve disminución de la capacidad fluorescente (Tabla 3.2). Sin embargo, el reemplazamiento de dichos aldehídos por grupos dadores (metoxi), aparte de desplazar la banda fluorescente más hacia el NIR (> 700 nm) por la interacción resonante de su par de electrones, provoca un desplazamiento batocrómico de la banda fluorescente (alrededor de 10 nm) con la polaridad del medio, solvatocromismo contrario al registrado en absorción,^[51] de ahí el aumento del desplazamiento de Stokes (> 1000 cm^{-1}). Tal y como se ha señalado anteriormente, la presencia

de grupos dadores (metoxi en 2 y 6) y aceptores (trifluorometil en 3 y 5) en la misma estructura favorece procesos de transferencia de carga especialmente tras la excitación. Como consecuencia el estado excitado difiere más del estado fundamental (aumento del desplazamiento de Stokes), se hace más polar y de ahí el desplazamiento batocrómico de la fluorescencia. Sin embargo, dicha separación de cargas implica más carácter ICT lo que se traduce en una reducción de la capacidad fluorescente especialmente en medios polares (del 73% con formaldehído en 2 y 6 al 13% al reemplazarlo por metoxi en metanol, Tabla 3.2).

La influencia del ICT se hace más patente a medida que aumenta el carácter *push-pull* del colorante, es decir, al introducir grupos dadores o aceptores en la posición *meso* (Tabla 3.2). Así, el reemplazamiento de 8-*o*-tolilo por 8-*p*-metoxifenilo o 8-*p*-trifluorometilfenilo en derivados con metoxi en posiciones β provoca mayores desplazamientos batocrómicos en fluorescencia (emisión hasta 725 nm) al aumentar la polaridad del medio, y como consecuencia, menores capacidades fluorescentes ($< 10\%$), conjuntamente con curvas de decaimiento rápidas y biexponenciales en los disolventes polares. Los mapas de potencial electrostático muestran claramente el cambio en la distribución de la densidad electrónica que inducen los sustituyentes. Así, la densidad electrónica del derivado 8-*o*-tolil-BODIPY (Figura 3.10.a) se distribuye siguiendo la tendencia típica de BODIPYs (Figura 1.3.b, capítulo 1), localizando densidad de carga negativa (color rojo) en el puente de unión BF_2 y positiva (color azul) alrededor de la posición 8. Sin embargo, la presencia de 8-*p*-trifluorometilfenil-BODIPY (Figura 3.10.b) y en menor medida de 8-*p*-metoxifenil-BODIPY (Figura 3.10.c) reorganiza dicha distribución. El puente BF_2 adquiere menor densidad de carga negativa (el color rojo se atenúa), la cual se desplaza hacia los grupos trifluorometilo (regiones amarillas, Figura 3.10.b), mientras que los grupos metoxi adquieren densidad de carga positiva (región azul, Figura 3.10.c). Todo ello indica que se produce un efecto *push-pull* mayor en el derivado con grupos trifluoroacetoxi (aceptores), en posiciones 3, 5 y 8, y metoxi (dadores), en las posiciones 2 y 6 (Figura 3.10.b). De hecho, de toda la serie de BODIPYs por extensión periférica de la deslocalización, este es el cromóforo con las propiedades fotofísicas más sensibles a la polaridad del medio (hecho experimental indicativo de procesos ICT), es decir, con emisión más desplazada a la zona NIR, pero en contrapartida con la menor eficiencia fluorescente de todos los BODIPYs estudiados (Tabla 3.2).

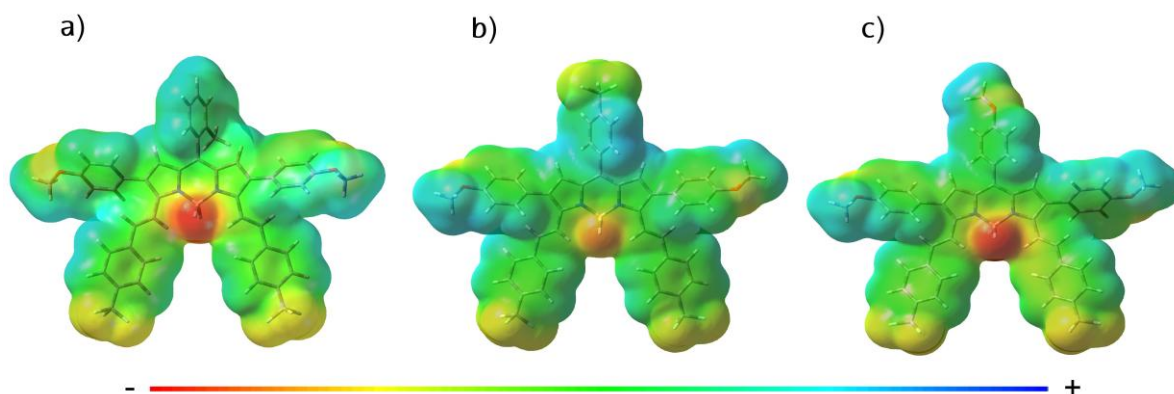


Figura 3.10. Mapas de los potenciales electrostáticos (rojo negativo y azul positivo) sobre la densidad electrónica de los derivados 2-/6- metoxifenil sustituidos y meso- a) o-tolil, b) p-CF₃-fenil y c) p-metoxifenil sustituidos.

De hecho, los BODIPYs del presente capítulo con el menor carácter *push-pull* (derivados con grupos aldehído en 2 y 6) muestran altas eficiencias láser en torno al 45-60% con fotoestabilidades del 100% (después de 50000 pulsos), lo que postula a estos derivados como colorantes láser prometedores en la región espectral roja. Si a esto le unimos las ya citadas fuertes bandas de absorción a 355 nm que facilitan el bombeo, se puede concluir que estos nuevos BODIPYs funcionalizados por reactividad ortogonal pueden desbancar a los láseres de colorante comerciales en la región espectral roja del visible y NIR.

De forma general, la combinación de grupos dadores y aceptores de electrones en estructuras de BODIPY extendidas mediante grupos aromáticos en las posiciones 3 y 5 es una estrategia adecuada para desplazar la banda a menores energías (absorción hasta 670 nm y fluorescencia hasta 725 nm), pero la capacidad fluorescente se resiente por la inducción de procesos ICT. Por tanto, y desde el punto de vista láser es necesario conseguir un balance entre inducir la suficiente separación de carga para conseguir mayores desplazamientos batocrómicos, pero sin que sea demasiada y limite la eficiencia láser del colorante.

El trabajo del presente capítulo ha sido aceptado en la revista *Chemistry European Journal* (2015) para su publicación, cuyo artículo se adjunta en el Anexo II al final de la memoria y donde se puede encontrar información más detallada de la caracterización fotofísica y láser de los BODIPYs con desplazamiento al rojo por la extensión de la deslocalización en la periferia del cromóforo.

Bibliografía

- [1] Terpetschnig, E.; Wolfbeis, O. S.; *Near-Infrared Dyes for High Technology Applications*, ed. Dihne, S.; Resch-Gender, U.; Wolfbeis, O. S.; Kluwer Academic, Dordrecht, **1998**.
- [2] Ntziachristos, V.; Ripoll, J.; Wang, L. H. V.; Weissleder, R.; *Nat. Biotechnol.*, **2005**, *23*, 313.
- [3] Ni, Y.; Wu, J.; *Org. Biomol. Chem.*, **2014**, *12*, 3774.
- [4] Qian, G.; Wang, Z. Y.; *Chem. Asian J.*; **2010**, *5*, 1006.
- [5] Bessette, A.; Hanan, G. S.; *Chem. Soc. Rev.*, **2014**, *43*, 3342.
- [6] Turan, I. S.; Cakmak, F. P.; Yildirim, D. C.; Cetin-Atalay, R.; Akkaya, E. U.; *Chem. Eur. J.*, **2014**, *20*, 16088.
- [7] Dolmans, D. E. J. G. J.; Fukumura, D.; Jain, R. K.; *Nat. Rev. Cancer*, **2003**, *3*, 380.
- [8] Huang, Z.; *Technol. Cancer Res. Treat.*, **2005**, *4*, 283.
- [9] Kamkaew, A.; Lim, S. H.; Lee, H. B.; Kiew, L. V.; Chung, L. Y.; Burgess, K.; *Chem. Soc. Rev.*, **2013**, *42*, 77.
- [10] Yuan, A.; Wu, J.; Tang, X.; Zhao, L.; Xu, F.; Hu, Y.; *J. Pharm. Sci.*, **2013**, *102*, 6.
- [11] Hilderbrand, S. A.; Weissleder, R.; *Curr. Opin. Chem. Biol.*, **2010**, *14*, 71.
- [12] Ethirajan, M.; Chen, Y. H.; Joshi, P.; Pandey, R. K.; *Chem. Soc. Rev.*, **2011**, *40*, 340.
- [13] Yuan, L.; Lin, W.; Zheng, K.; He, L.; Huang, W.; *Chem. Soc. Rev.*, **2013**, *42*, 622.
- [14] Yuan, L.; Lin, W.; Zhao, S.; Gao, W.; Chen, B.; He, L.; Zhu, S.; *J. Am. Chem. Soc.*, **2012**, *134*, 13510.
- [15] http://reflexions.ulg.ac.be/cms/c_41432/en/light-against-cancer
- [16] Umezawa, K.; Citterio, D.; Suzuki, K.; *Anal. Sci.*, **2014**, *30*, 327.
- [17] Haugland, R. P.; *The Handbook: A Guide to Fluorescent Probes and Labeling Technologies*, **2010**, Invitrogen Corp., Eugene.
- [18] Ballou, B.; Ernst, L. A.; Waggoner, A. S.; *Curr. Med. Chem.*, **2005**, *12*, 795.
- [19] Umezawa, K.; Nakamura, Y.; Makino, H.; Citterio, D.; Suzuki, K.; *JACS*, **2008**, *130*, 1550.
- [20] Loudet, A.; Burgess, K.; *Chem. Rev.*, **2007**, *107*, 4891.
- [21] Lu, H.; Mack, J.; Yang, Y.; Shen, Z.; *Chem. Soc. Rev.*; **2014**, *43*, 4778.
- [22] Roznyatovskiy, V. V.; Lee, C. H.; Sessler, J. L.; *Chem. Soc. Rev.*, **2013**, *42*, 1921.
- [23] Umezawa, K.; Matsui, A.; Nakamura, Y.; Citterio, D.; Suzuki, K.; *Chem. Eur. J.*, **2009**, *15*, 1096.
- [24] Ulrich, G.; Ziesel, R.; Harriman, A.; *Angew. Chem. Int. Ed.*, **2008**, *47*, 1184.
- [25] Boens, N.; Leen, V.; Dehaen, W.; *Chem. Soc. Rev.*, **2012**, *41*, 1130.
- [26] Sathyamoorthi, G.; Soong, M. L.; Ross, T. W.; Boyer, J. H.; *Heteroat. Chem.*, **1993**, *4*, 603.
- [27] Killoran, J.; Allen, L.; Gallagher, J. F.; Gallagher, W. M.; O'Shea, D. F.; *Chem. Commun.*, **2002**, 1862.
- [28] Gorman, A.; Killoran, J.; O'Shea, C.; Kenna, T.; Gallagher, W. M.; O'Shea, D. F.; *J. Am. Chem. Soc.*, **2004**, *126*, 10619.
- [29] Atilgan, S.; Ekmekci, Z.; Dogan, A. L.; Guc, D.; Akkaya, E. U.; *Chem. Commun.*, **2006**, *42*, 4398.
- [30] Burghart, A.; Kim, H. J.; Welch, M. B.; Thoresen, L. H.; Reibenspies, J.; Burgess, K.; Bergstrom, F.; Johansson, L. B. A.; *J. Org. Chem.*, **1999**, *64*, 7813.
- [31] Yamada, K.; Toyota, T.; Takakura, K.; Ishimaru, M.; Sugawara, T.; *New J. Chem.*, **2001**, *25*, 667.
- [32] Chen, J.; Burghart, A.; Derecskei-Kovacs, A.; Burgess, K.; *J. Org. Chem.*, **2000**, *65*, 2900.
- [33] Wada, M.; Ito, S.; Uno, H.; Murashima, T.; Ono, N.; Urano, T.; Urano, Y.; *Tetrahedron Lett.*, **2001**, *42*, 6711.
- [34] Shen, Z.; Röhr, H.; Rurack, K.; Uno, H.; Spieles, M.; Schulz, B.; Reck, G.; Ono, N.; *Chem. Eur. J.*, **2004**, *10*, 4853.
- [35] Nano, A.; Ziesel, R.; Stachelek, P.; Harriman, A.; *Chem. Eur. J.*; **2013**, *19*, 13528.
- [36] Shi, W.-J.; Lo, P.-C.; Singh, A.; Ledoux-Rak, I.; Ng, D. K. P.; *Tetrahedron*, **2012**, *68*, 8712.
- [37] Kolemen, S.; Bozdemir, O. A.; Cakmak, Y.; Barin, G.; Erten-Ela, S.; Marszalek, M.; Yum, J.-H.; Zakeeruddin, S. M.; Nazeeruddin, M. K.; Grätzel, M.; Akkaya, E. U.; *Chem. Sci.*, **2011**, *2*, 949.
- [38] Rurack, K.; Kollmannsberger, M.; Daub, J.; *Angew. Chem. Int. Ed.*, **2001**, *40*, 385.
- [39] Yu, Y.; Descalzo, A. B.; Shen, Z.; Röhr, H.; Liu, Q.; Wang, Y.; Spieles, M.; Li, Y.; Rurack, K.; You, X.; *Chem. Asian J.*; **2006**, *1*, 176.
- [40] Zhao, W. L.; Carreira, E. M.; *Angew. Chem. Int. Ed.*, **2005**, *44*, 1677.

- [41] Zhao, W. L.; Carreira, E. M.; *Chem. Eur. J.*, **2006**, *12*, 7254.
- [42] Goeb, S.; Ziesel, R.; *Org. Lett.*, **2007**, *9*, 737.
- [43] Descalzo, A. B.; Xu, H. J.; Xue, Z. L.; Hoffmann, K.; Shen, Z.; Weller, M. G.; You, X. Z.; Rurack, K.; *Organic Letters*, **2008**, *10*, 1581.
- [44] Leen, V.; Miscoria, D.; Yin, S.; Filarowski, A.; Molisho Ngongo, J.; Van der Auweraer, M.; Boens, N.; Dehaen, W.; *J. Org. Chem.*, **2011**, *76*, 8168.
- [45] Turro, N. J.; *Molecular Photochemistry*; W. A. Benjamín, Inc: New York, **1967**.
- [46] Ortiz, M. J.; García-Moreno, I.; Agarrabeitia, A. R.; Durán-Sampedro, G.; Costela, A.; Sastre, R.; López Arbeloa, F.; Bañuelos Prieto, J.; López Arbeloa, I.; *Phys. Chem. Chem. Phys.*, **2010**, *12*, 7804.
- [47] Duran-Sampedro, G.; Agarrabeitia, A. R.; García-Moreno, I.; Costela, A.; Bañuelos, J.; Arbeloa, T.; López Arbeloa, I.; Chiara, J. L.; Ortiz, M. J.; *Eur. J. Org. Chem.*, **2012**, 6335.
- [48] Buyukcakil, O.; Bozdemir, O. A.; Kolemen, S.; Erbas, S.; Akkaya, E. U.; *Org. Lett.*, **2009**, *11*, 4644.
- [49] García-Moreno, I.; Wang, L.; Costela, A.; Bañuelos, J.; López-Arbeloa, I.; Xiao, Y.; *ChemPhysChem*, **2012**, *13*, 3923.
- [50] Duran-Sampedro, G.; Agarrabeitia, A. R.; Garcia-Moreno, I.; Costela, A.; Bañuelos, J.; Arbeloa, T.; López-Arbeloa, I.; Chiara, J. L.; Ortiz, M. J.; *Eur. J. Org. Chem.*, **2012**, *32*, 6335.
- [51] Shandura, M. P.; Yakubovskiy, V. P.; Gerasov, A. O.; Kachkovsky, O. D.; Poronik, Y. M.; Kovtun, Y. P.; *Eur. J. Org. Chem.*, **2012**, 1825.

CAPÍTULO 4

BODIPYs EN LA REGIÓN AZUL DEL ESPECTRO VISIBLE

La necesidad de diseñar nuevos colorantes láser altamente eficientes y estables en la región azul del espectro visible es primordial para aplicaciones tecnológicas en optoelectrónica y dispositivos de almacenamiento^[1-6]. Actualmente, existen diversos colorantes orgánicos con emisión en dicha zona (Figura 4.1), pero generalmente muestran bajas eficiencias láser, poca estabilidad fotoquímica con un rápido fotoblanqueo y baja solubilidad en los disolventes más comunes^[7-12].

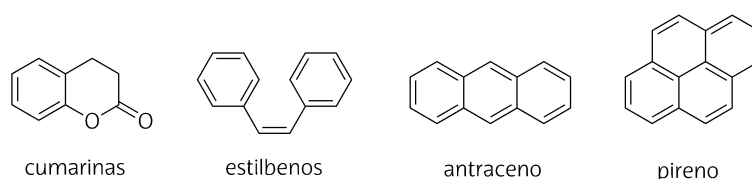


Figura 4.1. Estructuras generales de diversos fluoróforos que emiten en la región azul.

Tal y como se ha demostrado en los capítulos precedentes, la versatilidad sintética que ofrecen los colorantes BODIPY, permite modular la región de emisión a lo largo del espectro visible^[13], desde el verde-amarillo (500-590 nm en los capítulos 1-2) al naranja-rojo o NIR (590-725 nm en el capítulo 3)^[14]. Sin embargo, mientras que un desplazamiento batocrómico de las bandas espectrales se puede conseguir fácilmente extendiendo el sistema conjugado, un desplazamiento hipsocrómico no es tan trivial. De hecho, existen muy pocos estudios de

estructuras análogas al BODIPY con emisión centrada en la región espectral azul-verde (400-500 nm), y en la mayoría de los casos los resultados no han sido del todo satisfactorios en lo que se refiere a la eficiencia fluorescente y láser^[15-17]. Es por ello, que con el fin de cubrir todo el espectro visible con una única familia de colorantes se pretende obtener BODIPYs con emisión en el azul. Así, en este capítulo se analizan las propiedades fotofísicas y láser más representativas de una serie de BODIPYs con heteroátomos (N, O y S) en la posición *meso* (secciones 4.1-4.3), que sorprendentemente muestran la deseada emisión azul (Figura 4.2). Posteriormente y con vistas a mejorar más si cabe su eficiencia fluorescente y láser, se presenta el efecto de la metilación de las posiciones α (sección 4.4).

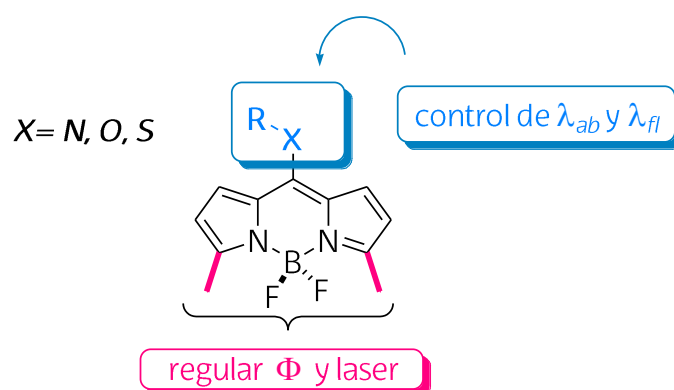


Figura 4.2. Estructura general de los BODIPYs azules estudiados en el presente capítulo.

Todos los colorantes analizados en este capítulo han sido sintetizados por el grupo del Prof. Eduardo Peña de la Universidad de Guanajuato (México) y en los 4 artículos adjuntos al Anexo III al final de la memoria, se encuentran los detalles tanto sintéticos como de las completas caracterizaciones fotofísicas y láser realizadas.

4.1. 8-AMINO BODIPYs

Los amino-BODIPYs del presente capítulo (Figura 4.3) constan de grupos amino en posición *meso* del cromóforo BDP con diferente grado de sustitución (primarias, secundarias o terciarias) y funcionalización (alifáticas, aromáticas o cíclicas).

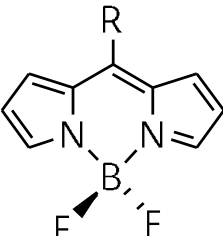
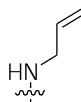
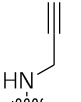
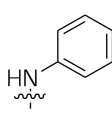
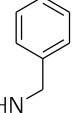
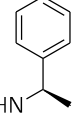
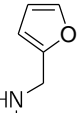
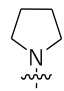
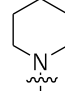
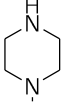
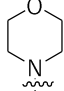
Grado de sustitución		R			
Amina 1 ^a		-NH ₂			
	alifáticas	-NHMe			-NHC(CH ₃) ₃
	aromáticas				
Amina 3 ^{as}	alifáticas	-N(CH ₃) ₂			
	cíclicas				

Figura 4.3. Estructuras moleculares de los 8-aminoBODIPYs.

En primer lugar, se analizan las propiedades fotofísicas del colorante más simple con una amina primaria en la posición 8 y posteriormente, se presenta el efecto general del resto de sustituciones por aminas secundarias o terciarias. En el presente apartado se consideran las características fotofísicas, electroquímicas y las propiedades láser más representativas de los 8-aminoBODIPYs, mientras que en los artículos adjuntos al Anexo III al final de la memoria se analizan en detalle todas estas características.

4.1.1. BODIPY sustituido por amina primaria en *meso*

En principio, cabría esperar que el par de electrones libres del grupo amino (dador de electrones, $\sigma_p^+ = -1.30$)^[18] es susceptible de deslocalizarse en el cromóforo BDP, y por lo tanto, se esperaría un desplazamiento espectral hacia la región roja por efecto resonante. Sin embargo, su presencia en posición *meso* induce un considerable desplazamiento hipsocrómico de las bandas, especialmente en el espectro de absorción (hasta 95 nm en absorción y 65 nm en

fluorescencia respecto al BDP, Figura 4.4.a). Por eso, el 8-NH₂-BODIPY se caracteriza por altos desplazamientos de Stokes (de ~1500-3000 cm⁻¹), siendo ésta una de las características más interesantes de los colorantes para aplicaciones de carácter fotónico como la mejora de la señal láser, ya que disminuye las pérdidas en la cavidad resonante por los fenómenos de reabsorción/reemisión presentes a altas densidades ópticas. Adicionalmente, la inclusión del grupo amino provoca la disminución de la probabilidad del máximo de absorción (situándose en torno a 3·10⁴ M⁻¹cm⁻¹), aunque induce un ensanchamiento de las bandas espectrales y se pierde el hombro vibrónico típico en BODIPYs (Figura 4.4.a). Por su parte, la emisión fluorescente es inesperadamente muy eficiente (rendimientos cuánticos superiores al 90%)^[19]. Es decir, la presencia del 8-amino desplaza las bandas espectrales al límite azul del espectro visible, manteniendo una fuerte emisión fluorescente en torno a 440 nm.

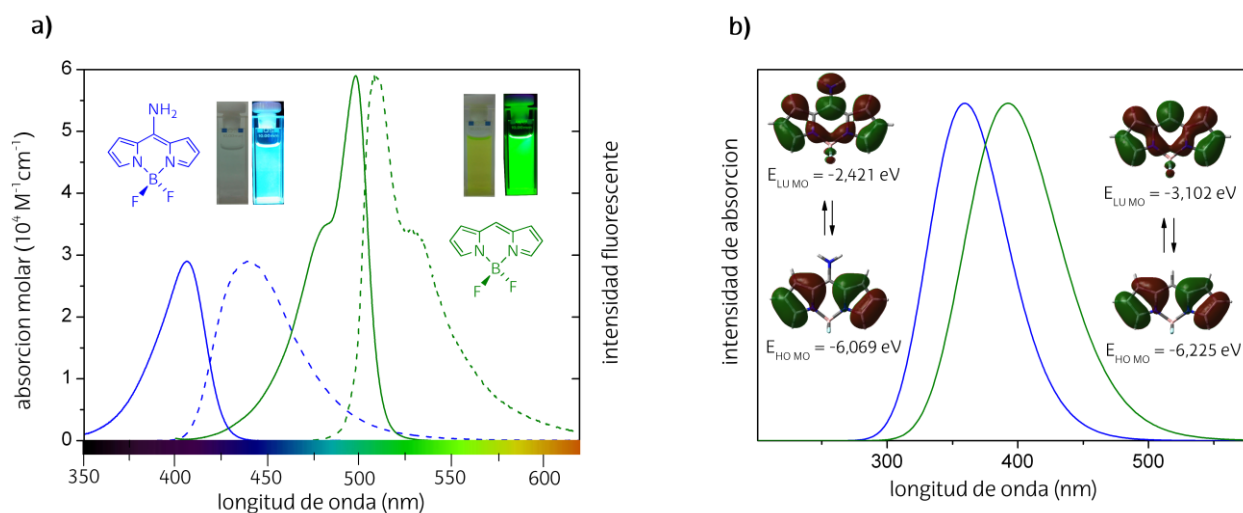


Figura 4.4. a) Espectros de absorción y emisión fluorescente normalizados en acetato de etilo del 8-aminoBODIPY (azul) vs BDP (verde, capítulo 1). Se insertan fotografías bajo luz ambiente y luz UV. b) Simulación del espectro de absorción del 8-aminoBODIPY (azul) vs BDP (verde), junto con los mapas de densidad electrónica de los correspondientes orbitales moleculares.

La incorporación del grupo amino en *meso* induce una mayor sensibilidad de las bandas espectrales al efecto del disolvente con respecto al BDP de referencia (Tabla 4.1). Así se siguen observando desplazamientos hipsocrómicos al aumentar la polaridad del medio, pero más marcados (de hasta 30 nm en absorción y 20 nm en fluorescencia al pasar de ciclohexano a metanol), mientras que en medios próticos (trifluoroetanol o agua) se observa un desplazamiento batocrómico, especialmente manifiesto en fluorescencia^[19]. Esta última tendencia se atribuye a una interacción específica, tipo enlace de hidrógeno entre el par de

electrones no-enlazantes del amino en 8 y los protones del disolvente, disminuyendo la capacidad dadora de la amina y por lo tanto, el desplazamiento espectral.

Tabla 4.1. Propiedades fotofísicas del BODIPY sustituido por amina primaria en meso vs BDP, en función de la polaridad del disolvente (*c-hex*: ciclohexano, *MetOH*: metanol, *F₃-EtOH*: 2,2,2-trifluoroetanol).

Derivado	Disolvente	λ_{ab} (nm)	ϵ_{max} ($10^4 M^{-1}cm^{-1}$)	λ_{fl} (nm)	$\Delta\nu_{St}$ (cm^{-1})	ϕ	τ (ns)	k_{fl} ($10^8 s^{-1}$)	k_{nr} ($10^8 s^{-1}$)
	<i>c-hex</i>	503.5	7.6	510.5	265	0.96	6.47	1.48	0.06
	<i>MetOH</i>	497.0	5.8	507.0	395	0.87	7.33	1.18	0.18
	<i>F₃-EtOH</i>	497.0	6.1	505.0	325	0.86	8.23	1.04	0.17
	<i>c-hex</i>	429.0	1.0	456.5	1410	0.96	4.49	2.14	0.09
	<i>MetOH</i>	399.0	2.6	437.5	2200	0.92	4.39	2.09	0.18
	<i>F₃-EtOH</i>	402.5	2.4	457.5	2980	0.94	5.86	1.60	0.10

La simulación teórica también predice un desplazamiento espectral a mayores energías respecto al BDP de referencia por la presencia de 8-amino en concordancia con las tendencias experimentales (Figura 4.4.b). Dicho aumento del salto energético es consecuencia del incremento de la energía del orbital LUMO, mientras que la energía del HOMO permanece prácticamente inalterada (Figura 4.4.b). El efecto dador de electrones del grupo amino desestabiliza el estado LUMO debido a que dicho estado localiza una alta densidad electrónica en la posición 8 en la que se incorpora el amino.

Sin embargo, la simulación teórica predice un desplazamiento hipsocrómico bastante menor que el experimental. Este hecho, conjuntamente con el cambio de la forma de los espectros (ensanchamiento), indica que existe una reorganización en la deslocalización electrónica del cromóforo como consecuencia de la interacción resonante con la amina. Así se ha propuesto que la disposición coplanar entre el amino en 8 y el indaceno permite una interacción resonante entre ambas entidades, que en vez de aumentar la deslocalización del sistema da lugar a la formación de una nueva estructura resonante (tipo-hemicianina) más corta que la normal de cianina, ya que se centra en un solo pirrol (Figura 4.5). La estabilización de esta forma mesomérica es la responsable del desplazamiento de las bandas al azul.

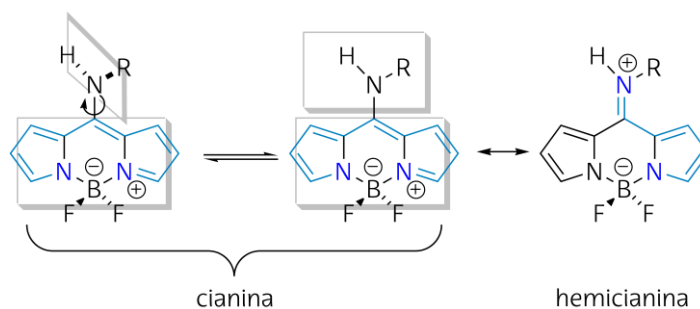


Figura 4.5. Estructuras del sistema π deslocalizado del 8-aminoBODIPY (en color azul se muestra la cadena responsable de la emisión).

Estos resultados obtenidos con la amina primaria ponen de manifiesto que el 8-NH₂-BODIPY es un candidato óptimo para ser empleado como colorante láser en la región azul. De hecho, se han llegado a alcanzar eficiencias láser del 62% en torno a 450 nm, similares a las registradas para el cromóforo BDP de referencia. Bien es cierto que su fotoestabilidad (40%) se resiente respecto al BDP (98%) después de 100000 pulsos de excitación, pero aún así su comportamiento es excelente puesto que el bombeo del 8-NH₂-BODIPY tiene lugar en la región UV, que es la zona más energética y además implica mayor fotodegradación con respecto a los que se bombean en la región visible. De hecho, su fotoestabilidad es mayor que la de los colorantes comerciales usados en la región azul (por ejemplo, de las cumarinas).

En vista de los prometedores resultados obtenidos con la amina primaria, a continuación se analiza cómo influye el carácter dador del grupo amino en la fofofísica del cromóforo BODIPY. La modificación controlada en la funcionalización del heteroátomo (desde aminas primarias a terciarias en la Figura 4.3), permite modular las propiedades fotofísicas de estos nuevos derivados.

4.1.2. BODIPYs sustituidos por aminas secundarias en *meso*

La metilación de la amina aumenta su carácter dador de electrones (metilamino, $\sigma_p^+ = -1.81$)^[18], lo que se traduce en un aumento del desplazamiento al azul (de hasta 10 nm) con respecto al derivado con amina primaria^[19]. Además, en el 8-NHMe-BODIPY, y a diferencia del 8-NH₂-BODIPY, se registra una disminución en la capacidad fluorescente de aproximadamente el 85% al pasar de ciclohexano (apolar) a metanol (polar). Es más, en medios polares las curvas de desactivación fluorescente se analizan como biexponenciales donde domina el tiempo de vida corto (Tabla 4.2). Estas evidencias experimentales inducen a pensar que existe un proceso

extra de desactivación no-radiante, activado o favorecido en medios polares. En este caso se atribuye a la formación de un estado ICT no fluorescente, a causa del mayor carácter dador de la amina al metilarse, y que se estabiliza en medios polares por la separación de cargas inherente al ICT. De hecho, en medios ácidos (trifluoroetanol) se recupera en parte la capacidad fluorescente ($\phi = 23\%$ y $\tau = 1.42$ ns, Tabla 4.2), lo que confirma la presencia del estado ICT, ya que en disolventes ácidos la amina se protona disminuyendo así su carácter dador y reduciendo la influencia negativa de dicho proceso ICT de desactivación no-radiante en la capacidad fluorescente.

Tabla 4.2. Propiedades fotofísicas de los BODIPYs sustituidos por aminas alifáticas secundarias en meso, en función de la polaridad del disolvente (*c-hex*: ciclohexano, *MetOH*: metanol, *F₃-EtOH*: 2,2,2-trifluoroetanol). El sustituyente R corresponde a la estructura base de la Figura 4.3.

R	Disolvente	λ_{ab} (nm)	ϵ_{max} ($10^4 \text{ M}^{-1} \text{ cm}^{-1}$)	λ_{fl} (nm)	Δv_{St} (cm^{-1})	ϕ	τ (ns)	k_{fl} (10^8 s^{-1})	k_{nr} (10^8 s^{-1})
	<i>c-hex</i>	418.5	2.4	463.0	2310	0.70	4.67	1.50	0.64
	<i>MetOH</i>	394.5	3.0	440.0	2605	0.10	0.52*	1.91	17.2
	<i>F₃-EtOH</i>	393.0	2.8	449.0	3170	0.23	1.42*	1.62	5.41
	<i>c-hex</i>	422.5	2.3	474.0	2570	0.79	4.89	1.61	0.43
	<i>MetOH</i>	401.0	2.9	453.0	2860	0.19	0.54*	3.52	15.0
	<i>F₃-EtOH</i>	399.0	2.7	469.5	3765	0.42	1.15*	3.65	5.04
	<i>c-hex</i>	422.5	3.5	482.0	2935	0.93	5.34	1.74	0.13
	<i>MetOH</i>	405.0	3.3	464.5	3175	0.52	3.22	1.61	1.49
	<i>F₃-EtOH</i>	404.0	2.9	480.5	3950	0.88	6.34	1.39	0.19

*Decaimiento biexponencial, se muestra el tiempo de vida mayoritario.

De hecho, las propiedades electroquímicas y la simulación mecanocuántica, correlacionan el mayor desplazamiento hipsocrómico con un aumento de la capacidad dadora del amino en meso (Figura 4.6.a). Así en el voltagrama cíclico del 8-NHMe-BODIPY se registran picos de reducción más negativos (de -0.71 V en el BDP a -1.36 V en el 8-NHMe-BODIPY), que sugieren, un aumento de la energía del LUMO y por tanto del salto energético, tal y como se constata teóricamente y de acuerdo con las medidas fotofísicas.

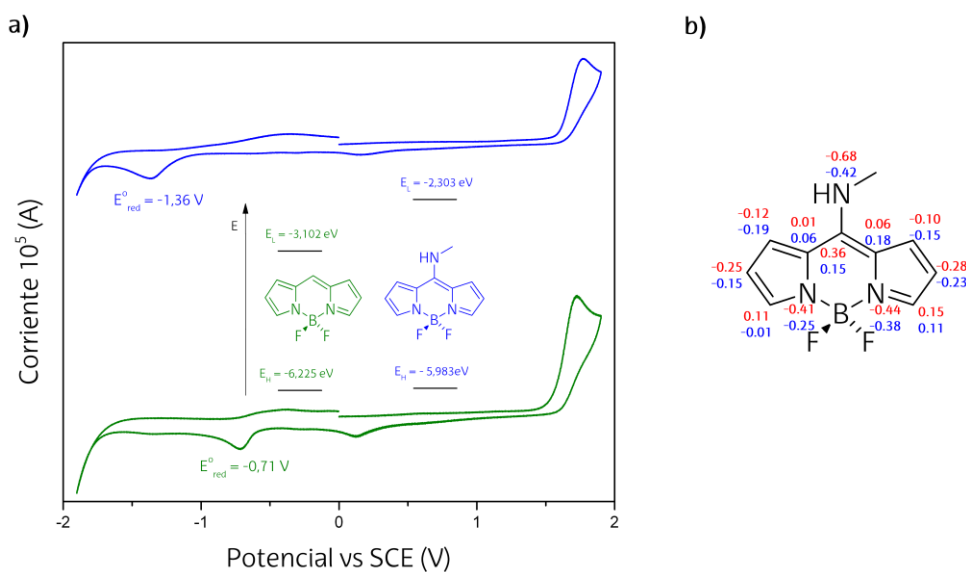


Figura 4.6. a) Voltagramas cíclicos del BDP (verde) y 8-metilaminoBODIPY (azul), junto con el diagrama energético de los correspondientes orbitales HOMO y LUMO. b) Distribución de la carga electrónica CHelpG en el estado fundamental (b3lyp/6-31g, en azul) y excitado (cis/6-31g, en rojo) del 8-metilaminoBODIPY.

Por otro lado, la presencia de un enlace doble (alilo) o triple (propargilo) en la amina secundaria disminuye la capacidad dadora de electrones de la misma y por ende el desplazamiento espectral al azul y la probabilidad de formación del ICT. Consecuentemente, las bandas espectrales no se sitúan tan al azul como en el 8-NHMe-BODIPY y la capacidad fluorescente es menos sensible a la polaridad del medio (Tabla 4.2). De hecho, el rendimiento cuántico del derivado con propargilamino en 8 disminuye en un 44% al pasar de un medio apolar a uno polar, mientras que en el 8-NHMe-BODIPY dicha disminución es de hasta un 85% (Tabla 4.2), lo que indica que la probabilidad de formación del estado ICT es menor a medida que aumenta el grado de instauración en la amina.

La presencia de la forma tipo-hemicianina, responsable del desplazamiento espectral al extremo azul del visible, se confirma mediante los espectros de ^1H - y ^{13}C -RMN, que asigna señales no-equivalentes a los átomos situados en posición simétrica de los anillos pirrólicos del indaceno^[15]. Es más, la distribución de cargas reafirma el cambio en la deslocalización del sistema de cianina a hemicianina, provocando que la distribución electrónica se vuelva asimétrica respecto a los pirroles especialmente en S_0 (Figura 4.6.b). Además, tras la excitación del 8-metilaminoBODIPY, el nitrógeno del grupo amino en *meso* adquiere más carga negativa (de -0.42 a -0.68) y la distancia del enlace C-N de la posición 8 aumenta (de 1.356 a 1.379 Å). Estos resultados, indican que la forma mesomérica tipo-hemicianina predomina en el estado

fundamental y es por eso que los desplazamientos hipsocrómicos de los 8-aminoBODIPYs en general son más pronunciados en los espectros de absorción.

Otra prueba experimental más del papel fundamental que juega el acoplamiento electrónico de la amina con el BODIPY para formar la hemicianina en la emisión azul se puede obtener al comparar el 8-aminoBODIPY con propargilo en la amina con su análogo donde la sustitución (metilos) en las posiciones adyacentes (1 y 7) proporciona un alto impedimento estérico y fija la amina perpendicular al indaceno (Figura 4.7 y ver la publicación *J. Org. Chem.* 2012 para más detalle). Así, el bloqueo del giro del grupo amino en 8 por impedimentos estéricos induce un menor desplazamiento hipsocrómico que el registrado para los BODIPYs amino sustituidos anteriormente citados (Figura 4.7). Es decir, aunque el carácter dador de electrones de la amina aumenta la energía del LUMO y con ello el salto energético, la disposición perpendicular entre el amino y el cromóforo (desacoplados electrónicamente) evita la formación de la hemicianina. De ahí que al introducir los metilos en 1 y 7 el desplazamiento al azul sea mucho menor que cuando no hay dicha sustitución. La ausencia de la deslocalización tipo hemicianina y el mayor peso de la forma cianina, se refleja en un incremento de la probabilidad de absorción ($\sim 5\text{-}6 \cdot 10^4 \text{ M}^{-1}\text{cm}^{-1}$) y un menor desplazamiento de Stokes ($\sim 1500\text{-}2000 \text{ cm}^{-1}$), más cercano al típico de los BODIPYs. A pesar de que un aumento en la rigidez del sistema generalmente aumenta la capacidad fluorescente, en el caso del 8-propargilaminoBODIPY tetrametilado se favorece un estado TICT (*Twisted Intramolecular Charge Transfer*)^[20], consecuencia de la disposición perpendicular entre ambas entidades que localiza el par de electrones en la amina. Dicho estado, desactiva fuertemente la capacidad fluorescente ya en disolventes apolares y más al aumentar la polaridad del medio (del 23% al 5%). De hecho, se han obtenido resultados similares en el derivado con un grupo voluminoso como el *tert*-butilo en la amina, donde también se impide la formación de la hemicianina (ver publicación *J. Org. Chem.* 2012 del Anexo III).

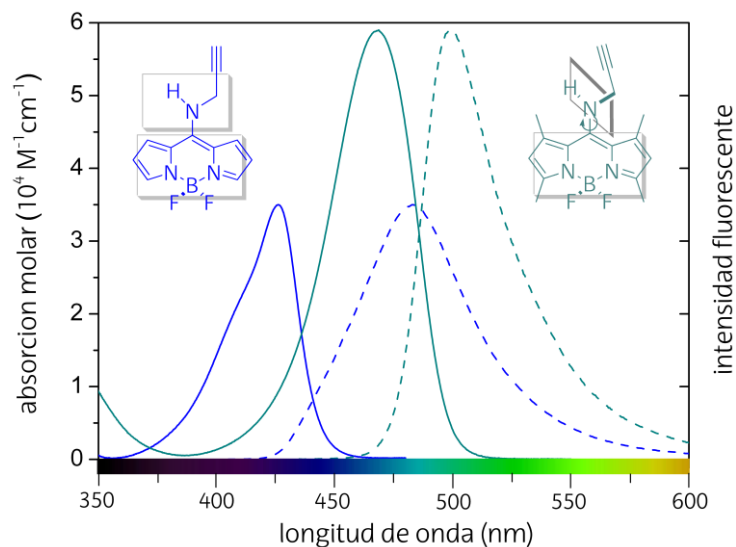
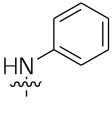
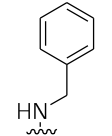
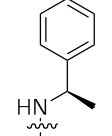
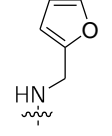


Figura 4.7. Espectros de absorción y emisión fluorescente normalizados en ciclohexano del 8-propargilaminoBODIPY con libertad de giro (en azul) y con el giro bloqueado (en verde-azulado).

Por otra parte, la presencia de grupos arilo en la amina (Figura 4.3, ver publicación *Chem Asian J.* del Anexo III para más detalle) no impiden la formación de la hemicianina y como consecuencia se observa el citado desplazamiento espectral al azul (Tabla 4.3). De hecho, se confirma por simulación mecanocuántica la disposición coplanar entre el amino y el cromóforo que se encuentran girados alrededor de 10° . Los rendimientos cuánticos de fluorescencia en medios apolares son muy altos (de casi hasta el 100%), pero de nuevo y en analogía al resto de aminas secundarias, la capacidad fluorescente depende de la polaridad del medio, en mayor medida que en los derivados con aminas alifáticas secundarias (Figura 4.8). De hecho, en el derivado que lleva la amina sustituida con metilbencilo, y por tanto la amina secundaria con mayor capacidad dadora de electrones, se llega a registrar una disminución del rendimiento cuántico de hasta el 95% de ciclohexano a metanol, donde la señal fluorescente es prácticamente nula y los tiempos de vida del orden de 300 ps. De nuevo el paso a un medio más ácido como el trifluoroetanol supone una mejora de la capacidad fluorescente por interacciones específicas con el amino que reducen la capacidad dadora del sustituyente (Tabla 4.3 y Figura 4.8). Esta batería de derivados de BODIPY con aminas secundarias confirman el papel fundamental que juega no sólo la formación de la hemicianina para modular la región de emisión sino también la activación de procesos ICT que limita la capacidad fluorescente del colorante según la polaridad del medio.

Tabla 4.3. Propiedades fotofísicas de los BODIPYs sustituidos por aminas aromáticas secundarias en meso, en función de la polaridad del disolvente (*c-hex*: ciclohexano, *MetOH*: metanol, *F₃-EtOH*: 2,2,2-trifluoroetanol). El sustituyente *R* corresponde a la estructura base de la Figura 4.3.

R	Disolvente	λ_{ab} (nm)	ϵ_{max} ($10^4 \text{ M}^{-1} \text{ cm}^{-1}$)	λ_{fl} (nm)	$\Delta\nu_{St}$ (cm^{-1})	ϕ	τ (ns)	k_{fl} (10^8 s^{-1})	k_{nr} (10^8 s^{-1})
	<i>c-hex</i>	423.0	4.3	480.0	2815	1.00	5.25	1.90	0.00
	<i>MetOH</i>	403.5	4.1	461.0	3105	0.16	0.92*	1.74	9.13
	<i>F₃-EtOH</i>	402.5	3.8	482.5	4110	0.43	3.07*	-	-
	<i>c-hex</i>	422.0	2.8	472.0	2490	1.00	4.92	2.03	0.00
	<i>MetOH</i>	403.0	2.3	453.5	2760	0.095	0.49*	1.84	18.5
	<i>F₃-EtOH</i>	401.0	2.0	460.0	3195	0.38	2.39*	-	-
	<i>c-hex</i>	424.0	4.2	475.0	2545	1.00	5.02	1.99	0.00
	<i>MetOH</i>	404.5	3.1	460.5	2995	0.054	0.32*	-	-
	<i>F₃-EtOH</i>	405.0	2.9	475.0	3630	0.20	1.38*	-	-
	<i>c-hex</i>	423.0	4.1	478.5	2745	0.98	5.24	1.87	0.04
	<i>MetOH</i>	403.0	3.4	464.0	3250	0.15	0.94*	1.60	9.04
	<i>F₃-EtOH</i>	402.0	3.5	483.0	4150	0.44	3.13*	-	-

*Decaimiento biexponencial, se muestra el tiempo de vida mayoritario.

Con respecto al comportamiento láser se observa que los BODIPYs con aminas secundarias presentan peores eficiencias y fotoestabilidades que las obtenidas con la amina primaria. Así, en el caso de aminas secundarias alifáticas la fotoestabilidad llega a ser del 20% después de 50000 pulsos y las eficiencias láser varían entre el 25-60%,^[19] mientras que en aminas secundarias aromáticas la eficiencia láser oscila entre el 25-44%, aunque se registran fotoestabilidades superiores al 65% tras 80000 pulsos. Sin embargo, en el derivado con mayor carácter dador (8-metilbencilaminoBODIPY) la eficiencia láser es del 14% y la fotoestabilidad del 30%. Es decir, parece haber una correlación no sólo entre la posición de la banda fluorescente y láser, sino también entre la probabilidad de los procesos no-radiantes (controlado por el ICT principalmente) y la fotoestabilidad; a medida que la amina es más dadora de electrones, más influencia del ICT y menos eficiencia y fotoestabilidad. Sin embargo, y a pesar de la ya mencionada disminución de la estabilidad láser, se siguen consiguiendo mejores resultados láser que los obtenidos con los colorantes comerciales de referencia en esta región espectral (cumarinas), sobre todo en lo que se refiere a fotoestabilidad^[15].

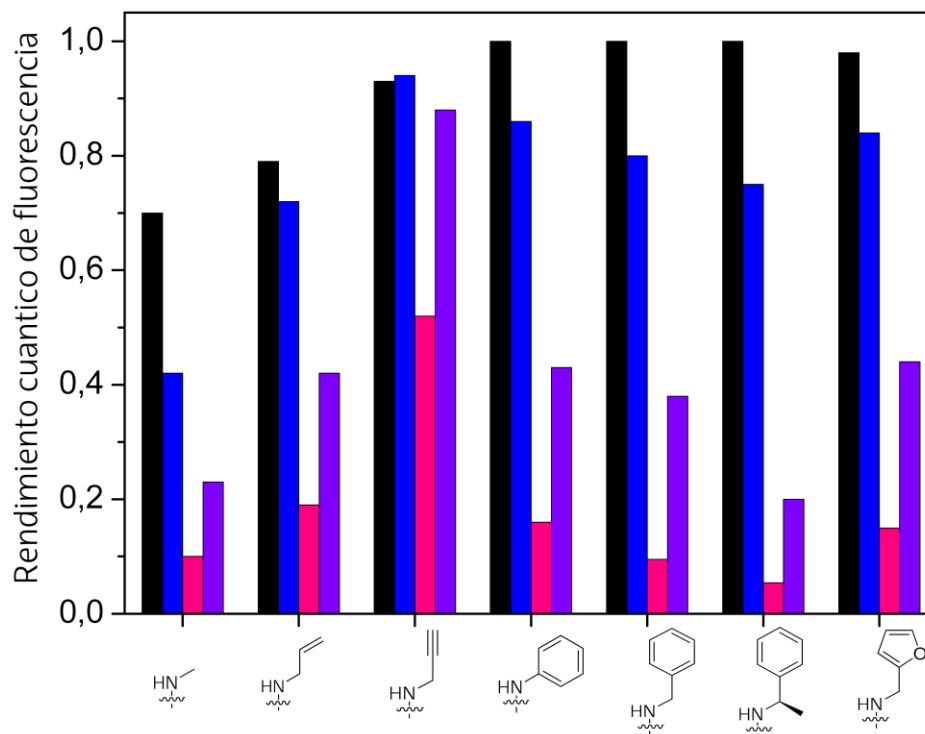


Figura 4.8. Rendimientos cuánticos de fluorescencia de los 8-BODIPYs sustituidos por aminas secundarias en función de la polaridad del medio: ciclohexano (negro), acetato de etilo (azul), metanol (rosa) y 2,2,2-trifluoroetanol (violeta).

4.1.3. BODIPYs sustituidos por aminas terciarias en *meso*

Para terminar con esta sección, se analiza la influencia de las aminas terciarias alifáticas y cíclicas en la posición *meso* (Figura 4.3, ver publicación *Chem Asian J.* del Anexo III para más detalle). La capacidad dadora del grupo dimetilamino ($\sigma_p^+ = -1.70$)^[18], apenas varía con respecto a la del metilamino ($\sigma_p^+ = -1.81$, en la sección 4.1.2)^[18], por lo que la posición de las bandas espectrales se mantiene prácticamente inalterada^[19] y la probabilidad de formación del estado ICT es similar (Tabla 4.4), tal y como queda patente en la disminución del rendimiento cuántico experimentada por el 8-NMe₂-BODIPY (alrededor del 81% vs 85% para el 8-NHMe-BODIPY) al aumentar la polaridad del medio (Figura 4.8 vs 4.9.a).

A diferencia de las aminas secundarias con grupos arilo (sección 4.1.2), en el caso de las aminas terciarias que forman parte de un ciclo (piperidina y pirrolidina), la incorporación del sustituyente voluminoso en 8 impide la disposición coplanar del grupo amino con el indaceno evitando así la deslocalización del par de electrones libres hacia el cromóforo. De hecho, la simulación teórica indica que estas aminas cíclicas se disponen giradas unos 26° (Figura 4.9.b),

dificultando la formación de la hemicianina y con ello dando lugar a un menor desplazamiento al azul (Tabla 4.4). Dicha disposición girada también sugiere mayor probabilidad de formación del estado ICT (o posible TICT) tal y como lo atestiguan las bajas capacidades fluorescentes registradas incluso en medios apolares, siendo menores que las de aminas secundarias (Figura 4.9).

Tabla 4.4. Propiedades fotofísicas de los BODIPYs sustituidos por aminas terciarias en meso, en función de la polaridad del disolvente (*c*-hex: ciclohexano, MetOH: metanol, F_3 -EtOH: 2,2,2-trifluoroetanol). El sustituyente R corresponde a la estructura base de la Figura 4.3.

R	Disolvente	λ_{ab} (nm)	ϵ_{max} ($10^4 M^{-1}cm^{-1}$)	λ_{fl} (nm)	$\Delta\nu_{St}$ (cm^{-1})	ϕ	τ (ns)	k_{fl} ($10^8 s^{-1}$)	k_{nr} ($10^8 s^{-1}$)
	<i>c</i> -hex	417.0	2.8	466.5	2545	0.49	4.65	1.05	1.09
	MetOH	396.0	2.7	438.0	2420	0.09	0.50*	1.80	18.2
	F_3 -EtOH	394.0	2.4	453.5	3330	0.26	1.36*	1.91	5.44
	<i>c</i> -hex	409.5	2.9	472.5	3245	0.051	-	-	-
	MetOH	391.5	2.4	454.5	3540	0.004	-	-	-
	<i>c</i> -hex	435.0	3.9	492.0	2670	0.069	1.23*	0.56	7.57
	MetOH	413.0	3.1	437.5	1360	0.001	-	-	-
	<i>c</i> -hex	440.0	2.9	498.0	2665	0.49	1.93	2.54	2.64
	MetOH	419.5	2.4	445.5	1380	0.006	-	-	-
	<i>c</i> -hex	439.5	4.2	496.0	2595	0.27	1.94*	1.39	3.76
	MetOH	419.5	2.6	452.0	1710	0.006	-	-	-

*Decaimiento biexponencial, se muestra el tiempo de vida mayoritario.

Por otro lado, la presencia de heteroátomos adicionales (N, O) en el ciclo afecta a la capacidad dadora de electrones de la amina ya que su electronegatividad provoca que se retire densidad electrónica del amino, disminuyendo su capacidad dadora (menor desplazamiento al azul, Tabla 4.4) y con ello la menor probabilidad de formación del estado ICT en medios apolares (son los derivados que presentan mayor rendimiento cuántico, alrededor del 30%-50%), si bien es cierto que la estabilización de dicho estado ICT en medios polares da lugar a emisiones prácticamente nulas (Figura 4.9.a).

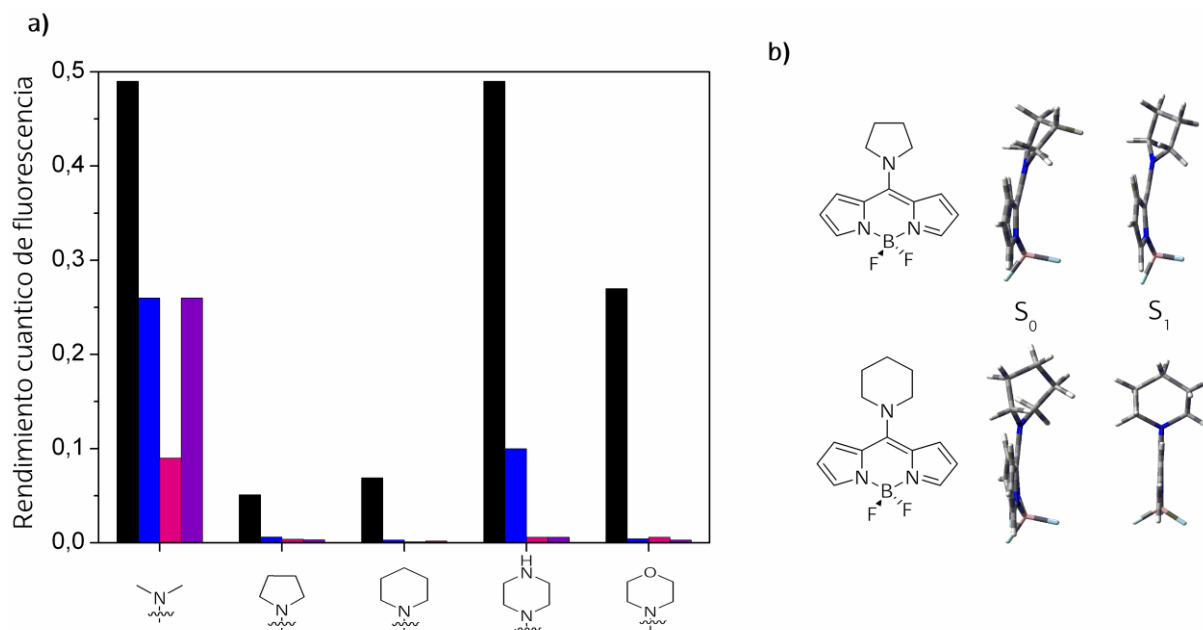


Figura 4.9. a) Rendimientos cuánticos de fluorescencia de los 8-BODIPYs sustituidos por aminas terciarias en función de la polaridad del medio: ciclohexano (negro), acetato de etilo (azul), metanol (rosa) y 2,2,2-trifluoroetanol (violeta). b) Geometrías optimizadas de los estados S_0 (b3lyp/6-31g) y S_1 (cis/6-31g) del 8-pirrolidinaBODIPY (arriba) y 8-piperidinaBODIPY (abajo).

Con el fin de confirmar inequívocamente la presencia de un estado ICT desde el grupo amino al BODIPY, especialmente cuando se incorporan aminas secundarias y terciarias al cromóforo, se realizaron medidas de fluorescencia a bajas temperaturas para el 8-pirrolidinaBODIPY. A 77K se disminuye el movimiento vibracional y se impide el rotacional, y los procesos activados que implican transferencia electrónica son menos probables. Así se observa un importante aumento de la intensidad fluorescente a medida que se disminuye la temperatura puesto que en estas condiciones es más difícil superar la barrera energética para poblar el ICT y se recupera la señal fluorescente del estado emisor LE (Figura 4.10). Teniendo en cuenta la fuerte desactivación fluorescente que ejerce el ICT a temperatura ambiente no es de extrañar que los derivados con amina terciaria no proporcionen señal láser.

Resumiendo, estos nuevos colorantes permiten modular las propiedades de emisión fluorescente hacia la región azul, en función del carácter dador del grupo amino en posición *meso* del cromóforo, para obtener colorantes láser basados en BODIPYs con óptimas prestaciones láser que desbancan a los medios activos comerciales empleados en dicha región. Así los derivados con aminas primarias proporcionan señal láser muy eficiente (hasta 62%) y estable, lo que supone paliar una de las mayores deficiencias de los colorantes láser disponibles en la región azul, mientras que en los derivados con aminas secundarias y terciarias su

comportamiento láser está limitado por la estabilización de un estado ICT no-fluorescente, especialmente en las aminas con mayor carácter dador de electrones y en medios polares.

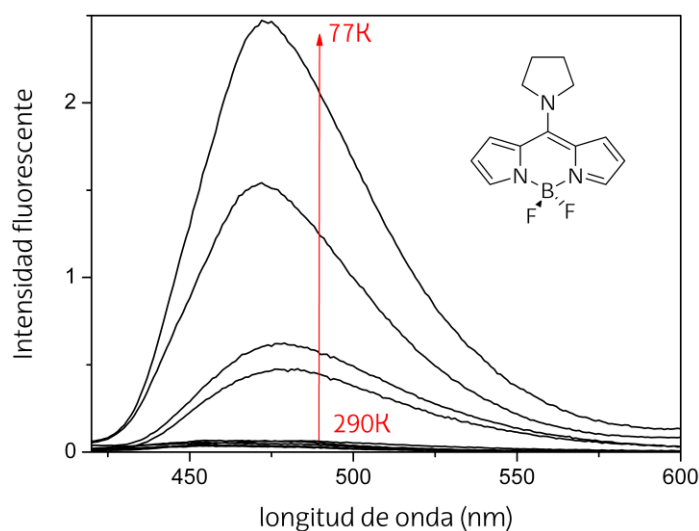


Figura 4.10. Intensidad de los espectros de fluorescencia del 8-pirrolidinaBODIPY en etanol en función de la temperatura.

4.2. 8-ALCOXI y 8-ARILOXI BODIPYs

En vista del efecto generado por la inclusión de grupos amino con diferente carácter dador en posición 8 y con intención de estudiar en profundidad la región espectral azul, se ha funcionalizado dicha posición con un heteroátomo como el oxígeno con menor carácter electronegativo. Así, en esta sección se analizan derivados de BODIPY con grupos alcoxi y ariloxi en la posición 8 (Figura 4.11). En primer lugar se analizan las propiedades fotofísicas del colorante más simple, con metoxi en *meso* (8-OMeBODIPY) y posteriormente se profundiza en el efecto de la sustitución del grupo oxo estudiando el resto de los alcoxi- y ariloxiBODIPYs. Este trabajo ha dado lugar a una publicación en *J. Org. Chem* 2013 (adjunta al Anexo III al final de la memoria) donde se interpretan los resultados de todos los derivados exhaustivamente.

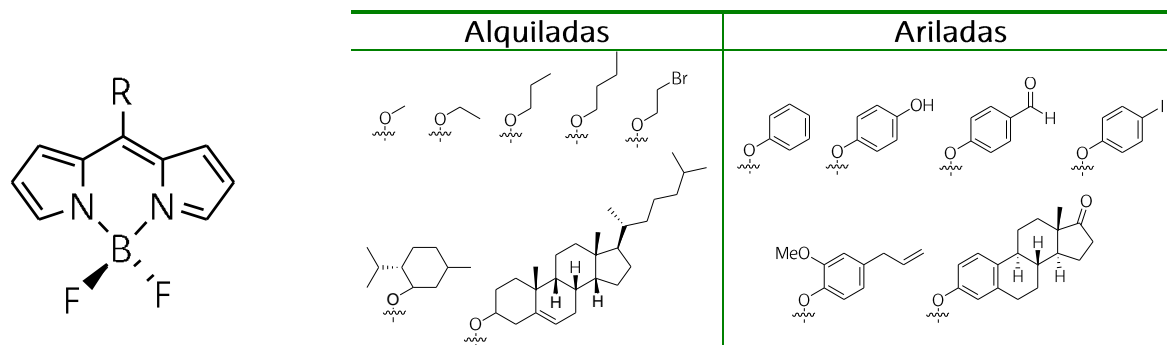


Figura 4.11. Estructuras moleculares de los 8-alcoxi- y 8-arioloxiBODIPYs.

4.2.1. 8-alcoxiBODIPYs

La menor electronegatividad del oxígeno supone que el sustituyente metoxi tenga menor carácter dador ($\sigma_p^+ = -0.78$)^[18] con respecto al metilamino ($\sigma_p^+ = -1.81$)^[18], lo que induce que el 8-OMeBODIPY sea más fácilmente reducible (-0.81 V vs -1.36 V en la Figura 4.12.a) y la desestabilización del orbital LUMO sea menor (-2.70 eV vs -2.30 eV en la Figura 4.12.b) que la del 8-NHMe-BODIPY.

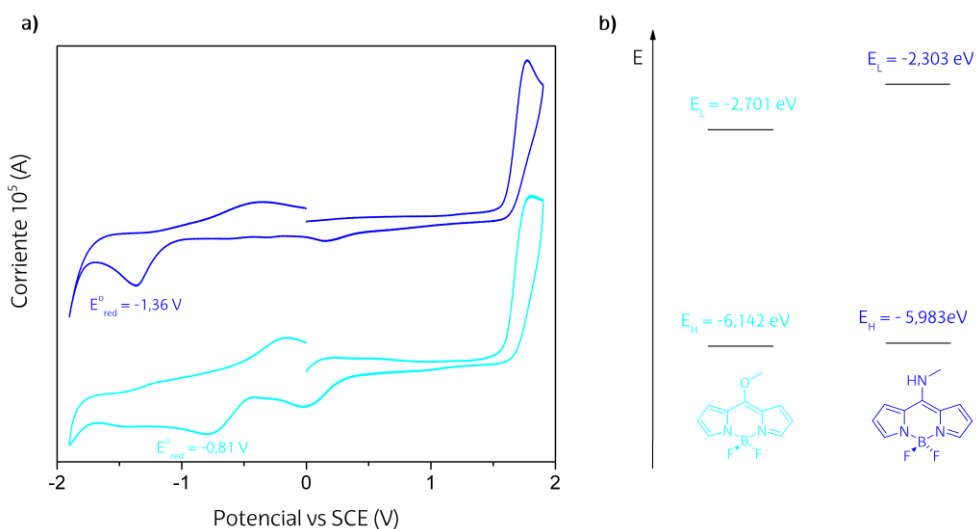


Figura 4.12. a) Voltagramas cíclicos y b) diagrama energético de los orbitales HOMO y LUMO del 8-metilaminoBODIPY (azul) vs 8-metoxiBODIPY (cian).

En todo caso el efecto dador del grupo metoxi en *meso* desestabiliza el LUMO y aumenta el potencial de reducción respecto al BDP de referencia, lo que se traduce en un desplazamiento espectral hipsocrómico (de ~55 nm en absorción y ~20 nm en fluorescencia con respecto al BDP) y un aumento del desplazamiento de Stokes (~2000 cm⁻¹, Tabla 4.5). Dicho desplazamiento a mayores energías es menos significativo que el registrado en el 8-NHMe-

BODIPY por la menor capacidad dadora del metoxi (Figura 4.13.a). En este caso la interacción resonante del par de electrones del grupo oxo con el indaceno también provoca una reorganización de la distribución electrónica y la generación de una nueva forma mesomérica denominada merocianina (Figura 4.13.b). El aumento de la probabilidad de absorción ($\sim 4\text{-}6 \cdot 10^4 \text{ M}^{-1}\text{cm}^{-1}$), junto con la recuperación del hombro vibrónico típico de BODIPYs, así como la disminución en la anchura espectral del 8-OMe-BODIPY con respecto a los amino derivados induce a pensar que la merocianina no influye tan severamente en las propiedades fotofísicas como la hemicianina, en concordancia con el menor desplazamiento al azul observado (Figura 4.13.a).

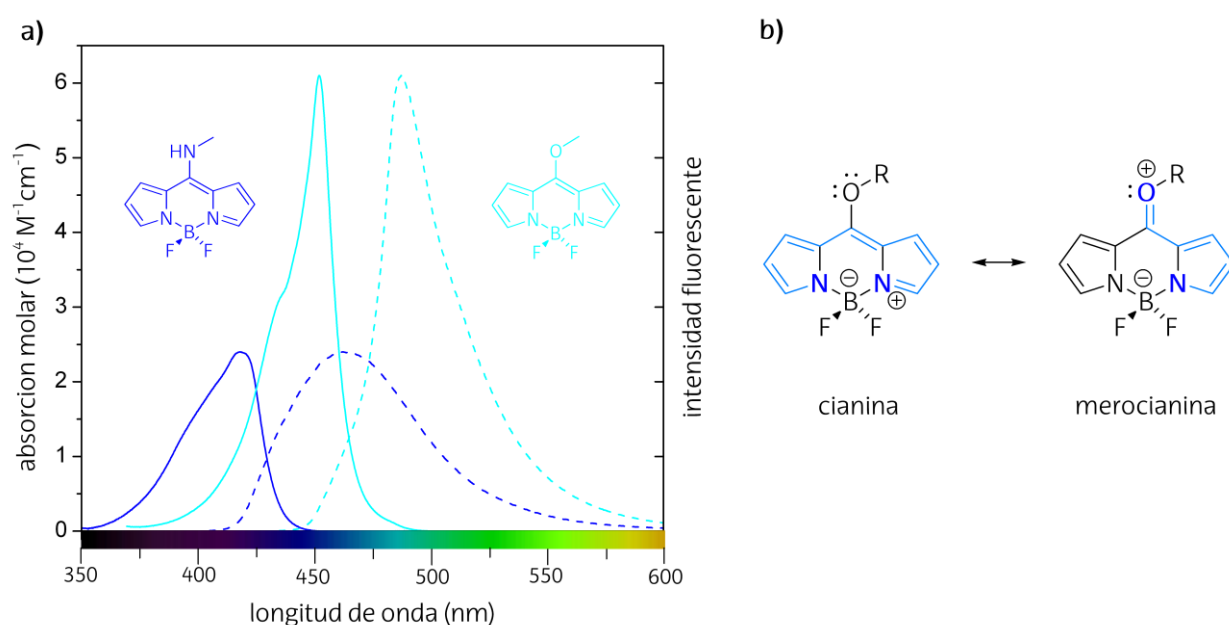
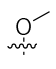
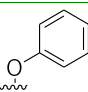


Figura 4.13. a) Espectros de absorción y emisión fluorescente normalizados en ciclohexano del 8-metoxiBODIPY (en cian) y 8-metilaminoBODIPY (en azul, sección 4.1). b) Estructuras del sistema π deslocalizado de los 8-alcoxiBODIPYs (en color azul se muestra la cadena responsable de la emisión).

Como consecuencia de la menor capacidad dadora del metoxi, se evita la formación del estado ICT presente especialmente en los derivados de BODIPY con aminas secundarias y terciarias, y por lo tanto, la capacidad fluorescente del 8-OMe-BODIPY se mantiene superior al 75% en todos los disolventes considerados. Se observa una leve disminución del rendimiento cuántico con la polaridad del medio (en torno al 11%), a la vez que el tiempo de vida aumenta (Tabla 4.5), todo ello considerado como una de las características generales de los BODIPYs (capítulo 1).

Tabla 4.5. Propiedades fotofísicas de los 8-BODIPYs sustituidos por grupos alcoxi y ariloxi más representativos, en función de la polaridad del disolvente (*c-hex*: ciclohexano, *MetOH*: metanol). El sustituyente *R* corresponde a la estructura base de la Figura 4.11.

R	Disolvente	λ_{ab} (nm)	ϵ_{max} ($10^4 \text{ M}^{-1} \text{ cm}^{-1}$)	λ_{fl} (nm)	$\Delta\nu_{St}$ (cm^{-1})	ϕ	τ (ns)	k_{fl} (10^8 s^{-1})	k_{nr} (10^8 s^{-1})
	<i>c-hex</i>	452.0	6.1	487.0	1590	0.84	5.41	1.55	0.29
	<i>MetOH</i>	441.0	4.6	485.5	2080	0.75	6.14	1.22	0.41
	<i>c-hex</i>	459.0	3.5	495.0	1585	0.97	5.78	1.68	0.05
	<i>MetOH</i>	441.0	3.1	485.0	2055	0.81	6.14	1.32	0.31

Las propiedades fotofísicas en el resto 8-alcoxi-BODIPYs considerados (Figura 4.11) son prácticamente idénticas a la descritas para el 8-OMe-BODIPY (ver ESI del *J. Org. Chem.* 2013 del Anexo III). Así, la capacidad fluorescente no se resiente ni por un aumento de la cadena alquílica (de metilo a butilo) ni por sustituyentes voluminosos, y se mantiene alta. Ni siquiera la presencia del átomo de bromo afecta a la capacidad fluorescente, que en principio podría favorecer el cruce intersistema por efecto del átomo pesado. De hecho, la simulación teórica predice que el bromo se dispone lo suficientemente lejos del cromóforo como para no influir en las propiedades fluorescentes.

4.2.2. 8-ariloxiBODIPYs

A continuación se analizan derivados de BODIPY donde se incorpora en la posición *meso* el grupo fenoxi, funcionalizado con grupos aceptores (formaldehído o yodo) y/o grupos dadores (estrona, metoxi, alilo o hidroxilo) (Figura 4.11).

En principio se podría esperar que la inclusión del fenoxi podría inducir una extensión de sistema π cromofórico hacia el fenilo y consecuentemente un desplazamiento de las bandas al rojo. Sin embargo, la simulación mecanocuántica predice un desacoplamiento electrónico entre el fenilo y el BODIPY (Figura 4.14.b), que sigue interaccionando con el par de electrones del grupo oxo, lo que posibilita la formación de la merocianina. Como consecuencia se sigue observando un desplazamiento hipsocrómico de las bandas espectrales, aunque menor (alrededor de 10 nm) que el registrado para 8-OMe-BODIPY (Figura 4.14.a). Esto es debido a la menor capacidad dadora del fenoxi ($\sigma_{p, OPh}^+ = -0.50$ vs $\sigma_{p, OMe}^+ = -0.78$)^[18], tal y como sugiere el cálculo de la energía de los orbitales moleculares, ya que la energía del LUMO del fenoxi derivado disminuye (-2.81 eV) con respecto a la de su análogo metoxi (-2.70 eV), mientras que

la energía del HOMO permanece inalterada (-6.14 eV). El derivado 8-fenoxiBODIPY muestra capacidades fluorescentes superiores al 80% y sigue la misma tendencia que la registrada en los 8-alcoxiBODIPYs caracterizada por pequeñas variaciones con la polaridad del medio (Tabla 4.5), típica de BODIPYs.

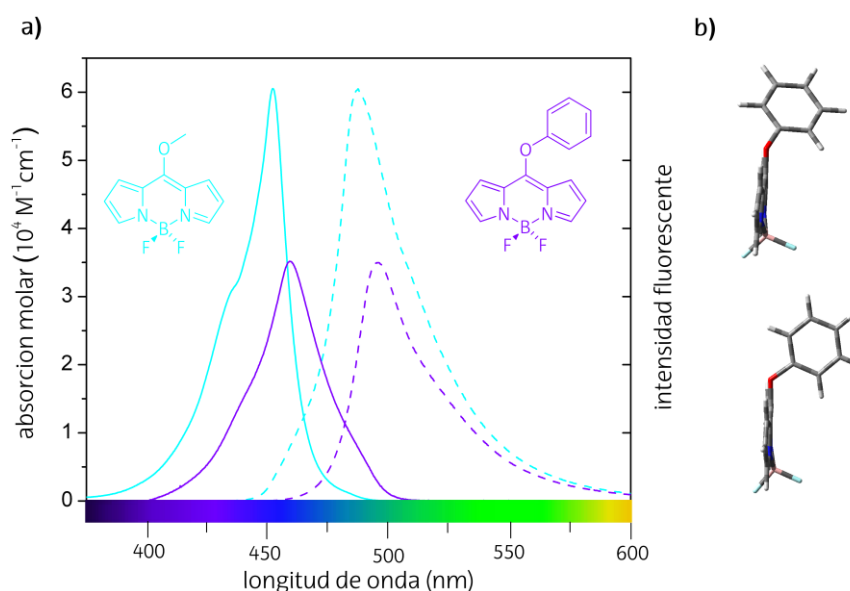


Figura 4.14. a) Espectros de absorción y fluorescencia normalizados en ciclohexano del 8-metoxiBODIPY (en cian) y 8-fenoxiBODIPY (en violeta). b) Geometría optimizada en S_0 (arriba) y S_1 (abajo) del 8-fenoxiBODIPY.

Respecto al resto de 8-ariloxiBODIPYs (ver *J. Org. Chem.* 2013 del Anexo III para más detalle), todos ellos mantienen rendimientos cuánticos superiores al 75% en medios apolares, pero la inclusión de grupos dadores/aceptores al fenilo (Figura 4.11) provocan que la capacidad fluorescente sea sensible al medio, de forma que llega a ser prácticamente nula incluso en medios polares apróticos (Figura 4.15). Es decir, la funcionalización del fenilo controla el carácter dador del grupo oxo y por ende la magnitud del desplazamiento espectral hipsocrómico y la facilidad para generar estados ICT. Así, un aumento de la capacidad aceptora de los sustituyentes (de yodo $\sigma_p^+ = 0.14$ a formaldehído $\sigma_p^+ = 0.73$)^[18] retira densidad electrónica del oxígeno siendo así los derivados que muestran menor desplazamiento al azul. Sin embargo, la presencia de entidades dadoras de electrones (estróna, metoxi, alilo o hidroxilo) en el grupo fenoxi induce una fuerte desactivación de la capacidad fluorescente por la activación del ICT en medios polares apróticos (Figura 4.15).

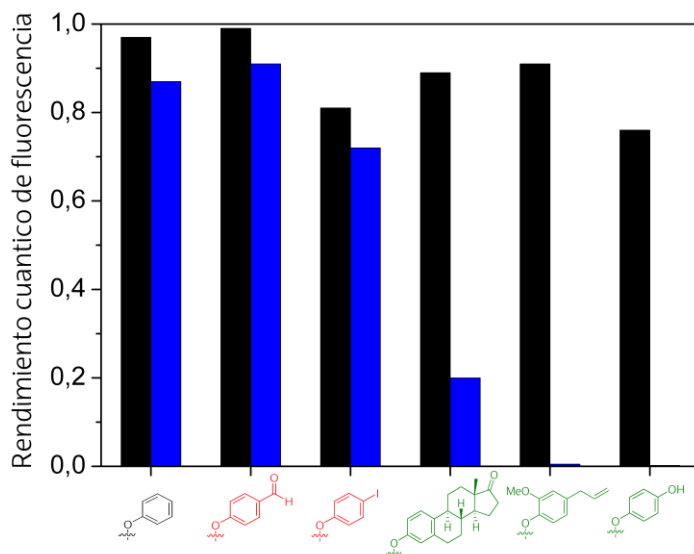


Figura 4.15. Rendimientos cuánticos de fluorescencia de los 8-arioloxiBODIPYs con grupos aceptores (en rojo) o dadores (en verde) en función de la polaridad del medio: ciclohexano (negro) y acetato de etilo (azul).

Resumiendo, la funcionalización del BDP en 8 con grupos alcoxi alifáticos o fenoxi también desplazan la emisión a mayores energías pero en menor medida que los 8-aminoBODIPYs. En contrapartida la disminución de la electronegatividad al reemplazar N por O dificulta la generación de estados ICT lo que supone que se obtengan altas capacidades fluorescentes (superiores al 70%) independientemente del medio, si bien es cierto que la incorporación de grupos fuertemente dadores o aceptores en el fenoxi pueden llegar a poblar el ICT con la consiguiente disminución de la respuesta fluorescente. Destacar los derivados funcionalizados con las biomoléculas colesterol y estrona, que presentan altas eficiencias fluorescentes (además, en el colesterol ϕ es independiente del medio considerado), lo que les convierte en candidatos óptimos para su empleo como marcadores fluorescentes. De hecho, los marcadores basados en BODIPYs generalmente presentan su emisión en la región amarilla-roja, por lo que podrían ser una variante complementaria en la región azul-verde.

4.3. 8-SULFO BODIPYs

Siguiendo el objetivo de modular de forma controlada la magnitud del desplazamiento espectral hacia mayores energías mediante la electronegatividad del heteroátomo incorporado en *meso*, en el siguiente colorante a considerar se reemplaza el O por S. El grupo tiometilo es menos dador de electrones ($\sigma_p^+ = -0.60$)^[18] que las anteriores funcionalizaciones por grupos

metoxi ($\sigma_p^+ = -0.78$)^[18] o metilamino ($\sigma_p^+ = -1.81$)^[18]. A diferencia de los resultados obtenidos con los sustituyentes NHMe y OMe, que inducen un aumento del potencial de reducción así como de la energía del LUMO conforme al carácter dador del heteroátomo, en el caso del 8-SMeBODIPY se disminuye ligeramente tanto el potencial como la energía del LUMO respecto al del BDP de referencia (Figura 4.16).

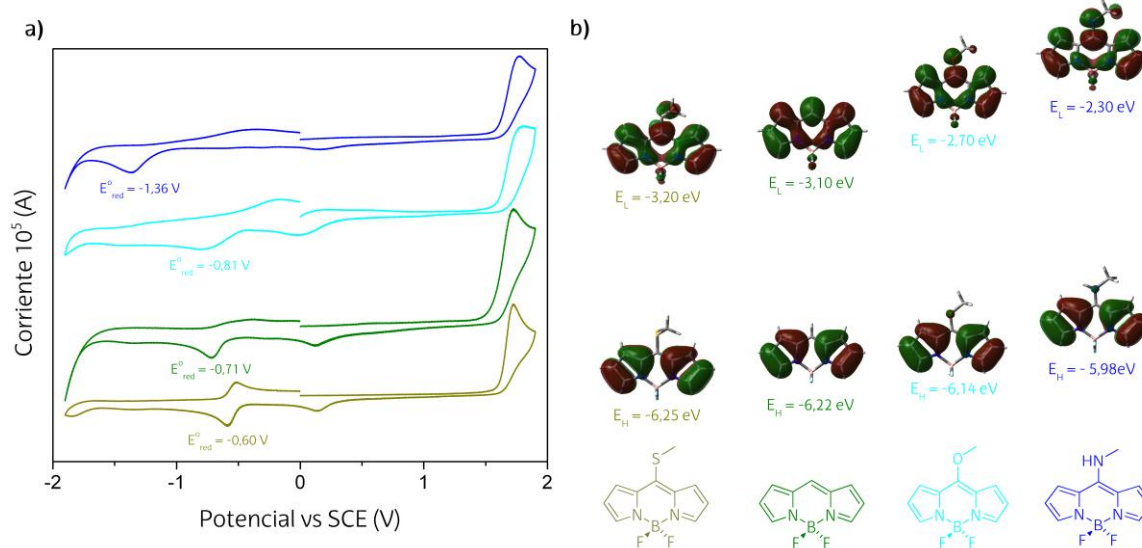


Figura 4.16. a) Voltagramas cíclicos y b) diagrama energético de los orbitales HOMO y LUMO del 8-tiometilBODIPY, BDP, 8-metoxiBODIPY y 8-metilaminoBODIPY.

El máximo del espectro de absorción del 8-SMeBODIPY registra un desplazamiento a mayores energías (~ 10 nm) con respecto al BDP. Sin embargo, el espectro de fluorescencia se desplaza batocrómicamente (~ 20 nm con respecto al BDP, Figura 4.17), en concordancia con la disminución tanto del potencial de reducción (-0.60 V) como de la energía del LUMO (-3.20 eV), contrariamente al resto de 8-heteroBODIPYs (Figura 4.16). De hecho, en el espectro de absorción del 8-SMe-BODIPY se obtiene un hombro a menores energías (Figura 4.17), que se hace más prominente en medios apolares (ver la publicación *ChemPhysChem* del Anexo III para más detalle). Estas evidencias, sugieren que la presencia del tiometilo cambia la probabilidad de las transiciones vibracionales, haciendo que adquieran más importancia las más energéticas. Por lo tanto, el hombro vibrónico de la banda de absorción a menores energías debe corresponder realmente a la transición Franck-Condon $S_0 \rightarrow S_1$ mientras que el máximo debería asignarse al modo vibrónico (esta interpretación se explica en más detalle en la sección 4.4). En consecuencia y aunque experimentalmente el máximo de absorción registrado supone un desplazamiento espectral hipsocrómico con respecto al BDP (Figura 4.17),

realmente la transición Franck-Condon es batocrómica, en concordancia con las medidas electroquímicas y la simulación teórica.

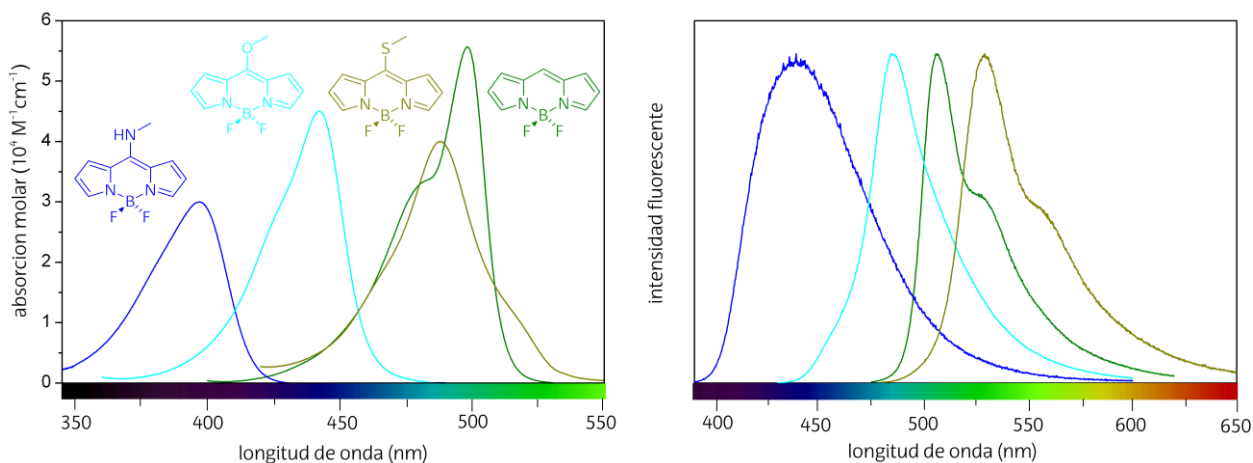


Figura 4.17. Espectros de absorción (izquierda) y emisión fluorescente (derecha) normalizados en etanol del 8-metilaminoBODIPY, 8-metoxiBODIPY, 8-sulfoBODIPY vs BDP.

4.4. METILACIÓN DE LAS POSICIONES α EN LOS 8-HETEROBODIPYs.

En vista de que la simple sustitución en *meso* del BDP por heteroátomos (N, O, S) con distinto carácter dador cubre un amplio rango espectral desde el azul al naranja, se ha intentado mejorar aún más la capacidad fluorescente de los derivados por la metilación en las posiciones 3 y 5. De hecho, la sustitución en estas posiciones α es altamente recomendada para mejorar la desactivación de forma radiante en BODIPYs^[21].

Efectivamente, la metilación de la posición α mejora sensiblemente las propiedades fotofísicas de los BODIPYs (ver la publicación *ChemPhysChem* del Anexo III para más detalle), principalmente en lo que se refiere a la capacidad fluorescente (Figura 4.18).

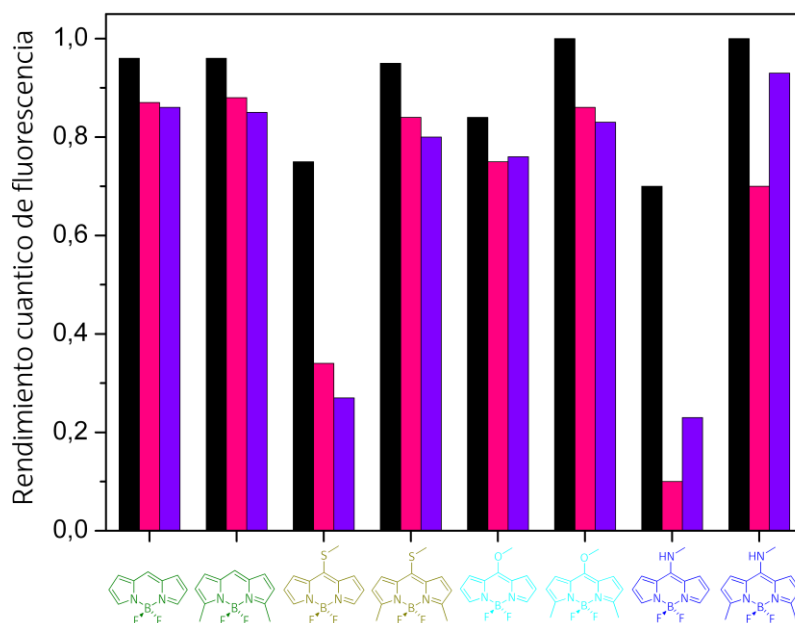


Figura 4.18. Rendimientos cuánticos de fluorescencia de los BODIPYs con heteroátomos en meso y la metilación de las posiciones α en función de la polaridad del medio: ciclohexano (negro), metanol (rosa) y 2,2,2-trifluoroetanol (violeta).

El efecto del 8-heteroátomo en los BODIPYs 3,5-metilados es similar al registrado en los colorantes homólogos sin metilar. Sin embargo, el desplazamiento hipsocrómico de las bandas espectrales se reduce (hasta 20 nm en el 8-NHMe-BODIPY) por el efecto inductivo dador de los grupos metilo, que compensa en parte el desplazamiento a mayores energías que provoca el 8-heteroátomo (Figura 4.19).

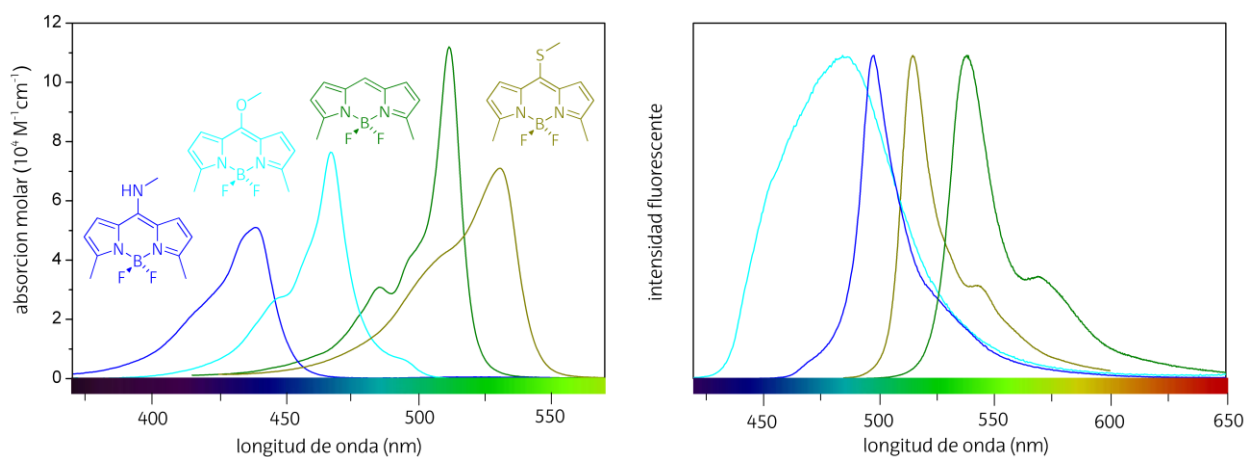


Figura 4.19. Espectros de absorción (izquierda) y emisión fluorescente (derecha) normalizados en ciclohexano de los 8-heteroBODIPYs con metilación en posición α .

El caso del 8-SMe-BODIPY es especialmente curioso ya que sus propiedades espectrales cambian ostensiblemente con el grado de alquilación del cromóforo. La metilación de las posiciones α del 8-SMe-BODIPY da lugar a desplazamientos claramente batocrómicos con respecto al BDP en medios apolares, presentando la forma típica de BODIPYs (con un hombro vibrónico a mayores energías, Figura 4.19). Sin embargo, al cambiar la polaridad del medio la forma del espectro cambia notablemente (Figura 4.20.a). Tal y como se menciona en la anterior sección 4.3, donde se analiza el 8-SMe-BODIPY sin metilación en las posiciones α , se observa dicho desplazamiento batocrómico en fluorescencia, pero un "aparente" desplazamiento hipsocrómico en absorción ya que dicho máximo realmente no corresponde a la transición Franck-Condon sino que es debido a un incremento de la probabilidad de las transiciones vibracionales más energéticas (Figura 4.17). Es más, dicha asignación se constata al bloquear la disposición coplanar entre el tiometilo y el BDP por la metilación adicional en las posiciones 1 y 7 cromofóricas, que da lugar a la progresión vibracional típica de la transición electrónica de BODIPYs incluso en medios polares (Figura 4.20.b). Así, la disposición perpendicular impide el acoplamiento electrónico del heteroátomo con el BDP, por lo que domina la transición $S_0 \rightarrow S_1$ debido a la deslocalización tipo cianina, mientras que a mayores energías del máximo se manifiesta el hombro vibrónico típico en BODIPYs. Por lo tanto, se justifica que la formación de la nueva forma mesomérica por la deslocalización del tiometilo en el cromóforo (en la Figura 4.20.a se muestra dicha nueva forma resonante) altera las transiciones vibracionales, siendo ésta forma la responsable de los cambios en la forma de los espectros.

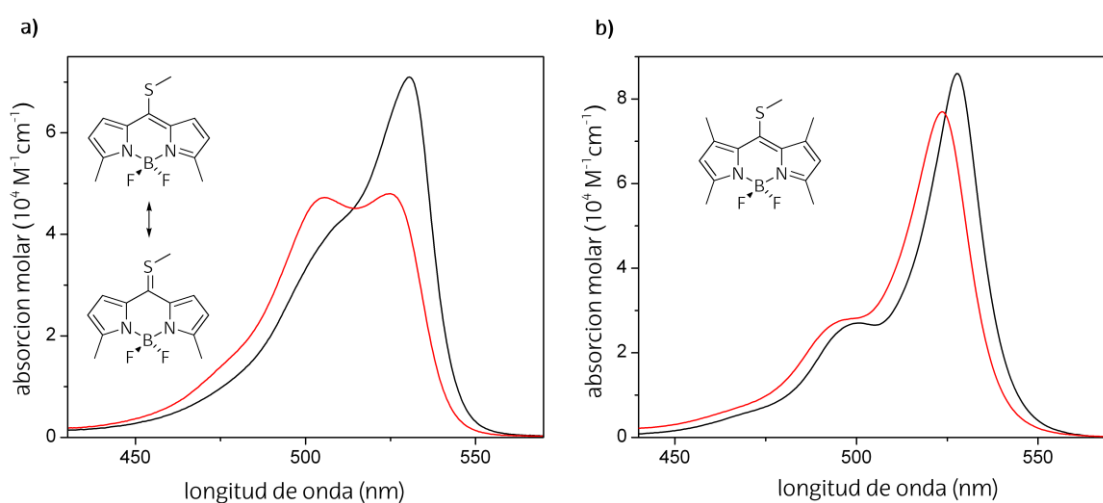


Figura 4.20. Espectros de absorción en ciclohexano (negro) y etanol (rojo) del **a)** 3,5-metil-8-tiometilBODIPY y **b)** 8-tiometilBODIPY tetrametilado.

En toda la serie de BODIPYs α -metilados, se registra un aumento de la probabilidad de absorción (especialmente en el 8-NHMe-BODIPY donde la mejora es de hasta prácticamente el doble) y se obtienen rendimientos cuánticos del 100% en medios apolares. Todo ello confirma que la metilación de las posiciones α no sólo mejora la emisión fluorescente sino que atenúa la activación del proceso ICT provocado por el carácter dador del heteroátomo en *meso*, ya que el efecto inductivo de los metilos en posición α provoca que el cromóforo sea peor aceptor de electrones. De hecho, la señalada disminución del 85% del rendimiento cuántico (de ciclohexano a metanol) registrado en el 8-NHMe-BODIPY por el ICT (sección 4.1.2), se palia por la metilación de las posiciones α , siendo la disminución fluorescente del 30% (Figura 4.18). En el artículo *ChemPhysChem* 2013 adjunto al Anexo III se puede consultar más información respecto al efecto global del heteroátomo y de la mejora en la capacidad fluorescente por la metilación.

La caracterización láser se correlaciona con los resultados fotofísicos, resultando en desplazamientos batocrómicos de la emisión láser y un aumento de la eficiencia por la metilación de las posiciones 3 y 5 (Figura 4.21). Cabe destacar un incremento de la eficiencia láser del 8% al 29% en el 8-NHMe-BODIPY tras la metilación (Figura 4.21), de acuerdo a la disminución de la probabilidad de formación del proceso ICT y fotoestabilidades que aumentan del 20% al 46% en los correspondientes 8-NHMe-BODIPYs (tras 18000 y 40000 pulsos, respectivamente).

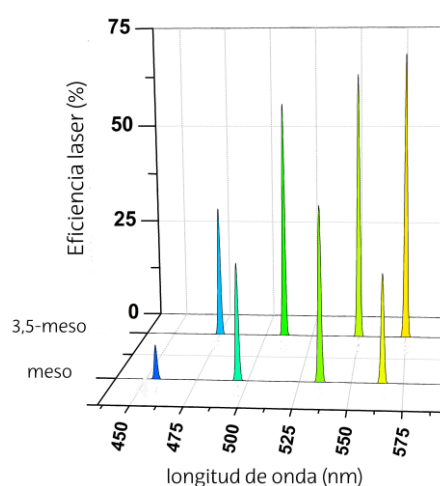


Figura 4.21. Diagrama de la eficiencia láser en acetato de etilo de los BODIPYs con heteroátomos en *meso* y los correspondientes metilados en posición α (8-NHMeBODIPYs en azul, 8-OMeBODIPYs en azul-verdoso, BDPs en verde y 8-SMeBODIPYs en amarillo).

Por lo tanto, se deduce que la alquilación de las posiciones 3 y 5 permite obtener un incremento de la capacidad fluorescente y láser, mientras se mantiene el desplazamiento al azul (aunque en menor medida que los análogos sin metilar). Además, se modera la formación del ICT especialmente favorecido en medios polares y tan perjudicial en la capacidad fluorescente de los BODIPYs. En resumen, en este capítulo se ha demostrado que la presencia de heteroátomos de diferente electronegatividad o con capacidad dadora de electrones controlada por el patrón de sustitución, junto con la metilación en las posiciones clave 3 y 5, es una estrategia adecuada para conseguir colorantes láser con óptimas prestaciones y emisión modulable desde el verde-amarillo hasta el azul, desbancando a las familias de colorantes láser existentes comercialmente en esas regiones espectrales.

El presente capítulo ha dado lugar a cuatro publicaciones que se adjuntan al Anexo III al final de la memoria, de las cuales en *The Journal of Organic Chemistry* (2012) y en *Chemistry – An Asian Journal* (2013) se caracterizan las propiedades fotofísicas y láser de los amino-BODIPYs, en *The Journal of Organic Chemistry* (2013) se caracterizan los alcoxi-BODIPYs y en el *ChemPhysChem* (2013) se da una visión global del efecto del tipo de heteroátomos (N, O, S) así como del efecto de la alquilación en posición 3 y 5 del cromóforo.

Bibliografía

- [1] *Tunable Laser Applications*, 2nd ed. (Ed.: Duarte, F. J.), CRC Press, Boca Raton, 2009.
- [2] Hu, Y.; Wex, B.; Perkovic, M. W.; Neckers, D. C.; *Tetrahedron*; 2008, 64, 2251.
- [3] Schiedel, M.-S.; Briehn, C. A.; Bäuerle, P.; *Angew. Chem.*; 2001, 113, 4813.
- [4] Schiedel, M.-S.; Briehn, C. A.; Bäuerle, P.; *Angew. Chem. Int. Ed.*; 2001, 40, 4677.
- [5] Mondal, R.; Shah, B. K.; Neckers, D. C.; *J. Org. Chem.*; 2006, 71, 4085.
- [6] Pron, A.; Zhou, G.; Norouzi-Arasi, H.; Baumgarten, M.; *Org. Lett.*; 2009, 11, 3550.
- [7] Brackmann, U.; *Laser Dyes*, Lambda Physik AG, Germany, 3rd ed, 2000.
- [8] Valeur, B.; *Molecular Fluorescence: Principles and Applications*, Wiley-VCH, Weinheim, 2002.
- [9] Moorthy, J. N.; Natarajan, P.; Venkatakrishnan, P.; Huang, D.-F.; Chow, T. J.; *Org. Lett.*; 2007, 9, 5215.
- [10] Adhikari, R. M.; Neckers, D. C.; Shah, B. K.; *J. Org. Chem.*; 2009, 74, 3341.
- [11] Iida, A.; Yamaguchi, S.; *Chem. Commun.*; 2009, 3002.
- [12] Tong, Q.-X.; Lai, S.-L.; Chan, M.-Y.; Zhou, Y.-C.; Kwong, H.-L.; Lee, C.-S.; Lee, S.-T.; *Chem. Mater.*; 2008, 20, 6310.
- [13] Umezawa, K.; Matsui, A.; Nakamura, Y.; Citterio, D.; Suzuki, K.; *Chem. Eur. J.*; 2009, 15, 1096.
- [14] Ulrich, G.; Goeb, S.; De Nicola, A.; Retailleau, P.; Ziessel, R.; *J. Org. Chem.*; 2011, 76, 4489.
- [15] Gómez-Durán, C. F. A.; García-Moreno, I.; Costela, A.; Martín, V.; Sastre, R.; Bañuelos, J.; López Arbeloa, F.; López Arbeloa, I.; Peña-Cabrera, E.; *Chem. Commun.*; 2010, 46, 5103.
- [16] Roacho, R. I.; Metta-Magaña, A.; Portillo, M. M.; Peña-Cabrera, E.; Pannell, K. H.; *J. Org. Chem.*; 2013, 78, 4245.
- [17] Bañuelos, J.; López Arbeloa, F.; Martínez, V.; Liras, M.; Costela, A.; García Moreno, I.; López Arbeloa, I.; *Phys. Chem. Chem. Phys.*; 2011, 13, 3437.
- [18] Hansch, C.; Leo, A.; Taft, R. W.; *Chem. Rev.*, 1991, 91, 165.
- [19] Bañuelos, J.; Martín, V.; Gómez-Durán, C. F. A.; Arroyo Córdoba, I. J.; Peña-Cabrera, E.; García-Moreno, I.; Costela, A.; Pérez-Ojeda, M. E.; Arbeloa, T.; López Arbeloa, I.; *Chem. Eur. J.*; 2011, 17, 7261.
- [20] Grabowski, Z. R.; Rotkiewicz, K.; Rettig, W.; *Chem. Rev.*; 2003, 103, 3899.
- [21] Mukherjee, S.; Thilagan, P.; *RSC Adv.*; 2015, 5, 2706.

CAPÍTULO 5

BODIPYs SENSIBLES A LA POLARIDAD DEL MEDIO

A lo largo de la presente memoria ha quedado demostrado que los BODIPYs presentan propiedades únicas y fácilmente modulables para su aplicación como eficientes colorantes láser en prácticamente cualquier rango del espectro visible. En algunos de los fluoróforos analizados en las secciones precedentes se indicó la inducción de procesos de transferencia de carga (ICT) por el patrón de sustitución (por ejemplo por la presencia de heteroátomos con alta capacidad dadora de electrones en la posición *meso*, ver capítulo 4). Dichos procesos fofofísicos desactivan la emisión fluorescente especialmente en medios polares y son indeseables desde el punto de vista de la aplicación láser. Sin embargo, la influencia en principio negativa para la emisión fluorescente, permite aplicar este tipo de fluoróforos en el campo de sensores^[1-5]. De hecho, en la última década se ha prestado un interés particular al desarrollo de dispositivos moleculares donde las propiedades ópticas del fluoróforo responden al estímulo ambiental perseguido^[6-10] (Figura 5.1). Se han considerado diversas estrategias a tal fin^[11-12], entre las que cabe destacar: la inducción de procesos de transferencia electrónica fotoinducida (procesos PET), para generar “interruptores” moleculares (*molecular switch on/off*)^[13] que detecten la presencia de la molécula de interés; o los fenómenos de transferencia de carga o la formación de excimeros (*excited dimer*) o exciplejos (*excited charge transfer complex*)^[14], para obtener sondas moleculares que monitoricen las propiedades fisicoquímicas ambientales. En el caso de los interruptores (Figura 5.1.a), la unión del analito de interés (catión, anión, ...) al fluoróforo provoca una fuerte disminución de la señal fluorescente (apagado por el proceso PET) o un

aumento de la misma (encendido por la inhibición del proceso PET). Mientras que en el caso de las sondas la detección tiene lugar por el cambio en la capacidad fluorescente del colorante o por la inducción de nuevas bandas espectrales (bien sea en absorción o en fluorescencia) al poblarse el estado ICT (Figura 5.1.b) o por medio de la formación del excimero (Figura 5.1.c). Algunas sondas, permiten llevar a cabo la monitorización de la propiedad ambiental incluso a simple vista (Figura 5.1.b-c).

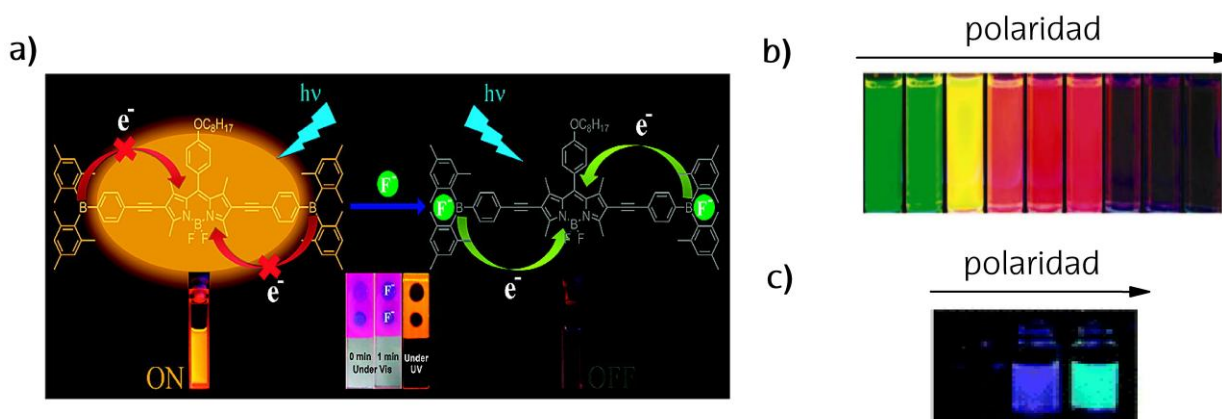


Figura 5.1. Ejemplos de a) "molecular switch" por la activación de procesos PET^[15] y b) sondas de polaridad por la activación del ICT^[16] o c) por la formación del excimero^[17].

El presente capítulo se centra en el desarrollo de sondas de polaridad mediante la inducción de procesos ICT en BODIPYs, de forma que sus propiedades fotofísicas (capacidad fluorescente o longitud de onda fluorescente) son sensibles a dicha propiedad del medio que rodea al colorante. Dicho estado ICT se genera después de la excitación y desactiva fuertemente la emisión fluorescente del estado localmente excitado (LE), especialmente en medios polares (Figura 5.2). Esto es debido a la separación de cargas inherente al ICT que provoca que dicho estado se caracterice por un alto momento dipolar y por tanto se establezca en disolventes polares. Si la probabilidad de recombinación de cargas es relativamente alta se puede detectar la emisión propia del ICT, sin embargo, si dicha probabilidad es baja se pierde la emisión e incluso se puede llegar a poblar el estado de separación de cargas (CS, que es un estado "oscuro"), que origina una drástica pérdida de la señal fluorescente del colorante (Figura 5.2).

5.1. TRANSFERENCIA DE CARGA EN BODIPYs

La inserción de grupos con capacidad dadora o aceptora de electrones, así como la posición del núcleo cromofórico donde se incorporen, inducen cambios significativos en las propiedades fluorescentes del BODIPY, ya que el núcleo cromofórico se puede comportar tanto como aceptor como dador de electrones según la funcionalización en la promoción de estados ICT. Es por ello que en este apartado se analizan en primer lugar las propiedades fotofísicas de colorantes donde se une directamente sustituyentes dadores (amino) o aceptores (nitro) de electrones a las posiciones α o β del núcleo del indaceno (sección 5.1.1), para posteriormente analizar otra serie de BODIPYs donde se incorporan una batería de grupos con diferente carácter dador o aceptor de electrones en la posición *meso*, pero separados del cromóforo por un espaciador metileno (sección 5.1.2).

5.1.1. Sustitución directa en las posiciones α o β

En la presente sección se procede al análisis de derivados de BODIPY asimétricos con sustitución alquílica en un solo pirrol o con un grupo *para*-tolilo con libertad de giro en posición 8, a los que se les ha insertado grupos fuertemente dadores (amino, $\sigma_p^+ = -1.30$)^[18] o aceptores de electrones (nitro, $\sigma_p^+ = 0.79$)^[18] en posición α o β (Figura 5.3). En el presente apartado se consideran los aspectos fotofísicos y láser más relevantes de estos derivados, mientras que en el artículo adjunto al Anexo IV de *RSC Advances 2013* se puede consultar la información detallada de los mismos.

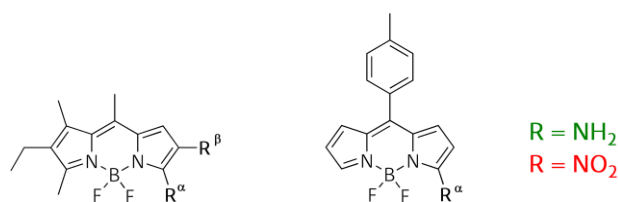


Figura 5.3. Estructuras del alquil-BODIPY asimétrico (izquierda) y 8-tolilBODIPY (derecha) con sustitución por grupos dadores (amino, verde) o aceptores (nitro, rojo) en posición α o β .

La asimetría del colorante BODIPY de referencia con sustitución alquílica, origina cierta separación de carga entre los pirroles que constituyen el esqueleto de indaceno. Dicha distribución asimétrica de la densidad electrónica provoca una reducción de la probabilidad de absorción hasta en un 55% ($\sim 2\text{-}3 \cdot 10^4 \text{ M}^{-1}\text{cm}^{-1}$) con respecto al BDP sin alquilar, a la vez que el

rendimiento cuántico de fluorescencia adquiere mayor sensibilidad con la polaridad del medio (disminución de ϕ del 21% de ciclohexano a metanol en el alquil-BODIPY, con respecto al 9% registrado en el BDP). Por otra parte, la presencia de un arilo en posición 8 con posibilidad de libre rotación provoca un fuerte aumento de la conversión interna, lo que está relacionado con la flexibilidad de la estructura molecular. Como consecuencia, la capacidad fluorescente se resiente considerablemente ($\phi < 0.05$ y $\tau < 400$ ps). Una prueba del papel de este mecanismo de relajación no-radiante es que este tipo de derivados de BODIPY con 8-arilo se han usado como sondas de viscosidad, donde dicha propiedad se monitoriza por el aumento del rendimiento cuántico o tiempo de vida de fluorescencia que experimenta el colorante al pasar a un medio más viscoso, ya que se dificulta el libre giro del 8-fenilo^[19].

5.1.1.1. Funcionalización con amino

En el capítulo 4, se constató que el acoplamiento electrónico del grupo dador de electrones amino con el BODIPY a través de la posición *meso* provocaba pronunciados desplazamientos espectrales hipsocrómicos y en el caso de la sustitución por aminas más dadoras o más impedidas estéricamente, se promovía la activación de un proceso ICT que desactiva la fluorescencia.

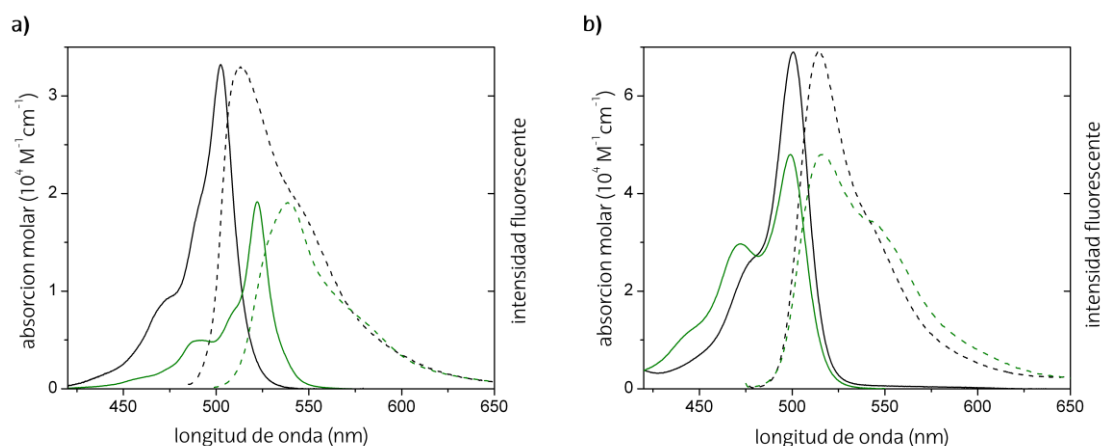
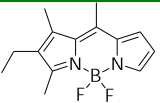
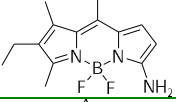
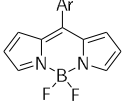
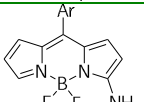


Figura 5.4. Espectros de absorción y fluorescencia normalizados en ciclohexano de los α -amino derivados (verde) del a) alquil-BODIPY y b) 8-tolilBODIPY de referencia (negro).

Sin embargo, la interacción resonante del amino en posición α del alquil-BODIPY induce un desplazamiento batocrómico de las bandas espectrales (~ 20 nm, Figura 5.4.a). Es más, a pesar del fuerte carácter dador de electrones del grupo amino, la capacidad fluorescente se

sigue manteniendo elevada independientemente del medio considerado ($\phi > 70\%$, Tabla 5.1), lo que indica que no se puebla ningún estado ICT. Por tanto, la disminución de la probabilidad de absorción ($\epsilon_{\max} < 2 \cdot 10^4 \text{ M}^{-1}\text{cm}^{-1}$, Tabla 5.1) y la ligera menor capacidad fluorescente del amino derivado respecto al alquil-BODIPY de referencia se atribuye a la mayor asimetría del colorante al incorporar el α -amino en el pirrol no alquilado. En concordancia con estos resultados fotofísicos obtenidos, se registra una moderada eficiencia láser del 29%. Señalar que en este caso el derivado con amino en β no era estable por la formación de un equilibrio de tautomería imina-enamina que destruye el sistema π deslocalizado.

Tabla 5.1. Propiedades fotofísicas del alquil y 8-tolil-BODIPY de referencia con los correspondientes NH_2 derivados, en función de la polaridad del disolvente (*c-hex*: ciclohexano, *MetOH*: metanol). El sustituyente *Ar* corresponde al fragmento *p*-metilfenilo.

Derivado	Disolvente	λ_{ab} (nm)	ϵ_{max} ($10^4 \text{ M}^{-1}\text{cm}^{-1}$)	λ_{fl} (nm)	$\Delta\nu_{\text{St}}$ (cm^{-1})	ϕ	τ (ns)	k_{fl} (10^8 s^{-1})	k_{nr} (10^8 s^{-1})
	<i>c-hex</i>	504.0	3.3	515.0	760	0.96	5.46	1.75	0.07
	<i>MetOH</i>	495.5	2.5	512.5	660	0.76	5.78	1.31	0.41
	<i>c-hex</i>	522.0	1.9	538.0	570	0.97	4.44	2.18	0.07
	<i>MetOH</i>	510.0	0.9	534.0	880	0.74	4.54	1.62	0.58
	<i>c-hex</i>	500.5	6.9	516.0	600	0.036	0.34	1.05	28.3
	<i>MetOH</i>	496.0	6.1	513.5	685	0.018	0.20	0.91	49.8
	<i>c-hex</i>	499.0	4.8	515.5	640	0.017	0.09	1.93	110.5
	<i>MetOH</i>	456.0	2.9	515.0	2510	0.013	0.07	1.82	149.7

Curiosamente, la misma funcionalización (grupo amino en posición 3) en el 8-tolil-BODIPY origina cambios diferentes en la fotofísica. A pesar de que debe tener lugar un aumento de la interacción resonante, apenas se observan desplazamientos espectrales (Figura 5.4.b). Sin embargo, la capacidad fluorescente se resiente ($\phi < 0.03$ y $\tau < 150 \text{ ps}$) por un aumento de los procesos no-radiantes ($k_{\text{nr}} > 70 \cdot 10^8 \text{ s}^{-1}$) más allá de la propia conversión interna asignada al giro del fenilo. Este comportamiento se atribuye a un proceso de desactivación no-radiante extra que se asigna a un proceso de ICT desde el amino al BODIPY, que en este caso actúa como aceptor. El hecho de que el ICT se active en el 8-tolil-BODIPY y no en el alquil-BODIPY indica que la sustitución del BODIPY juega un papel importante. Es decir, el efecto inductivo dador de electrones de la alquilación del BODIPY (en este caso metilo en posición 1, 3 y 8, y etilo en 2) supone que el cromóforo sea peor aceptor de electrones que el BDP sólo con tolilo en 8. De

forma que este último derivado es más susceptible de generar procesos ICT por aminación directa.

5.1.1.2. Funcionalización con nitro

En contraposición a la aminación del alquil-BODIPY de la sección anterior, la nitración del colorante en las mismas posiciones induce desplazamientos hipsocrómicos e importantes cambios en la forma espectral (Figura 5.5.a). Así, los espectros son más anchos a pesar de la disminución de la intensidad en la zona de menores energías del espectro de absorción, especialmente en disolventes polares. El espectro de fluorescencia sigue siendo imagen especular del de absorción y su forma no cambia con la longitud de onda de excitación, como tampoco se observan nuevas bandas de emisión a menores energías (consultar *RSC Advances 2013* junto al Anexo IV para más información). Todo esto induce a pensar que dichos cambios espectrales no se deben a nuevas bandas atribuibles a un proceso de ICT, sino más bien a un cambio en la probabilidad de transición vibracional por el acoplamiento electrónico con el grupo nitro, tal y como se comentó previamente para el 8-SMe-BODIPY del capítulo 4 (sección 4.4).

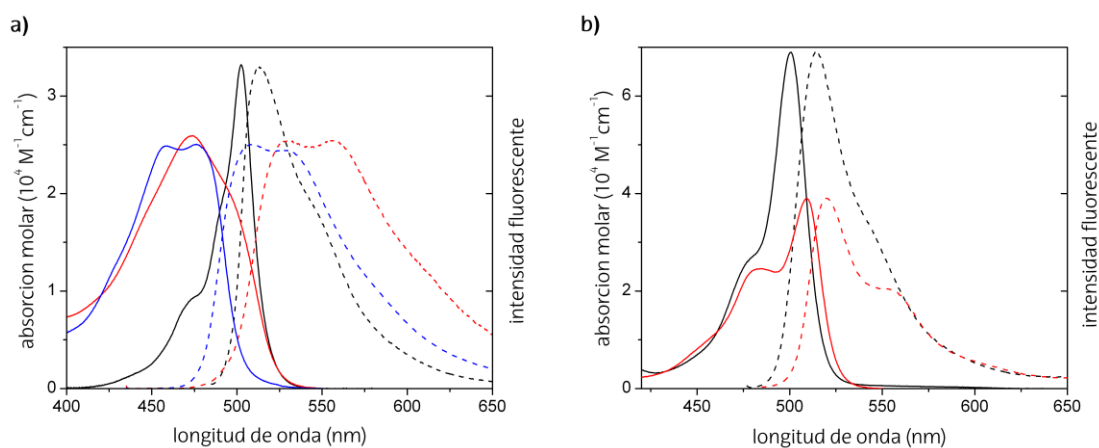
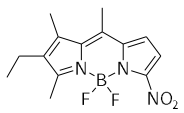
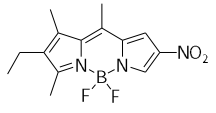
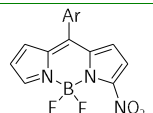


Figura 5.5. Espectros de absorción y fluorescencia normalizados en ciclohexano de los α - (rojo) y β -nitro derivados (azul) del **a)** alquil-BODIPY y **b)** 8-tolilBODIPY de referencia (negro).

A pesar de que los cambios en la forma espectral no son debidos a un estado ICT, dicho estado si que está presente por la nitración tal y como se refleja en la dependencia de la capacidad fluorescente de los nitro derivados con la polaridad de medio. Así, la población del ICT provoca una disminución del 97% y 68% (de ciclohexano a metanol, Tabla 5.2) en el α - y

β -NO₂-alquilBODIPY, respectivamente. Es más, mientras que en un mismo medio apolar se registra una capacidad fluorescente del 53% en el β -NO₂ derivado, en el análogo con α -NO₂ es de apenas un 17%, lo que indica la importancia de la posición cromofórica donde se inserta la funcionalización. La incorporación del grupo nitro atractor en posición α del BDP supone un aumento del momento dipolar de la molécula (Figura 5.6) y por lo tanto, mayor carácter de transferencia de carga. De hecho, es posible que en este caso la transferencia de carga esté tan favorecida en medios polares que se forme un estado de separación de cargas (CS, Figura 5.2) y de ahí la eficiente desactivación de la emisión fluorescente del cromóforo (ϕ de tan solo el 0.5% en metanol, Tabla 5.2).

Tabla 5.2. Propiedades fotofísicas de los correspondientes NO₂ derivados del alquil- y 8-tolilBODIPY, en función de la polaridad del disolvente (*c-hex*: ciclohexano, *MetOH*: metanol).

Derivado	Disolvente	λ_{ab} (nm)	ϵ_{max} (10 ⁴ M ⁻¹ cm ⁻¹)	λ_{fl} (nm)	ϕ	τ (ns)	k_{fl} (10 ⁸ s ⁻¹)	k_{nr} (10 ⁸ s ⁻¹)
	<i>c-hex</i>	474.0	2.5	530.5 556.0	0.174	1.53	1.11	5.42
	<i>MetOH</i>	462.5	2.0	530.5	0.005	0.05*	-	-
	<i>c-hex</i>	458.0 476.0	2.4	509.0 530.0	0.53	3.13	1.70	1.49
	<i>MetOH</i>	446.5	2.1	509.5 526.5	0.17	1.54	1.10	5.39
	<i>c-hex</i>	509.0	3.9	519.0	0.131	1.02	1.29	8.5
	<i>MetOH</i>	505.5	2.6	525.5	0.038	0.53	0.72	18.1

*Decaimiento biexponencial, se muestra el tiempo de vida mayoritario.

Por otro lado, la nitración del 8-tolilBODIPY da lugar a rendimientos cuánticos de fluorescencia superiores al derivado de referencia en medios apolares (13% vs 4%, respectivamente). A diferencia del amino derivado, un grupo aceptor como el nitro retira densidad electrónica del cromóforo y con ello, disminuye la desactivación por conversión interna de la rotación del fenilo en *meso*, recuperando parcialmente la capacidad fluorescente. De hecho, esta es una de las razones por lo que generalmente la sustitución en las posiciones 3 y 5 se postula como una de las más indicadas para aumentar la capacidad fluorescente, especialmente en BODIPYs con flexibilidad estructural que contienen grupos aromáticos con libre giro en la posición *meso*. Aún así, el ICT sigue estando vigente y se registra una disminución del 71% de la capacidad fluorescente con la polaridad del medio al insertar el nitro

en posición α del 8-tolil-BODIPY (Tabla 5.2). Recalcar que contrariamente a la aminación, la influencia del ICT en la fotofísica por la nitración es más notoria en el alquil-BODIPY que en el 8-tolilBODIPY. Este hecho se puede razonar de forma análoga a la aminación. Es decir, con el grupo nitro el cromóforo actúa como dador de electrones y la alquilación del pirrol favorece el carácter dador de electrones del BODIPY respecto a la simple arilación en 8, y con ello la población del estado ICT.

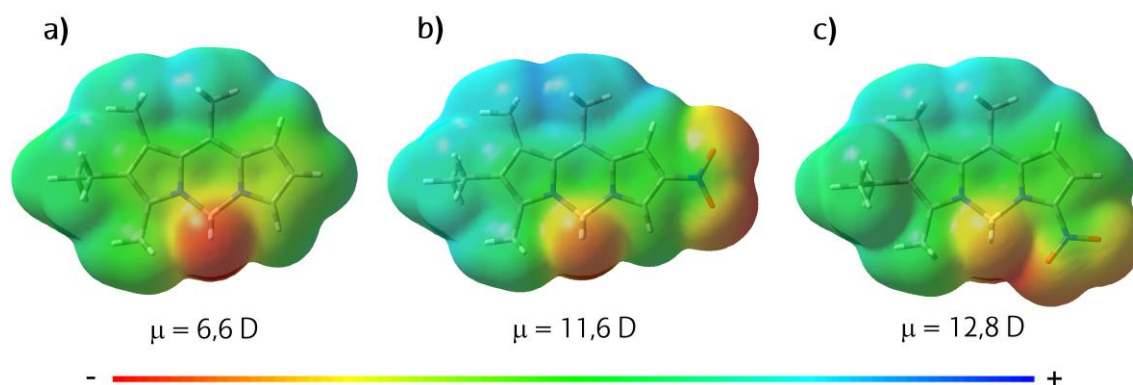


Figura 5.6. Mapas del potencial electrostático (rojo negativo y azul positivo) de la densidad electrónica del a) alquilBODIPY y los derivados b) β -NO₂ y c) α -NO₂ sustituidos, junto con los correspondientes momentos dipolares.

Por tanto, hay que resaltar que la aminación o nitración directa del BODIPY da lugar a procesos de ICT, cuya desactivación fluorescente depende tanto de la posición de sustitución como del carácter dador/aceptor del cromóforo. En este caso, la monitorización de la polaridad del medio tendría lugar por la variación de la capacidad fluorescente del colorante, ya que disminuiría progresivamente a medida que aumente la polaridad ambiental.

5.1.2. Sustitución en posición *meso* con espaciador metileno

En el capítulo anterior se constató que la posición *meso* es muy sensible al efecto del sustituyente, tal y como lo demuestran los fuertes cambios espectrales observados por el acoplamiento electrónico de heteroátomos (N, O, S) unidos directamente al BODIPY en dicha posición. En esta sección se ha continuado con la funcionalización en la posición 8 de una serie de BODIPYs comerciales (PM546, PM567 y PM597, analizados en el capítulo 2) pero usando tanto grupos dadores (dimetilamino) como aceptores (metoxicarbonil, halógenos, nitro,

sulfonil) de electrones separados del cromóforo por un grupo metileno (Figura 5.7). A continuación se representan los resultados más relevantes, mientras que en el artículo adjunto al Anexo IV de *Organic Letters 2014* se recoge la información detallada de las propiedades fotofísicas, electroquímica y la simulación mecanocuántica de estos derivados.

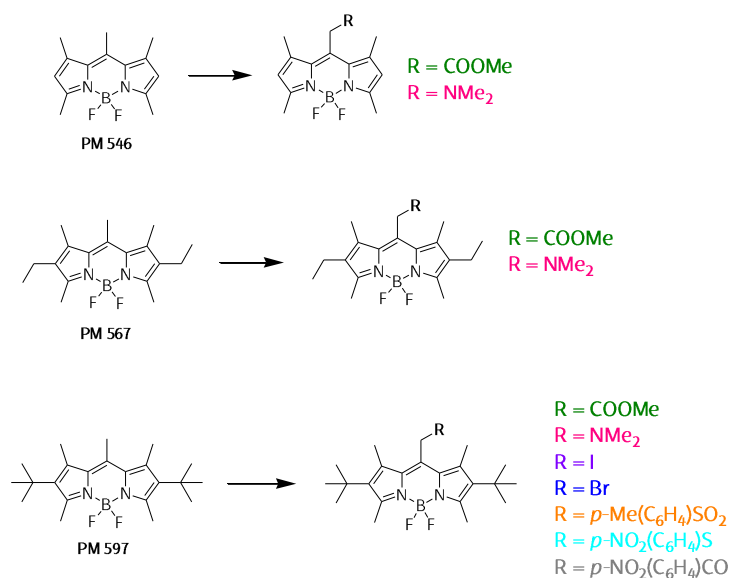


Figura 5.7. Estructuras de los pirrometenos comerciales con funcionalización en meso.

La razón del impacto que ejerce la funcionalización en la posición 8 se basa generalmente en la fuerte variación en la densidad electrónica que experimenta dicha posición con la excitación; de tener un nodo en el HOMO a localizar una alta densidad en el LUMO. Sin embargo, en los presentes derivados el espaciador metileno impide la interacción resonante del sustituyente con el cromóforo. En consecuencia, y a pesar de incorporar grupos fuertemente dadores (NMe₂, $\sigma_p^+ = -1.70$)^[18] o aceptores (CO₂Me, $\sigma_p^+ = 0.49$)^[18], las energías de los orbitales frontera varían levemente respecto a los de referencia (Figura 5.8.a) y los desplazamientos espectrales son mucho más moderados que en los registrados en los 8-heteroBODIPYs del capítulo 4. De hecho, las bandas espectrales presentan desplazamientos batocrómicos debido a una ligera estabilización del LUMO en ambos casos que se asigna al carácter inductivo atractor de ambos grupos.

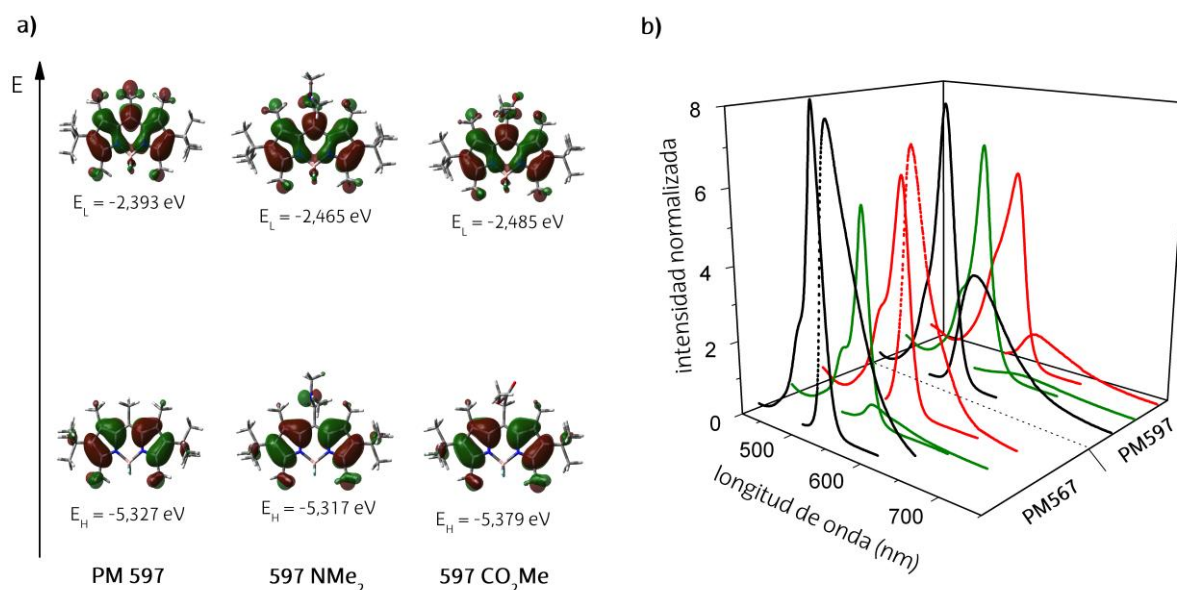


Figura 5.8. a) Diagrama de energías de los orbitales HOMO y LUMO de los derivados más representativos del PM597. b) Espectros de absorción y fluorescencia de los pirrometenos comerciales más representativos (en negro) con funcionalización por grupos dadores (dimetilamino, en verde) o aceptores (metoxicarbonil, en rojo) en THF.

En cuanto a la capacidad fluorescente, se observa que la presencia de grupos dadores de electrones como el amino promueve una drástica disminución del rendimiento fluorescente, a pesar de estar separado del cromóforo por un metileno. Dicho mecanismo extra de desactivación no-radiante se asigna a un proceso ICT (Figura 5.8.b y 5.9). De hecho, se ha comprobado que la protonación del dimetilamino desactiva dicho proceso recuperándose en parte la capacidad fluorescente del cromóforo, lo cual es una constatación de procesos de transferencia electrónica desde el amino al BODIPY, ya que al protonar el par de electrones localizado en el N está menos disponible para ser cedido^[20]. Sin embargo, la presencia de grupos fuertemente aceptores de electrones (por ejemplo a modo representativo, el metoxicarbonilo), también separados por un metileno del cromóforo provoca efectos contrarios según el BODIPY al que se unan. Así, mientras que en los derivados de PM546 y PM567 la capacidad fluorescente se mantiene después de dicha funcionalización en 8, en el derivado del PM597 la eficiencia fluorescente decae ostensiblemente (Figura 5.9).

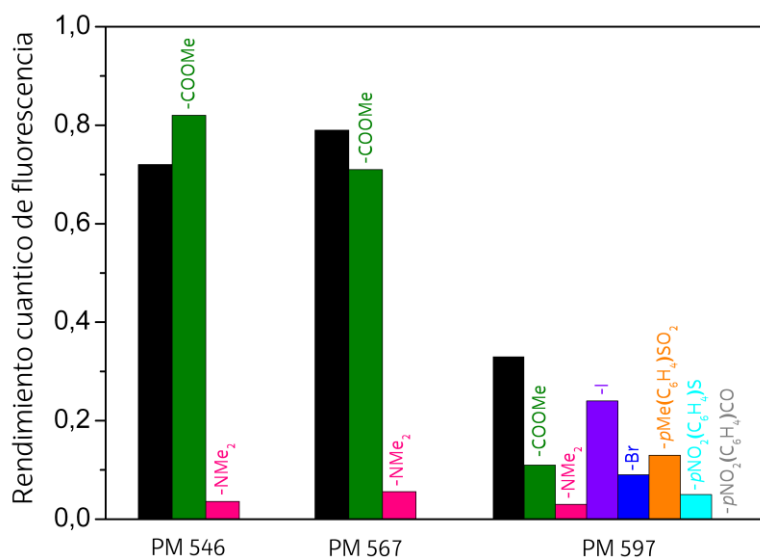


Figura 5.9. Rendimientos cuánticos de fluorescencia de los BODIPYs comerciales (en negro) y los correspondientes derivados en tetrahidrofurano (se adjuntan los fragmentos del sustituyente R correspondiente a las estructuras de la Figura 5.7).

Tal y como se ha explicado en el capítulo 2 (sección 2.1), la presencia de grupos *tert*-butilo en posición 2 y 6 (PM597 y PM597-8C9) induce un aumento del desplazamiento de Stokes consecuencia de una distorsión de la planaridad acentuada tras la excitación, de ahí su menor capacidad fluorescente respecto al resto de derivados comerciales alquilados (PM546 y PM567). Dicho patrón de sustitución implica que el PM597 sea el BODIPY con el carácter más dador de electrones de todos los considerados (*tert*-butilo vs etilo en PM567) ya que al aumentar la ramificación del alquilo éste adquiere mayor efecto inductivo dador de electrones. Como consecuencia el PM597 es el colorante más susceptible de formar estados ICT ante la presencia de grupos aceptores. Por lo tanto, la presencia de grupos tipo metoxicarbonilo en posición 8 del PM597 origina una disminución evidente de la capacidad fluorescente (del 33% al 11%, respectivamente), no observada en los derivados PM546 y PM567 (Figura 5.10). Es más, dicho descenso es más patente en medios polares, una prueba más de la población del ICT. Reseñar el papel fundamental que juega la posición de funcionalización, puesto que dicha desactivación de la fluorescencia registrada para el PM597 con metoxicarbonilo en la posición 8 y con metileno de espaciador, no tiene lugar si el mismo sustituyente se incorpora en la posición 3 del análogo estructural PM597-8C9 (ver la discusión del PM597-8C9 de referencia en el capítulo 2). Estos resultados postulan a la posición *meso* como el sitio cromóforico más sensible al efecto del sustituyente, incluso cuando el grupo funcional no está unido directamente al núcleo de BODIPY.

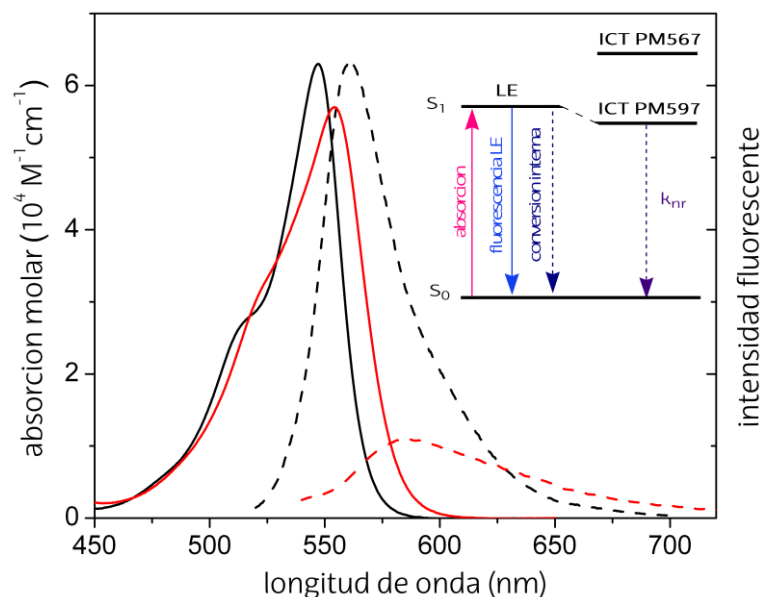


Figura 5.10. Espectros de absorción y fluorescencia normalizados en THF del PM567 (negro) y PM597 (rojo) 8-metilen-metoxicarbonil sustituidos.

La desactivación fluorescente originada por el proceso ICT en las propiedades fotofísicas de esta serie de derivados, se ve reflejada en las medidas electroquímicas. Por un lado, la incorporación de grupos dadores (NMe_2) induce variaciones en oxidación con la aparición de dos picos irreversibles (Figura 5.11). Por tanto, el colorante es más fácilmente oxidable de acuerdo con la transferencia electrónica desde el amino al BODIPY. Es más, la aproximación entre los picos de oxidación y reducción de los amino derivados se correlaciona con un menor salto energético (de ~ 0.08 eV, Figura 5.8.a) y por lo tanto un desplazamiento espectral batocrómico con respecto al correspondiente pirrometeno de referencia. Por otro lado, los grupos aceptores (COOMe) promueven cambios en la reducción con la aparición de dos picos irreversibles, lo que sugieren derivados más fáciles de reducir, en concordancia con transferencia electrónica desde el BODIPY al metoxicarbonilo (Figura 5.11). Señalar que el derivado del PM597 es más fácilmente reducible (pico de reducción desplazado a menores potenciales respecto al PM567) en concordancia con la mayor probabilidad de ICT detectada para el PM597.

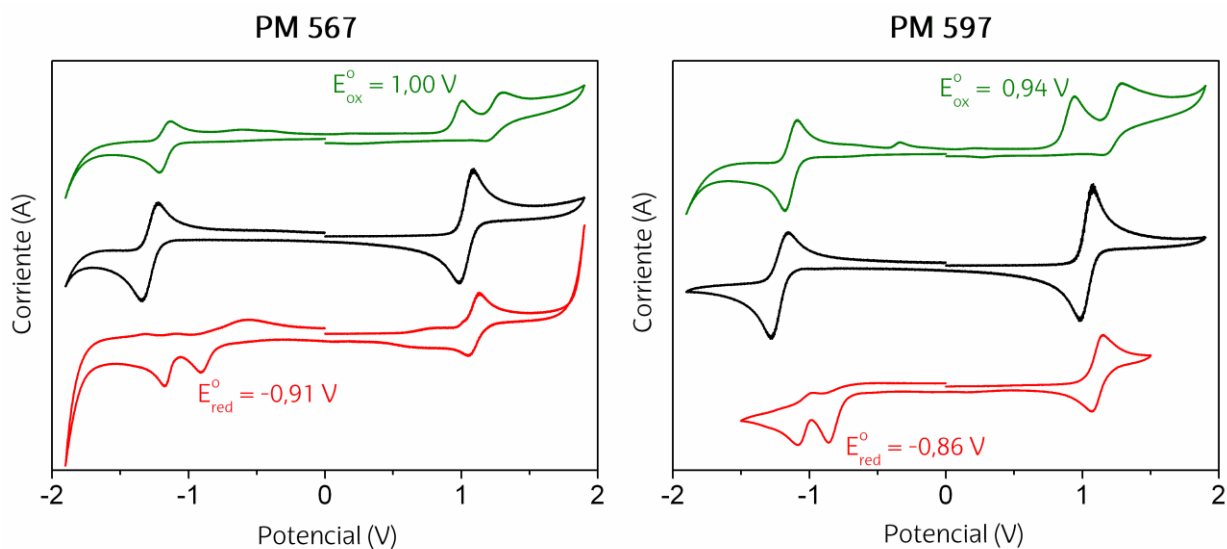


Figura 5.11. Voltagramas cíclicos de los pirrometenos PM567 y PM597 comerciales (negro) con los correspondientes derivados meso metileno sustituidos por grupos dadores (dimetilamino, verde) o aceptores (metoxicarbonilo, rojo).

Por tanto, y al igual que en los BODIPYs aminados o nitrados, la inducción de procesos ICT permite monitorizar la polaridad del medio en base a la disminución de la capacidad fluorescente que experimenta el colorante. Como consecuencia de este estudio se ha conseguido recopilar información de los factores estructurales y electrónicos que permiten activar el proceso ICT. En vista de que la posición *meso* es la más indicada para fomentar dichos procesos, en la siguiente sección se presenta un derivado de BODIPY que también funciona como sonda de polaridad, pero donde dicha propiedad se puede monitorizar de forma visual y reversible.

5.2. SONDA DE POLARIDAD COLORIMÉTRICA

En esta sección se analiza la caracterización fotofísica más destacable del colorante multicromofórico obtenido por la incorporación de pireno en la posición 8 del BODIPY, mientras que en el artículo adjunto al Anexo IV de *RSC Advances 2011* se analiza la información del cromóforo considerado. El correspondiente espectro de absorción consta de una banda correspondiente a la transición $S_0 \rightarrow S_1$ del BDP (centrada a 505 nm) y una serie de bandas con una marcada estructura vibracional en la región ultravioleta, típica de las transiciones electrónicas $S_0 \rightarrow S_n$ del pireno (Figura 5.12). El hecho de que el espectro sea la suma de las bandas de cada entidad molecular indica que, a pesar de la libertad de giro del 8-pireno, éste no

interacciona por resonancia con el BODIPY, y cada cromóforo mantiene su identidad después de la unión covalente. De hecho, la simulación mecanocuántica predice un desacoplamiento electrónico de ambos en el estado fundamental con una disposición girada del pireno respecto al plano del indaceno (unos 63°). Como consecuencia cada cromóforo puede ser excitado selectivamente. Por un lado, la excitación directa del BODIPY ($\lambda_{exc} = 480 \text{ nm}$) en ciclohexano, da lugar a la típica banda de emisión centrada a 520 nm , con una capacidad fluorescente del 30% y tiempos de vida del orden de 1.93 ns . Dicha disminución de la capacidad fluorescente se atribuye al aumento de conversión interna ($k_{nr} \sim 4 \cdot 10^8 \text{ s}^{-1}$) que provoca la citada flexibilidad estructural por el libre giro del 8-arilo.

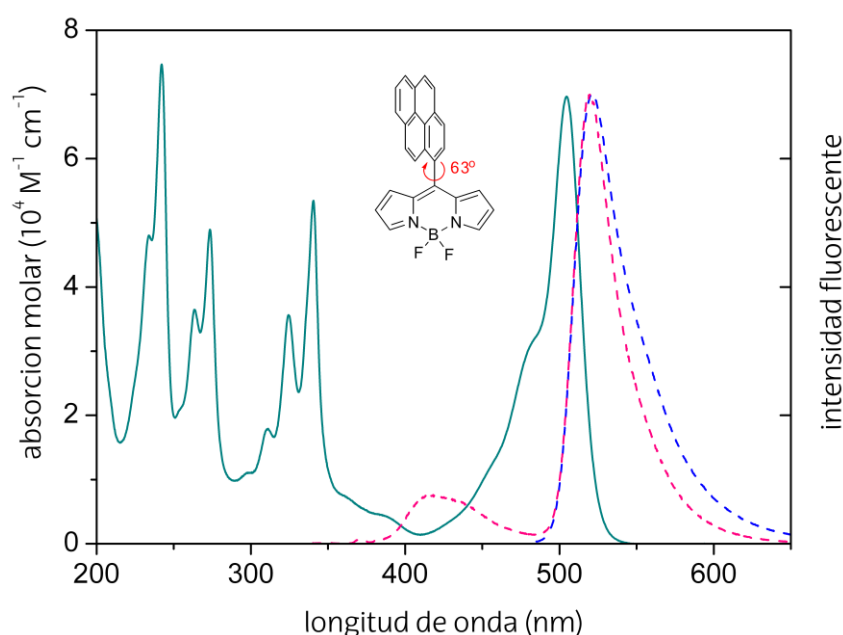


Figura 5.12. Espectros de absorción (azul-verdoso) y emisión fluorescente ($\lambda_{exc} = 340 \text{ nm}$ en rosa y $\lambda_{exc} = 480 \text{ nm}$ en azul) normalizados en ciclohexano del 8-pirenoBODIPY.

Por otra parte, la excitación selectiva del pireno en la región ultravioleta ($\lambda_{exc} = 340 \text{ nm}$), da lugar a la banda de emisión propia del pireno (420 nm) pero fuertemente desactivada a favor de una brillante emisión en 520 nm atribuible al BODIPY (Figura 5.12). De hecho, y bajo excitación ultravioleta, en medios apolares tiene lugar un proceso de transferencia de energía de excitación intra-EET del pireno (dador) al BODIPY (aceptor) a través del enlace. Esto se confirma mediante las medidas a bajas temperaturas (donde se ralentiza la transferencia electrónica), dado que se pierde la emisión del BODIPY mientras que la del pireno se sigue manteniendo (ver la publicación *RSC Adv. 2011* adjunto al Anexo IV para más información y el capítulo 6 para los detalles de los procesos de transferencia de energía). Por lo tanto, es posible

registrar la emisión del BODIPY excitando en una amplia ventana espectral; bien sea directamente al BODIPY o en la región UV donde se sitúan las bandas de absorción del pireno.

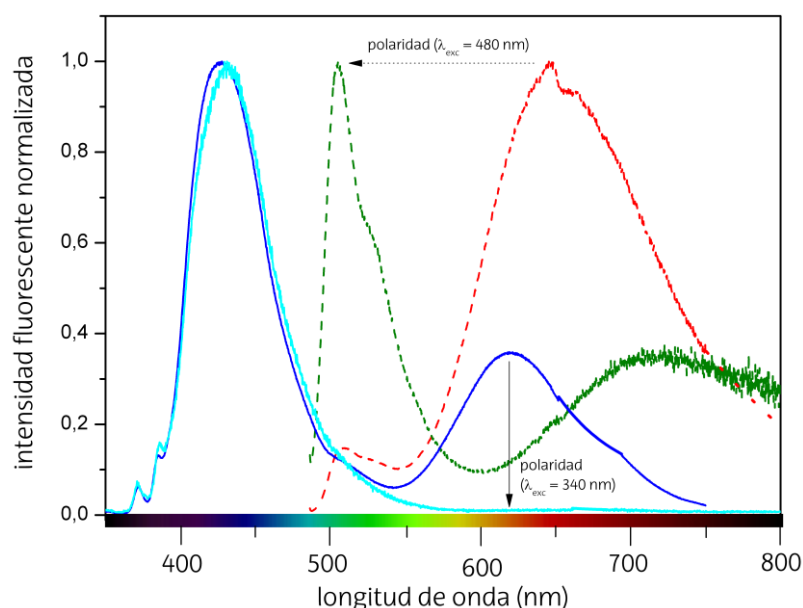


Figura 5.13. Intensidad de emisión fluorescente normalizada del 8-pirenoBODIPY en función de la polaridad del disolvente (acetato de etilo, colores azul oscuro y rojo; metanol, colores azul cian y verde) excitando a $\lambda_{exc} = 340$ nm (línea sólida) y $\lambda_{exc} = 480$ nm (línea punteada).

Las propiedades fluorescentes de la diada cambian considerablemente al aumentar la polaridad del disolvente. Así, la excitación directa del BODIPY en un medio de polaridad moderada como el acetato de etilo da lugar a una fuerte bajada de la intensidad fluorescente a 520 nm y la aparición de una nueva banda ancha situada a 650 nm atribuible a un proceso ICT, en este caso fluorescente^[21-23] (Figura 5.13). Más aún, un aumento de la polaridad del medio (metanol) provoca un desplazamiento batocrómico de la emisión del ICT (de 650 nm a 700 nm, recordar el típico solvatocromismo positivo de los estados ICT), a la vez que la señal fluorescente se hace muy débil. Esto probablemente se deba a que la estabilización de dicho estado en medios polares induce que la separación de cargas esté tan favorecida que se puebla el estado "oscuro" CS (Figura 5.2), resultando en una pérdida global de la señal fluorescente de la diada. Señalar que las mismas tendencias espectrales se observan bajo excitación UV (Figura 5.13). Así, en acetato de etilo se observa la señal propia del pireno pero débil (a 420 nm) y una considerable disminución de la intensidad de la banda del BODIPY (a 520 nm) con la aparición de la nueva banda del ICT (Figura 5.13), mientras que en metanol únicamente se detecta la emisión del pireno. Por lo tanto, bajo excitación UV la EET tiene lugar desde el pireno al estado ICT pasando por el LE del BODIPY.

Por tanto, en este caso según la polaridad del medio se observa un fuerte desplazamiento espectral de la emisión. Este hecho permite desarrollar una sonda de polaridad donde dicha característica ambiental se puede monitorizar a simple vista bajo irradiación. Para constatar este fenómeno se midió la fluorescencia de la diada bajo excitación directa del BODIPY en mezclas de THF/hexano. Así se observa que mientras en medios apolares (hexano al 90% en la Figura 5.14) domina la emisión verde típica del BODIPY, a medida que se incrementa gradualmente la polaridad de la mezcla por la adición de THF se observa un viraje del color de emisión a violeta de acorde a la emisión del ICT en la región menos energética (0% hexano en la Figura 5.14).

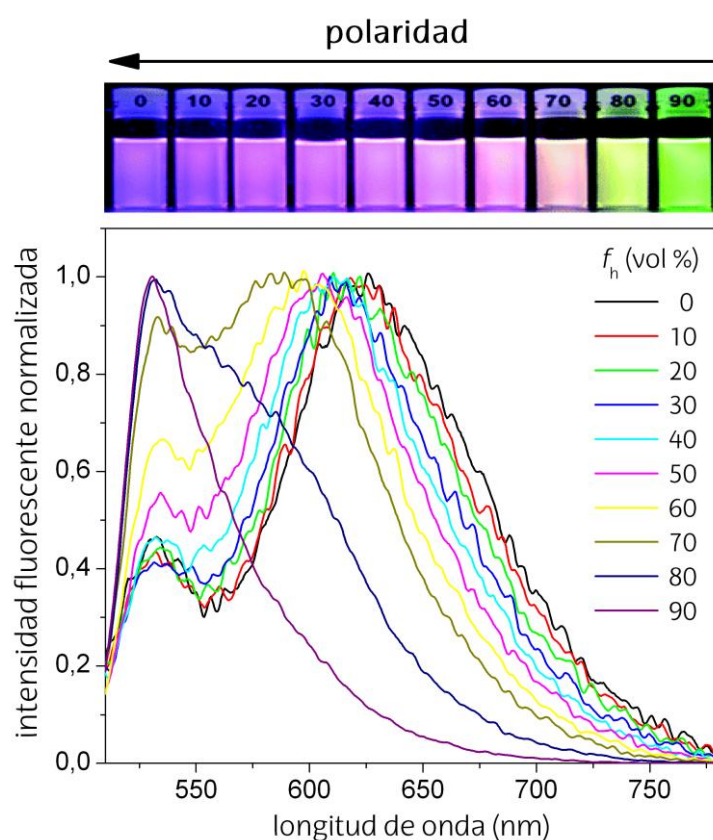


Figura 5.14. Fotografías bajo luz UV del 8-pirenoBODIPY en mezcla THF/hexano (se inserta las fracciones en volumen del disolvente apolar hexano), junto con los espectros de fluorescencia normalizados en altura.

Resumiendo, el 8-pireno-BODIPY es una alternativa fácil y directa para evaluar la polaridad del ambiente que rodea el colorante, puesto que, a diferencia de los derivados analizados en la sección 5.1, el estado ICT inducido por el pireno, que actúa como dador de electrones en la posición clave 8, es fluorescente, lo que permite evaluar a simple vista bajo irradiación la polaridad del medio.

El presente capítulo ha dado lugar a tres publicaciones en *RSC Advances* (2011), *RSC Advances* (2013) y *Organic Letters* (2014), que se adjuntan en el Anexo IV al final de la memoria y donde se puede encontrar información más detallada de la ruta de síntesis y de caracterización fotofísica, mecanocuántica, electroquímica y láser de los BODIPYs analizados.

Bibliografía

- [1] Loudet, A.; Burgess, K.; *Chem. Rev.*, **2007**, *107*, 4891.
- [2] Ulrich, G.; Zissel, R.; Harriman, A.; *Angew. Chem. Int. Ed.*; **2008**, *47*, 1184.
- [3] Turfan, B.; Akkaya, E.; *Org. Lett.*, **2002**, *4*, 2857.
- [4] Xu, W.; Bai, J.; Peng, J.; Samanta, A.; Divyanshu; Chang, Y.-T.; *Chem. Commun.*, **2014**, *50*, 10398.
- [5] Bossi, M.; Belov, V.; Polyakova, S.; Hell, S. W.; *Angew. Chem. Int. Ed.*; **2006**, *45*, 7462.
- [6] Natali, M.; Giordani, S.; *Chem. Soc. Rev.*, **2012**, *41*, 4010.
- [7] Yang, Z.; Cao, J.; He, Y.; Yang, J. H.; Kim, T.; Peng, X.; Kim, J. S.; *Chem. Soc. Rev.*, **2014**, *43*, 4563.
- [8] Lee J.-S.; Kang, N.-Y.; Kim, Y. K.; Samanta, A.; Feng, S.; Kim, H. K.; Vendrell, M.; Park, J. H.; Chang, Y.-T.; *J. Am. Chem. Soc.*, **2009**, *131*, 10077.
- [9] Feringa, B. L.; *J. Org. Chem.*, **2007**, *72*, 6635.
- [10] Boens, N.; Leen, V.; Dehaen, W.; *Chem. Soc. Rev.*, **2012**, *41*, 1130.
- [11] De Silva, A. P.; Gunaratne, H. Q. N.; Gunnaugsson, T.; Huxley, A. J. M.; McCoy, C. P.; Rademacher, J. T.; Rice, T. E.; *Chem. Rev.*, **1997**, *97*, 1515.
- [12] Rurack, K.; Resch-Genger, U.; *Chem. Soc. Rev.*, **2002**, *31*, 116.
- [13] Feringa, B. L.; Browne, W. R.; *Molecular Switches*, **2011**, Wiley-VCH Verlag GmbH & Co.
- [14] Rurack, K.; *Spectrochim. Acta Part A*, **2001**, *57*, 2161.
- [15] Sun, H.; Dong, X.; Liu, S.; Zhao, Q.; Mou, X.; Yang, H.; Huang, W.; *J. Phys. Chem. C.*, **2011**, *115*, 19947.
- [16] Hu, R.; Lager, E.; Aguilar, A.; Liu, J.; Lam, J. W. Y.; Sung, H. H. Y.; Williams, I. D.; Zhong, Y.; Wong, K. S.; Peña-Cabrera, E.; Tang, B. Z.; *J. Phys. Chem. C*, **2009**, *113*, 15845.
- [17] Cho, D. W.; Cho, D. W.; *New J. Chem.*, **2014**, *38*, 2233.
- [18] Hansch, C.; Leo, A.; Taft, R. W.; *Chem. Rev.*, **1991**, *91*, 165.
- [19] Alamiry, M. A. H.; Benniston, A. C.; Copley, G.; Elliot, K. J.; Harriman, A.; Stewart, B.; Zhi, Y.-G.; *Chem. Mater.*, **2008**, *20*, 4024.
- [20] Tian, M.; Peng, X.; Feng, F.; Meng, S.; Fan, J.; Sun, S.; *Dyes and Pigments*, **2009**, *81*, 58.
- [21] Hu, R.; Lager, E.; Aguilar-Aguilar, A.; Liu, J.; Lam, J. W. Y.; Sung, H. H. Y.; Williams, I. D.; Zhong, Y.; Wong, K. S.; Peña-Cabrera, E.; Tang, B. Z.; *J. Phys. Chem. C*, **2009**, *113*, 15845.
- [22] López Arbeloa, F.; López Arbeloa, T.; López Arbeloa, I.; *Trends Photochem. Photobiol.*, **1994**, *3*, 145.
- [23] Grabowski, Z. R.; Rotkiewicz, K.; Rettig, W.; *Chem. Rev.*, **2003**, *103*, 3899.

CAPÍTULO 6

MULTICROMÓFOROS BODIPY-CUMARINA

Una de las mayores limitaciones de los BODIPYs, y de la mayoría de los colorantes láser, es su bajo desplazamiento de Stokes. En general, los fluoróforos con alta capacidad fluorescente presentan una estructura rígida y la excitación no conlleva una significativa reorganización geométrica. Por tanto hay un alto solapamiento de los espectros de absorción y fluorescencia que provoca, por un lado, una disminución de la eficiencia fluorescente y láser en medios de alta densidad óptica (tales como los requeridos en la cavidad resonante para la amplificación de la emisión estimulada) por la mayor probabilidad de los procesos de reabsorción y reemisión. Por otro lado, la sensibilidad en los procesos de detección mediante microscopía fluorescente también se ve afectada por la cercanía espectral de la región de excitación y monitorización.

Una de las alternativas para conseguir alejar la zona de absorción/excitación respecto a la de emisión, es la unión covalente de dos o más cromóforos con bandas espectrales en diferentes regiones del espectro visible y que sean susceptibles de dar lugar a procesos de transferencia de energía de excitación (EET, *Excitation Energy Transfer*) no-radiantes. Señalar que los anteriormente citados procesos de reabsorción/reemisión también implican transferencia de energía pero de forma radiante. En la nueva entidad multicromofórica uno de

los fragmentos debe actuar como el componente encargado de la absorción de luz y de transferir la energía (dador, D) a otro fragmento (aceptor, A) que es excitado indirectamente y es el emisor final de luz. Ambos fluoróforos están covalentemente unidos por medio de un espaciador, el cual juega un papel fundamental^[1-2]. Es decir, el diseño molecular es primordial en este tipo de estructuras ya que si el espaciador permite una fuerte interacción intermolecular (límite de fuerte acoplamiento)^[3], en realidad lo que se obtiene es un nuevo cromóforo con nuevas bandas espectrales como resultado de la interacción resonante entre las nubes electrónicas del dador y acepto. Alternativamente, si el espaciador (por ejemplo, por medio de impedimentos estéricos) no permite interacción molecular entre ambos fluoróforos (límite de acoplamiento muy débil)³ cada uno de los fragmentos mantiene su identidad y sus propias bandas espectrales, a pesar de la unión covalente. En este último régimen (Figura 6.1), puede tener lugar la transferencia de energía por resonancia de fluorescencia (FRET, *Fluorescence Resonance Energy Transfer*)^[4-5]. Este mecanismo intramolecular también llamado de largo alcance y que tiene lugar a través del espacio, requiere de un acoplamiento dipolo-dipolo de los colorantes D y A implicados. Existen diversos factores que controlan su eficiencia como la absorción molar del acepto, el tiempo de vida del dador y el rendimiento cuántico de fluorescencia del dador, pero los más importantes son el solapamiento espectral entre el espectro de emisión del dador y el espectro de absorción del acepto^[6], la orientación relativa de sus momentos dipolares de transición electrónica y la distancia D-A (Figura 6.1). En los sistemas multicromofóricos, donde el proceso de EET es intramolecular y la unión covalente dispone ambos fragmentos muy cerca se pueden alcanzar eficiencias de EET muy altas (de prácticamente el 100%)^[7-8]. Tal y como se puede constatar a lo largo del presente capítulo, el diseño racional del colorante multicromofórico permite tener EET entre los fragmentos tanto cuando la interacción entre ellos es fuerte como muy débil. A pesar de que en esta memoria no se describen todos los procesos de transferencia de energía, se debe indicar que hay acoplamientos intermedios, así como otros mecanismos de transferencia como la colisional (o Dexter)^[9] o el que se produce a través del enlace (TBET, *Through-Bond Energy Transfer*)^[10-11].

En general, los BODIPYs presentan una fuerte absorción $S_0 \rightarrow S_1$ en la región verde-amarilla, sin embargo la probabilidad de absorción de las transiciones más energéticas que aparecen en el UV/azul son mucho más débiles. Por lo tanto, con el fin de cubrir eficientemente la excitación del BODIPY mediante radiación UV/azul, se sugiere la combinación de distintos BODIPYs y cumarinas, lo que posibilita la generación láser de estos multicromóforos a través de la radiación del tercer armónico del láser Nd:YAG a 355 nm. Los cromóforos de benzopirano (conocidos comúnmente como cumarinas, Figura 6.2) se caracterizan por absorber en el

UV/azul y por un marcado carácter de ICT inducido por el grupo amino o hidroxilo principalmente tras la excitación (colorantes tipo *push-pull*). Su principal desventaja es su baja fotoestabilidad bajo el bombeo con radiación UV^[12-15], aunque mediante los sistemas multicromofóricos propuestos en el presente capítulo, la cumarina no sufre tanta fotodegradación puesto que la energía de excitación se transfiere eficientemente al BODIPY.

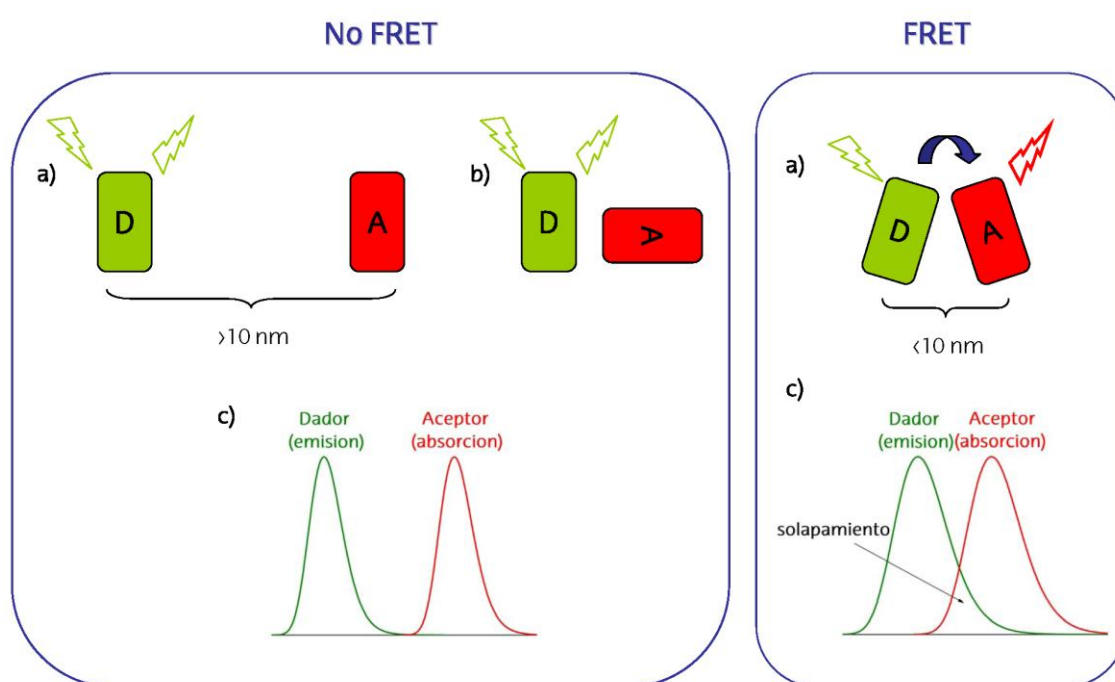


Figura 6.1. Esquema de las condiciones de a) distancia, b) orientación y c) solapamiento espectral de los fluoróforos dador (D) y aceptor (A) que proporcionen procesos FRET.^[16]

El solapamiento espectral de la cumarina y el BODIPY es el adecuado para promover procesos FRET de forma que tras la excitación en el UV del grupo dador (cumarina) se puede obtener la emisión en el visible del grupo aceptor (BODIPY). Con ello y desde el punto de vista láser, este tipo de sistemas son más versátiles ya que pueden ser bombeados tanto en el UV como en el visible, se puede aumentar la fotoestabilidad del BODIPY ya que no es bombeado directamente sino indirectamente desde la cumarina y se disminuye la probabilidad de procesos de reabsorción/reemisión. Además, también son potencialmente interesantes desde el punto de vista biofotónico ya que tras el correspondiente doblado de frecuencia de la emisión láser obtenida (520-680 nm), se consiguen fotones UV (250-340 nm), que permiten estudiar mecanismos de degradación de biomoléculas implicadas en procesos cancerígenos bajo idénticas condiciones a las de la exposición a la luz solar.

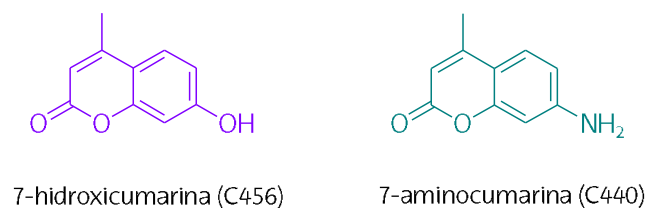


Figura 6.2. Estructuras de las cumarinas empleadas en el presente trabajo.

Por tanto, en el presente capítulo se van a analizar las propiedades fotofísicas y los mecanismo de EET que tienen lugar en BODIPYs funcionalizados en distintas posiciones (en el puente de boro, sección 6.1, y posiciones pirrólicas α , sección 6.2) con diferentes tipos (amino- e hidroxí-cumarina, Figura 6.2) y número (mono- y disustitución) de cumarinas.

Los colorantes analizados en este capítulo han sido sintetizados por el grupo de la Prof. M^a Jose Ortiz de la UCM. A continuación, se exponen los resultados más significativos de la serie de BODIPYs analizados, aunque en el artículo adjunto al Anexo V al final de la memoria (*Phys. Chem. Chem. Phys.* 2015) se especifica toda la metodología sintética y se discute en detalle la caracterización electroquímica, fotofísica y láser, además de la interpretación de la simulación mecanocuántica.

6.1. DIADA BODIPY-CUMARINA

En esta sección se analiza la fotofísica de la diada constituida por el PM567 (estudiado en el capítulo 2, y que actúa como aceptor) tras la sustitución de los átomos de flúor por el oxígeno de la 7-hidroxycumarina (C456, como dador). El espectro de absorción del multicromóforo es prácticamente la suma de la absorción visible del PM567 (510 nm) y el doble de la absorción UV (320 nm) del C456, ya que dispone de dos unidades cumarínicas (Figura 6.3.a).

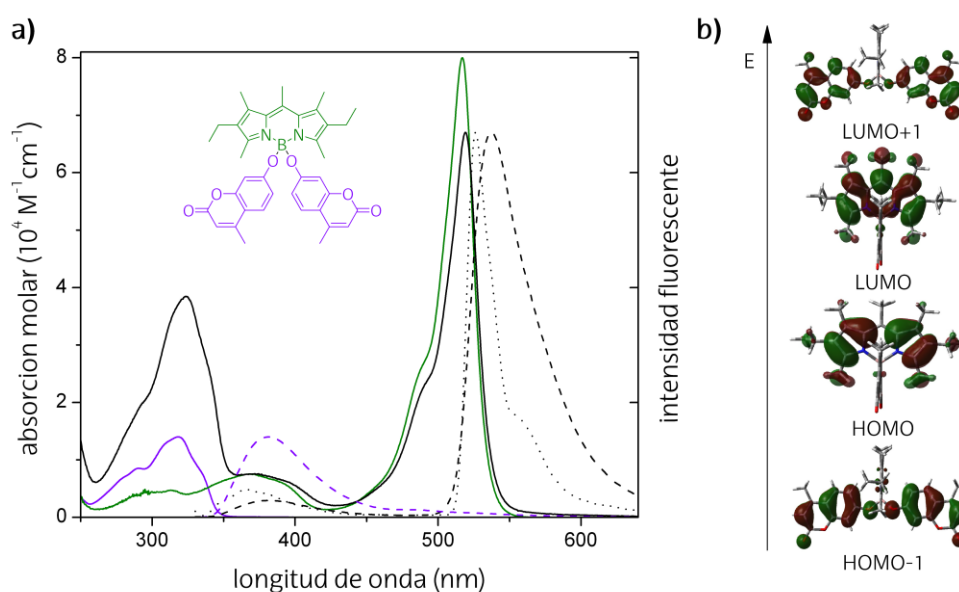


Figura 6.3. a) Espectros de absorción y fluorescencia (a temperatura ambiente línea rayada y a 77K línea punteada) bajo irradiación UV ($\lambda_{exc} = 325$ nm) de la 7-hidroxycumarina (violeta), PM567 (verde) y resultante de la unión covalente de ambos (negro) en etanol. b) Mapas de densidad electrónica de los orbitales moleculares del sistema PM567-cumarina.

Por lo tanto, los cromóforos que constituyen la diada se comportan como dos entidades independientes (límite de acoplamiento electrónico muy débil) que pueden ser excitadas selectivamente. Tal y como se comprobó en el capítulo 2, los sustituyentes incorporados al átomo de boro del BDP (reemplazando los átomos de flúor) no participan en la deslocalización del sistema π . De hecho, la simulación del espectro de absorción consta de una transición H-1 \rightarrow L+1 más energética y asignada exclusivamente a la cumarina, junto con otra transición HOMO \rightarrow LUMO en el visible y localizada sólo en el BODIPY (Figura 6.3.b). Es más, la caracterización electroquímica confirma la ausencia de interacción electrónica entre los fragmentos, puesto que las curvas de oxidación/reducción son idénticas a las de los correspondientes fragmentos de partida tras la unión covalente (Figura 6.4).

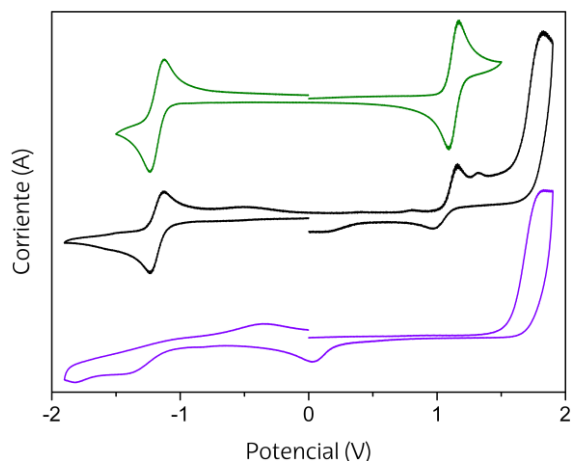


Figura 6.4. Voltagramas cíclicos de la diada PM567-cumarina (negro) y los correspondientes fragmentos de PM567 (verde) y 7-hidroxycumarina (violeta).

Por lo tanto, la separación electrónica de los fragmentos permite excitarlos selectivamente tanto en la región UV ($\lambda_{\text{exc}} = 325 \text{ nm}$, cumarina) como en el visible ($\lambda_{\text{exc}} = 490 \text{ nm}$, BODIPY). En ambos casos se registra una eficiente y dominante emisión del BODIPY (82% vs 84% del PM567 tras la excitación del pirrometeno) y el proceso de transferencia de energía de la cumarina al BODIPY podría considerarse del 100%, tal y como lo demuestra la emisión residual de la cumarina tras su excitación directa (Figura 6.3.a). La distancia predicha teóricamente entre los núcleos cromofóricos D-A es de $\sim 5 \text{ \AA}$, lo que posibilita una eficiente EET intramolecular. Teniendo en cuenta la ausencia de interacción resonante, el solapamiento espectral entre la emisión de la cumarina (dador) y la absorción del PM567 (aceptor) en la Figura 6.3.a, y la flexibilidad del enlace B-O que permite el giro de la cumarina y no restringe su orientación, el proceso EET debe de tener lugar por un mecanismo FRET. Con el fin de confirmar experimentalmente esta asignación se realizaron medidas de fluorescencia a bajas temperaturas (Figura 6.3.a) donde los procesos electrónicos (como el TBET, que requieren una energía de activación) se ralentizan considerablemente. Se comprueba, que la eficiencia de EET es muy similar a 77K y a temperatura ambiente, por lo tanto se ratifica la presencia del mecanismo FRET en la diada PM567-C456, como el responsable de que el sistema molecular actúe como una antena recolectando luz en un amplio intervalo espectral (UV-verde) y proporcionando exclusivamente emisión verde.

En cuanto a la caracterización láser, también se obtiene una significativa mejoría, puesto que se registra un aumento de la eficiencia láser de la diada (del 45% vs 20% en el PM567) tras el bombeo en la región UV, junto con una fotoestabilidad del 25% después de 50000 pulsos de excitación.

6.2. HÍBRIDOS BODIPY-CUMARINA

Con el fin de tener más información de la relación estructura-fotofísica, se ha procedido a analizar colorantes multicromofóricos donde una o dos unidades de la aminocumarina (C440) o hidroxycumarina (C456) se unen directamente por el heteroátomo (N u O, respectivamente) en la posición α de diversos BODIPYs que difieren en la sustitución de la posición *meso* (Figura 6.5), donde presentan arilos con el giro restringido (*mesitilo*), anillos con libre giro (*para*-tolilo) o grupos aceptores de electrones (trifluorometilo).

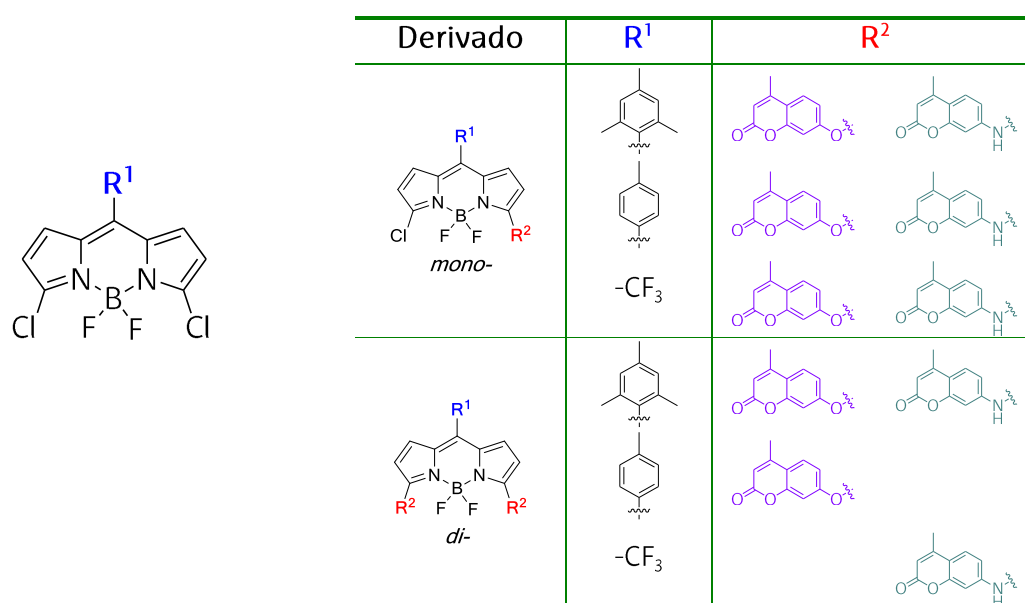
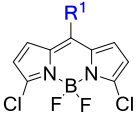
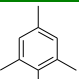
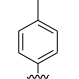


Figura 6.5. Estructuras de los híbridos BODIPY-cumarina mono- y di-sustituidos.

La capacidad fluorescente de los híbridos BODIPY-cumarina analizados en la presente sección está condicionada por el patrón de sustitución en posición 8 del BODIPY de partida. Así, la destacable capacidad fluorescente del 94% registrada en el 8-mesitilBODIPY clorado en las posiciones α , se debe a la *orto*-metilación del 8-arilo que impide su libre giro, mientras que en el 8-tolilBODIPY la libertad de giro del anillo (ver capítulo 5, sección 5.1.1) da lugar a capacidades fluorescentes del 25%, por un aumento de la conversión interna que se ve paliado en parte por la cloración en las posiciones 3 y 5 (Tabla 6.1). La presencia del 8-trifluorometilo en el cromóforo BODIPY da lugar a un desplazamiento batocrómico de las bandas espectrales (~30-35 nm, Tabla 6.2) como resultado de la estabilización preferencial del orbital LUMO por el efecto atractor del sustituyente, y mantiene una alta capacidad fluorescente (82%) a pesar de su carácter electrónico y estar anclado al cromóforo en la posición *meso*, la más sensible al efecto del sustituyente (ver el caso del PM650 con 8-ciano en el capítulo 2).

Tabla 6.1. Propiedades fotofísicas en acetato de etilo de los BODIPYs de referencia.

Derivado	R ¹	λ_{ab} (nm)	ϵ_{max} (10 ⁴ M ⁻¹ cm ⁻¹)	λ_{fl} (nm)	$\Delta\nu_{St}$ (cm ⁻¹)	ϕ	τ (ns)	k_{fl} (10 ⁸ s ⁻¹)	k_{nr} (10 ⁸ s ⁻¹)
		511.5	10.7	521.5	375	0.94	5.90	1.6	0.10
		509.5	10.3	522.0	470	0.25	1.93	1.3	3.9
	-CF ₃	545.0	6.8	552.0	230	0.82	6.77	1.2	0.26

A continuación se analizan principalmente los resultados de los híbridos derivados del 8-mesitilBODIPY, ya que es el que presenta la funcionalización completa, y tomando éste como referencia se hará mención al resto de derivados del 8-tolilBODIPY y 8-CF₃BODIPY. Para más detalle del análisis fotofísico, electroquímico o de la simulación mecanocuántica realizada para estos derivados ver el artículo *Phys. Chem. Chem. Phys.* 2015 adjunto al Anexo V al final de la memoria.

6.2.1. Híbridos mono-sustituidos

En general, los espectros de absorción de los híbridos obtenidos por la unión de la cumarina al correspondiente BODIPY de partida a través del N u O en la posición α cromofórica (Figura 6.5), constan de una banda dominante en la región visible, correspondiente a la transición $S_0 \rightarrow S_1$ del BODIPY, seguida de una serie de bandas en la región ultravioleta que se asignan al solapamiento de las transiciones $S_0 \rightarrow S_i$ más energéticas del propio BODIPY junto con las de los correspondientes fragmentos de las cumarinas (Figura 6.6).

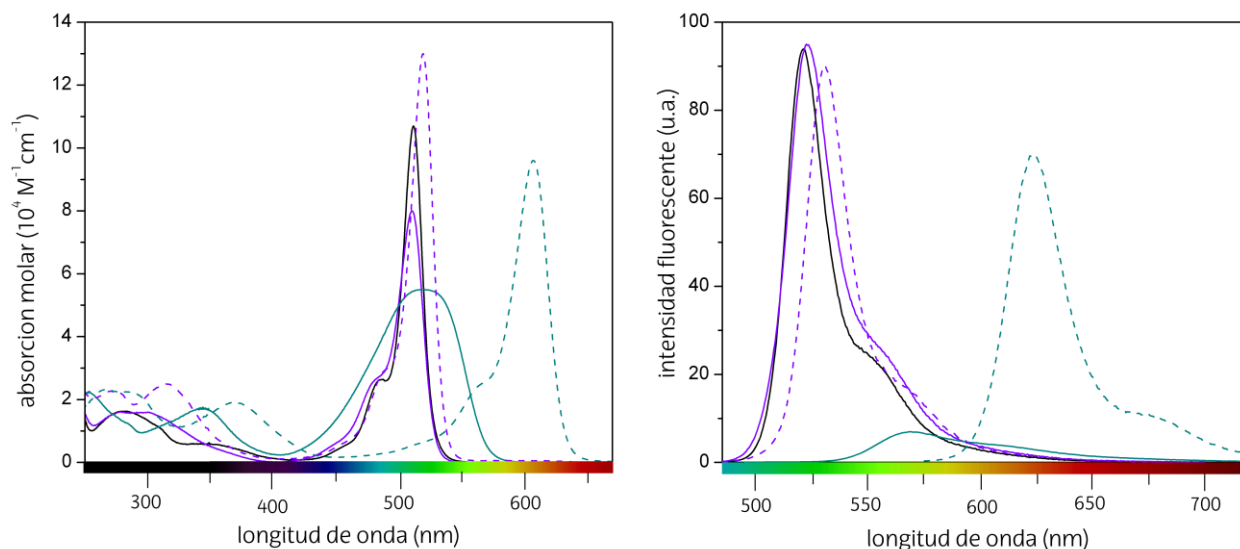


Figura 6.6. Espectros de absorción y fluorescencia (bajo excitación directa del BODIPY en el visible) de los híbridos BODIPY-cumarina del derivado 8-mesitilBDP más representativo (negro). Las líneas punteadas representan los derivados disustituidos y los colores corresponden a la sustitución por las cumarinas de la Figura 6.2 (7-hidroxycumarina en violeta y 7-aminocumarina en azul-verdoso).

Sin embargo, el marcado carácter dador de la aminocumarina provoca un notable ensanchamiento y disminución de la banda de absorción en todos los derivados monosustituidos ($\epsilon_{\text{max}} < 8 \cdot 10^4 \text{ M}^{-1} \text{ cm}^{-1}$, Figura 6.6 y Tabla 6.2). Estos cambios espectrales indican una interacción resonante entre la cumarina y el BODIPY, siendo esta interacción electrónica mucho más significativa en el caso de la aminocumarina (Figura 6.7.b) que con la hidroxycumarina (Figura 6.7.a), lo cual se atribuye al mayor carácter dador del N (heteroátomo menos electronegativo que el O). El fuerte acoplamiento electrónico entre ambas entidades promueve la reorganización del sistema π dando lugar a un aumento de la deslocalización, lo que impide la excitación selectiva de cada cromóforo. Por lo tanto, el mecanismo FRET que tenía lugar en la sección anterior al anclar la cumarina en el boro, no es operativo cuando la conexión a través del heteroátomo tiene lugar directamente en el indaceno.

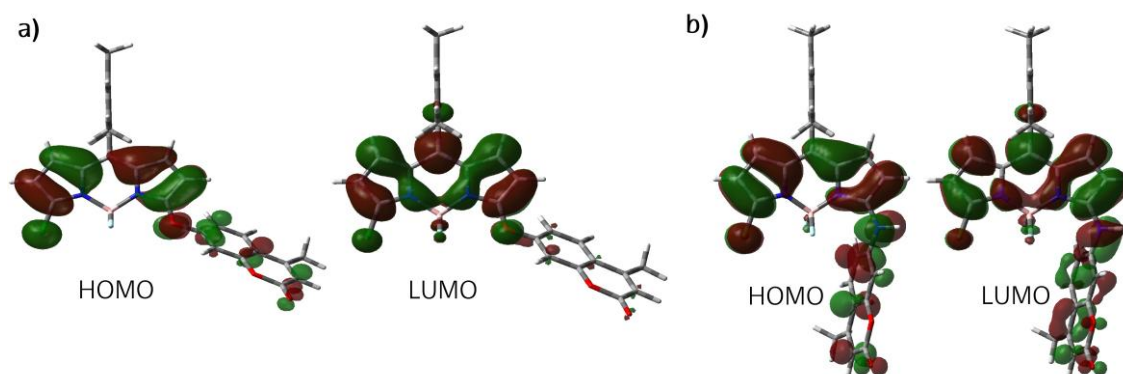


Figura 6.7. Mapas de densidad electrónica de los orbitales moleculares de los correspondientes híbridos BODIPY-cumarina monosustituídos del 8-mesitilBDP por la a) 7-hidroxycumarina o b) 7-aminocumarina.

En consecuencia la monosustitución por hidroxycumarinas, da lugar a bandas fluorescentes (tanto bajo excitación UV como visible) con posición y eficiencia similar al 8-mesitilBODIPY de referencia (<95%, Tabla 6.2). Sin embargo, en los correspondientes derivados monosustituídos del 8-tolilBODIPY y 8-CF₃BODIPY se registra una disminución de la capacidad fluorescente del 36% y 50%, respectivamente (Tabla 6.1 vs 6.2). No hay que olvidar que en la posición α opuesta hay un átomo de cloro que es un buen aceptor, y que por lo tanto, puede promover la activación de procesos ICT.

Tabla 6.2. Propiedades fotofísicas en acetato de etilo de los híbridos BODIPY-cumarina monosustituídos.

	λ_{ab} (nm)	ϵ_{max} (10 ⁴ M ⁻¹ cm ⁻¹)	λ_{fl} (nm)	$\Delta\nu_{St}$ (cm ⁻¹)	ϕ	τ (ns)	k_{fl} (10 ⁸ s ⁻¹)	k_{nr} (10 ⁸ s ⁻¹)
	510.5	8.0	522.5	450	0.95	4.48	2.1	0.11
	519.5	5.5	569.0	1675	0.07	0.28*	2.5	33.2
	510.0	4.6	525.0	560	0.16	0.84	1.9	10.0
	524.0	4.5	577.0	1750	0.04	0.28	1.4	34.3
	537.0	6.4	555.0	605	0.41	2.81	1.5	2.1
	520.5	3.7	-	-	-	-	-	-

*Decaimiento biexponencial, se muestra el tiempo de vida mayoritario.

Sin embargo, la monosustitución del 8-mesitilBODIPY por aminocumarinas, con mayor carácter dador, impulsa un desplazamiento batocrómico de la fluorescencia (~ 50 nm, más fuerte que el registrado en absorción, Figura 6.6), lo que se traduce en un incremento del desplazamiento de Stokes (~ 1700 cm^{-1} , Tabla 6.2), así como una pronunciada disminución de la capacidad fluorescente ($\ll 7\%$, Tabla 6.2). Dicho resultado refuerza la generación de procesos ICT como consecuencia de la sustitución asimétrica (resultados similares se han obtenido por la aminación de 8-tolilBODIPY en el capítulo 5, sección 5.1.1). De hecho, en la serie del 8- CF_3 BODIPY, el derivado monosustituido con aminocumarina da lugar a una nula señal fluorescente como resultado de la mayor separación de cargas que induce la presencia adicional de CF_3 aceptor en *meso*, a parte del cloro en posición 5.

6.2.2. Híbridos di-sustituidos

La disustitución promueve desplazamientos espectrales batocrómicos que son especialmente importantes en los derivados con aminocumarinas (de hasta 100 nm, Figura 6.6 y Tabla 6.3), debido a un aumento de la deslocalización del sistema π . De hecho, la caracterización electroquímica indica que la fuerte interacción electrónica de la aminocumarina con el BODIPY, promueve la disminución del potencial de oxidación (de 1.70 V en el 8-mesitilBDP de referencia a 0.63 V, Figura 6.8) y como consecuencia una disminución del salto energético (mayor proximidad entre los picos de reducción y oxidación).

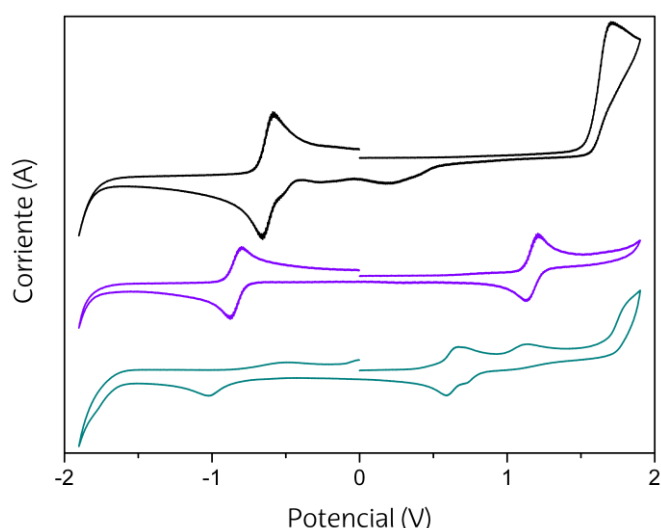
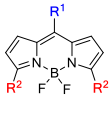
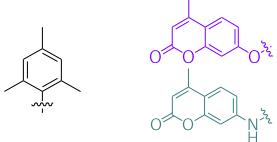
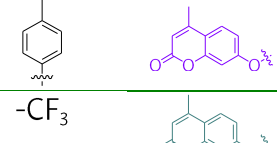
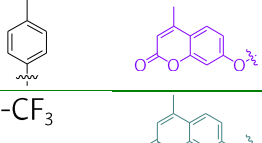
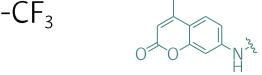


Figura 6.8. Voltagramas cíclicos del 8-mesitilBODIPY (negro) y los correspondientes derivados disustituidos por la hidroxycumarina (violeta) o aminocumarina (azul-verdoso).

El anclaje de dos unidades de hidroxycumarina al 8-mesitilBODIPY no origina cambios significativos (apenas un leve desplazamiento espectral y un aumento de la probabilidad de absorción, Figura 6.6), manteniéndose la alta capacidad fluorescente del colorante (en torno al 90%, Tabla 6.3). A diferencia del derivado monosustituido con aminocumarina del 8-mesitilBODIPY (sección 6.2.1), que se caracterizaba por un pronunciado ensanchamiento espectral (Figura 6.6) y una evidente disminución de la capacidad fluorescente (Tabla 6.2), la disustitución con aminocumarina no sigue dicha tendencia (Figura 6.9). Es decir, a pesar de la presencia de dos unidades de aminocumarina y por tanto del mayor carácter dador de los sustituyentes, la sustitución simétrica no sólo favorece la capacidad fluorescente, puesto que se remueven todos los cloros (la parte aceptora de electrones) con lo que se suprime en gran medida el estado ICT, sino que los espectros también recuperan la progresión vibracional típica de BODIPYs. Como consecuencia, se obtiene un colorante láser adecuado con emisión en el rojo centrada en 623 nm y con capacidades fluorescentes superiores al 70% (Figura 6.6 y Tabla 6.3).

Tabla 6.3. Propiedades fotofísicas en acetato de etilo de los híbridos BODIPY-cumarina disustituidos.

 R^1 R^2	λ_{ab} (nm)	ϵ_{max} ($10^4 M^{-1}cm^{-1}$)	λ_{fl} (nm)	$\Delta\nu_{St}$ (cm^{-1})	ϕ	τ (ns)	k_{fl} ($10^8 s^{-1}$)	k_{nr} ($10^8 s^{-1}$)
	519.5	13.0	530.0	380	0.90	3.78	2.4	0.26
	607.0	9.6	623.5	435	0.70	3.83	1.8	0.78
	517.5	4.2	532.0	525	0.36	1.56	2.3	4.1
 $-CF_3$	642.5	5.3	665.0	525	0.73	2.50	2.9	1.1

En concordancia, e independientemente de la incorporación de hidroxí- o aminocumarina, la disustitución en los correspondientes 8-tolil- y 8- CF_3 -BODIPY de referencia, da lugar a un incremento de la capacidad fluorescente con respecto al derivado monosustituido (columnas sin relleno de la Figura 6.9), como resultado de la citada menor probabilidad de procesos ICT. Dicho incremento es especialmente notable en el correspondiente derivado con el grupo CF_3 en *meso*, donde la capacidad fluorescente por la

disustitución de la aminocumarina llega a ser del 70% (Tabla 6.3), mientras que la monosustitución da lugar a un derivado con una emisión nula (Figura 6.9). Por lo tanto, este último colorante completaría a los estudiados en el capítulo 3 proporcionando excelentes propiedades fotofísicas, ya que absorbe a 642 nm y emite eficientemente a 665 nm, es decir, dentro de la ventana biológica.

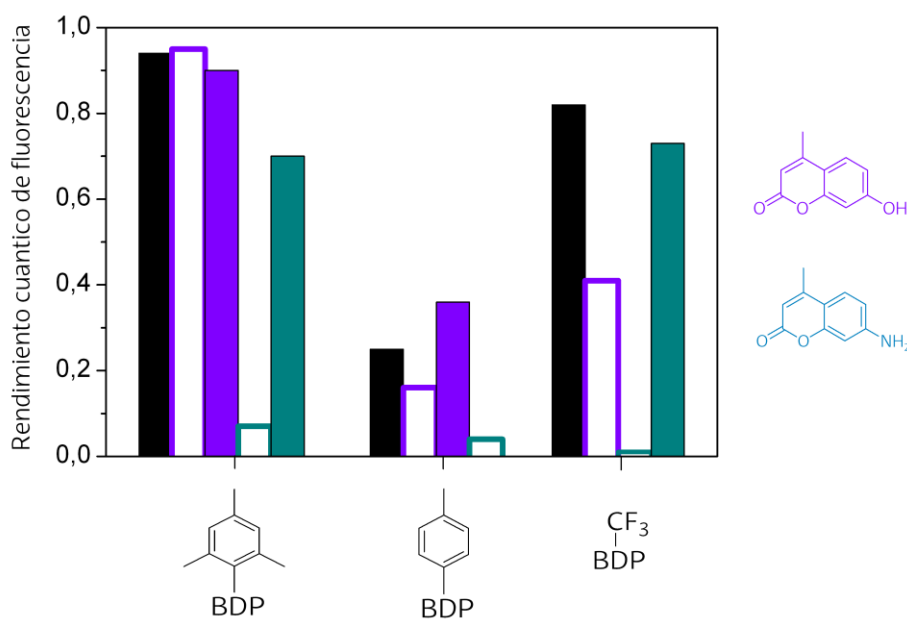


Figura 6.9. Rendimientos cuánticos de fluorescencia de los híbridos BODIPY-cumarina mono- (columnas sin relleno) y di-sustituidos (columnas con relleno) en las posiciones α en acetato de etilo, así como de sus respectivos colorantes de referencia (columnas negras). Se incluyen las estructuras de las correspondientes cumarinas.

Por otro lado, el aumento de la probabilidad de absorción registrada en la región más energética de los presentes híbridos BODIPY-cumarina posibilita el bombeo en el UV y la obtención de una eficiente emisión láser en el visible, desde 550 nm a 680 nm según el patrón de sustitución del cromóforo. De hecho, la eficiencia láser del 8-mesitilBODIPY (22%) aumenta hasta el 46% y 51%, tras la unión de una o dos unidades de hidroxycumarina, respectivamente. La fotoestabilidad láser también mejora como consecuencia de la excitación indirecta. Así, por ejemplo, se obtienen fotoestabilidades del 40% (mono-) y 55% (di-sustitución) tras 50000 pulsos de excitación UV para estos mismos colorantes.

Hay que reseñar que a pesar de que las cumarinas destacan por su baja fotoestabilidad tras su bombeo en la región UV, el presente capítulo muestra claramente los beneficios que supone el anclaje de cumarina en las propiedades fotofísicas y láser del BODIPY. Por un lado, la unión de ambas entidades por el átomo de boro hace posible la emisión del BODIPY por excitación indirecta en el UV a través de un eficiente proceso FRET desde la cumarina. Por el contrario, un aumento de la deslocalización sobre la posición α del BDP en función del carácter dador de la cumarina y aceptor del BODIPY, permite la modulación de la emisión y capacidad fluorescente del colorante. Así, la disustitución en posiciones simétricas por aminocumarinas promueve un fuerte desplazamiento hacia la región roja, a la vez que evita procesos de ICT, garantizando una brillante emisión. Por lo tanto, la característica fotodegradación de las cumarinas es solventada por el diseño de este tipo de sistemas multicromofóricos o híbridos BODIPY-cumarina.

El presente capítulo ha dado lugar a la publicación en *Phys. Chem. Chem. Phys.* 2015, que se adjunta en el Anexo V al final de la memoria, donde se analiza detalladamente la caracterización fotofísica, mecanocuántica, electroquímica y láser de los sistemas BODIPY-cumarina analizados.

Bibliografía

- [1] Albinsson, B.; Martensson, J.; *J. Photochem. Photobiol. A*, **2008**, *9*, 138.
- [2] Fan, J.; Hu, M.; Zhan, P.; Peng, X.; *Chem. Soc. Rev.*, **2013**, *42*, 29.
- [3] Valeur, B.; Berberan-Santos, M. N.; *Molecular Fluorescence: Principles and Applications*, Wiley-vch, Weinheim, **2013**.
- [4] Ziessel, R.; Ulrich, G.; Olivier, J. H.; Bura, T.; Sutter, A.; *Chem. Commun.*, **2010**, *46*, 7978.
- [5] Yilmaz, M. D.; Bozdemir, O. A.; Akkaya, E. U.; *Org. Lett.*, **2006**, *8*, 2871.
- [6] Lakowicz, J. R.; *Principles of Fluorescence Spectroscopy*, Kluwer/Plenum, New York, 2nd edn, **1999**.
- [7] Collado, D.; Remón, P.; Vida, Y.; Najera, F.; Sen, P.; Pischel, U.; Perez-Inestrosa, E.; *Chem. Asian J.*, **2014**, *9*, 797.
- [8] Bai, D.; Benniston, A. C.; Hagon, J.; Lemmetyinen, H.; Tkachenko, N. V.; Clegg, W.; Harrington, R. W.; *Phys. Chem. Chem. Phys.*, **2012**, *14*, 4447.
- [9] Dexter, D. L.; *J. Chem. Phys.*, **1953**, *21*, 836.
- [10] Bandichhor, R.; Petrescu, A. D.; Vespa, A.; Kier, A. B.; Schroeder, F.; Burgess, K.; *J. Am. Chem. Soc.*, **2006**, *128*, 10688.
- [11] Han, J.; Jose, J.; Mei, E.; Burgess, K.; *Angew. Chem., Int. Ed.*, **2007**, *46*, 1684.
- [12] Wagner, B. D.; *Molecules*, **2009**, *14*, 210.
- [13] Schäfer, F. P.; *Dye Lasers*, Springer-Verlag, New York, 3rd ed, **1990**.
- [14] Duarte, F. J.; Hillman, L. W.; *Dye Laser Principles*, Academic, New York, **1990**.
- [15] López Arbeloa, F.; López Arbeloa, I.; López Arbeloa, T.; *Handbook of Advanced Electronic and Photonic Materials and Devices*, ed. H. S. Nalwa, Academic Press, San Diego, **2001**, vol. 7.
- [16] Broussard, J. A.; Rappaz, B.; Weeb, D. J.; Brown, C. M.; *Nature protocols*, **2013**, *8*, 265.

CONCLUSIONES GENERALES

Los resultados experimentales y teóricos detallados en la presente memoria muestran claramente la versatilidad de la familia de colorantes basados en el cromóforo BDP. Así es viable desarrollar fluoróforos a la carta, es decir, diseñar estrategias sintéticas que permitan funcionalizar selectivamente y con una amplia variedad de grupos, para inducir el proceso fotofísico deseado que facilite la aplicación del colorante en diversos campos científicos. El trabajo realizado ha permitido acumular un amplio conocimiento de cómo el patrón de la estructura molecular modula las propiedades fotofísicas del colorante según la posición donde se incorpore el sustituyente. De tal manera, que nos encontramos en posición de sugerir a priori las modificaciones estructurales más convenientes según la aplicación donde interese utilizar un fluoróforo. En los puntos siguientes se listan los aspectos más relevantes de cada capítulo con vista a la aplicación de BODIPYs como medios activos de láseres sintonizables o sondas moleculares fluorescentes.

- A pesar de que en general el BODIPY destaca por su alta capacidad fluorescente y láser, sus prestaciones son susceptibles de ser mejoradas mediante el reemplazamiento de los átomos de flúor unidos al boro por grupos aceptores. De esta manera se consiguen medios activos mejorados con prestaciones láser optimizadas en el intervalo espectral que comprende la región visible del verde-amarillo.
- La extensión de la deslocalización del sistema π por la fusión de anillos aromáticos al núcleo BDP o por la funcionalización periférica del mismo mediante grupos aromáticos con grupos dadores/aceptores de electrones, permite ampliar el rango de acción de los BODIPYs hacia la región roja del visible. Destacar que los láseres de colorante obtenidos son mucho más brillantes y estables que los existentes comercialmente en dicha región (oxazinas o cianinas), de gran interés desde el punto de vista biofotónico.

- Alternativamente la presencia de heteroátomos (nitrógeno y oxígeno) en la posición *meso* promueve un destacable desplazamiento espectral hacia la región azul, que es modulable en base a la electronegatividad del heteroátomo y el patrón de sustitución de la amina o el alcoxi. Como resultado, se obtienen colorantes láser óptimos en la región más energética del espectro visible, cuyo comportamiento desbancan a los existentes comercialmente (cumarinas) especialmente en términos de fotoestabilidad. Resumiendo, las excelentes propiedades fotofísicas y láser de los BODIPY se han extendido tanto al azul como al rojo, es decir, con una única familia de colorantes es posible cubrir satisfactoriamente toda la región visible.
- Destacar la importancia tanto de la rigidez estructural (especialmente en la posición *meso*) como principalmente de la sustitución simétrica en las posiciones pirrólicas α , que además de mejorar la capacidad fluorescente, da lugar a desplazamientos batocrómicos más pronunciados.
- La inducción de procesos de transferencia de carga sensibles a la polaridad del disolvente fomenta la generación de sondas de polaridad mediante la monitorización de la capacidad fluorescente del colorante o el cambio de color de la luz emitida, según el carácter electrónico del sustituyente y la posición cromofórica funcionalizada. La posición *meso* se postula como la más sensible para la activación de procesos de transferencia de carga ante la presencia de grupos dadores o aceptores de electrones.
- El diseño de nuevos colorantes láser multicromofóricos, basados en la combinación de BODIPYs y cumarinas, permite absorber eficientemente radiación de luz en un amplio intervalo espectral, y obtener emisión estable desde la región verde hasta la roja, independientemente de la longitud de onda de bombeo debido a la presencia de procesos de transferencia de energía.

Una prueba clara del interés suscitado por los resultados presentados en esta memoria y de su calidad son los 11 artículos (Q1) publicados como consecuencia de esta tesis doctoral en revistas científicas internacionales de referencia en campos tales como la química orgánica, química física, química multidisciplinar y materiales. De hecho, varios de los BODIPYs reportados a lo largo de la memoria han despertado el interés de empresas (Sirah y Lasing). Además, fruto de esta tesis se pretende publicar otros trabajos, tal y como se detalla en el apartado de "Perspectivas futuras".

PERSPECTIVAS FUTURAS

Esta tesis doctoral ha demostrado la enorme versatilidad de los BODIPYs; tras un diseño molecular adecuado es posible obtener colorantes que se adapten a la aplicación requerida. En esta memoria, se han empleado como medios activos de láseres modulables, eficientes y estables, o con fines bioquímicos, como sensores o sondas fluorescentes. Además, se ha justificado que el conocimiento de las propiedades fotofísicas y su dependencia con el patrón de sustitución de la estructura básica del BODIPY es esencial para entender su comportamiento en la aplicación perseguida y mejorar sus prestaciones. Como consecuencia, el potencial de estos colorantes es enorme y todavía quedan retos por explorar, es decir, modificaciones estructurales que puedan dar lugar a la aplicación de estos colorantes en nuevos ámbitos científicos y tecnológicos.

De hecho, durante la realización de esta tesis doctoral se han estudiado otras estructuras BODIPY, cuyos resultados se están reflejando actualmente en los correspondientes artículos que se pretenden enviar a publicar próximamente. El análisis de estos nuevos sistemas no se ha incluido en el cuerpo principal de la memoria ya que ésta se ha desarrollado en forma de compendio de publicaciones científicas. A continuación se detalla brevemente dichos sistemas moleculares, así como el objetivo perseguido:

- Se ha empleado la reacción de Vilsmeier-Hack para introducir grupos formilo y enamina en posiciones específicas de diversos BODIPYs de partida, con vistas a su aplicación láser y eventualmente como sensores de aniones. Estos nuevos derivados son excelentes precursores para ser postfuncionalizados y desarrollar nuevos colorantes.
- Se ha constatado recientemente un gran interés por el desarrollo de colorantes capaces de dar señal fluorescente en estado sólido. Por ello y partiendo de la base de los *O*-BODIPYs analizados en el capítulo 2, se han diseñado colorantes muy rigidizados mediante la introducción de grupos voluminosos (mesitilos, *tert*-butilos y diacilo en el boro para que sea espiránico) en la misma estructura. El impedimento estérico impide el apilamiento π - π que desactiva fuertemente la eficiencia fluorescente. Estudios en agua de dichos BODIPYs hidrofóbicos constatan la inducción de agregados fluorescentes tipo J (orientación cabeza-cola). De hecho, estos colorantes han dado lugar a una emisión láser dual.
- Siguiendo la línea marcada en el capítulo 6, se han estudiado estructuras multicromofóricas basadas sólo en BODIPYs (bisBDPs). Con ello se ha determinado el efecto del espaciador (polifenilo, fluoreno, ferroceno o tiofeno) y de la rigidez estructural controlada por el grado de alquilación de cada unidad de BODIPY. La dependencia de la eficiencia fluorescente con la flexibilidad estructural posibilita el uso de estos fluoróforos como sensores de viscosidad.
- En relación con el punto anterior, y considerando que la absorción y emisión del BODIPY se puede desplazar bien sea al rojo (capítulo 3) o al azul (capítulo 4), se han diseñado estructuras donde se combinan covalentemente BODIPYs con absorciones en distintas zonas espectrales. Esto ha posibilitado también recolectar luz en un amplio intervalo espectral (del azul al amarillo) dando lugar exclusivamente la emisión de luz roja por sucesivos procesos de transferencia de energía intramolecular. Más aún, la disposición ortogonal de los fragmentos permite la generación de oxígeno singlete a partir del estado triplete, sin que se pierda del todo la señal fluorescente (de hecho el compuesto *lasea*). Es decir, esta antena molecular es especialmente interesante para biomedicina en teragnosis, ya que puede ser monitorizada como sonda fluorescente por bioimagen (diagnóstico), a la vez que actúa como fotosensibilizador para destruir las células tumorales (terapia fotodinámica).

Por último, y en relación a su aplicación como sondas fluorescentes, hay que mencionar que los BODIPYs aparecen como una óptima elección ya que su emisión se puede desplazar fuertemente al extremo rojo del visible (tal y como se demuestra en el capítulo 3 y 6 donde se detallan los colorantes NIR-BODIPYs) lo que permite excitarlos con luz roja que penetra eficientemente en los tejidos. Por lo tanto, se posibilita una excitación selectiva y eficiente, proporcionando una mayor sensibilidad en la detección por biomagen, ya que se evita la autofluorescencia de las biomoléculas. Además, la ya citada versatilidad sintética de los BODIPYs, posibilitaría la postfuncionalización de las estructuras con sistemas π extendidos para su anclaje selectivo a la biomolécula de interés.

Además de los trabajos anteriormente citados y que están pendientes de publicación, se están diseñando y analizando nuevas estructuras de BODIPY fruto de la estrecha colaboración que mantenemos con los grupos de investigación especializados en síntesis y caracterización láser.

ERANSKINAK / ANEXOS

I Eranskina (2. Kapitulua) / Anexo I (Capítulo 2)

1. Artikulua / Artículo 1: *Chem. Eur. J.*, 2014, 20, 2646
2. Artikulua / Artículo 2: *Adv. Funct. Mater.*, 2013, 23, 4205

II Eranskina (3. Kapitula) / Anexo II (Capítulo 3)

3. Artikulua / Artículo 3: *Chem. Eur. J.*, 2015

III Eranskina (4. Kapitulua) / Anexo III (Capítulo 4)

4. Artikulua / Artículo 4: *J. Org. Chem.*, 2012, 77, 5434
5. Artikulua / Artículo 5: *Chem. Asian J.*, 2013, 8, 2691
6. Artikulua / Artículo 6: *J. Org. Chem.*, 2013, 78, 5867
7. Artikulua / Artículo 7: *ChemPhysChem*, 2013, 14, 4134

IV Eranskina (5. Kapitulua) / Anexo IV (Capítulo 5)

8. Artikulua / Artículo 8: *RSC Adv.*, 2013, 3, 1547
9. Artikulua / Artículo 9: *Org. Lett.*, 2014, 16, 4364
10. Artikulua / Artículo 10: *RSC Adv.*, 2011, 1, 677

V Eranskina (6. Kapitulua) / Anexo V (Capítulo 6)

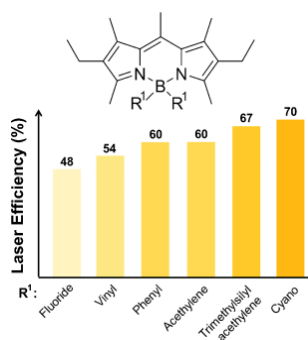
11. Artikulua / Artículo 11: *PhysChemChemPhys*, 2015, 17, 8239

2. Kapitulum I ERANSKINA / ANEXO I al Capítulo 2

1. Artikulua / Artículo 1:

First highly efficient and photostable *E* and *C* derivatives of 4,4-difluoro-4-bora-3a,4a-diaza-*s*-indacene (BODIPY) as dye lasers in the liquid phase, thin films, and solid-state rods

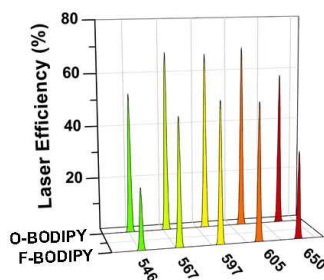
Chemistry – A European Journal, **2014**, *20*, 2646



2. Artikulua / Artículo 2:

Carboxylates versus Fluorines: boosting the emission properties of commercial BODIPYs in liquid and solid media

Advanced Functional Materials, **2013**, *23*, 4205



Laser Chemistry

First Highly Efficient and Photostable *E* and *C* Derivatives of 4,4-Difluoro-4-bora-3a,4a-diaza-*s*-indacene (BODIPY) as Dye Lasers in the Liquid Phase, Thin Films, and Solid-State RodsGonzalo Duran-Sampedro,^[a] Ixone Esnal,^[c] Antonia R. Agarrabeitia,^[a] Jorge Bañuelos Prieto,^[c] Luis Cerdán,^[b] Inmaculada García-Moreno,^{*[b]} Angel Costela,^[b] Iñigo Lopez-Arbeloa,^[c] and María J. Ortiz^{*[a]}

Abstract: A new library of *E*- and *C*-4,4-difluoro-4-bora-3a,4a-diaza-*s*-indacene (BODIPY) derivatives has been synthesized through a straightforward protocol from commercially available BODIPY complexes, and a systematic study of the photophysical properties and laser behavior related to the electronic properties of the B-substituent group (alkynyl, cyano, vinyl, aryl, and alkyl) has been carried out. The replacement of fluorine atoms by electron-withdrawing groups enhances the fluorescence response of the dye, whereas electron-donor groups diminish the fluorescence efficiency. As a consequence, these compounds exhibit enhanced laser action with respect to their parent dyes, both in liquid solution and in the solid phase, with lasing efficiencies under transversal pumping up to 73% in liquid solution and 53% in a solid

matrix. The new dyes also showed enhanced photostability. In a solid matrix, the derivative of commercial dye PM597 that incorporated cyano groups at the boron center exhibited a very high lasing stability, with the laser emission remaining at the initial level after 100 000 pump pulses in the same position of the sample at a 10 Hz repetition rate. Distributed feedback laser emission was demonstrated with organic films that incorporated parent dye PM597 and its cyano derivative. The films were deposited onto quartz substrates engraved with appropriate periodical structures. The *C* derivative exhibited a laser threshold lower than that of the parent dye as well as lasing intensities up to three orders of magnitude higher.

Introduction

Tunable lasers are an important tool in a wide variety of fields such as spectroscopy, photochemistry, material diagnosis, medicine, or integrated optical devices. Organic dye molecules offer clear advantages over other commercially available multi-wavelength laser sources such as low cost, ample spectral coverage over the visible region of the electromagnetic spectrum, and high conversion efficiency.^[1]

Among the numerous classes of highly fluorescent dyes used as the active media of tunable lasers, the family of difluoroboron dipyrromethene complexes, or BODIPYs, is one with the highest potential.^[2] Their development has acquired great importance in the last two decades owing to the excellent and easily modulated photophysical properties of these fluorophores.^[3] As a consequence, they are also intensively applied as fluorescent probes in biological systems, photosensitizers for photodynamic therapy, and as materials for incorporation into electroluminescent devices.^[2a,4]

The incorporation of appropriate functional groups into the chromophore could lead to new photophysical processes or large spectral shifts; therefore, depending on the desired application, one should carefully choose the kind of substituents and the position in which they will be incorporated into the BODIPY. A strategy that causes a substantial increase of the potential applications of the chromophore BODIPY is the substitution of fluorine atoms.^[3a-c] Thus, a wide variety of new BODIPYs have been synthesized by means of fluorine displacement by alkyl or aryl groups (*C*-BODIPYs), ethynyl groups (*E*-BODIPYs), and alkoxy or aryloxy groups (*O*-BODIPYs).^[5] The introduction of these functional groups leads to an increase in the Stokes shift as well as to the improved chemical and photochemical stability of these fluorophores, thereby opening the way to a new class of highly luminescent dyes.

[a] G. Duran-Sampedro, Prof. A. R. Agarrabeitia, Prof. M. J. Ortiz
Departamento de Química Orgánica I
Facultad de Ciencias Químicas, Universidad Complutense
28040 Madrid (Spain)
Fax: (+34) 913944103
E-mail: mjortiz@quim.ucm.es

[b] Dr. L. Cerdán, Prof. I. García-Moreno, Prof. A. Costela
Instituto de Química-Física "Rocasolano" (IQFR), CSIC
Serrano 119, 28006 Madrid (Spain)
Fax: (+34) 915642431
E-mail: i.garcia-moreno@iqfr.csic.es

[c] I. Esnal, Dr. J. Bañuelos Prieto, Prof. I. Lopez-Arbeloa
Departamento de Química Física, UPV-EHU
Apartado 644, 48080 Bilbao (Spain)

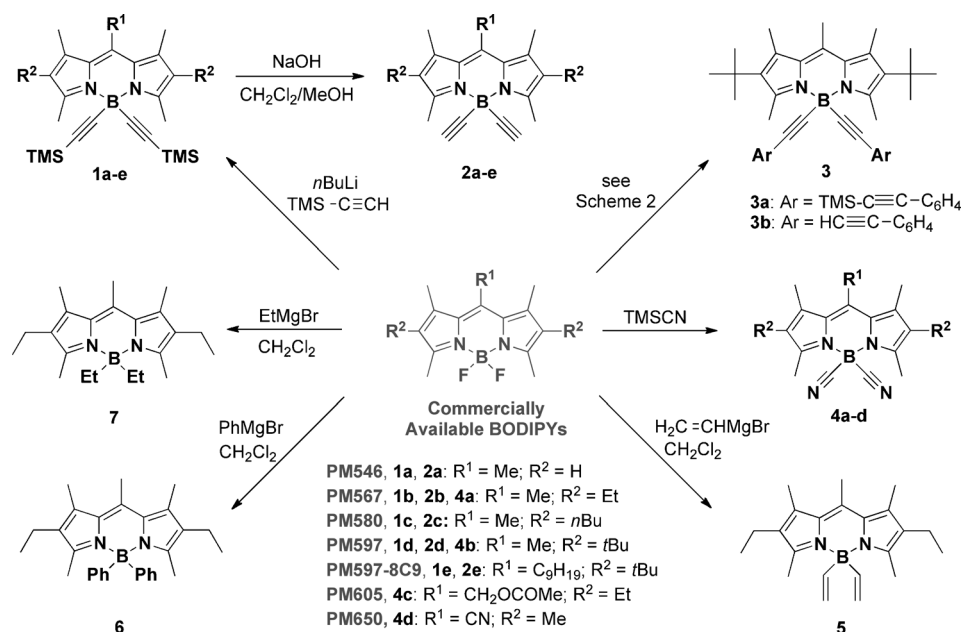
Supporting information for this article is available on the WWW under <http://dx.doi.org/10.1002/chem.201303579>.

Despite the considerable volume of work on the synthesis and applications of this type of fluorophores, there are few reports on their optical and lasing properties.^[5c,d] In this field, our research group has described the synthesis and characterization of the emission properties of a set of *O*-BODIPYs in which two carboxylate groups are connected to the boron center in place of the fluorine atoms. It was shown that these dyes are highly fluorescent and exhibit enhanced laser action with respect to their *F*-BODIPY analogues, both in liquid solution and the solid phase.^[5c]

Considering these results, in the present work we have synthesized a new library of *E*- and *C*-BODIPY derivatives (named 1–7 in Scheme 1) from the commercially available BODIPYs and we have carried out a systematic study of their photophysical properties and laser behavior related to the electronic properties of the B-substituent group (alkynyl, cyano, vinyl, aryl, and alkyl). As far as we know, there is only one precedent on lasing performance of *E*-BODIPYs by Ray et al. in which it is revealed that this substitution at the boron center does not significantly improve the laser efficiency but enhances the photostability owing to their lower reaction rates with ¹O₂ and lower ¹O₂ generation capacity.^[5d] However, the new BODIPY derivatives synthesized herein through a straightforward protocol exhibit lasing efficiencies up to four times higher than those recorded for the corresponding commercial dyes with high photostability in the liquid phase, the bulk solid state, and in thin films.

Results and Discussion

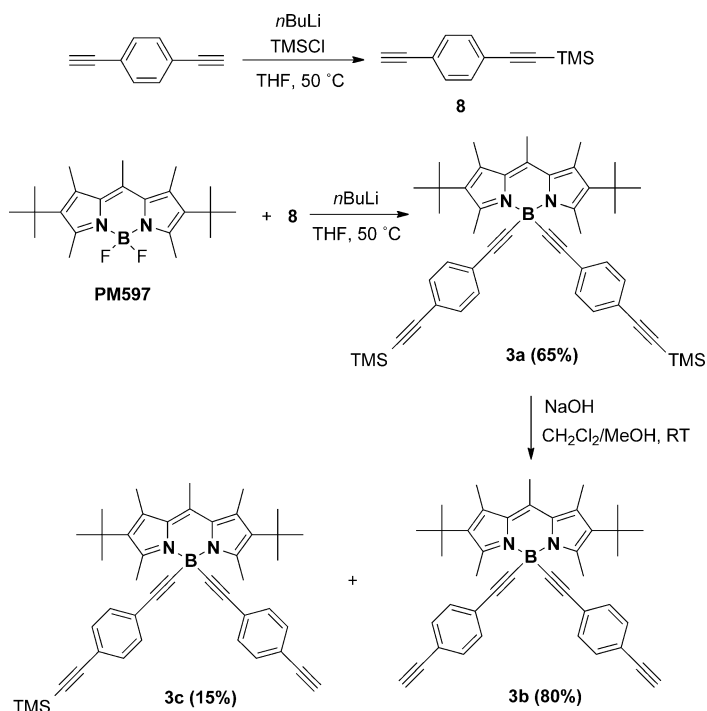
BODIPY dyes 1–7 were successfully obtained from commercially available dyes PM546, PM567, PM580, PM597, PM597-8C9, PM605, and PM650 with organolithium, Grignard reagents, or trimethylsilyl cyanide (TMSCN) as nucleophilic agents depending upon the desired change in the boron atom. BODIPY derivatives **1b**,^[6] **2b**,^[6] and **6**^[7] were synthesized by the methods previously described. Dyes **1a–e** were prepared in good yield by the introduction of two trimethylsilylacetylene units by using an excess amount of the corresponding organolithium derivative, generated in situ from trimethylsilylacetylene and *n*-butyllithium. No monosubstituted derivatives were formed under the reaction conditions. Removal of the trimethylsilyl groups using an excess amount of NaOH afforded **2a–e** as the major products. Only compound **2a** was obtained in addition to a small percentage of the monoprotected derivative.



Scheme 1. Molecular structures of commercial dyes and their analogues 1–7 synthesized in this work.

The reaction of PM597 with mono-TMS-protected 1,4-diethynylbenzene **8** gave *E*-BODIPY **3a** in good yield. The removal of the TMS protection yielded a mixture of dideprotected derivative **3b** (80%) and monodeprotected derivative **3c** (15%), which were separated by means of flash chromatography on silica (Scheme 2).

Replacement of the fluorine atoms by cyano groups (compounds **4a–d**) was carried out by the reaction of BODIPY with TMSCN in the presence of AlCl₃ as Lewis acid (compounds **4a**



Scheme 2. Synthesis of BODIPYs **3a–c**.

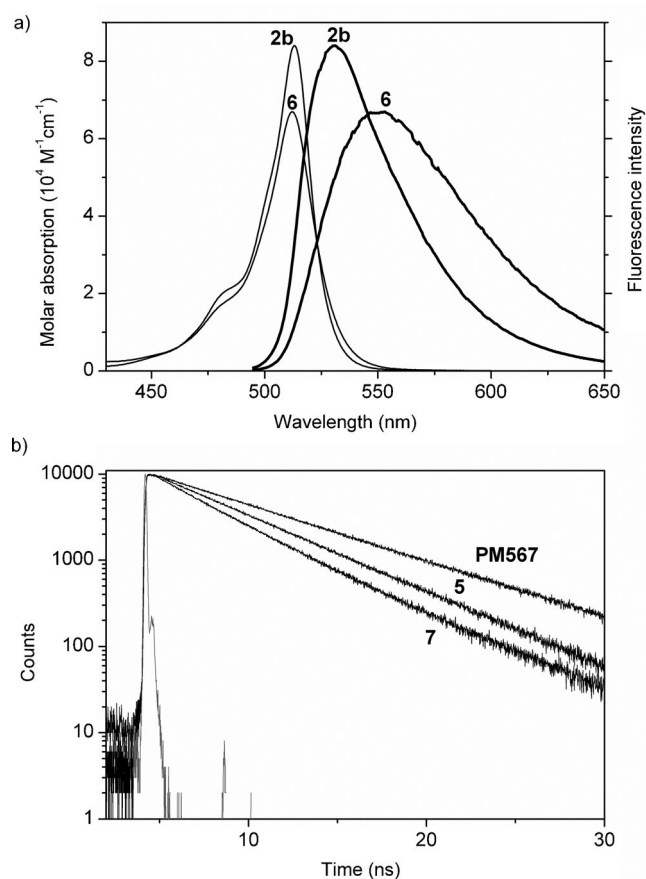


Figure 2. a) Absorption and normalized fluorescence (bold) spectra in ethyl acetate of PM567 derivatives bearing acetylene (**2b**) and phenyl (**6**) groups. b) Fluorescence decay curves of PM567 derivatives bearing vinyl (**5**) and ethyl (**7**) groups.

	ΔE_{ab} [eV]	ΔE_{fl} [eV]	$\Delta \nu_{st}$ [cm^{-1}]
PM567	2.91	2.87	380
2b	2.94	2.89	445
6	2.92	2.77	1210
5	2.95	2.88	580
7	2.99	2.83	1265
PM597	2.87	2.73	1170
PM597-8C9	2.84	2.62	1795

tion. Such theoretically suggested loss of planarity correlates well with the evolution of the nonradiative rate constant (Table S1 in the Supporting Information).

To address the opposite influence of the electron donor (harmful to the fluorescence capacity) and acceptor (slightly beneficial) groups, which are attached to boron in the *E*- and *C*-BODIPYs, we simulated the charge-density distribution in some selected compounds (Figure S3 in the Supporting Information). In a previous study on *O*-BODIPYs, we concluded that although the boron atom does not take part in the delocalized π system, its substitution determines the charge distribution

through the whole chromophore and hence the aromaticity of the π system (evaluated by the bond-length alternation (BLA) parameter,^[10] data included in Figure S3 in the Supporting Information).

The presence of acetylene groups leads to a higher positive charge in the boron atom and a slightly lower charge alternation through the core, with little influence on the aromaticity (similar BLA and fluorescence capacity to their corresponding reference *F*-BODIPYs). An increase in the electron-donor ability of the substituent (cyano groups) implies a strong rearrangement of the charge distribution, which results in a more aromatic chromophore, as reflected in the BLA parameter (i.e., 0.023 for compound **4a**), which is the lowest among all the BODIPYs reported herein. Accordingly, the derivatives with a cyano group at the boron atom (**4a–4d**) yield the highest fluorescence capacity. However, a progressive increase in the electron-donor ability of the substituent (from acetylene to ethyl) results in less aromatic dyes (BLA = 0.027, 0.029, and 0.031 for compounds **2b**, **5**, and **7**, respectively), which is in agreement with the registered lower fluorescence efficiencies. Especially remarkable is the asymmetric disposition of the phenyl rings in compound **6**. This should be a consequence of the steric hindrance between their *ortho*-hydrogen and the methyl groups in the 3- and 5-positions (Figure S1 in the Supporting Information). As a result, one of the rings acquires a high positive charge (Figure S3 in the Supporting Information) and leads to a less aromatic dye (BLA = 0.028), thereby reducing the fluorescence capacity.

Whereas the lengthening of the alkyl chain (from ethyl to butyl) at the 2- and 6-positions of PM567 to yield PM580 has a minor effect on the photophysical properties, important changes are noticed when the aliphatic chain is enlarged (from one methylene to nine) at the 8-position of PM597 to yield PM597-8C9 (Figure 1 and Table S1 in the Supporting Information). The photophysical properties of PM597 were controlled by the steric hindrance induced by the *tert*-butyl groups, which leads to a loss of planarity in the chromophore. As consequence, the nonradiative rate constant (from $0.28 \times 10^8 \text{ s}^{-1}$ in PM567 to $1.23 \times 10^8 \text{ s}^{-1}$ in PM597) and the Stokes shift (from 550 to 1330 cm^{-1} , respectively) increased significantly. These trends seem to be more evident upon grafting a linear chain at the 8-position, because the nonradiative rate (k_{nr}) enhances up to $7.9 \times 10^8 \text{ s}^{-1}$, thereby reducing the fluorescence quantum yield and lifetime (0.10 and 1.14 ns). In addition, the Stokes shift increases up to 2330 cm^{-1} as a result of a stronger bathochromic shift in the fluorescence band (placed at 595 nm, also theoretically predicted in Table 1).

The optimized geometries show that the linear chain in PM597-8C9 adopts a linear disposition, far away from the indacene core (Figure S1 in the Supporting Information). However, its presence seems to enhance the steric hindrance and a drastic geometrical rearrangement takes place after excitation. As a result, the chromophore geometry is highly distorted and a deviation of planarity up to 30° is predicted. Overall, such loss of planarity implies lower aromaticity, but surprisingly, the opposite happens in the compounds that bear 2,6-*tert*-butyl. In fact, the BLA parameters suggest that these compounds

Table 2. Lasing efficiencies of commercial BODIPY dyes and their C-BODIPY derivatives in different solvents at the dye concentrations that optimize their laser action of solutions in ethyl acetate (λ_{exc} : pumping wavelength).

Solvent	$\lambda_{\text{exc}} = 355 \text{ nm}$										$\lambda_{\text{exc}} = 532 \text{ nm}$																
	PM546	1 a	2 a	PM567	1 b	2 b	4 a	5	6	7	PM580	1 c	2 c	PM597	1 d	2 d	3 a	3 b	4 b	PM597-8C9	1 e	2 e	PM605	4 c	PM650	4 d	PM650-F-CN
EtOAc	23	58	52	48	67	60	68	54	60	30	57	65	63	53	70	63	73	68	73	55	62	59	55	68	35	45	36
Acetone	14	56	49	36	65	57	65	45	56	25	57	63	62	50	67	62	71	65	70	52	59	56	57	69	31	40	30
MeOH				34	58	54	61		52		51	61	57	54	63	59	69	63	68	47	59	54	55	66	12	30	22
EtOH	18	58	50	36	62	56	63	44	54	27				51	65	61	69	60	67				56	67			
F ₃ -EtOH														56	63	57	70	62	65				51	61	27	38	28
CH ₂ Cl ₂											50	61	59							50	60	56					
THF											59	66	64														

(PM597 and PM597-8C9) become more aromatic as the excited-state distortion increases (BLA of 0.022 and 0.019, respectively). These evolutions have been previously reported and explained in terms of the “loose-bolt” or Brunings–Corwin effect, in which the lower planarity by constrained geometries implies a lower resonance energy, thereby placing the excited and ground states energetically closer.^[11] Therefore, the strong bending of the chromophore in the excited state should be the reason for the important shift of the emission band towards higher energies and, at the same time, the reason for the reduction of the fluorescence efficiency in those compounds that bear *tert*-butyl groups at the 2- and 6-positions (PM597 and mainly PM597-8C9). In these dyes, further replacement of the fluorine atoms by acetylene (**1 e**, **2 e**) slightly ameliorates the fluorescence capacity, in line with the previously discussed *E*- and C-BODIPYs.

Lasing properties

Liquid phase

According to their absorption properties, the lasing properties of PM546 and its derivatives **1 a** and **2 a** were studied under pumping at 355 nm, whereas all the other dyes studied here were pumped at 532 nm. The dye concentrations in the lasing studies are in the millimolar range, as required by our experimental conditions of transversal excitation and strong focusing of the incoming pump radiation. In this way, the pump radiation is totally absorbed within the first millimeter of the solution to obtain an emitted laser beam with a near-circular cross-section.

To optimize the laser action, for the different dyes we first analyzed the dependence of their laser emission on dye concentration in ethyl acetate. The results obtained by varying the dye concentrations over the range 0.3 to 10 mM, depending on the dye, while keeping all the other experimental parameters constant, are collected in Table S2 in the Supporting Information. In all cases the dyes followed the typical behavior, with the lasing efficiency (defined as the ratio between the energy of the dye laser output and the pump energy incident on the sample surface) first increasing with dye concentration until a maximum value is reached. Increasing the dye concentration beyond this point results in a decrease in the lasing efficiency that can be related to reabsorption/reemission processes,

which become increasingly important as the dye concentration rises. The optimum value of the dye concentration thus determined was then used to prepare dye solutions in a number of polar protic and polar aprotic solvents to analyze the effect of the nature of the solvent on the laser properties of the different derivatives. The results obtained are collected in Table 2.

The observed lasing efficiencies within the different families of *E*- and C-BODIPYs correlate well with their photophysical properties, determined in more diluted solutions (Tables S1 and S2 in the Supporting Information): higher lasing efficiency corresponds in general to a lower nonradiative rate constant. The few exceptions to this general rule (i.e., in the PM580 family) can be understood in terms of the effect of the much higher dye concentration in the solutions utilized in the laser experiments.

The lasing properties of the new dyes follow a dependence on the solvent character similar to that exhibited by the commercial ones, with the lasing efficiencies being higher in polar aprotic solvents than in polar protic ones. It can be seen in Table 2 that, with the exception of dye **7**, in all cases the lasing efficiency of the derivatives is higher than that of the commercial parent dye. The highest lasing efficiencies were obtained with the derivatives that incorporate cyano groups (compounds **4 a–d**), which is in agreement with their photophysical behavior discussed above. The improvement in their fluorescence capacity was owing to the action of the cyano group counteracting the charge separation as a result of the increased electron-donor ability of the cyano substituent. The effect of the unsaturation degree of the alkyl chains attached to the boron atom, discussed in detail above, is also clearly indicated by the lasing data. Thus, the change from acetylene (compound **2 b**) to vinyl (**5**) and to ethyl (**7**), which produces a reversal of the electronic behavior from electron donor to acceptor as well as an increased geometrical distortion in the excited-state geometry of those compounds, takes place in accord with a decrease in the lasing efficiency following the sequence $\text{Eff}(\mathbf{2b}) > \text{Eff}(\mathbf{5}) > \text{Eff}(\mathbf{7})$ (Table 2).

An important parameter for any practical application of dye lasers is their lasing photostability under repeated pumping. Table 3 collects the data on the decrease in the laser-induced fluorescence intensity under transversal excitation of a capillary that contains dye solutions in ethyl acetate (see the Experi-

Table 3. Intensity of the laser-induced fluorescence emission (I) after 100 000 pump pulses for dyes in ethyl acetate solution.

	$\lambda_{\text{exc}} = 355 \text{ nm}$										$\lambda_{\text{exc}} = 532 \text{ nm}$														
	PM546	1a	2a	PM567	1b	2b	4a	6	7	PM580	1c	2c	PM597	1d	2d	3a	3b	4b	PM597-8C9	1e	2e	PM605	4c	PM650	4d
I [%] ^[a]	60	92	76	17	55	70	100	100	50	48	84	70	85	100	94	65	72	100	30 ^[b]	100	100	20 ^[c]	100	80	75

[a] I [%] = 100 (I/I_0), with I_0 being the initial intensity. [b] After 60 000 pump pulses. [c] After 40 000 pump pulses.

mental Section) after a given number (n) of pump pulses for both the commercial dyes and their derivatives synthesized in the present work. Dye PM546 and its derivatives **1a** and **2a** were pumped at 355 nm and at 5 Hz repetition rate. All the other dyes were pumped at 532 nm and at a 10 Hz repetition rate. The pump energy was 5 mJ in all cases. Dyes **4a–c**, which exhibited the highest lasing efficiencies and the best photophysical behavior, also were the most photostable, with their laser-induced fluorescence emission remaining at the initial level after 100 000 pump pulses. This stability is significantly higher than that of the corresponding commercial dyes (PM567, PM597, and PM605). Compound **4d**, which is the derivative of the *meso*-cyano-substituted dye PM650, exhibits lower photostability than **4a–c**, thereby reflecting the presence of the ICT state in PM650 with its harmful effects on laser performance and stability.^[8]

Bulk solid state

The excellent laser performance exhibited by the new dyes in liquid solution led us to explore their behavior as photonic materials, either in bulk as solid-state dye lasers (SSDLs) or incorporated into thin-film structures. First, we analyzed the laser behavior of the dyes incorporated into bulk solid samples cast in a cylindrical shape, thereby forming rods 10 mm in diameter and 10 mm in length (for more details, see the Supporting Information). The dyes chosen to perform this study were **4a–4c** because of their excellent lasing properties in liquid solution, and their behavior as SSDLs was compared with the corresponding parent dyes PM567, PM597, and PM605, respectively. As matrix material we chose poly(methylmethacrylate) (PMMA) because it mimics ethyl acetate, the solvent in which those dyes produced the highest lasing efficiencies (Table 2). In addition, PMMA has very high transparency, high laser damage threshold, very good chemical compatibility with the chosen dyes, and, most importantly from a practical point of view, the final production costs would be low owing to its cheapness. The dye concentration in the matrix was that which optimized the lasing efficiency in ethyl acetate (Table S2 in the Supporting Information).

Table 4 contains the lasing performance of the selected dyes. The lasing efficiencies of the C-BODIPYs enhanced significantly those obtained with the corresponding commercial parent dyes, and correlate with those obtained in liquid solution, with the efficiency of dye **4b** being the highest. These efficiencies are lower than those obtained in liquid solution, probably owing to the fact that the finishing of the surface of the solid samples relevant to the laser operation was not laser-

Table 4. Lasing properties of dyes incorporated into solid PMMA matrices.^[a]

Dye	Eff [%]	λ_1 [nm]	I_n [%]	n
PM567	34	566	30	100 000
4a	49	568	96	100 000
PM597	36	585	85	100 000
4b	53	588	100	100 000
PM605	37	595	0	65 000
4c	51	597	80	100 000

[a] Eff: lasing efficiency; λ_1 : peak laser emission wavelength; I_n [%]: intensity of the laser output after n pump pulses in the same position of the sample; I_n [%] = 100 × (I_n/I_0), with I_0 being the initial intensity.

grade, so that higher efficiencies are to be expected with laser-grade surfaces.

To assess the photostability of the new materials, we followed the evolution of their laser emission under repeated pumping in the same position of the sample at a repetition rate of 10 Hz. All three derivatives demonstrated a much higher photostability than the parent dyes, with dye **4b**, which has a laser emission that remains at the initial level after 100 000 pump pulses in the same position of the sample, exhibiting the best behavior once again. These results show that the newly developed C-BODIPYs are excellent candidates to achieve SSDLs with greatly improved performance.

Thin films

As a proof of concept, we also assessed the laser properties of the new BODIPYs operated as dye-doped polymer thin-film lasers, since over the last few years there has been a growing interest in the development of these types of devices because of their potential applications as coherent light sources suitable for integration in spectroscopic and sensing devices.^[12]

Given the outstanding laser properties shown by derivative **4b** both in liquid and the solid state, we decided to choose this dye and its parent dye PM597 as reference to develop the thin-film laser. The host matrix was PMMA. Thin films approximately 800–850 nm thick were prepared from solution by solving adequate amounts of dye and PMMA in chloroform, and the resulting solutions were spin-coated onto quartz substrates. The complete details on the sample preparation and evaluation can be found in the Supporting Information.

To obtain sufficient pump absorption and gain in the thin films, dye concentrations were selected to render an absorbance of 0.08 at the pump wavelength (532 nm). This means concentrations of 19 and 23 mM for PM597 and derivative **4b**,

respectively. Such high concentrations are prone to give rise to self-quenching^[13] (mirrored as band displacements and reduction in fluorescence quantum yield and extinction coefficients) and aggregate formation^[11] (appearance of new absorption bands). To assess the extent of both phenomena, the absorption and emission spectra of both dyes were collected (Figure 3). Even at these high dye concentrations, the absorp-

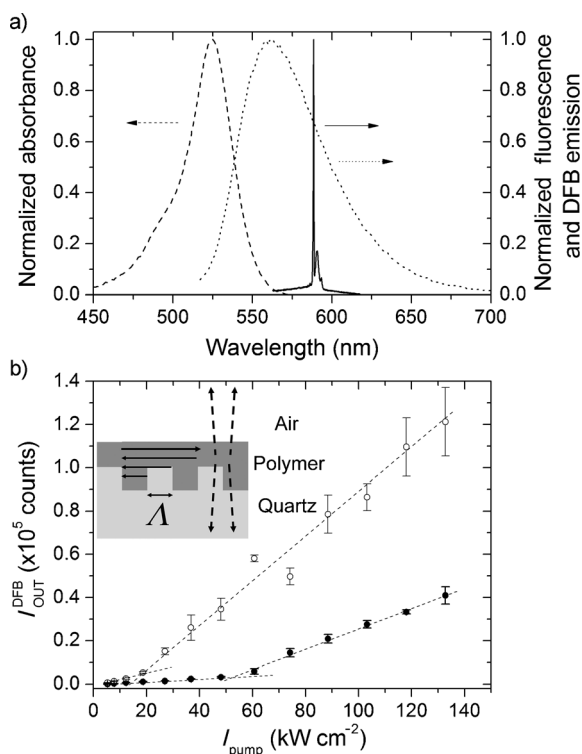


Figure 3. a) Absorption (dashed line), fluorescence ($\lambda_{\text{exc}} = 500$ nm, dotted line), and laser spectra (solid line) of derivative **4b** (23 mM) doped in PMMA. b) DFB output intensity as a function of pump intensity from thin films of commercial PM597 19 mM (filled circles) and derivative **4b** (23 mM; hollow circles) doped in PMMA. Inset: sketch of DFB laser. The arrows represent in-plane feedback owing to second-order diffraction (solid arrows) and out-coupled laser emission owing to first-order diffraction (dashed arrow).

tion and fluorescence spectra are redshifted by 2.5 and 0.5 nm, respectively, with respect to the ones registered with the dilute solutions, whereas the band shapes are unchanged (i.e., there are no new spectral features; compare Figures 2a and 3a). Nevertheless, the extinction coefficients of PM597 and derivative **4b** are reduced from 7.7 and $6.7 \times 10^4 \text{ M}^{-1} \text{ cm}^{-1}$ (2×10^{-6} M in EtOAc) to approximately 6.2 and $5.2 \times 10^4 \text{ M}^{-1} \text{ cm}^{-1}$ (≈ 20 mM in PMMA), respectively. The fluorescence quantum yield was not measured for the thin films, so it cannot be compared with the one in dilute solutions, but it will be arguably lower in the thin films. The previous facts indicate that dyes PM597 and derivative **4b** will suffer from a certain amount of self-quenching (but no aggregation) in the thin films, but we will see that it is not enough to prevent laser action from taking place.

To obtain resonant oscillation within the thin film, we made use of distributed feedback (DFB) owing to Bragg scattering in periodic structures (Figure 3b, inset).^[14] The emission wave-

length (λ_{DFB}) in DFB lasers is given by the Bragg condition $m \cdot \lambda_{\text{DFB}} \approx 2n_{\text{eff}} \Lambda$, in which m is the diffraction order in which the device operates, n_{eff} is the effective refractive index experienced by the propagating mode, and Λ is the period of the refractive index modulation (Figure 3b, inset). By working with the second-order $m = 2$, $\lambda_{\text{DFB}} \approx n_{\text{eff}} \Lambda$, the second-order diffraction provides in-plane feedback, and the laser light is diffracted out of the surface of the film perpendicular to the plane of the waveguide through first-order diffraction (Figure 3b, inset). The fundamental transverse electric (TE_0) propagating mode in waveguides approximately 800–850 nm thick with a refractive index of 1.4900 (PMMA), deposited onto a quartz substrate ($n = 1.456$), experiences an effective refractive index $n_{\text{eff}} = 1.472$.^[15] By taking into account that the resonant wavelength must be in the emission window of the selected dyes ($\lambda_{\text{DFB}} \approx 590$ nm), a substrate with modulation period $\Lambda = 400$ nm was used. For the present experiments, the quartz substrate was scribed by e-beam lithography^[16] with a squared grating (Figure 3b, inset) of period $\Lambda = 400$ nm, a duty cycle of 50%, and a depth of 100 nm. These waveguides might sustain a second propagating mode, the fundamental transverse magnetic (TM_0) mode, which does not participate in the laser process. We have excited the samples with the pump polarization parallel to the grating grooves so that the transition dipole moment of the emitting molecules and the grating wave vector (which is perpendicular to the grooves and parallel to the structure) fully overlap. This way the laser threshold of the TE_0 mode is maximally reduced.^[17]

By pumping the devices well above the threshold ($I_{\text{pump}} = 130 \text{ kW cm}^{-2}$), DFB laser emission with a linewidth of approximately 0.2 nm centered at 587.6 (PM597) and 588.5 nm (derivative **4b**) was obtained (Figure 3a), which is in agreement with the Bragg resonant wavelength expected for the chosen corrugated substrate and film thickness. The difference in the emission wavelengths is consistent with the slight changes in the sample thicknesses ($\approx \pm 50$ nm) owing to the deposition process, which modifies the effective refractive index n_{eff} and, in turn, the resonant wavelength.

Figure 3b shows the dependence of the DFB laser intensity on the pump intensity (light/light curve) for the samples doped with PM597 (filled circles) and derivative **4b** (hollow circles). From this plot one can determine the laser thresholds, which are the points in which there is a change in slope in the light/light curve. From the data in Figure 3b it can be seen that derivative **4b** not only has a lower DFB laser threshold than the parent dye (20 versus 55 kW cm^{-2}) but presents a threefold enhancement in the output intensity when pumped well above threshold ($I_{\text{pump}} = 130 \text{ kW cm}^{-2}$), which is in agreement with the results obtained in bulk and liquid media.

Conclusion

We have successfully designed and synthesized new *E*- and *C*-BODIPYs through a straightforward protocol from the commercially available BODIPYs. The experimental trends of the fluorescence efficiencies with the electron-donor/-acceptor properties of the substituents (Hammett parameter) at the boron

atom are properly rationalized by means of theoretical calculations in terms of the charge distribution and aromaticity (BLA) and excited-state geometry. Accordingly, the replacement of fluorine atoms by electron-acceptor moieties improves the fluorescence performance of commercial BODIPYs, whereas the electron-donor ones are harmful and lead to distorted geometries that enhance the nonradiative relaxation pathways.

The newly synthesized *E*- and *C*-BODIPYs exhibit enhanced laser action with respect to their parent dyes, both in liquid and in the solid phase, with the lasing properties correlating well with their photophysical behavior. The highest lasing efficiencies, up to 73% in the liquid phase and up to 53% in solid matrix under demanding transversal pumping conditions, were obtained with the derivatives that incorporated cyano groups at the boron center. These same derivatives also proved to be the most photostable, with stabilities significantly higher than that of the corresponding commercial dyes. Particularly relevant was the behavior of dye **4b** in solid matrix, which exhibited a very high lasing stability, with the laser emission remaining at the initial level after 100 000 pump pulses in the same position of the sample at 10 Hz repetition rate.

DFB laser emission was demonstrated with organic films that incorporated parent dye PM597 and its derivative **4b**, deposited onto quartz substrates engraved with appropriate periodical structures. Derivative **4b** exhibited a laser threshold lower than that of the parent dye as well as lasing intensities up to three orders of magnitude higher.

These results show that the newly developed *E*- and *C*-BODIPYs are excellent candidates to achieve SSDLs with much improved performance.

Experimental Section

BODIPY dyes PM546, PM567, PM580, PM597, P597-8C9, PM605, and PM650 were purchased from Exciton and used as received (purity >99%). Experimental procedures, characterization, and NMR spectra of the new dyes as well as quantum mechanical simulations, preparation of laser samples, and methods followed to analyze the photophysical and laser properties in the liquid and solid phase are described in detail in the Supporting Information.

Acknowledgements

This work was supported by the Ministerio de Economía y Competitividad (projects MAT2010-20646-C04-01, MAT2010-20646-C04-02, and MAT2010-20646-C04-04) and Gobierno Vasco (project IT339-10), which is also thanked by I.E. for a contract (SPE12UN140 and SPE13UN). G.D.-S thanks the MICINN for a predoctoral scholarship (FPI, cofinanced by Fondo Social Europeo).

Keywords: donor–acceptor systems · dyes/pigments · laser chemistry · photophysics · polymers

[1] a) *Dye Laser Principles* (Eds.: F. J. Duarte, L. W. Hillman), Academic Press, New York, 1990; b) *Tunable Lasers Handbook* (Ed.: F. J. Duarte), Academic Press, New York, 1995; c) *Tunable Laser Applications*, 2nd ed. (Ed.: F. J.

Duarte), CRC, Boca Raton, 2009; d) I. D. W. Samuel, G. A. Turnbull, *Chem. Rev.* 2007, 107, 1272–1295.

- [2] a) M. Benstead, G. H. Mehl, R. W. Boyle, *Tetrahedron* 2011, 67, 3573–3601; b) Y. Xiao, D. Zhang, X. Qian, A. Costela, I. García-Moreno, V. Martín, M. E. Pérez-Ojeda, J. Bañuelos, L. Gartzia, I. López Arbeloa, *Chem. Commun.* 2011, 47, 11513–11515; c) J. Bañuelos, V. Martín, C. F. A. Gómez-Duran, I. J. Arroyo Cordoba, E. Peña-Cabrera, I. García-Moreno, A. Costela, M. E. Pérez-Ojeda, T. Arbeloa, I. López Arbeloa, *Chem. Eur. J.* 2011, 17, 7261–7270; d) G. Duran-Sampedro, A. R. Agarrabeitia, I. García-Moreno, A. Costela, J. Bañuelos, T. Arbeloa, I. López Arbeloa, J. L. Chiara, M. J. Ortiz, *Eur. J. Org. Chem.* 2012, 6335–6358.
- [3] a) T. Bura, P. Retailleau, R. Ziessel, *Angew. Chem.* 2010, 122, 6809–6813; *Angew. Chem. Int. Ed.* 2010, 49, 6659–6663; b) C. Thivierge, A. Loudet, K. Burgess, *Macromolecules* 2011, 44, 4012–4015; c) C. A. Osorio-Martínez, A. Urías-Benavides, C. F. A. Gómez-Durán, J. Bañuelos, I. Esnal, I. López Arbeloa, E. Peña-Cabrera, *J. Org. Chem.* 2012, 77, 5434–5438; d) Y. Yang, Q. Guo, H. Chen, Z. Zhou, Z. Guo, Z. Shen, *Chem. Commun.* 2013, 49, 3940–3942.
- [4] a) A. Loudet, K. Burgess, *Chem. Rev.* 2007, 107, 4891–4932; b) R. Ziessel, G. Ulrich, A. Harriman, *New J. Chem.* 2007, 31, 496–501; c) G. Ulrich, R. Ziessel, A. Harriman, *Angew. Chem.* 2008, 120, 1202–1219; *Angew. Chem. Int. Ed.* 2008, 47, 1184–1201; d) F. L. Arbeloa, J. Bañuelos, V. Martínez, T. Arbeloa, I. L. Arbeloa, *Trends Phys. Chem.* 2008, 13, 101–122; e) A. C. Benniston, G. Copley, *Phys. Chem. Chem. Phys.* 2009, 11, 4124–4131; f) N. Boens, V. Leen, W. Dehaen, *Chem. Soc. Rev.* 2012, 41, 1130–1172; g) S. G. Awuah, Y. You, *RSC Adv.* 2012, 2, 11169–11183; h) A. Kamkaew, S. H. Lim, H. B. Lee, L. V. Kiew, L. Y. Chung, K. Burgess, *Chem. Soc. Rev.* 2013, 42, 77–88.
- [5] For example, see: a) S.-L. Niu, C. Massif, G. Ulrich, P.-Y. Renard, A. Romieu, R. Ziessel, *Chem. Eur. J.* 2012, 18, 7229–7242; b) A. Kaloudi-Chantzea, N. Karakostas, F. Pittler, C. P. Raptopoulou, N. Glezos, G. Pistolis, *Chem. Commun.* 2012, 48, 12213–12215; c) G. Durán-Sampedro, A. R. Agarrabeitia, L. Cerdán, M. E. Pérez-Ojeda, A. Costela, I. García-Moreno, I. Esnal, J. Bañuelos, I. López Arbeloa, M. J. Ortiz, *Adv. Funct. Mater.* 2013, 23, 4195–4205 and references cited therein; d) K. K. Jagtap, N. Shivran, S. Mula, D. B. Naik, S. K. Sarkar, T. Mukherjee, D. K. Maity, A. K. Ray, *Chem. Eur. J.* 2013, 19, 702–708; e) R. Ziessel, G. Ulrich, A. Haefele, A. Harriman, *J. Am. Chem. Soc.* 2013, 135, 11330–11344.
- [6] C. Goze, G. Ulrich, R. Ziessel, *Org. Lett.* 2006, 8, 4445–4448.
- [7] L. Yang, R. Simionescu, A. Lough, H. Yan, *Dyes Pigm.* 2011, 91, 264–267.
- [8] F. Lopez Arbeloa, J. Bañuelos, V. Martínez, T. Arbeloa, I. Lopez Arbeloa, *Int. Rev. Phys. Chem.* 2005, 24, 339–374.
- [9] I. García-Moreno, L. Wang, A. Costela, J. Bañuelos, I. Lopez Arbeloa, Y. Xiao, *ChemPhysChem* 2012, 13, 3923–3931.
- [10] G. Bourhill, J. L. Bredas, L. T. Cheng, S. R. Marder, F. Meyers, J. W. Perry, B. G. Tiemann, *J. Am. Chem. Soc.* 1994, 116, 2619–2620.
- [11] a) L. J. E. Hofer, R. J. Grabenstetter, E. O. Wiig, *J. Am. Chem. Soc.* 1950, 72, 203–209; b) M. Dekhtyar, W. Rettig, M. Szczepan, *Phys. Chem. Chem. Phys.* 2000, 2, 1129–1136; c) J. Bañuelos Prieto, F. López Arbeloa, V. Martínez, T. Arbeloa, I. López Arbeloa, *J. Phys. Chem. A* 2004, 108, 5503–5508; d) A. Costela, I. García-Moreno, M. Pintado-Sierra, F. Amat-Guerri, R. Sastre, M. Liras, F. López Arbeloa, J. Bañuelos Prieto, I. López Arbeloa, *J. Phys. Chem. A* 2009, 113, 8118–8124.
- [12] C. Grivas, M. Pollnau, *Laser Photonics Rev.* 2012, 6, 419–462.
- [13] F. López Arbeloa, T. López Arbeloa, I. López Arbeloa, I. García-Moreno, A. Costela, R. Sastre, F. Amat-Guerri, *Chem. Phys.* 1998, 236, 331–341.
- [14] T. T. Vu, M. Dvorko, E. Y. Schmidt, J.-F. Audibert, P. Retailleau, B. A. Trofimov, R. B. Pansu, G. Clavier, R. Méallet-Renault, *J. Phys. Chem. C* 2013, 117, 5373–5385.
- [15] Online 1D multilayer slab waveguide mode solver by Dr. Manfred Hammer, <http://wwwhome.math.utwente.nl/hammer/oms.html>.
- [16] G. A. Turnbull, A. Carleton, G. F. Barlow, A. Tahraoui, T. F. Krauss, K. A. Shore, I. D. W. Samuel, *J. Appl. Phys.* 2005, 98, 023105.
- [17] D. Wright, E. Brasselet, J. Zyss, G. Langer, W. Kern, *J. Opt. Soc. Am. B* 2004, 21, 944–950.

Received: September 10, 2013

Revised: November 18, 2013

Published online on January 22, 2014

Carboxylates versus Fluorines: Boosting the Emission Properties of Commercial BODIPYs in Liquid and Solid Media

Gonzalo Durán-Sampedro, Antonia R. Agarrabeitia, Luis Cerdán, M. Eugenia Pérez-Ojeda, Angel Costela, Inmaculada García-Moreno,* Ixone Esnal, Jorge Bañuelos, Iñigo López Arbeloa, and María J. Ortiz*

A new and facile strategy for the development of photonic materials is presented that fulfills the conditions of being efficient, stable, and tunable laser emitters over the visible region of spectrum, with the possibility of being easily processable and cost-effective. This approach uses poly(methyl methacrylate) (PMMA) as a host for new dyes with improved efficiency and photostability synthesized. Using a simple protocol, fluorine atoms in the commercial (4,4-difluoro-4-bora-3a,4a-diaza-s-indacene) (F-BODIPY) by carboxylate groups. The new O-BODIPYs exhibit enhanced optical properties and laser behavior both in the liquid and solid phases compared to their commercial analogues. Lasing efficiencies up to 2.6 times higher than those recorded for the commercial dyes are registered with high photostabilities since the laser output remain at 80% of the initial value after 100 000 pump pulses in the same position of the sample at a repetition rate of 30 Hz; the corresponding commercial dye entirely loses its laser action after only 12 000 pump pulses. Distributed feedback laser emission is demonstrated with organic films incorporating new O-BODIPYs deposited onto quartz substrates engraved with appropriated periodical structures. These dyes exhibit laser thresholds up to two times lower than those of the corresponding parent dyes with lasing intensities up to one order of magnitude higher.

1. Introduction

Presently, the development of photonic materials fulfilling the conditions of being efficient, stable and tunable emitters over the visible region of the electromagnetic spectrum, with the possibility of being easily processable, and cost-effective, is an area of active research driven by the wide range of possible practical applications. Over the last years, a vast amount of work has been carried out on materials engineering, designing and synthesizing semiconductor polymers and organic, hybrid and inorganic systems nano- and mesostructured, doped with organic dyes and quantum dots.^[1] Nevertheless, despite this extensive activity up to now none of the obtained materials happens to meet all the above requirements at the same time.

Our research group has contributed greatly to this effort, developing solid state dye lasers (SSDL) both in bulk matrices and waveguiding thin films, on the basis of organic and/or hybrid materials doped with dyes with emission covering the

spectral region from 550 up to 730 nm.^[2] Albeit we have demonstrated lasing efficiencies as high as 60% in some particular case, the materials we have developed exhibit on average efficiencies of about 30% with photostabilities that being higher than those reported by other researchers, demand nonetheless an improvement in order to guarantee the implementation of these materials in practical applications. In addition, our work has shown that there is not an universal material that optimizes the lasing behavior of all the different dyes, but that a specific dye/host combination is needed for each chromophore, which is determined by the photophysical and photochemical chromophore's properties.

Here, we propose a new and facile strategy for the development of laser materials economically affordable with optimized emission properties in the visible region of the spectrum. This approach implies the utilization of a commercial polymer (poly(methyl methacrylate), PMMA) competitive in cost and easily processable, as host for dyes with improved efficiency and photostability. The chromophores are new derivatives of a

G. Durán-Sampedro, Prof. A. R. Agarrabeitia,
Prof. M. J. Ortiz
Departamento de Química Orgánica I
Facultad de Ciencias Químicas
Universidad Complutense
28040, Madrid, Spain
E-mail: mjortiz@quim.ucm.es



Dr. L. Cerdán, M. E. Pérez-Ojeda, Prof. A. Costela,
Prof. I. García-Moreno
Departamento de Sistemas de Baja Dimensionalidad
Superficies y Materia Condensada
Instituto Química-Física "Rocasolano"
C.S.I.C., Serrano 119, 28006 Madrid, Spain
E-mail: i.garcia-moreno@iqfr.csic.es
I. Esnal, Dr. J. Bañuelos, Prof. I. López Arbeloa
Departamento de Química Física
Facultad de Ciencias y Tecnología
Universidad del País Vasco-EHU
Apartado 644, E-48080-Bilbao, Spain

DOI: 10.1002/adfm.201300198

single family of commercial dyes obtained following a simple and general synthesis protocol, which exhibits high reaction yields. The selected family of dyes was that of the so-called *F*-BODIPYs (4,4-difluoro-4-bora-3a,4a-diaza-*s*-indacene), developed in the late 1980s and early 1990s by Boyer and co-workers, because they exhibit high fluorescence quantum yields, intense absorption, and tunable emission wavelength^[3] as well as high chemical versatility to be functionalized.^[2b,4] Currently, these dyes have numerous applications such as fluorescent probes in biological systems, photosensitizers for photodynamic therapy, and as materials for incorporation into electroluminescent devices.^[5]

Among the numerous modifications in the BODIPY core, the replacement of one or both of the fluorine atoms in *F*-BODIPYs has become an active area. Thus, a wide variety of BODIPY dyes have been synthesized via fluorine displacement by alkyl or aryl derivatives (*C*-BODIPY),^[5a-c,6] ethynyl groups (*E*-BODIPY),^[5a-c,6e,7] and alkoxy or aryloxy derivatives (*O*-BODIPY),^[5a-c,6c,6f-g,8] including *O*-chelated BODIPYs.^[9] In addition, new types of boron modifications as borenium cations,^[10] CN-BODIPY,^[6a] *H*-BODIPY^[10] and *Cl*-BODIPY,^[6d,6g-h] have also been reported.

In one recent publication the authors evaluated the replacement of one or both of the fluorine atoms in 4,4-difluoro-1,3,5,7-tetramethyl-4-bora-3a,4a-diaza-*s*-indacene by acetoxy (AcO) groups in order to study the effect of an electron-withdrawing carboxylate on the boron atom in BODIPY, and they found that mono- and di-AcO substituted BODIPYs exhibited excellent fluorescence quantum yields and photostabilities.^[11] Furthermore, the AcO modification on boron resulted in significantly improved water solubility, which is highly desirable for biological applications.^[11] In another report about the stability of the BODIPY fluorophore under acidic and basic conditions, a 4,4-dichloroacetoxy BODIPY was formed when 4,4-dimethoxy-2,6-diethyl-1,3,5,7-tetramethyl-4-bora-3a,4a-diaza-*s*-indacene was mixed with an excess of dichloroacetic acid in CH₂Cl₂.^[6f] However, no fluorescence study of this compound was explored.

Based on these observations, in the present work we report the synthesis and emission properties characterization of a library of *O*-BODIPYs 1–10 (Figure 1) from commercially available BODIPYs, in which two carboxylate (acetoxy or trifluoroacetoxy) groups are connected to the boron center in the place of the fluorine atoms. It is shown that these dyes are highly fluorescent and exhibit enhanced laser action with respect to their *F*-BODIPY analogues, both in liquid solution and solid phase. To investigate in depth the influence of the acetoxy substitutions on the BODIPY emission properties we have also synthesized, as a proof of concept, new *O*-BODIPYs via fluorine displacement by other carboxylate groups with different electronic character such as acryloyloxy, propioloyloxy, methoxy, or 4-nitrophenoxy groups (11–14).

2. Results and Discussion

2.1. Synthesis

BODIPY dyes 1–14 were successfully obtained from commercially available dyes^[12] PM546, PM567, PM597, PM605 and PM650 through nucleophilic substitution reactions of fluorine

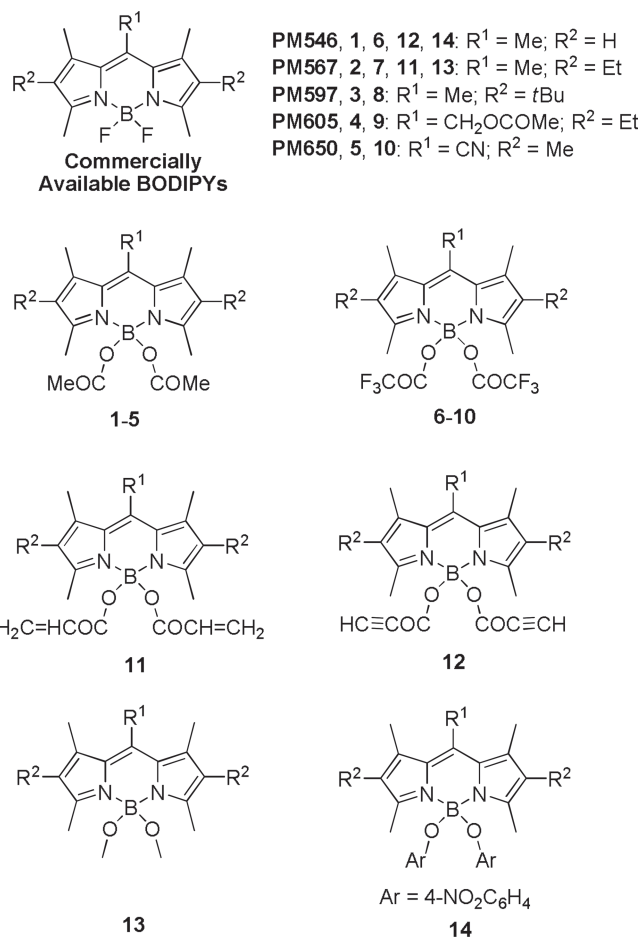
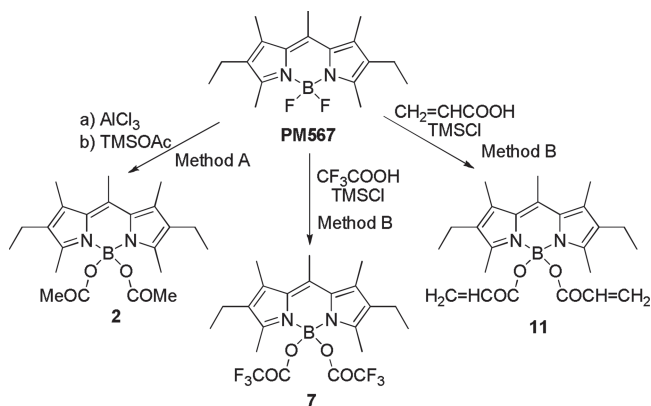


Figure 1. Molecular structures of dyes synthesized herein and their parent dyes.

atoms in the BF₂-group. Thus, 4,4-diacetoxy BODIPYs 1,2,4 and 5 were prepared with moderate yields by treating 20 equiv of TMSOAc with 1 equiv of PM546, PM567, PM605 or PM650, respectively, in presence of 3–4 equiv of AlCl₃ as Lewis acid (method A). In all these cases the monosubstituted derivative is not isolated. The dye 3 could not be synthesized by this method, so that an alternative procedure (method B) was used for their preparation involving the generation in situ of TMSOAc from acetic acid and TMSCl, in the absence of AlCl₃. Method B was also used in the synthesis of 4,4-bis(trifluoroacetoxy) BODIPYs 6,7 and 9 by adding of TMSOCOCF₃, generated in situ from trifluoroacetic acid and TMSCl, to the BODIPYs PM546, PM567 and PM605, respectively. 4,4-Bis(acryloyloxy) BODIPY 11 was prepared by reacting of PM567 with TMSOCOCH = CH₂, generated in situ from acrylic acid and TMSCl (method B), and this same method was used in the preparation of 12 from PM546 with propargylic acid and TMSCl. Scheme 1 shows the synthesis of the dyes 2,7 and 11 from commercial BODIPY PM567.

Surprisingly, treatment of PM597 with TMSOCOCF₃ in 1,2-dichloroethane resulted in a mixture of 15 (10%) and 6 (22%) by loss of one or both *tert*butyl groups present in the starting compound (Scheme 2). Therefore, we were decided to develop an alternative procedure (method C). Thus, BODIPY8



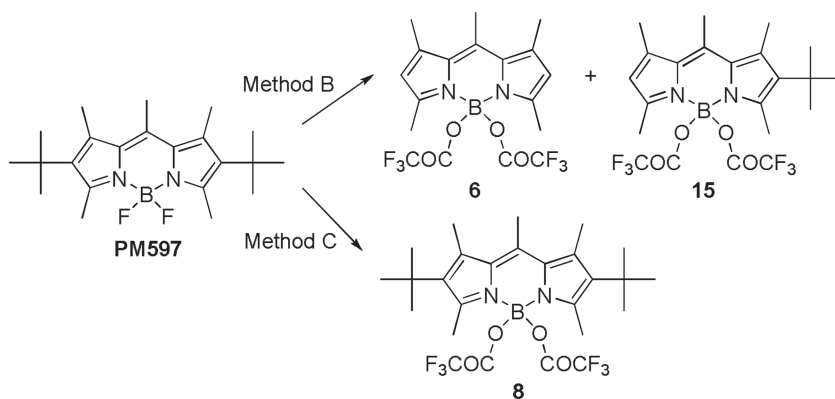
Scheme 1. Synthetic routes of derivatives **2**, **7**, and **11** from parent dye PM567.

was achieved by treatment of BODIPY PM597 with AlCl_3 in 1,2-dichloroethane and subsequent addition of TMSOCOCF_3 , generated in situ as above (Scheme 2). Similarly, compound **10** was successfully obtained from PM650 with moderate yield.

In addition, two other analogues, 4,4-dimethoxy **13**,^[6f] and 4,4-bis(4-nitrophenyl) **14** were synthesized according to procedure described in the literature or through the method A mentioned above.

2.2. Photophysical Properties

The selected commercial BODIPY laser dyes span a wide region of the visible spectrum; hence, the emission can be tuned from the green-yellow to the red as it is illustrated in **Figure 2**. The progressive bathochromic shift of the spectral bands is due to inductive donor effects of the alkyl groups at positions 2 and 6 (PM567 and PM597 vs PM546) or the electron withdrawing character of methylenacetoxo (PM605) or cyano (PM650) groups at position 8, which lead to a net stabilization of the LUMO molecular orbital.^[4a] Except for the PM650 derivative, where a fluorescence quenching intramolecular charge transfer state is operative,^[4a] these BODIPYs outstand by their bright and stable emission. For this reason, the set of derivatives from PM650 will be discussed later on.



Scheme 2. Synthetic routes of derivatives **6**, **8**, and **15** from parent dye PM597.

At first sight, the replacement of the fluorine atoms by alkoxy or aryloxy derivatives should have minor influence on the photophysical properties of the chromophore since the BF_2 group does not take part in the delocalized π -system and acts as a bridge to keep the planarity and rigidity of the indacene core. For this reason, as is shown in **Table 1**, the positions of the spectral bands of the new *O*-BODIPYs are almost those of their respective *F*-BODIPY counterparts. Besides, the solvent effect on the photophysical properties follows the normal trends previously described for *F*-BODIPYs (Table S1–S4 in the Supporting Information); i.e., small hypsochromic spectral shifts with the solvent polarity and low dependency of the fluorescence quantum yield with the solvent characteristics.

Moreover, and as a common rule except for the dyes **13** and **14** that will be discussed later on, the fluorescence quantum yield and lifetime of the new *O*-BODIPYs increase with respect to the commercial ones, ameliorating the emission properties of the commercial *F*-BODIPYs, which were considered as a benchmark in fluorescence and laser behavior in the middle energetic part of the visible spectrum (Table 1).^[6b,11] The enhancement of the emission properties of the *O*-BODIPYs depends on the electronic character of the carboxylate groups connected to the boron center in the following manner: while the fluorine displacement by the electron withdrawing acetoxy group (**1-4**) maintains or slightly improves the high fluorescent ability of the BODIPYs, a further increase in the electron acceptor character of the substituent via the inclusion of trifluoroacetoxy groups (**6-9**) leads to an even more significant improvement on the fluorescence quantum yield, which reaches nearly the unit in some solvents. Moreover, the same statement holds true for the attachment of other electron withdrawing carboxylate groups, such as acryloyloxy (**11**) or propioloyloxy (**12**).

It is noteworthy to remark the important improvement achieved in the fluorescent efficiency of PM597 through the replacement of fluorine atoms by carboxylate groups, thus, its fluorescence quantum yield increases from 0.43 up to 0.58 and 0.76 for its **3** and **8** *O*-BODIPYs derivatives, respectively (Table 1). The photophysical properties of the parent PM597 are controlled by the sterical hindrance induced by the *tert*-butyl groups at positions 2 and 6, which twists the planarity of the chromophore leading to an increase of both the internal conversion probability and the Stokes shift with respect to other planar BODIPYs such as, for instance, PM567. The **3** and **8** derivatives exhibit lower non-radiative rate constant than PM597, which could be related to the influence of the carboxylate group in the molecular geometry.

Overall, quantum mechanics calculations predict that the carboxylates are symmetrically disposed up and down the indacene core, both in the ground and excited state (**Figure 3**). Whereas the planarity of most of the *O*-BODIPYs remains the same regarding to their parent *F*-BODIPYs, a slight increase in the planarity is predicted for the PM597 derivatives since the dihedral angles, accounting for the pyrrole disposition with respect to the central ring, increase in around 3° in the excited state. However,

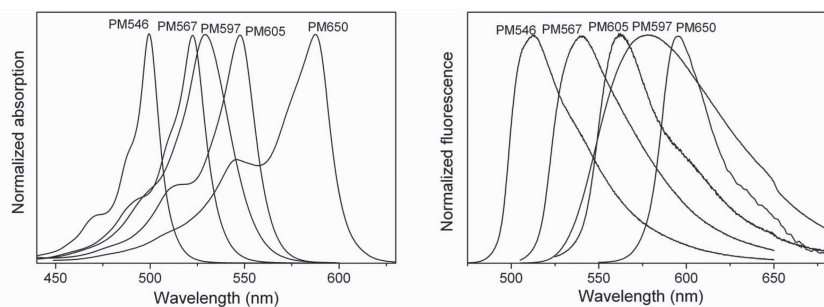


Figure 2. Normalized absorption and fluorescence spectra of commercial *F*-BODIPYs in a common solvent (cyclohexane).

such enhancement seems to be not strong enough to explain the important reduction observed in the internal conversion processes upon displacement of fluorine by carboxylate in the PM597 dye.

On the other hand, the photophysics behavior of the new *O*-BODIPY dyes depends strongly on the electronic character of the carboxylates substituent. Thus, the replacement of fluorine in PM567 by an electron donor methoxy group (**13**) has the opposite effect on the photophysical behavior with respect to that induced by electron withdrawing carboxylates since the presence of the $-\text{OCH}_3$ groups leads to a small reduction in the fluorescence quantum yield of the chromophore.

The opposite influence of the carboxy groups in the fluorescence quantum yield depending on their electronic character was analyzed in terms of the charge distribution in the corresponding excited states (Figure S1–S4 in the Supporting Information). In fact, the linkage of carboxylates to the boron atom implies a rearrangement in the chromophoric charge

distribution, as it is reflected for PM567 in Figure 3. The acetoxy group behaves as an electron acceptor group (Hammett parameter, $\sigma_p = 0.31$).^[13] Thus, its attachment to the boron leads to an increase of the positive charge in this last atom, while the oxygen acquires a negative charge much higher than of the fluorine in the corresponding *F*-BODIPYs. Such trend is more pronounced as the electron withdrawing character of the carboxylate substituent increases, for instance, in the case of the trifluoroacetoxy group ($\sigma_p = 0.46$). However, the replacement of fluorine atoms by electron donor methoxy groups ($\sigma_p = -0.27$) leads to the opposite behavior; the positive charge in the boron atom decrease and the oxygen results less negatively charged (Figure 3).

This rearrangement of the electronic charges around the boron atom determines the charge distribution of the chromophore (usually described as a cyclic cyanine). In fact, the negative charge of the aromatic nitrogen atoms decreases upon the presence of carboxylate groups (Figure 3 and Figure S1–S4 in the Supporting Information). This trend suggests that the electron lone pair is less localized in the nitrogen and tends to be more delocalized through the cyanine system. Furthermore, the charge alternation is softened, which is also indicative of higher delocalization. In addition, the aromatic character of the chromophore can be roughly evaluated by means of the Bond Length Alternation (BLA) parameter, which is defined as the difference between the average carbon-carbon bond lengths of alternative single and double bonds in the chromophoric π -system.^[14] Regarding the corresponding values for

Table 1. Photophysical properties of commercial *F*-BODIPYs (PM546, PM567, PM597 and PM605) and their corresponding *O*-BODIPYs in cyclohexane; absorption (λ_{ab}) and fluorescence (λ_{fl}) wavelength at the maximum, Stokes shift ($\Delta\nu_{St}$), molar absorption at the maximum (ϵ_{max}), fluorescence quantum yield (ϕ) and lifetime (τ), and radiative (k_{fl}) and non-radiative (k_{nr}) rate constants. The full photophysical data in several media are collected in the Supporting Information (Table S1–S4).

	λ_{ab} [nm]	ϵ_{max} [$10^4 \text{ M}^{-1} \text{ cm}^{-1}$]	λ_{fl} [nm]	$\Delta\nu_{St}$ [cm^{-1}]	ϕ	τ [ns]	k_{fl} [10^{-8} s^{-1}]	k_{nr} [10^{-8} s^{-1}]
PM546	499.5	9.7	509.5	400	0.91	5.23	1.74	0.17
1	501.0	9.5	508.0	275	0.91	5.40	1.68	0.17
6	502.0	10.2	509.5	295	0.95	5.52	1.72	0.10
12	502.0	8.2	511.0	350	0.99	5.62	1.76	0.02
14	499.5	11.6	511.0	450	0.89	5.94	1.50	0.18
PM567	522.5	9.3	537.0	520	0.88	5.60	1.57	0.21
2	522.0	8.5	537.0	535	0.84	5.71	1.47	0.28
7	525.5	7.8	541.5	565	0.94	6.25	1.50	0.10
11	523.5	8.1	541.0	620	0.90	5.98	1.50	0.17
13	522.0	8.0	539.5	620	0.81	5.64	1.44	0.34
PM597	529.0	8.1	571.0	1395	0.43	3.91	1.10	1.46
3	530.5	7.0	573.0	1400	0.58	4.58	1.27	0.92
8	532.5	5.4	571.0	1265	0.76	5.99	1.27	0.40
PM605	547.5	8.6	561.0	435	0.74	6.27	1.18	0.41
4	548.5	8.0	563.0	470	0.76	6.37	1.19	0.38
9	551.0	7.8	564.0	420	0.80	6.99	1.14	0.28

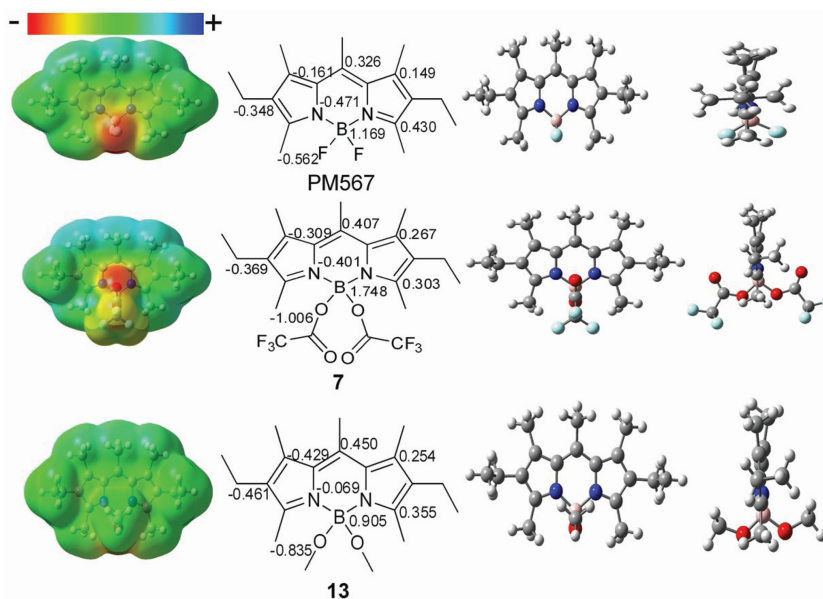


Figure 3. Electrostatic potential maps, ChelpG charge distribution (the corresponding data for the symmetrical counterpart in the chromophore are not included) in the excited state and the corresponding excited state geometries (at two different views) for PM567 dye and its derivatives **7** (trifluoroacetoxy) and **13** (methoxy). The electronic density distributions for all the derivatives are collected in Figure S1–S5 in the Supporting Information.

the *F*-BODIPYs and their respective *O*-BODIPYs, listed in Figure S1–S4 in the Supporting Information, the BLA parameter for dyes bearing acetoxy groups remains similar to that of their parent BODIPY (i.e., compound **2** (0.0227) vs PM567 (0.0222), in Figure S2, Supporting Information), but decreases for the derivatives bearing trifluoroacetoxy groups (i.e., compound **7** (0.0192) in Figure S2, Supporting Information). This tendency of the BLA parameter points out a higher aromaticity of the chromophore induced by the presence of electron withdrawing carboxylates, in good concordance with the enhancement of the fluorescence quantum yield experimentally observed. However, the presence of methoxy groups with electron donor character leads to an enhancement in the BLA parameter (0.0260 for compound **13** in Figure S2, Supporting Information) in line with the recorded decrease in the fluorescence efficiency. This evolution is even more pronounced for the PM597 derivatives **3** and **8** (0.0225, 0.0217 and 0.0181, respectively in Figure S3 in the Supporting Information). This fact, together with the slight increase in its planarity, could explain why this dye is the most sensitive system to the fluorine replacement by carboxylates.

On the other hand, aryloxy groups (4-nitrophenoxy) have also been attached to the boron of PM546 (compound **14**), replacing the fluorine atoms. While in apolar solvents the fluorescence efficiency keeps similar to the parent PM546 (Table 1), an increase in the polarity of the surrounding environment implies a progressive decrease of the fluorescence quantum yield, becoming almost negligible in the most polar solvents (from 0.89 in *c*-hexane to 0.05 in F_3 -ethanol, Table S1 in the Supporting Information). At the same time, as is reflected in Figure 4, the fluorescence decay gets faster and eventually biexponential with a dominating lifetime of 0.18 ns, which reaches a contribution higher than 97% in F_3 -ethanol (Table S1

in the Supporting Information). The presence of such fast lifetime indicates the presence of an extra non-radiative deactivation pathway, which is getting a higher influence as the solvent polarity increases and leads to very low fluorescence quantum yield in those media, in contrast to the rest of related *O*-BODIPYs where the fluorescence efficiency remains almost constant regardless of the solvent properties. Such fluorescence quenching in compound **14** and mainly in polar media suggests the activation of an intramolecular charge transfer (ICT) state from the BODIPY core to the nitro group, which is characterized by its strong electron withdrawing ability ($\sigma_p = 0.78$). In fact, the presence of ICT states induced by the direct attachment of nitro groups to the BODIPY core have been previously reported.^[15] Therefore, although we have concluded before that the replacement of fluorine by electron withdrawing alcoxy

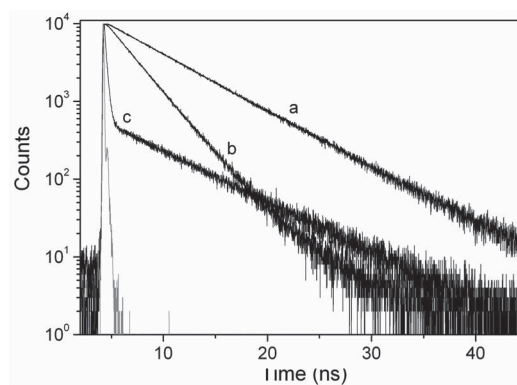


Figure 4. Fluorescence decay curves of compound **14** in a) cyclohexane, b) methanol, and c) trifluoroethanol.

Table 2. Photophysical properties of the PM650 and its corresponding O-BODIPYs (**5** and **10**) in cyclohexane and methanol. The full photophysical data in several media are collected in Supporting Information (Table S5).

	λ_{ab} [nm]	ϵ_{max} [10 ⁻⁴ M ⁻¹ cm ⁻¹]	λ_{fl} [nm]	ΔV_{St} [cm ⁻¹]	ϕ	τ [ns]	k_{fl} [10 ⁻⁸ s ⁻¹]	k_{nr} [10 ⁻⁸ s ⁻¹]
PM650								
c-hexane	589.5	5.3	599.5	290	0.36	4.67	0.77	1.37
Methanol	587.5	4.1	609.0	605	0.060	1.29	0.46	7.29
5								
c-hexane	588.5	4.5	600.5	340	0.39	5.19	0.75	1.17
Methanol	589.0	3.7	610.0	585	0.073	1.54 ^{a)}	0.47	6.02
10								
c-hexane	591.0	3.8	599.0	225	0.47	5.99	0.78	0.88
Methanol	591.0	2.7	609.5	515	0.11	2.23	0.49	3.99

^{a)}Main component (>98%) of the biexponential fit of the decay.

ameliorates the fluorescence of the dye, if the electron acceptor capacity of these substituent groups is too high, it could give rise to an extra non-radiative pathway (ICT), which quenches the fluorescence emission mainly in polar media.

Whereas all the above commented F-BODIPYs, were characterized by a bright fluorescence regardless of the media, the emission properties of the PM650 are limited by the presence of an ICT state induced by the electron withdrawing cyano group ($\sigma_p = 0.66$) attached at position 8 (in a similar way to compound **14**).^[4a] Thus, the fluorescence efficiency of this fluorophore, especially in polar solvents, is lower than that exhibited by other commercial BODIPYs (Table 2 and Figure S5 in the Supporting Information). Furthermore, it was previously reported the unstability of PM650 dye in certain solvents (most of them characterized as electron donors)^[16] since its solutions were completely bleached after some hours or days, depending of the solvent nature, as result of a specific interaction of the cyano group and those solvents. For this reason, all data listed for the derivatives of PM650 have been registered just after sample preparation.

In general, the replacement of the fluorine by carboxylates in PM650 follows the above commented trends for alkylated BODIPYs; thus, the presence of acetoxy (**5**) and mainly trifluoroacetoxy (**10**) improves the fluorescence capacity of the dye (Table 2). However, the presence of the quenching ICT process limits the fluorescence performance of these derivatives in polar media, and, although the fluorescence quantum yield is ameliorated it is still too low (around 0.1 in methanol in the best case, Table S5 in the Supporting Information) to achieve good laser performance. Whereas the presence of such quenching ICT state is harmful for the laser performance, it enables to apply PM650 and their O-BODIPYs derivatives as polarity sensors. The stabilization of the ICT state depends markedly of the solvent polarity, thus, the polarity of the surrounding environment can be monitored by means of the decrease in the fluorescence efficiency in such media or the change in the fluorescence colour (followed just with a naked eye) if the ICT state emits.^[17] On the other hand, compounds **5** and **10** show also a lack of stability, even more pronounced than in the parent commercial PM650 and after few hours most of the solutions are

bleached. Overall, the HOMO molecular orbital is stabilized when changing from F-BODIPYs to O-BODIPYs. Nevertheless, the carbon of the cyano gets a higher positive charge (from 0.463 in PM650 to 0.511 and 0.516 in compounds **5** and **10**, respectively, Figure S5 in the Supporting Information), whereas the nitrogen gets a slight higher negative charge. Therefore, the specific interaction of the cyano (through its carbon) with electron donor solvents should be more feasible in the O-BODIPYs, explaining its lower chemical stability than the reference PM650.

Summarizing, the replacement in the BODIPY core of fluorine atoms by electron withdrawing carboxylates is a good strategy to improve the fluorescence behavior, since it leads to more aromatic chromophores and, consequently, an enhanced laser action both in liquid and solid phase is expected.

2.2.1. pH-Dependence and Solubility Studies

To accomplish the characterization of the new O-BODIPYs their pH stability and water solubility were carefully studied. As a proof of concept, we detail the results achieved for the derivatives **1** and **6** related to the behavior exhibited by their parent dye PM546, under otherwise identical experimental conditions. The pH-dependence experiments of the BODIPY fluorophores **1** and **6** reveals that these BODIPYs were less degraded in acidic and basic conditions than the commercial PM546 (Figure S6 in the Supporting Information). This behavior could be understood taking into account that the BF₂ bridge is the most labile position of the BODIPY and, consequently, it could be the most suitable position to be attacked by acids or bases. It seems that the charge redistribution around the boron atom (increase of its positive charge) upon the replacement of fluorine by carboxylates strengthens the ionic B–N bond leading to dyes more robust to extreme pHs. In fact, theoretical calculations predict a slight decrease in such bond length (except for PM650) from ≈ 1.54 to 1.51 induced by the presence of trifluoroacetoxy groups.

Moreover, a solubility study was carried out with the BODIPYs above mentioned. The results obtained show that compounds **1** and **6** are more soluble in water than the parent

Table 3 Lasing properties of commercial *F*-BODIPYs and their new derivatives at the dye concentrations that optimize their laser action in ethyl acetate solutions. [c]: dye concentration; Eff: lasing efficiency (ratio between the energy of the laser output and the pump energy incident on the sample surface); λ_l : peak wavelength of the laser emission; Intensity of the laser-induced fluorescence emission (I_n) after n pump pulses for dyes in ethyl acetate solution λ_{exc} : pumping wavelength.

	$\lambda_{exc} = 355 \text{ nm}, 5 \text{ Hz}$										$\lambda_{exc} = 532 \text{ nm}, 10 \text{ Hz}$									
	PM546	1	6	12	14	PM567	2	7	11	13	PM597	3	8	PM605	4	9	PM650	5	10	
[c]/mM	2.5	3.8	7.5	2.5	2.5	1.5	1.5	0.6	1.5	9	0.5	0.9	0.9	0.6	0.6	0.6	0.9	1.4	0.5	
Eff (%)	23	43	53	59	16	48	63	68	65	59	53	59	65	55	60	67	35	50	55	
λ_l /nm	541	544	541	542	541	566	566	562	563	565	588	586	587	586	591	592	657	655	661	
I_n (%) ^{a)}	60	100	100	100	50	17	98	100	90	30	85	100	100	20	65	91	80	30	50	
$n/1000$	100	100	100	100	100	100	100	100	100	100	100	100	100	40	70	100	100	50	70	

^{a)} I_n (%) = 100 (I_n/I_0), with I_0 being the initial intensity.

PM546. Thus, while the PM546 is hydrophobic and it is not soluble in water, the dyes **1** and **6** exhibit 20 and 35 $\mu\text{g}/\text{mL}$, respectively, solubility in water, which is an important additional advantage of *O*-BODIPYs, in terms of their biological applications.

2.3. Lasing Properties

2.3.1. Liquid Phase

According to the absorption properties of the new BODIPYs (Table 1 and 2), their lasing properties were studied under pumping at 355 nm (dyes **1**, **6**, **12** and **14**, analogues of PM546) and 532 nm (all the other derivatives). Under our experimental conditions (transversal excitation and strong focusing of the incoming pump radiation) the concentration of the dyes should be in the millimolar range, to ensure total absorption of the pump radiation within the first millimeter at most of the solution, in order to obtain an emitted beam with near-circular cross-section and optimize the lasing efficiency (ratio between the energy of the dye laser output and the pump energy incident on the sample surface). To determine the dye concentration that optimizes the laser emission for the different derivatives, first the dependence of their laser emission on the corresponding dye concentrations was analyzed in ethyl acetate by varying the optical densities from 4 to 40, while keeping all the other experimental parameters constant. **Table 3** summarizes the concentrations that produced the highest lasing efficiencies in each case as well as the corresponding lasing wavelengths.

It can be appreciated in Table 3 that in all cases the lasing efficiency of the derivatives is higher than that of the commercial parent dye, with the highest lasing efficiencies being obtained in the derivatives incorporating trifluoroacetoxy groups (**6**–**10**).

Following the photophysical analysis, the actual effect of the solvent on the dye laser action was analyzed in solutions of polar protic and polar aprotic solvents. Although the photophysical studies showed that the new derivatives exhibited their highest fluorescence capacity when dissolved in apolar solvent-hexane, the low solubility of the synthesized *O*-BODIPYs in this solvent prevented preparation of solutions of the dyes in *c*-hexane at the concentration required for laser experiments under the pumping conditions selected in the present work. In all the other solvents, each dye was dissolved at the concentration that was found to optimize its emission in ethyl acetate (that is, the concentrations tabulated in Table 3).

In **Table 4** are presented the lasing properties of the new *O*-BODIPYs as a function of the solvent, together with those of the corresponding parent dyes. The lasing behavior of the new compounds is in good agreement with their photophysical properties (Table S1–S5 in the Supporting Information). In the acetoxy derivatives **1**–**4** the photophysics changes little in the different solvents and so does the lasing efficiency, which nevertheless improves in general that of the parent dyes, in accordance with the improvement of the fluorescence capacity of those derivatives with respect to the parent dyes.

As discussed in the previous section, the inclusion of the trifluoroacetoxy groups in the BODIPYs further enhanced the fluorescence capacity of the parent dyes. Correspondingly, derivatives **6**–**9** exhibit consistently higher lasing efficiencies

Table 4. Lasing efficiencies for the commercial *F*-BODIPY dyes and their new derivatives in different solvents. λ_{exc} : pumping wavelength.

Solvent	$\lambda_{exc} = 355 \text{ nm}$										$\lambda_{exc} = 532 \text{ nm}$									
	PM546	1	6	12	14	PM567	2	7	11	13	PM597	3	8	PM605	4	9	PM650	5	10	
F_3 -ethanol ^{a)}	39	47	40			30	47	49	45	39	56	54	58	51	57	61	27	33	38	
Methanol	45	58	49	5		34	54	58	53	48	54	52	60	55	58	60	12	27	31	
Ethanol	44	56	50	7		36	52	59	57	51	51	52	59	56	60	64		21	25	
Ethyl acetate	23	43	53	59	16	48	63	68	61	59	53	59	65	55	60	67	35	50	55	
Acetone	14	37		52	14	36	55	57	60	55	50	53	60	57	59	65	31	44	49	

^{a)} F_3 -ethanol: 2,2,2-trifluoroethanol

than compounds 1–4. In the compounds 7–9, the highest lasing efficiencies (an impressive 65–67%) are obtained in ethyl acetate, which is the solvent where those dyes have the highest quantum yield and radiative rate constant as well as the lowest nonradiative rate constant. In compound 6, the highest quantum yield and radiative rate constant and the lowest nonradiative rate constant are achieved in methanol, and thus it is in this solvent where the highest lasing efficiency (58%) is observed.

The derivatives of PM567 with acryloyloxy (**11**) and methoxy (**13**) groups do not improve the lasing efficiencies demonstrated with the trifluoroacetoxy derivative 7, in accordance with their lower fluorescence quantum yields and higher nonradiative rate constants, albeit compound 11 improves slightly the emission efficiency of derivative 2, also in agreement with the slightly better photophysical parameters of 11 as compared with 2 (Table S2 in the Supporting Information). In the group of dyes pumped at 355 nm, compound 12, derivative of PM546 incorporating propiloxy groups, exhibits much higher lasing efficiencies than the parent dye and the other derivatives, with the exception of compound 6, which has better laser emission in polar protic solvents. This behavior reflects the photophysical properties: as can be seen in Table S1 in the Supporting Information, in polar protic solvents 6 has higher quantum yields and lower nonradiative constants than 12, but the contrary happens in polar aprotic solvents. Compound 14, on the other hand, is the one with the poorest lasing performance as a result of the fluorescence quenching processes discussed above, when considering the photophysical properties of the new derivatives.

Regarding dye PM650 and its derivatives 5 and 10, as we have discussed in the previous section their emission properties are limited by the presence of an ICT state, which results in low fluorescence quantum yields in polar media. As a result their lasing efficiencies are lower than those of the other compounds pumped at 532 nm. As seen in Table S5 (Supporting Information), the fluorescence performance of these dyes is somewhat improved in polar aprotic solvents, which correlates with their higher lasing efficiencies in ethyl acetate and acetone, as compared with those observed in F_3 -ethanol, methanol and ethanol.

An important parameter for any practical application of the dye lasers is their lasing photostability under repeated pumping. In Table 3 are collected data on the decrease of the laser-induced fluorescence intensity, under transversal excitation of capillary containing dye solutions in ethyl acetate (see Experimental Section), after a given number n of pump pulses, for both the commercial dyes and their derivatives synthesized in the present work. Dye PM546 and its derivatives 1 and 6 were pumped at 355 nm and 5 Hz repetition rate. All the other dyes were pumped at 532 nm and 10 Hz repetition rate. The pump energy was in all cases 5 mJ.

It has to be remarked that all the newly synthesized *O*-BODIPYs are more photostable than the corresponding *F*-BODIPYs, with the exception of 14 and derivatives of PM650, which lower stability reflects their lower chemical stability, due to the mechanism discussed above, when analyzing their photophysical properties.

2.3.2. Bulk Solid State

The excellent laser performance exhibited by the new dyes in liquid solution led us to explore their behavior as photonic materials, either in bulk as SSDLs or incorporated into

Table 5. Lasing properties of dyes incorporated in solid PMMA matrices. Eff: lasing efficiency; λ_l : peak laser emission wavelength; I_n (%): intensity of the laser output after n pump pulses in the same position of the sample, $I_n(\%) = 100(I_n/I_0)$, where I_0 is the initial intensity.

Dye	Eff [%]	λ_l [nm]	I_{100000} [%] ^{a)}	I_n [%] ^{b)}	n
PM567	34	566	30	0	12000
2	49	568	80	0	40000
7	56	568	100	80	100000
11	47	567	100	0	100000

^{a)}Pumping at 10 Hz; ^{b)}Pumping at 30 Hz.

waveguiding structures. To this end, as a proof of concept, we chose dye PM567 as reference with which to compare the laser behavior of derivatives 2 and 7 under identical experimental conditions. As matrix material we chose PMMA because it mimics ethyl acetate, the solvent in which those dyes exhibited the highest lasing efficiencies in liquid solution (Table 4). The dye concentration in the matrix was that which optimized the lasing efficiency in ethyl acetate (Table 3). We have seen in previous work^[18] that the covalent bonding of the chromophore to the polymeric matrix improves significantly the dye photostability because new channels are open to dissipate the excess energy released to the medium as heat. To check out the effect of this mechanism in the present case, PMMA matrices were also prepared incorporating dye 11, which is an *O*-derivative of PM567 with acrylic bonds that allow the covalent bonding of the dye to the polymeric chains.

Table 5 collects the lasing performance of the different dyes. The lasing efficiencies of the new materials based on PMMA doped with *O*-BODIPYs enhance significantly those recorded with the commercial PM567 and correlate with those obtained in liquid solution, with the efficiency of dye 7 being the highest and being maintained the relationship: Eff (PM567) < Eff (**11**) < Eff (**2**) < Eff (**7**). These efficiencies are lower than those obtained in liquid solution, probably due to the fact that the finishing of the surface of the solid samples relevant to the laser operation was not laser-grade, so that higher efficiencies are to be expected with laser-grade surfaces.

To assess the photostability of the new materials we followed the evolution of their laser emission under repeated pumping in the same position of the sample at 10 Hz repetition rate. All the three derivatives demonstrated a much higher photostability than the parent dye PM567 (Table 5). After 100 000 pump pulses, the emission of compound 2 dropped by 20%, but the lasing intensity of both derivatives 7 and 11 remained constant at the initial level. Trying to distinguish more clearly the photostability behavior of the different dyes, we decided to subject the dyes to more drastic pumping conditions. We had demonstrated in previous work that the accumulation of heat into polymeric SSDLs increases significantly with the pumping repetition rate, resulting in a decrease in the lasing photostability.^[19] Consequently, we proceeded to pump the SSDLs at 30 Hz repetition rate. The results are collected in the last two columns of Table 5. To facilitate comparison of the results obtained in a more intuitive way, the actual evolution of the

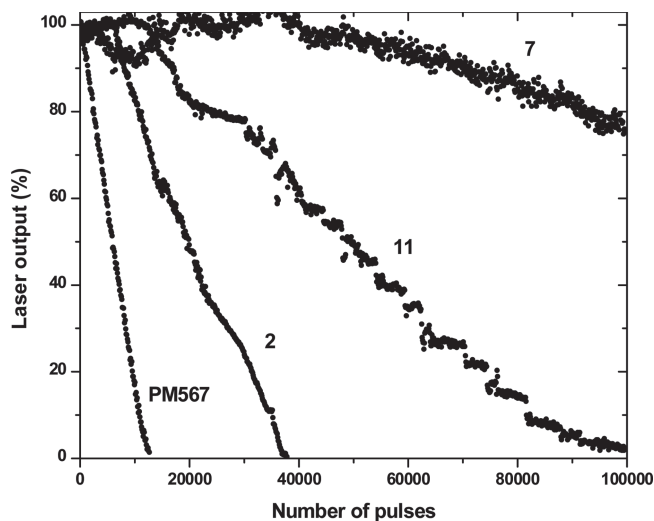


Figure 5. Normalized laser output as a function of the number of pump pulses in the same position of the sample of parent dye PM567 and its derivatives **2**, **7** and **11**. Pump energy and repetition rate: 3.5 mJ pulse⁻¹ and 30 Hz, respectively.

laser emission of the different dyes at 30 Hz repetition rate is shown in **Figure 5**.

Compound **11** being covalently bonded to the polymeric chains improves the heat dissipation and, consequently, the lasing photostability with respect to dye **2**, which is merely solved into the matrix. However, the highest photostability is achieved with PMMA doped with dye **7**, with a drop in its emission intensity of just 20% after 100,000 pump pulses. These unexpected results can be understood in the light of the photophysics of compounds **7** and **11** (Table S2 in the Supporting Information). While the fluorescence quantum yield and radiative rate constant of compound **7** in ethyl acetate are just somewhat higher than those of compound **11**, the nonradiative rate constant of **7** is much lower than that of **11**. That means that the energy not converted into laser emission, which appears in the medium as heat, is much lower in **7** than in **11**, which more than compensates the higher dissipation rates in the matrix doped with the covalently bonded dye **11**.

2.3.3. Thin Films

In the previous section, we have studied the laser properties of the newly synthesized dyes operated as conventional two-mirror lasers. Nevertheless, there has been significant work over the last few years exploring the development of organic thin film lasers based on dye doped polymers because of their potential applications as coherent light sources suitable for integration in optoelectronic and disposable spectroscopic and sensing devices.^[1d] In order to explore the suitability of the newly synthesized dyes for integrated devices, we implemented distributed feedback (DFB) lasers, the most common resonator type for organic thin film lasers.^[1a]

In DFB lasers, light propagating in a waveguide mode of the organic film is Bragg-scattered by a wavelength-scale periodic modulation of the refractive index in the film, substrate, or both, to create a diffracted wave propagating in the counter

propagating waveguide mode. The propagating and counter propagating modes will destructively interfere with each other at a given wavelength to create a photonic stopband at which light propagation is forbidden. This optical gap, whose width depends on the refractive index contrast of the periodic modulation, is centered at a wavelength λ_B , satisfying the Bragg condition, $m\lambda_B = 2 n_{\text{eff}}\Lambda$, where m is an integer that represents the order of the diffraction, n_{eff} is the effective refractive index of the waveguide, which represents a geometrical average of the refractive indices of the three layers of the waveguide, and Λ is the period of the modulation.^[1a] Working with the second order $m = 2$, the resonant wavelength is equal to $n_{\text{eff}}\Lambda$, and light is diffracted out of the surface of the film perpendicular to the plane of the waveguide. That is, the second-order structure provides a surface-emitted output coupling of the laser light via first-order diffraction while providing in-plane feedback via second-order diffraction (Figure S7a in Supporting Information).

The fundamental transverse electric (TE₀) propagating mode in a waveguide 1 μm thick with refractive index 1.4900 (PMMA), deposited onto a quartz substrate ($n = 1.456$), experiences an effective refractive index $n_{\text{eff}} \approx 1.477$, as calculated with a waveguide mode solver,^[20] in the range 550–600 nm. Hence, if dye doped PMMA thin films are deposited on substrates with modulation periods $\Lambda_1 = 386$ nm and $\Lambda_2 = 400$ nm, second-order photonic stopbands centered at $\lambda_{B1} \approx 570$ nm and $\lambda_{B2} \approx 590$ nm, respectively, will be obtained. As λ_{B1} and λ_{B2} match the emission windows of the PM567 and PM597 families, respectively, we choose these dyes to implement the DFB lasers.

Two compounds of each family were chosen, the commercial compounds as the references and the derivatives with trifluoroacetoxy groups (compounds **7** and **8**), which showed the best laser performances both in liquid and bulk media. In order to better compare the laser performances, the dye concentrations were selected to render similar absorbance (Abs ≈ 0.055) at the pumping wavelength (532 nm), enough to provide the needed gain while avoiding the undesirable effects of dye aggregation.

In agreement with the estimated Bragg resonant wavelengths, when the devices were pumped well above threshold DFB laser emission was obtained around 570 nm, for samples with PM567 and **7**, and around 590 nm, for samples with PM597 and **8** (**Figure 6a**).

Explicitly, the laser peaks were centered at 569.3 nm for PM567, 571.6 nm for **7**, 589.3 nm for PM597 and 590.4 nm for **8**. The differences in the emission wavelengths between each group of samples have its origin in the slight differences in the sample thicknesses, which modifies the effective refractive index n_{eff} and, in turn, the resonant wavelength.

Figure 6b,c show the dependence of the DFB emission intensity on the pump intensity for the samples doped with PM567 derivatives and PM597 derivatives, respectively. At low pump intensities there is just fluorescence and the emission grows linearly. Once the threshold is reached, the intensity of the emission grows superlinearly with the pump intensity, and the emission linewidth collapses to a mere 0.2 nm (**Figure 6a**). From the data in **Figure 6b** it is seen that the sample with **7** not only has a lower laser threshold than that with PM567 (1.7 against 2.5 kW cm⁻²) but presents an output intensity up to an order of magnitude higher, in agreement with the results

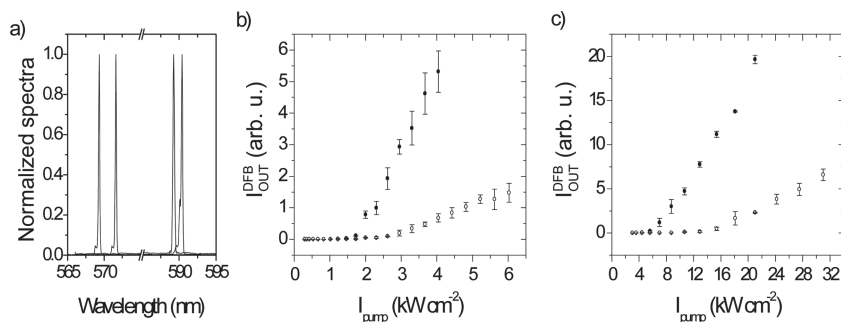


Figure 6. a) From left to right, DFB laser spectra of commercial PM567, derivative **7**, commercial PM597 and derivative **8** doped in PMMA. b) Output intensity as a function of pump intensity for commercial PM567 35 mM (hollow circles) and derivative **7** 25 mM (filled circles) doped in PMMA. c) Output intensity as a function of pump intensity for commercial PM597 25 mM (hollow circles) and derivative **8** 30 mM (filled circles) doped in PMMA.

observed in bulk media. Analogous results are obtained when comparing the samples with **8** and PM597 (Figure 6c). In this case the sample with **8** presents a laser threshold of 6 kW cm^{-2} , to be compared to the 14.5 kW cm^{-2} needed to excite laser emission in the sample with PM597.

3. Experimental Section

BODIPY dyes PM546, PM567, PM597, PM605 and PM650 were purchased from Lasing, S. A. and used as received.^[12] New BODIPYs **1–12** and **14** were synthesized by modification of methods previously described.^[8a,11] Compound **13**^[6f] was synthesized according to procedure described in the literature.

Characterization of the new dyes as well as quantum mechanical simulations, preparation of laser samples, methods followed to analyze the photophysical and laser properties in liquid and solid phase and procedures to pH and solubility studies are described in detail in the Supporting Information.

4. Conclusions

The development of O-BODIPYs from commercial dyes is a successful strategy to obtain optimized laser dyes. The replacement of the fluorines by electron acceptor carboxylate groups ameliorate the fluorescence efficiency, reaching in some cases values around 100%; hence, these novel BODIPYs would be promising candidates to achieve tunable lasers at different regions of the visible with improved performance. To confirm this possibility, the lasing performance of the new derivatives in liquid solution and solid state was assessed and compared with that of the parent dyes.

The lasing efficiencies of the new compounds correlate well with their photophysical properties: all the derivatives exhibit a lasing efficiency higher than that of the commercial parent dye (except **14**, derivative of PM546 with aryloxy groups, in agreement with its lower fluorescence capability), with the highest lasing efficiencies being obtained in the derivatives incorporating trifluoroacetoxy groups.

To assess the laser behavior of the new dyes in solid state, dye PM567 and its derivatives **2**, **7**, and **11** were incorporated into solid matrices of PMMA. The lasing efficiencies of the

O-BODIPYs were in all cases higher than that of the parent dye, and correlate with those obtained in liquid solution. Thus, the highest efficiency, 56%, was obtained with compound **7**. Compound **7** also exhibited a very high lasing stability, with the laser emission remaining at 80% of its initial value after 100 000 pump pulses in the same position of the sample at 30 Hz repetition rate.

DFB laser emission was demonstrated with organic films incorporating trifluoroacetoxy derivatives **7** and **8**, deposited onto quartz substrates engraved with appropriated periodical structures. Both derivatives exhibited laser thresholds lower than those of the parent dyes as well lasing intensities up to one order of magnitude higher. In

view of the easy synthetic assembly, and the large number of described BODIPY laser dyes, we are confident that this powerful approach can be extended to other dyes of this family, furthering their practical application in optical and sensing fields.^[21]

Supporting Information

Supporting Information is available from the Wiley Online Library or from the author.

Acknowledgements

This work was supported by Projects MAT2010-20646-C04-01, MAT2010-20646-C04-02, MAT2010-20646-C04-04 and TRACE 2009-0144 of the Spanish Ministerio de Ciencia e Innovación (MICINN), actually Spanish Ministerio de Economía y Competitividad (MINECO). I.E. thanks the Gobierno Vasco for a predoctoral contract IT339-10. L.C., M.E.P.-O. and G.D.-S. thank MICINN for a predoctoral scholarship (FPI, cofinanced by Fondo Social Europeo).

Received: January 17, 2013

Revised: February 6, 2013

Published online: March 26, 2013

- [1] a) I. D. W. Samuel, G. A. Turnbull, *Chem. Rev.* **2007**, *107*, 1272; b) H. Zou, S. Wu, J. Shen, *Chem. Rev.* **2008**, *108*, 3893; c) D. Bera, L. Qian, T.-K. Tseng, P. H. Holloway, *Materials* **2010**, *3*, 2260; d) C. Grivas, M. Pollnau, *Laser Photonics Rev.* **2012**, *6*, 419.
- [2] a) A. Costela, I. García-Moreno, R. Sastre, in *Tunable Laser Applications*, (Ed: F. J. Duarte), CRC Press, Boca Raton, FL **2009**, Ch. 3, pp 97–120; b) O. García, L. Garrido, R. Sastre, A. Costela, I. García-Moreno, *Adv. Funct. Mater.* **2008**, *18*, 2017; c) O. García, R. Sastre, I. García-Moreno, V. Martín, A. Costela, *J. Phys. Chem. C* **2008**, *112*, 14710; d) I. García-Moreno, A. Costela, V. Martín, M. Pintado-Sierra, R. Sastre, *Adv. Funct. Mater.* **2009**, *19*, 2547; e) A. Costela, I. García-Moreno, L. Cerdán, V. Martín, O. García, R. Sastre, *Adv. Mater.* **2009**, *21*, 4163; f) L. Cerdán, A. Costela, I. García-Moreno, O. García, R. Sastre, D. Muñoz, J. de Abajo, *Macromol. Chem. Phys.* **2009**, *210*, 1624; g) R. Sastre, V. Martín, L. Garrido, J. L. Chiara, B. Trastoy, O. García, A. Costela, I. García-Moreno, *Adv. Funct. Mater.* **2009**, *19*, 3307; h) E. Enciso, A. Costela,

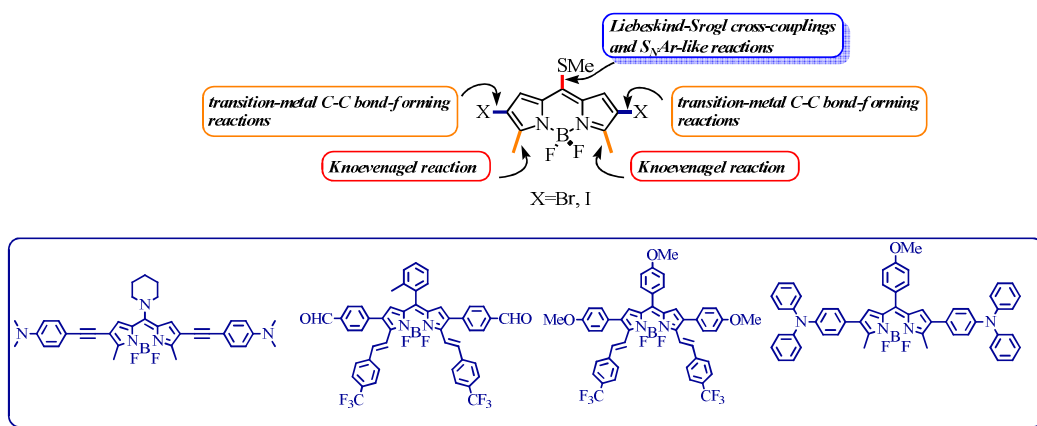
- l. García-Moreno, V. Martín, R. Sastre, *Langmuir* **2010**, *26*, 6154; i) L. Cerdán, A. Costela, I. García-Moreno, O. García, R. Sastre, *Opt. Express* **2010**, *18*, 10247; j) V. Martín, J. Bañuelos, E. Enciso, I. López Arbeloa, A. Costela, I. García-Moreno, *J. Phys. Chem. C* **2011**, *115*, 3926; k) M. E. Pérez-Ojeda, C. Thivierge, V. Martín, A. Costela, K. Burgess, I. García-Moreno, *Opt. Mater. Express* **2011**, *1*, 243; l) M. E. Pérez-Ojeda, B. Trastoy, I. López Arbeloa, J. Bañuelos, A. Costela, I. García-Moreno, J. L. Chiara, *Chem. Eur. J.* **2011**, *17*, 13258; m) L. Cerdán, A. Costela, G. Durán-Sampedro, I. García-Moreno, M. Calle, J. de Abajo, G. A. Turnbull, *J. Mater. Chem.* **2012**, *22*, 8938; n) L. Cerdán, A. Costela, I. García-Moreno, *Org. Electron.* **2012**, *13*, 1463; o) L. Cerdán, A. Costela, I. García-Moreno, J. Bañuelos, I. López Arbeloa, *Laser Phys. Lett.* **2012**, *9*, 426; p) L. Cerdán, E. Enciso, V. Martín, J. Bañuelos, I. López Arbeloa, A. Costela, I. García-Moreno, *Nat. Photonics* **2012**, *6*, 621; q) L. Cerdán, A. Costela, G. Durán-Sampedro, I. García-Moreno, *Appl. Phys. B* **2012**, *108*, 839.
- [3] a) T. G. Pavlopoulos, M. Shah, J. H. Boyer, *Appl. Opt.* **1988**, *27*, 4998; b) M. Shah, K. Thangaraj, M. L. Soong, L. T. Wolford, J. H. Boyer, I. R. Politzer, T. G. Pavlopoulos, *Heteroatom. Chem.* **1990**, *1*, 389; c) T. G. Pavlopoulos, J. H. Boyer, M. Shah, K. Thangaraj, M. L. Soong, *Appl. Opt.* **1990**, *29*, 3885; d) T. G. Pavlopoulos, J. H. Boyer, K. Thangaraj, G. Sathyamoorthi, M. P. Shah, M. L. Soong, *Appl. Opt.* **1992**, *31*, 7089; e) J. H. Boyer, A. M. Haag, G. Sathyamoorthi, M. L. Soong, K. Thangaraj, T. G. Pavlopoulos, *Heteroatom. Chem.* **1993**, *4*, 39.
- [4] a) F. Lopez Arbeloa, J. Bañuelos, V. Martinez, T. Arbeloa, I. Lopez Arbeloa, *Int. Rev. Phys. Chem.* **2005**, *24*, 339; b) O. Garcia, R. Sastre, D. del Agua, A. Costela, I. Garcia-Moreno, *Chem. Mater.* **2006**, *18*, 601; c) I. Garcia-Moreno, F. Amat-Guerri, M. Liras, A. Costela, L. Infantes, R. Sastre, F. Lopez Arbeloa, J. Bañuelos Prieto, I. Lopez Arbeloa, *Adv. Funct. Mater.* **2007**, *17*, 3088; d) A. Costela, I. Garcia-Moreno, M. Pintado-Sierra, F. Amat-Guerri, R. Sastre, M. Liras, F. Lopez Arbeloa, J. Bañuelos Prieto, I. Lopez Arbeloa, *J. Phys. Chem. A* **2009**, *113*, 8118; e) M. J. Ortiz, I. Garcia-Moreno, A. R. Agarrabeitia, G. Duran-Sampedro, A. Costela, R. Sastre, F. Lopez Arbeloa, J. Bañuelos Prieto, I. Lopez Arbeloa, *Phys. Chem. Chem. Phys.* **2010**, *12*, 7804; f) J. Bañuelos Prieto, A. R. Agarrabeitia, I. Garcia-Moreno, I. Lopez-Arbeloa, A. Costela, L. Infantes, M. E. Perez-Ojeda, M. Palacios-Cuesta, M. J. Ortiz, *Chem. Eur. J.* **2010**, *16*, 14094; g) Y. Xiao, D. Zhang, X. Qian, A. Costela, I. Garcia-Moreno, V. Martin, M. E. Perez-Ojeda, J. Bañuelos, L. Gartzia, I. Lopez Arbeloa, *Chem. Commun.* **2011**, *47*, 11513; h) J. Bañuelos, V. Martin, C. F. A. Gomez-Duran, I. J. Arroyo Cordoba, E. Peña-Cabrera, I. Garcia-Moreno, A. Costela, M. E. Perez-Ojeda, T. Arbeloa, I. Lopez Arbeloa, *Chem. Eur. J.* **2011**, *17*, 7261; i) G. Duran-Sampedro, A. R. Agarrabeitia, I. Garcia-Moreno, A. Costela, J. Bañuelos, T. Arbeloa, I. López Arbeloa, J. L. Chiara, M. J. Ortiz, *Eur. J. Org. Chem.* **2012**, *32*, 6335.
- [5] a) A. Loudet, K. Burgess, *Chem. Rev.* **2007**, *107*, 4891; b) R. Ziessel, G. Ulrich, A. Harriman, *New J. Chem.* **2007**, *31*, 496; c) G. Ulrich, R. Ziessel, A. Harriman, *Angew. Chem. Int. Ed.* **2008**, *47*, 1184; d) F. L. Arbeloa, J. Bañuelos, V. Martinez, T. Arbeloa, I. L. Arbeloa, *Trends Phys. Chem.* **2008**, *13*, 101; e) A. C. Benniston, G. Copley, *Phys. Chem. Chem. Phys.* **2009**, *11*, 4124; f) M. Benstead, G. H. Mehl, R. W. Boyle, *Tetrahedron* **2011**, *67*, 3573; g) N. Boens, V. Leen, W. Dehaen, *Chem. Soc. Rev.* **2012**, *41*, 1130; h) S. G. Awuah, Y. You, *RSC Adv.* **2012**, *2*, 11169; i) A. Kamkaew, S. H. Lim, H. B. Lee, L. V. Kiew, L. Y. Chung, K. Burgess, *Chem. Soc. Rev.* **2013**, *42*, 77.
- [6] a) L. Li, B. Nguyen, K. Burgess, *Bioorg. Med. Chem. Lett.* **2008**, *18*, 3112; b) C. Bonnier, W. E. Piers, A. Al-Sheikh Ali, A. Thompson, M. Parvez, *Organometallics* **2009**, *28*, 4845; c) S. M. Crawford, A. Thompson, *Org. Lett.* **2010**, *12*, 1424; d) T. W. Hudnall, T.-P. Lin, F. P. Gabbaï, *J. Fluorine Chem.* **2010**, *131*, 1182; e) G. Ulrich, S. Goeb, A. De Nicola, P. Retailleau, R. Ziessel, *J. Org. Chem.* **2011**, *76*, 4489; f) L. Yang, R. Simionescu, A. Lough, H. Yan, *Dyes Pigments* **2011**, *91*, 264; g) T. Lundrigan, S. M. Crawford, T. S. Cameron, A. Thompson, *Chem. Commun.* **2012**, *48*, 1003; h) T. Lundrigan, A. Thompson, *J. Org. Chem.* **2012**, *78*, 757.
- [7] a) L. Bonardi, G. Ulrich, R. Ziessel, *Org. Lett.* **2008**, *10*, 2183; b) A. Nagai, J. Miyake, K. Kokado, Y. Nagata, Y. Chujo, *J. Am. Chem. Soc.* **2008**, *130*, 15276; c) A. Harriman, L. Mallon, R. Ziessel, *Chem. Eur. J.* **2008**, *14*, 11461; d) T. Rousseau, A. Cravino, T. Bura, G. Ulrich, R. Ziessel, J. Roncali, *Chem. Commun.* **2009**, 1673; e) A. Harriman, L. J. Mallon, K. J. Elliot, A. Haefele, G. Ulrich, R. Ziessel, *J. Am. Chem. Soc.* **2009**, *131*, 13375; f) J.-H. Olivier, A. Haefele, P. Retailleau, R. Ziessel, *Org. Lett.* **2010**, *12*, 408; g) T. Bura, P. Retailleau, R. Ziessel, *Angew. Chem. Int. Ed.* **2010**, *49*, 6659; h) T. Bura, R. Ziessel, *Org. Lett.* **2011**, *13*, 3072; i) S. Rihn, M. Erdem, A. De Nicola, P. Retailleau, R. Ziessel, *Org. Lett.* **2011**, *13*, 1916; j) S. Zhu, N. Dorh, J. Zhang, G. Vegesna, H. Li, F.-T. Luo, A. Tiwari, H. Liu, *J. Mater. Chem.* **2012**, *22*, 2781; k) J.-S. Lu, S.-B. Ko, N. R. Walters, S. Wang, *Org. Lett.* **2012**, *14*, 5660.
- [8] a) C. Tahtaoui, C. Thomas, F. Rohmer, P. Klotz, G. Duportail, Y. Mély, D. Bonnet, M. Hibert, *J. Org. Chem.* **2007**, *72*, 269; b) Y. Tokoro, A. Nagai, Y. Chujo, *Tetrahedron Lett.* **2010**, *51*, 3451; c) C. A. Wijesinghe, M. E. El-Khouly, N. K. Subbaiyan, M. Supur, M. E. Zandler, K. Ohkubo, S. Fukuzumi, F. D'Souza, *Chem. Eur. J.* **2011**, *17*, 3147; d) B. Brizet, A. Eggenspieler, C. P. Gros, J. M. Barbe, C. Goze, F. Denat, P. D. Harvey, *J. Org. Chem.* **2012**, *77*, 3646.
- [9] a) A. K. Parhi, M.-P. Kung, K. Ploessl, H. F. Kung, *Tetrahedron Lett.* **2008**, *49*, 3395; b) C. Ikeda, S. Ueda, T. Nabeshima, *Chem. Commun.* **2009**, 2544; c) A. Kubo, Y. Minowa, T. Shoda, K. Takeshita, *Tetrahedron Lett.* **2010**, *51*, 1600; d) S. Rausaria, A. Kamadulski, N. P. Rath, L. Bryant, Z. Chen, D. Salvemini, W. L. Neumann, *J. Am. Chem. Soc.* **2011**, *133*, 4200; e) Y. Tomimori, T. Okujima, T. Yano, S. Mori, N. Ono, H. Yamada, H. Uno, *Tetrahedron* **2011**, *67*, 3187.
- [10] a) C. Bonnier, W. E. Piers, M. Parvez, T. S. Sorensen, *Chem. Commun.* **2008**, 4593; b) C. Bonnier, W. E. Piers, M. Parvez, *Organometallics* **2011**, *30*, 1067.
- [11] X.-D. Jiang, J. Zhang, T. Furuyama, W. Zhao, *Org. Lett.* **2012**, *14*, 248.
- [12] Laser grade, Exciton. They were used as received with a purity >99%.
- [13] C. Hansch, A. Leo, R. W. Taft, *Chem. Rev.* **1991**, *91*, 165.
- [14] G. Bourhill, J.-L. Brédas, L.-T. Cheng, S. R. Marder, F. Meyers, B. W. Perry, B. G. Tiemann, *J. Am. Chem. Soc.* **1994**, *116*, 2619.
- [15] I. Esnal, J. Bañuelos, I. López Arbeloa, A. Costela, I. García-Moreno, M. Garzón, A. R. Agarrabeitia, M. J. Ortiz, *RSC Adv.* **2013**, *3*, 1547.
- [16] J. Bañuelos, T. Arbeloa, M. Liras, V. Martinez, F. López Arbeloa, *J. Photochem. Photobiol. A* **2006**, *184*, 298.
- [17] a) A. P. de Silva, H. Q. N. Gunaratne, T. Gunlaugsson, A. J. M. Huxley, C. P. McCoy, J. T. Rademacher, T. E. Rice, *Chem. Rev.* **1997**, *97*, 1515; b) K. Rurack, U. Resch-Genger, *Chem. Soc. Rev.* **2002**, *31*, 116; c) H. Sunahara, Y. Urano, H. Kojima, T. Nagano, *J. Am. Chem. Soc.* **2007**, *129*, 5597; d) J. Bañuelos, I. J. Arroyo-Cordoba, I. Valois-Escamilla, A. Alvarez-Hernández, E. Peña-Cabrera, R. Hu, B. Z. Tang, I. Esnal, V. Martínez, I. López Arbeloa, *RSC Adv.* **2011**, *1*, 677.
- [18] A. Costela, I. García-Moreno, R. Sastre, *Phys. Chem. Chem. Phys.* **2003**, *5*, 4745.
- [19] a) A. Costela, I. García-Moreno, D. del Agua, O. García, R. Sastre, *Appl. Phys. Lett.* **2004**, *85*, 2160; b) A. Costela, I. García-Moreno, D. del Agua, O. García, R. Sastre, *J. Appl. Phys.* **2007**, *101*, 073110.
- [20] Online 1D multilayer slab waveguide mode solver by Dr. Manfred Hammer. <http://wwwhome.math.utwente.nl/~hammer/oms.html> (accessed March 2013).
- [21] M. J. Ortiz, A. R. Agarrabeitia, M. Garzón Sanz, I. García-Moreno, A. Costela, G. Durán-Sampedro, Spanish Patent Application no. 201200871, **2012**.

3. Kapitulum II ERANSKINA / ANEXO II al Capítulo 3

3. Artikulua / Artículo 3:

Near IR BODIPY dyes *a la carte*. Programmed orthogonal functionalization of rationally designed building blocks.

Aceptado en *Chemistry European Journal* en 2015



Near IR BODIPY Dyes *a la Carte*. Programmed Orthogonal Functionalization of Rationally Designed Building Blocks

Cesar F. A. Gómez-Durán,^[a] Ixone Esnal,^[b] Ismael Valois-Escamilla,^[a] Arlette Urías-Benavides,^[a] Jorge Bañuelos,^{*[b]} Iñigo López Arbeloa,^[b] Inmaculada García-Moreno,^[c] Eduardo Peña-Cabrera^{*[a]}

Abstract: Herein, we report the synthesis of polyfunctional BODIPY building blocks suitable to be subjected to several reaction sequences with complete chemoselectivity, which allowed the preparation of complex BODIPY derivatives in a versatile and programmable manner. The reactions included: the Liebeskind-Srogl cross-coupling reaction (LSCC), S_NAr, Suzuki, Sonogashira, and Stille couplings and a desulfative reduction of the MeS- group. This novel synthetic protocol is a powerful route to design a library of compounds with tailored photophysical properties for advanced applications. In this context, it is noteworthy the straightforward and cost-less strategies to shift the BODIPY emission deep into the near infrared spectral region but retaining high fluorescence quantum yields as well as highly efficient and stable laser action. These new dyes outperform the lasing behaviour of dyes considered benchmarks over the red spectral region, overcoming the important drawbacks exhibited by these commercial laser dyes: low absorption at the standard pump wavelengths (355 and 532 nm) and/or poor photostability.

Introduction

One of the most important aspects in organic synthesis is chemoselectivity, that is, the selective preferential reaction of a functional group in the presence of other(s) of similar reactivity. Complete control over it, saves steps in the overall synthetic plan since there is no need for protecting groups. A particular type of chemoselectivity that has been used mainly in transition-metal catalyzed transformations is the so-called orthogonal reactivity. It is defined as the activation of a single reactive site in over others in a polyfunctional substrate by the judicious selection of the reaction conditions (Figure 1).^[1]

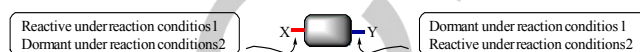
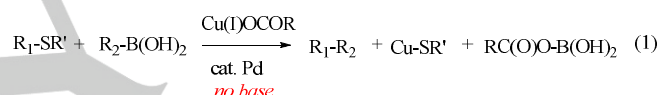


Figure 1. General structure of a substrate with orthogonal reactivity

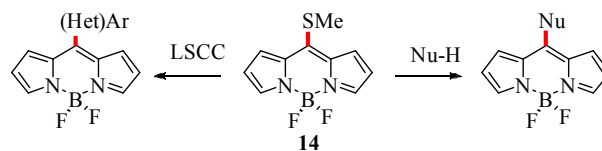
There are several successful examples in the literature of substrates that display such property).^[2-14]

A more recent member in the transition-metal catalyzed cross-coupling reaction arena is the Liebeskind-Srogl cross-coupling reaction (LSCC).^[15] In a general way, it consists of the Pd-catalyzed, Cu(I)-mediated reaction or thioorganics with nucleophilic reagents such as organostannanes and boronic acids under neutral conditions (eq 1).



This very feature rapidly prompted chemists to design building blocks that contained both halogens as well as the thioether moiety. Under the neutral LSCC reactions conditions, the halogen-C bonds would be rendered inactive since a base is required to activate the boronic acid to participate in (for example) the Suzuki-Miyaura pathway. On the other hand, the S-C bonds would be inactive under the Suzuki-Miyaura or similar reactions since it requires the Cu(I) thiophilic co-factor to weaken the initially formed Pd-SR bond after the oxidative addition.^[16]

The LSCC has been used to efficiently functionalize the *meso*-position of 8-methylthioBODIPY **14**. The methylthio group has proven to be an excellent handle not only in Pd-catalyzed reactions, but also as an efficient leaving group in S_NAr-like reactions (Scheme 1).^[17]



Scheme 1. Reactivity of methylthioBODIPY **14**

In the context of our ongoing program to modify at will the BODIPY (Borondipyrromethene^[18]) core, we envisioned that the principle of orthogonal reactivity would be suitable to tailor its structure in order to produce derivatives with particular properties, amenable for different applications. Why would that be important? Due to the well-documented remarkable properties of BODIPYs,^[19] there is a continued effort to design

[a] Dr. C. F. A. Gómez-Durán, Dr. I. Valois Escamilla, Dr. A. Urías-Benavides, Prof. E. Peña-Cabrera
Departamento de Química
Universidad de Guanajuato
Col. Noria Alta S/N, Guanajuato GTO 36050, Mexico
E-mail: eduardop@ugto.mx

[b] I. Esnal, Dr. J. Bañuelos, Prof. I. López Arbeloa
Departamento de Química Física
Universidad del País Vasco (UPV/EHU)
Apto. 644, 48080 Bilbao, Spain.
E-mail: jorge.banuelos@ehu.es

[c] Prof. I. García-Moreno
Departamento de Sistemas de Baja Dimensionalidad, Superficies y Materia Condensada
Instituto de Química Física "Rocasolano", CSIC
Serrano 119, 28006 Madrid, Spain

Supporting information for this article is given via a link at the end of the document.

new analogues with specific properties of solubility, absorption, emission, quantum yield, and such. Hence, numerous BODIPY-related applications have appeared in the literature.^[20-27] Additionally, an excellent review was published recently on further applications of BODIPYs as well as different methods of halogenation.^[28]

Against that background, we prepared BODIPY **15a,b** (Figure 2). This compound features several reactive sites on the periphery of the main core,^[29] i.e., the methylthio group at the *meso*-position, two bromine atoms at the 2- and 6-positions and two methyl groups at positions 3 and 5. We reasoned that, for the aforementioned reasons, the *meso*-position would be activated under a specific set of conditions where neither the halogens nor the methyl groups would react. Then, bromine-bearing carbon atoms would engage in transition-metal catalyzed C-C bond-forming reactions such as Stille, Suzuki and Sonogashira, hence the orthogonal reactivity. Furthermore, the methyl groups would participate in the Knoevenagel reaction with aldehydes to extend the conjugation to produce a red shift in the final products.^[30] BODIPYs **15a,b** also possess two additional reactive sites, i.e., the B-F bonds. The replacement of the F atoms by alkoxy, phenoxy,^[31] alynyl,^[32] aryl,^[33] heteroaryl,^[34] Cl,^[35] and carboxylate moieties,^[36] has been reported, however, these transformations, though interesting, lie beyond the scope of this paper.

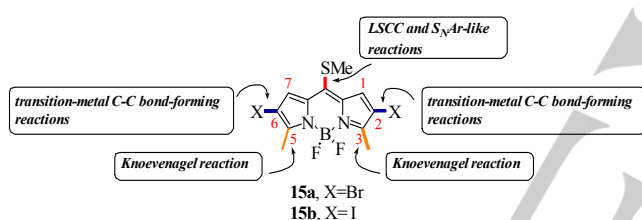


Figure 2. Different reaction sites of **15a,b**

The synthesis of fluorescent dyes within the spectral window 650-900 nm is one of the most active research areas^[37] since they are widely applied in several fields from analytical chemistry as fluorescence probes^[38] to lasers^[39] or in biomedicine for fluorescence imaging or photodynamic therapy.^[40] Indeed, this kind of dyes have distinct advantages for sensing purposes such as reduced background signal and scattering, which improves the sensibility, less interference from impurities or surrounding biomolecules, and deep penetration of the excitation laser irradiation into skin and tissues. Although a number of long-wavelength emitting commercial dyes are available, they have major drawbacks related to overlapping absorption and emission bands, which affects the sensibility limit, low energy gap between molecular orbitals, which enhances the nonradiative pathways increasing the photodegradation rate, low absorption at the standard excitation wavelengths, low water solubility, and high tendency to aggregate.

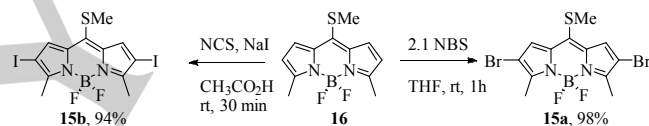
BODIPYs are outstanding as a promising and successful alternative to shift the emission deep into the red spectral region while keeping their efficiency and photostability.^[41] In fact, the

simple BODIPY core has been an excellent scaffold to assay the common synthetic strategies of long-wavelength fluorescent dyes such as the attachment of electron-donating and/or withdrawing moieties at the periphery to promote push-pull motif,^[42] the extension of the conjugated π -system through pendant aromatic chains,^[43] the conformationally restricted and rigid architectures by fusing aryl rings^[44] and/or the replacement of the central carbon by aza groups.^[45]

In this paper we follow the protocol described above, based on the orthogonal reactivity of the BODIPY scaffold to design a library of new BODIPY dyes with the most efficient and stable emission ever recorded in the 650-780 nm spectral region. Our approach provides facile and cost-effective strategy to overcome some of the most important drawbacks associated with commercial red-emitting laser dyes.

Results and Discussion

Synthesis of 15a,b. The preparation of **15a,b** were carried out in a straightforward manner. **15a** was prepared by reacting the Biellmann BODIPY **16**^[46] with NBS in THF at rt with a 98% yield, whereas **15b** was obtained in 94% yield, after treating **16** with *N*-Chlorosuccinimide (NCS) and NaI in acetic acid (Scheme 2).^[47]

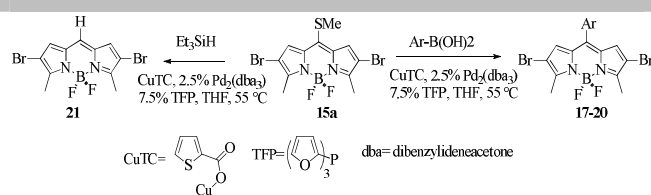


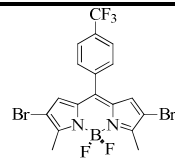
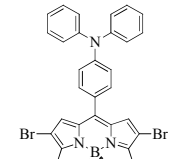
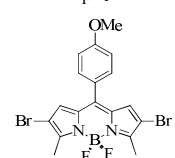
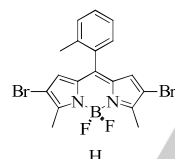
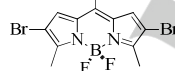
Scheme 2. Synthesis of BODIPYs **15a,b**

Functionalization of the *meso*-position. The *meso*-position was selectively functionalized in three different ways, i.e., via the LSCC with arylboronic acids, via a desulfative reduction of the MeS-group,^[17b] and via a S_NAr -like reaction with amines. The results of the first two transformations are shown in Table 1.

This step was crucial to our hypothesis, due to the fact that in this stage, the *meso*-position becomes differentiated from the bromine-bearing C atoms (2- and 6-positions). The yields in the cases studied ranged from good to excellent for both electron-withdrawing and electron-rich boronic acids. Sterically demanding 2-tolylboronic acid reacted smoothly with **15a** to produce **20** in good yield. The desulfative Liebeskind-Fukuyama reaction (entry 5) also occurred selectively and efficiently to reduce the MeS group demonstrating that the underlying principle of orthogonal reactivity also applies to this process. It is important to mention that in all of the reactions shown in Table 1, trace amounts of other colored compounds were observed, however, they were formed in such minute amounts, that it was impossible to unambiguously characterize them.

The third reaction used to functionalize the *meso*-position of **15a,b** was the S_NAr -like reaction with different amines (Table 2).

Table 1. Selective LSCC and desulfurative reaction on **15a**


Entry	Time (h)	% yield ^[a]	Product	Cmpd
1	1	81		17
2	2.5	93		18
3	1	60		19
4	2	83		20
5	4	75		21

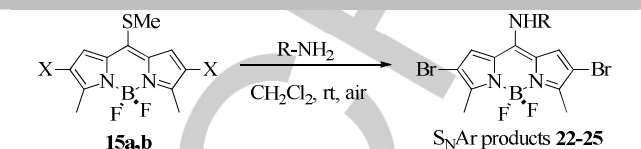
^[a] Isolated yields. Typical run: **15a** (1 equiv), arylboronic acid (3 equiv), CuTC (3 equiv), Pd₂(dba)₃ (2.5%), TFP (7.5%). For the case of **21**, 3 equiv of Et₃SiH were used.

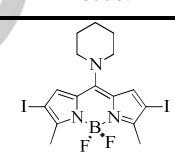
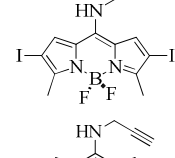
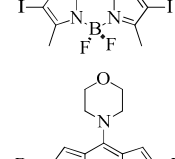
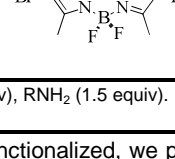
In this process, the only susceptible site for a nucleophilic attack is the *meso*-position since the negative charge that develops upon the amine attack, would be stabilized by the BODIPY N atoms previously to the expulsion of the MeS group (Figure 3).

**Figure 3.** Proposed reaction mechanism for the formation of *meso*-aminoBODIPYs

Neither the 2- nor 6-position, albeit bearing a Br atom, are reactive towards an S_NAr reaction since the negative charge resulting from the attack of the amino group at the said positions would never be stabilized by the BODIPY N atoms. Thus, both

primary and secondary amines smoothly reacted at room temperature under air in acetonitrile.

Table 2. Selective S_NAr-like reaction of **15a,b**.


Entry	X	Time (h)	% yield ^a	Product	Cmpd
1	I	1	81		22
2	I	2.5	93		23
3	I	1	60		24
4	Br	2	83		25

^a Isolated yields. Typical run: **15a,b** (1 equiv), RNH₂ (1.5 equiv).

Once the *meso*-position was functionalized, we proceeded to elaborate the 2- and 6-position.

Sequence LSCC-Suzuki. Selected examples of the LSCC products of Table 1 were chosen as starting materials to carry out the Suzuki reaction. The results are illustrated in Table 3.

Electron-deficient arylboronic acids reacted faster than their electron-rich counterparts, especially with electron-rich BODIPY partners (entries 1, 3, 7). The overall yields in the series studied do not show a clear pattern with respect to the electronic nature of either the *meso*-substituent on the BODIPY core, or that of the arylboronic acid. Likewise, the reaction does work, albeit with modest yields, no matter what the electronic properties of either partner.

Sequence S_NAr-Suzuki. Next, we proceeded to carry out the Suzuki coupling on electron-rich 8-morpholinoBODIPY **25** (Table 4).

A striking difference was observed in the reaction time. When electron-poor boronic acids were used, the reactions went to completion within 4h, on the other hand, when electron-rich boronic acids were utilized, the reactions became very sluggish, with reaction times of 12 and 26h (entries 1 and 4). A similar pattern was observed in Table 3. The % yields of this process remained within a narrow range in the cases analyzed (65-80%).

Table 3. Products from the sequence LSCC.Suzuki.

Entry	LSCC starting material	Ar ₂	Time (h)	% yield ^[a]	LSCC-Suzuki product	Cmpd
1	18		3.0	63		26
2	18		6.0	52		27
3	18		3.0	43		28
4	17		7.5	49		29
5	17		7.0	41		30
6	17		4.0	51		31
7	19		2.5	44		32
8	19		5.0	38		33
9	19		6.0	50		34

^[a] Isolated yields. Typical run: LSCC starting material (1.0 equiv), boronic acid (3.0 equiv), Pd₂(dba)₃ (10%), Cy₃PHBF₄ (40%), Cs₂CO₃ (4.0 equiv).

Sequence LSCC-Stille. LSCC product **17** was chosen as starting material to study the Stille coupling with some organostannanes. The results are included in Table 5.

This process was not as general as the others studied. Only 2-thienyl- and 2-methoxy-4-thiazolylstannane produced the desired product in modest yield. Two of the representative examples that did not work are shown. In all of the unsuccessful cases, it appeared that the product was being generated, but after a short while, the reaction went to complete decomposition to give an untreatable dark material that did not move from the TLC baseline even with polar eluents. We are not clear at the present time of the factors that govern the Stille coupling using **17**. The reasons that the products would be inherently unstable are not apparent at this point, i.e., product **29** was uneventfully obtained following the LSCC-Suzuki sequence (see Table 3, entry 4). Moreover, there are cases of Stille couplings using halogenated BODIPYs as starting materials.^[48]

Sequence S_NAr-Sonogashira. The initial attempts with brominated aminoBODIPY **25** rendered very sluggish reactions; therefore, we turned our attention to the iodinated analogues. For this process, two starting materials were chosen, one with a primary amino group at the *meso*-position **23**, and another with a secondary amino group **22**. This selection was made in order to explore if the extend of the conjugation of the nitrogen lone pair of the BODIPY^[17k] core would significantly modify the outcome of the Sonogashira reaction. We have demonstrated that, in compounds such as **23**, the amino group exhibits a significant electron-donation onto the BODIPY core owing to the ability of the amino group to adopt a nearly planar conformation with respect to the BODIPY moiety. On the other hand, the amino group in **22** places itself in a twisted conformation in relation to the BODIPY core, thereby reducing the electron-donation. The results are illustrated in Table 6.

After the analysis of these results, it becomes apparent that, the richer the BODIPY core, the shorter the reaction times (entries 1-4). Also, the less electron-rich the BODIPY core, the slightly better chemical yields were obtained (entries 5-8).

Sequence LSCC-Knoevenagel. LSCC starting materials **17**, **19**, and **20** were chosen to be further elaborated via the Knoevenagel reaction.^[49]

Table 4. Products from the sequence S _N -Ar-Suzuki					
Entry	Ar	Time (h)	% yield ^[a]	S _N Ar-Suzuki product	Cmpd
1		12.0	80		35
2		3.5	65		36
3		4.0	72		37
4		26	75		38
^[a] Isolated yields. Typical run: BODIPY 25 (1 equiv), boronic acid (3.0 equiv), Pd ₂ (dba) ₃ (10%), Cy ₃ P.HBF ₄ (40%), Cs ₂ CO ₃ (4.0 equiv)					

Table 5. Products from the sequence LSCC-Stille					
Entry	(Het)Ar	Time (h)	% yield ^[a]	LSCC-Stille product	Cmpd
1		4.0	49		39
2		3.0	47		40
3		1	Dec.		41
4		1	Dec.		29
^[a] Isolated yields. Typical run: BODIPY 17 (1 equiv), PdCl ₂ (PPh ₃) ₂ (10%), P(<i>t</i> -Bu) ₃ (20%), CuI (10%). Dec.: Decomposition (see text)					

The Knoevenagel reaction took place smoothly in the three substrates to provide the expected products. We realize that the number of examples in Table 7 is small to be able to draw a trend, but it is apparent that BODIPY **17** showed the highest reactivity and %yield presumably because the acidity of its methyl protons is higher than those of **19** and **20** by virtue of having more electron-withdrawing groups on its periphery.

Sequence LSCC-Knoevenagel-Suzuki. The three products from the LSCC-Knoevenagel sequence were used as starting materials; one having an electron-donating group at the *meso*-position **52**, one with an electron-withdrawing group **50**, and another with a neutral group, but with restricted rotation **51** (Table 8). Two boronic acids with different electronic properties were chosen, 4-methoxyphenyl- and 4-formylphenylboronic acid.

In general, the yields of the Suzuki couplings were modest, obtaining the highest ones when the *meso*-position was occupied by an electron-withdrawing group (entries 3 and 4). There was no evident influence in the yields of the nature of the boronic acids employed. The lowest yield (entry 2) represents that of two individual Suzuki couplings with a 50% yield each. It is important to underscore that, even though the chemical yields of this step were modest, the richness of functional groups is exceptional. The flexibility of this methodology was demonstrated.

Photophysical properties

As was emphasized in the introduction, the photophysical and laser characterization was focused on the new dyes with emission in the red-near NIR spectral window (Table 7 and 8), due to its special novelty and technological relevance. The fully functionalized **53-58** BODIPYs (Table 8) show sharp and intense spectral bands located at the red-edge of the visible spectrum (Figure 4). In all the herein reported dyes the bathochromic shift with regard to the simplest core is beyond 150 nm, as result of an extended delocalized π -system, which is reflected also in a higher molar absorption coefficient (surpassing $10^5 \text{ M}^{-1} \text{ cm}^{-1}$ in most cases). It is noteworthy the remarkable increase of the absorption band placed at around 350 nm (usually assigned to the S₀→S₂ transition) due to the interaction of the peripheral aromatic chains with the chromophoric core (Figure S1 in ESI). It is also noticeable that this strong UV absorption allows the use of different excitation sources spanning the UV-Vis region, which is a key property for photonic purposes. The calculated molecular orbitals show an extended conjugated π -system through the aromatic moieties attached at positions 3/5, and 2/6, being more efficient through the former chromophoric positions (Figure 4). As a rule, the promotion from the HOMO to the LUMO implies transfer of electronic charge from the pendant aromatic units to the dypirromethene framework, mainly from the aromatic moieties attached at positions 2 and 6, which contribution to the LUMO is almost null.^[50]

Table 6. Products from the sequence S_NAr -Sonogashira

Entry	S_NAr s.mat.	Time (h)	% Yield ^[a]	S_NAr -Sonogashira product	Cmpd
1	23	3.0	75		42
2	23	1.0	60		43
3	23	1.0	40		44
4	23	0.5	50		45
5	22	7.0	80		46
6	22	6.0	60		47
7	22	0.5	55		48
8	22	12.0	40		49

^[a] Isolated yields. Typical run: BODIPY **22** or **23** (1 equiv), alkyne (3 equiv), Pd(PPh₃)₂Cl₂ (9.5%), PPh₃ (20%), CuI (10%).

Table 7. Products from the sequence LSCC-Knoevenagel

Entry	LSCC s. mat.	Time (h)	% Yield ^a	LSCC-Knoevenagel product	Cmpd
1	17	1.0	86		50
2	20	2.5	63		51
3	19	4.0	70		52

^[a] Isolated yields. Typical run: LSCC starting mat. (1 equiv), aldehyde (4 equiv), acetic acid (0.3mL), piperidine (0.3 mL).

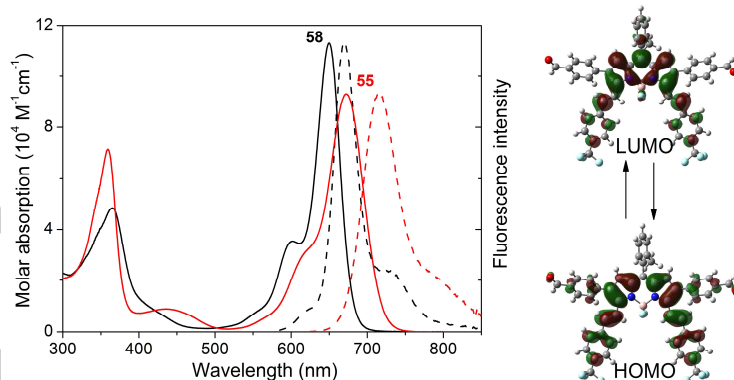


Figure 4. Absorption and normalized fluorescence (dashed) spectra of dyes **55** and **58** in cyclohexane. The frontier orbitals of the former dye are included to show the extended polymethine π -system.

Table 8. Products from the sequence LSCC-Knoevenagel-Suzuki

Entry	LSCC-Knoevenagel s. mat.	Ar ₂ -	Time (h)	% Yield ^[a]	LSCC-Knoevenagel-Suzuki product	Cmpd
<p style="text-align: center;">LSCC-Knoevenagel s. mat. + Ar₂B(OH)₂ $\xrightarrow[\text{THF/H}_2\text{O}, 55^\circ\text{C}]{\text{Pd}_2(\text{dba})_3, \text{Cy}_3\text{P}, \text{HBF}_4, \text{Cs}_2\text{CO}_3}$ LSCC-Knoevenagel-Suzuki products 53-58</p>						
1	52		21	36		53
2	52		7.0	25		54
3	50		8.5	67		55
4	50		9.0	60		56
5	51		6.0	37		57
6	51		4.0	48		58

^[a] Isolated yields. Typical run: LSCC-Knoevenagel s. material (1 equiv), boronic acid (3.0 equiv), Pd₂(dba)₃ (10%), Cy₃PHBF₄ (40%), Cs₂CO₃ (4.0 equiv).

All these red-emitting BODIPYs bear the same aromatic arm at positions 3 and 5 but differ in the peripheral units placed at 2 and 6 positions, and especially at position 8, which probably is the most sensitive one to the substituent effect regarding fluorescence response. In the following lines, we will analyze in depth the impact of the modification of chromophoric structure on the photophysical signatures of the dye.

At a first sight, the dyes bearing an *ortho*-substituted aryl at 8-position (**57**, **58**) should be the most suitable for improved fluorescence efficiency, since this methyl group might hinder the free motion of the phenyl ring and suppress its associated nonradiative relaxation pathway.^[51] In fact, the ring is twisted 72° with respect to the indacene plane, a geometrical disposition in which the electronic coupling is totally avoided. As consequence, dye **58** shows a strong absorption ($\epsilon_{\text{max}} > 10^5 \text{ M}^{-1} \text{ cm}^{-1}$) and effective emission (87%, almost insensitive to the solvent

As pointed out in the introduction, the presence of electron donor/acceptor moieties in the BODIPY framework should have a deep impact in both the spectral band positions and the fluorescence signatures. In fact, the replacement of the electron-withdrawing formyl group (dye **58**) by the strong electron donor methoxy group (dye **57**) at positions 2 and 6, exerts a more pronounced bathochromic shift but reduces the fluorescence efficiency and lifetimes mainly in polar media (Table 9). The presence of a donor (methoxy) and electron-attracting (trifluoromethyl) entities in the same structure infers a “push-pull” character to the dye. As stated above, the excitation from HOMO to LUMO implies electronic transfer from the aromatic arms at position 2 and 6 to the BODIPY core. Accordingly, such behaviour should be strengthened by the presence of electron-releasing groups in such position, leading to further bathochromic shift. Nonetheless, unlike typical BODIPYs, the emission band shifts bathochromically with the solvent polarity (around 10 nm) leading to a markedly increase of the Stokes shift (up to 1090 cm^{-1} in methanol). Thus, the excited state

properties) centred at 670 nm (Table 9), in spite of the proximity of the ground and excited states. Overall one of the main reasons of the lack of fluorescence emission of long-wavelength emitting dyes is the internal conversion deactivation. The low energy gap in the red-NIR spectral region enhances the overlap between the vibrational levels of the S_0 and S_1 states, and hence the nonradiative relaxation pathways are more feasible. Nonetheless, the lowering in the energy gap of dye **58** implies high radiative rate constant (up to $1.9 \times 10^8 \text{ s}^{-1}$), whereas the nonradiative probability remains low (lower than $0.7 \times 10^8 \text{ s}^{-1}$). As result, the recorded fluorescence lifetimes (around 4.5 ns) are similar to those recorded for typical BODIPYs working in more energetic spectral regions. Therefore, the herein reported molecular architectures are ideal to shift the emission deep into the red, whereas retaining almost the high fluorescence efficiency characteristic of BODIPY (Table 9).

evolves from a cyanine-like π -system, characterized by a negative solvatochromism of the fluorescence band (*i.e.*, dye **58**), to a charge transfer one with positive solvatochromism by the coexistence of an electron-donor methoxy (push) and an electron-withdrawing trifluoromethyl (pull) groups in the same structure (*i.e.*, dye **57**).^[52] At the same time and, as a consequence of this induced charge separation, the fluorescence quantum yield (from 61% to 13%) and lifetime (from 4.2 ns to 1.2 ns) of dye **57** progressively drop on increasing the solvent polarity (Table 9).

Similar trends are also recorded, in higher or lower extent, from all other BODIPYs bearing electron-acceptor substituents (dyes **54** and **56**) or electron-donor groups (dyes **53** and **55**, respectively) (Table 9). It is noteworthy that in these sets of derivatives, the fluorescence efficiency registered in apolar media is quite high (up to 67%) in spite of the allowed free rotation of the 8-aryl group. It seems that the removal of electronic density from the central *meso* chromophoric position by the delocalization extension through the 3 and 5 positions

Table 9. Photophysical properties of the fully functionalized BODIPYs **53–58** in apolar cyclohexane (c-hex) and polar methanol (MeOH); absorption (λ_{ab}) and fluorescence (λ_{fl}) wavelength, Stokes shift ($\Delta\nu_{\text{St}}$), molar absorption coefficient at the maximum (ϵ_{max}), fluorescence quantum yield (ϕ) and lifetime (τ). More data are included in Table S1 in ESI.

Dye	λ_{ab} (nm)	ϵ_{max} ($10^4 \text{ M}^{-1} \text{ cm}^{-1}$)	λ_{fl} (nm)	$\Delta\nu_{\text{St}}$ (cm^{-1})	ϕ	τ (ns)	k_{fl} (10^8 s^{-1})	k_{nr} (10^8 s^{-1})
53 <i>c-hex</i> <i>MeOH</i>	661.0	8.5	696.0	760	0.47	4.46	1.05	1.20
	653.0	6.8	703.0	1090	0.11	1.50 (70%) 0.62 (30%)	-	-
54 <i>c-hex</i> <i>MeOH</i>	645.0	5.9	662.5	410	0.58	4.51	1.28	0.93
	638.0	5.6	661.0	545	0.49	4.40	1.11	1.16
55 <i>c-hex</i> <i>MeOH</i>	672.5	9.3	715.0	885	0.47	3.70	1.27	1.43
	664.5	8.7	726.0	1275	0.06	0.73 (99%) 3.08 (1%)	-	-
56 <i>c-hex</i> <i>MeOH</i>	666.5	11.3	699.0	700	0.67	4.60	1.45	0.72
	659.0	10.3	699.0	870	0.39	3.18	1.22	1.92
57 <i>c-hex</i> <i>MeOH</i>	665.0	10.9	701.0	770	0.61	4.25	1.43	0.92
	657.5	8.9	708.0	1090	0.13	1.20	1.09	7.25
58 <i>c-hex</i> <i>MeOH</i>	650.0	11.3	670.0	460	0.87	4.61	1.90	0.28
	644.0	10.4	668.0	560	0.73	4.36	1.67	0.62

decreases the nonradiative deactivation pathway via the vibrational coupling of the aryl with the indacene core.^[53] As a matter of fact, an increase of the solvent polarity in those derivatives of the 8-*para*-trifluoromethyl-phenyl or 8-*para*-methoxy-phenyl, bearing also *para*-methoxy-phenyl groups at positions 2 and 6 (dyes **55** and **53**, respectively), leads to more red-shifted emission bands, higher Stokes shifts, lower fluorescence quantum yields, and lifetimes (even the decay should be fitted as biexponential, Figure 5) as result of an increase of the nonradiative deactivation processes induced by the charge separation (Table 9). Noticeably, such evolution is softened replacing the methoxy groups, at position 2 and 6, by substituents with no electron-releasing character, such as the formyl group (dye **56** and **54**). Thus, relatively high fluorescence quantum yield can be attained even in polar solvents (around 40-50%) since the fluorescence quenching in these media is less efficient as result of a lower "push-pull" character of the transition (Table 9).

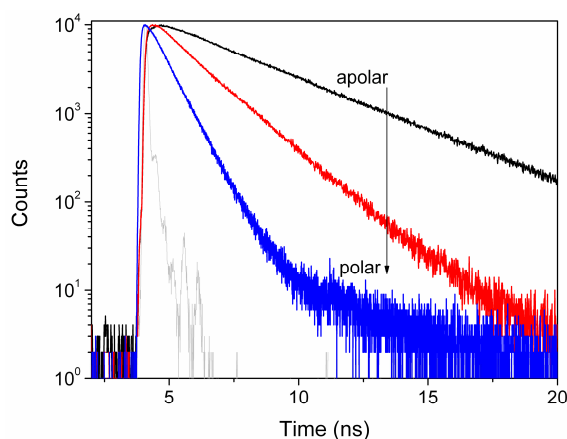


Figure 5. Fluorescence decay curves of dye **55** with regard to the solvent polarity; from cyclohexane to ethyl acetate and methanol.

The aforementioned charge transfer character of dyes, which combine strong electron- acceptor and donor end groups, is nicely reflected in Figure 6 through the electrostatic potential maps theoretically calculated for some representative red dyes. While in **57** (with an aryl ring at 8-position) the negative charge is located mainly in the BF₂ bridge (red region), as is typical in alkylated-BODIPYs, and the positive charge around the 8-phenyl group, the presence of an electron-releasing group (methoxy in **53**) or a withdrawing one (trifluoromethyl in **55**) grafted in *para* position of the 8-phenyl infers a "push-pull" character to the dye. As result, the charge distribution is rearranged and new centres in which negative or positive charge is located are induced (Figure 6). In fact, in these derivatives the BF₂ bridge carries less negative charge (the red colour is lighter) since it is shifted to the electron-withdrawing trifluoromethyl end groups (yellow regions) located at both 8 and 3,5 positions (dye **55**) and, alternatively, the positive charge is located around the methoxy groups (blue regions) especially when it is also linked to the 8-phenyl unit (dye **53**). The charge transfer character is more evident in dye **55**, where the "push-pull" effect, induced by the

presence in the same molecule of two peripheral methoxy groups and three trifluoromethyl units, leads to a decrease of the negative charge in the dipyrromethene core (greener), which is reflected in a more efficient quenching and faster deactivation of the excited state (Figure 5 and Table 9).

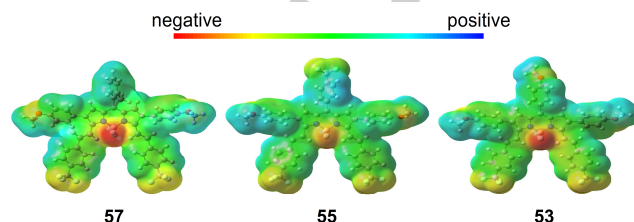


Figure 6. Electrostatic potential mapped onto the electronic density for the compounds bearing *para*-methoxyphenyl at positions 2 and 6 and *para*-trifluoromethylstyryl at positions 3 and 5, but *ortho*-methylphenyl (**57**), *para*-trifluoromethylphenyl (**55**) and *para*-methoxyphenyl (**53**) at 8-position.

Therefore, in order to achieve dyes with their emission pushed towards the red as much as possible while keeping a high fluorescence response, a compromise between both structural parameters, the presence of electron donor/acceptors groups and the extended π -system through aromatic frameworks, should be reached. The promotion of "push-pull" effects in the dye together with extended π -systems is a good strategy to achieve emissions in the red-edge. However, the molecular design should be considered that a too strong charge transfer, albeit is very efficient pushing the emission deep into the red, could be deleterious for the fluorescence efficiency mainly in polar environment.

In this context, it is also noteworthy the photonic behaviour of the brominated precursors of the above set of compounds as red-emitting dyes (**50-52**). It is widely known that heavy atoms should be avoided to achieve highly fluorescent dyes because of the enhancement of intersystem crossing processes. However, it must be stressed that all these brominated compounds at positions 2 and 6 exhibit high fluorescence efficiencies, up to 81% (Table 10), albeit less shifted to the red than the above mentioned fully extended derivatives (Figure 7 and Figure S2 in ESI). Moreover, even in the derivatives bearing trifluoromethyl or methoxy end groups at *meso* position, high fluorescence quantum yields are recorded regardless of the solvent (up to 70% in methanol, Table S2 in ESI) since the above mentioned "push-pull" effect is drastically reduced and the BODIPY retains its cyanine-like delocalization. Therefore, using orthogonal reactivity as synthetic strategy for selected functionalization of the BODIPY core, the usually avoided bromine atoms are also adequate to attain bright red-emitting dyes probably because the spin-orbit coupling in an π -extended chromophore should be less efficient. To get a deeper insight into such behaviour we have also considered the corresponding derivative **20** without aromatic chains at the 3 and 5 positions. In this last dye, the bromine atoms decrease the fluorescence quantum yield from 81% in the related **51** to 41%, owing to an enhancement of the nonradiative pathways (Table 10). The simulated energy levels

reveal that, in dye **20**, three triplet states lie down its singlet emitting state (Figure 7), which makes the intersystem crossing more feasible from a thermodynamic point of view due to its low singlet-triplet energy gap (0.04 eV). The energy of the triplet states and the singlet-triplet energy gap rises up as the π -system is extended (dye **51**) and, of course, by removal of the bromine atoms (dye **57**). Therefore, these brominated BODIPYs, besides being excellent framework for further functionalization or as linking point for target entities, as is demonstrated in the present work, they are suitable scaffolds to develop bright red emitting dyes.

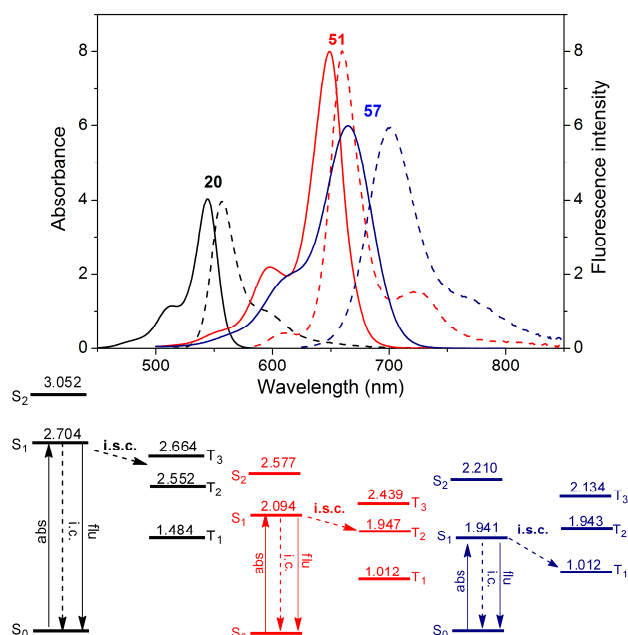


Figure 7. Normalized absorption and fluorescence (dashed) spectra scaled by their fluorescence efficiency of dyes **20**, **51** and **57**. The corresponding energy diagram in eV including singlet and triplet states is also added.

Table 10. Photophysical properties of the brominated BODIPYs **50-52** in cyclohexane. The data of **20** is included for comparison. Additional data are listed in Table S2 in ESI.

	λ_{ab} (nm)	ϵ_{max} ($10^4 M^{-1}cm^{-1}$)	λ_{fl} (nm)	$\Delta\nu_{St}$ (cm^{-1})	ϕ	τ (ns)	k_{fl} ($10^8 s^{-1}$)	k_{nr} ($10^8 s^{-1}$)
50	656.5	11.6	672.0	350	0.62	4.53	1.36	0.84
51	649.0	12.4	660.0	255	0.81	4.60	1.76	0.41
52	645.0	11.6	656.0	260	0.81	4.56	1.77	0.42
20	544.5	11.1	557.0	410	0.41	3.74	1.09	1.58

Lasing properties

The lasing properties of the new BODIPYs were studied under pumping at 532 nm, which is the usual pump wavelength for dyes emitting in the red spectral region. However, and according to the absorption properties of the new dyes, only derivative **20** is suitable for excitation at this wavelength since the orthogonal functionalization of the BODIPY core induces a significant bathochromic shift of its absorption bands locating the maximum

absorption within the 630-680 nm spectral region and leaving the absorption coefficients at 532 nm below $3000 M^{-1} cm^{-1}$. In turn, this orthogonal functionalization induces a strong absorption in the UV region (Figure 4 and S1 and S2 in ESI), which allows pumping these derivatives at 355 nm, which is other usual pump wavelength for laser dyes, especially for those dyes with emission in the blue-green spectral region although it is much less common radiation to excite dyes with red-shifted emission. These new dyes allow overcoming one of the major limitations exhibited by red-emitting commercial dyes such as its low absorption at standard pumping wavelengths, such as 355 and 532 nm, which imposes the use of high concentrations leading to solubility, quenching and aggregation problems, all with detrimental effect on the laser action.

To optimize the laser action, we first analyze the dependence of the laser emission on the dye concentration in ethyl acetate solutions with optical densities (1 cm path length) in the range 1-35 while keeping constant all other experimental parameters. Under our experimental conditions (transversal excitation and strong focusing of the incoming pump radiation) the concentration of the dyes should be in the millimolar range, to ensure total absorption of the pump radiation within the first millimeter at most of the solution, in order to obtain an emitted beam with near-circular cross-section and optimize the lasing efficiency (defined as the ratio between the energy of the dye laser output and the pump energy incident on the sample surface).

Under the selected experimental conditions, broad-line-width laser emission with pump threshold energy approximately 0.6 mJ, divergence of 5 mrad and pulse duration of 8 ns full width at half maximum (FWHM) is obtained from the new dyes when placed in a simple plane-plane non-tunable resonator. The lasing properties recorded with the optimal concentration for each dye are presented in Table 11. The lasing behavior of the new dyes shows good correlation with their photophysical properties: the higher the fluorescence quantum yield, the higher the lasing efficiency; the longer the fluorescence wavelength, the "redder" the lasing emission; the lower the nonradiative rate constant, the higher the lasing photostability.

The new dyes lase with high efficiencies, ranging from

33% (dye **55**) up to 60% (dye **58**), including the brominated derivatives whose efficiencies are between 49% (dye **50**) and 56% (dye **52**). In this context, it is noteworthy the peculiar behavior of some derivatives, such as **57**, **53** and **55**, because although they exhibit low fluorescence quantum yields, 30%, 25% and 17%, respectively, reach efficiencies as high as 43%. As it was discussed in the photophysical properties section, these three dyes show: a) high Stokes shift (up to $1170 cm^{-1}$), which reduces reabsorption/reemission processes and, thus, their deleterious effect in the laser action and b) very short fluorescence lifetimes (below to 1.71 ns), which lead to radiative rate constants similar to those observed for the other dyes. The combination of these factors in the same molecule is responsible for some of the unique lasing properties exhibited by these new BODIPY dyes.

Table 11. Lasing properties of new BODIPY dyes at the dye concentration that optimize the laser action in ethyl acetate solutions. [c]: dye concentration; Eff: lasing efficiency (ratio between the energy of the laser output and the pump energy incident on the sample surface); λ : peak wavelength of the laser emission; Intensity of the laser-induced fluorescence emission (I_n) after 50 000 pump pulses at 10 Hz repetition rate

	50	51	52	53	54	55	56	57	58
[c]/mM	0.5	0.8	0.9	0.8	0.9	0.6	0.4	0.6	0.7
Eff(%)	49	55	56	38	47	33	46	43	60
λ /nm	695	680	670	728	685	760	717	740	700
I_n (%) ^[a]	100	100	100	89	100	84	100	93	100

^[a] I_n (%) = 100 (I_n/I_0) with I_0 being the initial intensity

Regarding the lasing wavelength, the effective control of both the orthogonal reactivity of BODIPY framework and the electron-donor strength of the substitution pattern, allow modulating the lasing emission of these novel dyes over a wide range (670-740 nm) in the red-NIR spectral region. While brominated derivatives have the laser emission centered on the red region of the spectrum (670-695 nm), their substitution at position 2 and 6 pushes the lasing wavelength towards the NIR spectral region (685-740 nm) (Figure 8). In fact, the tuning capability of the new BODIPYs, one of the most important features of laser dyes, is determined by placing their liquid solutions in the grazing-incidence grating tunable resonator. Tunable laser emission with a linewidth of the order of 0.15 cm^{-1} , and a tuning range of up to 120 nm was thus recorded, and the spectral region 660-750 nm can be continuously covered with narrow-linewidth laser radiation by using these new dyes.

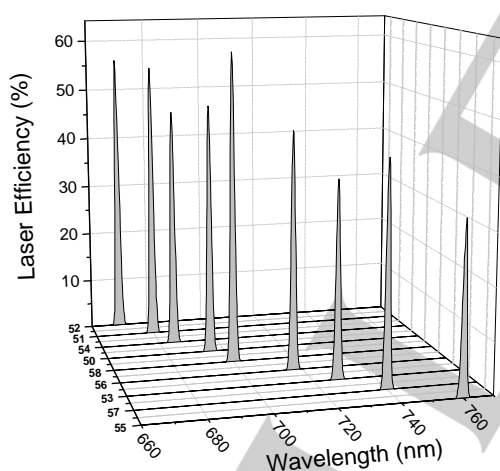


Figure 8. Lasing emission spectra of the new BODIPY dyes in ethyl acetate solution recorded under transversal pumping at 355 nm.

Following the photophysical analysis, the actual effect of the solvent on the laser action was analyzed in solutions of a polar protic solvent such as methanol and an apolar solvent such as *c*-hexane. Although the photophysical studies showed that the new derivatives exhibited their highest fluorescence capacity when dissolved in *c*-hexane, the low solubility of the new BODIPYs in this solvent prevented preparation of solutions at the concentration required for laser experiments under the

pumping conditions selected in the present work. In methanol, each dye was dissolved at the concentration that was found to optimize its emission in ethyl acetate (that is, the concentrations tabulated in Table 11). Once again, the lasing behavior of the new compounds is in good agreement with their photophysical properties (see Tables S1-S2 in ESI). On the one hand, the laser action of the brominated derivatives as well as those dyes with formyl as end group grafted at positions 2 and 6 (**58** and **54**), appear to be independent on the nature of the solvent. On the other hand, the laser efficiency of the other derivatives in methanol is slightly lower (≈ 1.2 times) than that recorded in ethyl acetate.

An important parameter for any practical application of the dye lasers is their lasing photostability under repeated pumping. In Table 11 are collected data on the decrease of the laser-induced fluorescence intensity, under transversal excitation of capillary containing dye solutions in ethyl acetate (see Experimental section), after 50 000 pump pulses at 10 Hz repetition rate. Even under drastic pumping conditions, all the new BODIPYs results to be highly photostable dyes, since, they maintain their initial laser output without sign of degradation or, in the worst scenario, the laser emission drops by less than 20% during the pumping process.

To put the present results in perspective, the lasing parameters of commercial dyes, which lase in the same region as the newly synthesized dyes, were also measured under similar experimental conditions (Table 12). This aim requires analyzing the laser emission from ethyl acetate solutions of at least 7 commercial dyes to cover 80 nm in the red spectral region (650-730 nm), such as Cresyl Violet (650 nm); Oxazine 720 (675 nm), LDS698 (695 nm), NileBlue (700 nm), LDS 722 (715 nm), LDS 730 (725 nm) and Oxazine 725 (730 nm).

Table 12. Lasing properties of commercial laser dyes, with emission in the same spectral region than the new BODIPYs, in ethyl acetate solution transversally pumped at 532 nm.

	Cresyl Violet	OX 720	LDS 698	Nile Blue	LDS 722	LDS 730	OX 725
[c]/mM	10	9	8	10	8	10	10
Eff(%)	29	22	38	20	32	35	28
λ /nm	650	675	695	700	715	725	730
I_n (%)	0	0	0	0	0	0	0
$n/1000$	3	4	50	8	20	50	5

The first drawback of these dyes is their no absorption in the UV region and even their low molar absorption coefficients at 532 nm, which requires preparing high concentrated solutions, in the order of 10 mM. Under these experimental conditions, the commercial dyes exhibit lasing efficiencies ranging from 22-38% (Table 12), much lower than those achieved with the new BODIPYs, as can be clearly seen in Figure 9. But what is more important, these commercial dyes are much more unstable than the new BODIPYs since none remains at its initial laser output after 50 000 pump pulses. In fact, four of them lose completely their emission after just 8 000 pulses, and the laser action from the commercial dyes that prove to be more photostable, such as LDS 698 and LDS 730, drops to 50% of its initial value after 30000 pulses.

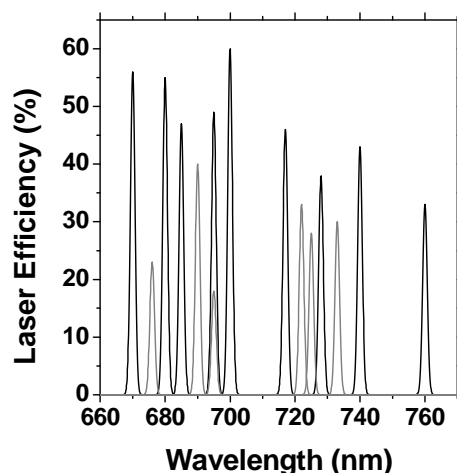


Figure 9. Laser efficiency of the new BODIPYs (dark line) and the commercial dyes (grey line) with emission in the same spectral region

Conclusions

Herein, we have described the synthesis of polyfunctional BODIPY building blocks (**15a,b**) suitable to be subjected to several reaction sequences with complete chemoselectivity, which allowed the preparation of complex BODIPY derivatives in a versatile and programmable manner. The reactions included: Liebeskind-Srogl (LSCC), Suzuki, Sonogashira, and Stille cross-coupling reactions, S_NAr , and a desulfurative reduction of the MeS- group. It is clear, however, that many others can be attempted, for example, the MeS group can be transthiolated^[17r] or displaced by C-centered soft nucleophiles.^[17q] The halogen-bearing C atoms may engage in a host of transition metal-catalyzed reactions such as the Negishi and Hiyama cross-couplings, in C-heteroatom bond-forming processes, polymerizations, and such. In addition to the reactions shown in this contribution, as mentioned in the introduction, both **15a,b** possess two additional B-F bonds that would offer even more reaction sites that can be used, for example, to modify the solubility properties of the new derivatives. These additional transformations not only will enrich the basic knowledge of BODIPYs, but also will broaden the possibilities of their applications.

In fact, this novel synthetic protocol has proved to be a powerful route to design a library of compounds with tailored photophysical properties for advanced applications. Such fine control of the molecular structure prompted us to design red-emitting laser dyes based on the BODIPY core. The extension of the delocalized π -system is probably the most recommended strategy to shift the spectral bands to the red part of the visible region, while ensuring a bright emission. Even the brominated derivatives result an optimal alternative, since some of the herein reported brominated dyes show emission peaked at around 680 nm with fluorescence quantum yields as high as 87%. The combination of such methodology with electron-rich substituents grafted to BODIPY core provides additional bathochromic shifts (up to 710 nm) but inducing “push-pull”

effects deleterious for fluorescence efficiency. Therefore, from the photophysical point of view, a rational balance has to be achieved between bathochromic shift and fluorescence response to optimize the performance of red-emitting BODIPYs.

The new library of BODIPYs exhibit outstanding laser performance under transversal pumping at 355 nm, with high efficiencies, up to 60%, and high photostability, remaining their laser emission without sign of degradation after 50 000 pump pulses at 10 Hz repetition rate, and wavelength-finely tunable emission covering a wide red-NIR spectral region (650-750 nm). The laser action of the new dyes outperforms the lasing behaviour of dyes considered to be benchmarks over the red spectral region, shortcoming the important drawbacks exhibited by these commercial laser dyes: low absorption at the standard pump wavelengths (355 and 532 nm) and/or poor photostability. In fact, to the best of our knowledge, the laser behaviour of the new BODIPYs is the topmost achieved for organic, inorganic and hybrid dyes with emission in the red-NIR spectral region, furthering their practical application, in the mid-term, in both optoelectronic and biophotonic fields.

Experimental Section

Synthetic procedures and characterization data, photophysical and computational results, NMR spectra of the new compounds are included in the Supporting Information.

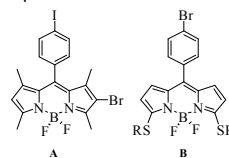
Acknowledgements

This work was supported by Ministerio de Economía y Competitividad (Projects MAT2014-51937-C3-1 and C3-03) and Gobierno Vasco (Project IT339-10), which is also thanked by a contract for I. E. We thank CONACyT (Grants 129572 and 123732). C. F. A. G.-D. and A. U.-B. thank CONACyT for graduate scholarships. I. V.-E. thanks CONACyT for postdoctoral fellowship. Donation of **16** by Cuantico de Mexico is greatly appreciated.

Keywords: BODIPY • synthesis • NIR dyes • photophysics • laser

- [1] N. Hadei, G. T. Achonduh, C. Valente, C. J. O'Brien, M.G. Organ, *Angew. Chem. Int. Ed.* **2011**, *50*, 3896-3899.
- [2] J. Terao, H. Todo, S. A. Begum, H. Kuniyasu, N. Kambe, *Angew. Chem. Int. Ed.* **2007**, *46*, 2086-2089.
- [3] O. Vechorkin, D. Barmaz, V. Proust, X. Hu, *J. Am. Chem. Soc.* **2009**, *131*, 12078-12079.
- [4] a) A. F. Littke, C. Dai, G. C. Fu, *J. Am. Chem. Soc.* **2000**, *122*, 4020-4028; b) X. Zhang, A. Liu, W. Chen, *Org. Lett.* **2008**, *10*, 3849-3852.
- [5] R. A. Altman, A. M. Hyde, X. Huang, S. L. Buchwald, *J. Am. Chem. Soc.* **2008**, *130*, 9613-9620.
- [6] a) M. Tobisu, T. Shimasaki, N. Chatani, *Angew. Chem. Int. Ed.* **2008**, *47*, 4866-4869; b) K.W. Quasdorf, X. Tian, N. K. Garg, *J. Am. Chem.*

- Soc. **2008**, *130*, 14422-14423; c) B.-T. Guan, Y. Wang, B.-J. Li, D.-G. Yu, Z.-J. Shi, *J. Am. Chem. Soc.* **2008**, *130*, 14468-14470.
- [7] a) H. Noguchi, K. Hojo, M. Suginoe, *J. Am. Chem. Soc.* **2007**, *129*, 758-759; b) H. Noguchi, T. Shioda, C. M. Chou, M. Suginoe, *Org. Lett.* **2008**, *10*, 377-380; c) E. P. Gillis, M. D. Burke, *J. Am. Chem. Soc.* **2007**, *129*, 6716-6717; d) E. P. Gillis, M. D. Burke, *J. Am. Chem. Soc.* **2008**, *130*, 14084-14085; e) S. J. Lee, K. C. Gray, J. S. Paek, M. D. Burke, *J. Am. Chem. Soc.* **2008**, *130*, 466-468.
- [8] S. R. Chemler, D. Trauner, S. J. Danishefsky, *Angew. Chem. Int. Ed.* **2001**, *40*, 4544-4568.
- [9] a) S. Darses, J.-P. Genet, *Eur. J. Org. Chem.* **2003**, 4313-4327; b) G. A. Molander, N. Ellis, *Acc. Chem. Res.* **2007**, *40*, 275-286; c) G. A. Molander, D. L. Sandrock, *J. Am. Chem. Soc.* **2008**, *130*, 15792-15793.
- [10] S. I. Ngi, K. Cherry, V. Héran, L. Commeiras, J.-L. Parrain, A. Duchêne, M. Abarbri, J. Thibonnet, *Chem. Eur. J.* **2011**, *17*, 13692-13696.
- [11] X. Liu, Y. Sun, B. B. Y. Hsu, A. Lorbach, L. Qi, A. J. Heeger, G. C. Bazan, *J. Am. Chem. Soc.* **2014**, *136*, 5697-5708.
- [12] F. Zhao, Y.-F. Zhang, J. Wen, D.-G. Yu, J.-B. Wei, Z. Xi, Z.-J. Shi, *Org. Lett.* **2013**, *15*, 3230-3233.
- [13] K. Itami, D. Yamazaki, J. Yoshida, *J. Am. Chem. Soc.* **2004**, *126*, 15396-15397.
- [14] D. Qiu, S. Wang, S. Tang, H. Meng, L. Jin, F. Mo, Y. Zhang, J. Wang, *J. Org. Chem.* **2014**, *79*, 1979-1988.
- [15] H. Prokopová, C. O. Kappe, *Angew. Chem. Int. Ed.* **2009**, *48*, 2276-2286 and references therein.
- [16] a) M. Koley, L. Wimmer, M. Schnürch, M. D. Mihovilovic, *Eur. J. Org. Chem.* **2011**, 1972-1979; b) C. M. Counciller, C. C. Eichman, N. Proust, J. P. Stambuli, *Adv. Synth. Catal.* **2011**, *353*, 79-83; c) V. Gembus, J.-F. Bonfanti, O. Querolle, P. Jubault, V. Levacher, C. Hoarau, *Org. Lett.* **2012**, *14*, 6012-6015; d) A. Aguilar-Aguilar, E. Peña-Cabrera, *Org. Lett.* **2007**, *9*, 4163-4166; e) N. Kaval, B. K. Singh, D. S. Ermolat'ev, S. Claerhout, V. S. Parmar, J. Van der Eycken, E. Van der Eycken, *J. Comb. Chem.* **2007**, *9*, 446-453; f) G. Bouscary-Desforges, A. Bombrun, J. K. Augustine, G. Bernardinelli, A. Quattropani, *J. Org. Chem.* **2012**, *77*, 243-252; g) M. Čerňová, R. Pohl, B. Klepetářová, M. Hocek, *Synlett* **2012**, *23*, 1305-1308; h) L. Maingot, O. Dehbi, F. Buron, M. Aadil, M. Aksira, G. Guillaume, *Synlett* **2012**, *23*, 2449-2452; i) J. F. Hooper, R. D. Young, I. Pernik, A. S. Weller, M. C. Willis, *Chem. Sci.* **2013**, *4*, 1568; j) C. Kusturin, L. S. Liebeskind, H. Rahman, K. Sample, B. Schweitzer, J. Srogl, W. L. Neumann, *Org. Lett.* **2003**, *5*, 4349-4352.
- [17] a) E. Peña-Cabrera, A. Aguilar-Aguilar, M. González-Domínguez, E. Lager, R. Zamudio-Vázquez, J. Godoy-Vargas, F. Villanueva, *Org. Lett.* **2007**, *9*, 3985-3988; b) I. J. Arroyo, R. Hu, G. Merino, B. Z. Tang, E. Peña-Cabrera, *J. Org. Chem.* **2009**, *74*, 5719-5722; c) E. Lager, J. Liu, A. Aguilar-Aguilar, B. Z. Tang, E. Peña-Cabrera, *J. Org. Chem.* **2009**, *74*, 2053-2058; d) R. Hu, E. Lager, A. Aguilar-Aguilar, J. Liu, J. W. Y. Lam, H. H. Y. Sung, I. D. Williams, Y. Zhong, K. S. Wong, E. Peña-Cabrera, B. Z. Tang, *J. Phys. Chem. C.* **2009**, *113*, 15845-15853; e) I. J. Arroyo, R. Hu, B. Z. Tang, F. I. López, E. Peña-Cabrera, *Tetrahedron* **2011**, *67*, 7244-7250; f) C. F. A. Gómez-Durán, I. García-Moreno, A. Costela, V. Martín, R. Sastre, J. Bañuelos, F. López Arbeloa, I. López Arbeloa, E. Peña-Cabrera, *Chem. Comm.* **2010**, *46*, 5103-5105; g) J. Bañuelos, V. Martín, C. F. A. Gómez-Durán, I. J. Arroyo-Córdoba, E. Peña-Cabrera, I. García-Moreno, A. Costela, M. A. Pérez-Ojeda, T. Arbeloa, I. López Arbeloa, *Chem. Eur. J.* **2011**, *17*, 7261-7270; h) J. Bañuelos, I. J. Arroyo-Córdoba, I. Valois-Escamilla, A. Alvarez-Hernández, E. Peña-Cabrera, R. Hu, B. Z. Tang, I. Esnal, V. Martínez, I. López Arbeloa, *RSC Adv.* **2011**, *1*, 677-684; i) M. E. Pérez-Ojeda, V. Martín, A. Costela, I. García-Moreno, I. J. Arroyo-Córdoba, E. Peña-Cabrera, *Appl. Phys. B* **2012**, *106*, 911-914; j) J. O. Flores-Rizo, I. Esnal, C. A. Osorio-Martínez, C. F. A. Gómez-Durán, J. Bañuelos, I. López Arbeloa, K. H. Pannell, A. J. Metta-Magaña, E. Peña-Cabrera, *J. Org. Chem.* **2013**, *78*, 5867-5877; k) C. A. Osorio-Martínez, A. Urías-Benavides, C. F. A. Gómez-Durán, J. Bañuelos, I. Esnal, I. López Arbeloa, E. Peña-Cabrera, *J. Org. Chem.* **2012**, *77*, 5434-5438; l) R. I. Roacho, A. J. Metta-Magaña, E. Peña-Cabrera, K. H. Pannell, *J. Phys. Org. Chem.* **2013**, *26*, 345-351; m) R. I. Roacho, A. J. Metta-Magana, M. Portillo, E. Peña-Cabrera, K. H. Pannell, *J. Org. Chem.* **2013**, *78*, 4245-4250; n) J. Han, O. Gonzalez, A. Aguilar-Aguilar, E. Peña-Cabrera, K. Burgess, *Org. Biomol. Chem.* **2009**, *7*, 34-36; o) M. L. Betancourt-Mendiola, E. Peña-Cabrera, S. Gil, K. Chulvi, L. E. Ochando, A. M. Costero, *Tetrahedron* **2014**, *70*, 3735-3739; p) M. R. Martínez-Gonzalez, A. Urías-Benavides, E. Alvarado-Martínez, J. Cristobal Lopez, A. M. Gómez, M. del Rio, I. García, A. Costela, J. Bañuelos, T. Arbeloa, I. López Arbeloa, E. Peña-Cabrera, *Eur. J. Org. Chem.* **2014**, *26*, 5659-5663; q) B. D. Gutiérrez-Ramos, J. Bañuelos, T. Arbeloa, I. López Arbeloa, P. E. González-Navarro, K.; Wrobel, L. Cerdán, I. García-Moreno, A. Costela, E. Peña-Cabrera, *Chem. Eur. J.* **2014**, *21*, 1755-1764; r) R. I. Roacho, A. Metta-Magaña, E. Peña-Cabrera, K. H. Pannell, *Org. Biomol. Chem.* **2015**, *13*, 995-999.
- [8] a) Molecular Probes Inc., Eugene, Oregon, USA; b) R. P. Haugland, *The Handbook. A Guide to Fluorescent Probes and Labeling Technologies*, 10th edn. Molecular Probes Inc., Eugene, Oregon, USA.
- [19] a) R. Ziessel, G. Ulrich, A. Harriman, *New J. Chem.* **2007**, *31*, 496-501; b) G. Ulrich, R. Ziessel, A. Harriman, *Angew. Chem. Int. Ed.* **2008**, *47*, 1184-1201; c) A. C. Benniston, G. Copley, *Phys. Chem. Chem. Phys.* **2009**, *11*, 4124-4131; d) A. Loudet, K. Burgess, *Chem. Rev.* **2007**, *107*, 4891-4932; e) T. E. Wood, A. Thompson, *Chem Rev.* **2007**, *107*, 1831-1861.
- [20] J. Lu, H. Fu, Y. Zhang, Z. J. Jakubek, Y. Tao, S. Suning Wang, *Angew. Chem. Int. Ed.* **2011**, *50*, 11658-11662.
- [21] Z. Zhang, B. Xu, J. Su, L. Shen, Y. Xie, H. Tian, *Angew. Chem. Int. Ed.* **2011**, *50*, 11654-11657.
- [22] P. Li, L. Fang, H. Zhou, W. Zhang, X. Wang, N. Li, H. Zhong, B. Tang, *Chem. Eur. J.* **2011**, *17*, 10520-10523.
- [23] N. Boens, W. Qin, M. Baruah, W. M. De Borggraeve, A. Filarowski, N. Smismod, M. Ameloot, L. Crovetto, E. M. Talavera, J. M. Alvarez-Pez, *Chem. Eur. J.* **2011**, *17*, 10924-10934.
- [24] T. Bura, N. Leclerc, S. Fall, P. Lévêque, T. Heiser, R. Ziessel, *Org. Lett.* **2011**, *13*, 6030-6033.
- [25] D.-R. Kim, H.-C. Ahn, W.-J. Lee, D.-R. Ahn, *Chem. Commun.* **2011**, *47*, 791-793.
- [26] a) J.-J. Lee, S.-C. Sung-Chan Lee, D. Zhai, Y.-H. Ahn, H. Y. Yeo, Y. L. Tana, Y.-T. Chang, *Chem. Commun.* **2011**, *47*, 4508-4510; b) W. Liu, F. Li, X. Chen, J. Hou, L. Yi, Y.-W. Wu, *J. Am. Chem. Soc.* **2014**, *136*, 4468-4471.
- [27] M.-R. Ke, S.-L. Yeung, D. K. P. Ng, W.-P. Fong, P.-C. Lo, *J. Med. Chem.* **2013**, *56*, 8475-8483.
- [28] a) N. Boens, V. Leen, W. Dehaen, *Chem. Soc. Rev.* **2012**, *41*, 1130-1172; b) V. Lakshmi, M. R. Rao, M. Ravikanth *Org. Biomol. Chem.*, **2015**, *13*, 2501.
- [29] There are two examples in the literature that contain two or more independent reactions sites:



However, these two examples not only exhibit limited applicability, but also not all of the reaction sites are located at the periphery of the bodipy core. See: a) L. Bonardi, G. Ulrich, R. Ziessel, *Org. Lett.* **2008**, *10*, 2183-2186; b) Ref. 17(n).

- [30] a) A. Coskun, E. U. Akkaya, *J. Am. Chem. Soc.* **2005**, *127*, 10464-10465; b) K. Rurack, M. Kollmannsberger, J. Daub, *Angew. Chem., Int. Ed.* **2001**, *40*, 385-387; c) A. Coskun, E. Deniz, E. U. Akkaya, *Org. Lett.* **2005**, *7*, 5187-5189; d) Z. Dost, S. Atilgan, E. U. Akkaya, *Tetrahedron* **2006**, *62*, 8484-8488; e) O. Buyukcakir, O. A. Bozdemir, S. Kolemen, S. Erbas, E. U. Akkaya, *Org. Lett.* **2005**, *7*, 5187-5189; f) S.

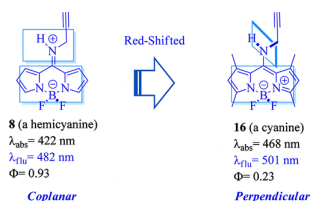
- Zhu, J. Zhang, G. K. Vegesna, R. Pandey, F.-T. Luo, S. A. Green, H. Liu, *Chem. Commun.* **2011**, *47*, 3508-3510; g) S. Kolemen, Y. Cakmak, S. Erten-Ela, Y. Altay, J. Brendel, M. Thelakkat, E. U. Akkaya, *Org. Lett.* **2010**, *12*, 3812-3815; h) S. Atilgan, T. Ozdemir, E. U. Akkaya, *Org. Lett.* **2008**, *10*, 4065-4067; i) Y. Cakmak, T. Nalbantoglu, T. Durgut, E. U. Akkaya, *Tetrahedron Lett.* **2014**, *55*, 538-540; j) A. Mirloup, P. Retailleau, R. Ziessel, *Tetrahedron Lett.* **2013**, *54*, 4456-4462.
- [31] B. Brizet, C. Bernhard, Y. Volkova, Y. Rousselin, P. D. Harvey, C. Goze, F. Denat, *Org. Biomol. Chem.* **2013**, *11*, 7729-7737.
- [32] R. Ziessel, G. Ulrich, A. Haefele, A. Harriman, *J. Am. Chem. Soc.* **2013**, *135*, 11330-11344.
- [33] C. Goze, G. Ulrich, L. J. Mallon, B. D. Allen, A. Harriman, *J. Am. Chem. Soc.*, **2006**, *128*, 10231-10239.
- [34] K. Kim, S. H. Choi, J. Jeon, H. Lee, J. O. Huh, J. Yoo, J. T. Kim, C.-H. Lee, Y. S. Lee, D. G. Churchill, *Inorg. Chem.* **2011**, *50*, 5351-5360.
- [35] T. Lundrigan, S. M. Crawford, T. S. Cameron, A. Thompson, *Chem. Commun.* **2012**, *48*, 1003-1005.
- [36] G. Durán-Sampedro, A. R. Agarrabeitia, L. Cerdán, M. E. Pérez-Ojeda, A. Costela, I. García-Moreno, I. Esnal, J. Bañuelos, I. López Arbeloa, M. J. Ortiz, *Adv. Funct. Mater.* **2013**, *23*, 4195-4205.
- [37] T. A. Fayed, *Reviews in Fluorescence*. Ed. D. D. Geddes, Springer, New York, 2011.
- [38] a) N. Johnsson, K. Johnsson, *ACS Chem Biol.* **2007**, *2*, 31-38; b) L. D. Davis and R. T. Raines, *ACS Chem. Biol.* **2008**, *3*, 142-155.
- [39] a) G. I. Jones, *Dye Lasers Principles*. Ed. F. J. Duarte and L. W. Hillman, Academic Press, New York 1990; b) G. Jones II, Z. Huang, S. Kumar, D. Pacheco, *Proc SPIE-Int. Soc. Opt. Eng.* **2002**, *4360*, 72-81.
- [40] a) A. Becker, C. Hassenius, K. Licha, B. Ebert, U. Sukowski, W. Semmler, B. Wiedenmann, C. Grotzinger, *Nat. Biotechnol.* **2001**, *19*, 327-331; b) F. V. Frangioni, *Curr. Opin. Chem. Biol.* **2003**, *7*, 626-634; c) V. Ntziachristos, J. Ripoli, L. H. V. Wang, R. Weissleder, *Nat. Biotechnol.* **2005**, *23*, 313-320.
- [41] a) A. Bessette, G. S. Hanan, *Chem. Soc. Rev.* **2014**, *43*, 3342-3405; b) H. Lu, J. Mack, Y. Yang, Z. Shen, *Chem. Soc. Rev.* **2014**, *43*, 4778-4823.
- [42] a) K. Krumova, G. Cosa, *J. Am. Chem. Soc.* **2010**, *132*, 17560-17569; b) T. Bura, P. Retailleau, G. Ulrich, R. Ziessel, *J. Org. Chem.* **2011**, *76*, 1109-1117; c) A. Martin, C. Long, R. J. Forster, T. E. Keyes, *Chem. Commun.* **2012**, *48*, 5617-5619.
- [43] a) A. Harriman, L. J. Mallon, S. Goeb, R. Ziessel, *Phys. Chem. Chem. Phys.* **2007**, *9*, 5199-5201; b) W. Qin, T. Rohand, W. Dehaen, J. N. Clifford, K. Driesen, D. Beljonne, B. Van Aberke, M. Van der Auweraer, N. Boens, *J. Phys. Chem. A* **2007**, *111*, 8588-8597; c) M. J. Ortiz, I. García-Moreno, A. R. Agarrabeitia, G. Durán-Sampedro, A. Costela, R. Sastre, F. López Arbeloa, J. Bañuelos, I. López Arbeloa, *Phys. Chem. Chem. Phys.* **2010**, *12*, 7804-7811; d) J. Li, B. Hu, G. Hu, X. Li, P. Lu, Y. Wang, *Org. Biomol. Chem.* **2012**, *10*, 8848-8859; e) M. Gupta, S. Mula, M. Tyagi, T. K. Ghanty, S. Murudkar, A. K. Ray, S. Chattopadhyay, *Chem. Eur. J.* **2013**, *19*, 17766-17772.
- [44] a) Z. Shen, H. Röhr, K. Rurack, H. Uno, M. Spieles, B. Schulz, G. Reck, N. Ono, *Chem. Eur. J.* **2004**, *10*, 4853-4871; b) K. Umezawa, Y. Nakamura, H. Makino, D. Citterio, K. Suzuki, *J. Am. Chem. Soc.* **2008**, *130*, 1550-1551; c) K. Umezawa, A. Matsui, Y. Nakamura, D. Citterio, K. Suzuki, *Chem. Eur. J.* **2009**, *15*, 1096-1106; d) A. Wakamiya, T. Murakami, S. Yamaguchi, *Chem. Sci.* **2013**, *4*, 1002-1007; e) T. Uppal, X. Hu, F. R. Fronczek, S. Maschek, P. Bobadova-Parvanova, M. G. H. Vicente, *Chem. Eur. J.* **2012**, *18*, 3893-3905; f) M. Nakamura, H. Tahara, K. Takahashi, T. Nagata, H. Uoyama, D. Kuzuhara, S. Mori, T. Okujima, H. Yamada, H. Uno, *Org. Biomol. Chem.* **2012**, *10*, 6840-6849; g) Y. Ni, W. Zeng, K.-W. Huang, J. Wu, *Chem Commun.* **2013**, *49*, 1217-1219.
- [45] a) J. Killoran, L. Allen, J. F. Gallagher, W. M. Gallagher, D. F. O'Shea, *Chem. Commun.* **2002**, 1862-1863; b) W. Zhao, E. M. Carreira, *Angew. Chem. Int. Ed.* **2005**, *44*, 1677-1679; c) W. Zhao, E. M. Carreira, *Chem. Eur. J.* **2006**, *12*, 7254-7263; d) A. Loudet, R. Bandichor, L. Wu, K. Burgess, *Tetrahedron* **2008**, *64*, 3642-3654.
- [46] T. V. Goud, A. Tutar, J.-F. Biellmann, *Tetrahedron* **2006**, *62*, 5084-5091.
- [47] T. Yamamoto, K. Toyota, N. Morita, *Tetrahedron Lett.* **2010**, *51*, 1364-1366.
- [48] a) A. Cihaner, F. Algi, *React. Funct. Polym.* **2009**, *69*, 62-67; b) T. Rohand, W. Qin, N. Boens, W. Dehaen, *Eur. J. Org. Chem.* **2006**, 4658-4663; c) V. Leen, D. Miscoria, S. Yin, A. Filarowski, J. M. Ngongo, M. Van der Auweraer, N. Boens, W. Dehaen, *J. Org. Chem.* **2011**, *76*, 8168-8176.
- [49] a) O. A. Bozdemir, Y. Cakmak, F. Sozmen, T. Ozdemir, A. Siemiarzczuk, E. U. Akkaya, *Chem. Eur. J.* **2010**, *16*, 6346-6351; b) G. Barin, M. D. Yilmaz, E. U. Akkaya, *Tetrahedron Lett.* **2009**, *50*, 1738.
- [50] I. García-Moreno, L. Wang, A. Costela, J. Bañuelos, I. López-Arbeloa, Y. Xiao, *ChemPhysChem* **2012**, *13*, 3923-3931.
- [51] a) S. Li, S. I. Yang, T. Ciringh, J. Seth, C. H. Martin III, D. L. Singh, D. Kim, R. R. Birge, D. F. Bocian, D. Holten, J. S. Lindsey, *J. Am. Chem. Soc.* **1998**, *120*, 10001-10017; b) F. López Arbeloa, J. Bañuelos, V. Martínez, T. Arbeloa, I. López Arbeloa, *Int. Rev. Phys. Chem.* **2005**, *24*, 339-374.
- [52] M. P. Shandura, V. P. Yakuboskyi, A. O. Gerasov, O. D. Kachkovsky, Y. M. Poronik, Y. P. Kovun, *Eur. J. Org. Chem.* **2012**, 1825-1834.
- [53] G. Durán-Sampedro, A. R. Agarrabeitia, I. García-Moreno, A. Costela, J. Bañuelos, T. Arbeloa, I. López Arbeloa, J. L. Chiara, M. J. Ortiz, *Eur. J. Org. Chem.* **2012**, 6335-6350.

4. Kapitulum III ERANSKINA / ANEXO III al Capítulo 4

4. Artikulua / Artículo 4:

8-AminoBODIPYs: Cyanines or Hemicyanines? The effect of the coplanarity of the amino group on their optical properties

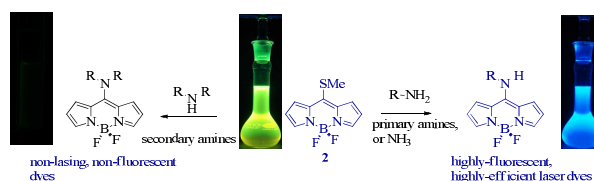
The Journal of Organic Chemistry, 2012, 77, 5434



5. Artikulua / Artículo 5:

Reaction of Amines with 8-MethylthioBODIPY: dramatic optical and laser response to amine substitution.

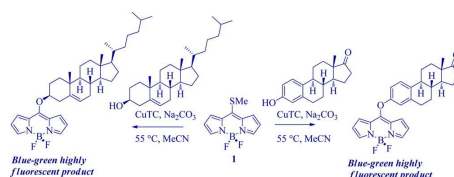
Chemistry – An Asian Journal, 2013, 8, 2691



6. Artikulua / Artículo 6:

8-Alkoxy- and 8-Aryloxy-BODIPYs: straightforward fluorescent tagging of alcohols and phenols

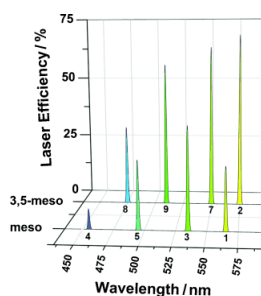
The Journal of Organic Chemistry, 2013, 78, 5867



7. Artikulua / Artículo 7:

Blue-to-orange color-tunable laser emission from tailored boron-dipyrrromethene dyes.

ChemPhysChem, 2013, 14, 4134



8-AminoBODIPYs: Cyanines or Hemicyanines? The Effect of the Coplanarity of the Amino Group on Their Optical Properties

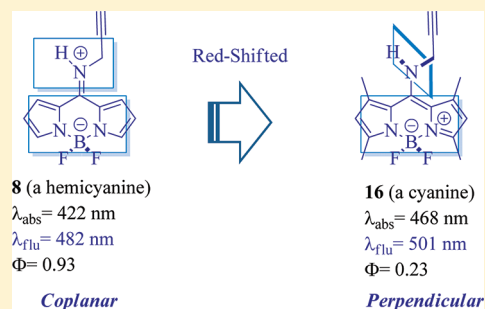
Carlos A. Osorio-Martínez,[†] Arlette Urías-Benavides,[†] C. F. Azael Gómez-Durán,[†] Jorge Bañuelos,[‡] Ixone Esnal,[‡] Iñigo López Arbeloa,^{*,‡} and Eduardo Peña-Cabrera^{*,†}

[†]Departamento de Química, Universidad de Guanajuato, Col. Noria Alta S/N, Guanajuato, GTO, 36050, Mexico

[‡]Departamento de Química Física, Universidad del País Vasco UPV/EHU, Aptdo. 644, 48080 Bilbao, Spain

Supporting Information

ABSTRACT: The role of the amino group twisting ability in the BODIPY photophysics for nonsterically hindered and constrained molecular structures was studied. When a coplanar disposition of the amino and the BODIPY core is feasible, a hemicyanine-like delocalized π -system gives rise to novel blue and efficient BODIPY laser dyes. The key role of such rotamer is confirmed by newly synthesized derivatives where the amino and the BODIPY core are electronically decoupled by steric repulsions.



BODIPYs¹ are small compounds that have unique properties: high quantum yields, excellent solubility in organic solvents, high absorption coefficients and stability.²

The structure of such compounds is described as the resonance hybrid of canonical forms 1 and 2 (Figure 1).

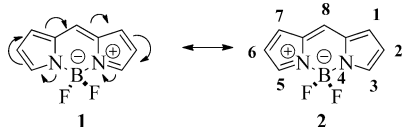
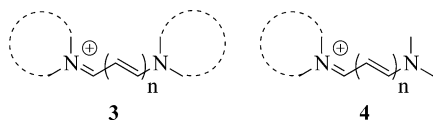


Figure 1. Resonance contributions to the BODIPY structure.

The core BODIPY structure resembles that of a cyanine 3. Cyanines are conjugated compounds that contain two nitrogen atoms, one of which is positively charged, connected by an odd number of carbon atoms.³ In the particular case that only one of the N atoms is part of a heterocycle (e.g., 4), the compound is termed hemicyanine.



Bielmann et al. reported the synthesis of 8-anilinoBODIPY 6 (eq 1). They proposed that 6 (a cyanine-like structure) was best represented by cross-conjugated canonical structure 7 (a hemicyanine-like structure).⁴

We later demonstrated that displacement of thiomethyl group in 5 by nonaromatic amines furnished a family of unprecedented highly fluorescent blue-emitting BODIPY dyes (Figure 2).⁵

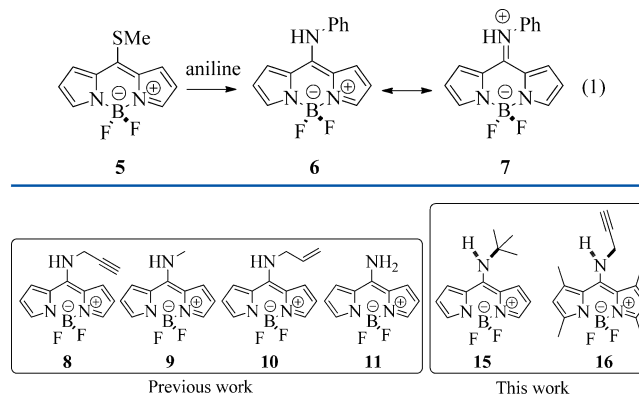


Figure 2. A new family of blue-emitting BODIPY dyes.

One of the questions we tried to answer was why 8–11 fluoresce in the blue edge of the visible spectrum. Quantum mechanical calculations indicated that the observed spectral shifts were due to the fact that an amino group at the 8-position generates a net destabilization of the LUMO state while leaving the HOMO unaltered.^{5b} This result was in direct contrast with 3-amino-substituted BODIPY derivatives, in which the HOMO–LUMO energy gap remained unchanged by the presence of the amino group in that position.⁶ Likewise, it was clear from the X-ray diffraction data of 6⁴ and 8^{5a} that the amino groups adopted a nearly planar geometry. Both ¹H and ¹³C NMR spectra of all of the amino derivatives (except for 11, vide infra) showed nonequivalent signals of the pyrrolic atoms.

Received: April 13, 2012

Published: May 21, 2012

The hypothesis that was proposed suggests that 8-amino-BODIPYs 7–11 were best described as coplanar rotamer 13, in which the lone-pair of the amino group is in the right orientation for efficient overlap with the π -system of the BODIPY core (Figure 3).

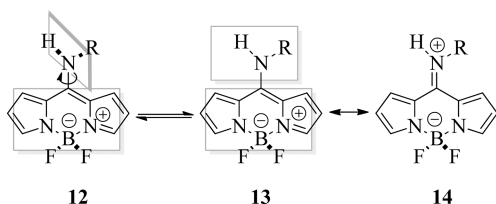


Figure 3. Rotamers of 8-aminoBODIPY dyes.

It follows, therefore, that once the N lone-pair is delocalized over the BODIPY core, *hemicyanine* structure 14 would be the dominant resonance contributor. Structure 14 would be now a cross-conjugated system, where the push–pull interaction of the pyrrole nitrogen atoms would be interrupted. This factor would cause a widening the HOMO–LUMO gap, thereby blue-shifting both the absorption and fluorescence bands. This model would explain the near planarity of the amino group observed on the X-ray diffraction data of 7–8. By the same token, it would explain the NMR spectra of 7–10, for a rigid 14 would render the pyrrole rings nonequivalent. 8-Amino-BODIPY 11 displays equivalent signals for the pyrrole rings in both ^1H and ^{13}C NMR spectra since its corresponding hemicyanine structure 14 ($\text{R} = \text{H}$) would still be symmetrical.

If our working hypothesis were true, a derivative in which the amino group was to be forced to remain perpendicular to the BODIPY ring (e.g., rotamer 12) should behave more like a typical cyanine-like BODIPY system, with both absorption and emission bands red-shifted.

Two 8-aminoBODIPY derivatives were designed to support our hypothesis: 8-*tert*-butylaminoBODIPY 15 and 8-propargylamino-1,3,5,7-tetramethylBODIPY 16.

These systems cannot adopt the coplanar conformation 13 because of steric repulsion of the amino-substituent with the atoms at both the 1- and 7-positions of the BODIPY core (Figure 4).

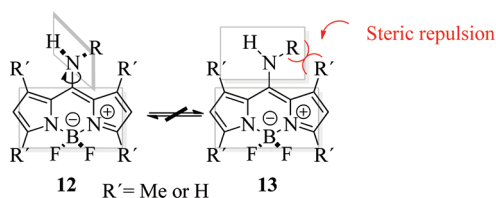
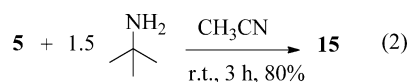


Figure 4. Preferred perpendicular rotamer 12.

Compound 15 was prepared according to the reported method (eq 2).^{4,5a,b}



The synthesis of 16 is illustrated in Scheme 1.

2,4-Dimethylpyrrole was reacted with thiophosgene to give highly colored 17. Methylation of 17 followed by complexation with BF_3 etherate gave 18. Finally, 16 was prepared by treating

18 with an excess of propargylamine at rt for 22 h in acetonitrile.

The aromatic section of the ^1H NMR spectra of 15 and 16 in CD_3CN is shown in Figure S1, Supporting Information (SI). For purposes of comparison, the spectrum of analogue 8^{5a} is also included.

The coplanar conformation that 8 adopts^{5a} renders the six BODIPY protons nonequivalent as can be observed in Figure S1 (SI) (middle). On the other hand, because of the aforementioned sterics arguments, both 15 (Figure S1 (SI), right) and 16 (Figure S1 (SI), left) adopt the perpendicular, plane-symmetric conformation. As a result, the BODIPY protons become magnetically equivalent, displaying only three and one signals, respectively.

The free twist of the amine group can be hindered by either adding bulky substituents (15) or by replacing the hydrogens of adjacent positions 1 and 7 of the BODIPY by methyl groups (16) (Figure 4). With regard to their counterparts, without such steric hindrance (9 and 8, respectively), quantum mechanical calculations (structural data for 8, 9, 15, and 16 amino derivatives are collected in Tables S2 and S3 (SI)) confirm the blockade of the amine in a twisted disposition (mainly in the excited state) with regard to the chromophoric plane, preventing a coplanar arrangement between the amine and the indacene chromophore (Figure 5). For instance, the calculated dihedral angle for the twist of the amine was $\sim 3^\circ$ for dye 8, according to a coplanar disposition (rotamer 13 in Figure 3); consequently, the amine electronic coupling with the chromophore is allowed, giving rise to a hemicyanine-like resonance structure where the amine is characterized by a sp^2 hybridization (rotamer 14 in Figure 3). The presence of such entity in related *meso* substituted BODIPYs has been previously reported.^{5,7} The twist angle for the sterically hindered derivative 16 increases up to $\sim 50^\circ$ (Table S2 (SI)) upon the methylation of the adjacent positions, which corresponds to a nonplanar sp^3 hybridization and a cyanine-like delocalized π -system (rotamer 12 in Figure 3). Similar results were obtained for pairs 9 and 15, where the amine was fixed in a perpendicular disposition in the excited state ($\sim 90^\circ$, Table S3 (SI)) by the presence of a bulky *tert*-butyl moiety in the amino group. Indeed, the theoretical simulation suggests that whereas in compound 9 an electronic coupling between the indacene core and the amino is allowed, in the sterically hindered derivative 15, such delocalization is interrupted (Figure 5). Thus, these sets of derivatives are adequate to evaluate the effect of coplanarity of the amino group on the photophysical properties of the BODIPY.

Previous results of related 8-amino derivatives showed also wide spectral bands placed at the blue region of the visible. This occurs because of the electron releasing effect of the amine group leading to an energy rise of the LUMO.⁵ Such blue-shift is not so pronounced for derivatives 15 and 16 in comparison with reference dyes 8 and 9 (Figure 6). In these last derivatives, the contribution of a rotamer characterized by a hemicyanine-like delocalized π -system is responsible for the large spectral shift to higher energies. Nonetheless, the constrained structure of 15 and 16, induced by the steric repulsion of their substitution pattern (Figure 4), hampers the required coplanar disposition of the amine and the BODIPY, consequently decreasing the formation probability of such hemicyanine and rendering a less pronounced blue-shift of the spectral bands (Figure 6). Furthermore, for nonconstrained amino substituted BODIPYs, a direct relationship between the electron donor

Scheme 1. Synthesis of 16

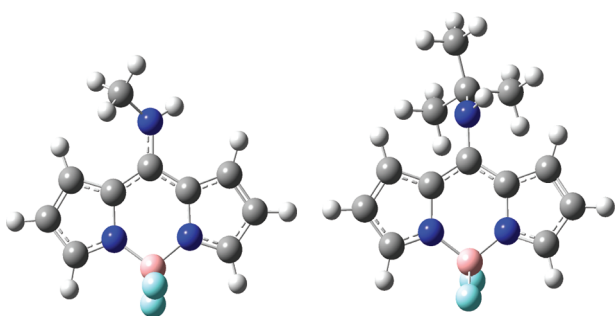
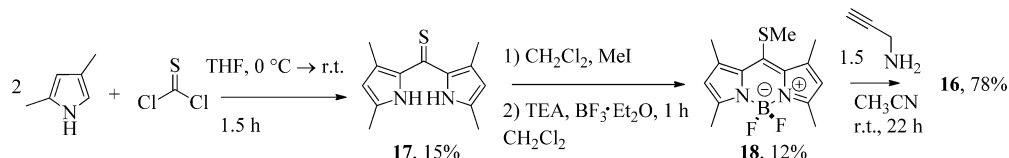


Figure 5. Optimized first excited state geometry for the fluorophores 9 and 15.

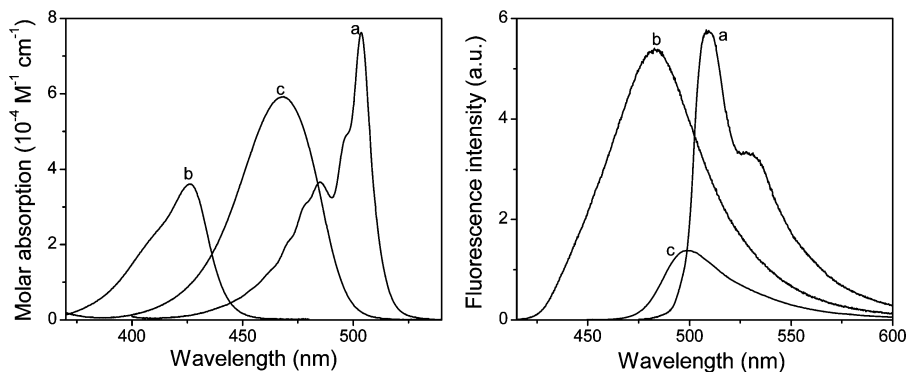
character of the amine and the extent of the spectral blue-shift has been established.^{5b} Accordingly, a larger spectral shift should be expected for derivative 15 (*N-tert-butyl*) than for dye 9 (*N-methyl*) because the *tert-butyl* substituent (Hammett parameter $\sigma_p^+ = -0.275$) has a higher donor capacity than the methyl ($\sigma_p^+ = -0.256$). This is not the case here, which indicates the influence of the formation of the hemicyanine in the spectral shift.

Table S1 (SI) summarizes the photophysical properties of 15 and 16. A comparison is made with their structural analogues 9 and 8 respectively, as well as with the parent BODIPY chromophore 1. In all amine derivatives, the blue-shift in absorption is much more evident than in fluorescence, leading to a clear enhancement in the Stokes shift. This is an important feature because BODIPYs are usually characterized by a close absorption and emission region, thus, the negative influence of reabsorption/reemission phenomena are of great relevance.² Most of the 8-amine derivatives (including 8 and 9) overcome such limitations while maintaining a high fluorescence efficiency.^{5b} Furthermore, although the absorption intensity (ϵ_{\max}) decreases by the presence of the amine, the overall absorption probability (described by the oscillator strength) remains similar to their reference BDP chromophore, because of their wider spectra.

As seen in Table S1 (SI), the derivatives with no sterically hindered amines (8 and 9) are characterized by bright blue emission with a fluorescence efficiency that is close to that of the BDP (at around 0.90). This can be explained in terms of the formation probability of the hemicyanine π -system (rotamer 14 in Figure 3). However, for a more electron donor amine (9), the fluorescence quantum yield and lifetime decreased in polar media because of the activation of an intramolecular charge transfer (ICT).^{5b}

On the other hand, restricting the movement of the amines (15 and 16) implies a larger absorption coefficient in comparison with their respective counterparts free from steric repulsions (9 and 8). These trends, and the registered spectral band blue-shift, were theoretically corroborated by quantum mechanics simulation of the absorption transition. The perpendicular conformation of the amine preventing its electronic coupling with the chromophore explains why the photophysics of derivatives 15 and 16 tends to that of the BODIPY 1. Nonetheless, this conformation of the 8-amine implies a drastic reduction in the fluorescence ability (Table S1 (SI)). Furthermore, in polar media such decrease is more evident, the fluorescence quantum yield tends to zero (<0.1), and the lifetimes become very short (lower than 1 ns, see Table S1 (SI)). In general, a more constrained geometry, that is, hindering the mobility of the functional groups attached to the chromophore, benefits fluorescence ability because it reduces the internal conversion processes, typically related with rigidity/flexibility of the fluorophore.⁸ However, in this study, entirely opposite features are achieved. Steric hindrance prevents a coplanar disposition of the amine and the BODIPY and consequently the formation of the hemicyanine, avoiding the high efficient blue emission signal observed in dyes 8 and 9. Alternatively, such twisted disposition seems to activate a new nonradiative pathway, responsible for the quenching of the fluorescence emission in the LE state.

Considering the electron donor character of the amine and the sensibility of the fluorescence quantum yield and lifetime with the solvent nature, such extra quenching process, mainly

Figure 6. Absorption (left) and fluorescence (right) spectra of diluted solutions of reference compound 1 (a) and its 8-amino derivatives 8 (b) and 16 (c) in *c*-hexane.

active in polar media, should be an intramolecular charge transfer (ICT) state, which should be nonfluorescent (no new emission bands were detected). Furthermore, considering the steric hindrance, which forces the amine into a more perpendicular disposition, it could be a twisted ICT state (TICT), where the donor and acceptor are electronically decoupled.⁹ The stabilization of this ICT state leads to the appearance of a fast component in the fluorescence decay curves (Table S1 (SI)). Such state has also been proposed for aniline substituted BODIPY derivatives.¹⁰ The fluorescence quenching effect of the ICT state is more obvious in derivative **15** than in **16**. In polar media, the former derivative is almost nonfluorescent, and the decay curves are better suited as a biexponential fit with fast lifetime (<0.1 ns).

The *tert*-butyl group electron releasing effect is higher than that of the propargyl; hence, the formation of the ICT state is further favored in derivative **15** in comparison with derivative **16**. In fact, the higher electron donor nature of the amine in the former entity is reflected in the shift of the spectral bands, which are placed deeper into the blue upon *tert*-butyl substitution in the amine.

In summary, two new rigid 8-aminoBODIPY dyes **15** and **16** were prepared. The disposition of the amino group at the *meso* position plays a key role on the photophysical properties of the BODIPYs. If the amine substituents are small enough or the chromophoric adjacent positions to the *meso* are not substituted, the amine can adopt a coplanar disposition and give rise to a hemicyanine-like delocalized π -system. Such entity is responsible for the spectral blue shift and is characterized by very high fluorescence efficiency, mainly in apolar media, allowing their use in tunable dye lasers. Nonetheless, if the amine motion is blocked, the coplanar rotamer cannot be achieved, and hence the hemicyanine formation is forbidden. Consequently, the blue shift is lower and an ICT state is activated because of the electron releasing ability and twisted disposition of the amine group. Such new state efficiently quenches the fluorescence emission of the BODIPY even in apolar environments.

EXPERIMENTAL SECTION

General Procedures. All reactions were performed under a dry N₂ atmosphere in oven- and/or flame-dried glassware unless otherwise noted. Analytical thin-layer chromatography was performed on Merck silica gel plates with F-254 indicator. THF was dried over activated 4 Å molecular sieves. Column chromatography was performed on 100–200 mesh silica gel.

Starting Materials. 8-ThiomethylBODIPY, thiophosgene, 2,4-dimethylpyrrole, methyl iodide, triethylamine, propargylamine, *tert*-butylamine, and BF₃·OEt₂ are commercially available and were used as received. **Caution!** Handling thiophosgene requires a fume hood and the container has to be kept tightly closed for storage. Thiophosgene is highly toxic.

Synthesis of Bis(3,5-dimethyl-1H-pyrrol-2-yl)methanethione **17.** A solution of 2,4-dimethylpyrrole (2.0 g, 21.0 mmol, 2.1 equiv) in dry tetrahydrofuran (20 mL) was added dropwise thiophosgene (1.15 g, 10.0 mmol, 1 equiv) at 0 °C. After TLC showed that the reaction went to completion (1.5 h), the reaction mixture was allowed to reach rt and was adsorbed on SiO₂-gel. After flash-chromatography (SiO₂-gel, EtOAc/hexanes gradient). The pure compound fraction was collected, which after removal of the solvents under reduced pressure yielded **17** (348.0 mg, 15%) as a crystalline orange red solid: TLC (30% EtOAc/hexanes, R_f = 0.5); mp 185–186 °C; IR (KBr, cm⁻¹) 3271 (s), 2916 (m), 1558 (s), 1531 (s), 1487 (s), 1439 (s), 1329 (m), 1259 (s), 1221 (s), 1138 (s); ¹H NMR (200 MHz, CDCl₃) δ 9.0 (1H, br s), 5.90 (d, J = 2.2 Hz, 2H), 2.24 (s, 6H), 2.05 (s, 6H); ¹³C NMR

(50 MHz, CDCl₃), δ 191.8, 137.5, 137.2, 127.8, 114.1, 13.6, 13.2. Anal. Calcd for C₁₃H₁₆N₂S: C, 67.20; H, 6.94; N, 12.06. Found: C, 67.16; H, 6.89; N, 12.10.

Synthesis of 5,5-Difluoro-1,3,7,9-tetramethyl-10-(methylthio)-5H-dipyrrolo[1,2-c:2',1'-f][1,3,2]diazaborinin-4-ium-5-uide **18.** To a solution of compound **17** (0.34 g, 1.46 mmol, 1 equiv) in anhydrous dichloromethane (1.5 mL) was added methyl iodide (0.46 mL, 7.4 mmol, 5 equiv) at rt. The reaction mixture was stirred for 24 h until completion (TLC monitoring). The solvent was removed under reduced pressure, and to the residue, dissolved in anhydrous dichloromethane (1.5 mL) under N₂ atmosphere at rt was added triethylamine (0.49 mL, 3.50 mmol, 2.4 equiv). After stirring for 30 min, BF₃·OEt₂ (0.47 mL, 4.9 mmol, 3.3 equiv) was added. The mixture was stirred for 30 min at rt. After the evaporation of solvents under reduced pressure, the crude product was adsorbed on SiO₂-gel. After flash-chromatography (SiO₂-gel, EtOAc/hexanes gradient), **18** (51.5 mg, 12%) was isolated as a dark red solid: TLC (30% EtOAc/hexanes, R_f = 0.8); mp 150–151 °C; IR (KBr, cm⁻¹) 3436 (m), 1535 (s), 1505 (s), 1471 (w), 1369 (w), 1299 (s), 1196 (s), 1221 (s); ¹H NMR (200 MHz, CDCl₃) δ 6.08 (s, 2H), 2.61 (s, 6H), 2.52 (s, 6H), 2.45 (s, 3H); ¹³C NMR (50 MHz, CDCl₃), δ 155.7, 143.8, 141.3, 122.5, 22.5, 17.2, 15.0, 14.4. Anal. Calcd for C₁₄H₁₇BF₂N₂S: C, 57.16; H, 5.82; N, 9.52. Found: C, 57.12; H, 5.89; N, 9.49.

Typical Procedure (TP) for the Addition of Amines to ThiomethylBODIPY Dyes. To a CH₃CN (2 mL) solution of the corresponding thiomethylBODIPY (either **5** or **18**, typically 20 mg) was added the corresponding amine (1.5 equiv) in a 20 mL scintillation vial under air. The vial was capped, and the mixture was stirred at rt until completion (TLC). Flash chromatography (SiO₂-gel, EtOAc/hexanes gradient) purification yielded the pure compounds.

5,5-Difluoro-1,3,7,9-tetramethyl-10-(prop-2-yn-1-ylamino)-5H-dipyrrolo[1,2-c:2',1'-f][1,3,2]diazaborinin-4-ium-5-uide **16.** According to TP: TLC (30% EtOAc/hexanes, R_f = 0.5); yellow crystals; mp 161–163 °C; yield 78% (16 mg); IR (KBr, cm⁻¹) 3423 (m), 3283 (m), 1571 (s), 1531 (s), 1508 (m), 1462 (w), 1392 (m), 1283 (w), 1221 (s); ¹H NMR (300 MHz, CDCl₃) δ 6.05 (s, 2H), 5.25 (br signal, 2H), 4.18 (dd, J₁ = 3.6 Hz, J₂ = 8.7 Hz, 2H), 2.51 (s, 6H), 2.42 (s, 2H); ¹³C NMR (75 MHz, CDCl₃), δ 150.7, 150.1, 134.3, 124.4, 119.4, 79.5, 75.16, 41.8, 15.4, 14.4. Anal. Calcd for C₁₆H₁₈BF₂N₃: C, 63.81; H, 6.02; N, 13.95. Found: C, 63.83; H, 6.09; N, 13.90.

10-(tert-Butylamino)-5,5-difluoro-5H-dipyrrolo[1,2-c:2',1'-f][1,3,2]diazaborinin-4-ium-5-uide **15.** According to TP: TLC (30% EtOAc/hexanes, R_f = 0.4); yellow crystals; mp 130–131 °C; yield 80% (17.6 mg); IR (KBr, cm⁻¹) 3369 (s), 2981 (w), 1582 (s), 1554 (s), 1457 (m), 1404 (m), 1381 (s), 1278 (m), 1225 (m); ¹H NMR (200 MHz, CDCl₃) δ 7.60 (s, 2H), 7.09 (s, 2H), 6.69 (br s, 1H), 6.47 (s, 2H), 1.70 (s, 9H); ¹³C NMR (50 MHz, CDCl₃), δ 148.0, 134.5, 124.0, 120.9, 114.4, 55.6, 29.2. Anal. Calcd for C₁₃H₁₆BF₂N₃: C, 59.35; H, 6.13; N, 15.97. Found: C, 59.41; H, 6.19; N, 15.91.

ASSOCIATED CONTENT

Supporting Information

Tables S1–S3 and Figure S1. Full photophysical data of the BDP chromophore and its 8-amino derivatives **8**, **9**, **15**, and **16** in different solvents ranging from apolar to polar/protic media. Theoretically calculated structural data of these amino derivatives, NMR spectra of the new compounds. This material is available free of charge via the Internet at <http://pubs.acs.org>.

AUTHOR INFORMATION

Corresponding Author

*E-mail: inigo.lopezARBelo@ehu.es; eduardop@ugto.mx.

Notes

The authors declare no competing financial interest.

■ ACKNOWLEDGMENTS

We thank CONACyT (Mexico, Grant 129572) and Gobierno Vasco (IT339-10, S-PE10UN65 and S-PE11UN064) for financial support. A.U.-B., C.F.A.G.-D., and C.A.O.-M. wish to thank CONACyT for scholarships. We also wish to thank Cuántico de México for kind donation of thiomethylBODIPY 5. The SGI/IZO-SGIker UPV/EHU is gratefully thanked for allocation of computational resources.

■ REFERENCES

- (1) Haugland, R. P. *Handbook of Fluorescent Probes and Research Chemicals*, 6th ed.; Molecular Probes: Eugene, OR, 1996.
- (2) (a) Boens, N.; Leen, V.; Dehaen, W. *Chem. Soc. Rev.* **2012**, *41*, 1130. (b) Benstead, M.; Mehl, G. H.; Boyle, R. W. *Tetrahedron* **2011**, *67*, 3573. (c) Loudet, A.; Burgess, K. *Chem. Rev.* **2007**, *107*, 4891. (d) Ulrich, G.; Ziessel, R.; Harriman, A. *Angew. Chem., Int. Ed.* **2008**, *47*, 1184. (e) Ziessel, R.; Ulrich, G.; Harriman, A. *New J. Chem.* **2007**, *31*, 496. (f) Wood, T. E.; Thompson, A. *Chem. Rev.* **2007**, *107*, 1831. (g) Benniston, A. C.; Copley, G. *Phys. Chem. Chem. Phys.* **2009**, *11*, 4124. (h) López Arbeloa, F.; Bañuelos, J.; Martínez, V.; Arbeloa, T.; López Arbeloa, T. *Int. Rev. Phys. Chem.* **2005**, *24*, 339.
- (3) Mishra, A.; Behera, R. K.; Behera, P. K.; Mishra, B. K.; Behera, G. B. *Chem. Rev.* **2000**, *100*, 1973.
- (4) Goud, T. V.; Tutar, A.; Biellmann, J.-F. *Tetrahedron* **2006**, *62*, 5084.
- (5) (a) Gómez-Durán, C. F. A.; García-Moreno, I.; Costela, A.; Martín, V.; Sastre, R.; Bañuelos, J.; López Arbeloa, F.; López Arbeloa, I.; Peña-Cabrera, E. *Chem. Commun.* **2010**, *46*, 5103. (b) Bañuelos, J.; Martín, V.; Gómez-Durán, C. F. A.; Arroyo-Cordoba, I. J.; Peña-Cabrera, E.; García-Moreno, I.; Costela, A.; Pérez-Ojeda, M. A.; Arbeloa, T.; López Arbeloa, I. *Chem.—Eur. J.* **2011**, *17*, 7261.
- (6) Bañuelos, J.; López Arbeloa, F.; Arbeloa, T.; Salleres, S.; Vilas, J. L.; Amat-Guerri, F.; Liras, M.; López Arbeloa, I. *J. Fluoresc.* **2008**, *18*, 899.
- (7) (a) Yakubovskiy, V. P.; Shandura, M. P.; Kovtun, Y. P. *Dyes Pigm.* **2010**, *87*, 17. (b) Kim, K.; Jo, C.; Easwaramoorthi, S.; Sung, J.; Kim, D. H.; Churchill, D. G. *Inorg. Chem.* **2010**, *48*, 4881.
- (8) (a) Wang, Y.-W.; Descalzo, A. B.; Shen, Z.; You, X.-Z.; Rurack, K. *Chem.—Eur. J.* **2010**, *16*, 2887. (b) Vu., T. T.; Badré, S.; Dumas-Verdes, C.; Vachon, J.-J.; Julien, C.; Audebert, P.; Senosutrova, E. Y.; Schmidt, E. Y.; Trofimov, B. A.; Pansu, R. B.; Clavier, G.; Méallet-Renault, R. *J. Phys. Chem. C* **2009**, *113*, 11844. (c) Zheng, Q.; Xu, G.; Prasad, P. N. *Chem.—Eur. J.* **2008**, *14*, 5812.
- (9) Grabowski, Z. R.; Rotkiewicz, K.; Rettig, W. *Chem. Rev.* **2003**, *103*, 3899.
- (10) Kollmannsberger, M.; Rurack, K.; Resch-Genger, U.; Baub, J. J. *Phys. Chem. A* **1998**, *102*, 10211.

Reaction of Amines with 8-MethylthioBODIPY: Dramatic Optical and Laser Response to Amine Substitution**

Ixone Esnal,^[a] Arlette Urías-Benavides,^[b] C. F. Azael Gómez-Durán,^[b] Carlos A. Osorio-Martínez,^[b] Inmaculada García-Moreno,^[c] Angel Costela,^[c] Jorge Bañuelos,*^[a] Nerea Epelde,^[a] Iñigo López Arbeloa,^[a] Rongrong Hu,^[d] Ben Zhong Tang,^[d] and Eduardo Peña-Cabrera*^[b]

Abstract: A thorough study of the photophysical and laser properties of 8-aminoboron dipyrromethene dyes was undertaken to determine the role of amine substitution and spatial disposition on the properties of the dyes. It was found that the fluorescent and laser response varied significantly. Although primary amines give rise to highly fluorescent products at the blue edge of the visible region, secondary amines yield nonfluorescent analogues in polar media. The crystal structures

of two analogues are reported and described. Steric hindrance and the higher electron-releasing ability of the amine favor the formation of a quenching intramolecular charge-transfer state. Accordingly, boron dipyrromethene derivatives with primary amines exhibited laser emission with efficien-

cies of up to 44%. Besides, the more efficient derivative was also the most photostable, leading to a significant improvement in the lasing performance with regard to previously reported 8-aminoboron dipyrromethene derivatives. An increase in the solvent polarity, and mainly the presence of tertiary cyclic amines, led to a dramatic decrease or even the loss of the laser action.

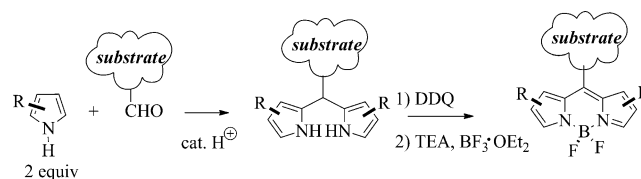
Keywords: charge transfer • dyes/pigments • fluorescence • heterocycles • laser chemistry

Introduction

Boron dipyrromethene (BODIPY)-related reports continue to grow in the chemical literature mainly for two reasons: 1) synthetic chemists are developing new methods to tailor the properties of the BODIPY core (1) by introducing several functional groups around its periphery,^[1] and 2) new

and exciting applications derive from these novel analogues.^[2]

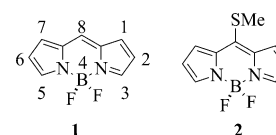
The most common way to build the BODIPY fragment into the substrate of interest is based upon the well-known Lindsey method.^[3] This method relies upon the acid-catalyzed condensation of pyrrole, or its alkylated derivatives, with a formyl group previously attached to the molecule of interest. Oxidation with 2,3-dichloro-5,6-dicyano-1,4-benzoquinone (DDQ) and $\text{BF}_3 \cdot \text{OEt}_2$ coordination yield the final product (Scheme 1).



Scheme 1. Typical Lindsey method to build the BODIPY core into a substrate molecule. TEA = triethylamine.

Despite its practicality, this method is not suitable for complex molecules that possess functional groups that are sensitive to acids, oxidation, or Lewis acids.

Our groups have demonstrated the usefulness of methylthioBODIPY (2)^[4]. A host



[a] I. Esnal, Dr. J. Bañuelos, N. Epelde, Prof. I. López Arbeloa
Departamento de Química Física
Universidad del País Vasco (UPV/EHU)
aptdo. 644, 48080 Bilbao (Spain)
E-mail: jorge.banuelos@ehu.es

[b] A. Urías-Benavides, Dr. C. F. A. Gómez-Durán,
Dr. C. A. Osorio-Martínez, Prof. E. Peña-Cabrera
Departamento de Química, Universidad de Guanajuato
Col. Noria Alta S/N. Guanajuato, Gto. Mexico, 36050 (Mexico)
E-mail: eduardop@ugto.mx

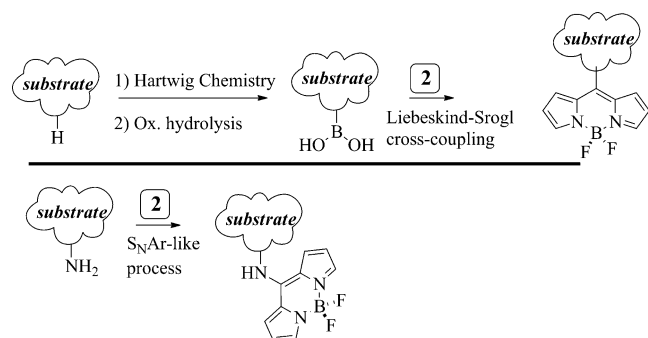
[c] Prof. I. García-Moreno, Prof. A. Costela
Sistemas de Baja Dimensionalidad
Superficies y Materia Condensada
Instituto de Química-Física "Rocasolano"
CSIC. Serrano 119, 28006 Madrid (Spain)

[d] Dr. R. Hu, Prof. B. Zhong Tang
Department of Chemistry
The Hong Kong University of Science and Technology
Clear Water Bay, Kowloon, Hong Kong (P.R. China)

[**] BODIPY = boron dipyrromethene.

Supporting information for this article is available on the WWW under <http://dx.doi.org/10.1002/asia.201300760>.

of different boronic acids react under neutral conditions with **2** in a palladium-catalyzed, copper(I)-mediated reaction (the Liebeskind–Srogl cross-coupling reaction^[5],^[6]). In addition to being an excellent partner in cross-coupling reactions, the methylthio group can be displaced in a S_NAr -like process by amines to give highly emitting dyes that fluoresce at the blue edge of the visible spectrum; a property unknown for BODIPY dyes until recently.^[7] These new findings provide new opportunities for functionalization of complex molecules. Two new strategies are conceptually possible (Scheme 2). In one, a boronate ester may be introduced into

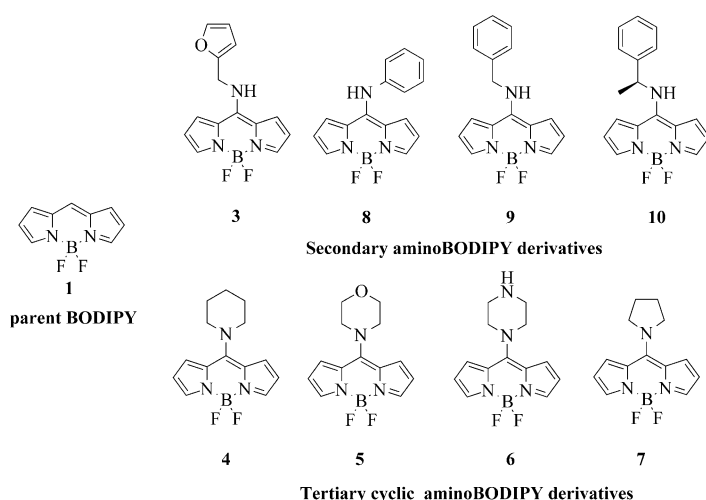


Scheme 2. Two new conceptually protocols for the fluorescent tagging of complex molecules.

the target molecule by using Hartwig chemistry.^[8] The boronate ester would then be oxidatively hydrolyzed to yield the target, suitably functionalized molecule for fluorescent tagging. In the other, more straightforward, strategy, if the target molecule has an amine (either primary or secondary, see below), it would react directly with **2** to give the desired product. This approach is of particular importance owing to large number of natural (and non-natural) products containing one or more amino groups that are particularly suitable for labeling.

Being aware of the potential for the quick tagging of complex molecules through an amino group, we decided to extend the study of our previous reports to a larger number of amines with different substitution patterns (Scheme 3).

An additional and important motivation for this contribution lies in the fact that the development of highly efficient and stable blue-emitting dyes, to overcome some of the most important shortcomings of available chromophores, is of great technological importance for modern optical, analytical, electronic, and biological applications. In fact, many organic dyes with emission in the blue spectral region suffer from low efficiency and rapid chemical photobleaching,^[9] which has impaired the practical implementation of blue-emitting lasers based on dyes. On the other hand, certain BODIPY dyes are excellent laser dyes in the yellow–green (and even red, after proper structural modifications) spectral region to the point of currently being considered as the benchmark against which to compare the lasing performance of organic dyes in that spectral region. Thus, the



Scheme 3. Structures of the 8-aminoBODIPY dyes studied herein.

question arises as to whether it would be possible to extend the operation of these dyes towards the blue region of the spectrum, while retaining their excellent lasing performance.

In previous papers,^[7] we demonstrated that, by attaching different amino groups at the 8-position of a fully unsubstituted BODIPY (**1**), blue-emitting BODIPY dyes are obtained, some of which exhibited very high fluorescence quantum yields and large Stokes shifts, leading to highly efficient laser emission with photostabilities much higher than those exhibited by current dyes with emission in the same spectral region. The present work hopes to provide a deeper insight into the role of amino substitution (electron-releasing ability and spatial disposition) on the photophysical and lasing properties of BODIPY dyes. To this end, we looked for the best structural modifications to enhance the photonic performance at the blue region or to make the fluorescence sensitive to a certain solvent property (i.e., polarity/acidity).

Results and Discussion

Synthesis

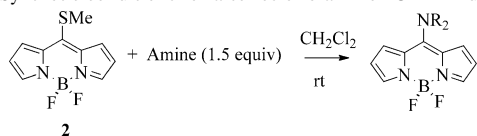
The synthesis of 8-aminoBODIPY dyes was carried out as previously reported.^[7] Thus, derivative **2** was treated with a variety of amines to give the desired products (Table 1).

The synthesis was very efficient and straightforward, as well as being a spot-to-spot procedure, which facilitated the purification process. The reduced nucleophilicity of aniline was reflected in the lower yield and longer reaction time of the formation of **8**.^[4] Both primary and secondary amines reacted within a few minutes with high yields. Tertiary amines did not react.

Photophysical Properties in Solution

A number of BODIPY dyes were prepared with different amino groups at the 8-position with different substitution patterns (Scheme 3).

Table 1. Synthetic conditions for a series of 8-aminoBODIPY dyes.



Entry	Amine	Reaction time [min]	Yield ^[a] [%]	Product
1	furfurylamine	15	85	3
2	piperidine	20	93	4
3	morpholine	10	95	5
4	piperazine	5	96	6
5	pyrrolidine	30	95	7
6	aniline	90	35	8
7	benzylamine	40	94	9
8	(S)-(-)- α -methylbenzylamine	40	90	10

[a] Yield of isolated product.

Secondary 8-AminoBODIPY Derivatives (Compounds **3**, **8**, **9**, and **10**)

The presence of the electron-donating amine group at the *meso* position resulted in a significant blueshift of the spectral bands; this was more important for absorption (Figure 1). As a result, these derivatives are characterized by a large Stokes shift (up to 2500–3000 cm^{-1}). These tendencies are in agreement with the results obtained for derivatives with monoalkylated amines.^[7b] Such displacement of the spectral bands towards higher energies was rationalized

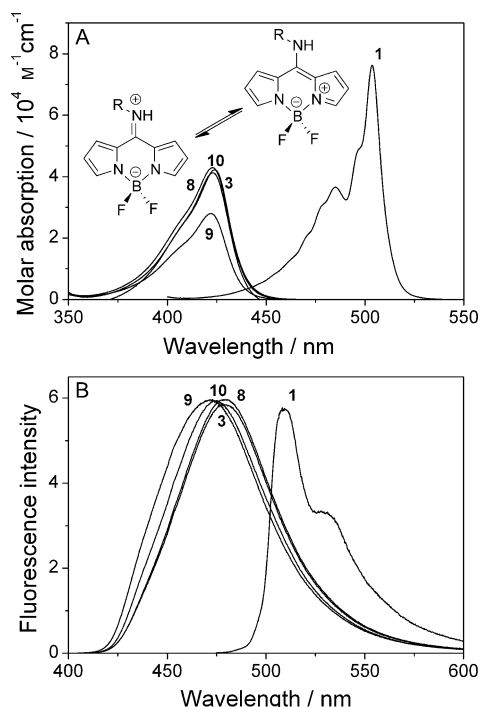


Figure 1. Absorption (A) and fluorescence (B) spectra of reference compound **1** and its derivatives with secondary amines (**3**, **8**, **9** and **10**) in *c*-hexane. Inset: the 8-amino-induced resonant hemicyanine structure from the cyanine one.

in terms of an increase in the LUMO energy (Figure S1 in the Supporting Information), owing to electron-releasing ability of the amine, and the formation of a hemicyanine-like π system (Figure 1), owing to electronic coupling with the chromophoric core. Those BODIPY derivatives with the most electron-donating amines (methylaryl or methylbenzyl substituents) exhibit greater instability of the LUMO. Moreover, in spite of the presence of the aryl rings, the optimized geometries indicate that the amine is coplanar to the chromophore (Figure S2 in the Supporting Information), which enables the formation of the hemicyanine, the delocalized system of which is shorter than the normal cyclic cyanine in BODIPY. The presence of this mesomeric form was confirmed by previously reported NMR spectra.^[7]

The electrochemical properties of a selected representative derivative of secondary amines (compound **3**) were analyzed by cyclic voltammetry. Reference compound **1** showed an irreversible oxidation at 1.72 V and a quasi-reversible reduction at -0.71 V (Figure 2). Whereas the oxidation wave

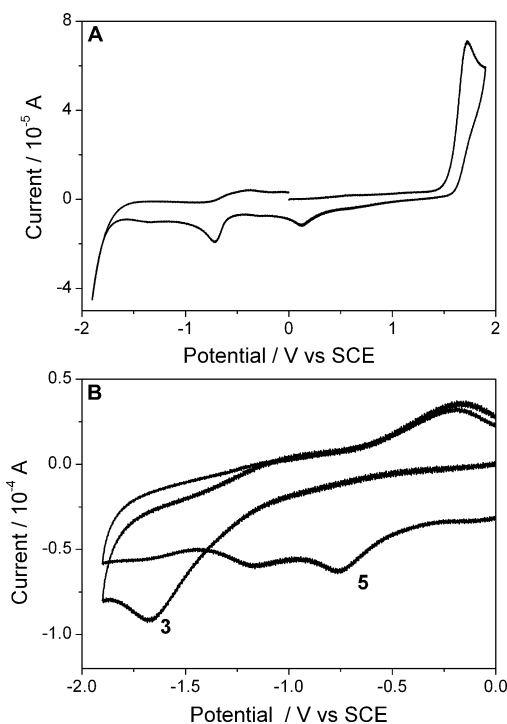


Figure 2. Cyclic voltammograms (scan rate of 0.1 V s^{-1} in the negative direction) of compound **1** (A, 1 mM) and compounds **3** and **5** (B; 0.5 mM, only the reduction potential) in acetonitrile with tetrabutylammonium hexafluorophosphate (TBAPF₆) as the supporting electrolyte.

remained almost unaltered in the presence of the amine, the reduction peak was shifted towards more negative values for compound **3** (-1.67 V). Thus, amination implies that the compound is more difficult to reduce because its electron-donating ability causes instability in the corresponding radical anion. Such behavior supports strong electronic coupling between both entities and the theoretical increase in the

Table 2. Photophysical data of the parent BODIPY dye and the secondary 8-aminoBODIPY derivatives in *c*-hexane and methanol.^[a]

	λ_{ab} [nm]	ϵ_{max} (<i>f</i>) [10^4 M ⁻¹ cm ⁻¹]	λ_{fl} [nm]	ϕ	τ [ns]	k_{fl} [10^8 s ⁻¹]	k_{nr} [10^8 s ⁻¹]
<i>c</i> -hexane							
1	503.5	7.6 (0.38)	510.5	0.96	6.47	1.48	0.06
8	423.0	4.3 (0.38)	480.0	1.00	5.25	1.90	0.00
9	422.0	2.8 (0.25)	472.0	1.00	4.92	2.03	0.00
10	424.0	4.2 (0.35)	475.0	1.00	5.02	1.99	0.00
3	423.0	4.1 (0.35)	478.5	0.98	5.24	1.87	0.04
methanol							
1	497.0	5.8 (0.39)	507.0	0.87	7.33	1.18	0.18
8	403.5	4.1 (0.45)	461.0	0.16	0.92 ^[b]	1.74	9.13
9	403.0	2.3 (0.23)	453.5	0.09	0.49 ^[b]	1.84	18.6
10	404.5	3.1 (0.33)	460.5	0.05	0.32 ^[b]	–	–
3	403.0	3.4 (0.36)	464.0	0.15	0.94 ^[b]	1.60	9.04

[a] Photophysical data: absorption (λ_{ab}) and fluorescence wavelength (λ_{fl}), molar absorption (ϵ_{max}), oscillator strength (*f*), fluorescence quantum yield (ϕ), lifetime (τ), and radiative (k_{fl}) and nonradiative (k_{nr}) deactivation rate constants. The full photophysical data in other solvents are listed in Table S1 in the Supporting Information. [b] Main component of the decay curve; the corresponding rate constants are calculated from this lifetime only when its contribution to the decay curve is higher than 98%.

LUMO energy suggested above as reasons for the enhancement in the energy gap.

The main photophysical data for the novel BODIPY derivatives with monofunctionalized amines are listed in Table 2. The results obtained exhibit the same tendencies as those previously reported for the derivative with the 8-methylamino moiety.^[7b] Indeed, the fluorescence capacity showed a marked dependence on the nature of the solvent. Thus, the new BODIPYs are highly fluorescent in apolar media, such as *c*-hexane (up to 100%), but in polar media both the fluorescence quantum yields (down to 10%) and lifetimes (around hundreds of picoseconds) drastically decline. In polar media, the fluorescence decay curves were analyzed as biexponentials, with the main decay (which is the one listed in Table 2) characterized by a short lifetime, and the minor decay (with a much lower contribution) by a long lifetime (≈ 4 ns), which is reminiscent of that of BODIPY. Such evolution is clearer in compounds **9** and **10**, which contain the more electron-donating amines (benzylamine and methyl benzylamine).

These results suggest the presence of an extra deactivation process, in particular, a nonfluorescent (no new bands are detected) intramolecular charge-transfer state (ICT). The population of such state depends markedly on the polarity of the environment; thus, the quenching of the fluorescence emission from the locally excited state (LE) by the ICT is more efficient in polar media. The presence of this ICT state is supported by augmentation of the fluorescence capacity in protic media (such as F₃-ethanol) with respect to other polar solvents (Table S1 in the Supporting Information), because the electron pair of the amino group is more fixed, owing to specific interaction with these protic solvents, leading to a decrease in the electron-donating capacity of the amine and the ICT probability.

Accordingly, the short lifetime of the biexponential decay curve in polar media is attributed to deactivation of the LE through ICT and the long reminiscent lifetime is attributed

to the relaxed LE. Such assignment is supported by the dependence of the contribution of the lifetimes to the multiexponential adjustment on the wavelength selected to monitor the deactivation curves. Thus, at wavelengths longer than the maximum of the emission (detection wavelength placed in a region closer to the possible ICT emission), the contribution of the short lifetime to the decay curve increases considerably (data not shown). In the next section, the conducting temperature-dependence measurements provide further evidence of the operative ICT state.

Tertiary 8-AminoBODIPY Derivatives (Compounds 4–7)

As expected, the spectral bands of these derivatives are blueshifted relative to reference compound **1** (Figure 3). However, the extension of such a hypsochromic shift was smaller (with the exception of derivative **7**) than that recorded previously for secondary amines. Indeed, the reduction potential in compound **5** decreases (less negative, -1.17 V; Figure 2) with regard to counterpart **3**, with second-

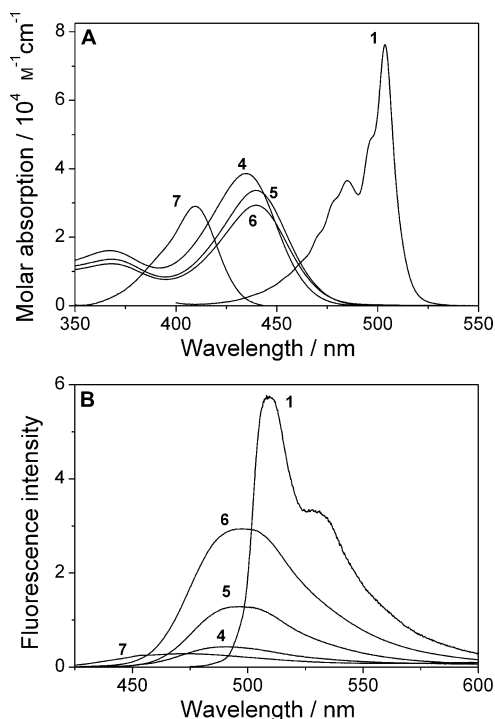


Figure 3. Absorption (A) and fluorescence (B) spectra of reference BODIPY **1** and its derivatives 8-substituted by tertiary cyclic amines (**4**, **5**, **6**, and **7**) in *c*-hexane.

dary amines (−1.67); this is indicative of a reduced energy gap. Although tertiary amines have a higher electron-donating character, they take part in the ring, which implies steric hindrance with adjacent positions of the core. Indeed, the optimized geometries (Figure S2 in the Supporting Information) indicate that cyclic amines are twisted around 26° and are out of the indacene plane (the secondary counterparts were around 10° and almost coplanar). As result of accommodation of the cyclic amine, the planarity of the chromophore is distorted (up to 20° along the transverse axis). Therefore, the coplanar arrangement between the amine and BODIPY is hindered, which reduces the probability of the formation of the hemicyanine, and consequently, lowering of the magnitude of the spectral blueshift (Figure 3). Further evidence is provided by compound **7**, which contains the smallest cycle (pyrrolidine). In this case, steric hindrance should be lower and enable a coplanar disposition of the amine, leading to a greater contribution from the hemicyanine form. Compound **7** shows the largest blueshift of all compounds studied herein.

Table 3 collects the main photophysical data of the tertiary 8-aminoBODIPYs in *c*-hexane and methanol. A com-

parison of the results in Tables 2 and 3 shows clearly an important decrease in both the fluorescence capacity (which is negligible in polar media) and the lifetimes in the derivatives with cyclic amines, even in apolar solvents, such as *c*-hexane. This decrease is particularly noticeable if there are no other heteroatoms in the cyclic amines. It is likely that the presence of heteroatoms (O and N) in the ring (**5** and **6**) removes electron density from the amine, and hence, decreases the probability of the formation of the ICT state. Steric hindrance (discussed above) could not only decrease the probability of the formation of the hemicyanine form, but also cause the electron-donating amino group to be positioned such that it is more orthogonal to the BODIPY chromophore to alleviate the steric hindrance; thus favoring the formation of an ICT state (probably a twisted intramolecu-

lar charge-transfer state (TICT)). Moreover, theoretical calculations confirm twisting of the amine and reveal a loss of planarity in the chromophore, owing to accommodation of the bulky cyclic amine. Such geometrical distortion is usually related to an enhancement of the internal conversion processes. Consequently, even in apolar media, in which the ICT state is less favored, derivatives **5** and **6** have a lower fluorescence capacity than the secondary 8-aminoBODIPY dyes. In polar media, the fluorescence emission was almost negligible for all disubstituted cyclic amines. The dynamics of the ICT process in these solvents should be very fast (tens of picoseconds, under the temporal resolution of the photon counter), indicating that such a processes is highly favored.^[10]

Some authors have reported the influence of the ring size of amine-containing cycles in the photophysical properties of chromophores (i.e., rosamine and naphthalimides).^[11] They concluded that charge transfer was more feasible in the bigger cycles; N-atom inversion is hindered in the smaller rings. Surprisingly, a new, weak fluorescence band appeared at around 600 nm, after the emission from the LE state, only for compound **7** (which has the smallest ring), when dissolved in apolar *c*-hexane (Figure 4). This band could be attributed to emission from the ICT state. Furthermore, some authors have claimed that the ICT state can eventually evolve into an exciplex-like state upon coulombic interactions (harpooning effect).^[12] Such an entity causes a weak and redshifted emission and has even been reported for some BODIPYs if ICT takes part.^[13]

Such a new band was no longer detected upon changing the solvent to a more polar one, although the decrease in the fluorescence emission was also very clear and drastic (Figure 4). Thus, further stabili-

Table 3. Photophysical data of the parent BODIPY dye and its tertiary 8-amino derivatives in the *meso* position in *c*-hexane and methanol. Full photophysical data are reported in Table S2 in the Supporting Information.

	λ_{ab} [nm]	ϵ_{max} (<i>f</i>) [$10^4 \text{ M}^{-1} \text{ cm}^{-1}$]	λ_n [nm]	ϕ	τ [ns]	k_n [10^8 s^{-1}]	k_{nr} [10^8 s^{-1}]
<i>c</i> -hexane							
1	503.5	7.6 (0.38)	510.5	0.96	6.47	1.48	0.06
7	409.5	2.9 (0.26)	472.5	0.05	0.04 ^[a]	12.5	237
6	440.0	2.9 (0.44)	498.0	0.49	1.93	2.54	2.64
5	439.5	4.2 (0.36)	496.0	0.27	1.94 ^[a]	1.39	3.76
4	435.0	3.9 (0.41)	492.0	0.07	1.23 ^[a]	0.56	7.57
methanol							
1	497.0	5.8 (0.39)	507.0	0.87	7.33	1.18	0.18
7	391.5	2.4 (0.26)	454.5	0.004	–	1.90	474
6	419.5	2.4 (0.41)	445.5	0.006	–	–	–
5	419.5	2.6 (0.38)	452.0	0.006	–	–	–
4	413.0	3.1 (0.43)	437.5	0.001	–	–	–

[a] Main component of the decay curve; the corresponding rate constants are calculated from this lifetime only when its contribution to the decay curve is higher than 98%. The fluorescence lifetimes of compounds **4**–**7** in methanol were below the temporal resolution of our picosecond photon counter (around 30–40 ps).

parison of the results in Tables 2 and 3 shows clearly an important decrease in both the fluorescence capacity (which is negligible in polar media) and the lifetimes in the derivatives with cyclic amines, even in apolar solvents, such as *c*-hexane. This decrease is particularly noticeable if there are no other heteroatoms in the cyclic amines. It is likely that the presence of heteroatoms (O and N) in the ring (**5** and **6**) removes electron density from the amine, and hence, decreases the probability of the formation of the ICT state. Steric hindrance (discussed above) could not only decrease the probability of the formation of the hemicyanine form, but also cause the electron-donating amino group to be positioned such that it is more orthogonal to the BODIPY chromophore to alleviate the steric hindrance; thus favoring the formation of an ICT state (probably a twisted intramolecu-

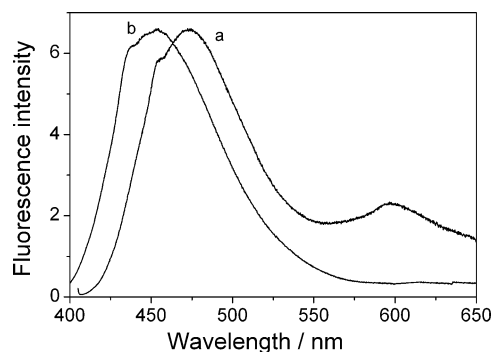


Figure 4. Normalized fluorescence spectra of dilute solutions of **7** in (2 μM) of *c*-hexane (a) and methanol (b).

zation of the ICT (by more electron-donating amines or more polar solvents) suppresses its fluorescence emission. This apparent mismatch can be rationalized when considering that the stabilization of the ICT does not imply a stronger emission, rather the opposite, because the ICT state is energetically close to the ground state. The closer the proximity of the electronic state, the highest the probability of internal conversion, in terms of the energy gap law. Moreover, heating a solution of compound **7** in *c*-hexane led to a concomitant decrease in the ICT fluorescence band, because vibrational coupling is enhanced (Figure S3 in the Supporting Information). Furthermore, ICT stabilization by solvent polarization could give rise to a nonfluorescent charge-separation (CS) state that hampers detection of the ICT fluorescence. Similar trends were claimed for a BODIPY derivative with 8-aniline forced to be perpendicular through steric hindrance.^[14]

Summing up, the feasibility of ICT formation should control not only the fluorescence behavior, but also laser performance. Therefore, we conducted temperature-dependence fluorescence measurements to unambiguously assign fluorescence quenching to ICT. The cooling of compound **5** down to 77 K led to a large increase in the fluorescence signal (Figure 5). Usually, a temperature decrease enhances fluorescence efficiency because the vibrational motion is

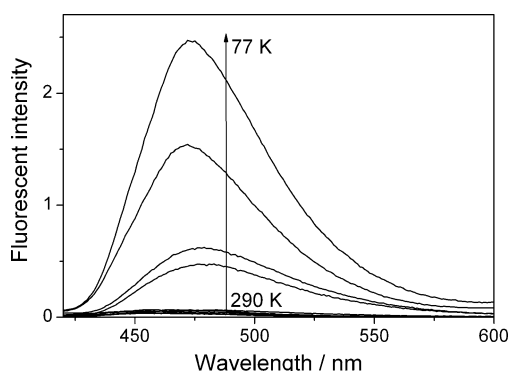


Figure 5. Fluorescence spectra of compound **5** in ethanol from 290 to 77 K.

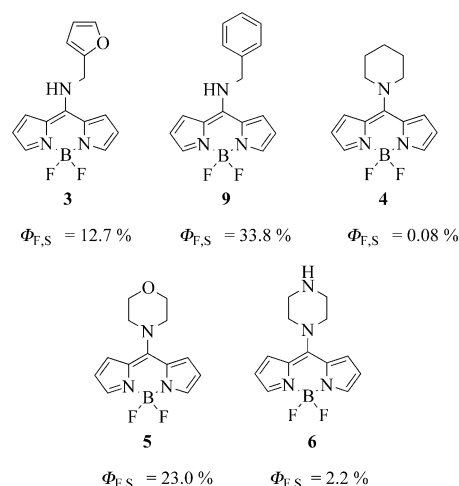
hindered, and hence, internal conversion is reduced. However, in the present case, the huge improvement of the fluorescence emission after freezing the sample indicates that the quenching process present at room temperature is no longer taking place. Similar results were also obtained for compound **3**, which contains a secondary amine (data not shown). Considering that ICT is an activated process, at low enough temperatures its population is avoided; thus confirming the key role of such a process in the photophysical properties of mono- and disubstituted cyclic 8-aminoBODIPYs.

Finally, a careful comparison of the optical properties of the 8-aminoBODIPYs prepared so far (primary, secondary, and tertiary amines) shows that there is an evident trend in the fluorescent response of the product, according to the

nature of the amino groups. Indeed, if the dyes are irradiated at $\lambda = 366$ nm (Figure 6), primary amines and ammonia yield highly fluorescent dyes, whereas secondary and aromatic amines give nonemissive products (ICT stabilization), thereby providing a basis for their utilization as an amine chemodosimeter.

Solid-State Emission

Solid-state quantum yields ($\Phi_{F,S}$) for compounds **3–6** and **9** were measured by means of a calibrated integrating sphere. Relatively high $\Phi_{F,S}$ values were deduced from measurements of the secondary aminoBODIPYs. For example, the $\Phi_{F,S}$ values of **9** and **3** were 33.8 and 12.7%, respectively. Meanwhile, tertiary aminoBODIPY derivatives **4** and **6** have low $\Phi_{F,S}$ value of 0.08 and 2.2%, respectively (Scheme 4).



Scheme 4. Quantum yield of selected aminoBODIPYs in the solid state.

X-ray Study

Single-crystal structures of secondary aminoBODIPY **9** and tertiary aminoBODIPY **5** were obtained to gain detailed information about the solid-state molecular structures (Figure 7). The BODIPY core is almost coplanar and the nitrogen atom substituted on the 8-position of BODIPY lies on the same plane in both **9** and **5**, whereas the phenyl ring in compound **9** is twisted out of the plane. The packing modes of these two compounds are different. In the single-crystal structure of **9** (Figure 7C), the plane-to-plane distance of two closest BODIPY moieties is 3.700 Å and the two BODIPY moieties are staggered. A distance of 2.286 Å was observed between the amino proton and one fluorine atom; this indicates hydrogen-bonding interactions. Such hydrogen bonding connects molecules through the parallel direction of the BODIPY plane. Different from **9**, the single-crystal structure of **5** adopts a head-to-tail packing mode (Figure 7D). The plane-to-plane distance of the closest BODIPY moieties is 3.776 Å and the BODIPY cores were



Figure 6. Fluorescent response of the 8-aminoBODIPY dyes to the nature of the amino group (solutions in ethyl acetate, under excitation at $\lambda = 366$ nm).

highly overlapped along the perpendicular axis. A distance of 2.303 Å was observed between the oxygen atom on the morpholine ring and the proton on the 3-position of BODIPY, indicating intramolecular interactions along the parallel axis of the BODIPY plane. Taking these intermolecular interactions and steric hindrance into account, molecules of **5** packed in a closer manner in the crystal state than that of **9**, which may quench the solid-state emission. Hence, it has a smaller Φ_{FS} value compared with **9**.

Lasing Properties

The lasing properties of representative examples of the new BODIPY derivatives were studied under pumping at $\lambda = 355$ nm, which is the usual pump wavelength for dyes emitting in the blue spectral region. Under our experimental conditions (transversal excitation and strong focusing of the incoming pump radiation, see the Experimental Section), the concentration of the dyes in different solvents should be in the millimolar range to ensure total absorption of the pump radiation within the first millimeter at most of the solution, to obtain an emitted beam with near-circular cross-section, and to optimize the lasing efficiency (ratio between the energy of the dye laser output and the pump energy incident on the sample surface). Although in all cases the highest fluorescence quantum yields of the new derivatives

were obtained in *c*-hexane, none of the dyes could be dissolved in this solvent at the concentrations required to obtain laser emission. The BODIPY derivatives with primary amines did exhibit laser emission in ethyl acetate, acetone, F₃-ethanol, and ethanol (Figure 8), with efficiencies correlated with their photophysical properties in dilute solutions (Table S1 in the Supporting Information): the higher the fluorescence quantum yield and the lower the nonradiative rate constant, the higher the lasing efficiency.

None of the derivatives with secondary amines exhibited laser action, even at the highest possible concentrations, as expected on account of their very low quantum yields and high nonradiative rate constants (Table S2 in the Supporting Information). Therefore, such correlation indicates that the lasing efficiency is controlled by the influence of the ICT state on the photophysics of the dye.

As shown in Figure 8, the highest lasing efficiencies were obtained in ethyl acetate, which is the more apolar solvent after *c*-hexane among the solvents used in this work, that is, in media where the probability of fluorescence quenching through ICT processes is reduced. The dependence of the laser action of BODIPY derivatives **8**, **9**, **10** and **3** on the corresponding dye concentrations was analyzed in ethyl acetate, which was the solvent in which the dyes exhibited the highest fluorescence quantum yield, together with the lowest nonradiative rate constant. It was found that, in all

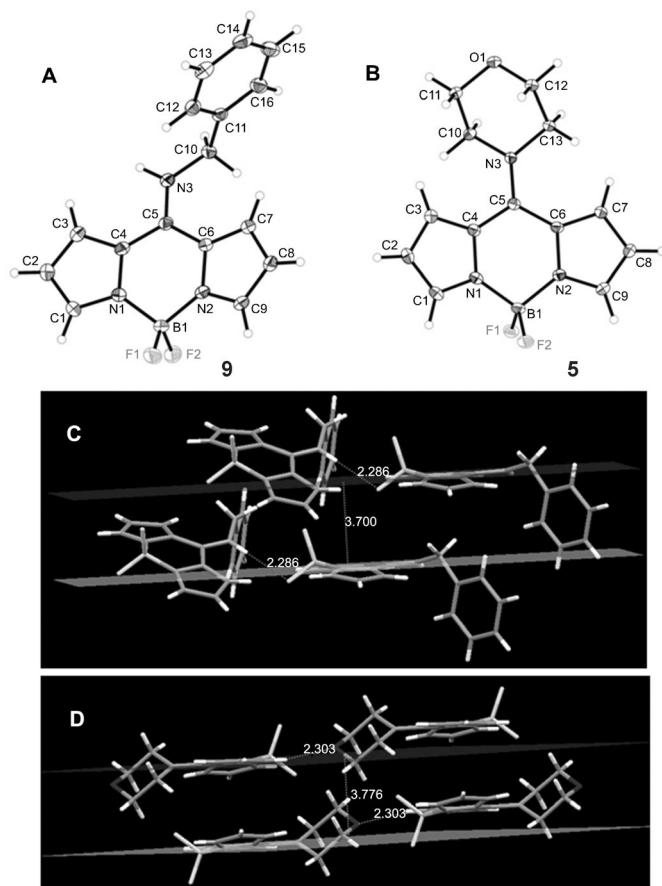


Figure 7. Single-crystal structures and crystal packing modes of **9** (A and C) and **5** (B and D).

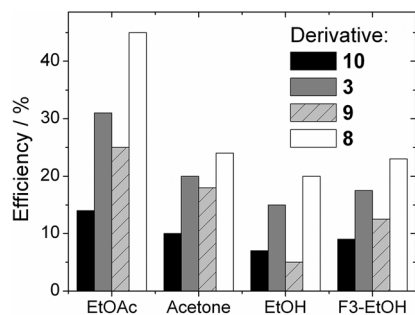


Figure 8. Lasing efficiencies of the new BODIPYs derivatives (**3**: grey, **8**: white, **9**: striped, and **10**: black) in different solvents under $\lambda = 355$ nm pumping.

cases, the optimum concentration was 4×10^{-3} M (Figure 9), with lasing efficiencies ranging from 14 (**10**) up to 44% (**8**).

An important parameter for any practical application of the dye lasers is their lasing photostability under repeated pumping. We studied the lasing photostability of the new BODIPY derivatives in ethanol because, in this solvent, the nonradiative constants of the dyes studied exhibit significant variations that correlate well with the photostability. Figure 10 depicts the actual evolution of the laser-induced

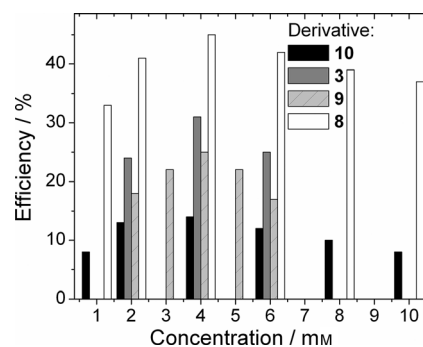


Figure 9. Dependence of the lasing efficiency of the new BODIPY derivatives (**3**: grey, **8**: white, **9**: striped, and **10**: black) on their concentration in ethyl acetate under 355 nm pumping.

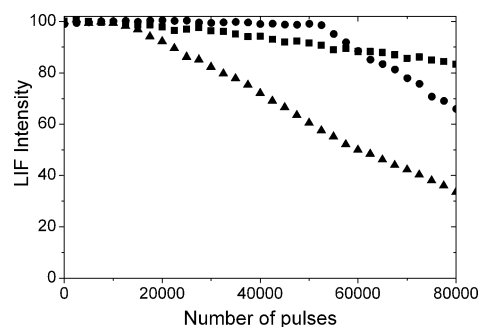


Figure 10. Normalized laser-induced fluorescence emission as a function of the number of pump pulses at a 5 Hz repetition rate for solutions of dyes **8** (■), **9** (●) and **10** (▲) in ethyl acetate under transversal pumping at $\lambda = 355$ nm.

fluorescence emission of dyes **8**, **9**, and **10** with the number of pump pulses at a 5 Hz repetition rate. There is an excellent correlation between the values of the nonradiative constants and the photostability: the lower the nonradiative rate constant, the higher the photostability. Figure 10 does not show the photostability of dye **3** because it is almost identical to that of **8**, which is in agreement with both dyes having the same value of nonradiative decay constant.

Dye **8** leads to improved efficiency and photostability over that previously obtained with 8-aminoBODIPY derivatives,^[7b] which in turn leads to significantly improved lasing performance compared with that of commercial coumarin dyes pumped under identical experimental conditions.^[7a,b] This fact highlights the potential of these dyes to act as laser emitters in the blue spectral region.

Conclusion

Eight new 8-aminoBODIPY dyes were efficiently prepared and an in-depth study was performed to understand the role of amine spatial disposition on the photophysical and lasing properties of BODIPY. Crystal structures of derivatives **9** and **5** were obtained. In both cases, the BODIPY core remained nearly planar, although the packing mode of **9** and **5**

differed from each other. In **9** the BODIPY moieties were staggered, whereas in **5** they adopted a head-to-tail arrangement.

These dyes were characterized by their emission at the blue edge of the visible region, owing to their hemicyanine-like delocalized π system. Whereas the attachment of aryl rings to the amine gave rise to improved fluorescence and lasing efficiencies in apolar media, the inclusion of the amine in a cycle resulted in a drastic decline in the fluorescence efficiency and the derivatives no longer lased. In the former monosubstituted amines, high fluorescence quantum yields (approaching the 100%) were achieved in apolar media and superseded commercial blue-emitting dyes in terms of their lasing performance. However, in polar media, a quenching ICT state was populated, which reduced their lasing ability. The quenching effect was even more apparent after attaching cyclic amines to the core. The induced steric hindrance twisted the amine and hampered electronic coupling with the chromophore. Consequently, the statistical weight of the hemicyanine resonant structure was reduced, leading to a lower blueshift of the spectral bands and fluorescence quenching by the ICT (reinforced by the higher electron donor ability of the tertiary amine) was more marked and caused the completely loss of the fluorescence signal in polar media. Therefore, the stabilization of the ICT process, which in turns depended on the substitution pattern of the amino group and the environment, determined the laser performance of these BODIPY derivatives working at the blue part of the visible spectrum.

Experimental Section

Materials

Solvents for laser and photophysical studies were of spectroscopic grade (Merck, Aldrich, or Sigma) and were used without purification; those used in synthetic work were purified by standard methods. Other reagents were from commercial sources and used as received. BODIPY **8** was prepared according to a literature procedure.^[4]

Photophysical, Electrochemical, and Quantum Mechanical Properties

The photophysical properties were recorded in dilute solutions (around 2×10^{-6} M), which were prepared by adding the corresponding solvent to the residue from an adequate amount of a concentrated stock solution in acetone after vacuum evaporation of this solvent. UV/Vis absorption and fluorescence spectra were recorded on a Varian model CARY 4E spectrophotometer and a SPEX Fluorolog 3-22 spectrofluorimeter, respectively. Fluorescence quantum yield (Φ) was obtained by using a solution of coumarin 1 in ethanol as a reference ($\Phi^r = 0.75$). Temperature-dependence measurements were performed by using a liquid-hydrogen-cooled cryostat (Oxford) and an external electronic temperature controller device for heating. Radiative decay curves were obtained with the time-correlated single-photon-counting technique (Edinburgh Instruments, model FL920, with picosecond time resolution). Fluorescence emission was monitored at the maximum emission wavelength after excitation at $\lambda = 370$ nm by means of a diode laser (PicoQuant, model LDH370) with 150 ps FWHM pulses. The fluorescence lifetime (τ) was obtained after the deconvolution of the instrumental response signal from the recorded decay curves by means of an iterative method. The goodness of the exponential fit was controlled by statistical parameters (chi-square, Durbin-Watson and the analysis of the residuals). The radiative (k_r) and nonradiative (k_{nr}) rate constants were calculated from the fluorescence quan-

tum yield and lifetime: $k_r = \Phi/\tau$ and $k_{nr} = (1-\Phi)/\tau$. The solid-state fluorescence quantum yields were determined on an integrating sphere, according to the method described by de Mello et al.^[15] A $\lambda = 325$ nm continuous-wave (CW) light from a He-Cd laser was used for optical pumping. The studied sample was placed inside the integrating sphere, in which light emission was redistributed isotropically over the interior surface of the sphere. An optical fiber collected light from the sphere and directed it to an Ocean Optics (Ocean Optics, Inc.) USB2000 miniature fiber optics spectrometer. The number of emitted photons was obtained by integrating the measured photoluminescence (PL) signal over the emission wavelengths. The response of the fiber and spectrometer detector system was normalized by using a calibrated light source.

Single-crystal X-ray diffraction intensity data were collected at 100 K on a Bruker-Nonices Smart Apex CCD diffractometer with graphite monochromated $\text{MoK}\alpha$ radiation. Processing of the intensity data was performed by using the SAINT and SADABS routines and the structures and refinements were achieved by using the SHELTL suite of X-ray programs (version 6.10).

CCDC 953705 (**9**) and CCDC 953706 (**9**) contain the supplementary crystallographic data for this paper. These data can be obtained free of charge from The Cambridge Crystallographic Data Centre via www.ccdc.cam.ac.uk/data_request/cif.

Electrochemical experiments (Metrohm Autolab) were performed by using a three-electrode setup with a platinum disk (diameter 3 mm) or layer (length 7.1 mm \times width 8 mm) working electrode, platinum wire as the counter electrode, and Ag/AgCl as the reference electrode. A 0.1 M solution of TBAPF₆ in dry acetonitrile was used as the electrolyte solvent in which the compounds were dissolved to achieve a concentration of 0.5–1 mM. All redox potentials were reported versus ferrocene as an internal standard. The solutions were purged with argon and all measurements were performed under an inert atmosphere.

Ground- and excited-state geometries were optimized at the B3LYP and CIS theory level respectively, by using the double valence basis set (6-31g), as implemented in Gaussian 09. The geometries were considered as energy minima when the corresponding frequency analysis did not give any negative values.

Laser Experiments

Liquid solutions of dyes were contained in 1 cm optical-path quartz cells carefully sealed to avoid solvent evaporation during experiments. The solutions of the newly synthesized dyes were transversely pumped at $\lambda = 355$ nm, with 5 mJ/pulse, 8 ns full-width at half maximum (FWHM) pulses from the third-harmonic of Q-switched Nd:YAG laser (Spectron SL282G) and at a repetition rate of up to 5 Hz. The exciting pulses were line-focused onto the cell, providing pump fluences on the active medium of 110 mJ cm^{-2} . The oscillation cavity (2 cm length) consisted of a 90% reflectivity aluminum mirror, with the lateral face of the cell as the output coupler.

The photostability of the dyes was evaluated by irradiating a solution (10 μL) in ethyl acetate under lasing conditions. The solutions were contained in a cylindrical Pyrex tube (1 cm height, 1 mm internal diameter) carefully sealed to avoid solvent evaporation during the experiments. Although the low optical quality of the capillary tube prevented laser emission from the dyes, information about photostabilities could be obtained by monitoring the decrease in laser-induced fluorescence intensity, excited transversally to the capillary tube, as a function of the number of pump pulses at a 5 Hz repetition rate. The fluorescence emission was monitored perpendicular to the exciting beam, collected by an optical fiber, and imaged onto the input slit of a monochromator (Acton Research corporation) and detected with a charge-coupled device (CCD) (SpectraMM:GS128B). The fluorescence emission was recorded by feeding the signal to the boxcar (Stanford Research, model 250) to be integrated before being digitized and processed by a computer. Each experiment was repeated at least three times. The estimated error in energy and photostability measurements was 10%.

Typical Procedure for the Aromatic Nucleophilic Substitution of 8-methylthioBODIPY 2 with Primary and Secondary Amines

All reactions were initiated with **2** (20.0 mg, 0.08 mmol) as the limiting reagent and the amine (0.13 mmol). In a 5 mL flask, compound **2** was dissolved in acetonitrile (2 mL) and the amine was added in one portion and allowed to stir at 25°C. The crude reaction mixture was dried in vacuo, the dry solid was transferred to a vial in which the solid was dissolved in dichloromethane and petroleum ether was added to carefully form two phases to promote crystallization of the solids.

Acknowledgements

This work was supported by the Ministerio de Economía y Competitividad (MEC) (MAT2010-20646-C04-01 and MAT2010-20646-C04-04, and TRACE 2009-0144). The Gobierno Vasco (IT339-10 project) is thanked for financial support and a research contract (SPE12UN140) for I.E. We also thank CONACyT (Mexico, Grant 129572). A.U.-B., C.F.A.G.-D., and C.A.O.-M. wish to thank CONACyT for scholarships. We also wish to thank Cuantico de México for the kind donation of 8-methylthioBODIPY 2. B.Z.T. thanks the Research Grants Council of Hong Kong (HKUST2/CRF/10).

- [1] a) R. Ziessel, G. Ulrich, A. Harriman, *New J. Chem.* **2007**, *31*, 496–501; b) G. Ulrich, R. Ziessel, A. Harriman, *Angew. Chem.* **2008**, *120*, 1202–1219; *Angew. Chem. Int. Ed.* **2008**, *47*, 1184–1201; c) A. C. Benniston, G. Copley, *Phys. Chem. Chem. Phys.* **2009**, *11*, 4124–4131; d) A. Loudet, K. Burgess, *Chem. Rev.* **2007**, *107*, 4891–4932; e) T. E. Wood, A. Thompson, *Chem. Rev.* **2007**, *107*, 1831–1861.
- [2] a) R. West, C. Panagabko, J. Atkinson, *J. Org. Chem.* **2010**, *75*, 2883–2892; b) T. Ehrenschwender, H.-A. Wagenknecht, *Synthesis* **2008**, 3657–3662; c) Y. Rio, W. Seitz, A. Gouloumis, P. Vazquez, J. L. Sessler, D. M. Guldi, T. Torres, *Chem. Eur. J.* **2010**, *16*, 1929–1940; d) M. Koepf, A. Trabolsi, M. Elhabiri, J. A. Wytko, D. Paul, A. M. Albrecht-Gary, J. Weiss, *Org. Lett.* **2005**, *7*, 1279–1282; e) C. Y. Lee, J. T. Hupp, *Langmuir* **2010**, *26*, 3760–3765; f) M. R. Rao, S. M. Mobin, M. Ravikanth, *Tetrahedron* **2010**, *66*, 1728–1734; g) M. Vendrell, G. G. Krishna, K. K. Ghosh, D. Zhai, J.-S. Lee, Q. Zhu, Y. H. Yau, S. G. Shochat, H. Kim, J. Chung, Y.-T. Chang, *Chem. Commun.* **2011**, *47*, 8424–8426; h) N. Boens, W. Qin, M. Baruah, W. M. De Borggraeve, A. Filarowski, N. Smisdom, M. Ameloot, L. Crovetto, E. M. Talavera, J. M. Alvarez-Pez, *Chem. Eur. J.* **2011**, *17*, 10924–10934; i) N. Boens, V. Leen, W. Dehaen, *Chem. Soc. Rev.* **2012**, *41*, 1130–1172; j) T. Cheng, T. Wang, W. Zhu, Y. Yang, B. Zeng, Y. Xu, *Chem. Commun.* **2011**, *47*, 3915–3917; k) J. Godoy, G. Vives, J. M. Tour, *Org. Lett.* **2010**, *12*, 1464–1467; l) J. Lu, H. Fu, Y. Zhang, Z. J. Jakubek, Y. Tao, S. Wang, *Angew. Chem.* **2011**, *123*, 11862–11866; *Angew. Chem. Int. Ed.* **2011**, *50*, 11658–11662; m) J. G. Baker, L. A. Adams, K. Salchow, S. N. Mistry, R. J. Middleton, S. J. Hill, B. J. Kellam, *Med. Chem.* **2011**, *54*, 6874–3887; n) T. Bura, N. Leclerc, S. Fall, P. Léveque, T. Heiser, R. Ziessel, *Org. Lett.* **2011**, *13*, 6030–6033; o) D. R. Kim, H.-C. Ahn, W.-J. Lee, D.-R. Ahn, *Chem. Commun.* **2011**, *47*, 791–793; p) A. P. Singh, K. M. Lee, D. P. Murale, T. Jun, H. Liew, Y.-H. Suh, D. G. Churchill, *Chem. Commun.* **2012**, *48*, 7298–7300; q) R. Wang, F. Yu, P. Liu, L. Chen, *Chem. Commun.* **2012**, *48*, 5310–5312; r) N. Sakamoto, C. Ikeda, M. Yamamura, T. Nabeshima, *Chem. Commun.* **2012**, *48*, 4818–4820.
- [3] R. W. Wagner, J. S. Lindsey, *Pure Appl. Chem.* **1996**, *68*, 1373–1380.
- [4] T. V. Goud, A. Tutar, J.-F. Biellmann, *Tetrahedron* **2006**, *62*, 5084–5091.
- [5] a) H. Prokopcová, C. O. Kappe, *Angew. Chem.* **2008**, *120*, 3732–3734; *Angew. Chem. Int. Ed.* **2008**, *47*, 3674–3676; b) H. Prokopcová, C. O. Kappe, *Angew. Chem.* **2009**, *121*, 2312–2322; *Angew. Chem. Int. Ed.* **2009**, *48*, 2276–2286.
- [6] a) E. Peña-Cabrera, A. Aguilar-Aguilar, M. González-Domínguez, E. Lager, R. Zamudio-Vázquez, J. Godoy-Vargas, F. Villanueva, *Org. Lett.* **2007**, *9*, 3985–3988; b) I. J. Arroyo, R. Hu, G. Merino, B. Z. Tang, E. Peña-Cabrera, *J. Org. Chem.* **2009**, *74*, 5719–5722; c) E. Lager, J. Liu, A. Aguilar-Aguilar, B. Z. Tang, E. Peña-Cabrera, *J. Org. Chem.* **2009**, *74*, 2053–2058; d) I. J. Arroyo, R. Hu, B. Z. Tang, F. I. López, E. Peña-Cabrera, *Tetrahedron* **2011**, *67*, 7244–7250; e) J. Bañuelos, I. J. Arroyo-Córdoba, I. Valois-Escamilla, A. Alvarez-Hernández, E. Peña-Cabrera, R. Hu, B. Z. Tang, I. Esnal, V. Martínez, I. López Arbeloa, *RSC Adv.* **2011**, *1*, 677–684.
- [7] a) C. F. A. Gómez-Durán, I. García-Moreno, A. Costela, V. Martín, R. Sastre, J. Bañuelos, F. López Arbeloa, I. López Arbeloa, E. Peña-Cabrera, *Chem. Commun.* **2010**, *46*, 5103–5105; b) J. Bañuelos, V. Martín, C. F. A. Gómez-Durán, I. J. Arroyo-Córdoba, E. Peña-Cabrera, I. García-Moreno, A. Costela, M. E. Pérez-Ojeda, T. Arbeloa, I. López Arbeloa, *Chem. Eur. J.* **2011**, *17*, 7261–7270; c) C. A. Osorio-Martínez, A. Urías-Benavides, C. F. A. Gómez-Durán, J. Bañuelos, I. Esnal, I. López Arbeloa, E. Peña-Cabrera, *J. Org. Chem.* **2012**, *77*, 5434–5438; d) R. I. Roacho, A. Metta-Magaña, M. M. Portillo, E. Peña-Cabrera, K. H. Pannell, *J. Org. Chem.* **2013**, *78*, 4245–4250.
- [8] J. M. Murphy, C. C. Tzschucke, J. F. Hartwig, *Org. Lett.* **2007**, *9*, 757–760.
- [9] a) *Laser Dyes*, 3rd ed. (Ed.: U. Brackmann), Lambda Physik AG, Göttingen, **2000**; b) *Molecular Fluorescence: Principles and Applications* (Ed.: B. Valeur), Wiley-VCH, Weinheim, **2002**; c) A. N. Fletcher, M. E. Pietrak, *Appl. Phys. B* **1985**, *37*, 151–157; d) S. Nad, M. Kumbhakar, H. Pal, *J. Phys. Chem. A* **2003**, *107*, 4808–4816; e) J. N. Moorthy, P. Natarajan, P. Venkatakrishnan, D.-F. Huang, T. J. Chow, *Org. Lett.* **2007**, *9*, 5215–5218; f) Q.-X. Tong, S.-L. Lai, M.-Y. Chan, Y.-C. Zhou, H.-L. Kwong, C.-S. Lee, S.-T. Lee, *Chem. Mater.* **2008**, *20*, 6310–6312; g) A. Lida, S. Yamaguchi, *Chem. Commun.* **2009**, 3002–3004; h) R. M. Adhikari, D. C. Neckers, B. K. Shah, *J. Org. Chem.* **2009**, *74*, 3341–3349.
- [10] A. C. Benniston, S. Clift, J. Hagon, H. Lemmetyinen, N. V. Tkachenko, W. Clegg, R. W. Harrington, *ChemPhysChem* **2012**, *13*, 3672–3681.
- [11] a) L. Xu, K. Burgess, *J. Org. Chem.* **2008**, *73*, 8711–8718; b) A. Saha, A. Samanta, *J. Phys. Chem. A* **2002**, *106*, 4763–4771; c) B. Bhattacharya, A. Samanta, *Chem. Phys. Lett.* **2007**, *442*, 316–321; d) K. A. Zachariasse, M. Grobys, T. von der Haar, A. Hebecker, Y. V. Illichev, O. Morawski, I. Rückert, W. Kühnle, *J. Photochem. Photobiol. A* **1997**, *105*, 373–383.
- [12] a) J. W. Verhoeven, *Pure Appl. Chem.* **1990**, *62*, 1585–1596; b) J. W. Verhoeven, T. Scherer, R. J. Willemsse, *Pure Appl. Chem.* **1993**, *65*, 1717–1722.
- [13] a) A. C. Benniston, A. Harriman, V. L. Whittle, M. Zelzer, R. W. Harrington, W. Clegg, *Photochem. Photobiol. Sci.* **2010**, *9*, 1009–1017; b) A. C. Benniston, G. Copley, H. Lemmetyinen, N. V. Tkachenko, *ChemPhysChem* **2010**, *11*, 1685–1692; c) S. Mula, K. Elliot, A. Harriman, R. Ziessel, *J. Phys. Chem. A* **2010**, *114*, 10515–10522.
- [14] M. Kollmannsberger, K. Rurack, U. Resch-Genger, J. Daub, *J. Phys. Chem. A* **1998**, *102*, 10211–10220.
- [15] J. C. de Mello, H. F. Wittmann, R. H. Friend, *Adv. Mater.* **1997**, *9*, 230–232.

Received: June 7, 2013

Published online: August 16, 2013

8-Alkoxy- and 8-Aryloxy-BODIPYs: Straightforward Fluorescent Tagging of Alcohols and Phenols

Juan O. Flores-Rizo,[†] Ixone Esnal,[‡] Carlos A. Osorio-Martínez,[†] César F. A. Gómez-Durán,[†] Jorge Bañuelos,[‡] Iñigo López Arbeloa,^{*,‡} Keith H. Pannell,[§] Alejandro J. Metta-Magaña,[§] and Eduardo Peña-Cabrera^{*,†}

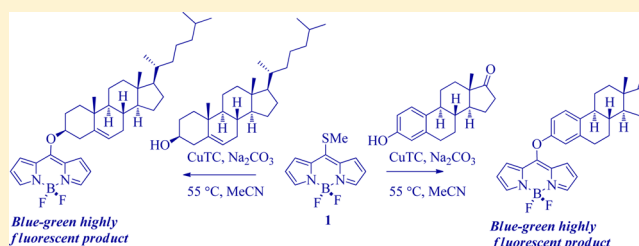
[†]Departamento de Química, Universidad de Guanajuato, Col. Noria Alta S/N, Guanajuato, Gto. 36050, Mexico

[‡]Departamento de Química Física, Universidad del País Vasco/EHU, Aptdo 644, 48080, Bilbao, Spain

[§]Department of Chemistry, The University of Texas at El Paso, 500 West University Avenue, El Paso, Texas 79968, United States

S Supporting Information

ABSTRACT: We demonstrate herein that both alcohols and phenols can be tagged with a BODIPY (borondipyrromethene) moiety to yield highly fluorescent products. Thus, 8-(methylthio)-BODIPY (**1**) undergoes an S_NAr -type reaction with a host of alcohols and phenols in the presence of a base and a Cu(I) additive. The BODIPY dyes bearing alkoxy or nonfunctionalized phenoxy moieties are characterized by a highly efficient fluorescence emission, regardless of the media, in the blue-green part of the visible region. Complementary to this, the presence of electron-donor groups at the aryl ring leads to an intramolecular charge-transfer process, which quenches the fluorescence mainly in polar media. In addition to simple alcohols and phenols, four natural products (eugenol, menthol, cholesterol, and estrone) were labeled in a simple fashion. X-ray structures of the cholesterol and estrone derivatives are discussed. In fact, the BODIPY bearing cholesterol stands out as a bright fluorescence biological marker.



INTRODUCTION

Applications seemingly unrelated such as the design of drug nanocarriers used in theranostics (area of research that combines diagnostic detection agents with therapeutic drug delivery carriers)¹ and recently reported conjugated materials used in solution-processed solar cells² have one thing in common: they both contain one or several BODIPY (borondipyrromethene) units. Among their most useful properties are strong absorbance in the visible wavelengths, narrow absorption bands, and tunable photophysics that can allow one to vary both the quantum yield (ϕ_F) and emission wavelength (λ_{em}).⁴ These types of dye have found ample use in biology⁵ and materials science,⁶ due to the fact that they can be grafted onto the substrate of interest, thereby making it fluorescent or fluorescent-prone.

After a seminal report by Biellmann et al. in 2006, which described the synthesis and optical properties of 8-(methylthio)-BODIPY (**1**),⁷ our research groups have demonstrated that such a compound can efficiently participate in a variety of useful chemical transformations.



For example, **1** participates in the Liebeskind–Srogl cross-coupling reaction⁸ with boronic acids to yield the correspond-

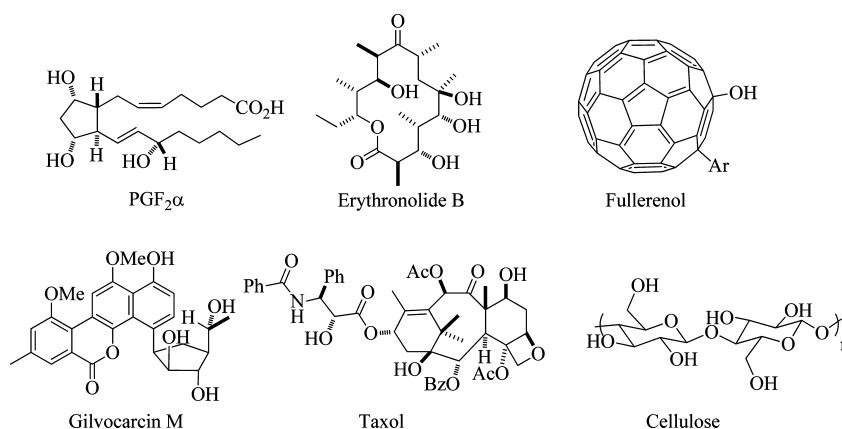
ing 8-substituted BODIPY derivatives.⁹ Also, the methylthio group can be replaced by a proton to produce the parent unsubstituted BODIPY system in almost quantitative yield.¹⁰ We have shown as well that the methylthio group could be substituted by primary and secondary amines to give highly fluorescent blue-emitting analogues, a property hitherto unknown for BODIPY dyes.¹¹ In this way, blue-emitting BODIPYs were developed with improving fluorescence and lasing performance with regard to commercially available laser dyes in that region. The reason for such unexpected behavior was that the BODIPY delocalized π system, characterized as a cyclic cyanine, changes to a hemicyanine-like system with the presence of the amino group. However, the fluorescence efficiency of the derivatives bearing secondary and tertiary amines was limited in polar media by the activation of a quenching intramolecular charge-transfer (ICT) process.

Although BODIPY dyes have been conjugated to many biologically relevant molecules,¹² a great synthetic effort has to be devoted to the modification of the BODIPY core in order to add a functional group that would allow the attachment to the target molecule under mild conditions. Alternatively, one can purchase the commercially available dyes³ already functionalized for the desired purposes, albeit at sky-high prices.

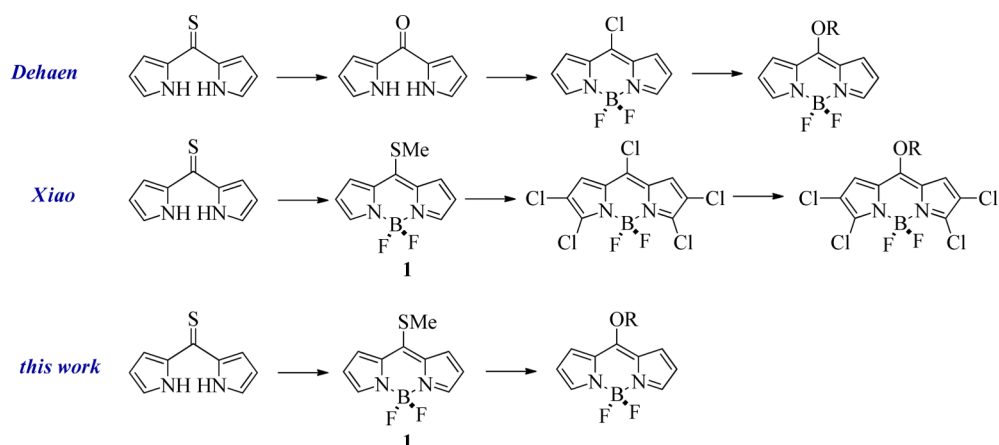
Received: March 2, 2013

Published: May 30, 2013

Chart 1. Hydroxylated Complex Products



Scheme 1. Different Ways To Prepare Alkoxy-BODIPYs



On the other hand, intriguing research possibilities have arisen that give the opportunity to tag hydroxylated complex molecules (i.e., the molecules in Chart 1) with a fluorescent moiety under mild reaction conditions.

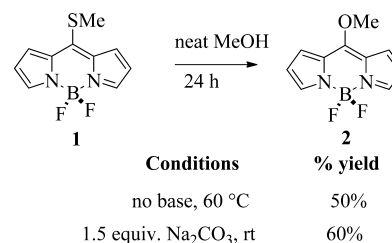
The mode of action of important drugs may be elucidated using highly sensitive fluorescent techniques. The fabrication of fluorescent new materials, with potentially very useful properties, may become a reality. In this context, we wish to disclose our efforts to *directly* attach alcohols and phenols to the BODIPY core via de displacement of the methylthio group to yield highly fluorescent dyes. Recently, both Dehaen and Xiao have reported the properties of a few examples of similar compounds by means of somewhat longer routes (Scheme 1).¹³

Herein, we have carried out a more comprehensive study of this family of compounds. In addition to demonstrating the synthetic utility of this methodology, we have introduced alkoxy and aryloxy groups in the *meso* BODIPY position with the aim to modulate the extension of the blue shift, looking for tailor-made BODIPYs in an almost unexploited region with this fluorophore. In contrast to the fluorescence behavior of the amino-BODIPYs in polar solvents, 8-alkoxy-BODIPYs developed herein excel by their bright green fluorescence, regardless of the media.

RESULTS AND DISCUSSION

Synthesis. Prompted by our reports of the mild S_NAr-like displacement of the methylthio group in **1** with amines,¹¹ we

set out to investigate similar displacement reactions with alcohols and phenols. In the initial trials, the desired product was obtained in 50% yield simply by stirring **1** in neat MeOH at 60 °C for 24 h. A slight yield increase (60%) was observed after 24 h at room temperature if 1.5 equiv of Na₂CO₃ was added (Scheme 2).

Scheme 2. Initial Reactions of **1** with Neat MeOH

Realizing that these results were useful only for simple alcohols, we decided to investigate a more general and efficient way to carry out the same transformation using stoichiometric amounts of the reactants. The transformation of a thiol ester into an ester has been reported in the literature.¹⁴ This process is mediated by soft metal cations: Hg(II), Cu(I), Cu(II), and Ag(I). Coordination of the metal cation with the sulfur atom in the thiol ester weakens the S–C bond, thereby facilitating the attack of the incoming alcohol. We hypothesized that a similar

reactivity might be displayed by **1**, drawing an analogy with thiol esters (Figure 1).

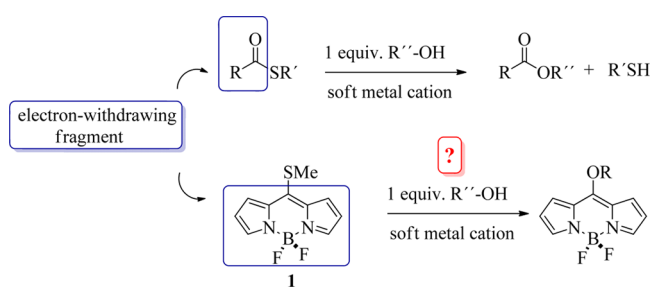
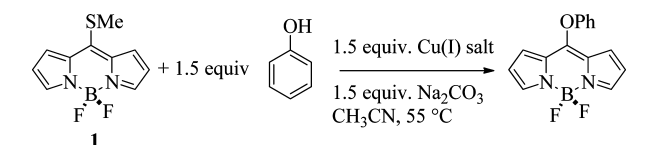


Figure 1. Analogy of the electronic properties of a thiol ester and those of **1**.

Since Cu(I) salts were considered to have the right combination of both low toxicity and cost, in comparison to other soft metal cations such as Hg(II), a survey of the reactivities of different Cu(I) salts was undertaken (Table 1).

Table 1. Survey of Cu(I) Salts on the Formation of 8-Alkoxy-BODIPY Dyes



entry	Cu(I) salt	conversion after 1 h (%) ^a
1	none	0
2	CuCl	34
3	CuCN	9
4	CuI	36
5	Cu(I)-3-methylsalicylate	67
6	CuI-SMe ₂	31
7	Cu(I)OP(O)Ph ₂	47
8	Cu(I)OTf	21
9	CuTC ^b	100 ^c

^aDetermined by ¹H NMR. ^bCopper(I) thiophene-2-carboxylate. ^c90% isolated yield.

Although the majority of the Cu(I) salts showed some degree of activity, it was clear that copper(I) thiophene-2-carboxylate (CuTC) was the most effective Cu(I) source, since the desired product was obtained in 90% isolated yield with a complete conversion in under 1 h. Although no mechanistic study was undertaken, it might be argued that the driving force for the CuTC-mediated reaction is the formation of a strong S–CuTC bond (45–55 kcal/mol), thereby labilizing further the C–S bond.¹⁵ The presence of a Cu(I) salt was essential, as demonstrated by the control experiment shown in entry 1. After the best reaction conditions were identified (CuTC, Na₂CO₃, CH₃CN), the generality of the process was investigated with a series of both alcohols and phenols (Table 2). In method 1, simple alcohols were used both as solvents and reactants, while in method 2, the alcohol or phenol was used in slight excess in CH₃CN.

Using method 1, simple alcohols added to **1** after only a few hours (entries 1–3) to yield the corresponding 8-alkoxy dyes in acceptable yields. However, for reasons at this point unclear to us, *i*-PrOH failed to give the desired product, for only decomposition was observed (entry 4). Using method 2,

aliphatic alcohols displaced the methylthio group of **1** in moderate yields (entries 5, 6, 8, and 13). This reaction appears to be sensitive to steric effects; primary alcohols added within 3–6 h, while menthol and cholesterol added only after 24 and 36 h, respectively. Triphenylcarbinol failed to give the product altogether (entry 15).

Phenols with different substitution patterns were added to **1** (entries 7, 9–12, and 14). Phenol was the most reactive nucleophile, since it efficiently added to **1** in 90% yield in less than 1 h (entry 7). Addition of either electron-withdrawing or electron-donating substituents resulted in longer reaction times and moderate yields, with no discernible apparent pattern, at least in the sample of examples examined. As in the aliphatic alcohol series, steric crowding had a deleterious effect; pyrogallol also failed to add (entry 15).

The functional group tolerance of particularly method 2 is worth mentioning. As is hinted by the examples presented herein, the potential of this method for numerous applications becomes clear. For instance, complex natural hydroxylated products (entries 8, 9, 12, and 13) can be rendered fluorescent in one step via a very simple reaction. Similarly, some of the products prepared in this work contain functional groups that can be used as connecting points with other target molecules or that can be interconverted to other species for a specific application: for example, the bromine atom in **6**, the allyl group in **9**, the formyl group in **10**, the *p*-iodo atom in **11**, the carbonyl group in **12**, and the *p*-OH group in **14**.

Optical Properties. With the results previously reported by us¹¹ for the 8-amino-BODIPY dyes as background, the properties of the new alkoxy and phenoxy derivatives are better understood. Figure 2 shows that both the absorption and fluorescence spectra of the methoxy derivative **2** are blue-shifted with regard to the parent BODIPY chromophore, but to a lesser extent than for the corresponding methylamino counterpart. Thus, while the amino substitution placed the absorption and emission bands at 418 and 463 nm, respectively, the alkoxy group placed them at 452 and 487 nm, enlarging the Stokes shift in relation to the parent BODIPY (Figure 2). Theoretical calculations confirm this tendency. In general, the inclusion of electron-donor substituents at the central position, characterized by a high enhancement of the electronic density upon excitation, increased the LUMO energy, whereas the HOMO remained almost unaltered (Figure 3). Such an increase of the energy gap depends on the electron-releasing ability of the substituent. Thus, the methoxy group (Hammett parameter $\sigma_p = -0.268$) has a lower electron-donor character in comparison with the methylamino group ($\sigma_p = -0.84$) and, consequently, the increase of the energy gap is lower with the former substituent. Reported electrochemical measurements for a similar 8-methoxy-BODIPY pointed out that the dye was more difficult to reduce, while the oxidation half-wave potential remained almost unaltered, confirming the increase cited above of the LUMO energy as the reason for the spectral blue shift.^{13b}

The hypsochromic shift induced by the presence of heteroatoms at the *meso* position is due to an important rearrangement of the electronic delocalization of the chromophore. The formation of a hemicyanine-like delocalized π system due to the electron coupling of the amine and the BODIPY core (Figure 4) explains the shift induced by the amino group.¹¹ According to this argument, a methoxy group should also be able to interact by resonance with the chromophore and, hence, enable the formation of a merocyanine-like delocalization. The optimized ground-state

Table 2. Scope and Limitations of the Reaction of Alcohols and Phenols with 1

Entry	R-OH/Method	Compound	Reaction time (h)	% Yield ^a	Entry	R-OH/Method	Compound	Reaction time (h)	% Yield ^a
1	MeOH Method 1		1	73	10			12	41
2	EtOH Method 1		3	62	11			5	57
3	Pr-OH Method 1		4	70	12			5	76
4	tPr-OH Method 1	-	-	-	13			36	60
5	Bu-OH Method 2		3	67	14			2.5	56
6	Br-CH ₂ -CH ₂ -OH Method 2		6	66	15		-	-	-
7	PhOH Method 2		0.9	90	16		-	-	-
8			24	53					
9			12	52					

^aIsolated yields.

geometry places the oxygen coplanar with the chromophore, making possible the required electron coupling favoring the new resonant structure. The formation of these hemi- and merocyanine delocalized π systems from the cyanine system, upon grafting an amino or methoxy group, should imply an important charge rearrangement, since both pyrroles are no longer equivalent. Accordingly, the shape of the spectral bands is altered (mainly in absorption, where these resonant structures prevail) and they become broader and have lower vibrational resolution (Figure 2). This feature is more evident

with the amino group, since the induced change in the chromophoric charge density by its higher electron-releasing ability is stronger (Figure 4).

The fluorescence quantum yield of the BODIPY 2 is very high (around 0.8), regardless of the surrounding environment. At this point, it is important to note that the primary amino derivatives were highly fluorescent; however, secondary and tertiary amines caused a decrease of the fluorescence capacity in polar solvents because of activation of a quenching ICT state. Taking into account that the formation of such a state depends

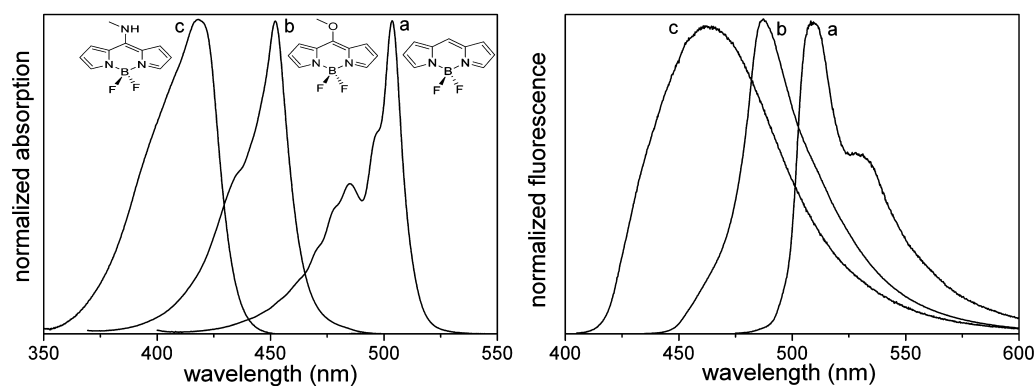


Figure 2. Normalized absorption and fluorescence spectra of BODIPY (a) and its methoxy (b) and methylamino (c) derivatives at central *meso* positions in cyclohexane.

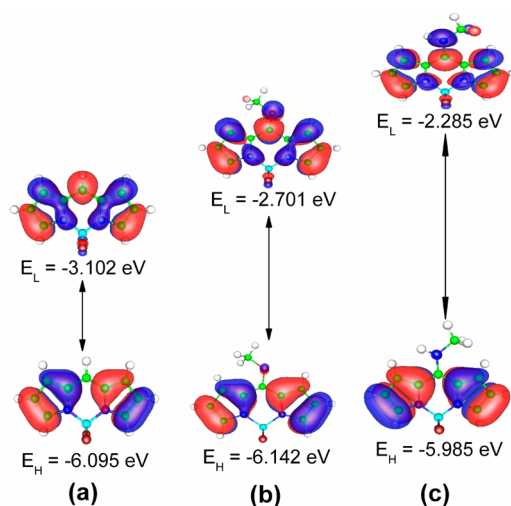


Figure 3. HOMO and LUMO eigenvalues for the parent BODIPY (a) and its derivatives bearing methoxy (b) and methylamino groups (c) at the central position.

directly on the electron-releasing ability of the donor unit, the population of the ICT state should be hampered by the

replacement of the methylamino group by the methoxy fragment. In fact, the high fluorescence efficiencies of dye 2 in all the considered solvents (Table 3) indicates that the ICT state is not taking place. This is a very important advantage, since 8-methoxy-BODIPY overcomes the limited fluorescence emission of 8-amino-BODIPYs in polar solvents.

Neither the length of the alkyl chain (from methyl to butyl) nor the size of the substituent (cf. 8 and 13) had a significant impact on photophysical properties, except for the fluorescent quantum yield that ranges from 0.80 to 0.95 (Table 3 and Figure 1S in the Supporting Information). Even the heavy bromine atom in 6 had no influence because of its location far from the BODIPY core. It should be pointed out that for the menthol derivative 8, with a more constrained structure due to steric hindrance, the fluorescence decay curve is better described as a growth and a decay. Such a growth component should be associated with the steric hindrance, which slows down the structural rearrangement upon excitation. Nonetheless, slight differences are observed in the fluorescence abilities among the aliphatic derivatives. Thus, from methoxy to propoxy the fluorescence quantum yield improves from 0.84 to 0.96 and 0.93, which could be due to the increase of the electron-donor character of the alkoxy group with the number

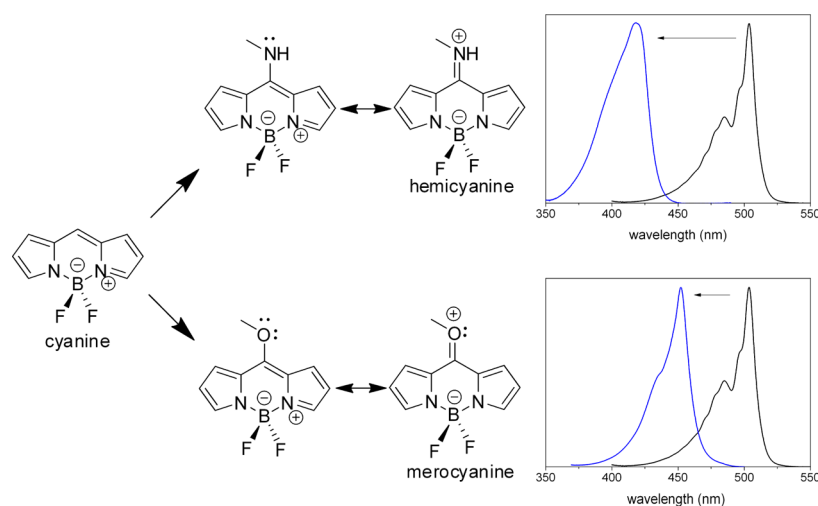


Figure 4. Hemicyanine and merocyanine resonance structures from a cyanine delocalized π system upon the incorporation of heteroatoms (nitrogen and oxygen, respectively), at the central position of the BODIPY. The corresponding spectral hypsochromic shift of each new resonant structure is also plotted.

Table 3. Photophysical Properties of the Parent Unsubstituted BODIPY and Its Derivatives Bearing Alkoxy Groups in a Common Apolar Solvent (Cyclohexane)^a

	λ_{ab} (nm)	ϵ_{max} (10^4 M ⁻¹ cm ⁻¹)	λ_{fl} (nm)	ϕ	τ (ns)	k_{fl} (10^8 s ⁻¹)	k_{nr} (10^8 s ⁻¹)
BODIPY	503.5	7.6	510.5	0.96	6.47	1.48	0.06
2 (cyclohexane)	452.0	6.0	487.0	0.84	5.41	1.55	0.29
2 (methanol)	441.0	4.6	485.5	0.75	6.14	1.22	0.41
8-MAB (cyclohexane)	418.5	2.4	463.0	0.70	4.67	1.50	0.64
8-MAB (methanol)	394.5	3.0	440.0	0.10	0.52	1.91	17.2
3	451.0	6.2	486.5	0.96	5.44	1.76	0.07
4	450.5	6.4	486.0	0.93	5.43	1.71	0.13
5	450.0	6.0	486.0	0.80	5.43	1.47	0.37
13	451.5	5.3	485.0	0.91	5.58	1.63	0.16
8	450.5	6.2	486.0	0.88	5.63	1.56	0.21
6	455.5	4.5	491.0	0.91	5.57	1.63	0.16

^aThe corresponding photophysical properties of 8-methylamino-BODIPY (8-MAB) have been included.^{11b} The data in a polar solvent (methanol) for methoxy and methylamino derivatives are also collected. The complete photophysical data in several solvents are included in Table 1S in the Supporting Information.

of methylene units. Accordingly, the merocyanine form is better stabilized and the fluorescence quantum yield is slightly ameliorated. However, a longer aliphatic chain (i.e., butoxy) leads to a more flexible structure, which favors the vibrational decay pathways, as is reflected in the increase in the nonradiative rate constant for compound **5** (Table 3). Therefore, all these derivatives are characterized by very high fluorescence quantum yields (>0.80) in all the solvents studied and should be ideal for the vast applications that make use of BODIPYs, i.e., as active media of tunable dye lasers, with the additional advantage of their large Stokes shift (>2000 cm⁻¹).

Of special interest is the cholesterol derivative **13**. In this case, the BODIPY core was successfully functionalized with a biomolecule, and the fluorescence properties of the chromophore remained unaltered. In brief, a fluorescence marker to monitor biological events has been developed with emission in the blue-green part of the electromagnetic spectrum. This region is not generally used in studies in most of the molecular probes based on BODIPYs (generally from yellow to red).

In addition to alcohols, several phenol derivatives have been prepared. First of all, the phenyl ring did not seem to participate in the delocalized π system of the indacene core, since the spectral band positions were similar to those of the alkoxy-BODIPYs (Figure 5); otherwise, a red-shifted emission

should have been observed corresponding to an extended delocalization. The optimized geometry revealed that the phenyl ring was twisted with respect to the oxo-BODIPY plane, hampering the electronic coupling (Figure 5). Instead, the lone pair of electrons on oxygen seems to still interact mainly with the BODIPY core, leading to the merocyanine (Figure 4), maintaining the previously discussed blue-shifted spectral bands. However, such hypsochromic shifts are slightly lower than the shifts in related aliphatic derivatives, as theoretically corroborated by the energy of the frontier orbitals (Figure 2S in the Supporting Information). This tendency is extrapolated to all phenoxy derivatives, especially those bearing electron-withdrawing substituents, such as dyes **10** and **11**, which should remove more electronic density from the oxygen (Figure 5). Therefore, the aromatic substituent could slightly remove the electronic density from the oxygen and consequently decrease the extension of the spectral blue shift.

Table 4 gives the photophysical properties of the aryloxy derivatives of BODIPY. It is worth noting that derivatives bearing hydroxyl, methoxy, or iodine at the phenyl ring were

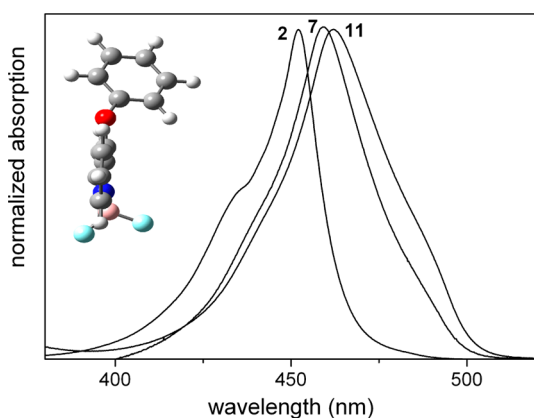


Figure 5. Normalized absorption spectra of BODIPY derivatives bearing methoxy (compound **2**), phenoxy (**7**), and *p*-iodophenoxy groups (**11**) in a common solvent (cyclohexane). The optimized ground-state geometry of **7** is also shown.

Table 4. Photophysical Properties of BODIPYs Bearing Different Aryloxy Substituents at the Meso Position in Apolar (Cyclohexane) and Polar/Protic (Trifluoroethanol) Solvents^a

	λ_{ab} (nm)	ϵ_{max} (10^4 M ⁻¹ cm ⁻¹)	λ_{fl} (nm)	ϕ	τ (ns)	k_{fl} (10^8 s ⁻¹)	k_{nr} (10^8 s ⁻¹)
Cyclohexane							
7	459.0	3.5	495.0	0.97	5.78	1.68	0.05
10	466.0	3.8	498.5	0.99	6.03	1.64	0.02
12	458.0	3.4	495.0	0.89	5.84	1.52	0.19
11	462.0	4.7	497.0	0.81	5.66	1.43	0.33
14	458.0	4.2	495.5	0.76	5.25	1.45	0.46
9	457.0	4.9	494.0	0.91	5.60	1.62	0.16
Trifluoroethanol							
7	449.0	2.9	491.5	0.54	4.71	1.04	1.08
10	456.0	0.7	494.5	0.81	7.68	1.05	0.25
12	448.0	2.9	488.5	0.005			
11	452.5	4.0	492.0	0.05	0.33	1.51	28.8
14	448.5	3.6	491.0	0.002			
9	448.5	3.8	484.0	0.001			

^aThe complete photophysical data in several solvents are included in Table 2S in the Supporting Information.

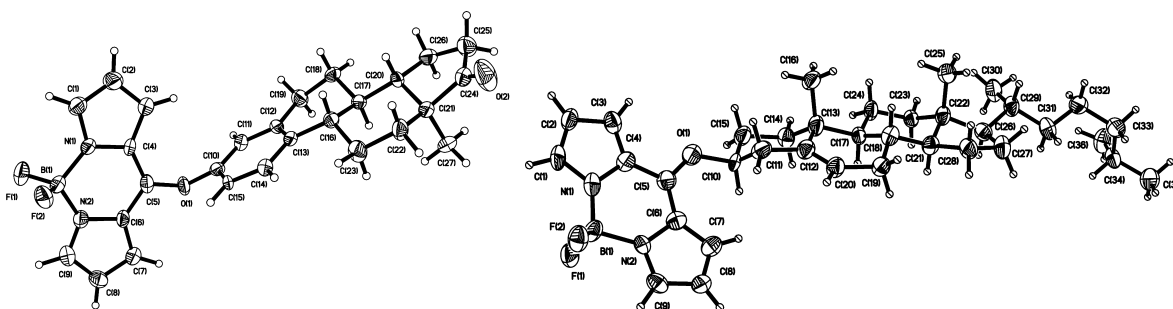


Figure 6. Conformations adopted in the crystal form for compounds **12** (left) and **13** (right). The ellipsoids are drawn at the 50% probability level.

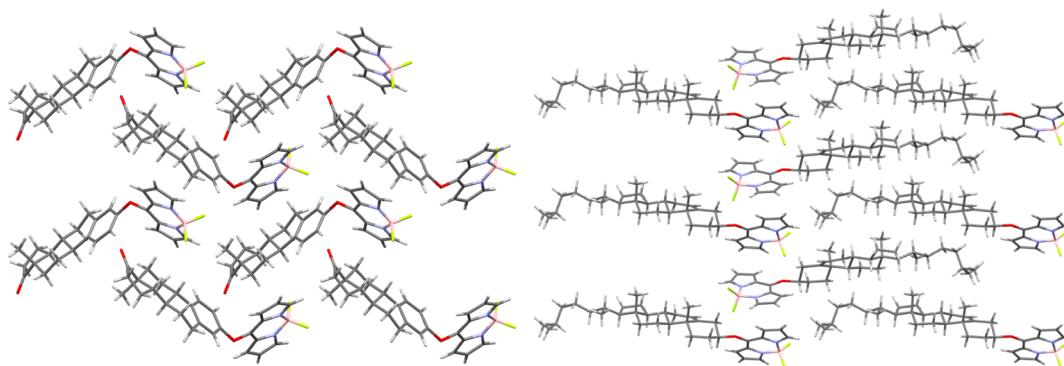


Figure 7. Crystal packing of **12** (left) and **13** (right) showing the difference between them due to the size of cholesterol in comparison to estrone.

not stable in nucleophilic solvents (such as alcohols and amides). Their photophysical properties change as the solution ages. Probably, these types of solvents act as reactants displacing the initial alkoxy or phenoxy fragments, which may behave as good leaving groups. No effort was made to pursue this observation. For this reason, these solvents were excluded from the photophysical characterization. The phenyl ring in **7** did not affect the fluorescence properties, and very high efficiencies were achieved (up to 0.97, Table 4) in all solvents. However, functionalization of the aryl group completely changes the situation. Substitution on the phenyl ring (i.e., **11**, **14**, **9**, and **12**) had a drastic effect on the fluorescence properties of the BODIPY, particularly when the substituent was characterized by its electron-releasing ability. Thus, although high fluorescence quantum yields were recorded in apolar media (approaching 1 in most cases), the emission efficiency strongly decreased in polar solvents (Table 4). The exception to this behavior was the formyl-substituted derivative **10**, with an electron-withdrawing group ($\sigma_p = 0.22$) at the *para* position of the aryl, where high fluorescence efficiencies were achieved in all considered media, in a way similar to that for the parent unsubstituted phenyl derivative **7**.

The presence of the electron-donor groups methoxy (**9**, $\sigma_p = -0.268$) and hydroxyl (**14**, $\sigma_p = -0.37$) in *ortho* and *para* positions of the phenyl ring, respectively, induced a strong quenching of the fluorescence emission even in low-polarity solvents (e.g., ethyl acetate, Table 2S in the Supporting Information). This is attributed to the formation of an ICT state that leads to a negligible emission in polar media (Table 4). Considering the evolution of the fluorescence efficiency with the solvent polarity for compound **11** (bearing a *p*-iodo group), an ICT should also take place in this derivative. The effect of the heavy atom should be very low because of its distant location from the chromophore. However, the iodine behaved like an electron acceptor ($\sigma_p = 0.35$) and the ICT

should occur from the BODIPY to the aryl fragment. Furthermore, the quenching effect of the ICT induced by the halogen (compound **11**) is less effective than that described above for compounds **9** and **14**, since higher fluorescence quantum yields are achieved for the former derivative in polar media (Table 4).

Dye **12** is structurally very similar to **13**. Both are functionalized with biomolecules (estrone and cholesterol, respectively), but their photophysical properties are quite different. The presence of cholesterol (cyclohexane attached to oxygen) leads to high fluorescence efficiencies regardless of the media (Table 3); on the other hand, the presence of estrone (phenyl linked to the oxygen) decreases the fluorescence ability of the derivative, especially in polar solvents (Table 4), in accord with the presence of a quenching ICT state. The phenyl ring can behave as an electron donor or acceptor depending on its substitution pattern, as we have stated before (i.e., donor in the presence of hydroxyl or acceptor with the attachment of iodine). In **12** the phenyl ring is fused to an aliphatic ring, increasing its electron-donor ability, which seems to be high enough to activate the ICT state.

To summarize, BODIPY derivatives bearing aliphatic alkoxy or phenoxy groups are characterized by high fluorescence efficiency in all media. Complementing this, the attachment of sufficiently strong electron-donating or -withdrawing groups (methoxy, hydroxyl, etc.) at the aryl ring leads to a fluorescence emission sensitive to the environment, making feasible their use as polarity sensors.

X-ray Structures of 12 and 13. Cholesterol is a very important organic structure, but previous crystal reports show that it is quite difficult structure to solve.¹⁶ Due to this feature, the number of crystal reports is scarce, and in order to modify some properties, functionalization at the OH has been carried out. This modification has an impact on the crystal structure, allowing a more efficient packing, therefore upgrading the

symmetry from P1 for the nonfunctionalized cholesterol to P2₁ and even P2₁2₁.¹⁷ For BODIPY 13, the space group is P2₁. Due to the fused polycyclic nature of the cholesterol, no changes in the conformation are observed with the functionalization; however, the alkyl chain attached to it has more freedom, which allows it to acquire a better orientation to maximize the packing.

As observed in other BODIPY systems,⁷ the O–C_{BODIPY} distance is shorter than the O–C_{chol} distance due to the merocyanine character of this oxygen (Figure 4). The distances in the BODIPY moiety are not statistically differentiable due to the equivalent resonance structures in the conjugate system. There is a small dihedral angle of 5.7° between the pyrrole rings, but the BODIPY moiety could be considered as planar. Cholesterol is tilted from this plane by about 39° (Figure 6).

The crystal packing is bilayer type, expected because of the amphiphilic character of this derivative (Figure 7). The short contact distances H...H in the cholesterol moiety range from 2.16 to 2.37 Å, showing that these contacts, albeit being unfavorable (considering the London forces), are present due to the stabilization energy introduced by the BODIPY fragment. The BODIPY moieties are arranged in a parallel fashion (Figure 7), although it is not a π – π interaction because the interplanar distance is 3.34 Å, but the offset is ~3.0 Å. The most important interactions are those formed by one of the fluorine atoms, which behaves as a bidentate HB acceptor (C3–H3...F1 = 2.53 Å and C11–H11B...F1 = 2.65 Å)¹⁸ generating a 2-D layer (the BODIPY layer or polar domain).

The conformation of the estrone moiety remains unchanged in BODIPY 12 (Figure 6). It can be compared to the reported structure of the unfunctionalized estrone by Busetta et al.¹⁹ However, the functionalization in this case, in contrast to that of cholesterol, reduces the symmetry of the crystal, bringing it from P2₁2₁2₁ to P2₁, because of the elimination of the hydroxyl group and further removal of the intramolecular HB between it and the carbonyl group.

The other difference with respect to derivative 13 is the size; estrone is smaller and thus the hydrophobic character is not as strong as in 13; therefore, the packing is different. In this derivative the bilayer arrangement is not the favored one, but a zigzag chain arrangement (Figure 7). However, as in 13, the strongest interactions are formed by the F atoms; in this case both F atoms participate in the HB to generate the 3-D structure (C7–H7...F1 = 2.36 Å, C22–H22...F2 = 2.52 Å, and C2–H2...F2 = 2.60 Å).²⁰ In addition, the tilt of the BODIPY moiety against the estrone mean plane is 79.6°.

CONCLUSIONS

We have successfully prepared a family of 8-alkoxy- and 8-aryloxy-BODIPY dyes in a straightforward manner in moderate to good yields. The substituents at the meso position carry functional groups that will allow further elaboration for specific applications. Four biomolecules (eugenol, menthol, cholesterol, and estrone) were easily attached to the BODIPY core, which demonstrates the usefulness of this method to label biologically relevant molecules.

The inclusion of heteroatoms at the central position of the BODIPY is an adequate strategy to achieve BODIPY-based blue-green emitting fluorophores. Furthermore, the proper selection of the heteroatom, in terms of its electronegativity, allows the modulation of the extension of the blue shift. Accordingly, the amino group induces a more pronounced spectral shift to higher energies than the alkoxy group.

However, the fluorescence performance of the mono- and disubstituted 8-amino-BODIPYs was limited in polar media. Herein, we show that 8-alkoxy-BODIPYs overcome such problems and display high fluorescence efficiencies irrespective of the media. The lower electron donor character of the alkoxy group, with regard to the amino group, prevents the formation of quenching intramolecular charge transfer states, which limits the fluorescence performance of the latter dyes in polar media. Of course, the inclusion of electron-donor or -acceptor substituents at the oxygen fragment can also lead to the formation of the ICT state, with the consequent reduction in fluorescence efficiency.

In summation, BODIPY dyes bearing heteroatoms (N and O) allow for a wide coverage of the visible electromagnetic region (from yellow to blue). Taking into account the reported BODIPYs with red-shifted emission, it is in fact possible to span the whole visible spectrum, by just choosing the adequate modification of the chromophoric core.

EXPERIMENTAL SECTION

Photophysical Properties. The photophysical properties were registered in dilute solutions (around 2×10^{-6} M), prepared by adding the corresponding solvent to the residue from the adequate amount of a concentrated stock solution in acetone, after vacuum evaporation of this solvent. The fluorescence spectra were corrected from the wavelength dependence of the detector sensibility. The fluorescence quantum yield (ϕ) was obtained using a 0.1 M NaOH aqueous solution of fluorescein ($\phi_r = 0.79$) as reference and corrected by the different refractive indexes of the solvents used for the sample and the reference. Radiative decay curves were registered with the time-correlated single-photon counting technique using a microchannel plate detector, with picosecond time resolution (~20 ps). Fluorescence emission was monitored at the maximum emission wavelength after excitation at 440 nm by means of a diode laser with 150 ps fwhm pulses. The fluorescence lifetime (τ) was obtained from the slope after the deconvolution of the instrumental response signal from the recorded decay curves by means of an iterative method. The goodness of the exponential fit was controlled by statistical parameters (χ^2 , Durbin–Watson, the analysis of the residuals). The radiative (k_r) and nonradiative deactivation (k_{nr}) rate constants were calculated by means of $k_r = \phi/\tau$ and $k_{nr} = (1 - \phi)/\tau$, respectively.

Theoretical Calculations. The ground-state geometry was optimized by the hybrid DFT method B3LYP, using a double-valence basis set (6-31G), as implemented in Gaussian 09. The geometry was considered as a minimum of energy after the analysis of the frequencies did not yield any negative value.

X-ray Diffraction Measurements. Each crystal was mounted on a glass fiber using Paratone, and its crystal data were acquired at room temperature and processed with the suite APEX 2.²¹ The structure solution was obtained through direct methods. Absorption corrections were applied. The hydrogens were placed by geometry and restrained to ride on the heavy atoms.

Synthesis and Characterization. ¹H and ¹³C NMR spectra were recorded on a 200 MHz spectrometer in deuteriochloroform (CDCl₃), with tetramethylsilane (TMS; 0.00 ppm ¹H, 0.00 ppm ¹³C), chloroform (7.26 ppm ¹H, 77.00 ppm ¹³C), acetonitrile-*d*₃ (1.94 ppm ¹H, 118.3, 1.3 ppm ¹³C), or acetone-*d*₆ (2.05 ppm ¹H, 206.0, 29.8 ppm ¹³C) as internal reference. Data are reported in the following order: chemical shift in ppm, multiplicity (br (broadened), s (singlet), d (doublet), t (triplet), q (quartet), sex (sextet), hep (heptet), m (multiplet), exch (exchangeable), app (apparent)), coupling constant *J* (Hz), and integration. Infrared spectra were recorded on a FTIR spectrophotometer; peaks are reported (cm⁻¹) with the following relative intensities: s (strong, 67–100%), m (medium, 40–67%), and w (weak, 20–40%). Melting points are not corrected. Mass spectrometry data were collected on a TOF analyzer.

Typical Method 1 (TM1). A Schlenk tube equipped with a stir bar under N₂ was charged with BODIPY 1 (0.10 g, 0.42 mmol, 1 equiv). The corresponding alcohol (5 mL) was added, and the mixture was stirred until the solids dissolved. The mixture was purged with N₂ for 5 min, whereupon CuTC (0.119 g, 0.63 mmol, 1.5 equiv) and Na₂CO₃ (0.07 g, 0.63 mmol, 1.5 equiv.) were added. The Schlenk tube was immersed in a preheated oil bath at 55 °C and the stirring continued until the consumption of the starting material. The solvent was removed in vacuo, and the crude material was adsorbed in SiO₂ gel. The product was purified by column chromatography using a hexane/EtOAc gradient. For purposes of characterization, the products were crystallized from CH₂Cl₂/hexanes.

Typical Method 2 (TM2). A Schlenk tube equipped with a stir bar under N₂ was charged with BODIPY 1 (0.10 g, 0.42 mmol, 1 equiv) and CH₃CN (6 mL). The mixture was purged with N₂ for 5 min, whereupon CuTC (0.119 g, 0.63 mmol, 1.5 equiv) and the corresponding alcohol or phenol was added (0.63 mmol, 1.5 equiv). The reaction mixture was stirred for 5 min, upon which Na₂CO₃ (0.07 g, 0.63 mmol, 1.5 equiv) was added. The Schlenk tube was immersed in a preheated oil bath at 55 °C and the stirring continued until the consumption of the starting material. The solvent was removed in vacuo, and the crude material was adsorbed in SiO₂ gel. The product was purified by column chromatography using a hexane/EtOAc gradient. For purposes of characterization, the products were crystallized from CH₂Cl₂/hexanes.

BODIPY 2: following TM1; product (68.5 mg, 73%) obtained as a yellow solid; *R*_f = 0.3 (30% EtOAc/hexanes); mp 137–139 °C; IR (KBr; cm⁻¹) 3127 (w), 3116 (w), 2925 (w), 1739 (w), 1559 (s), 1533 (s), 1465 (s), 1395 (s), 1366 (s), 1335 (m), 1291 (s), 1263 (s), 1231 (s), 1186 (m), 1131 (s), 1085 (s), 1002 (m), 971 (s), 938 (m), 866 (w), 779 (m), 730 (m), 647 (m), 551 (w), 443 (w); ¹H NMR (CDCl₃, 300 MHz) δ 7.74 (s, 2H), 7.37 (d, *J* = 6.0 Hz, 2H), 6.54 (s, 2H), 4.49 (s, 3H); ¹³C NMR (CDCl₃, 75 MHz) δ 162.00, 139.58, 126.22, 125.52, 116.69, 62.15.^{13a}

BODIPY 3: following TM1; product (62.0 mg, 62%) obtained as a yellow solid; *R*_f = 0.5 (30% EtOAc/hexanes); mp 118–119 °C; IR (KBr; cm⁻¹) 2925 (w), 1736 (w), 1558 (s), 1529 (m), 1474 (w), 1445 (s), 1402 (s), 1351 (m), 1331 (m), 1292 (s), 1262 (s), 1232 (m), 1151 (m), 1132 (s), 1100 (s), 1073 (s), 1008 (m), 960 (s), 787 (w), 861 (w), 763 (m), 728 (m), 643 (w), 582 (w), 435 (w); ¹H NMR (CDCl₃, 300 MHz) δ 7.66 (s, 2H), 7.27 (d, *J* = 3.6 Hz, 2H), 6.45 (d, *J* = 1.8 Hz, 2H), 4.68 (q, *J* = 7.2 Hz, 2H), 1.54 (t, *J* = 6.9 Hz, 3H); ¹³C NMR (CDCl₃, 75 MHz) δ 161.62, 139.371, 126.54, 125.54, 116.54, 71.51, 15.51; HRMS FABS (M + H⁺) calcd for C₁₁H₁₂BF₂N₂O 237.1011, found 237.1015.

BODIPY 4: following TM1; product (73.5 mg, 70%) obtained as a yellow solid; *R*_f = 0.4 (30% EtOAc/hexanes); mp 99–100 °C; IR (KBr; cm⁻¹) 3123 (w), 2972 (w), 2885 (w), 1730 (w), 1554 (s), 1471 (m), 1441 (s), 1399 (s), 1365 (m), 1333 (w), 1290 (m), 1264 (s), 1225 (s), 1151 (m), 1130 (s), 1096 (s), 1079 (s), 1040 (m), 995 (w), 970 (s), 862 (w), 769 (s), 728 (s), 644 (m), 583 (w), 453 (w); ¹H NMR (CDCl₃, 300 MHz) δ 7.73 (s, 2H), 7.34 (d, *J* = 3.6 Hz, 2H), 6.51 (d, *J* = 3.6 Hz, 2H), 4.66 (t, *J* = 6.0 Hz, 2H), 1.98 (m, 2H), 1.13 (t, *J* = 7.2 Hz, 2H); ¹³C NMR (CDCl₃, 75 MHz) δ 161.893, 139.45, 125.47, 116.53, 77.78, 23.395, 10.662; HRMS FABS (M + H⁺) calcd for C₁₂H₁₄BF₂N₂O 251.1167, found 251.1171.

BODIPY 5: following TM2; product (74.3 mg, 67%) obtained as yellow crystals; *R*_f = 0.6 (30% EtOAc/hexanes); mp 79–80 °C; IR (KBr, cm⁻¹) 3125 (w), 2963 (w), 1565 (s), 1474 (w), 1438 (m), 1405 (s), 1368 (w), 1350 (w), 1262 (s), 1226 (m), 1127 (m), 1094 (s), 1076 (m), 1043 (m), 992 (w), 968 (m), 768 (m), 730 (m); ¹H NMR (300 MHz, CDCl₃) δ 7.71 (s, 2H), 7.32 (s, 2H), 6.50 (s, 2H), 4.68 (m, *J* = 5.7 Hz, 2H), 1.93 (m, *J* = 6.6 Hz, 2H), 1.56 (m, *J* = 7.2 Hz, 2H), 1.03 (m, *J* = 6.6 Hz, 2H); ¹³C NMR (75 MHz, CDCl₃) δ 161.8, 139.3, 126.5, 125.5, 116.5, 75.4, 31.8, 19.3, 13.9; HRMS FABS (M + H⁺) calcd for C₁₃H₁₆BF₂N₂O 265.1324, found 265.1320.

BODIPY 6: following TM2; product (87.5 mg, 66%) obtained as a bright yellow solid; *R*_f = 0.4 (30% EtOAc/hexanes); mp 120.5–122.0 °C; IR (KBr; cm⁻¹) 2975 (w), 2940 (w), 2634 (w) 1709 (s), 1649 (s), 1545 (s), 1460 (m), 1422 (s), 1402 (m), 1365 (m), 1311 (w),

1276 (m), 1090 (s), 1012 (m), 982 (m), 967 (w), 946 (m), 778 (m), 759 (m), 646 (w), 660 (m), 586 (w); ¹H NMR (CDCl₃, 200 MHz) δ 7.77 (s, 1H), 7.35 (d, *J* = 4.0 Hz, 2H), 6.55 (s, 2H), 4.99 (t, *J* = 6 Hz, 2H), 3.77 (t, *J* = 6 Hz, 2H); ¹³C NMR (CDCl₃, 75 MHz) δ 160.30, 140.23, 126.38, 125.88, 74.01, 2810; HRMS FABS (M + H⁺) calcd for C₁₁H₁₁BBrF₂N₂O 315.0116, found 315.0119.

BODIPY 7: following TM2; product (107.5 mg, 90%) obtained as a bright yellow solid; *R*_f = 0.67 (30% EtOAc/hexanes); mp 129.8–131.4 °C; IR (KBr; cm⁻¹) 3122 (w), 1740 (w), 1573 (s), 1526 (m), 1486 (m), 1398 (s), 1364 (s), 1332 (w), 1283 (s), 1251 (s), 1225 (s), 1187 (w), 1118 (s), 1073 (s), 1040 (s), 960 (s), 868 (w), 786 (m), 768 (s), 721 (m), 694 (m), 638 (m), 568 (w), 478 (w); ¹H NMR (CDCl₃, 300 MHz) δ 7.74 (s, 2H), 7.52–7.47 (t, 2H, *J* = 7.32 Hz), 7.41–7.36 (t, 1H, *J* = 7.32 Hz), 7.24 (s, 2H), 6.67 (s, 2H), 6.39 (s, 2H); ¹³C NMR (CDCl₃, 75 MHz) δ 156.04, 141.08, 130.85, 130.85, 127.33, 126.457, 120.44, 117.08.^{13a}

BODIPY 8: following TM2; product (76.7 mg, 53%) obtained as a light olive green solid; *R*_f = 0.4 (30% EtOAc/hexanes); mp 149.4–250.4 °C; IR (KBr; cm⁻¹) 2944 (m), 2871 (m), 1550 (s), 1469 (m), 1428 (s), 1407 (s), 1322 (m), 1290 (m), 1256 (s), 1223 (s), 1186 (w), 1147 (w), 1126 (s), 1094 (s), 1076 (s), 1052 (m), 963 (s), 847 (w), 781 (m), 766 (m), 734 (m), 676 (w), 64 (m), 585 (w), 525 (w); ¹H NMR (CDCl₃, 300 MHz) δ 7.71 (s, 2H), 7.28 (s, 2H), 6.52 (s, 2H), 4.97 (m, 1H), 2.37 (d, *J* = 12.3 Hz, 1H), 2.09–0.745 (m, 17H); ¹³C NMR (CDCl₃, 75 MHz) δ 161.42, 139.03, 126.61, 124.88, 116.528, 85.56, 48.86, 40.01, 34.27, 31.77, 27.01, 24.08, 22.22, 20.78, 17.01; HRMS FABS (M + H⁺) calcd for C₁₉H₂₆BF₂N₂O 347.2106, found 347.2104.

BODIPY 9: following TM2; product (77.3 mg, 52%) obtained as a yellow solid; *R*_f = 0.7 (30% EtOAc/hexanes); mp 273–274 °C; IR (KBr, cm⁻¹) 3130 (w), 1637 (s), 1612 (m), 1569 (s), 1540 (s), 1513 (m), 1461 (m), 1413 (s), 1395 (s), 1380 (s), 1267 (m), 1235 (w), 1117 (m), 1032 (m), 944 (w), 792 (m); ¹H NMR (300 MHz, CDCl₃) δ 7.71 (s, 2H), 7.15 (d, *J* = 9 Hz, 1H), 6.88 (d, *J* = 3 Hz, 2H), 6.70 (d, *J* = 3 Hz, 2H), 6.37 (d, *J* = 3 Hz, 2H), 6.05–5.96 (m, 1H), 5.17–5.11 (m, *J* = 9 Hz, 2H), 3.72 (s, 3H), 3.46 (d, *J* = 6 Hz, 2H); ¹³C NMR (75 MHz, CDCl₃) δ 160.8, 150.6, 142.6, 141.0, 140.3, 136.8, 126.7, 125.5, 121.7, 121.5, 116.9, 116.7, 114.1, 56.3, 40.3; HRMS FABS (M + H⁺) calcd for C₁₉H₁₈BF₂N₂O₂ 355.1429, found 355.1423.

BODIPY 10: following TM2; product (53.6 mg, 41%) obtained as a bright yellow solid; *R*_f = 0.4 (30% EtOAc/hexanes); mp 195 °C dec; IR (KBr; cm⁻¹) 3114 (w), 2857 (w), 1695 (m), 1597 (m), 1565 (s), 1495 (m), 1473 (m), 1407 (s), 1395 (s), 1365 (m), 1332 (w), 1287 (m), 1255 (s), 1226 (s), 1202 (m), 1158 (w), 1124 (s), 1088 (s), 1065 (s), 1044 (m), 954 (s), 874 (w), 849 (w), 775 (m), 766 (m), 724 (w), 638 (w), 607 (w), 577 (w), 504 (w); ¹H NMR (CDCl₃, 300 MHz) δ 10.04 (s, 1H), 8.01 (d, *J* = 8.4 Hz), 7.80 (s, 2H), 7.41 (d, *J* = 8.7 Hz), 6.82 (s, 2H), 6.46 (s, 2H); ¹³C NMR (CDCl₃, 75 MHz) δ 189.16, 159.96, 141.35, 133.22, 131.06, 126.46, 125.45, 118.99, 116.57; HRMS FABS (M + H⁺) calcd for C₁₆H₁₂BF₂N₂O₂ 313.0960, found 313.0963.

BODIPY 11: following TM2; product (98.1 mg, 57%) obtained as yellow crystals; *R*_f = 0.6 (30% EtOAc/hexanes); mp 122–124 °C; IR (KBr, cm⁻¹) 3130 (w), 3109 (w), 2865 (w), 2353 (m), 2342 (m), 1569 (s), 1541 (s), 1414 (s), 1400 (s), 1263 (s), 1155 (m), 1120 (s), 1082 (s), 1053 (m), 1000 (w), 977 (m); ¹H NMR (200 MHz, CDCl₃) δ 7.79 (d, *J* = 9 Hz, 2H), 7.02 (d, *J* = 9 Hz, 2H), 6.75 (d, *J* = 3.6 Hz, 2H), 6.43 (s, 2H); ¹³C NMR (75 MHz, CDCl₃) δ 156.2, 141.7, 138.8, 128.1, 126.6, 122.3, 117.5, 114.3, 90.8; HRMS FABS (M + H⁺) calcd for C₁₅H₁₁BF₂IN₂O 410.9977, found 410.9975.

BODIPY 12: following TM2; product (147.0 mg, 76%) obtained as yellow crystals; *R*_f = 0.36 (30% EtOAc/hexanes); mp 202–204 °C; IR (KBr, cm⁻¹) 3120 (w), 3066 (w), 2943 (m), 2865 (w), 1718 (s), 1619 (w), 1582 (w), 1567 (s), 1538 (s), 1462 (m), 1409 (s), 1400 (s), 1380 (m), 1356 (w), 1287 (m), 1259 (s), 1165 (s), 1157 (w), 1115 (s), 970 (m); ¹H NMR (300 MHz, CDCl₃) δ 7.72 (s, 2H), 7.37 (d, *J* = 7.8 Hz, 1H), 7.00 (m, *J* = 7.8 Hz, 1H), 6.97 (s, 1H), 6.72 (s, 2H), 6.39 (s, 2H), 2.91 (s, 3H), 2.58–2.35 (m, 4H), 2.20–2.02 (m, 6H), 1.98–1.463 (m, 9H), 0.90 (s, 3H); ¹³C NMR (75 MHz, CDCl₃) δ 207.5, 159.9, 153.9, 140.8, 139.7, 139.0, 132.0, 127.6, 126.3, 120.0, 116.9, 115.6, 113.2, 50.8, 48.3, 44.4, 38.2, 36.2, 36.1, 31.8, 29.7, 26.5, 21.9, 14.2;

HRMS FABS ($M + H^+$) calcd for $C_{27}H_{28}BF_2N_2O_2$ 461.2212, found 461.2215.

BODIPY 13: following TM2; product (145.2 mg, 60%) obtained as yellow crystals; $R_f = 0.7$ (30% EtOAc/hexanes); mp 171–173 °C; IR (KBr, cm^{-1}) 2938 (w), 2893 (w), 2865 (w), 1738 (w), 1668 (w), 1565 (s), 1471 (w), 1431 (s), 1400 (s), 1371 (w), 1341 (w), 1290 (m), 1263 (s), 1225 (m), 1151 (w), 1126 (m), 1095 (s), 1075 (s), 1053 (w), 1000 (w), 972 (m), 766 (m), 728 (m); 1H NMR (300 MHz, $CDCl_3$) δ 7.62 (s, 2H), 7.19 (s, 2H), 6.42 (s, 2H), 5.4 (s, 1H), 2.57 (d, $J = 6$ Hz, 2H), 2.134–0.765 (m), 0.62 (s, 3H); ^{13}C NMR (75 MHz, $CDCl_3$) δ 160.9, 139.3, 138.8, 133.4, 132.3, 127.9, 126.9, 125.2, 124.4, 123.1, 116.6, 85.0, 75.3, 57.0, 56.5, 50.4, 42.6, 39.9, 38.9, 37.2, 36.5, 36.1, 32.2, 30.0, 28.2, 24.6, 24.2, 23.1, 21.4, 19.7, 19.0, 12.2; HRMS FABS ($M + H^+$) calcd for $C_{36}H_{35}BF_2N_2O$ 577.4141, found 577.4139.

BODIPY 14: following TM2; product (70.5 mg, 56%) obtained as yellow crystals; $R_f = 0.4$ (30% EtOAc/hexanes); mp 198–200 °C; IR (KBr, cm^{-1}) 3506 (w), 3129 (w), 1601 (w), 1568 (s), 1503 (s), 1399 (s), 1366 (m), 1289 (m), 1256 (s), 1230 (s), 1216 (w), 1188 (m), 1113 (s), 1088 (s), 1013 (m), 946 (w), 930 (m), 842 (w), 762 (s); 1H NMR (200 MHz, $CDCl_3$) δ 7.7 (s, 2H), 7.12 (d, $J = 9$ Hz, 2H), 6.92 (d, $J = 9$ Hz, 2H), 6.70 (m, $J = 4$ Hz, 2H), 6.40 (d, $J = 4$ Hz, 2H); ^{13}C NMR (75 MHz, $CDCl_3$) δ 154.9, 149.2, 140.7, 128.1, 126.4, 121.6, 117.2, 117.01, 116.5; HRMS FABS ($M + H^+$) calcd for $C_{15}H_{12}BF_2N_2O_2$ 301.0960, found 301.0964.

■ ASSOCIATED CONTENT

■ Supporting Information

Figures, tables, and CIF files giving 1H and ^{13}C NMR spectra of all the compounds described, full photophysical data in several solvents, calculated energies of the frontier orbitals, tables of atom coordinates and absolute energies, and crystallographic data. This material is available free of charge via the Internet at <http://pubs.acs.org>.

■ AUTHOR INFORMATION

Corresponding Author

*E-mail: inigo.lopezarbeloa@ehu.es (I.L.A.); eduardop@ugto.mx (E.P.-C.).

Notes

The authors declare no competing financial interest.

■ ACKNOWLEDGMENTS

We thank CONACyT (Grant 129572) for financial support. J.O.F.-R., C.A.O.-M., and C.F.A.G.-D. thank CONACyT for graduate scholarships. The Gobierno Vasco is thanked for a Ph.D. contract (I.E., IT339-10) and for financial support (SPE11UN064 and SPE12UN140). The Robert A. Welch Foundation, Houston, TX (Grant No. 0546), is also acknowledged. We also thank Cuantico de Mexico for a donation of I.

■ REFERENCES

- (1) (a) Sharma, A.; Neibert, K.; Sharma, R.; Hourani, R.; Maysinger, D.; Kakkar, A. *Macromolecules* **2011**, *44*, 521. (b) Calderera-Moore, M. E.; Liechty, W. B.; Peppas, N. A. *Acc. Chem. Res.* **2011**, *44*, 1061.
- (2) Bura, T.; Leclerc, N.; Fall, S.; L ev eque, P.; Heiser, T.; Retailleau, P.; Rihn, S.; Mirloup, A.; Ziessel, R. *J. Am. Chem. Soc.* **2012**, *134*, 17404.
- (3) Haugland, R. P. *The Handbook. A Guide to Fluorescent Probes and Labeling Technology*, 10th ed.; Molecular Probes: Eugene, OR, 2005.
- (4) (a) Ziessel, R.; Ulrich, G.; Harriman, A. *New J. Chem.* **2007**, *31*, 496. (b) Ulrich, G.; Ziessel, R.; Harriman, A. *Angew. Chem., Int. Ed.* **2008**, *47*, 1184. (c) Benniston, A. C.; Copley, G. *Phys. Chem. Chem. Phys.* **2009**, *11*, 4124. (d) Loudet, A.; Burgess, K. *Chem. Rev.* **2007**, *107*, 4891. (e) Wood, T. E.; Thompson, A. *Chem. Rev.* **2007**, *107*, 1831.

- (5) (a) Han, J.; Loudet, A.; Barhoumi, B.; Burghardt, R. C.; Burgess, K. *J. Am. Chem. Soc.* **2009**, *131*, 1642. (b) Kamiya, M.; Johnsson, K. *Anal. Chem.* **2010**, *82*, 6472. (c) Li, Z.; Mintzer, E.; Bittman, R. *J. Org. Chem.* **2006**, *71*, 1718. (d) Ariola, F. S.; Li, Z.; Cornejo, C.; Bittman, R.; Heikal, A. A. *Biophys. J.* **2009**, *96*, 2696. (e) Li, Z.; Bittman, R. *J. Org. Chem.* **2007**, *72*, 8376. (f) Ehrenschrwender, T.; Wagenknecht, H.-A. *J. Org. Chem.* **2011**, *76*, 2301. (g) Kim, D.-R.; Ahn, H.-C.; Leec, W.-J.; Ahn, D.-R. *Chem. Commun.* **2011**, *47*, 791. (h) Hornillos, V.; Carrillo, E.; Rivas, L.; Amat-Guerri, F.; Acuña, A. U. *Bioorg. Med. Chem. Lett.* **2008**, *18*, 6336. (i) Ojida, A.; Sakamoto, T.; Inoue, M.-a.; Fujishima, S.-h.; Lippens, G.; Hamachi, I. *J. Am. Chem. Soc.* **2009**, *131*, 6543. (j) Krumova, K.; Oleynik, P.; Karam, P.; Cosa, G. *J. Org. Chem.* **2009**, *74*, 3641. (k) Kowada, T.; Kikuta, J.; Kubo, A.; Ishii, M.; Maeda, H.; Mizukami, S.; Kikuchi, K. *J. Am. Chem. Soc.* **2011**, *133*, 17772. (l) Gonalves, M. S. T. *Chem. Rev.* **2009**, *109*, 190.

- (6) (a) Camerel, F.; Ulrich, G.; Barber a, J.; Ziessel, R. *Chem. Eur. J.* **2007**, *13*, 2189. (b) Warnan, J.; Buchet, F.; Pellegrin, Y.; Blart, E.; Odobel, F. *Org. Lett.* **2011**, *13*, 3944. (c) Ziessel, R.; Harriman, A. *Chem. Commun.* **2011**, *47*, 611. (d) Gust, D.; Moore, T. A.; Moore, A. L. *Acc. Chem. Res.* **2009**, *42*, 1890. (e) Rousseau, T.; Cravino, A.; Bura, T.; Ulrich, G.; Ziessel, R.; Roncali, J. *Chem. Commun.* **2009**, 1673. (f) Zrig, S.; R emy, P.; Andrioletti, B.; Rose, E.; Asselberghs, I.; Clays, K. *J. Org. Chem.* **2008**, *73*, 1563. (g) Alamiry, M. A. H.; Benniston, A. C.; Copley, G.; Elliott, K. H.; Harriman, A.; Stewart, B.; Zhi, Y.-G. *Chem. Mater.* **2008**, *20*, 4024. (h) Bozdemir, A.; B uy kca kir, O.; Akkaya, E. U. *Chem. Eur. J.* **2009**, *15*, 3843. (i) Warnan, J.; Pellegrin, Y.; Blart, E.; Odobel, F. *Chem. Commun.* **2012**, *48*, 675. (j) Xiao, Y.; Zhang, D.; Qian, X.; Costela, A.; Garcia-Moreno, I.; Martin, V.; Perez-Ojeda, M. E.; Ba uelos, J.; Gartzia, L.; L opez Arbeloa, I. *Chem. Commun.* **2011**, *47*, 11513.

- (7) Goud, T. V.; Tutar, A.; Biellmann, J.-F. *Tetrahedron* **2006**, *62*, 5084.

- (8) (a) Prokopcov a, H.; Kappe, C. O. *Angew. Chem., Int. Ed.* **2008**, *47*, 3674. (b) Prokopcov a, H.; Kappe, C. O. *Angew. Chem., Int. Ed.* **2009**, *48*, 2276.

- (9) (a) Pe a-Cabrera, E.; Aguilar-Aguilar, A.; Gonzalez-Dominguez, M.; Lager, E.; Zamudio-Vazquez, R.; Godoy-Vargas, J.; Villanueva-Garcia, F. *Org. Lett.* **2007**, *9*, 3985. (b) Arroyo, I. J.; Hu, R.; Tang, B. Z.; L opez, F. I.; Pe a-Cabrera, E. *Tetrahedron* **2011**, *67*, 7244.

- (10) Arroyo, I. J.; Hu, R.; Merino, G.; Tang, B. Z.; Pe a-Cabrera, E. *J. Org. Chem.* **2009**, *74*, 5719.

- (11) (a) G omez-Dur an, C. F. A.; Garc a-Moreno, I.; Costela, A.; Martin, V.; Sastre, R.; Ba uelos, J.; L opez Arbeloa, F.; L opez Arbeloa, I.; Pe a-Cabrera, E. *Chem. Commun.* **2010**, *46*, 5103. (b) Ba uelos, J.; V. Mart n, V.; G omez-Dur an, C. F. A.; Arroyo-Cordoba, I. J.; Pe a-Cabrera, E.; Garc a-Moreno, I.; Costela, A.; P erez-Ojeda, M. A.; Arbeloa, T.; L opez Arbeloa, I. *Chem. Eur. J.* **2011**, *17*, 7261. (c) Osorio-Mart nez, C. A.; Ur as-Benavides, A.; G omez-Dur an, C. F. A.; Ba uelos, J.; Esnal, I.; L opez Arbeloa, I.; Pe a-Cabrera, E. *J. Org. Chem.* **2012**, *77*, 5434.

- (12) (a) Kasurinen, J. *Biochem. Biophys. Res. Commun.* **1992**, *187*, 1594. (b) Ellena, J. F.; Le, M.; Ca iso, D. S.; Solis, R. M.; Langston, M.; Sankaram, M. B. *Drug Delivery* **1999**, *6*, 9. (c) Hendrickson, H. S.; Hendrickson, E. K.; Johnson, I. D.; Farber, S. A. *Anal. Biochem.* **1999**, *276*, 27. (d) Dahim, M.; Mizuno, N. K.; Li, X.-M.; Momsen, W. E.; Momsen, M. M.; Brockman, H. L. *Biophys. J.* **2002**, *83*, 1511. (e) Kaiser, R. D.; London, E. *Biochim. Biophys. Acta* **1998**, *1375*, 13.

- (13) (a) Leen, V.; Yuan, P.; Wang, L.; Boens, N.; Dehaen, W. *Org. Lett.* **2012**, *14*, 6150. (b) Wang, L.; Zhang, Y.; Xiao, Y. *RSC Adv.* **2013**, *3*, 2203.

- (14) (a) Masamune, S.; Hayase, Y.; Schilling, W.; Chan, W.-K.; Bates, G. S. *J. Am. Chem. Soc.* **1977**, *99*, 6756. (b) Masamune, S.; Kamata, S.; Schilling, W. *J. Am. Chem. Soc.* **1975**, *97*, 3515.

- (15) Musaeov, D. G.; Liebeskind, L. S. *Organometallics* **2009**, *28*, 4639.

- (16) (a) Shieh, H.-S.; Hoard, L. G.; Nordman, C. E. *Acta Crystallogr., Sect. B* **1981**, *37B*, 1538. (b) Hsu, L.-Y.; Kampf, J. W.; Nordman, C. E. *Acta Crystallogr., Sect. B* **2002**, *58*, 260.

- (17) In the following references the CCDC code is given first followed by the space group in brackets and then the corresponding

reference. [SEGPID, P1]: Polishchuk, A. P.; Yu, M.; Antipin, T. V.; Timofeeva, O. D.; Lavrentovich, A. S.; Kotel'chuk, L. A.; Taraborkin, L. A.; Struchkov, T. *Kristallografiya (Russ.) (Crystallogr. Rep.)* **1988**, *33*, 1134. [VAVBUR, P1]: Ikonen, S.; Jurcek, O.; Wimmer, Z.; Drasar, P.; Kolehmainen, E. *J. Mol. Struct.* **2012**, *1011*, 25. [DECHUO, P2₁]: Polishchuk, A. P.; Antipin, M.; Timofeeva, T. V.; Yu, T.; Struchkov, V.; Kulishov, I. *Khim. Fiz. (Russ.) (Sov. J. Chem. Phys.)* **1985**, *4*, 329. [FELBII, P2₁]: Powell, D. A.; Maki, T.; Fu, G. C. *J. Am. Chem. Soc.* **2005**, *127*, 510. [JABZER, P2₁]: Suh, I.-H.; Ko, T.-S.; Park, Y. J.; Yoon, Y. K.; Saenger, W. *Acta Crystallogr., Sect. C* **1988**, *C44*, 2163. [KOGPUR, P2₁]: Polishchuk, A. P.; Timofeeva, T. V.; Yu, M.; Antipin, G. R. G.; Kulishov, V. I.; Struchkov, T.; Payusova, I. K.; Tolmachev, A. V. *Zh. Strukt. Khim. (Russ.) (J. Struct. Chem.)* **1990**, *31*, 67–5. [SEGPOJ, P2₁]: Polishchuk, A. P.; Yu, M.; Timofeeva, T. V.; Lavrentovich, O. D.; Kotel'chuk, A. S.; Taraborkin, L. A.; Struchkov, Y. T. *Kristallografiya (Russ.) (Crystallogr. Rep.)* **1988**, *33*, 1134. [SUBHOM, P2₁2₁2₁]: Subrtova, V.; Petricek, V.; Maly, K. *Collect. Czech. Chem. Commun.* **1991**, *56*, 1983.

(18) The symmetry operators for F1 are $[-x, -1/2 + y, 2 - z]$ and $[1 - x, -1/2 + y, 2 - z]$, respectively.

(19) ESTRON10: Busetta, B.; Courseille, C.; Hospital, M. *Acta Crystallogr., Sect. B* **1973**, *29*, 298.

(20) Symmetry operators are $[-x, -1/2 + y, -z]$, $[1 - x, -1/2 + y, 1 - z]$, and $[1 + x, y, z]$, respectively.

(21) APEX2 v2010.7-0; Bruker AXS Inc., Madison, WI.

DOI: 10.1002/cphc.201300818

Blue-to-Orange Color-Tunable Laser Emission from Tailored Boron-Dipyrromethene Dyes

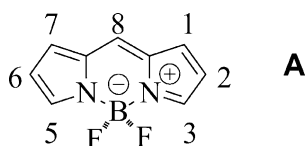
Ixone Esnal,^[a] Ismael Valois-Escamilla,^[b] César F. A. Gómez-Durán,^[b] Arlette Urías-Benavides,^[b] María L. Betancourt-Mendiola,^[b] Iñigo López-Arbeloa,^[a] Jorge Bañuelos,^{*[a]} Inmaculada García-Moreno,^[c] Angel Costela,^[c] and Eduardo Peña-Cabrera^{*[b]}

A series of *meso*-substituted boron-dipyrromethene (BODIPY) dyes are synthesized and their laser and photophysical properties systematically studied. Laser emission covering a wide visible spectral region (from blue to orange) is obtained by just changing the electron donor character of the heteroatom at position 8. The additional presence of methyl groups at positions 3 and 5 results in dyes with a photostability similar to

that of the unsubstituted dye but with much improved efficiency. Correlation of the lasing properties of the different dyes to their photophysical properties provides inklings to define synthetic strategies of new BODIPY dyes with enhanced efficiency and modulated wavelength emission over the visible spectral region.

1. Introduction

Boron-dipyrromethene (BODIPY)^[1] dyes have become the fluorophores of choice for many different applications. Their well-known properties include high quantum yields, high extinction coefficients, good solubility in common organic solvents^[2] and, if modified, in water.^[3] In addition to all of the above-mentioned properties, chemists have devoted a great effort in developing new methods to tailor the core structure **A** so that its properties could be tuned to the target application.



One of the properties most sought after is the emission response, that is, being able to induce either a bathochromic or hypsochromic shift as a result of a structural modification. Thus, different research groups have induced bathochromic

shifts, either by extending the conjugated system introducing aryl groups, double or triple bonds,^[4] or by building fused aromatic rings onto the BODIPY core system.^[5] However, we have recently observed that if one takes as a reference the parent unsubstituted BODIPY,^[6] it is possible to induce a profound shift, either bathochromic or hypsochromic, just by introducing a heteroatom at the 8-position.^[7] Moreover, as we disclose below, the photophysical and laser properties could be enhanced simply by introducing alkyl substitution at the 3- and 5-positions (Figure 1).^[8]

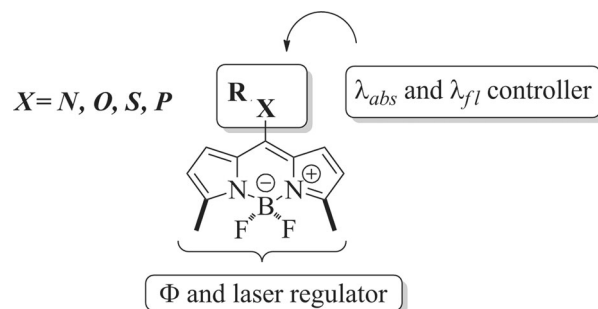


Figure 1. General structure of the BODIPY dyes studied in this work.

The general synthesis of these derivatives is possible starting from Biellmann's 8-methylthio-BODIPY derivatives **1–2**.^[9] We have demonstrated that these commercially available building blocks participate in both Liebeskind–Srogl cross-coupling^[10] and S_NAr -like processes (Scheme 1).^[7]

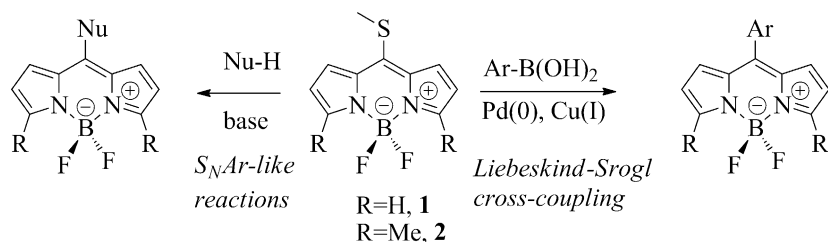
This implies that compounds as readily available as those depicted in Figure 1, could have two very useful handles to tailor their properties, that is, heteroatom substitution on the 8-position to modify both the absorption and emission properties, and alkyl substitution on both 3- and 5-positions to en-

[a] I. Esnal, Prof. I. López-Arbeloa, Dr. J. Bañuelos
Dpto. Química Física
Universidad del País Vasco (UPV/EHU)
Apto. 644, 48080 Bilbao (Spain)
E-mail: jorge.banuelos@ehu.es

[b] Dr. I. Valois-Escamilla, C. F. A. Gómez-Durán, A. Urías-Benavides,
M. L. Betancourt-Mendiola, Prof. E. Peña-Cabrera
Dpto. Química, Universidad de Guanajuato
Col. Noria Alta S/N, Guanajuato, GTO, 36050 (Mexico)
E-mail: eduardop@ugto.mx

[c] Prof. I. García-Moreno, Prof. A. Costela
Dpto. De Sistemas de Baja Dimensionalidad
Superficies y Materia Condensada
Instituto Química Física "Rocasolano"
Serrano 119, 28006, Madrid (Spain)

Supporting Information for this article is available on the WWW under
<http://dx.doi.org/10.1002/cphc.201300818>.



Scheme 1. Reactivity of 1 and 2.

hance the quantum yield (ϕ) and laser properties. The multi-step syntheses of BODIPYs with heteroatom substitution on other than the *meso*-position have been reported in the literature, and their optical properties described.^[11] We report herein, to the best of our knowledge, the first systematic study of the photophysical and laser properties of various *meso*-substituted BODIPY dyes with N, S, O, P, and H moieties as well as the influence of methyl substitution on the 3- and 5-positions on their laser properties.

2. Results and Discussion

The structures studied in this work are shown in Figure 2.

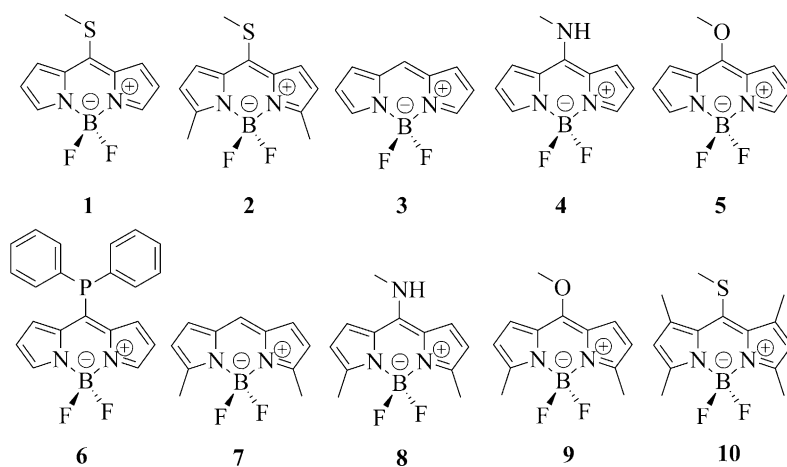


Figure 2. BODIPY dyes described herein; non-alkylated (1, 3–6) and with methyls at positions 3 and 5 (2, 7–10).

2.1. Synthesis

Compounds 1–5 and 10 were prepared according to literature procedures.^[6,7,9] Compounds 6–9 were prepared as shown in Equations (1)–(4).

Meso-diphenylphosphinoBODIPY 6 was prepared in 61% yield in a straightforward manner simply by adding an excess of PPh_2H to a tetrahydrofuran (THF) solution of 1 at room temperature (rt). This result demonstrates that in addition to N- and O-centered nucleophiles, phosphines also efficiently displace the MeS group from 1 under mild conditions. Utilizing the methodology developed in our group to prepare parent

BODIPY 3,^[6] its 3,5-dimethyl analogue 7 was obtained in 89% yield in less than one hour. Addition of a slight excess of aq. MeNH_2 to 2 in MeCN at rt yielded aminoBODIPY 8 in excellent yield. Finally, treating 2 with copper (I) 2-thiophenecarboxylate (CuTC) and Na_2CO_3 in neat MeOH at 55 °C produced highly colored BODIPY 9 in 78% yield

after 7 h.



2.2. Laser Properties

According to their absorption properties, which will be discussed below in detail, dyes 3, 4, 5, 7, 8, and 9 were pumped at 355 nm, whereas dyes 1, 2, and 6 required pumping at 532 nm. Under our experimental conditions of transversal excitation and strong focusing of the incoming pump radiation, dye concentrations in the millimolar range are required to ensure total absorption of the pump radiation within the first millimeter at most of the solution, to obtain an emitted beam with near-circular cross-section and optimize the lasing efficiency (ratio between the energy of the dye laser output and the pump energy incident on the sample surface). Except for compound 6, which did not lase, all the compounds studied in this work

emitted broad-band laser emission when placed in the simple plane-plane non-tunable resonator described in the Experimental Section. The bandwidth of the laser emission was in the range of 6–10 nm, much narrower than that due to fluorescence, and typical of a laser with many modes running simultaneously, due to the lack of wavelength-selection elements in the cavity.

To optimize the laser action, we first analyzed the dependence of the laser emission on the dye concentration in ethyl acetate solutions, and found the typical behavior where the lasing efficiency increases with dye concentration until a maxi-

mum value is reached. Increasing the dye concentration beyond this point results in a decrease of the lasing efficiency that can be related to reabsorption/reemission processes, which become increasingly important as the dye concentration rises. The optimum value of the dye concentration so determined was then used to prepare dye solutions in different solvents. The results obtained are collected in Table 1, where the

Table 1. Lasing properties ^[a] of the new BODIPY dyes in several solvents.							
Dye	C ^[b] [mM]	Data	F ₃ -EtOH	MeOH	EtOH	EtOAc	Acetone
Pump: 355 nm							
3	1	λ_L [nm]	535	537	538	537	538
		Eff [%]	50	42	48	55	31
		I_{40000} [%]				85	
7	4	λ_L [nm]	543	545	542	543	544
		Eff [%]	70	75	73	73	70
		I_{40000} [%]				68	
4	3	λ_L [nm]	461	457	457	459	457
		Eff [%]	7	4	6	8	5
		I_{18000} [%]				20	
8	8	λ_L [nm]	483	478	476	475	476
		Eff [%]	30	22	23	29	24
		I_{40000} [%]				46	
5	5	λ_L [nm]	490	492	493	492	490
		Eff [%]	24	26	28	30	28
		I_{40000} [%]				55	
9	10	λ_L [nm]	512	513	511	512	510
		Eff [%]	45	47	49	51	48
		I_{40000} [%]				70	
Pump: 532 nm							
1	2	λ_L [nm]	558	562	564	562	562
		Eff [%]	21	16	19	28	18
		I_{40000} [%]				20	
2	3	λ_L [nm]	570	573	574	572	573
		Eff [%]	60	72	74	78	84
		I_{40000} [%]				80	

[a] Eff: energy conversion efficiency; λ_L : peak wavelength of the laser emission; I_n : intensity of the dye laser output after n pulses with respect to its initial intensity I_0 , $I(\%) = (I/I_0) \times 100$. [b] C: dye concentration.

peak of the laser emission, the lasing efficiency, and the lasing stability are presented, as well as the corresponding optimal concentration of each dye. To facilitate the interpretation and comparison of the lasing results, we have graphically represented, in Figure 3, the laser emission of the different dyes in an ethyl acetate solution. In this figure, the height of the peaks is proportional to the lasing efficiency.

Depending on the heteroatom incorporated at position 8, the wavelength of the laser emission shifts to the blue or red with respect to the unsubstituted compound (dye 3). Thus, whereas the methylamino (4) and methoxy (5) groups lead to noticeable hypsochromic shifts, the methylthio moiety (1) does the contrary towards the red. Incorporation of methyl groups at positions 3 and 5 results in both an increase in the lasing efficiency and a red-shift of the emission of the compound with respect to that of the corresponding unsubstituted (at 3 and 5 positions) dye. In particular compound 4, which lases with low efficiency (8%), increases its laser efficiency up to 29% upon methylation at positions 3 and 5. Ethyl acetate showed to be

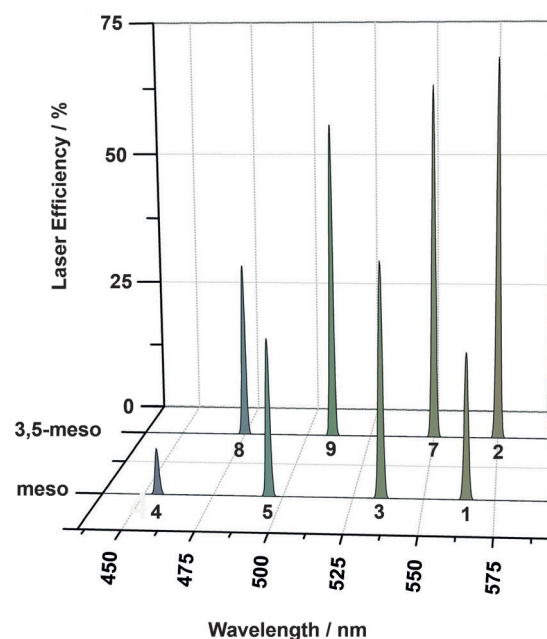


Figure 3. Efficiency of the laser emission of the different dyes *meso*-substituted and 3,5-*meso*-substituted in ethyl acetate solution. The numbers under the peaks identify the corresponding dye.

the best choice as a common solvent for all the new dyes, with dyes 7 and 2 exhibiting lasing efficiencies over 70% (Figure 3).

Table 1 also collects the value of the photostability of the different dyes under repeated pumping, which is a parameter of great importance for any practical applications of dye lasers. Dyes 4 and 1, which were the least efficient, are also the least photostable, with dye 4 in particular exhibiting a rather fast degradation. On the other hand, combination of the *meso* substitution with alkylation at strategic positions, such as 3 and 5, improves the photostability to values close to that of the unsubstituted dye 3.

Summing up, the BODIPYs designed herein are not only new laser dyes suitable to cover a wide visible spectral region (from blue to orange) by just changing the electron donor character of the 8-heteroatom (from N to S), but also stand out by their improved laser efficiency and photostability upon the simple additional presence of 3,5-methyl-groups. To understand the physics responsible for the laser behavior exhibited by these set of 8-heteroatom-substituted BODIPYs, their lasing properties were correlated to their photophysical properties. These correlations would provide useful inkings to define synthetic strategies of new BODIPY laser dyes with enhanced efficiency and modulated wavelength emission over the visible spectral region.

2.3. Photophysical Properties

The laser behavior of the new dyes correlates well with their photophysical properties in diluted solutions (see Tables S1–S3 in the Supporting Information, SI):

a) The position of the spectral bands markedly depends on the electronegativity of the heteroatom attached to the *meso* position of the BODIPY core (Figure 4). Thus, the grafting of methylamine and methoxy group (dyes 4 and 5) (Hammett parameter for chromophores bearing a delocalized positive

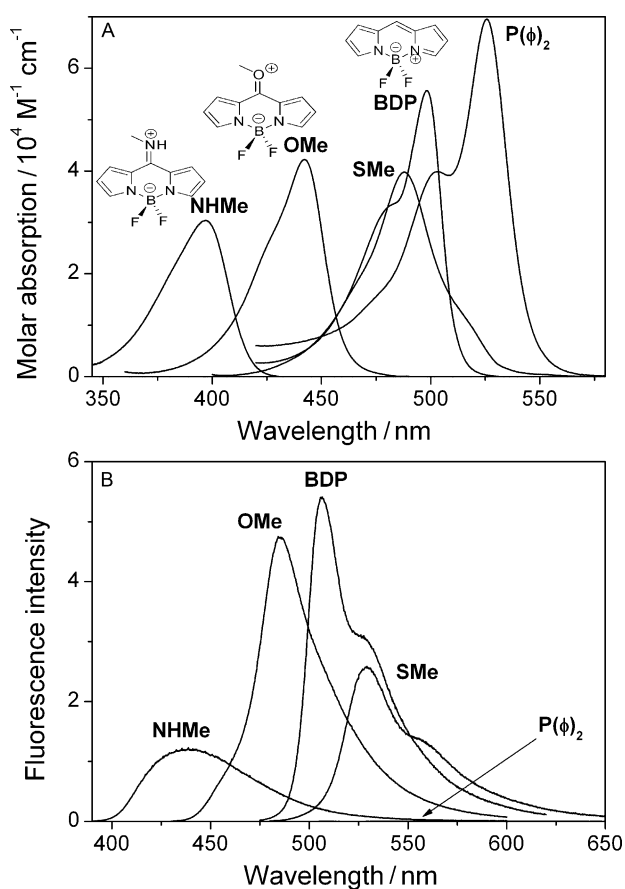


Figure 4. A) Absorption and B) fluorescence (area scaled by the fluorescence quantum yield) spectra of reference unsubstituted dye 3 and its 8-heteroatom derivatives in ethanol. For the sake of clarity, the functional groups attached to the *meso* position have been depicted (BDP is compound 3, NHMe 4, OMe 5, SMe 1 and $P(\phi)_2$ 6).

charge, $\sigma_p^+ = -1.81$ and -0.78 , respectively)^[12] led to a large hypsochromic shift of the spectral bands (i.e. 85 and 50 nm in absorption, respectively, with respect to the unsubstituted dye 3) because of the formation of a new delocalized π -system (Figure 5).^[7] Indeed, the simulated charge distribution (Figure S1) indicates that the heteroatoms induce an asymmetry in the electronic density between the pyrroles. The presence of such forms has been confirmed by conducting temperature-dependence NMR spectra.^[13]

Upon excitation of the 8-amine-BODIPY, the negative charge located at the nitrogen increases (from -0.42 to -0.68) and the N–C bond lengthens (from 1.356 to 1.379 Å). Therefore, the new resonance structures prevail in the ground state, explaining the highest hypsochromic shift in absorption, the broadening of such spectra and the large Stokes shift (up to 4000 cm^{-1}), as result of an important geometrical rearrange-

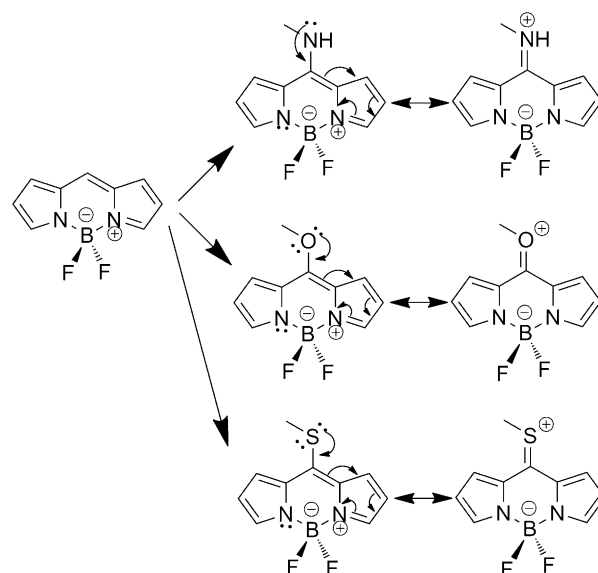


Figure 5. Resonance structures of the BODIPY core upon electronic coupling with methylamino, methoxy, and methylthio groups at position 8.

ment upon excitation (Figure 4). The replacement of such heteroatoms by a diphenylphosphino group gave rise to opposite spectral shifts (Figure 4), owing to its electron-withdrawing character ($\sigma_p^+ = 0.70$).

Electrochemical measurements (Figure S2) and quantum mechanical calculations agree with the above statements. The cyclic voltammogram of the reference BODIPY (dye 3) shows an irreversible oxidation wave (1.72 V) and a reduction wave (-0.71 V). The presence of 8-heteroatoms hardly alters the oxidation, but drastically affects the reduction potentials (Figure 6). Thus, an increase of the electron-releasing ability in the substituent group (i.e. from H to OMe and to NMe) leads to more negative reduction potentials (from -0.71 V to -0.81 and -1.36 V, respectively). Such evolution implies an increase of the lowest unoccupied molecular orbital (LUMO) energy, and consequently of the energy gap, in good concordance with the calculated energies of the frontier orbitals (Figure 6). On the contrary, the electron-withdrawing diphenylphosphino group leads to a stabilization of the LUMO state (compound 6).

b) With the exception of compound 6, all these novel BODIPYs exhibit a very high fluorescence quantum yield in the different media (Table 2), although the high electron-donor ability of the amine (dye 4) activates an intramolecular charge-transfer state (ICT) in polar media, which limits its fluorescence efficiency (Figure S3).^[7] In compound 6 several non-radiative deactivation mechanism could merge to explain its null fluorescence efficiency. The bulky diphenylphosphino group could rotate, thereby enhancing the internal conversion processes and allowing an electronic coupling with the chromophore.^[14] Such an interaction should not lead to any stabilized resonance form (like in dyes 4 and 5) and distorts the geometry of the BODIPY, as has been observed for the 8-vinyl and 8-styryl derivatives.^[10d,15] In these compounds, theoretical calculations pointed out an enhancement in the out-of-plane vibrational

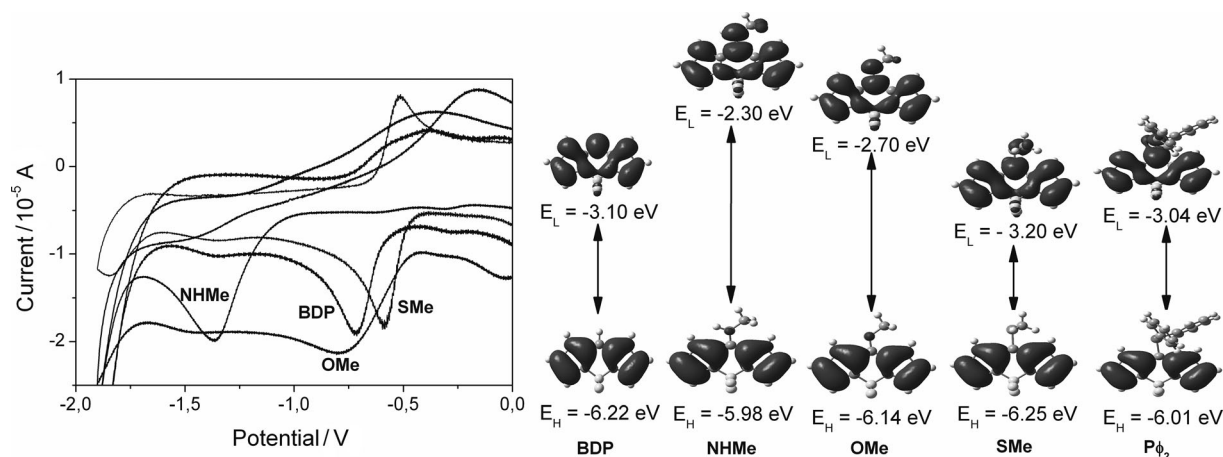


Figure 6. Reduction region of the cyclic voltammograms (positive scan, 0.2 V s^{-1}) of BODIPY **3** and its 8-heteroatom-substituted BODIPYs (dyes **1** (SMe), **4** (NHMe), and **5** (OMe)) in acetonitrile (0.5–1 mM), using TBAPF₆ 0.1 M as electrode. The corresponding energies of the HOMO and LUMO molecular orbitals are included for comparison.

	λ_{ab} [nm]	ϵ_{max} [$10^4 \text{ M}^{-1} \text{ cm}^{-1}$]	λ_{fl} [nm]	ϕ	τ [ns]	k_{fl} [10^8 s^{-1}]	k_{nr} [10^8 s^{-1}]
<i>c</i> -hexane							
3	503.5	7.6	510.5	0.96	6.47	1.48	0.06
4 (NHMe)	418.5	2.4	463.0	0.70	4.67	1.50	0.64
5 (OMe)	452.0	6.1	487.0	0.84	5.41	1.55	0.29
1 (SMe)	495.0	4.3	532.0	0.75	6.10	1.2	0.41
6 (P(ϕ) ₂)	528.5	7.4	553.5	0.003	-	-	-
ethanol							
3	498.0	5.6	508.0	0.90	7.02	1.28	0.14
4 (NHMe)	397.0	3.0	439.0	0.16	0.77 ^[b]	2.21	10.8
5 (OMe)	442.5	4.6	486.0	0.79	5.94	1.33	0.35
1 (SMe)	488.0	4.0	530.0	0.43	3.97	1.08	1.43
6 (P(ϕ) ₂)	525.5	6.9	559.0	0.001	-	-	-

[a] Variables: absorption (λ_{ab}) and fluorescence wavelength (λ_{fl}), molar absorption (ϵ_{max}), fluorescence quantum yield (ϕ), lifetime (τ), radiative (k_{fl}), and non-radiative (k_{nr}) deactivation rate constants. The full photophysical data in other solvents are listed in Tables S1–S3. [b] Main lifetime (contribution > 98%) of the biexponential fit.

methyl groups (fluorescence quantum yield up to 100%). The substitution at positions 3 and 5 improves the delocalization through the chromophore as is reflected by the enhancement of the absorption probability in all the methylated 8-heteroatom-substituted BODIPYs (Table 3). Indeed, theoretical calculations predict more planar geometries for the methylthio and methylamino derivatives upon methylation (i.e. the dihedral angle accounting for the chromophore's planarity increases from 172° in compound **4** to 180° in **8**), leading to a more rigid and delocalized chromophore.^[18]

motions of the pyrrols and the BF₂ bridge.^[16] In addition, the electron-withdrawing phosphorous atom could enable an ICT state, as has been reported for 8-cyano-BODIPYs.^[17]

c) Methylation at positions 3 and 5 reduces the hypsochromic shift of the spectral bands induced by the 8-substitution owing to the donor inductive effect of the methyl groups (Figure 4 and 7). The influence of the methylthio group is misleading since apparently opposite shifts are achieved in absorption, with regard to the reference BODIPY. This behavior will be discussed later in detail.

Moreover, the fluorescence efficiency of the new derivatives is noticeably ameliorated by these

The most striking feature is observed in polar media for the 8-amino-BODIPYs. The fluorescence efficiency of dye **4** is limited in polar solvents due to the ICT state (Table 2). However,

	λ_{ab} [nm]	ϵ_{max} [$10^4 \text{ M}^{-1} \text{ cm}^{-1}$]	λ_{fl} [nm]	ϕ	τ [ns]	k_{fl} [10^8 s^{-1}]	k_{nr} [10^8 s^{-1}]
<i>c</i> -hexane							
7	511.5	11.2	515.0	0.96	5.67	1.7	0.07
8 (NHMe)	439.0	5.1	484.5	1.00	4.25	2.4	0.00
9 (OMe)	467.0	7.7	497.5	1.00	4.80	2.1	0.00
2 (SMe)	530.5	7.1	538.0	0.95	6.53	1.5	0.08
ethanol							
7	507.0	9.1	512.5	0.88	6.15	1.4	0.20
8 (NMe)	416.5	4.0	454.0	0.81	3.52	2.3	0.54
9 (OMe)	459.5	5.8	496.5	0.87	5.30	1.6	0.25
2 (SMe)	505.5	4.8	536.0	0.87	6.70	1.3	0.19
	525.0						

[a] The full photophysical data are summarized in Tables S1–S3.

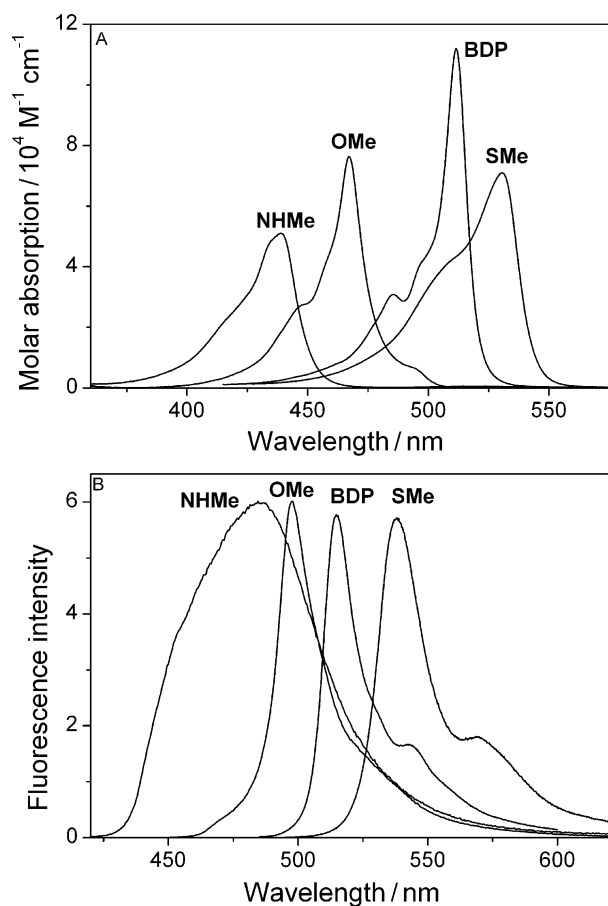


Figure 7. A) Absorption and B) fluorescence (area scaled by the fluorescence quantum yield) spectra of reference BODIPY (BDP is compound 3) and its 8-heteroatom derivatives bearing methyl groups at positions 3 and 5 in *c*-hexane (NHMe is compound 8, OMe 9 and SMe 2).

this process is suppressed by simple methylation at positions 3 and 5 (Table 3). As a result, the fluorescence quantum yields are clearly ameliorated (i.e. from 0.10 for compound 4 to 0.70 for compound 8 in methanol, Table S1). The inductive electron-donor character of the methyl groups could increase the electronic charge density in the chromophore. Consequently, the BODIPY is no longer a suitable electron acceptor for donors at the *meso* position, causing the suppression of the ICT population. The fluorescence-decay curves nicely reproduce the enhancement of the fluorescence in polar media by methylation at positions 3 and 5, and the lifetimes increase at those media, as a result of a lower non-radiative deactivation probability by the absence of ICT processes (Figure 8).

d) The presence of an 8-methylthio group leads to an apparent blue-shift in absorption for compound 1, but a red-shift is achieved upon additional methylation at positions 3 and 5 (compound 2), whereas the fluorescence bands are always red-shifted (in close agreement with the laser bands) with regard to the reference BODIPYs (3 and 7, respectively). Furthermore, a closer inspection of Figure 4 reveals, in the absorption band of compound 1, a shoulder at low energies. The solvent properties drastically influence the ratio between these two bands or shoulders (Figure S4), with the most energetic one prevail-

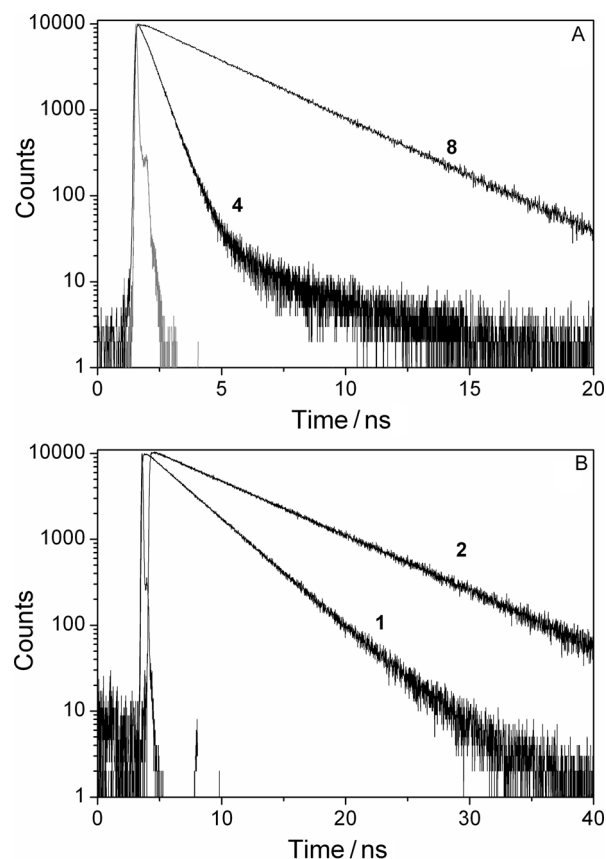


Figure 8. Fluorescence decay curves of: A) 8-methylamino (dye 4) and B) 8-methylthio-BODIPYs (dye 1) and their corresponding dimethylated derivatives at positions 3 and 5 (dyes 8 and 2, respectively) in methanol.

ing as the environmental polarity increases. In polar media, the 3,5-methyl derivative (dye 2) shows an absorption spectrum consisting of two bands with almost equal intensity. The excitation spectra match the absorption spectra (Figure S5). Besides, both the fluorescence and excitation spectra neither change with the excitation nor with the emission wavelengths, and therefore, no new entities are formed.

To clarify this behavior, we considered the tetramethyl derivative 10. Its absorption band shape matches—and fully reminds us of—the typical band shape of BODIPY (Figure 9). Substitution at the 1- and 7-positions infers steric hindrance to the 8-substituent, inducing an orthogonal disposition, which avoids the electronic coupling of the sulfur atom with the core, whereas the absence of those methyl groups should enable the resonance interaction. Thus, the main difference among these methylthio derivatives should be their spatial disposition at the *meso* position.

Then, the shape of the absorption spectrum induced by the presence of a methylthio substituent could be interpreted in terms of the stabilization of the new resonance structures, in a similar way to the amino and methoxy derivatives (dyes 4 and 5, respectively). Thus, the methylthio group is less electron donating than the amino or methoxy substituents, but if the electronic coupling is geometrically allowed, it should also give rise to an additional new resonance structure (Figure 5), albeit

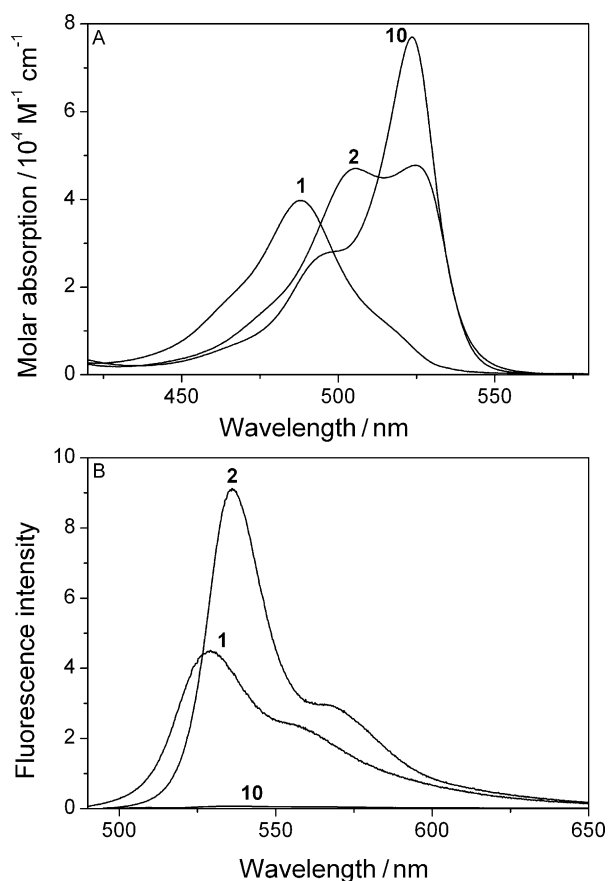


Figure 9. A) Absorption and B) fluorescence (scaled by the fluorescence efficiency) spectra of 8-methylthio-BODIPYs (1), 3,5-dimethylated (2) and tetramethylated analogue (10) in ethanol.

less stabilized than in the amino or methoxy counterparts. Accordingly, the more energetic band could be attributed to the resonance form, where the sulfur is delocalized to one pyrrole, and the less energetic one to the normal cyanine-like structure. Therefore, the shape of the absorption spectra should be the result of the contribution of each resonance form, which depends on the substitution pattern and the environmental properties. In fact, the new resonance structure is more polar and should be favored in polar media, where the contribution of the more energetic band increases (Figures 9 and S4). Moreover, upon methylation at positions 3 and 5 (compound 2), such a structure is less favored because the electron density in the BODIPY should increase and the core is less receptive to the electron lone pair of the sulfur atom. This fact explains that in compound 2 the two bands are better observed in polar media and their intensities are almost similar.

The above-commented balance between such two main resonance structures (Figure 4), owing to the electronic coupling of the methylthio group with the BODIPY core, could lead to additional non-radiative deactivation pathways and hence explain the lower fluorescence quantum yield of compound 1, with regard to the reference compound 3 and its methoxy counterparts (compound 5) in apolar media (Table 2). Moreover, in compound 1, the fluorescence efficiency further drops

in polar media, although less than in the amino derivative 4, where an ICT state is activated (Table 2). In these media, the resonance structure resulting from the delocalization of the methylthio fragment through the BODIPY obtains a higher relevance, as supported by the increase in the contribution of the more energetic absorption band. Nevertheless, the situation is completely reversed by the methylation at positions 3 and 5, which seems to be very profitable for the fluorescence efficiency (i.e. from 0.43 for compound 1 to 0.87 for 2 in ethanol, Tables 2 and 3). Indeed, compound 2, bearing also a 8-methylthio group, gives rise to high fluorescence quantum yields in all media and the fluorescence lifetimes recover the typical values of BODIPY (Figure 8 and Table S3).

3. Conclusions

A systematic study on both the photophysical and laser properties of a series of nine BODIPY dyes as a function of varied substitution at the 8, 3, and 5-positions was accomplished. *Meso*-substituents included N, O, S, P, and H fragments, and 3,5-positions containing either protons or methyl groups have been developed. These derivatives were prepared in a very efficient manner using the methodology previously developed in our groups from commercially available starting materials.

These sets of 8-heteroatom-substituted BODIPYs enable us to successfully cover the spectral region, from blue to orange, because of the launch of new delocalized π -systems (from cyanine to hemi- or merocyanine). However, the fluorescence and laser performance of the blue-emitting dyes (amino derivatives) in polar media is limited by the activation of an ICT quenching state. Nevertheless, such limitation is overcome by the incorporation of methyl groups at positions 3 and 5. Their inductive electron-donor character suppresses the ICT process, and highly fluorescent dyes (approaching 100%) are achieved (regardless of the medium) from blue to orange by attaching methylamino, methoxy, and methylthio groups. Laser emission covering the spectral range from 475 to 575 nm, with good efficiency and photostability, was demonstrated. In particular, the combination of heteroatoms at the *meso* position with alkylation at positions 3 and 5 resulted in dyes with a photostability similar to that of the unsubstituted dye, but with a much improved efficiency.

Experimental Section

BODIPYs 1, 2, 3, and 10 are commercially available or can be prepared according to the literature procedures.^[6,7,9] All the other reactants, ligands and catalysts are commercially available. BODIPYs 4 and 5 were prepared according to the literature procedures.^[7] Details of the synthesis and characterization of the other compounds (6–9) can be found in the SI.

Laser properties were measured under transversal pumping at 355 nm from the third-harmonic of a Q-switched Nd:YAG laser (Spectron SL282G) or at 532 nm from a frequency-doubled Q-switched Nd:YAG laser (Monocrom OPL-10). The photostability of the dyes was evaluated by monitoring the decrease in laser-induced fluorescence intensity, which was collected by an optical

fiber, and imaged onto the input slit of a monochromator (Acton Research corporation) and detected with a charge-coupled device (CCD) (SpectruMM:G5128B). The signal was fed to a boxcar (Stanford Research, model 250) to be integrated before being digitized and processed by a computer.

UV/Vis absorption and fluorescence spectra were recorded on a Varian model CARY 4E spectrophotometer and an SPEX Fluorolog 3-22 spectrofluorimeter, respectively. Radiative decay curves were registered by the time-correlated single-photon counting technique (Edinburgh Instruments, model FL920, with picosecond time resolution) exciting at 410 and 470 nm using a diode laser (Pico-Quant).

Electrochemical experiments (Metrohm Autolab) were performed using a three-electrode setup with a platinum disk or layer as the working electrode, a platinum wire as the counter electrode, and Ag/AgCl as the reference electrode.

Further details of the experimental conditions are included in the SI.

Acknowledgements

This work was supported by Projects MAT-2010-20646-01 and MAT-2010-20646-04 of the Spanish MICINN. Support from CONACYT (Grant 129572) is gratefully acknowledged. I.V.-E. wishes to thank CONACYT for a postdoctoral fellowship. I.E. thanks the Gobierno Vasco for a PhD contract (SPE12UN140 and IT339-10). C.F.A.G.-D., A.U.-B., and M.L.B.-M. wish to thank CONACYT for graduate fellowships. We also wish to thank Cuantico de México for the kind donation of 8-thiomethyl-BODIPY dyes 1 and 2.

Keywords: boron-dipyrromethene • charge transfer • cyanines • heteroatoms • lasers

- [1] R. P. Haugland, *The Handbook. A Guide to Fluorescent Probes and Labeling Technology*, 10th ed., Molecular Probes, Eugene, 2005.
- [2] a) R. Ziessel, G. Ulrich, A. Harriman, *New J. Chem.* **2007**, *31*, 496–501; b) G. Ulrich, R. Ziessel, A. Harriman, *Angew. Chem.* **2008**, *120*, 1202–1219; *Angew. Chem. Int. Ed.* **2008**, *47*, 1184–1201; c) A. C. Benniston, G. Copley, *Phys. Chem. Chem. Phys.* **2009**, *11*, 4124–4131; d) A. Loudet, K. Burgess, *Chem. Rev.* **2007**, *107*, 4891–4932; e) T. E. Wood, A. Thompson, *Chem. Rev.* **2007**, *107*, 1831–1861.
- [3] a) S. Lin Niu, G. Ulrich, R. Ziessel, A. Kiss, P.-Y. Renard, A. Romieu, *Org. Lett.* **2009**, *11*, 2049–2052; b) S. Zhu, J. Zhang, G. Vegesna, F.-T. Luo, S. A. Green, H. Liu, *Org. Lett.* **2011**, *13*, 438–441; c) T. Bura, R. Ziessel, *Org. Lett.* **2011**, *13*, 3072–3075; d) M. Tasiar, J. Murtagh, D. O. Frimannsson, S. O. McDonnell, D. F. O'Shea, *Org. Biomol. Chem.* **2010**, *8*, 522–525; e) M. Brellier, G. Duportail, R. Baati, *Tetrahedron Lett.* **2010**, *51*, 1269–1272; f) L. Li, J. Han, B. Nguyen, K. Burgess, *J. Org. Chem.* **2008**, *73*, 1963–1970.
- [4] a) J.-S. Lee, N.-Y. Kang, Y. K. Kim, A. Samanta, S. Feng, H. K. Kim, M. Vendrell, J. H. Parkand, Y.-T. Chang, *J. Am. Chem. Soc.* **2009**, *131*, 10077–10082; b) P. H. Lee, *Bull. Korean Chem. Soc.* **2008**, *29*, 261–264; c) G. Barin, M. D. Yilmaz, E. U. Akkaya, *Tetrahedron Lett.* **2009**, *50*, 1738–1740; d) O. A. Bozdemir, O. Büyükcakir, E. U. Akkaya, *Chem. Eur. J.* **2009**, *15*, 3830–3838; e) V. P. Yakubovskiy, M. P. Shandura, Y. P. Kovtun, *Eur. J. Org. Chem.* **2009**, 3237–3243; f) T. Bura, R. Ziessel, *Tetrahedron Lett.* **2010**, *51*, 2875–2879; g) T. Rousseau, A. Cravino, E. Ripaud, P. Leriche, S. Rihn, A. De Nicola, R. Ziessel, J. Roncali, *Chem. Commun.* **2010**, 46, 5082–5084; h) D. Zhang, Y. Wang, Y. Xiao, S. Qian, X. Qian, *Tetrahedron* **2009**, *65*, 8099–8103; i) D. T. Chase, B. S. Young, M. M. Haley, *J. Org. Chem.* **2011**, *76*, 4043–4051; j) Y. M. Poronik, V. P. Yakubovskiy, M. P. Shandura, Y. G. Vlasenko, A. N. Chernega, Y. P. Kovtun, *Eur. J. Org. Chem.* **2010**, 2746–2752.
- [5] a) Z. Shen, H. Röhr, K. Rurack, H. Uno, M. Spieles, B. Schulz, G. Reck, N. Ono, *Chem. Eur. J.* **2004**, *10*, 4853–4871; b) L. Zeng, C. Jiao, X. Huang, K.-W. Huang, W.-S. Chin, J. Wu, *Org. Lett.* **2011**, *13*, 6026–6029; c) L. Jiao, C. Yu, M. Liu, Y. Wu, K. Cong, T. Meng, Y. Wang, E. Hao, *J. Org. Chem.* **2010**, *75*, 6035–6038; d) T. Okujima, Y. Tomimori, J. Nakamura, H. Yamada, H. Uno, N. Ono, *Tetrahedron* **2010**, *66*, 6895–6900; e) M. A. Filatov, A. Y. Lebedev, S. N. Mukhin, S. A. Vinogradov, A. V. Cheprakov, *J. Am. Chem. Soc.* **2010**, *132*, 9552–9554; f) M. Wada, S. Ito, H. Uno, T. Murashima, N. Ono, T. Urano, Y. Urano, *Tetrahedron Lett.* **2001**, *42*, 6711–6713; g) V. Leen, W. Qin, W. Yang, J. Cui, C. Xu, X. Tang, W. Liu, K. Robeyns, L. Van Meervelt, D. Beljonne, R. Lazzaroni, C. Tonnelé, N. Boens, W. Dehaen, *Chem. Asian J.* **2010**, *5*, 2016–2026; h) C. Jiao, K.-W. Huang, J. Wu, *Org. Lett.* **2011**, *13*, 632–635; i) A. B. Descalzo, H.-J. Xu, Z.-L. Xue, K. Hoffmann, Z. Shen, M. G. Weller, X.-Z. You, K. Rurack, *Org. Lett.* **2008**, *10*, 1581–1584.
- [6] I. J. Arroyo, R. Hu, G. Merino, B. Z. Tang, E. Peña-Cabrera, *J. Org. Chem.* **2009**, *74*, 5719–5722.
- [7] For the case of 8-amino-substituted BODIPYs, see: a) C. F. A. Gómez-Durán, I. García-Moreno, A. Costela, V. Martín, R. Sastre, J. Bañuelos, F. López Arbeloa, I. López Arbeloa, E. Peña-Cabrera, *Chem. Commun.* **2010**, 46, 5103–5105; b) J. Bañuelos, V. Martín, C. F. A. Gómez-Durán, I. J. Arroyo-Córdoba, E. Peña-Cabrera, I. García-Moreno, A. Costela, M. E. Pérez-Ojeda, T. Arbeloa, I. López Arbeloa, *Chem. Eur. J.* **2011**, *17*, 7261–7270; c) C. A. Osorio-Martínez, A. Urias-Benavides, C. F. A. Gómez-Durán, J. Bañuelos, I. Esnal, I. López Arbeloa, E. Peña-Cabrera, *J. Org. Chem.* **2012**, *77*, 5434–5438. For the case of 8-alkoxy and 8-aryloxyBODIPYs, see: d) J. O. Flores-Rizo, I. Esnal, C. A. Osorio-Martínez, C. F. A. Gómez-Durán, J. Bañuelos, I. López Arbeloa, K. H. Pannell, A. Metta-Magaña, E. Peña-Cabrera, *J. Org. Chem.* **2013**, *78*, 5867–5877.
- [8] In a recent paper, Dehaen et al. described a modified synthesis of **1** and **9**, as well as other meso-heteroatom-substituted BODIPY dyes, however, just a superficial discussion of their properties was provided. See: V. Leen, P. Yuan, L. Wang, N. Boens, W. Dehaen, *Org. Lett.* **2012**, *14*, 6150–6153.
- [9] T. V. Goud, A. Tutar, J.-F. Biellmann, *Tetrahedron* **2006**, *62*, 5084–5091.
- [10] a) E. Peña-Cabrera, A. Aguilar-Aguilar, M. González-Domínguez, E. Lager, R. Zamudio-Vázquez, J. Godoy-Vargas, F. Villanueva, *Org. Lett.* **2007**, *9*, 3985–3988; b) E. Lager, J. Liu, A. Aguilar-Aguilar, B. Z. Tang, E. Peña-Cabrera, *J. Org. Chem.* **2009**, *74*, 2053–2058; c) I. J. Arroyo, R. Hu, B. Z. Tang, F. I. López, E. Peña-Cabrera, *Tetrahedron* **2011**, *67*, 7244–7250; d) J. Bañuelos, I. J. Arroyo-Córdoba, I. Valois-Escamilla, A. Alvarez-Hernández, E. Peña-Cabrera, R. Hu, B. Z. Tang, I. Esnal, V. Martínez, I. López Arbeloa, *RSC Adv.* **2011**, *1*, 677–684.
- [11] a) Y. Hayashi, S. Yamaguchi, W. Y. Cha, D. Kim, H. Shinokubo, *Org. Lett.* **2011**, *13*, 2992–2995; b) E. Fron, E. Coutiño-Gonzalez, L. Pandey, M. Sliwa, M. Van der Auweraer, F. C. De Schryver, J. Thomas, Z. Dong, V. Leen, M. Smet, W. Dehaen, T. Vosch, *New J. Chem.* **2009**, *33*, 1490–1496; c) W. Qin, V. Leen, T. Rohand, W. Dehaen, P. Dedecker, M. Van der Auweraer, K. Robeyns, L. Van Meervelt, D. Beljonne, B. Van Averbek, J. N. Clifford, K. Driesen, K. Binnemans, N. Boens, *J. Phys. Chem. A* **2009**, *113*, 439–447; d) O. Dilek, S. L. Bane, *J. Fluoresc.* **2011**, *21*, 347–354; e) V. Hornillos, E. Carrillo, L. Rivas, F. Amat-Guerri, A. U. Acuña, *Bioorg. Med. Chem. Lett.* **2008**, *18*, 6336–6339; f) A. Ojida, T. Sakamoto, M. Inoue, S. Fujishima, G. Lippens, I. Hamachi, *J. Am. Chem. Soc.* **2009**, *131*, 6543–6548; g) K. Tamanna, T. K. Khan, M. Ravikanth, *Tetrahedron* **2012**, *68*, 830–840; h) E. Deniz, G. C. Isbasar, O. A. Bozdemir, L. T. Yildirim, A. Siemiarzczuk, E. U. Akkaya, *Org. Lett.* **2008**, *10*, 3401–3403; i) T. Rohand, M. Baruah, W. Qin, N. Boens, W. Dehaen, *Chem. Commun.* **2006**, 266–268; j) J. Chen, M. Mizumura, H. Shinokubo, A. Osuka, *Chem. Eur. J.* **2009**, *15*, 5942–5949; k) D. Zhang, Y. Wen, Y. Xiao, G. Yu, Y. Liu, X. Qian, *Chem. Commun.* **2008**, 4777–4779; l) L. Li, B. Nguyen, K. Burgess, *Bioorg. Med. Chem. Lett.* **2008**, *18*, 3112–3116; m) O. Dilek, S. L. Bane, *Bioorg. Med. Chem. Lett.* **2009**, *19*, 6911–6913; n) V. Leen, T. Leemans, N. Boens, W. Dehaen, *Eur. J. Org. Chem.* **2011**, 4386–4396; o) V. Lakshmi, M. Ravikanth, *J. Org. Chem.* **2011**, *76*, 8466–8471; p) M. J. Ortiz, A. R. Agarrabeitia, G. Duran-Sampedro, J. Bañuelos Prieto, T. Arbeloa Lopez, W. A. Massad, H. A. Montejano, N. A. García, I. Lopez Arbeloa, *Tetrahedron* **2012**, *68*, 1153–1162.
- [12] C. Hansch, A. Leo, R. W. Taft, *Chem. Rev.* **1991**, *91*, 165–195.

- [13] R. I. Roacho, A. Metta-Magaña, M. M. Portillo, E. Peña-Cabrera, K. H. Pannell, *J. Org. Chem.* **2013**, *78*, 4245–4250.
- [14] F. Li, S. I. Yang, T. Ciringh, J. Seth, C. H. Martin III, D. L. Singh, D. Kim, R. R. Birge, D. F. Bocian, D. Holten, J. S. Lindsey, *J. Am. Chem. Soc.* **1998**, *120*, 10001–10017.
- [15] N. Shivran, S. Mula, T. K. Ghanty, S. Chattopadhyay, *Org. Lett.* **2011**, *13*, 5870–5873.
- [16] S. Chibani, B. L. Guennic, A. Charaf-Eddin, A. D. Laurent, D. Jacquemin, *Chem. Sci.* **2013**, *4*, 1950–1963.
- [17] F. López Arbeloa, J. Bañuelos, V. Martínez, T. Arbeloa, I. López Arbeloa, *ChemPhysChem* **2004**, *5*, 1762–1771.
- [18] a) A. Cui, X. Peng, J. Fan, X. Chen, Y. Wu, B. Guo, *J. Photochem. Photobiol. A* **2007**, *186*, 85–92; b) W. Qin, T. Rohand, W. Dehaen, J. N. Clifford, K. Driesen, D. Beljonne, B. Van Aberbeke, M. Van der Auweraer, N. Boens, *J. Phys. Chem. A* **2007**, *111*, 8588–8597.

Received: September 4, 2013

Revised: October 21, 2013

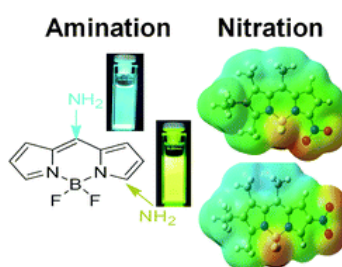
Published online on November 20, 2013

5. Kapituluko IV ERANSKINA / ANEXO IV al Capítulo 5

8. Artikulua / Artículo 8:

Nitro and amino BODIPYs: crucial substituents to modulate their photonic behavior.

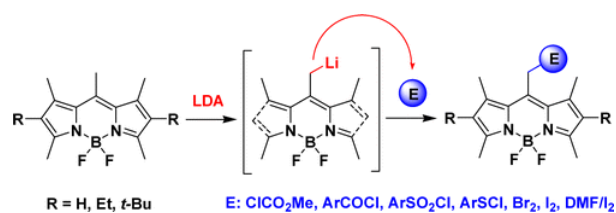
RSC Advances, 2013, 3, 1547



9. Artikulua / Artículo 9:

Selective lateral lithiation of methyl BODIPYs: synthesis, photophysics and electrochemistry of new *meso* derivatives.

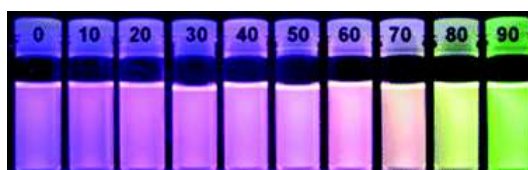
Organic Letters, 2014, 16, 4364



10. Artikulua / Artículo 10:

Modulation of the photophysical properties of BODIPY dyes by substitution at their *meso* position

RSC Advances, 2011, 1, 677



PAPER

Nitro and amino BODIPYS: crucial substituents to modulate their photonic behavior†

Cite this: *RSC Advances*, 2013, 3, 1547

Ixone Esnal,^a Jorge Bañuelos,^{*a} Iñigo López Arbeloa,^a Angel Costela,^b Inmaculada García-Moreno,^b Miguel Garzón,^c Antonia R. Agarrabeitia^c and María José Ortiz^c

The present work deals with the synthesis and photophysical, quantum mechanical, and lasing characterization of novel BODIPYs bearing amino and nitro groups at different positions in the core. The results emphasize the relevant role on the photophysical and lasing properties, not only of the attached functionality but also of the position in which is grafted, as well as the molecular structure of the indacene core. A wide part of the visible spectrum can be covered by the insertion of an amino group at position 3 (red shift) or 8 (blue shift). Furthermore, the electron withdrawing character of the nitro substituent induces intramolecular charge transfer processes, the efficiency of which depends on the position of the nitro group on the BODIPY core. All these experimental findings can be rationalized with the help of quantum mechanical calculations.

Received 15th November 2012,
Accepted 16th November 2012

DOI: 10.1039/c2ra22916a

www.rsc.org/advances

Introduction

The family of difluoroboradiazaindacenes, known by the trade name BODIPY, is currently considered as comprising some of the most useful and versatile fluorophores. The numerous applications of these compounds (biotechnology, electronics, *etc.*) require the design of new fluorophores with properties such as high stability, high fluorescence quantum yields, large Stokes shifts, and suitable absorption profiles, as well as incorporating substituents that optimize the function of these compounds in the different applications.¹ The incorporation of appropriate functional groups onto the chromophore could lead to new photophysical processes or large spectral shifts. Thus, the type of substituents and the position in which they are attached to the chromophore allow obtainment of, for example, a highly fluorescence dye in the red part of the visible spectrum or a system in which fluorescence properties are sensitive to a certain property of the surrounding environment. Therefore, one should choose carefully the kind of substituents and the position in which they will be incorporated to BODIPY, depending on the desired application.¹

Post-modification of the BODIPY core is a convenient method for the facile functionalization of these dyes. The extensive literature available on BODIPY dyes shows that substitution at all positions has been investigated.^{1–9} Several synthetic strategies have been used for this purpose, such as Knoevenagel-type condensation^{1a–c,g,2} and oxidative formylation of methyl-substituted BODIPYs,³ nucleophilic substitutions^{1a–c,g,4} and palladium coupling reactions^{1a,5} on halogenated BODIPYs, direct hydrogen substitution,⁶ the Liebeskind–Srögl reaction⁷ and electrophilic substitution reactions.^{1a,8} Furthermore, the replacement of fluoride atoms by carbon and oxygen nucleophiles or by other halogen atoms has been shown to be an important advance for the introduction of functionality.^{1a–c,2c,k,8b,9}

Functionalization at the 2,6-positions from 1,3,5,7-tetramethyl substituted BODIPYs can be achieved by electrophilic substitution reactions.^{1a,8} Thus, halogenation at these positions has been extensively studied.^{5f,8b–f} However, the nitration of BODIPYs has not attracted so much research interest as demonstrated by the few related publications in the literature. As we know, there is an example of nitration in the 2,6-positions of the commercial BODIPY core named PM546 (**A**),¹⁰ and there are several Japanese patents with two dinitro derivatives (**B**¹¹ and **C**¹²), but neither their syntheses nor their spectroscopic data have been described (Fig. 1). Moreover, electrophilic substitution reactions in pyrrole-unsubstituted BODIPYs have attracted relatively little research interest until very recently^{4h,8g–j} and, specifically, there is no study on the nitration reaction in this type of compound. In contrast, there are numerous examples of BODIPYs with nitro groups but not

^aDepartamento de Química Física, Universidad País Vasco (UPV-EHU), Aptdo. 644, 48080, Bilbao, Spain

^bDepartamento de Sistemas de Baja Dimensionalidad, Superficies y Materia Condensada, Instituto Química-Física “Rocasolano”, CSIC, Serrano 119, 28006 Madrid, Spain

^cDepartamento de Química Orgánica I, Facultad de Ciencias Químicas, Universidad Complutense, 28040, Madrid, Spain

† Electronic Supplementary Information (ESI) available: details of the synthesis route, NMR spectra, photophysical data. See DOI: 10.1039/c2ra22916a

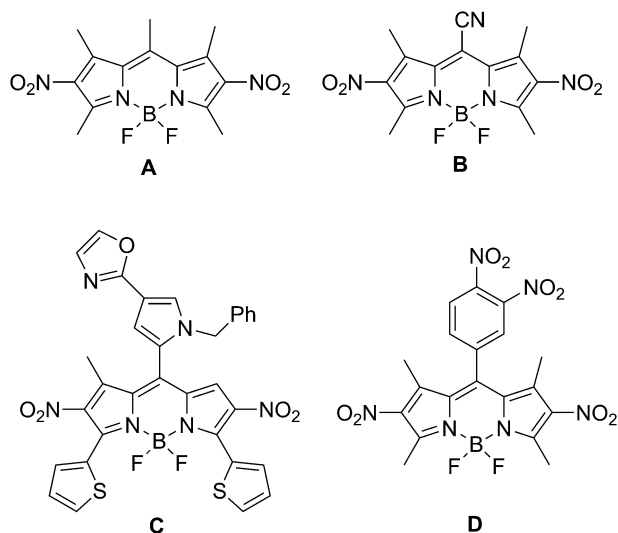


Fig. 1 Chemical structures for 2,6-dinitro-1,3,5,7-substituted BODIPYs (**A**, **B** and **C**), and 8-dinitroaryl BODIPY (**D**).

directly attached to the BODIPY core (**D**),^{1a,13} and most of them are used as precursors of amino groups (Fig. 1).

In this work we report the synthesis of new nitro derivatives of two different BODIPY scaffolds, by electrophilic substitution and subsequent reduction to the corresponding amino derivatives (Fig. 2). This library of new dyes allows us to analyze in detail the dependence of their optical properties on the nature and position of the substituents linked to a symmetric and asymmetric BODIPY core.

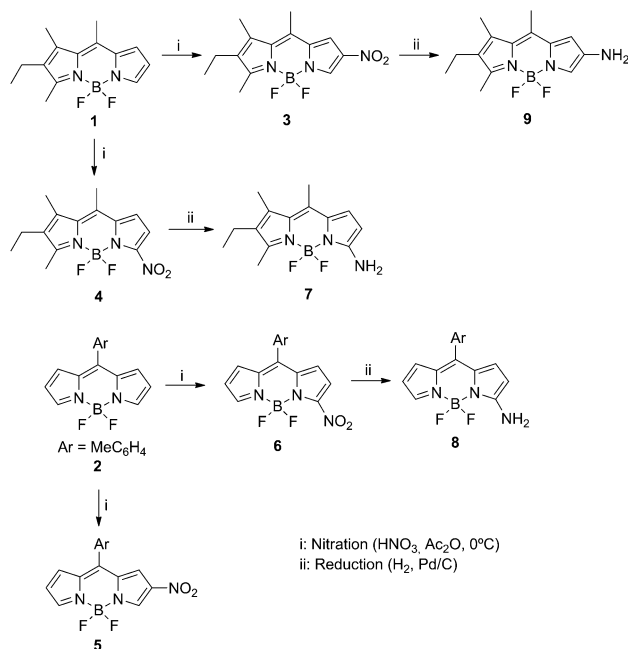


Fig. 2 Starting BODIPYs (**1**, **2**) and core-nitro and amino BODIPY dyes (**3–9**) studied in this work.

Furthermore, the present work provides new insight into the effect of the molecular structure on the photophysical properties of the resulting chromophore. The nitration of BODIPYs induces new photophysical processes such as charge transfer phenomena, the influence on the optical properties of which is strongly dependent on the type of substituent, as well as the position where it is anchored to the chromophore. Therefore, the correct selection of functional groups and the most convenient position to graft them to the core allows the design of tailor-made BODIPY for the desired application, ranging from BODIPY covering a wide part of the visible part of the spectrum (amino substitution) to fluorophores sensitive to the environmental properties (nitro substitution). Moreover, these derivatives should be excellent scaffolds to further functionalization, leading to a wide battery of available structures based on BODIPY.

Results and discussion

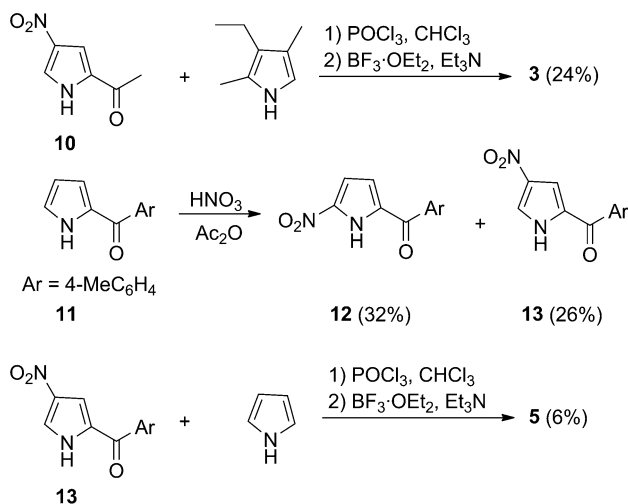
Synthesis

Nitration of the BODIPY core has been carried out by electrophilic substitution reaction. Thus, the reaction of BODIPY dye **1**¹⁴ with 2 equiv. HNO_3 in Ac_2O at 0°C gave a mixture of 6-nitro derivative **3** (11%) and 5-nitro derivative **4** (37%), which were separated *via* flash chromatography on silica. A similar result was obtained from pyrrole-unsubstituted BODIPY **2**¹⁵ with 4 equiv. HNO_3 in Ac_2O , yielding 2-nitro derivative **5** (6%) and 3-nitro derivative **6** (36%). No other nitro BODIPY was formed under these reaction conditions. Increasing the amount of HNO_3 gave a complex mixture of nitro products.

Due to the low yields obtained from β -nitro derivatives **3** and **5**, we carried out the independent synthesis of these compounds from nitro pyrrole precursors (Scheme 1). Thus, the reaction of 2-acetyl-4-nitro-1*H*-pyrrole (**10**)¹⁶ and 3-ethyl-2,4-dimethyl-1*H*-pyrrole with phosphorus oxychloride in CHCl_3 , followed by treatment with $\text{BF}_3 \cdot \text{OEt}_2$ in the presence of triethylamine, gave a moderate yield of BODIPY **3**. For the preparation of BODIPY **5**, we carried out the nitration of (1*H*-pyrrol-2-yl) (4-tolyl) methanone (**11**),¹⁷ yielding a mixture of (5-nitro-1*H*-pyrrol-2-yl) (4-tolyl) methanone (**12**) and (4-nitro-1*H*-pyrrol-2-yl) (4-tolyl) methanone (**13**), which were separated *via* flash chromatography on silica. The condensation of compound **13** and pyrrole with phosphorus oxychloride, followed by treatment with $\text{BF}_3 \cdot \text{OEt}_2$ in the presence of triethylamine allowed us to isolate BODIPY **5**, but, as in the direct nitration of BODIPY **2**, with a very low yield (Scheme 1). In addition, this compound was very unstable and its photophysical study was not possible. The amino BODIPYs **7** and **8** were readily obtained by reduction of the nitro to the amino group in the presence of molecular hydrogen and a solid catalyst with a quantitative good yield. However, BODIPY **9** could not be isolated because it decomposes quickly.

Photophysical properties

The photophysical properties of the parent compound **1** have been previously analyzed as a function of the solvent nature.¹⁴



Scheme 1 Independent synthesis of BODIPYs **3** and **5**.

Its photophysics were conditioned by the asymmetric substitution pattern, which reduces the absorption probability, while its fluorescence efficiency remained high, close to 100% in apolar solvents (Table 1). In addition, the asymmetric charge distribution in the pyrroles, induced by the substitution pattern, increased the non-radiative deactivation pathway and led to a moderate fluorescence quenching in polar media (around 25%), not reflected in the fluorescence lifetime. This behavior was a consequence of a concomitant decline in the radiative rate constant (parallel to the decrease in the molar absorption) and an enhancement of the non-radiative deactivation rate constants with the solvent polarity, which further favored the charge separation between the pyrroles.

Amino substitution. With respect to the parent dye **1**, the presence of an amino group at position 5 (compound **7**) red-shifts the spectral bands (around 20 nm), owing to the electron donor ability of the amine, which enhances the delocalized electronic density in the chromophoric core (Table 1 and Fig. 3, left). Similar red shifts have been reported for BODIPYs bearing amino groups at positions 3 and 5.¹⁸ The 5-amino substituent increases the asymmetry in the charge distribution with the consequent decrease in the absorption probability of the new derivative **7**. Alternatively the fluorescence quantum yield remains high in apolar media, whereas it significantly decreases in polar media, following the same dependence on the solvent polarity to that previously observed for the

Table 1 Photophysical properties of compound **1** and its 5-amino derivative (**7**) in apolar (cyclohexane) and polar media (methanol). The full photophysical data in other solvents are collected in Table S1 (ESI[†])

	λ_{ab} (nm)	ϵ_{max} ($M^{-1} cm^{-1}$)	λ_{fl} (nm)	ϕ	τ (ns)
1					
c-Hexane	504.0	33000	515.0	0.96	5.46
Methanol	495.5	25000	512.5	0.76	5.78
7					
c-Hexane	522.0	19000	538.0	0.97	4.44
Methanol	510.0	9000	534.0	0.74	4.54

reference dye **1** (Table 1). In fact, the electron releasing capacity of the amino at position 5 is not strong enough to induce a charge transfer state, which usually drastically quenches the fluorescence emission of BODIPYs. Theoretical simulations do not suggest an electronic density shift from the amino to the BODIPY core upon excitation, and the frontier orbital contour maps keep the normal features of the fluorophore, but extended to the amino group.

The inclusion of the same group at position 6 (compound **9**) gave rise to a very unstable product, with fast degradation, losing the spectral bands typical of BODIPY. The electronic coupling of the amino at such a position could give rise to the formation of an emamine-imine tautomeric equilibrium (Scheme S1, ESI[†]) destroying the delocalized π -system of the chromophore. Therefore, entirely different results were obtained by changing the position in which the amino group was attached. Such a key role of the substitution position on the optical properties is reinforced by previous results reported by a BODIPY bearing just an amino group in the *meso* position.^{7e,19} While the presence of this group in position 5 led to a slight bathochromic shift of the spectral bands, the substitution at position 8 induced a large blue shift (Fig. 3, right).

The reason for such opposite behavior can be understood through the theoretical simulation of the electronic distribution in the frontier orbitals involved in the corresponding spectral transition. With independence of the substitution, the electronic density at position 5 of the BODIPY core is nearly similar in the HOMO and LUMO states (Fig. 3). Thus, the 5-amino substituent only increased the delocalization of the π -system, red-shifting the spectral bands. However, the electronic density at position 8 of the BODIPY core increases significantly upon excitation from the HOMO to the LUMO state, highlighting the *meso* position as being very sensitive to substituent effects. Then, the electron donor amine linked at the 8-position raised up the energy of the LUMO state, leaving the HOMO state unaltered,¹⁹ and, consequently, leading to an increase of the energy gap, which is reflected in the blue-shift of the spectral bands.

Nitro substitution. Following an opposite behavior to that previously described for amino substitution, the presence of a nitro group at position 5 (compound **4**) as well as at 6 (compound **3**) gave rise to a hypsochromic shift of the absorption band due to its electron withdrawing character (Fig. 4), which removes part of the electronic density delocalized through the BODIPY core. Nonetheless, the most striking feature induced by nitro substitution is a drastic change in the shape of both the absorption and fluorescence spectra. Indeed, the absorption bands seem to be split into two transitions, behavior that becomes clearer in fluorescence, where very broad emission bands were registered.

Taking into account the strong electron-withdrawing character of the substituent, one could wonder that this photophysical behavior is related to the presence of an intramolecular charge transfer (ICT) state, active even in the ground state. However, the influence of the ICT on the spectral bands is not well defined, since absorption transitions attributed to ICT have been reported as red-shifted and as blue-shifted, with respect to the locally excited (LE) state.²⁰

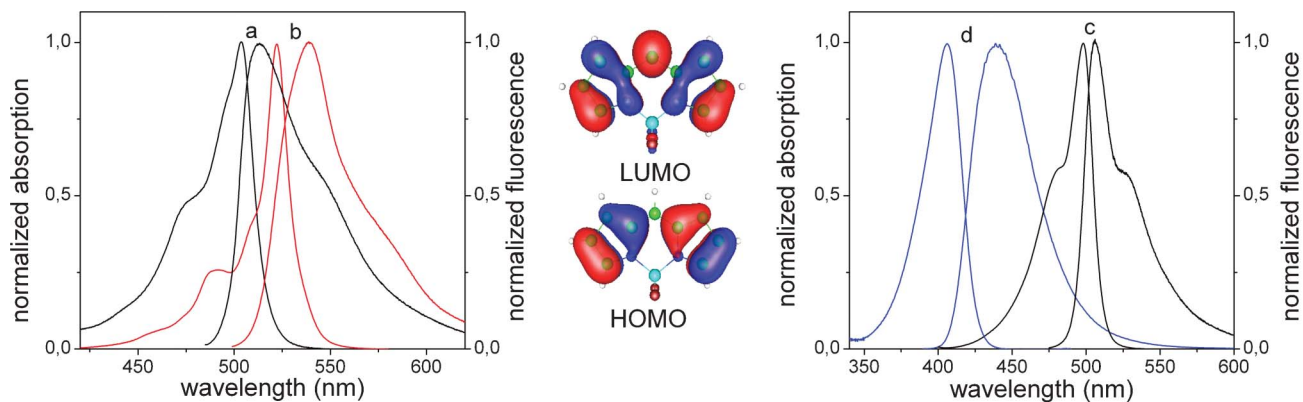


Fig. 3 (Left) Absorption and fluorescence spectra of the alkylated BODIPY **1** (a) and its 5-amino substituted derivative **7** (b). (Right) For comparison purposes, the corresponding spectral bands of the fully unsubstituted BODIPY dye (named as BDP) and its 8-amino derivative ((c) and (d), respectively)^{7c,19} are included. For the sake of clear understanding of the opposite spectral shifts induced by the amino group depending on the grafting position, the HOMO and LUMO contour maps of the BODIPY core are also included.

More clearly perceptible is the dependence of the ICT states on the solvent nature, since they are stabilized in polar media due to their high dipole moment. Thus, their spectral bands are very sensitive to the solvent polarity and usually show large Stokes shifts in polar solvents.

However, the spectra of these nitro derivatives are characterized by small Stokes shifts and low solvatochromism. Indeed, the presence of such a possible second band becomes less evident in polar media, whereas the spectral transitions involving ICT states usually appear clearer, as the polarity of the solvent increases. Moreover, the fluorescence spectra and fluorescence decay curves of these nitro-substituted BODIPYs do not change with the excitation wavelength (or emission wavelength in the later case), and also their excitation spectra perfectly match the absorption ones, regardless of the emission wavelength. All this evidence allows rejection of the hypothesis of the presence of an ICT state as the origin of the apparent spectral splitting, which could be more related to the

change in the vibrational structure of the bands induced by the nitro group, because of the following features: (a) the vibrational resolution appears clearer in apolar media; (b) there is only one emitting entity, since the spectral bands and the decay curves are independent of the excitation and emission wavelengths; (c) the solvatochromism of the spectra is quite low (see Fig. S1 in the ESI†), and (d) theoretical simulation of the absorption spectrum only predicts one transition in the visible region.

Regarding the fluorescence properties, the presence of the nitro group reduced the fluorescence efficiency and the lifetime of the BODIPY, as shown in Table 2 and Fig. 5. Such a decrease was more evident in polar media, where the fluorescence decay is faster. This trend is more dramatic in compound **4**, because in the most polar media the fluorescence ability becomes negligible and the corresponding decay curve has to be deconvoluted as biexponential, with a dominating short lifetime (around 50 ps in methanol). The marked sensitivity of the fluorescence quantum yield and decay curve on the solvent polarity can be related to the presence of an extra non-radiative deactivation pathway in these media.

Taking into account the strong electron-withdrawing ability of the nitro group, the reason for the fluorescence quenching should be an ICT state, built up from the LE state. The presence of an ICT has been discussed before to explain the shape of the spectra. Although such a hypothesis was discarded as an explanation of the spectral splitting, it does not mean that the ICT is not taking place in the excited state. From the above discussion, it is clear that the ICT state is not formed in the ground state. Nonetheless, it can be populated in the excited state, but with absence of self-emission, which allows the maintenance of the vibrational resolution of the absorption spectrum in the fluorescence one. Therefore, the formation of an ICT state upon excitation in the nitro derivatives **3** and **4** explains the decrease in fluorescence ability. Generally, the ICT states are characterized by a poor or negligible emission, since they are placed at lower energies than the LE state and non-radiative deactivation is more

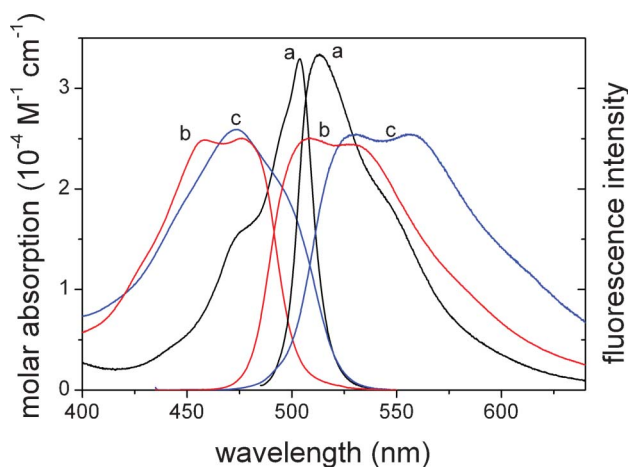


Fig. 4 Absorption and fluorescence spectra of compound **1** (a) and its nitro derivatives **3** (b) and **4** (c).

Table 2 Photophysical properties of reference compound **1** and its nitro derivatives (**3** and **4**) in cyclohexane and methanol. The full photophysical data in several solvents are listed in Table S2 (ESI†)

	λ_{ab} (nm)	ϵ_{max} ($M^{-1} cm^{-1}$)	λ_{fl} (nm)	ϕ	τ (ns)	k_{fl} ($10^{-8} s^{-1}$)	k_{nr} ($10^{-8} s^{-1}$)
c-Hexane							
1	504.0	33000	515.0	0.96	5.46	1.75	0.07
3	458.0	24000	509.0	0.53	3.13	1.70	1.49
	476.0	24000	530.0				
4	474.0	25000	530.5	0.17	1.53	1.11	5.42
			556.0				
Methanol							
1	495.5	25000	512.5	0.76	5.78	1.31	0.41
3	446.5	21000	509.5	0.17	1.54	1.10	5.39
			526.5				
4	462.5	20000	530.5	0.005	0.05 (91%) 1.73 (9%)	—	—

feasible. In fact, in some derivatives, the ICT emission is weakly detected in non-polar media. The ICT stabilization in polar media implies a loss of its fluorescence emission, because the consequent red-shift favors the non-radiative deactivation from the ICT state.^{20a} Moreover, the charge transfer could be as feasible as a “dark” charge separation (CS) state could be populated from the ICT state. In this state the charge transfer is so high that the charges are fixed and the electronic delocalization is stopped, hence contributing further to the loss of fluorescence emission.

The fluorescence quenching ability of the ICT state induced by the nitro group depends on the chromophoric position at which it is attached. In fact, its inclusion at position 5 led to a more drastic decrease in the fluorescence efficiency and lifetime than at position 6. Generally, in BODIPYs the dipole moment is located along the transversal axis with the positive charge density placed around the central position 8 and the negative charge density at the fluorine atoms (Fig. 6). Thus, the charge separation should be more effective upon incorporation of an electron acceptor group (nitro) at the bottom part of the BODIPY (position 5, compound **4**) than at the rest of the positions (*i.e.*, position 6, compound **3**). In fact, the presence of the nitro substituent significantly increases the theoretically calculated dipole moment of the molecule, from 6.6 D of the parent compound **1** to 11.6 D for derivative **3** and up to 12.8 D

for compound **4** (Fig. 6). These results indicate that the quenching effect of the ICT is more important in the derivative **4** where, in polar media, the fluorescence almost disappears (<0.01). Moreover, in this last derivative the decay curve becomes biexponential, with a main component characterized by a very fast lifetime (around 50 ps), which is attributed to the quenching of the fluorescence LE state by the ICT state, and a residual contribution of a lifetime around 1.5–2 ns, resembling that of the LE state. In more polar solvents such as 2,2,2-trifluoroethanol, the fluorescence quantum yield decreases, making an accurate deconvolution of the corresponding decay curve impossible.

Consequently, the nitro derivatives described herein work as polarity sensors due to the ICT state. They do not represent good laser dyes but, apart from being excellent starting points for further functionalization, they are very sensitive to the environmental polarity.

Amino and nitro derivatives of 8-tolyl BODIPY 2. The photophysics of the reference compound **2** are controlled by the presence of the phenyl ring in the *meso* position. The absence of substituents at adjacent positions enables free rotation of the aryl group. Such a motion greatly increased the internal conversion process, owing to vibrational couplings, causing a drastic decrease of the BODIPY fluorescence ability ($\phi < 0.05$ and $\tau < 400$ ps; see Table S3, ESI†). Moreover,

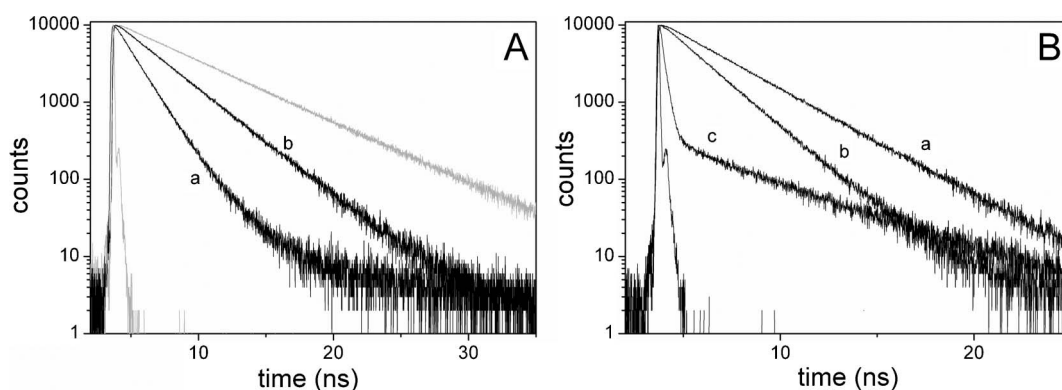


Fig. 5 (A) Fluorescence decay curve of compound **1** (grey) and its nitro derivatives **3** (b) and **4** (a) in cyclohexane. (B) Decay curves of compound **2** as a function of the solvent; cyclohexane (a), acetone (b) and F₃-ethanol (c).

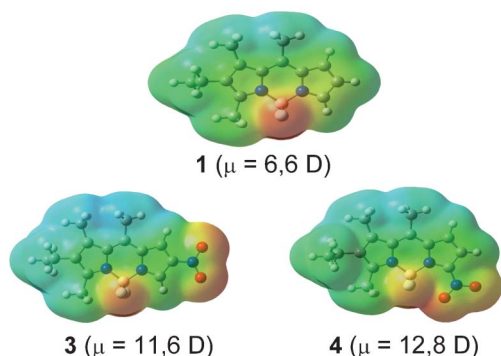


Fig. 6 Electrostatic potential mapped onto the electronic density for compound **1** and its nitro derivatives **3** and **4**. The corresponding calculated dipole moments are also included.

interaction between the phenyl and indacene electronic clouds could not be discarded and could further take part in the non-radiative deactivation processes.²¹

While the presence of an amine at position 5 in asymmetric compound **1** (dye **7**) led to a bathochromic spectral shift and kept the high fluorescence ability of the BODIPY, the presence of such a group in the 8-tolyl-BODIPY core (compound **8**) gave completely opposite results: a slight hypsochromic shift and a lower fluorescence efficiency ($\phi < 0.03$ and $\tau < 150$ ps; see Table S3, ESI†). Therefore, in this case, the electron releasing ability of the amine substituent increases the non-radiative deactivation processes. This donor resonant effect should increase the electronic charge at the BODIPY core, and hence, the deleterious effect in fluorescence of the phenyl free motion should be more important than in the above amino derivatives without such an 8-aryl group. The molecular orbitals of compound **8**, depicted in Fig. 7, show that transition from the HOMO to the LUMO state implies a shift of electronic density from the amino-BODIPY core to the phenyl ring. Considering the electron donor character of the amine and the ability of the phenyl group to behave as donor or acceptor depending on its substitution, the additional presence of a quenching ICT state should be operative. Indeed, in the most acidic media (2,2,2-trifluoroethanol), where the amine can be protonated and its electron donor ability should be lower, the highest fluorescence quantum yield is achieved, in concordance with a lower formation probability of the ICT state.

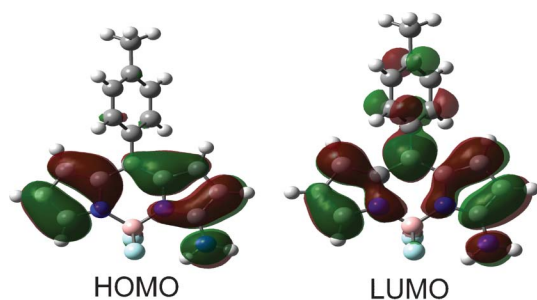


Fig. 7 HOMO and LUMO contour maps of compound **8**.

The vibrational resolution of the spectral bands upon nitration of the reference 8-tolyl-BODIPY (compound **6**) was not so marked as previously observed in the nitro derivatives of compound **1**. In this case, the spectral bands are similar to that shown by BODIPY dyes (see Fig. S2, ESI†), although they became broader in polar media. Once more, these features confirm that the nitro group tends to alter the vibrational resolution of the electronic transitions, and reinforce the above interpretation of the absence of spectral bands from any ICT state for derivative **6**, as well for **3** and **4**.

Surprisingly, whereas the nitration of alkyl BODIPY was very harmful to the fluorescence efficiency, the nitration of the 8-tolyl-BODIPY at position 5 (compound **6**) ameliorates the fluorescence ability of the chromophore (Fig. 8). The electron withdrawing character of the nitro group removes electronic density from the chromophore, including from the central position. Thus, the effect of the aryl free motion is reduced and the fluorescence efficiency is somewhat recovered.

The essential role of the electron character of the substituent in the fluorescence ability of derivatives bearing bulky groups with free motion should be noted. Taking into account the fact that the internal conversion processes have been associated with the structural rigidity/flexibility, the electron donor moieties (*i.e.* amine) increase the negative influence of such rotational freedom on the fluorescence while the electron acceptor ones (*i.e.* nitro) counteract this non-radiative pathway. To this aim, the most effective positions to be substituted are 3 and 5 (beginning and end of the delocalized π -system of the BODIPY).^{8j,15}

Following a similar behavior to that previous described and discussed for the nitro derivatives **3** and **4**, in the case of compound **6**, the electron withdrawing effect of the nitro group was so high that, in the more polar environments, the mentioned ICT state is more stabilized and effectively quenches its fluorescence emission (Fig. 8). In fact, the fluorescence quantum yield of dye **6** in methanol clearly

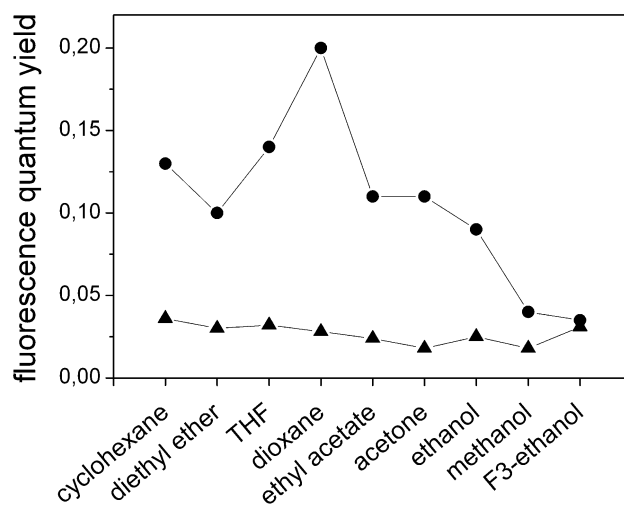


Fig. 8 Evolution of the fluorescence quantum yield of reference compound **2** (triangles) and its nitro derivative **6** (circles) in several solvents ordered by their polarity.

drops, to values as low as those of the reference compound **2**, and, simultaneously, the lifetime becomes shorter (around 500 ps in methanol, Table S3, ESI†). It should be mentioned that the decay curve of the nitro-derivative **6** is described as monoexponential even in polar media, while the nitration of compound **1** at the same position 5 (compound **4**) gave rise to a biexponential decay in polar solvents. Such behaviour should be related to the inherent high internal conversion probability induced by the aryl free motion in the derivatives of compound **2**, which reduces the influence of the ICT process in the fluorescence decay of dye **6**.

Lasing properties

The position of the absorption bands of the derivatives with amino substitution allows for studying their lasing properties under pumping at 532 nm. Under our experimental conditions (transversal excitation and strong focusing of the incoming pump radiation, see experimental section), the concentration of the dyes in the different solvents for the lasing studies should be in the millimolar range, so that the incoming pump radiation penetrates the sample (*i.e.* is absorbed) to a depth similar to that of the thickness of the pump stripe at the input face of the cell onto which the pumping radiation is focused (about 0.3 mm). This gives rise to an emitted beam with a near-circular cross-section and optimizes the lasing efficiency (ratio between the energy of the dye laser output and the pump energy incident on the sample surface).

Compound **9**, where the amino group was at position 6, was very unstable, as discussed above, when dealing with its photophysical properties, and its lasing behavior could not be characterized. Thus, only the lasing properties of compound **7**, with the amino group at position 5, could be studied. Although the highest fluorescence quantum yield of this compound was obtained in cyclohexane (Table S1, ESI†), it could not be dissolved in this apolar solvent at the concentrations required to obtain laser emission. Thus, the dependence of the laser emission on the concentration of the solvent was studied in ethyl acetate, which was the solvent where compound **7** exhibits the next highest quantum yield. It was found (Table 3) that the optimum concentration was 1.4×10^{-3} M, rendering a lasing efficiency of 29%. Lower and higher concentrations resulted in decreased lasing efficiency. This behavior of the emission efficiency is typical of lasing dyes. The lasing efficiency first increases with dye concentration up to a point from where further increases in concentration result in a decrease in the lasing efficiency, due to the increase in

reabsorption/re-emission processes. The growing importance of reabsorption/re-emission processes with dye concentration is also reflected in the progressive red-shift of the wavelength of the laser emission.

In Table 3 are also presented the efficiency and peak wavelength of the laser emission of compound **7** in polar aprotic and polar protic solvents at the determined optimum dye concentration. The lasing efficiencies correlate well with the dye photophysical properties in diluted solutions (Table S1, ESI†): the higher the fluorescence quantum yield, the higher the lasing efficiency, with the lowest efficiency being obtained in polar protic solvents. In this regard, it should be indicated that no laser emission was observed when the solvent was 2,2,2-trifluoroethanol.

Due to the hypsochromic shift of the absorption bands in the nitro derivatives, their lasing properties were first studied under pumping at 355 nm, which is the usual pump wavelength for dyes emitting in the blue spectral region. Once again, although the highest fluorescence quantum yields of the nitro derivatives **3** and **4** were obtained in apolar solvent cyclohexane, these compounds could not be dissolved in this solvent at the high concentrations needed for laser operation under the transversal pumping arrangement.

Compound **4** did not exhibit laser action, even under our drastic pumping conditions, which was to be expected taking into account the low fluorescence efficiency of this dye in all solvents (see Table S2, ESI†). Compound **3** did exhibit laser action, albeit with efficiencies of less than 10% under the 355 nm pumping (Table 4). From Table S2, ESI† and Fig. 3, it is seen that although the absorption bands of the nitro derivatives are blue shifted, away from the typical pump wavelength of 532 nm, the shift is not enough to move the bands as far away as 355 nm, so that absorption at this wavelength is rather low. Higher lasing efficiency would be expected if the nitro derivatives are pumped at or near the maximum of their absorption bands. Thus, we used a Coumarin 460-based dye laser, working at 450 nm (see experimental section), to pump compound **3** at the peak of its absorption band. As can be seen in Table 4, under these conditions the lasing efficiency of this compound in ethyl acetate doubled to 18%. This lasing efficiency is still lower than those obtained with the amino derivatives (Table 3), as is to be expected given the lower fluorescence quantum yields of

Table 3 Maximum wavelength of the laser emission (λ_{la}) and lasing efficiency (Eff) of compound **7** as a function of the concentration in ethyl acetate and in different solvents at a given concentration. Pump wavelength was 532 nm

Solvent	<i>c</i> (mM)	λ_{la} (nm)	Eff (%)
Ethyl acetate	0.8	563	24
	1.4	564	29
	1.9	568	20
	2.8	568	14
Methanol	1.4	558	12
Acetone	1.4	573	20
DCM	1.4	576	23

Table 4 Maximum wavelength of the laser emission (λ_{la}) and lasing efficiency (Eff) of compound **3** as a function of the concentration in ethyl acetate and in different solvents at a given concentration

Solvent	λ_{pump}^a (nm)	<i>c</i> (mM)	λ_{la} (nm)	Eff (%)
Ethyl acetate	355	2.2	534	9
	355	4.5	539	7
	355	6.7	540	4
Ethyl acetate	450	2.2	537	11
	450	4.5	538	18
	450	6.7	540	16
	450	4.5	534	8
Methanol	450	4.5	539	5

^a λ_{pump} : pump wavelength.

compound **3** with respect to those of compound **7** (Tables S1 and S2, ESI†). When compound **3** is dissolved in acetone or methanol its lasing efficiency decreases, in good correlation with the photophysical properties (lower fluorescence quantum yields in these solvents than in ethyl acetate).

The 8-tolyl BODIPYs, derivatives of compound **2** with amino or nitro groups at position 4 (compounds **8** and **6**, respectively), have very low fluorescence quantum yields (Table S3, ESI†) in all solvents and, correspondingly, their laser emission was very inefficient. Under 355 nm pumping and at the optimum concentration of 2×10^{-3} M, compound **8** lased at 550 nm with an efficiency of just 1%, whereas compound **6**, which has somewhat higher fluorescence quantum yields, emitted laser radiation at 563 nm with an efficiency of 4%.

Conclusion

The present work highlights the essential role of the nature and position of the substituent, as well as the molecular structure of the indacene core, in the optical properties of BODIPYs. In this sense, the same functional group may lead to entirely opposite results, just by varying the position in which it is incorporated to the chromophore and/or the molecular structure of the core. The amine group at position 3 led to a modest red shift, but the same group at position 8 led to a large hypsochromic shift. On the other hand, the strong withdrawing character of the nitro group induced intramolecular charge transfer processes in the excited state, where the quenching effect over the fluorescence emission depends strongly on the position in which it is added to the indacene core. In spite of this, laser action has been demonstrated in both amine and nitro derivatives, with lasing properties exhibiting good correlation with the photophysical properties.

Furthermore, the amino and nitro derivatives described herein are excellent precursors, from a synthetic point of view, to design BODIPY derivatives with different functionalizations.

Experimental section

Materials

Starting materials and reagents used in the preparation of BODIPYs are commercially available. The solvents were dried and distilled before use.

Synthesis of BODIPY 1–9

BODIPY dyes **1**¹⁴ and **2**¹⁵ were synthesized by the methods previously described. These compounds were transformed in the corresponding nitro BODIPYs **3–6** by treatment with $\text{HNO}_3/\text{Ac}_2\text{O}$. By means of a catalytic hydrogenation over Pd on charcoal, the nitro derivatives **4** and **6** can be easily reduced to the corresponding amino BODIPYs **7** and **8**. The syntheses and spectroscopic data for all compounds are described in the ESI.†

Characterization of the new dyes

Spectral data of the known compounds were in accordance with the literature data. Flash column chromatography was performed using silica gel Merck 60 (230–400 mesh). ^1H and ^{13}C NMR spectra were recorded with a Bruker Avance-DPX-300 spectrometer (300 MHz for ^1H and 75 MHz for ^{13}C) and a Bruker Avance III spectrometer (700 MHz for ^1H and 176 MHz for ^{13}C). Chemical shift multiplicities are reported as s = singlet, d = doublet, t = triplet, q = quartet and m = multiplet. IR spectra (in cm^{-1}) were recorded in a Bruker Tensor-27-FTIR spectrophotometer. Melting points were determined in open capillaries and are uncorrected. High resolution mass spectra were determined by ESI (electrospray ionization) in a FTMS Bruker APEX Q IV and by EI (electron impact) in a Thermofisher MAT 95 XP (see ESI†).

Photophysical properties

The photophysical properties were registered in dilute solutions (around 2×10^{-6} M), prepared by adding the corresponding solvent to the residue from the adequate amount of concentrated stock solution in acetone, after vacuum evaporation of this solvent. UV-Vis absorption and fluorescence spectra were recorded on a Varian model CARY 4E spectrophotometer and a SPEX Fluorolog 3-22 spectrofluorimeter, respectively. The fluorescence spectra were corrected from the wavelength dependence of the detector sensibility. The fluorescence quantum yield (ϕ) was obtained using a methanolic solution of PM567 as a reference ($\phi^{\text{F}}=0.91$). Radiative decay curves were registered with the time correlated single-photon counting technique (Edinburgh Instruments, model FL920) using a microchannel plate detector (Hamamatsu C4878), with picosecond time resolution (~ 20 ps). Fluorescence emission was monitored at the maximum emission wavelength after excitation at 410, 440 and 470 nm by means of a diode laser (PicoQuant, model LDH410, 440 and 470, respectively) with 150 ps FWHM pulses. The fluorescence lifetime (τ) was obtained from the slope after the deconvolution of the instrumental response signal from the recorded decay curves by means of an iterative method. The closeness of the exponential fit was controlled by statistical parameters (chi-square, Durbin–Watson and the analysis of the residuals). The radiative (k_{r}) and non-radiative deactivation (k_{nr}) rate constants were calculated by means of: $k_{\text{r}} = \phi/\tau$ and $k_{\text{nr}} = (1 - \phi)/\tau$, respectively.

Laser experiments

Liquid solutions of dyes were contained in 1 cm optical-path length cells, which were carefully sealed to avoid solvent evaporation during the experiments. The dye solutions were transversely pumped with nanosecond pulses either at 532 nm (6 ns FWHM and 5.5 mJ/pulse) or at 355 nm (8 ns FWHM and 3.5 mJ/pulse). The source of the 532 nm pulses was a frequency-doubled Q-switched Nd:YAG laser (Monocrom OPL-10). The 355 nm pulses were the third harmonic of a Q-switched Nd:YAG laser (Spectron SL282G). In both cases the excitation pulses were line-focused onto the cell, providing pump fluences on the active medium of 180 mJ cm^{-2} and 110 mJ cm^{-2} for 532 nm and 355 nm pumping, respectively. The

oscillation cavity (2 cm in length) consisted of a 90% reflectivity back aluminum mirror and the lateral face of the cell as an output coupler. Experiments were also performed at a pump wavelength of 450 nm, with 12 ns, 3 mJ pulses from a dye laser (ethanolic solution of Coumarin 460 pumped with the Spectron SL282G 355 nm pulses). The energy of dye and pump laser pulses was measured with GenTec ED-100A and ED-200 pyroelectric energy meters. The spectral characteristics of the laser emission were determined by collecting a fraction of the emission by an optical fiber attached to the input slit of a spectrograph/monochromator (SpectraPro-300i, Acton Research Corporation) equipped with a charge-coupled device (CCD)/SpectruMM:GS 128B).

Acknowledgements

This work was supported by Projects MAT2010-20646-C04-01, -02 and -04 and TRACE 2009-0144 of the Spanish Ministerio de Economía y Competitividad (MINECO). Ixone Esnal thanks the Gobierno Vasco for predoctoral contracts (S-PE10UN65, SPE11UN064, SPE12UN140 and IT339-10)

References

- (a) A. Loudet and K. Burgess, *Chem. Rev.*, 2007, **107**, 4891–4932; (b) R. Ziessel, G. Ulrich and A. Harriman, *New J. Chem.*, 2007, **31**, 496–501; (c) G. Ulrich, R. Ziessel and A. Harriman, *Angew. Chem., Int. Ed.*, 2008, **47**, 1184–1201; (d) F. L. Arbeloa, J. Bañuelos, V. Martínez, T. Arbeloa and I. L. Arbeloa, *Trends Phys. Chem.*, 2008, **13**, 101–122; (e) A. C. Benniston and G. Copley, *Phys. Chem. Chem. Phys.*, 2009, **11**, 4124–4131; (f) M. Benstead, G. H. Mehl and R. W. Boyle, *Tetrahedron*, 2011, **67**, 3573–3601; (g) N. Boens, V. Leen and W. Dehaen, *Chem. Soc. Rev.*, 2012, **41**, 1130–1172.
- (a) K. Rurack, M. Kollmannsberger and J. Daub, *Angew. Chem., Int. Ed.*, 2001, **40**, 385–387; (b) O. Buyukcakir, O. A. Bozdemir, S. Kolemen, S. Erbas and E. U. Akkaya, *Org. Lett.*, 2009, **11**, 4644–4647; (c) O. A. Bozdemir, R. Guliyev, O. Buyukcakir, S. Selcuk, S. Kolemen, G. Gulseren, T. Nalbantoglu, H. Boyaci and E. U. Akkaya, *J. Am. Chem. Soc.*, 2010, **132**, 8029–8036; (d) T. Bura, P. Retailleau and R. Ziessel, *Angew. Chem., Int. Ed.*, 2010, **49**, 6659–6663; (e) S. Kolemen, O. A. Bozdemir, Y. Cakmak, G. Barin, S. Erten-Ela, M. Marszalek, J.-H. Yum, S. M. Zakeeruddin, M. K. Nazeeruddin, M. Grätzel and E. U. Akkaya, *Chem. Sci.*, 2011, **2**, 949–954; (f) T. Bura, P. Retailleau, G. Ulrich and R. Ziessel, *J. Org. Chem.*, 2011, **76**, 1109–1117; (g) O. A. Bozdemir, S. Erbas-Cakmak, O. O. Ekiz, A. Dana and E. U. Akkaya, *Angew. Chem., Int. Ed.*, 2011, **50**, 1–7; (h) H. He, P.-C. Lo, S.-L. Yeung, W.-P. Fong and D. K. P. Ng, *Chem. Commun.*, 2011, **47**, 4748–4750; (i) T. Bura, D. Hablot and R. Ziessel, *Tetrahedron Lett.*, 2011, **52**, 2370–2374; (j) N. Boens, W. Qin, M. Baruah, W. M. De Borggraeve, A. Filarowski, N. Smisdom, M. Ameloot, L. Crovetto, E. M. Talavera and J. M. Alvarez-Pez, *Chem.–Eur. J.*, 2011, **17**, 10924–10934; (k) S. Zhu, J. Zhang, G. Vegesna, A. Tiwari, F.-T. Luo, M. Zeller, R. Luck, H. Li, S. Green and H. Liu, *RSC Adv.*, 2012, **2**, 404–407; (l) J.-H. Olivier, J. Barberá, E. Bahaidarah, A. Harriman and R. Ziessel, *J. Am. Chem. Soc.*, 2012, **134**, 6100–6103; (m) C. W. Evans, M. J. Latter, D. Ho, S. A. M. A. Peerzade, T. D. Clemons, M. Fitzgerald, S. A. Dunlop and K. S. Iyer, *New J. Chem.*, 2012, **36**, 1457–1462.
- A. Haeefe, C. Zedde, P. Retailleau, G. Ulrich and R. Ziessel, *Org. Lett.*, 2010, **12**, 1672–1675.
- (a) T. Rohand, M. Baruah, W. Qin, N. Boens and W. Dehaen, *Chem. Commun.*, 2006, 266–268; (b) L. Li, B. Nguyen and K. Burgess, *Bioorg. Med. Chem. Lett.*, 2008, **18**, 3112–3116; (c) Ö. Dilek and S. L. Bane, *Tetrahedron Lett.*, 2008, **49**, 1413–1416; (d) E. Fron, E. Coutiño-Gonzalez, L. Pandey, M. Sliwa, M. Van der Auweraer, F. C. De Schryver, J. Thomas, Z. Dong, V. Leen, M. Smet, W. Dehaen and T. Vosch, *New J. Chem.*, 2009, **33**, 1490–1496; (e) W. Qin, V. Leen, W. Dehaen, J. Cui, C. Xu, X. Tang, W. Liu, T. Rohand, D. Beljonne, B. Van Averbeke, J. N. Clifford, K. Driesen, K. Binnemans, M. Van der Auweraer and N. Boens, *J. Phys. Chem. C*, 2009, **113**, 11731–11740; (f) L. Jiao, C. Yu, M. Liu, Y. Wu, K. Cong, T. Meng, Y. Wang and E. Hao, *J. Org. Chem.*, 2010, **75**, 6035–6038; (g) L. Jiao, C. Yu, T. Uppal, M. Liu, Y. Li, Y. Zhou, E. Hao, X. Hu and M. G. H. Vicente, *Org. Biomol. Chem.*, 2010, **8**, 2517–2519; (h) V. Leen, T. Leemans, N. Boens and W. Dehaen, *Eur. J. Org. Chem.*, 2011, **23**, 4386–4396; (i) O. Dilek and S. L. Bane, *J. Fluoresc.*, 2011, **21**, 347–354; (j) M. Zhang, E. Hao, J. Zhou, C. Yu, G. Bai, F. Wang and L. Jiao, *Org. Biomol. Chem.*, 2012, **10**, 2139–2145; (k) X. Li, S. Huang and Y. Hu, *Org. Biomol. Chem.*, 2012, **10**, 2369–2372; (l) G. Ulrich, A. Haeefe, P. Retailleau and R. Ziessel, *J. Org. Chem.*, 2012, **77**, 5036–5048.
- (a) T. Rohand, W. Qin, N. Boens and W. Dehaen, *Eur. J. Org. Chem.*, 2006, 4658–4663; (b) W. Qin, T. Rohand, W. Dehaen, J. N. Clifford, K. Driesen, D. Beljonne, B. Van Averbeke, M. Van der Auweraer and N. Boens, *J. Phys. Chem. A*, 2007, **111**, 8588–8597; (c) S. Rihn, P. Retailleau, N. Bugsaliewicz, A. De Nicola and R. Ziessel, *Tetrahedron Lett.*, 2009, **50**, 7008–7013; (d) R. Guliyev, A. Coskun and E. U. Akkaya, *J. Am. Chem. Soc.*, 2009, **131**, 9007–9013; (e) O. A. Bozdemir, Y. Cakmak, F. Sozmen, T. Ozdemir, A. Siemiarczuk and E. U. Akkaya, *Chem.–Eur. J.*, 2010, **16**, 6346–6351; (f) M. J. Ortiz, I. Garcia-Moreno, A. R. Agarrabertia, G. Duran-Sampedro, A. Costela, R. Sastre, F. López Arbeloa, J. Bañuelos Prieto and I. López Arbeloa, *Phys. Chem. Chem. Phys.*, 2010, **12**, 7804–7811; (g) C. Thivierge, J. Han, R. M. Jenkins and K. Burgess, *J. Org. Chem.*, 2011, **76**, 5219–5228; (h) T. K. Khan and M. Ravikant, *Tetrahedron*, 2011, **67**, 5816–5824; (i) Y. Wu, X. Ma, J. Jiao, Y. Cheng and C. Zhu, *Synlett*, 2012, **23**, 778–782.
- (a) C. Thivierge, R. Bandichhor and K. Burgess, *Org. Lett.*, 2007, **9**, 2135–2138; (b) J. Chen, M. Mizumura, H. Shinokubo and A. Osuka, *Chem.–Eur. J.*, 2009, **15**, 5942–5949; (c) V. Leen, V. Zaragozaí Gonzalvo, W. M. Deborggraeve, N. Boens and W. Dehaen, *Chem. Commun.*, 2010, **46**, 4908–4910; (d) V. Leen, M. Van der Auweraer, N. Boens and W. Dehaen, *Org. Lett.*, 2011, **13**, 1470–1473; (e) B. Verbelen, V. Leen, L. Wang, N. Boens and W. Dehaen, *Chem. Commun.*, 2012, **48**, 9129–9131.
- (a) T. V. Goud, A. Tutar and J.-F. Biellmann, *Tetrahedron*, 2006, **62**, 5084–5091; (b) E. Peña-Cabrera, A. Aguilar-Aguilar, M. González-Domínguez, E. Lager, R. Zamudio-

- Vázquez, J. Godoy-Vargas and F. Villanueva-García, *Org. Lett.*, 2007, **9**, 3985–3988; (c) J. Han, O. Gonzalez, A. Aguilar-Aguilar, E. Peña-Cabrera and K. Burgess, *Org. Biomol. Chem.*, 2009, **7**, 34–36; (d) E. Lager, J. Liu, A. Aguilar-Aguilar, B. Z. Tang and E. Peña-Cabrera, *J. Org. Chem.*, 2009, **74**, 2053–2058; (e) C. F. A. Gómez-Durán, I. García-Moreno, A. Costela, V. Martín, R. Sastre, J. Bañuelos, F. López Arbeloa, I. López Arbeloa and E. Peña-Cabrera, *Chem. Commun.*, 2010, **46**, 5103–5105; (f) I. J. Arroyo, R. Hu, B. Z. Tang, F. I. López and E. Peña-Cabrera, *Tetrahedron*, 2011, **67**, 7244–7250.
- 8 (a) L. Li, J. Han, B. Nguyen and K. Burgess, *J. Org. Chem.*, 2008, **73**, 1963–1970; (b) L. Bonardi, G. Ulrich and R. Ziesel, *Org. Lett.*, 2008, **10**, 2183–2186; (c) Ö. A. Bozdemir, O. Büyükcakir and E. U. Akkaya, *Chem.-Eur. J.*, 2009, **15**, 3830–3838; (d) K. Krumova and G. Cosa, *J. Am. Chem. Soc.*, 2010, **132**, 17560–17569; (e) S. Rihn, M. Erdem, A. De Nicola, P. Retailleau and R. Ziesel, *Org. Lett.*, 2011, **13**, 1916–1919; (f) R. P. Sabatini, T. M. McCormick, T. Lazarides, K. C. Wilson, R. Eisenberg and D. W. McCamant, *J. Phys. Chem. Lett.*, 2011, **2**, 223–227; (g) C. Yu, L. Jiao, H. Yin, J. Zhou, W. Pang, Y. Wu, Z. Wang, G. Yang and E. Hao, *Eur. J. Org. Chem.*, 2011, 5460–5468; (h) L. Jiao, W. Pang, J. Zhou, Y. Wei, X. Mu, G. Bai and E. Hao, *J. Org. Chem.*, 2011, **76**, 9988–9996; (i) Y. Hayashi, S. Yamaguchi, W. Y. Cha, D. Kim and H. Shinokubo, *Org. Lett.*, 2011, **13**, 2992–2995; (j) M. J. Ortiz, A. R. Agarrabeitia, G. Duran-Sampedro, J. Bañuelos Prieto, T. Arbeloa Lopez, W. A. Massad, H. A. Montejano, N. A. García and I. Lopez Arbeloa, *Tetrahedron*, 2012, **68**, 1153–1162.
- 9 (a) A. Harriman, L. Mallon and R. Ziesel, *Chem.-Eur. J.*, 2008, **14**, 11461–11473; (b) T. W. Hundnall, T.-P. Lin and F. P. Gabbañ, *J. Fluorine Chem.*, 2010, **131**, 1182–1186; (c) J.-H. Olivier, A. Haefele, P. Retailleau and R. Ziesel, *Org. Lett.*, 2010, **12**, 408–411; (d) C. A. Wijesinghe, M. E. El-Khouly, J. D. Blakemore, M. E. Zandler, S. Fukuzumi and F. D'Souza, *Chem. Commun.*, 2010, **46**, 3301–3303; (e) T. Bura and R. Ziesel, *Org. Lett.*, 2011, **13**, 3072–3075; (f) X.-D. Jiang, J. Zhang, T. Furuyama and W. Zhao, *Org. Lett.*, 2012, **14**, 248–251; (g) T. Lundrigan, S. M. Crawford, T. S. Cameron and A. Thompson, *Chem. Commun.*, 2012, **48**, 1003–1005.
- 10 M. Shah, K. Thangaraj, M.-L. Soong, L. T. Wolford, J. H. Boyer, R. Politzer and T. G. Pavlopoulos, *Heteroat. Chem.*, 1990, **1**, 389–399.
- 11 T. Suzuki, T. Tanaka, I. Higashiguchi and A. Oda, *JP Patent 11176572*, 1999.
- 12 K. Takuma, T. Misawa, K. Sugimoto, T. Nishimoto, H. Tsukahara and K. Takuma, *JP Patent 10273504*, 1998.
- 13 T. Tachikawa, N. Wang, S. Yamashita, S.-C. Cui and T. Majima, *Angew. Chem., Int. Ed.*, 2010, **49**, 8593–8597.
- 14 J. Bañuelos Prieto, A. R. Agarrabeitia, I. Garcia-Moreno, I. Lopez-Arbeloa, A. Costela, L. Infantes, M. E. Perez-Ojeda, M. Palacios-Cuesta and M. J. Ortiz, *Chem.-Eur. J.*, 2010, **16**, 14094–14105.
- 15 A. Cui, X. Peng, J. Fan, X. Chen, Y. Wu and B. Guo, *J. Photochem. Photobiol., A*, 2007, **186**, 85–92.
- 16 H. Oda, T. Hanami, T. Iwashita, M. Kojima, M. Itoh and Y. Hayashizaki, *Tetrahedron*, 2007, **63**, 12747–12753.
- 17 A. R. Katritzky, K. Suzuki, S. K. Singh and H.-Y. He, *J. Org. Chem.*, 2003, **68**, 5720–5723.
- 18 W. Qin, V. Leen, T. Rohand, W. Dehaen, P. Dedecker, M. Van der Auweraer, K. Robeyns, L. Van Meervelt, D. Beljonne, B. Van Averbeke, J. N. Clifford, K. Driesen, K. Binnemans and N. Boens, *J. Phys. Chem. A*, 2009, **113**, 439–447.
- 19 J. Bañuelos, V. Martin, C. F. A. Gómez-Durán, I. J. Arroyo-Córdoba, E. Peña-Cabrera, I. García-Moreno, A. Costela, M. E. Pérez-Ojeda, T. Arbeloa and I. López Arbeloa, *Chem.-Eur. J.*, 2011, **17**, 7261–7270.
- 20 (a) M. Kollmannsberger, K. Rurack, U. Resch-Genger and J. Daub, *J. Phys. Chem. A*, 1998, **102**, 10211–10220; (b) Z. R. Grabowski, K. Rotkiewicz and W. Rettig, *Chem. Rev.*, 2003, **103**, 3899–4032; (c) W. Qin, M. Baruah, M. Van der Auweraer, F. C. De Schryver and N. Boens, *J. Phys. Chem. A*, 2005, **109**, 7371–7384.
- 21 H. L. Kee, C. Kirmaier, L. Yu, P. Thamyongkit, W. J. Youngblood, M. E. Calder, L. Ramos, B. C. Noll, D. F. Bocian, W. E. Scheidt, R. R. Birge, J. S. Lindsey and D. Holten, *J. Phys. Chem. B*, 2005, **109**, 20433–20443.

Selective Lateral Lithiation of Methyl BODIPYs: Synthesis, Photophysics, and Electrochemistry of New *Meso* Derivatives

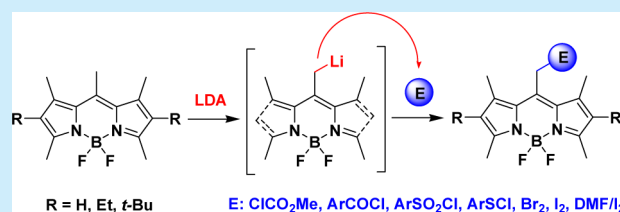
Eduardo Palao,[†] Santiago de la Moya,^{*,†} Antonia R. Agarrabeitia,[†] Ixone Esnal,[‡] Jorge Bañuelos,[‡] Íñigo López-Arbeloa,[‡] and María J. Ortiz^{*,†}

[†]Departamento de Química Orgánica I, Facultad de Ciencias Químicas, Universidad Complutense de Madrid, Ciudad Universitaria s/n, 28040 Madrid, Spain

[‡]Departamento de Química Física, Universidad del País Vasco-EHU, Apartado 644, 48080 Bilbao, Spain

S Supporting Information

ABSTRACT: Selected *meso* BODIPYs (chemically reactive, difficult to obtain by established procedures, or photophysically or electrochemically attractive) have been obtained by unprecedented selective lateral lithiation of 8-methylBODIPYs. The physical study of the obtained new *meso* BODIPYs reveals interesting tunable properties related to the activation of intramolecular charge-transfer processes, endorsing the new synthetic methodology as useful for the development of smarter BODIPY dyes for technological applications.



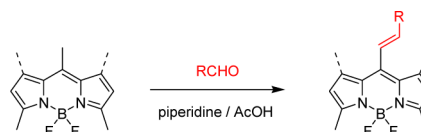
4,4-Difluoro-4-bora-3a,4a-diaza-*s*-indacene (BODIPY) dyes are a well-known family of fluorophores with significant use in lasing, sensing, bioimage, photodynamic therapy, or optoelectronics, among other valuable photonic applications.¹ This is due to three main factors: (1) excellent photophysical properties coming from the BODIPY chromophore, (2) high solubility in organic solvents improving processability steps required for the development of specific dyed materials (i.e., organic films), and (3) a core that can be selectively functionalized, allowing the fine modulation of its photophysical signature.^{1–5} In relation with the latter, some of the most successful BODIPY transformations involve selective electrophilic aromatic substitution (generally halogenations at C2/6, but also at other positions),² nucleophilic aromatic substitution (mainly of halogen at C3/5),³ nucleophile substitution at boron (mainly to prepare *C*- and *O*-BODIPYs),⁴ as well as metal-catalyzed C–C cross couplings in different positions (mainly involving haloBODIPYs and palladium).⁵

C8-functionalized (*meso*) BODIPYs constitute an important subclass within the BODIPY family due to their success in certain photonic applications (e.g., molecular probing or ratiometric sensing by fluorescence signaling).⁶ Some functionalities (e.g., bromoalkyl or chloroalkyl) can be introduced in the BODIPY *meso* position when its core is being constructed (i.e., before boron complex formation).⁷ However, interesting *meso* BODIPYs for specific photophysical applications cannot be easily achieved by this way.⁸ This fact has promoted a special interest in the development of synthetic procedures to *meso* BODIPYs from more accessible BODIPY precursors.⁹

Along these lines, it is known that 8-methylBODIPYs undergo Knoevenagel-like reaction with aldehydes to yield the corresponding *meso*-alkenyl derivatives.¹⁰ Interestingly, it is also known that 3,5,8-trimethylBODIPY and 1,3,5,7,8-pentamethyl-BODIPY undergo the reaction regioselectively at the *meso*

methyl (Scheme 1),^{10b} which demonstrates the higher enamine-like reactivity of that methyl when compared with those located

Scheme 1. Knoevenagel-like Reactivity of Selected 8-MethylBODIPYs



at C3/5 or C1/7. These results prompted us to investigate the selective enamine-like chemistry of 8-methylBODIPYs, aimed at expanding the available synthetic methods to valuable *meso* BODIPYs.

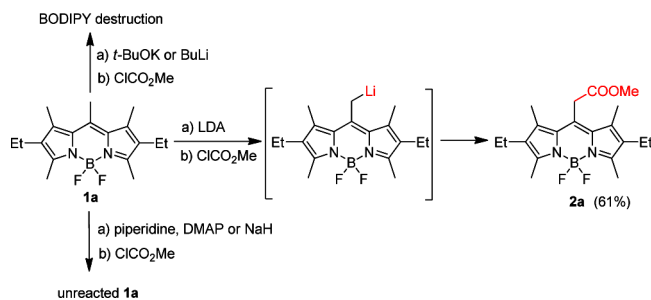
Our first objective was to explore the acylation of 8-methylBODIPYs, since the expected 8-(2-oxoethyl)BODIPYs are unknown and potentially interesting due to the well-known chemistry and photophysics of the carbonyl group. For this purpose, commercial **1a** was used as starting *meso*-methyl BODIPY and highly reactive methyl chloroformate as acylating reagent (Scheme 2). Different common bases and reaction conditions were explored (see Scheme 2; note that five methyl groups are potentially reactive).

Treatment of **1a** with piperidine, DMAP, or NaH in different solvents and conditions and then addition of methyl chloroformate resulted in the recovery of **1a** (Scheme 2). On the other hand, the use of *t*-BuOK or BuLi led to the destruction of the BODIPY framework. In the case of *t*-BuOK, *O*-nucleophilic attack on the boron center, and then boron

Received: May 26, 2014

Published: August 25, 2014

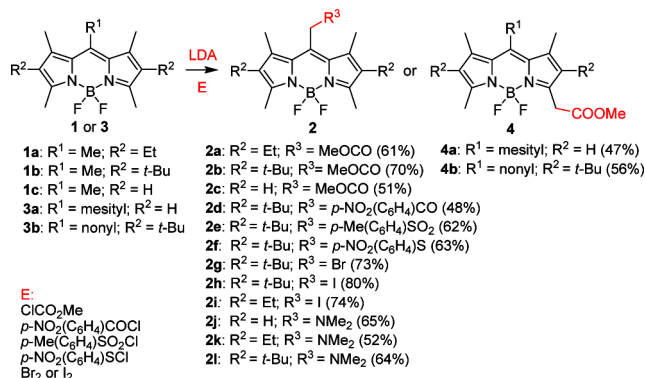
Scheme 2. Approaches for Methoxycarbonylation at *Meso* Methyl in **1a** (See the Supporting Information for More Details)



decomplexation during the final hydrolysis step, should explain the observed result (the corresponding unstable dipyrromethene was detected by NMR).¹¹ For BuLi, C-nucleophilic attack at C8, giving place to an undetected difluoroboradipyrromethane salt, is a highly plausible explanation for the observed BODIPY destruction.¹²

Satisfactorily, the use of LDA resulted in the formation of **2a** (Scheme 2), which constitutes the first example of BODIPY chemistry based on its selective lateral lithiation.¹³ To study the scope of this procedure, different BODIPYs and electrophiles (E) were essayed (Scheme 3).

Scheme 3. Selective Lithiation–Functionalization of **1** and **3** (See the Supporting Information for Details)



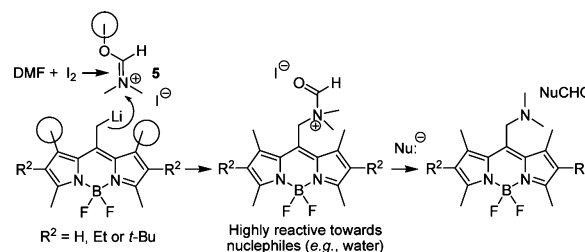
The initially tested BODIPYs were the commercially available PMS67, PMS97, and PMS46 (**1a–c**, respectively), while the initially chosen E (molecular halogens, and acyl, sulfonyl, and sulfonyl chlorides) were selected on the basis of the potential chemical,¹⁴ electrochemical,¹⁵ or photophysical interest¹⁶ of the expected reaction products. All the conducted reactions took place selectively at the *meso* position (see **2a–i** in Scheme 3), with the exception of the halogenation reaction of **1c**, which gave place to the corresponding 2,6-dihalobODIPY^{2a} (iodination was tested). This result is explained by the appropriate location of unsubstituted BODIPY positions (CH) with respect to the lithiated methyl,¹⁷ joined to the known BODIPY ability to undergo electrophilic aromatic substitution at C2/C6.² It must be noted nonetheless that, in the rest of the essayed cases, neither functionalization at a different methyl nor polyfunctionalization was detected.

Expectedly, the absence of *meso*-methyl entails the selective lithiation of methyl group at C3/C5, yielding the corresponding functionalized BODIPY after electrophilic treatment. Thus, the methoxycarbonylation of *meso*-mesitylated **3a** selectively yielded

4a (Scheme 3). More interesting is the related reaction of *meso*-nonylated **3b**, since α -functionalization of the *meso* group is now possible (Scheme 3). However, the decrease of the acidity, and also the increase of the sterical hindrance, of the nonyl C8-methylene explains the observed formation of **4b**.

Trying to find appropriate conditions to achieve the *meso*-methyl halogenation of **1c**, we observed that the use of *N,N*-dimethylformamide/I₂ (DMF/I₂) surprisingly led to the formation of **2j** (see Scheme 3). It must be noted that DMF alone does not react as electrophile in the used reaction conditions (see the Supporting Information, SI). The same reactivity was tested for **1a** and **1b** (products **2k** and **2l**, respectively, in Scheme 3). Although the observed reactivity is striking (unprecedented up to our knowledge), it should be noted that all the obtained dimethylamino derivatives were isolated with good yields (52–65%, see Scheme 3). This fact discards the possible initial formation of the corresponding iodoBODIPY (e.g., **2i**), giving place to the observed final product by reaction with dimethylamine as a trace reagent in the reaction media. Nonetheless, the presence of dimethylamine has been also discarded (see the SI). On the other hand, the observed dimethylamination does not work when DMF/Br₂ is used instead of DMF/I₂ (**1a** and **1b** were tested). In this case, *meso*-methyl bromination takes place exclusively (probably due to the higher electrophilic character of bromine). Moreover, no reaction was observed when *N,N*-diisopropylformamide (DIPF) was used instead of DMF. These results suggest that iminium cation **5** (formed by the electrophilic attack of iodine on the formamide carbonyl) is involved as the *N*-electrophilic reagent quenching the lithiated BODIPY (Scheme 4; see the SI for experimental evidence supporting the proposed mechanism).

Scheme 4. Reactivity of Laterally Lithiated BODIPYs with DMF/I₂ (Circles Highlight Steric Hindrance)



The “inverted” reactivity of **5** (*N*- instead of *C*-electrophile) is explained by a double-regioselective control exerted by both reactive partners. Thus, the bulky iodine of **5** blocks its carbon center against the nucleophilic attack of an, also hindered, lithiated BODIPY, which results in the preferential reaction of the nitrogen center (Scheme 4). Thus, shielding the nitrogen of **5**, by changing its methyl groups by isopropyls (DIPF instead of DMF), results in the observed lack of reactivity.

The photophysics of the new *meso* BODIPYs was found to be ruled by the electron-donating/withdrawing properties of the group located at the *meso* methyl and the BODIPY core itself. Thus, the strong *n* electron-donating dimethylamino group of **2j–l**, albeit separated from the BODIPY core by a methylene unit, promotes a drastic fluorescence quenching in these derivatives when compared to the corresponding parent (unsubstituted) BODIPYs (e.g., see **2k** vs **1a**, and **2l** vs **1b** in Table 1; see also Table S1 and Figures S1–S3, SI). This result can be explained by the activation of an intramolecular charge-

Table 1. Photophysical Properties of *meso*-BODIPYs 2a,b and 2k,l and Parent BODIPYs 1a,b^{a,b}

	λ_{ab} (nm)	ϵ_{max} (M ⁻¹ cm ⁻¹)	λ_{fl} (nm)	ϕ	τ_1 (ns)	$\Delta\nu_{St}$ (cm ⁻¹)
1a	518.5	83000	534.0	0.79	5.63	560
2a	547.0	63000	563.0	0.71	6.13	520
2k	536.0	57000	547.0	0.05	0.24 ^c	375
1b	525.0	78000	566.5	0.33	4.15	1395
2b	554.0	57000	586.0	0.11	1.29 ^c	985
2l	541.5	66000	602.0	0.03	0.39 ^c	1855

^aTetrahydrofuran solution. ^bFor full detailed data, see Table S1 (Supporting Information). ^cMain lifetime from biexponential fits.

transfer (ICT) process. Indeed, the fluorescence efficiency was recovered after protonation (**2j** was tested).^{6b,g} Conversely, the introduction of electron-withdrawing methoxycarbonyl at the *meso* methyl in **1a** and **1c**, to give **2a** and **2c**, respectively, retains the fluorescence ability of the parent BODIPY (cf. **2a** vs **1a** in Table 1 and in Figure S1, SI; cf. **2c** vs **1c** in Table S1 and Figure S2, SI). The same fact occurs when methoxycarbonyl is introduced at the C5-methyl instead of the *meso* methyl (see **4a** in Table S1, SI). However, locating the same group at the *meso* methyl in di-*tert*-butylated **1b**, to give **2b**, quenches the fluorescence (cf. **2b** vs **1b** in Table 1 and in Figure S3, SI). The last effect is also observed by locating the same group at the C5-methyl in **1b** (see **4b** in Table S1, SI).

Interestingly, it was observed that all the derivatives of di-*tert*-butylated **1b** bearing electron-withdrawing groups at the *meso* methyl (**2b–f**) are characterized by a poor fluorescence response as well, mainly in polar media (see Table S1, SI). This **1b** effect must be caused by the increased electron-donating ability of the BODIPY core, by the branched *tert*-butyl groups, which switches on an ICT process from the BODIPY core to the electron-withdrawing group located at *meso* methyl. Note the higher inductive effect (+I) of *tert*-butyl (**1b** derivatives) when compared with ethyl (**1a** derivatives) or hydrogen (**1c** derivatives).

The absence of red-shifted emission bands or new absorption bands for these **1b** derivatives suggests that the involved ICT state is not fluorescent, and it is not directly populated, but through to the locally excited (LE) state (see **2b** in Figure 1). This nonfluorescent de-excitation of the LE state should be favored in polar media, as it is observed (see Table S1, SI) due to the higher stabilization of the polar ICT state.

It is important to highlight here that the population of the ICT state, from the BODIPY core to the electron-withdrawing group

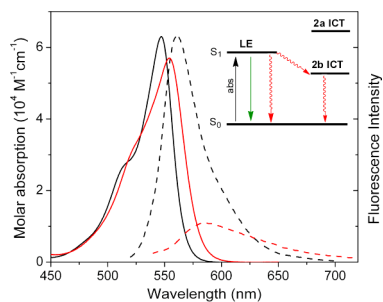


Figure 1. Absorption (bold) and fluorescence (dashed) spectra of **2a** (black) and **2b** (red) in tetrahydrofuran (see the Supporting Information for details) and energy diagram explaining differential fluorescence behavior by ICT process (radiative processes in green, nonradiative in red).

at the C8-methyl, is promoted when the electron-donating ability of the BODIPY is high enough (as it occurs in **2b** by the presence of the *tert*-butyl groups); otherwise, the process is thermodynamically nonviable (cf. **2a** vs **2b** in Figure 1), allowing the detection of an efficient fluorescence signal.

The photophysical effect caused by the halogenation at the *meso* methyl in **1b**, to give **2g** or **2h**, is noteworthy. The photophysics of **1b** are controlled by the steric hindrance exerted by the *tert*-butyls, which distorts the chromophore planarity, mainly in the excited state leading to large Stokes shifts (Table 1). However, halogenated **2g** and **2h** exhibit low Stokes shifts (see Table S1, SI), suggesting lower differential distortion upon excitation. On the other hand, the higher fluorescence efficiency of iodinated **2h** when compared with brominated **2g** (24% vs 9%, see Table S1, SI) suggests lower ICT ability for the former due to the less electronegative character of iodine.

The noticeable influence of the *meso*-methyl groups on modulating the photophysics of the corresponding non-substituted parent BODIPY is also observed in the modulation of the electrochemistry (Figure 2 and Figures S4–S6, SI). Thus,

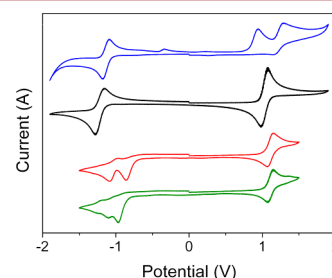


Figure 2. Cyclic voltammograms of **1b** (black), **2l** (blue), **2b** (red), and **2e** (green) in acetonitrile (see the Supporting Information for details).

the introduction of the *n* electron-donating dimethylamino group alters the oxidation wave of the parent BODIPY (two irreversible oxidation peaks appear in the anodic region), whereas the reversible shape of the cathodic wave is almost the same (e.g., **2l** vs **1b** in Figure 2). The lower oxidation potential of the dimethylaminated derivatives agrees with the ICT process (BODIPY-core reductive) proposed for these compounds. Moreover, their oxidation and reduction waves are now closer, suggesting lower energy gap by HOMO-state destabilization, in agreement also with their spectral red-shifts when compared to the corresponding parent (e.g., see **2l** vs **1b** in Table S1 and also in Figure S3, SI).

Oppositely, electron-withdrawing groups (e.g., methoxycarbonyl or halogen) alter the reduction ability of the parent nonsubstituted BODIPY: irreversible reduction peaks appear at smaller potentials in the cathodic region, whereas the oxidation ability remains almost unchanged^{7d} (e.g., see **2b** and **2e** vs **1b** in Figure 2). The easier reduction also explains the red shifts observed in these *meso* BODIPYs (electron-withdrawing substituted) when compared to their parents (LUMO-state stabilization).

In summary, a new synthetic method to achieve *meso* BODIPYs is described. This method involves the selective lateral lithiation of 8-methylBODIPY precursors, followed by electrophilic capture of the formed azaenolate-like organolithium. The procedure works well for different electrophiles, with the exception of highly reactive Br₂ or I₂ when reacting with nonentirely substituted BODIPY substrates (polyhalogenation takes place). Interestingly, DMF/I₂ is demonstrated to cause the

dimethylamination of the studied *meso*-methyl-lithiated BODIPYs. Lateral lithiation–functionalization of BODIPYs can also take place selectively in 3-methylBODIPYs, but in this case the absence of *meso* methyl is necessary. The physical study of the new *meso* BODIPYs demonstrates that their photophysical and electrochemical properties can be finely tuned by key structural modifications. The obtained compounds range from highly fluorescent dyes to almost nonemitting systems by the promotion of ICT, which, in turn, makes them valuable for sensing purposes. Finally, we are convinced that the reported new BODIPY reactivity, based on its selective lateral lithiation, will be highly useful for the future development of smarter BODIPYs for technological applications.

■ ASSOCIATED CONTENT

Supporting Information

Detailed experimental procedures, NMR spectra, photophysical and electrochemical data, and experimental evidence supporting the mechanism in Scheme 4. This material is available free of charge via the Internet at <http://pubs.acs.org>.

■ AUTHOR INFORMATION

Corresponding Authors

*E-mail: santmoya@ucm.es.

*E-mail: mjortiz@ucm.es.

Notes

The authors declare no competing financial interest.

■ ACKNOWLEDGMENTS

Financial support from the MINECO (MAT2010-20646-C04-02 and -04) of Spain is gratefully acknowledged. I.E. thanks Gobierno Vasco for a research contract (IT339-10).

■ REFERENCES

- (1) (a) Loudet, A.; Burgess, K. *Chem. Rev.* **2007**, *107*, 4891. (b) Ulrich, G.; Ziessel, R.; Harriman, A. *Angew. Chem., Int. Ed.* **2008**, *47*, 1184. (c) Benstead, M.; Mehl, G. H.; Boyle, R. W. *Tetrahedron* **2011**, *67*, 3573. (d) Boens, N.; Leen, V.; Dehaen, W. *Chem. Soc. Rev.* **2012**, *41*, 1130. (e) Kamkaew, A.; Lim, S. H.; Lee, H. B.; Kiew, L. V.; Chung, L. Y.; Burgess, K. *Chem. Soc. Rev.* **2013**, *42*, 77.
- (2) For example, see: (a) Bonardi, L.; Ulrich, G.; Ziessel, R. *Org. Lett.* **2008**, *10*, 2183. (b) Ozlem, S.; Akkaya, E. U. *J. Am. Chem. Soc.* **2009**, *131*, 48. (c) Thivierge, C.; Han, J.; Jenkins, R. M.; Burgess, K. *J. Org. Chem.* **2011**, *76*, 5219. (d) Jiao, L.; Pang, W.; Zhou, J.; Wei, Y.; Mu, X.; Bai, G.; Hao, E. *J. Org. Chem.* **2011**, *76*, 9988. (e) Rihn, S.; Erdem, M.; De Nicola, A.; Retaillieu, P.; Ziessel, R. *Org. Lett.* **2011**, *13*, 1916. (f) Ortiz, M. J.; Agarrabeitia, A. R.; Durán-Sampedro, G.; Bañuelos, J.; Arbeloa López, T.; Massad, W. A.; Montejano, H. A.; García, N. A.; López Arbeloa, I. *Tetrahedron* **2012**, *68*, 1153.
- (3) For example, see: (a) Rohand, T.; Baruah, M.; Qin, W.; Boens, N.; Dehaen, W. *Chem. Commun.* **2006**, 266. (b) Li, L.; Nguyen, B.; Burgess, K. *Biorg. Med. Chem. Lett.* **2008**, *18*, 3112. (c) Leen, V.; Leemans, T.; Boens, N.; Dehaen, W. *Eur. J. Org. Chem.* **2011**, 4386. (d) Leen, V.; Miscoria, D.; Yin, S.; Filarowski, A.; Ngongo, J. M.; Van der Auweraer, M.; Boens, N.; Dehaen, W. *J. Org. Chem.* **2011**, *76*, 8168. (e) Sánchez-Carnerero, E. M.; Moreno, F.; Maroto, B. L.; Agarrabeitia, A. R.; Bañuelos, J.; Arbeloa, T.; López-Arbeloa, I.; Ortiz, M. J.; de la Moya, S. *Chem. Commun.* **2013**, 49, 11641. (f) Jiang, T.; Zhang, P.; Yu, C.; Yin, J.; Jiao, L.; Dai, E.; Wang, J.; Wei, Y.; Mu, X.; Hao, E. *Org. Lett.* **2014**, *16*, 1952.
- (4) For example, see: (a) Ziessel, R.; Ulrich, G.; Haefele, A.; Harriman, A. *J. Am. Chem. Soc.* **2013**, *135*, 11330. (b) Durán-Sampedro, G.; Agarrabeitia, A. R.; Cerdán, L.; Pérez-Ojeda, M. E.; Costela, A.; García-Moreno, I.; Esnal, I.; Bañuelos, J.; López Arbeloa, I.; Ortiz, M. J. *Adv.*

Funct. Mater. **2013**, *23*, 4195. (c) G. Durán-Sampedro, G.; Esnal, I.; Agarrabeitia, A. R.; Bañuelos, J.; Cerdán, L.; García-Moreno, I.; Costela, A.; López Arbeloa, I.; Ortiz, M. J. *Chem.—Eur. J.* **2014**, *20*, 2646. (d) Sánchez-Carnerero, E. M.; Moreno, F.; Maroto, B. L.; Agarrabeitia, A. R.; Ortiz, M. J.; Vo, B. G.; Muller, G.; de la Moya, S. *J. Am. Chem. Soc.* **2014**, *136*, 3346.

(5) For example, see: (a) Rohand, T.; Qin, W.; Boens, N.; Dehaen, W. *Eur. J. Org. Chem.* **2006**, 4658. (b) Yin, S.; Leen, V.; Snick, S. V.; Boens, N.; Dehaen, W. *Chem. Commun.* **2010**, 46, 6329. (c) Ortiz, M. J.; García-Moreno, I.; Agarrabeitia, A. R.; Durán-Sampedro, G.; Costela, A.; Sastre, R.; Lopez Arbeloa, F.; Bañuelos Prieto, J.; Lopez Arbeloa, I. *Phys. Chem. Chem. Phys.* **2010**, *12*, 7804. (d) Lakshmi, V.; Ravikanth, M. *Dyes Pigments* **2013**, *96*, 665. (e) Rihn, S.; Erden, M.; De Nicola, A.; Retaillieu, P.; Ziessel, R. *Org. Lett.* **2011**, *13*, 1916. (f) Durán-Sampedro, G.; Palao, E.; Agarrabeitia, A. R.; de la Moya, S.; Boens, N.; Ortiz, M. J. *RSC Adv.* **2014**, *4*, 19210.

(6) For example, see: (a) Zeng, L.; Miller, E. W.; Pralle, A.; Isacoff, E. Y.; Chang, C. J. *J. Am. Chem. Soc.* **2006**, *128*, 10. (b) Tian, M.; Peng, X.; Feng, F.; Meng, S.; Fan, J.; Sun, S. *Dyes Pigments* **2009**, *81*, 58. (c) Rosenthal, J.; Lippard, S. J. *J. Am. Chem. Soc.* **2010**, *132*, 5536. (d) Li, P.; Xie, T.; Duan, X.; Yu, F.; Wang, X.; Tang, B. *Chem.—Eur. J.* **2010**, *16*, 1834. (e) Li, P.; Fang, L.; Zhou, H.; Zhang, W.; Wang, X.; Li, N.; Zhong, H.; Tang, B. *Chem.—Eur. J.* **2011**, *17*, 10520. (f) Royzen, M.; Wilson, J. J.; Lippard, S. J. *J. Inorg. Biochem.* **2013**, *118*, 162. (g) Oshikawa, Y.; Ojida, A. *Chem. Commun.* **2013**, 49, 11373.

(7) For example, see: (a) Kálai, T.; Hideg, K. *Tetrahedron* **2006**, *62*, 10352. (b) Guliyev, R.; Buyukcakir, O.; Sozmen, F.; Bozdemir, O. A. *Tetrahedron Lett.* **2009**, *50*, 5139. (c) Wang, D.; Fan, J.; Gao, X.; Wang, B.; Sun, S.; Peng, X. *J. Org. Chem.* **2009**, *74*, 7675. (d) Krumova, K.; Cosa, G. *J. Am. Chem. Soc.* **2010**, *132*, 17560. (e) Genovese, D.; Bonacchi, S.; Juris, R.; Montalti, M.; Prodi, L.; Rampazzo, E.; Zaccheroni, N. *Angew. Chem., Int. Ed.* **2013**, *52*, 5965. (f) Xie, R.; Yi, Y.; He, Y.; Liu, X.; Liu, Z.-X. *Tetrahedron* **2013**, *69*, 8541. (g) Heisig, F.; Gollos, S.; Freudenthal, S. J.; El-Tayeb, A.; Iqbal, J.; Müller, C. E. *J. Fluoresc.* **2014**, *24*, 213.

(8) For example, see: Flores-Rizo, J. O.; Esnal, I.; Osorio-Martínez, C. A.; Gómez-Durán, C. F. A.; Bañuelos, J.; López Arbeloa, I.; Panell, K. H.; Metta-Magaña, A. J.; Peña-Cabrera, E. *J. Org. Chem.* **2013**, *78*, 5867.

(9) For example, see: (a) Peña-Cabrera, E.; Aguilar-Aguilar, A.; González-Domínguez, M.; Lager, E.; Zamudio-Vázquez, R.; Godoy-Vargas, J.; Villanueva-García, F. *Org. Lett.* **2007**, *9*, 3985. (b) Osorio-Martínez, C. A.; Urías-Benavides, A.; Gómez-Durán, C. F. A.; Bañuelos, J.; Esnal, I.; López Arbeloa, I.; Peña-Cabrera, E. *J. Org. Chem.* **2012**, *77*, 5434. (c) Leen, V.; Yuan, P.; Wang, L.; Boens, N.; Dehaen, W. *Org. Lett.* **2012**, *14*, 6150. (d) Wang, J.; Vicente, M. G. H.; Fronczek, F. R.; Smith, K. M. *Chem.—Eur. J.* **2014**, *20*, 5064.

(10) (a) Shivran, N.; Mula, S.; Ghanty, T. K.; Chattopadhyay, S. *Org. Lett.* **2011**, *13*, 5870. (b) Palao, E.; Agarrabeitia, A. R.; Bañuelos-Prieto, J.; Arbeloa López, T.; Lopez-Arbeloa, I.; Armesto, D.; Ortiz, M. J. *Org. Lett.* **2013**, *15*, 4454.

(11) Smithen, D. A.; Baker, A. E. G.; Offman, M.; Crawford, S. M.; Cameron, S.; Thompson, A. *J. Org. Chem.* **2012**, *77*, 3439.

(12) Crawford, S. M.; Thompson, A. *Org. Lett.* **2010**, *12*, 1424.

(13) Clark, R. D.; Jahangir, A. *Org. React.* **1995**, *47*, 1.

(14) As example, 8-(iodomethyl)BODIPYs are valuable key intermediates to interesting dyes by nucleophilic substitution: (a) Kálai, T.; Hideg, K. *Tetrahedron* **2006**, *62*, 10352. (b) Guliyev, R.; Buyukcakir, O.; Sozmen, F.; Bozdemir, O. A. *Tetrahedron Lett.* **2009**, *50*, 5139. On the other hand, note the chemical possibilities of the rich carbonyl chemistry.

(15) As an example, for the red-ox properties of related oxygenated BODIPYs, see ref 7d.

(16) The lack of procedures to date for obtaining a broad series of *meso* BODIPYs has avoided the study on the influence exerted by certain functional groups located at the *meso* position (e.g., carbonyl) on the BODIPY photophysics.

(17) Mathieu, J.; Gros, P.; Fort, Y. *Chem. Commun.* **2000**, 951.

Cite this: *RSC Advances*, 2011, 1, 677–684

www.rsc.org/advances

PAPER

Modulation of the photophysical properties of BODIPY dyes by substitution at their *meso* position.†

Jorge Bañuelos,^{*a} Ismael J. Arroyo-Córdoba,^b Ismael Valois-Escamilla,^c Alejandro Alvarez-Hernández,^c Eduardo Peña-Cabrera,^b Rongrong Hu,^d Ben Zhong Tang,^d Ixone Esnal,^a Virginia Martínez^a and Iñigo López Arbeloa^a

Received 7th April 2011, Accepted 27th June 2011

DOI: 10.1039/c1ra00020a

We report the photophysical properties of new BODIPY derivatives monosubstituted at the central position. The presence of different functional groups induced the appearance of new photophysical processes in BODIPY dyes, such as intramolecular charge or energy transfer. These phenomena are sensitive to solvent properties (mainly the polarity) and have a potential use as fluorescent probes. Adequate modifications in their molecular structure or in the environment polarity can modulate the emission region of these fluorophores in the visible spectral region. Specifically, different processes and photophysical behaviors can be achieved depending on the excited chromophore and/or the solvent characteristics in a bichromophoric pyrene-BODIPY system.

Introduction

4,4-difluoro-4-bora-3a,4a-diaza-s-indacene dyes (henceforth abbreviated as BODIPY) are widely known active media of tunable dye lasers, generally in the green-yellow part of the visible spectral region.¹ BODIPY dyes efficiently absorb electromagnetic radiation and emit sharp fluorescence bands, usually characterized by high fluorescence quantum yields, in some cases close to the unit.² Due to their quasi-aromatic electron delocalization, the intersystem crossing probability is very low,³ dismissing the triplet-triplet absorption ability in these dyes; probably the main factor which reduces the laser efficiency of many laser dyes. Moreover, BODIPY dyes have excellent chemical and thermal stabilities. All these factors contribute to the important application of BODIPY dyes in photonics and as fluorescent probes in many biological systems.⁴ The synthesis of new BODIPY derivatives with adequate aromatic substituents can extend the chromophoric π -system and shifts the emission band to the red.⁵ Thus, photoactive materials with a wide range of the visible spectral region can be achieved with the same laser dye family.

Since the discovery of BODIPY at the beginning of the 90s as efficient laser dyes,⁶ BODIPY fluorophores are widely used in light harvesting arrays or antenna systems, as energy injectors or acceptors to collect and transport the light to a reaction centre, or as sensitizers in solar cells.⁷ However, probably the most successful application is as fluorescence probes or sensors to monitor the evolution of biological processes, to characterize the surrounding environment of biomolecules or to recognize the presence of certain analytes.⁸ Indeed, there is a huge variety of functionalized BODIPY dyes to study biochemistry processes in biological systems (DNA, proteins, lipids and so on).⁹ Most BODIPY-probes are based on the possibility of modulating their photophysical behaviour by the incorporation of appropriate functional groups in the molecular structure of the chromophore. Typically, the photophysics of BODIPY dyes are quite insensitive to the solvent properties,² but the presence of adequate substituents induces new photophysical processes, which can be sensitive to certain environmental characteristics.

The present work is focused in the controlled modification of the photophysical properties of BODIPY dyes by the inclusion of appropriate substituents at the *meso* position of the BODIPY core. This central position is the most sensitive one to the substituent effect because an important modification in the electronic density localized at this *meso* position takes place upon excitation. The new BODIPY derivatives considered in this work are depicted in Scheme 1. The aim of the 8-alkyl derivatives (compounds 1–3) was to shift the emission band of the BODIPY chromophore to the blue part of the visible region, a barely exploited region with BODIPY. Additionally, different aromatic groups: *p*-bromophenyl (4), triphenylaminethiophene (5) and pyrene (6) were included in the search for new photophysical phenomena sensitive to the solvent and to expand the applicability of BODIPY dyes.

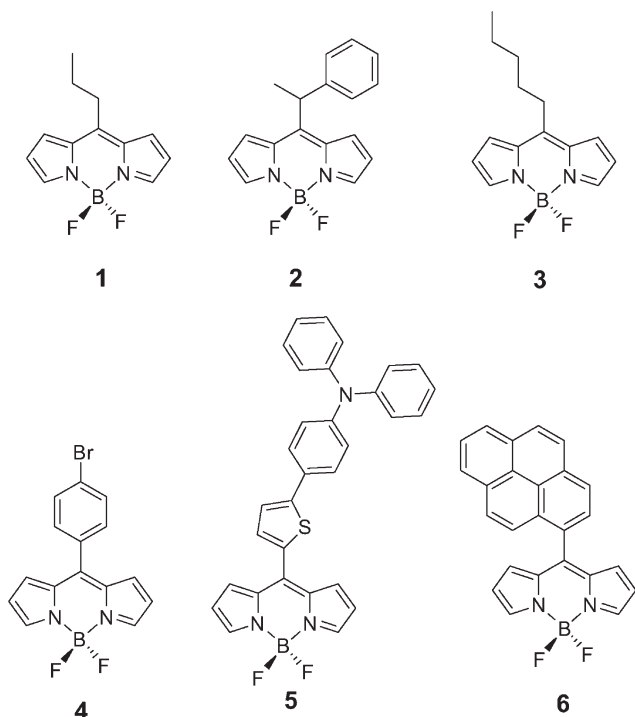
^aDepartamento Química Física, Universidad del País Vasco, -EHU, Apartado 644, 48080-Bilbao, Spain. E-mail: jorge.bañuelos@ehu.es; Fax: +34946013500; Tel: +34946015384

^bDepartamento Química, Universidad de Guanajuato. Col. Noria Alta, Guanajuato, Gto. 36050, Mexico. E-mail: eduardop@quijote.ugto.mx

^cCentro Investigaciones Químicas, Universidad Autónoma del Estado de Hidalgo. Carretera Pachuca-Tulancingo Km. 4.5. Cd. Universitaria, Mineral de la Reforma, Hidalgo 42076, Mexico. E-mail: alvarez@uaeh.edu.mx

^dDepartment of Chemistry, Hong Kong University of Science and Technology, Clear Water Bay, Kowloon, Hong Kong, China. E-mail: tangbenz@ust.hk

† Electronic supplementary information (ESI) available: Complementary photophysical data and theoretical results. See DOI: 10.1039/c1ra00020a



Scheme 1 Molecular structure of BODIPY derivatives

Experimental

BODIPY derivatives **4–6** were prepared as previously described.¹⁰ The preparation of derivatives **1–3** will be reported elsewhere. The photophysical properties of the new BODIPY derivatives (**1–6**, Scheme 1) were explored in diluted solutions (2×10^{-6} M) using solvents (spectroscopy grade), from apolar to polar and polar/protic, in 1 cm optical pathway quartz cuvettes. The samples in different media were prepared by adding the corresponding solvent to an adequate amount of a concentrated stock solution (*ca.* 10^{-3} M) of the corresponding dye in acetone, after vacuum evaporation of the solvent.

UV-Vis absorption and fluorescence spectra were recorded on a Varian model CARY 4E spectrophotometer and a SPEX Fluorolog 3–22 fluorimeter, respectively. The fluorescence quantum yield (ϕ) was obtained using a methanolic solution of adequate commercial BODIPY dyes as reference. Radiative decay curves were registered with the time correlated single-photon counting technique (Edinburgh Instruments, model FL920) with a time resolution of 30 ps by means of a multichannel plate detector (Hamamatsu MCP C4878). The emission was monitored with a double monochromator at the maximum emission wavelength after excitation at 370 or 470 nm, depending on the dye, by means of pulsed diode lasers (PicoQuant, model LDH370 and 470, respectively) with recorded wide pulses of 150 ps and operating at 20 MHz repetition rate. The measured fluorescence decay curves were deconvoluted from the instrument response function (recorded by a LUDOX scatter) and determined from the slope of the exponential fit by means of iterative software supplied with the instruments. The goodness of the fit was described by the chi-square statistical parameter and by the analysis of the residual distribution. The

radiative (k_r) and non-radiative (k_{nr}) rate constants were calculated by means of ϕ/τ and $(1 - \phi)/\tau$, respectively.

Quantum mechanic calculations were performed by Gaussian 09 software. The ground and excited state geometries were fully optimized with the B3LYP (Density Functional Theory, DFT) and *ab initio* CIS methods respectively, using in both cases the double valence 6-31G basis set. Absorption properties were predicted by the Time Dependent (TD-B3LYP) method and semiempirical ZINDO method as the Franck–Condon transition from the ground states. The solvent effect was considered by the Polarizable Continuum Model (PCM).

Results and Discussion

Alkyl-BODIPY (**1–3**).

Monosubstituted alkyl BODIPY dyes bearing *n*-propyl, *n*-pentyl and 1-phenylethyl groups at the *meso* position (Scheme 1) showed the typical absorption and emission bands of BODIPY chromophore.¹¹ They were located at around 495 and 505 nm, respectively (Fig. 1), at slightly higher energies with respect to unsubstituted BODIPY (505 nm and 515 nm, respectively). Such hypsochromic shifts can be related to the inductive effect of the alkyl groups. Indeed, quantum mechanical calculations suggest that the electron density at the central 8-carbon of the BODIPY chromophore increases upon excitation (Fig. 1).² Consequently the inductive effect +I of the alkyl groups will raise up the energy of the LUMO state with regard to the HOMO, slightly increasing the energy gap between both states. The small bathochromic shift (around 5 nm) observed for dye **2** with respect to the other *n*-alkyl analogs (**1** and **3**), should be ascribed to the presence of the phenyl group, which reduces the inductive donor character of the substituent, recovering the spectral band position of the parent BODIPY core. In fact, the calculated energy gap slightly increases (0.1 eV) for dye **2**.

The photophysical behaviour of these derivatives (Table 1) were very similar to that of the 8-unsubstituted chromophore,¹¹ with a high fluorescence quantum yield ($\phi > 0.90$) and lifetime

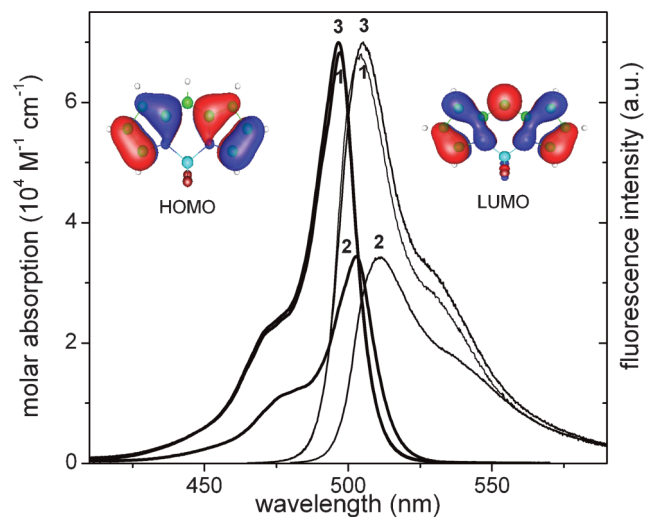


Fig. 1 Absorption and fluorescence normalized spectra of dye **1**, **2** and **3** in diluted (2×10^{-6} M) solutions of *c*-hexane. Electronic density in the HOMO and LUMO state of the unsubstituted BODIPY.

Table 1 Photophysical properties of compounds **1–3** in a common solvent (c-hexane). The full data are listed in Table 1 in Supporting Information.

BODIPY	λ_{ab} (nm)	ϵ_{max} ($10^4 \text{M}^{-1} \text{cm}^{-1}$)	λ_{fl} (nm)	$\Delta\nu_{\text{St}}$ (cm^{-1})	ϕ	τ (ns)	k_{fl} (10^8s^{-1})	k_{nr} (10^8s^{-1})
BDP	503.5	7.6	510.5	265	0.96	6.47	1.48	0.06
1	497.0	6.8	505.0	315	0.95	6.23	1.52	0.08
2	503.0	3.4	512.0	355	0.92	6.65	1.38	0.12
3	496.5	7.0	506.5	385	0.97	6.50	1.49	0.04

absorption (λ_{abs}) and fluorescence (λ_{fl}) wavelength, Stokes shift ($\Delta\nu_{\text{St}}$), molar absorption coefficient (ϵ_{max}), fluorescence quantum yield (ϕ) and lifetime (τ), radiative (k_{fl}) and non-radiative (k_{nr}) rate constant.

($\tau > 6$ ns), leading to a high radiative rate constant ($k_{\text{fl}} > 1.4 \times 10^8 \text{s}^{-1}$) and a low non-radiative deactivation process ($k_{\text{nr}} < 0.1 \times 10^8 \text{s}^{-1}$), a short Stokes shift ($\Delta\nu_{\text{St}} < 400 \text{cm}^{-1}$) and a high molar absorption coefficient ($\epsilon_{\text{max}} \sim 7 \times 10^4 \text{M}^{-1} \text{cm}^{-1}$). As an exception, dye **2** showed an unusual low molar absorption coefficient.

The solvent dependence of the photophysical parameters of these derivatives (see Table S1, ESI[†]) was as commonly observed for an 8-unsubstituted derivative, with short displacement of the absorption and fluorescence bands to lower energies from apolar to polar and protic solvents. The fluorescence capacity did not depend practically on the nature of the solvent.

Consequently, alkylation at the *meso* position of the BODIPY core did not damage its excellent fluorescence capacity.

p-bromophenyl-BODIPY (**4**)

The presence of the electron withdrawing *p*-bromophenyl group at central position of the BODIPY chromophore (Scheme 1) induced important changes in the photophysical behavior. Fig. 2 shows a large bathochromic shift of **4** in the absorption and fluorescence bands (around 80–90 nm) and a decrease in the fluorescence lifetime compared with **1** (Fig. 2).

As mentioned, the *meso* position was very sensitive to the presence of substituents with electronic acceptor/donor character, since an important increase in the electronic density at this position took place when an electron jumped from the HOMO to the LUMO state, the involved molecular orbitals in the $S_0 \rightarrow S_1$ spectral transition (Fig. 1). Therefore, important spectral shifts are expected by the incorporation of substituents with high electron donor/acceptor ability at this central position. In the present case, the electron withdrawing Br atom stabilized the LUMO state more extensively than the HOMO state, and hence the energy gap between both states decreased.

Table 2 summarizes the photophysical parameters of compound **4** in several solvents, covering the complete apolar, polar and polar/protic range. Although the molar absorption coefficient of this dye remained high ($\epsilon_{\text{max}} \sim 7.7 \times 10^4 \text{M}^{-1} \text{cm}^{-1}$), both the fluorescence quantum yield ($\phi \sim 0.4$) and the lifetime ($\tau \sim 3$ ns) decreased with respect to those values of its alkyl partners (Table 1) in not very acid protic solvents. These changes are mainly due to an increase in the non-radiative deactivation rate constant ($k_{\text{nr}} \sim 2 \times 10^8 \text{s}^{-1}$) rather than to a decrease in the radiative deactivation ($k_{\text{fl}} \sim 1.3 \times 10^8 \text{s}^{-1}$). The increase in the non-radiative deactivation may be due to an augmentation to the internal conversion and/or intersystem crossing processes. For instance, the presence of the Br atom could imply an increase in the intersystem crossing probability by the heavy atom effect. However, the Br atom is attached to the BODIPY

chromophore by a phenyl group, and consequently its intramolecular heavy atom effect should be very low.

Therefore, the reduction in the fluorescence capacity should be mainly assigned to an increase in the internal conversion process, probably due to the rotational motion of the phenyl group directly linked to the BODIPY core. Indeed, it has been demonstrated that the free rotation of a phenyl group attached at the central 8-position of BODIPY core drastically reduces the fluorescence capacity of the chromophore,¹² but when this rotational motion is reduced (for instance, by the incorporation

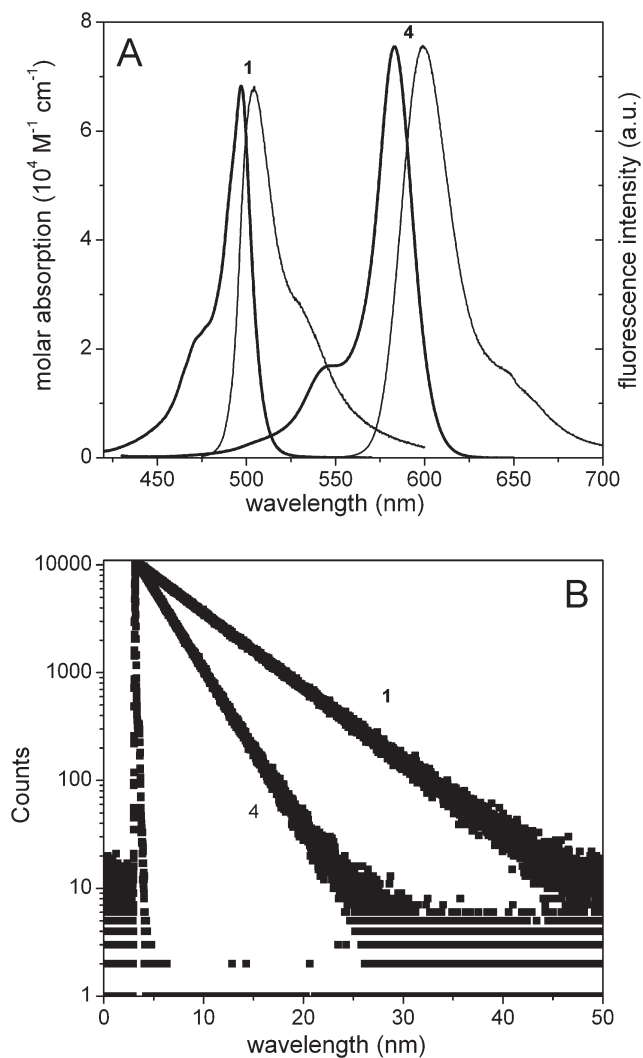


Fig. 2 Absorption and fluorescence spectra (A) and decay curve (B) of compound **4** in diluted solutions of c-hexane. The corresponding spectra and curve of dye **1** are also included for comparison.

Table 2 Photophysical data of compound **4** in different environments; from apolar (c-hexane) to polar (ethyl acetate and acetone) and polar/protic (ethanol, methanol and trifluoroethanol) solvents.

Solvent	λ_{ab} (nm)	ϵ_{max} ($10^4 M^{-1} cm^{-1}$)	λ_{fl} (nm)	$\Delta\nu_{St}$ (cm^{-1})	ϕ	τ (ns)	k_{fl} ($10^8 s^{-1}$)	k_{nr} ($10^8 s^{-1}$)
F ₃ -ethanol	574.0	7.5	591.5	525	0.54	5.40	1.00	0.85
methanol	577.5	7.7	597.0	570	0.40	3.53	1.13	1.70
ethanol	579.0	7.5	598.5	525	0.43	3.74	1.15	1.52
acetone	578.5	7.6	599.0	595	0.39	3.31	1.17	1.84
ethyl acetate	579.0	7.9	599.0	580	0.39	3.46	1.12	1.76
c-hexane	583.0	7.5	600.0	485	0.39	2.89	1.35	2.11

of methyl groups at the *ortho* position of the phenyl group and/or at the 1- and 7-position of the BODIPY core) the fluorescence ability of the chromophore is recovered.¹³

The highest values of the fluorescence quantum yield and lifetime were achieved in polar/protic media due to a decrease in the non radiative rate constant (Table 2). This dependency of the k_{nr} value on the solvent characteristics confirms that the non-radiative deactivation from the excited state is due to internal conversion mechanisms rather than intersystem crossing processes.

From these results it can be concluded that dye **4** can operate as an active medium of dye lasers emitting at the red part of the visible region. Furthermore, improvement in the lasing efficiency could be obtained with a more constricted structure, for instance by restricting the intramolecular rotational motion of the *p*-Br-phenyl group by attaching bulky groups at the *ortho* positions of the phenyl group and/or at the 1- and 7- positions of the BODIPY ring.

Triphenylaminethiophene-BODIPY (**5**)

The derivative bearing a thiophene group, α -substituted with a triphenylamine (TPA) unit, at the *meso* position of the BODIPY core (Scheme 1), presents a clear change in the shape of its absorption spectrum, as shown in Fig. 3. In fact, as well as the typical absorption band of alkyl-BODIPYs, centered at around 520 nm, a new shoulder appeared at a lower energy (around 570 nm in c-hexane). This new band became much more evident and bathochromically shifted in polar media, suggesting the formation of a new absorbing entity characterized by a high dipole moment. Roncali and coworkers have studied the formation of intramolecular charge transfer (ICT) complexes between TPA-thiophene and several π -conjugated systems by UV-Vis spectroscopy.¹⁴ The authors point out the high electron donor capacity of such a group and that the intensity and position of the absorbing complexes depends on the electron acceptor properties of the π -system attached to the thiophene group. In compound **5**, the same donor unit is present at the *meso* position of the BODIPY core, which can act as an electron acceptor. The HOMO - 1 and LUMO molecular orbitals are exclusively located in the BODIPY, while the HOMO and LUMO + 1 are located in the TPA-thiophene (Fig. S1, ESI[†]). Consequently, the new absorption band placed at lower energies should be assigned to an intramolecular charge transfer (ICT) complex formed between the TPA-thiophene partner and the BODIPY core, which already exists in the ground state (*i.e.*, transition from the HOMO in the donor TPA-thiophene to the LUMO in the acceptor BODIPY). Such an ICT complex is characterized by a high dipole moment and is further stabilized in polar media. Theoretical simulation was not able

to reproduce such new bathochromic band (Table S2, ESI[†]), even in polar solvent.

The excitation at the BODIPY absorption band (490 nm) leads to a broad fluorescence band, centered at 600 nm in c-hexane (Fig. 3). Consequently, compound **5** is characterized by a large Stokes shift ($2565 cm^{-1}$), much higher than the typical

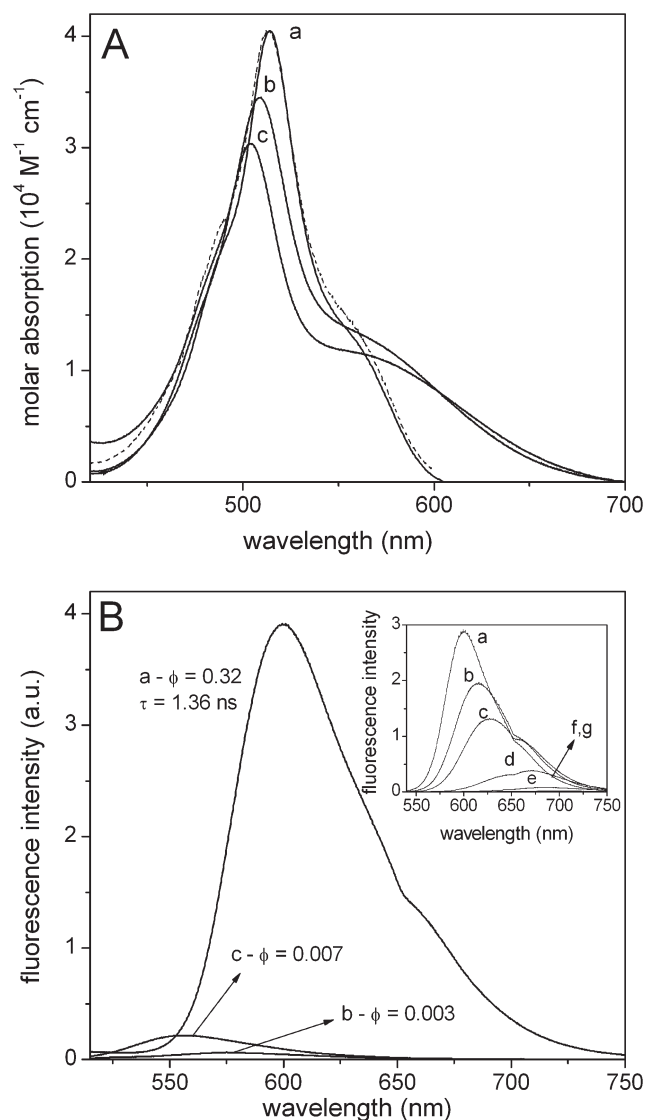


Fig. 3 Absorption and excitation (dashed line) (A) and fluorescence (B) spectra of compound **5** in c-hexane (a), acetone (b) and F₃-ethanol (c). Inset: evolution of the fluorescence spectra in ethyl acetate/c-hexane mixtures with different volume fractions of ethyl acetate: a-0%, b-5%, c-10%, d-25%, e-50%, f-75% and g-100%.

one for alkyl-BODIPY dyes (around 500 cm^{-1}). The fluorescence quantum yield ($\phi = 0.32$) and lifetime ($\tau = 1.36\text{ ns}$) were reduced by more than 50% compared to the values of the alkyl-BODIPY derivatives as a result of an important increase in the probability of the non-radiative deactivation processes ($k_{\text{nr}} = 5 \times 10^8\text{ s}^{-1}$).

The shape and position of the emission band did not change with the excitation wavelength, even after exciting the new CT absorption band (around 570 nm). The corresponding excitation spectrum perfectly matched the absorption one (Fig. 3). All this experimental evidence indicates that the fluorescence band is due to the emission from the excited state of the ICT complex, which can be populated either by direct excitation (570 nm) or from the locally excited (LE) state of BODIPY (490 nm) after electron transfer from the donor TPA-thiophene. The fluorescence decay curve after excitation at 470 nm was analyzed as monoexponential, without any grown-in component, suggesting a very fast population (faster than the time resolution of our single photon counter, $\sim 30\text{ ps}$) of the ICT state.

Polar environments further reduced the fluorescent ability of this derivative and it became nearly non-fluorescent in the most polar media ($\phi < 0.01$ in F_3 -ethanol, Fig. 3). Just a weak remnant fluorescence band was observed at $550\text{--}600\text{ nm}$, depending on the solvent, after the excitation at the main absorption band. Generally, the ICT states were stabilized in polar media due to their high dipole moment. However, the charge transfer process can be so favored that it leads to a charge separation (CS) ionic state (zwitterionic form), which is not fluorescent and quenches the emission from the CT complex. Thus, in polar media only a remnant emission was observed at shorter wavelengths (for wide excitation and emission slits), which should be ascribed to the weak emission from the LE state.

The CT nature of the emissive species was confirmed by the evolution of the fluorescence band in *c*-hexane/ethyl acetate mixtures. Indeed, a progressive increase in the solvent polarity by increasing the ethyl acetate content led to a red shift of the emission band and a concomitant decrease of the fluorescence intensity (inset Fig. 3). In pure ethyl acetate the fluorescence band is nearly negligible.

Taking into account that the fluorescence efficiency of this derivative is very sensitive to the solvent polarity, it can be potentially used as a fluorescent probe to monitor environmental polarity, achieving a red fluorescence emission in apolar environments, but nearly no fluorescence signal in polar media.

Pyrene-BODIPY dyad (**6**)

Finally, we considered the influence of a pyrene chromophore, attached also at the *meso* position, on the photophysics of the BODIPY (Scheme 1). The UV-Vis absorption spectrum of this dye, depicted in Fig. 4, is characterized by a strong ($\epsilon_{\text{max}} \sim 7 \times 10^4\text{ M}^{-1}\text{ cm}^{-1}$) band in the visible region (centered at around 505 nm), attributed to the BODIPY core, and several UV bands assignable to different $S_0 \rightarrow S_n$ electronic transitions of the pyrene chromophore with their typical and clear vibrational structure. In this UV region (around 370 nm) the BODIPY also presents weak absorption bands (Fig. S2, ESI†). This result suggests that there is no electronic interaction between the two moieties in the ground state. Indeed, the optimized geometry

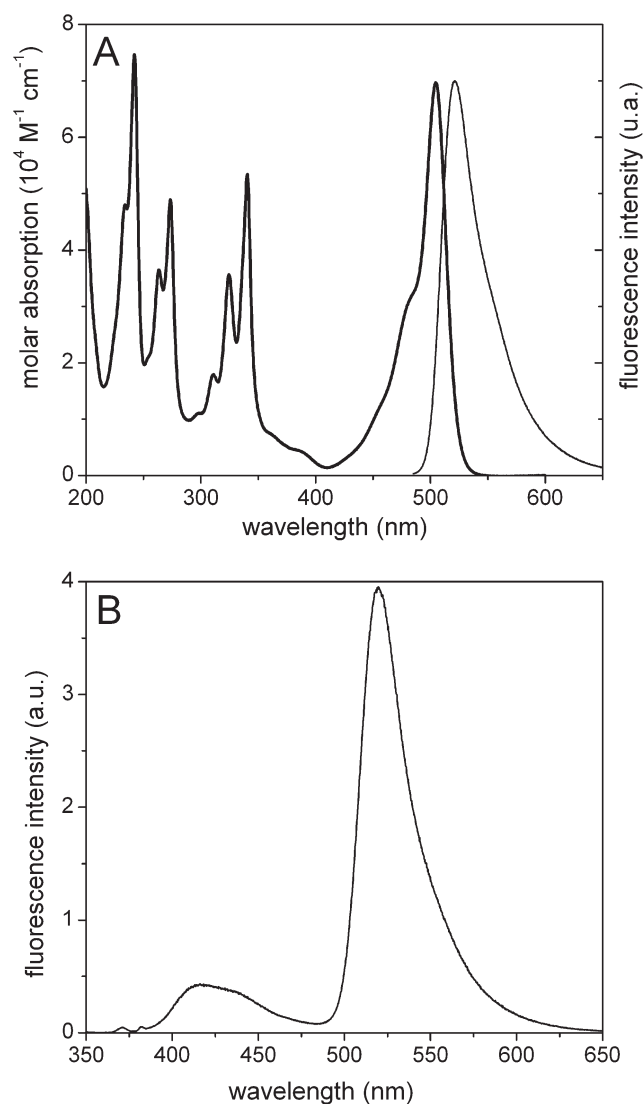


Fig. 4 UV-Vis absorption and fluorescence, under $\lambda_{\text{exc}} = 480\text{ nm}$ (A) and under $\lambda_{\text{exc}} = 340\text{ nm}$ (B), spectra of compound **6** in *c*-hexane.

places the pyrene at a 63° with respect to the BODIPY fragment, without altering the BODIPY core planarity. Thus, the π -electronic clouds of both chromophores do not overlap and both chromophoric systems are independent of each other. These trends are theoretically confirmed since similar absorption properties to the BDP chromophore are predicted upon the presence of the pyrene, corroborating the nearly negligible effect of such unit, at least in the ground state.

The direct excitation of the $S_0\text{--}S_1$ absorption band of the BODIPY chromophore at the visible region (480 nm) provides the typical fluorescent emission of the BODIPY core. In *c*-hexane this emission band is placed at 520 nm (Fig. 4) with a modest fluorescence quantum yield ($\phi = 0.30$) and low lifetime ($\tau = 1.93\text{ ns}$), owing to a high non-radiative deactivation rate constant ($k_{\text{nr}} = 3.6 \times 10^8\text{ s}^{-1}$). Probably, the pyrene group can have some freedom to rotate, like in other 8-aromatic-BODIPY dyes,¹³ enhancing the non-radiative deactivation processes. Blocking such internal movement, by the substitution at the adjacent positions to the *meso*, places the chromophore in a more rigid and perpendicular disposition, improving the fluorescent ability.¹⁵

On the other hand, the UV excitation (340 nm) at the pyrene moiety gave rise to a weak fluorescent band at around 420 nm, typical of the pyrene chromophore, and an intense emission band in the visible region (520 nm), attributed to the BODIPY core (Fig. 4). These results suggest an intramolecular excitation energy transfer process (intra-EET) from the donor pyrene to the acceptor BODIPY. The excitation energy transfer from pyrene to BODIPY is not total since a remnant emission from the pyrene fluorophore is observed in the emission spectrum. The mechanism of the intra-EET process can be assigned to through-bond or through-space interactions. Although the spectral overlap between the emission of the donor pyrene and the S_0 - S_1 absorption of the BODIPY is small, the possibility of Förster type EET through the S_0 - S_2 and higher energies absorption bands of the BODIPY (see Fig. S2, ESI†) has been reported.¹⁶ Furthermore, the mutual orientation of the transition dipole moments of the chromophores in compound **6** is also adequate. To properly assess the operating mechanism in the intra-EET process we have measured the fluorescence spectra at low temperatures (down to 77 K, Fig. S3, ESI†). At low temperatures the electron transfer (involved in the through-bond EET) should be stopped while the EET *via* dipole-dipole coupling should still take place. The intra-EET of compound **6** disappeared lowering the sample temperature, confirming that the intra-EET process in compound **6** takes place through-bond.¹⁷

As a consequence, the visible BODIPY fluorescence emission of this bichromophoric system can be monitored far away from the excitation of the pyrene at the UV, reducing the detection of the excitation light scattering and improving the use of this dye as a fluorescent probe, mainly in biochemical systems where the size of biological entities (proteins, membranes, cells, etc) can induce high scattering of the excitation light.

While the absorption spectrum of compound **6** was nearly solvent independent, the fluorescence properties of this derivative presented a marked dependency on the nature of the solvent. The theoretically predicted geometries in apolar (cyclohexane) and polar (methanol) media are very close, with similar twist angles for the pyrene in both the ground and excited states. Fig. 5 shows the fluorescence spectrum of compound **6** in several polar and polar/protic solvents after direct excitation at the BODIPY core in the visible region (480 nm). Besides the normal emission of the BODIPY core at 510 nm, which was strongly quenched, a new emission band appeared at longer wavelengths. The intensity and position of the new band depended on the solvent. In ethyl acetate this emission band was intense and placed at around 650 nm with a fluorescence lifetime of 3.5 ns. The new red band became less intense in more polar and protic solvent (in F_3 -ethanol practically disappears) and progressively shifted to lower energies (around 700 nm in acetone or methanol). In these solvents, the decay curves are analyzed as biexponentials with a short lifetime of 50 ps and a moderate lifetime of 1 ns with similar statistical weights. As occurs in compound **5**, the HOMO is placed in the pyrene, whereas the LUMO in the BODIPY (Fig. S1, ESI†).

These results clearly show that upon excitation there is an important interaction between both chromophoric systems in polar media giving rise to a new emission band. Taking into account the solvatochromic shift of this band (from 650 in ethyl acetate to 700 nm in methanol), the new emitting species would

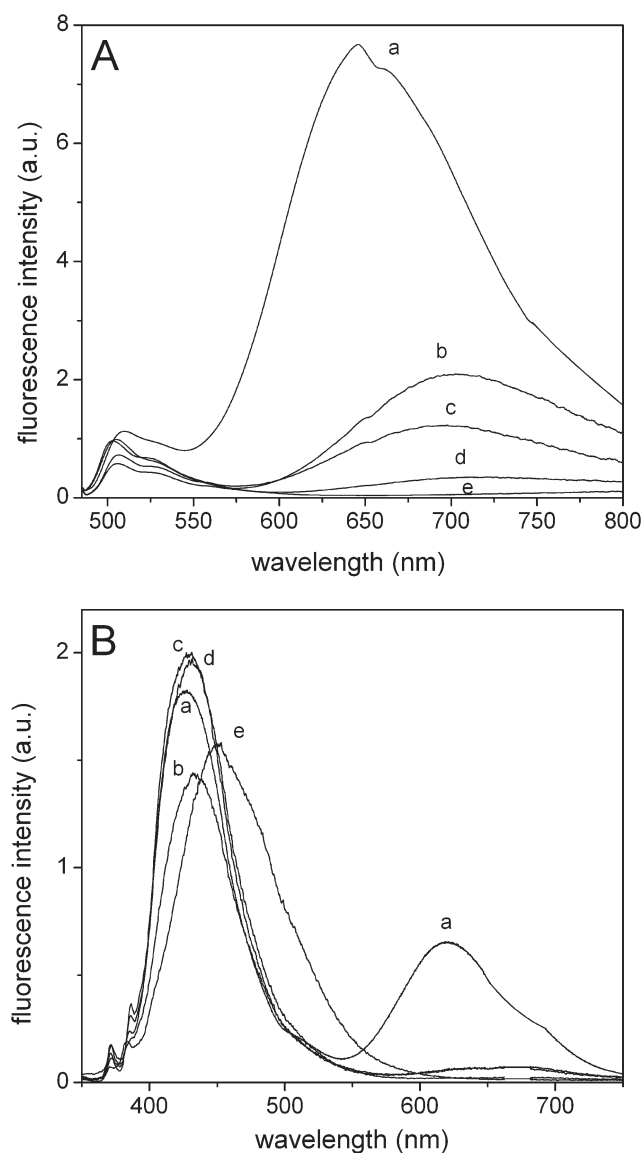


Fig. 5 Fluorescence spectra, exciting at 480 nm (A) and 340 nm (B), of compound **6** in ethyl acetate (a), acetone (b), ethanol (c), methanol (d), and F_3 -ethanol (e).

be characterized by an important dipole moment, and its excited state is stabilized in polar media. Excimer emission of the pyrene is discarded since the measurements are carried out in diluted solutions. At first impression, the formation of an exciplex is rather improbable in view of the excited state optimized geometry, since pyrene and BODIPY are located in planes twisted 72° , therefore, avoiding any cofacial arrangements between them. However, it has been previously suggested that exciplex-like emission occurs even in rigid donor-acceptor systems.¹⁸ In these cases, the intramolecular charge transfer state can convert into an exciplex-like state upon a Coulombic interaction (harpooning effect),¹⁹ causing a weak and red-shifted emission. Probably this approach occurs in compound **6**, where the red emission detected in polar media could be attributed to an exciplex-like emission with a marked charge transfer character. Surprisingly, this emission was slightly favored at low temperatures, matching results previously reported.^{18c}

In fact, in compound **6**, the BODIPY core may serve as an electron acceptor (A) while the pyrene ring is somewhat electron donor (D). Molecules with such as D–A structures often show interesting optical properties, *e.g.*, solvatochromism.²⁰ In non-polar solvents, the LE state of the BODIPY luminogen emits intense green light. Increasing the solvent polarity brings the luminogens from the LE states to the intramolecular charge transfer (ICT) state, and probably afterwards to the exciplex, causing a large bathochromic shift in the emission color and also a dramatic decrease in the emission efficiency.^{20,21}

To examine whether the ICT process is involved in **6** in polar solvents, we systematically changed the polarity of the media by admixing polar THF and nonpolar hexane in different ratios (Fig. 6). When the hexane fraction (f_h) in the THF/hexane mixture increased from 0 to 90%, the emission color of **6** changed gradually from magenta to orange, then yellow, and finally to green.

The visible observation was verified by the spectroscopic analysis. The absorption spectrum of **6** in THF solution was similar to that recorded in *c*-hexane (Fig. 4). However, the emission of **6** was very sensitive to solvent polarity change (Fig. 6). In pure THF, the emission spectrum of **6** ($\lambda_{\text{exc}} = 480$ nm) was dominated by its ICT emission at 626 nm. Its LE emission appeared as a small shoulder at 531 nm. When the f_h value in the solvent mixture was progressively increased from 0 to 70%, the ICT peak moved continuously to 603 nm, while the LE peak remained the same. Both the ICT and LE peaks were intensified upon hexane addition. In the solvent mixture with 80 vol % hexane, the LE emission was dominated in the spectrum, while the ICT emission diminished to a weak shoulder. The ICT peak disappeared when the hexane content reached 90 vol %, and the spectrum only exhibited an LE emission at

531 nm (Fig. 6). Indeed, in pure hexane, the emission at 532 nm was characterized by a fluorescence quantum yield that was 4.6-fold higher than that in pure THF (from 0.028 in THF to 0.13 in hexane).

The fluorescence behavior under UV excitation (340 nm) was also strongly dependent on the solvent. In polar media, the dominant band was the emission from the pyrene. The emission from the LE state of the BODIPY core, previously detected in apolar solvents, is no longer obtained in polar media and just a weak signal from the ICT state (except in ethyl acetate where it was more intense) was detected (Fig. 5). In a previous work about a similar system but with the pyrene placed perpendicular to the BODIPY due to steric reasons, no emission from the pyrene was detected due to efficient intra-EET in all the solvents.¹⁵ However, in compound **6**, where the pyrene had some freedom to oscillate, the intra-EET process most likely populates the LE state of the BODIPY but the further stabilization of the ICT state in the polar media quenches the LE state.

Summarizing, compound **6** is a very versatile dye: in apolar media the visual emission of the BODIPY core can be monitored far away from the excitation of the pyrene chromophore in the UV by means of a through-bond intra-EET process, whereas in polar media the green–red emission from a ICT state can be modulated depending on the nature of the solvent. So, this compound can be used as fluorescence probe to monitor environmental polarity. Besides, the blue emission from the pyrene can be achieved in polar/protic solvents under UV excitation and blue and red emission can coexist in media with moderate polarity (*i.e.* ethyl acetate).

Conclusions

The emission from BODIPY dyes can be modulated by the incorporation of appropriate substituents at the *meso* 8-position. The attachment of different aromatic groups (triphenylamine, thiophene *p*-substituted phenyl, and pyrene) can induce new processes which could be sensitive to solvent properties. In this way new fluorescence probes based on BODIPY fluorophore can be developed.

The bichromophoric pyrene-BODIPY system shows an intramolecular energy transfer process in apolar media with an interesting green emission after UV excitation. In polar media, the formation of an ICT- state, which probably evolves to an exciplex state due to the harpooning effect, shifts the emission band to the red. Blue emission from the pyrene chromophore can be achieved after UV irradiation when the energy transfer process is blocked and the emission from the ICT exciplex is quenched, for instance in polar/protic media. Consequently, blue/green/red emissions can be obtained from this derivative depending on excitation conditions and on the solvent.

Acknowledgements

This work was supported by *Ministerio de Ciencia e Innovación*, projects MAT2007-65778-C02-02 and MAT2010-20646-C04-03. Part of this work was supported by Grant GTO-2007-C02-69094 (CONCyTEG, Mexico). V. Martínez thanks the *Gobierno Vasco* (IT339-10) for postdoctoral contract.

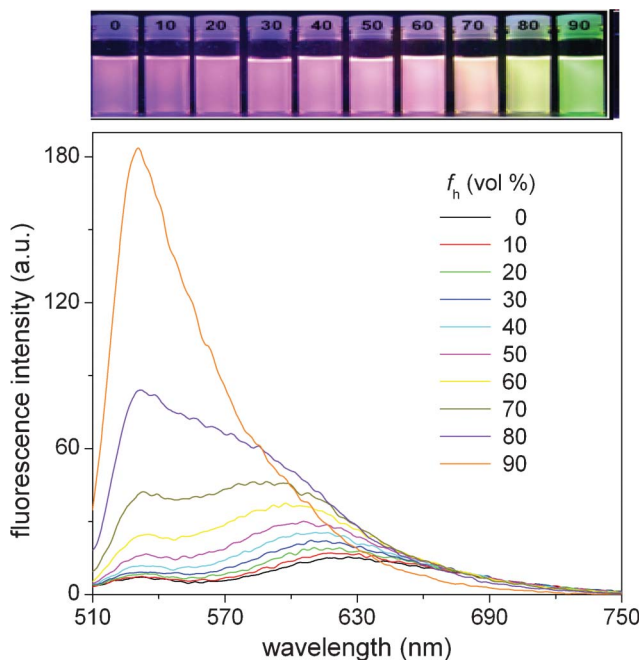


Fig. 6 Photographs (under UV illumination) and emission spectra of **6** (under visible light excitation) in THF/hexane mixtures with different fractions of hexane (f_h , vol %). Solution concentration: 10 μM .

References

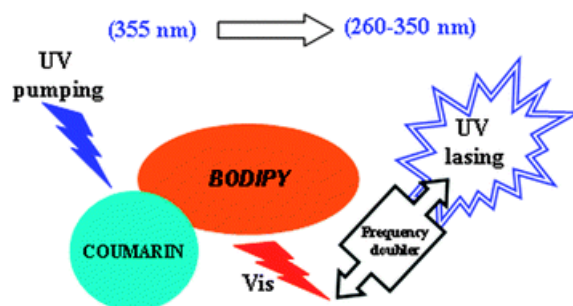
- (a) E. Yariv and R. Reisfeld, *Opt. Mater.*, 1999, **13**, 49–54; (b) M. Ahmad, T. A. King, D.-K. Ko, B. H. Cha and J. Lee, *J. Phys. D: Appl. Phys.*, 2002, **35**, 1473–1476; (c) A. Costela, I. García-Moreno and R. Sastre, *Phys. Chem. Chem. Phys.*, 2003, **5**, 4745–4763; (d) Y. Yang, M. Wang, G. Qian, Z. Wang and X. Fan, *Opt. Mater.*, 2004, **24**, 621–628; (e) A. Costela, I. García-Moreno, M. Pintado-Sierra, F. Amat-Guerri, R. Sastre, M. Liras, F. López Arbeloa, J. Bañuelos and I. López Arbeloa, *J. Phys. Chem. A*, 2009, **113**, 8118–8124.
- (a) R. Y. Lai and A. J. Bard, *J. Phys. Chem. B*, 2003, **107**, 5036–5042; (b) F. López Arbeloa, J. Bañuelos, V. Martínez, T. Arbeloa and I. López Arbeloa, *Int. Rev. Phys. Chem.*, 2005, **24**, 339–374; (c) A. D. Quartarolo, N. Russo and E. Sicilia, *Chem.–Eur. J.*, 2006, **12**, 6797–6803; (d) A. Cui, X. Peng, J. Fan, X. Chen, Y. Wu and B. Chuo, *J. Photochem. Photobiol., A*, 2007, **186**, 85–92; (e) W. Qin, T. Rohand, W. Dehaen, J. N. Clifford, K. Driesen, D. Beljonne, B. Van Averbeke, M. Van der Auweraer and N. Boens, *J. Phys. Chem. A*, 2007, **111**, 8588–8597; (f) M. A. H. Alamiry, A. C. Benniston, G. Copley, K. J. Elliot, A. Harriman, B. Stewart and Y.-G. Zhi, *Chem. Mater.*, 2008, **20**, 4024–4032; (g) F. López Arbeloa, J. Bañuelos, V. Martínez, T. Arbeloa and I. López Arbeloa, *Trends in Physical Chemistry*, 2008, **13**, 101–122.
- (a) A. A. Gorman, I. Hamblett, T. A. King and M. D. Rahn, *J. Photochem. Photobiol., A*, 2000, **130**, 127–132; (b) T. G. Pavlopoulos, *Prog. Quantum Electron.*, 2002, **26**, 193–224.
- (a) A. Loudet and K. Burgess, *Chem. Rev.*, 2007, **107**, 4891–4932; (b) T. E. Wood and A. Thompson, *Chem. Rev.*, 2007, **107**, 1831–1861; (c) G. Ulrich, R. Ziessel and A. Harriman, *Angew. Chem. Int. Ed.*, 2008, **47**, 1185–1201; (d) A. C. Benniston and G. Copley, *Phys. Chem. Chem. Phys.*, 2009, **11**, 4124–4131; (e) M. Benstead, G. H. Mehl and R. W. Boyle, *Tetrahedron*, 2001, **67**, 3573–3601.
- (a) K. Umezawa, A. Matsui, Y. Nakamura, D. Citterio and K. Suzuki, *Chem.–Eur. J.*, 2009, **15**, 1096–1106; (b) M. J. Ortiz, I. García-Moreno, A. R. Agarrabeitia, G. Durán-Sampedro, A. Costela, R. Sastre, F. López Arbeloa and I. López Arbeloa, *Phys. Chem. Chem. Phys.*, 2010, **12**, 7804–7811; (c) V. R. Donuru, S. Zhu, S. Green and H. Liu, *Polymer*, 2010, **51**, 5359–5368; (d) V. Leen, W. Qin, W. Yang, J. Cui, C. Xu, X. Tang, W. Liu, K. Robeyns, L. Van Meervelt, D. Beljonne, R. Lazzaroni, C. Tonnele, N. Boensa and W. Dehaen, *Chem.–Asian J.*, 2010, **5**, 2016–2026.
- (a) J. H. Boyer, A. Haag, M. L. Soong, K. Thangaraj and J. H. Boyer, *Appl. Opt.*, 1991, **30**, 3788–3789; (b) J. H. Boyer, A. M. Haag, G. Sathyamoorthi, M. L. Soong, K. Thangaraj and T. G. Pavlopoulos, *Heteroat. Chem.*, 1993, **4**, 39–49.
- (a) R. W. Wagner, J. S. Lindsey, J. Seth, V. Palaniappan and D. F. Bocian, *J. Am. Chem. Soc.*, 1996, **118**, 3996–3997; (b) R. K. Lammi, A. Ambroise, T. Balasubramanian, R. W. Wagner, D. F. Bocian, D. Holten and J. S. Lindsey, *J. Am. Chem. Soc.*, 2000, **122**, 7579–7591; (c) F. D'Souza, P. M. Smith, M. E. Zandler, A. L. McCarty, M. Itou, Y. Araki and O. Ito, *J. Am. Chem. Soc.*, 2004, **126**, 7898–7907; (d) A. Harriman, L. J. Mallon, S. Goeb and R. Ziessel, *Phys. Chem. Chem. Phys.*, 2007, **9**, 5199–5201; (e) T. Rousseau, A. Cravino, E. Ripaud, P. Leriche, S. Rihn, A. De Nicola, R. Ziessel and J. Roncali, *Chem. Commun.*, 2010, **46**, 5082–5084; (f) S. Kolemen, Y. Cakmak, S. Erten-Elä, Y. Altay, J. Brendel, M. Thelakkat and E. U. Akkaya, *Org. Lett.*, 2010, **12**, 3812–3815; (g) O. A. Bozdemir, Y. Cakman, F. Sozmen, T. Ozdemir, A. Siemiarczuk and E. U. Akkaya, *Chem.–Eur. J.*, 2010, **16**, 6346–6351.
- (a) C. Goze, G. Ulrich, L. Charbonnière, M. Cesario, T. Prangé and R. Ziessel, *Chem.–Eur. J.*, 2003, **9**, 3748–3755; (b) J. L. Bricks, A. Kovalchuk, C. Trieflinger, M. Nofz, M. Büschel, A. I. Tolmachev, J. Daub and K. Rurack, *J. Am. Chem. Soc.*, 2005, **127**, 13522–13529; (c) T. Kálai and K. Hideg, *Tetrahedron*, 2006, **62**, 10352–10360; (d) H. Sunahara, Y. Urano, H. Kojima and T. Nagano, *J. Am. Chem. Soc.*, 2007, **129**, 5597–5604; (e) H. Lu, S. Zhang, H. Liu, Y. Wang, Z. Shen, C. Liu and X. You, *J. Phys. Chem. A*, 2009, **113**, 14081–14086; (f) X. Qian, Y. Xiao, Y. Xu, X. Guo, J. Qian and W. Zhu, *Chem. Commun.*, 2010, **46**, 6418–6436; (g) O. A. Bozdemir, R. Guliyev, O. Buyukcakir, S. Onur, S. Kolemen, G. Gulseren, T. Nalbantoglu, H. Boyaci and E. U. Akkaya, *J. Am. Chem. Soc.*, 2010, **132**, 8029–8036.
- (a) R. P. Haugland, *Handbook of Fluorescent Probes and Research Chemicals*, Molecular Probes, Eugene, OR, 1999; (b) M. L. Metzker, J. Lu and R. A. Gibbs, *Science*, 1996, **271**, 1420–1422; (c) S. A. Farber, M. Pack, S.-Y. Ho, I. D. Johnson, D. S. Wagner, R. Dosch, M. C. Mullins, H. S. Hendrickson, E. K. Hendrickson and M. E. Halpern, *Science*, 2001, **292**, 1385–1388; (d) J.-S. Lee, N.-Y. Kang, Y. K. Kim, A. Samanta, S. Feng, H. K. Kim, M. Vendrell, J. H. Park and Y.-T. Chang, *J. Am. Chem. Soc.*, 2009, **131**, 10077–10082.
- (a) E. Peña-Cabrera, A. Aguilar-Aguilar, M. González-Domínguez, E. Lager, R. Zamudio-Vázquez, J. Godoy-Vargas and F. Villanueva-García, *Org. Lett.*, 2007, **9**, 3985–3988; (b) E. Lager, J. Liu, A. Aguilar-Aguilar, B. Z. Tang and E. Peña-Cabrera, *J. Org. Chem.*, 2009, **74**, 2053–2058.
- (a) I. J. Arroyo, H. Rongrong, G. Merino, B. Z. Tang and E. Peña-Cabrera, *J. Org. Chem.*, 2009, **74**, 5719–5722; (b) C. F. A. Gómez-Durán, I. García-Moreno, A. Costela, V. Martín, R. Sastre, R. Sastre, J. Bañuelos, F. López Arbeloa, I. López Arbeloa and E. Peña-Cabrera, *Chem. Commun.*, 2010, **46**, 5103–5105.
- (a) F. Li, S. I. Yang, Y. Ciringh, J. Seth, C. H. Martin, D. L. Singh, D. Kim, R. R. Birge, D. F. Bocian, D. Holten and J. S. Lindsey, *J. Am. Chem. Soc.*, 1998, **120**, 10001–10017; (b) A. Burghart, H. Kim, M. B. Welsch, L. H. Thoresen, J. Reibenspies and K. Burgess, *J. Org. Chem.*, 1999, **64**, 7813–7819; (c) J. Chen, A. Burghart, A. Derecskei-Kovacs and K. Burgess, *J. Org. Chem.*, 2000, **65**, 2900–2906; (d) H. L. Kee, C. Kirmaier, L. Yu, P. Thamyongkit, W. J. Youngblood, M. E. Calder, L. Ramos, B. C. Noll, D. F. Bocian, W. R. Scheidt, R. R. Birge, J. S. Lindsey and D. Holten, *J. Phys. Chem. B*, 2005, **109**, 20433–20443.
- (a) J. Bañuelos, F. López Arbeloa, V. Martínez, T. Arbeloa, F. Amat-Guerri, M. Liras and I. López Arbeloa, *Chem. Phys. Lett.*, 2004, **385**, 29–35; (b) S. Badré, V. Monnier, R. Méallet-Renault, C. Dumas-Veides, E. Y. Schmidt, A. I. Mikhaleva, G. Laurent, G. Levi, A. Ibañez, B. A. Trofimov and R. B. Pansu, *J. Photochem. Photobiol., A*, 2006, **183**, 238–246; (c) Q. Zheng, G. Xu and P. N. Prasad, *Chem.–Eur. J.*, 2008, **14**, 5812–5819.
- P. Leriche, P. Frère, A. Cravino, O. Alévêque and J. Roncali, *J. Org. Chem.*, 2007, **72**, 8332–8336.
- R. Ziessel, C. Goze, G. Ulrich, M. Césario, P. Retailleau, A. Harriman and J. P. Rostron, *Chem.–Eur. J.*, 2005, **11**, 7366–7378.
- (a) A. Harriman, G. Izzet and R. Ziessel, *J. Am. Chem. Soc.*, 2006, **128**, 10231–10239; (b) A. Harriman, L. J. Mallon, S. Goeb, G. Ulrich and R. Ziessel, *Chem.–Eur. J.*, 2009, **15**, 4553–4564.
- (a) C.-W. Wan, A. Burghart, J. Chen, F. Bergström, L. B.-A. Johansson, M. F. Wolford, T. G. Kim, M. R. Topp, R. M. Hochtrasser and K. Burgess, *Chem.–Eur. J.*, 2003, **9**, 4430–4441; (b) T. G. Kim, J. C. Castro, A. Loudet, J. G.-S. Jiao, R. M. Hochtrasser, K. Burgess and M. R. Topp, *J. Phys. Chem. A*, 2006, **110**, 20–27; (c) M. A. H. Alamiry, A. Harriman, L. J. Mallon, G. Ulrich and R. Ziessel, *Eur. J. Org. Chem.*, 2008, 2774–2782; (d) R. Ziessel and A. Harriman, *Chem. Commun.*, 2011, **47**, 611–631.
- (a) T. Scherer, I. H. M. Van Stokkum, A. M. Brouwer and J. W. Verhoeven, *J. Phys. Chem.*, 1994, **98**, 10539–10549; (b) B. Wegewijs, J. W. Verhoeven and S. E. Braslavsky, *J. Phys. Chem. A*, 1996, **100**, 8890–8894; (c) S. Mula, K. Elliot, A. Harriman and R. Ziessel, *J. Phys. Chem. A*, 2010, **114**, 10515–10522.
- (a) J. W. Verhoeven, T. Scherer and R. J. Willemsse, *Pure Appl. Chem.*, 1993, **65**, 1717–1722; (b) J. W. Verhoeven, *Pure Appl. Chem.*, 1990, **62**, 1585–1596; (c) A. C. Benniston, A. Harriman, V. L. Whittle, M. Zelzer and R. W. Harrington, *Photochem. Photobiol. Sci.*, 2010, **9**, 1009–1017.
- R. Hu, E. Lager, A. Aguilar-Aguilar, J. Liu, J. W. Y. Lam, H. H. Y. Sung, I. D. Williams, Y. Zhong, K. S. Wong, E. Peña-Cabrera and B. Z. Tang, *J. Phys. Chem. C*, 2009, **113**, 15845.
- (a) F. López Arbeloa, T. López Arbeloa and I. López Arbeloa, *Trends Photochem. Photobiol.*, 1994, **3**, 145–155; (b) Z. R. Grabowski, K. Rotkiewicz and W. Rettig, *Chem. Rev.*, 2003, **103**, 3899–4032.

6. Kapitulum V ERANSKINA / ANEXO V al Capítulo 6

11. Artikulua / Artículo 11:

Coumarin/BODIPY hybrids by heteroatom linkage: versatile, tunable and photostable dye lasers for UV irradiation

Physical Chemistry Chemical Physics, 2015, 17, 8239





Cite this: *Phys. Chem. Chem. Phys.*,
2015, 17, 8239

Coumarin–BODIPY hybrids by heteroatom linkage: versatile, tunable and photostable dye lasers for UV irradiation†

I. Esnal,^a G. Duran-Sampedro,^b A. R. Agarrabeitia,^b J. Bañuelos,^{*a} I. García-Moreno,^c M. A. Macías,^d E. Peña-Cabrera,^d I. López-Arbeloa,^a S. de la Moya^{*b} and M. J. Ortiz^b

Linking amino and hydroxycoumarins to BODIPYs through the amino or hydroxyl group lets the easy construction of unprecedented photostable coumarin–BODIPY hybrids with broadened and enhanced absorption in the UV spectral region, and outstanding wavelength-tunable laser action within the green-to-red spectral region (~520–680 nm). These laser dyes allow the generation of a valuable tunable UV (~260–350 nm) laser source by frequency doubling, which is essential to study accurately the photochemistry of biological molecules under solar irradiation. The tunability is achieved by selecting the substitution pattern of the hybrid. Key factors are the linking heteroatom (nitrogen vs. oxygen), the number of coumarin units joined to the BODIPY framework and the involved linking positions.

Received 13th January 2015,
Accepted 23rd February 2015

DOI: 10.1039/c5cp00193e

www.rsc.org/pccp

Introduction

Solar ultraviolet (UV) photons constitute one of the most ubiquitous and potent environmental carcinogens. For this reason, a great deal of work concerning the photophysics and photochemistry of the excited states created in key biomolecules (*e.g.*, nucleic acids) upon exposure to UV light is being conducted, since such states are at the beginning of the complex chain of biochemical events that culminates in photocarcinogenesis.¹ However, more accurate experiments are urgently needed to understand the dynamics of these excited states, which have been stymied by the lack of suitable laser sources providing efficient, stable and tunable UV radiation within the range of 250–350 nm. An attractive approach to overcome this drawback involves the design of new laser dyes with strong UV absorption and highly efficient and stable emission in the visible (Vis) spectral region (500–700 nm), since it constitutes

the only way to generate, efficiently and without undesired re-absorption/re-emission processes, the required tunable UV laser radiation by frequency doubling, and even with ultra-short pumping pulses.

Since it is still difficult to judiciously design single laser dyes fulfilling the mentioned requirements, a powerful strategy is the construction of molecular energy-transfer arrays (coupled or cassette systems) able to undergo efficient excitation energy transfer (EET) from UV-absorbing donors to a covalently-linked Vis-emitting laser dye acting as the acceptor partner. To address this issue, we were prompted to develop unprecedented laser dyes featuring the direct covalent integration of UV-absorbing coumarin (1*H*-chromen-2-one) chromophores into Vis-emitting BODIPY (4,4-difluoro-4-bora-3*a*,4*a*-diazas-indacene) ones (Fig. 1).

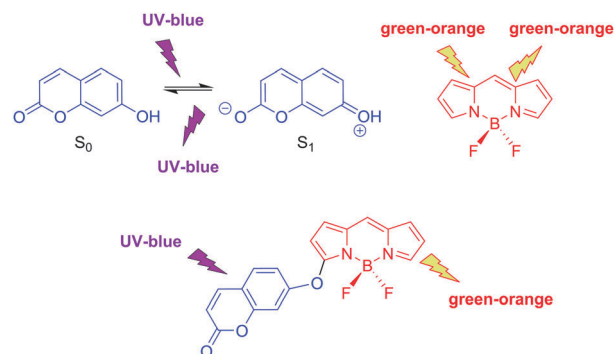


Fig. 1 Simple push-pull 7-hydroxycoumarin (blue) and BODIPY (red) chromophores, and a hybrid system based on them.

^a Depto. de Química Física, Universidad del País Vasco-EHU, Apartado 644, 48080, Bilbao, Spain. E-mail: jorge.bañuelos@ehu.es

^b Depto. de Química Orgánica I, Facultad de CC. Químicas, Universidad Complutense de Madrid, Ciudad Universitaria s/n, 28040, Madrid, Spain. E-mail: santmoya@ucm.es

^c Depto. de Sistemas de Baja Dimensionalidad, Superficies y Materia Condensada, Instituto de Química-Física "Rocasolano", C.S.I.C., Serrano 119, 28006, Madrid, Spain

^d Depto. de Química, Universidad de Guanajuato, Col. Noria Alta s/n, Guanajuato, 36050, Mexico

† Electronic supplementary information (ESI) available: General experimental details, synthetic procedures and characterization data, Fig. S1–S5, Tables S1 and S2, as well as copies of the NMR spectra recorded from new compounds. See DOI: 10.1039/c5cp00193e

Coumarins are an interesting family of fluorescent dyes;² among them, amino and hydroxycoumarin derivatives (mainly 7-amino and 7-hydroxycoumarins) are especially significant because their photophysical signatures are ruled by internal charge transfer (ICT) upon light absorption (classic push-pull dyes, see Fig. 1),³ which is valuable for developing certain applications (e.g., fluorescent sensing by ICT modulation).⁴ Moreover, simple amino and hydroxycoumarins are characterized by absorbing and emitting in the UV/blue-edge spectral region, taking the emission place with relatively large quantum yield,⁵ which has been used for developing blue dye lasers.² However, coumarins are not as photostable as other common laser dyes, and they usually undergo bleaching under long UV pumping.⁶

On the other hand, BODIPYs constitute a recognized family of Vis-emitting dyes with noticeable utility in the development of a plethora of photonic tools,⁷ due to their excellent photophysical properties, high solubility in organic solvents improving dyed-material processability (e.g., in the preparation of organic films), and possibility of selective functionalization to finely modulate their physical properties.⁷ The usually large molar-absorption coefficients (ϵ) and high fluorescence quantum yields (ϕ) of BODIPYs have promoted their application as fluorescent dyes for lasing.^{7d,8} On the other hand, the characteristic green/orange-edge emission of the BODIPY chromophore should be highly interesting for developing tunable UV lasers by frequency doubling. However, two important drawbacks limit this application: low absorption in the UV spectral region, and small Stokes shifts enabling undesired re-absorption/re-emission processes.

Despite the outstanding and spectrally-complementary photophysical properties of BODIPYs and coumarins, cassettes combining both chromophores are scarce.⁹ Thus, the unique two molecular coumarin-BODIPY cassettes described up to now were attained by linking a naked coumarin (non aminated, nor hydroxylated) to a BODIPY chromophore, hence without heteroatom linkage.^{9b} On the other hand, non-cassette coumarin-BODIPY hybrids obtained by fusing,^{10a} or by linking through a hydrocarbonated spacer,^{4,10b} both moieties are described to exhibit interesting photophysical properties (e.g., ICT processes giving place to large Stokes shifts), which are useful for developing certain photonic tools.^{4,10} It should be noted that none of these systems have been evaluated as laser dyes. Furthermore, challenging coumarin-BODIPY hybrids involving push-pull amino or hydroxycoumarins covalently linked to the BODIPY chromophore through the amino or hydroxyl heteroatom (note the possibility of ICT processes involving both chromophores) are unknown.

All the above mentioned prompted us to develop the latter coumarin-BODIPY hybrids (e.g., see hybrid based on 7-hydroxycoumarin shown in Fig. 1). The main goals of these new molecular dyes should be: (1) a strong UV-blue absorption enabling an efficient green-orange fluorescence and laser, (2) the possibility of emission modulation by tuning ICT processes involving both chromophores¹¹ and, (3) enhanced photostability of the involved chromophores by its mutual covalent linkage,^{8a,b} which is especially interesting in the case of the photounstable coumarin partner.

Result and discussion

Synthesis

For our purpose, we chose the coumarin-BODIPY structures shown in Fig. 2 (i.e., 1-4dX and 2-4mX, with X = A, B or C). These structural designs were selected on the basis of synthetic accessibility, and possibility of cassette behavior (1dX case) or photophysics modulation by tuning ICT processes (rest of the cases).

Dicoumarin-substituted O-BODIPY 1dA was straightforwardly obtained from commercial 2,6-diethyl-1,3,5,7,8-pentamethyl-BODIPY (PM567, 1), a known strongly fluorescent green-emitting dye,¹² by AlCl₃ promoted substitution of fluorine^{8c,13} by the corresponding coumarin (see Fig. 3). On the other hand, monocoumarin- and dicoumarin-substituted BODIPYs 2mX and 2dX, 3mX and 3dX, and 4mX and 4dX were obtained by controlled aromatic nucleophilic substitution in 3,5-dichloro-BODIPYs (mono or disubstitution),¹⁴ using the corresponding coumarin (AH, BH or CH) as the nucleophile, and 3,5-dichloro-8-(*p*-tolyl)BODIPY (2),^{14a} 3,5-dichloro-8-mesitylBODIPY (3)¹⁵ or 3,5-dichloro-8-(trifluoromethyl)BODIPY (4)^{14b} as the corresponding starting BODIPY. The latter dihaloBODIPYs were selected on the basis of their synthetic accessibility (Fig. 3), and the different stereoelectronic influence of their *meso* groups (R) in the photophysics of the BODIPY chromophore. On the other hand, the coumarins used as nucleophiles in the mentioned halogen (fluorine or chlorine) substitutions were commercial 7-hydroxy-4-methyl-2H-chromen-2-one (AH), 7-amino-4-methyl-2H-chromen-2-one (BH) and 4-hydroxy-2H-chromen-2-one (CH).

Chlorine substitutions on less-activated 2 and 3 (when compared to trifluoromethylated 4) with less nucleophilic hydroxycoumarins AH and CH (when compared to aminocoumarin BH) required specific base catalysis (see Fig. 3). On the other hand, since highly activated 4 was tested to decompose under the employed basic conditions, chlorine substitutions on it (especially by using less activated hydroxycoumarins) were promoted by microwave (MW) irradiation (see Fig. 3). Finally, the synthesis of disubstituted derivatives (2dX) required stronger reaction conditions (e.g., longer times; see ESI[†]) because the involved monosubstituted intermediates (2mX) are less activated than the

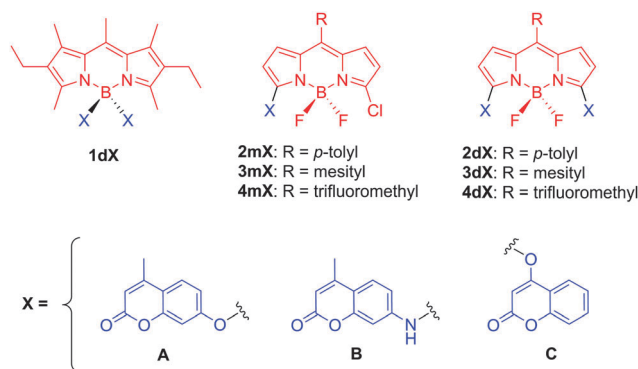


Fig. 2 Selected structural designs for coumarin-BODIPY hybrids (up, X = A, B or C), and corresponding coumarin moieties (down).

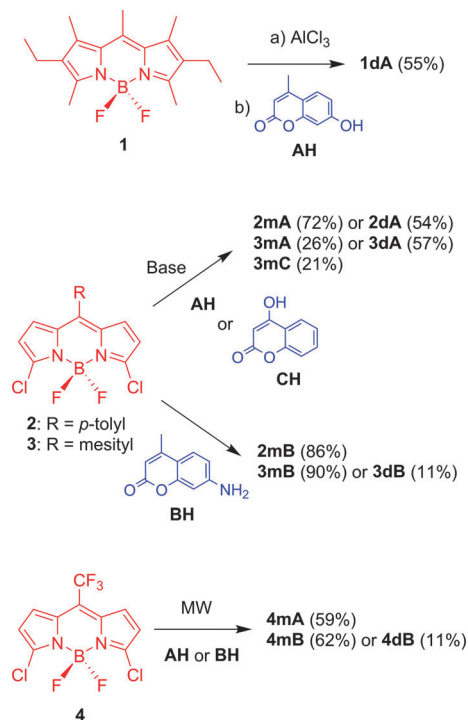


Fig. 3 Synthesis of coumarin-BODIPY hybrids (see ESI† for experimental details). Yields in parentheses.

corresponding starting dichloroBODIPYs. This fact is especially significant in the case of the amino derivatives (note the less electron-withdrawing effect of nitrogen when compared with oxygen), and explains the low yield when obtaining **3dB** (null in the case of **2dB**), and the use of MW irradiation for obtaining **4dB** (together with **4mB**) from **4** (see Fig. 3).

Photophysics

The absorption spectrum of **1dA** was almost the sum of the absorptions of the individual chromophores involved in its molecular structure, as shown by its comparison with the spectra recorded for **1** and **AH** (double concentration for the latter since two coumarins are involved in **1dA**, see Fig. 4). Therefore, no noticeable electronic coupling between chromophores exists in **1dA**, at least at its ground state, as it was expected by the role of the linking boron in the BODIPY partner. Indeed, boron is an advisable linking position to develop molecular cassettes based on BODIPY, since it does not participate in the cyanine-like π -system of the BODIPY chromophore, but provides rigidity to it.¹⁶ Theoretical calculations (B3LYP/6-31g) conducted on **1dA** (see ESI†) also support the claimed electronic isolation of chromophores. Thus, the conducted time dependent quantum mechanical simulation (see ESI†) predicts the involvement of molecular orbitals placed exclusively at the coumarin moiety, or at the BODIPY one, for the main electronic transitions associated with each absorption band (UV and Vis) of **1dA** (see Fig. S1 in ESI†). This photophysical result is also supported by electrochemical measurements (see ESI†). Thus, the oxidation and reduction waves recorded in the cyclic voltammogram of **1dA** match almost

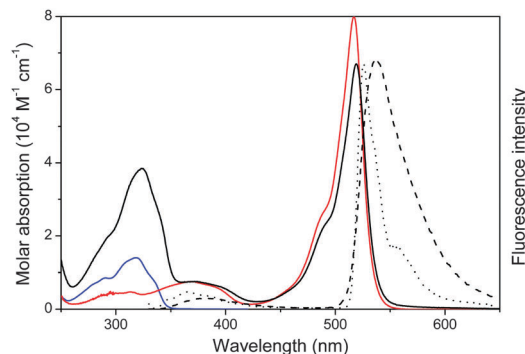


Fig. 4 Absorption spectra (bold) of **1dA** (black), **1** (red) and **AH** (blue), and normalized fluorescence spectra of **1dA** (dashed at room temperature; dotted at 77 K) upon UV irradiation (325 nm) in ethanol (see ESI† for experimental details).

perfectly with those registered for each individual parent molecules **1** and **AH** (see Fig. S2 in ESI†).

In this regime, very weak electronic-coupling limit, the cassette-required selective excitation of chromophores should be feasible. In fact, exciting the BODIPY or the coumarin chromophore in **1dA** (Vis or UV irradiation, respectively) leads to the typical fluorescent BODIPY signature (see Fig. 4). Noticeably, the characteristic high quantum yield of the BODIPY chromophore was maintained by UV excitation ($\phi = 82\%$, see Table S1 in ESI†). Moreover, the observed coumarin-BODIPY intramolecular EET process is highly efficient (approaching the 100%), as demonstrated by the residual emission from the coumarin chromophore, despite its direct excitation (see Fig. 4). The short donor-acceptor distance (~ 5 Å between chromophoric centers, as predicted theoretically) ensures a fast and efficient quenching of the donor by the EET to the acceptor BODIPY.

The EET in **1dA** should take place by the Förster resonance energy-transfer (FRET) mechanism,¹⁷ taking into account: (1) the feasible spectral overlap of the emission transitions of the coumarin donor not only with the UV absorption transitions of the acceptor BODIPY (*e.g.*, $S_0 \rightarrow S_2$),¹⁸ but also with the Vis ones, although in less extension (see Fig. S3 in ESI†); (2) the spatial proximity of the involved chromophores; (3) the lack of orbital overlap avoiding the electronic exchange required by the through-bond energy-transfer (TBET) mechanism,¹⁹ due to the spacing imposed by the tetrahedral boron. Indeed, the EET efficiency of **1dA** was practically the same when decreasing the temperature, even at 77 K, where the electronic-exchange mechanism (an energy-activated process) is virtually nullified.²⁰ The hypsochromic shift and narrowing of the fluorescence signal upon freezing the sample (Fig. 4) is merely due to the low temperature, which lowers the relaxation of the excited state upon irradiation, and hinders the vibrational motion.

Regarding hybrids based on **2** (see Fig. 2), their fluorescence response is limited by the rotational free motion of the *p*-tolyl moiety, which drastically enhanced the probability of de-excitation by internal conversion ($\phi = 25\%$ for **2**; see Fig. 5, and Table S1 in ESI†).²¹ Linking hydroxycoumarin **AH** to BODIPY **2**, to generate

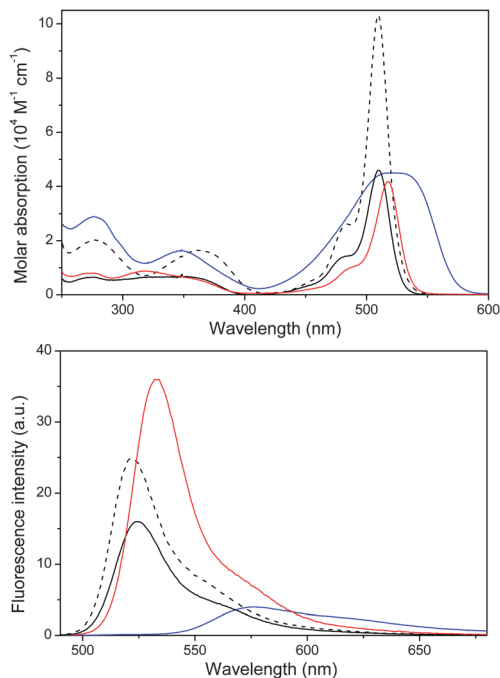


Fig. 5 Absorption (up) and fluorescence (down, upon Vis irradiation) spectra of **2** (dashed), **2mA** (black), **2mB** (blue) and **2dA** (red) in ethyl acetate (see ESI[†] for experimental details).

hybrid **2mA**, gives rise to a slight decrease in the quantum yield of the BODIPY emission upon Vis irradiation, but without noticeable changes in the shape and position of both the absorption and the emission band (*cf.* **2** and **2mA** in Fig. 5, and in Table S1 in ESI[†]). However, the replacement of the oxygen linkage of **2mA** by nitrogen in **2mB** decreases significantly the fluorescence ($\phi = 4\%$), shifts the spectral bands towards the red (mainly in fluorescence, up to ~ 55 nm), and broadens them (mainly in absorption); (see Fig. 5, and Table S1 in ESI[†]).

The mentioned effect observed in **2mB** must result from a strong electronic coupling between the aminocoumarin and the BODIPY due to the involved nitrogen linkage. Additionally, the nitrogen must promote an ICT process, from the coumarin to the BODIPY, due to its known electron-donating ability (note its +K conjugative effect). The ICT must be also favored by the electron-withdrawing effect exerted by the chlorine (strong $-I$ inductive effect) on the BODIPY chromophore. Indeed, the computed frontier orbitals (B3LYP/6-31g; see ESI[†]) for amino-coumarin-based **2mB** are extended through the whole molecular structure (see Fig. S4 in ESI[†]), which supports an ICT process by the HOMO \rightarrow LUMO transition. However, the frontier orbitals for hydroxycoumarin-based **2mA**, where the more-electronegative less-conjugative oxygen linkage is involved, shows that the coumarin-BODIPY electronic interaction is much weaker. In fact, the computed frontier orbitals for hybrid **2mA** are mainly located at the BODIPY core, with a small contribution of the oxygen atom (see Fig. S4 in ESI[†]). As a consequence of the transfer of electronic density from the coumarin fragment to the BODIPY moiety, not only the fluorescence efficiency decreases, but also the fluorescence lifetimes become faster (see data collected in Table S1 in

ESI[†]). The ICT-character of the emitting state implies also an increase of the deactivation rate constants, especially the non-radiative one. Thus, the amino connection induces a more pronounced fluorescence-quenching than the oxygen linkage, due to the less electron-donor character of the latter. Likely, the higher charge-separation promoted in the former case further enhances the non-radiative deactivation probability.

Noticeably, linking an additional AH moiety in **2mA**, to generate hybrid **2dA**, boosts the fluorescence quantum up to 36%, producing also a modest red shift in both the absorption and the emission bands (see Fig. 5, and Table S1 in ESI[†]). In agreement with this observation, we have previously demonstrated that symmetrically substituting the 8-(*p*-tolyl)BODIPY chromophore with electronegative atoms at the C3 and C5 BODIPY positions ameliorates the negative effect produced by the aryl motion.²¹ Noteworthy, the time dependent simulations of **2**, **2mA**, **2mB** and **2dA** (see Table S2 in ESI[†]) also predict the observed shifts of the absorption bands as a consequence of an increase in the HOMO energy. These agreements of the theoretical predictions with the experimental findings confirm the goodness of the conducted computations.

Although hybrids **2mA**, **2mB** and **2dA** are not able to work as real cassettes because the excitation energy is truly delocalized over both BODIPY and coumarin moieties, especially in nitrogen-linked **2mB** where the electron coupling is more important (*cf.* frontier orbitals in Fig. S4 in ESI[†]), the UV irradiation gives rise to the same Vis emission observed upon Vis irradiation, without detecting the emission signal from the coumarin. However, the observed EET cannot be adequately described by a FRET mechanism, due to the demonstrated high electronic interaction between coumarin and BODIPY moieties (highlighted also by the noticeable different absorption spectra for hybrids and corresponding individual chromophores; *cf.* the Vis absorptions of **2mB** and **2** in Fig. 5). Thus, the EET observed in these hybrids really lies in a coherent process, where the excitation oscillates back and forth between the donor coumarin and the acceptor BODIPY. In these cases, where an electronic mechanism takes place (strong coupling limit), the EET process is extremely fast and efficient.

Restricting the conformation motion of the phenyl ring in *meso*-arylBODIPYs, *via* the sterical hindrance induced by *ortho* methyl groups in the aryl moiety, is known to increase the BODIPY fluorescence by decreasing the probability of non-radiative deactivation pathways (*cf.* **2** and **3** in Table S1 in ESI[†]). Thus, mesityl-based hydroxycoumarin hybrids **3mA** and **3dA** are more fluorescent than the corresponding *p*-tolyl analogues **2mA** and **2dA**. Indeed, the fluorescence quantum yields of **3mA** and **3dA** are similar to those obtained for parent **3** (higher than 90%; see Fig. 6 and Table S1 in ESI[†]). The same effect is observed when the 7-hydroxycoumarin moiety of **3mA** is substituted by the 3-hydroxycoumarin moiety in **3mC** (see Table S1 in ESI[†]). However, the strong electronic interaction provided by the nitrogen linkage, when compared with the oxygen one, makes the aminocoumarin-based **3mB** to lose fluorescence ability ($\phi = 7\%$), probably due to the same ICT process invoked for **2mB**. Indeed, the absorption band of **3mB** is broader,

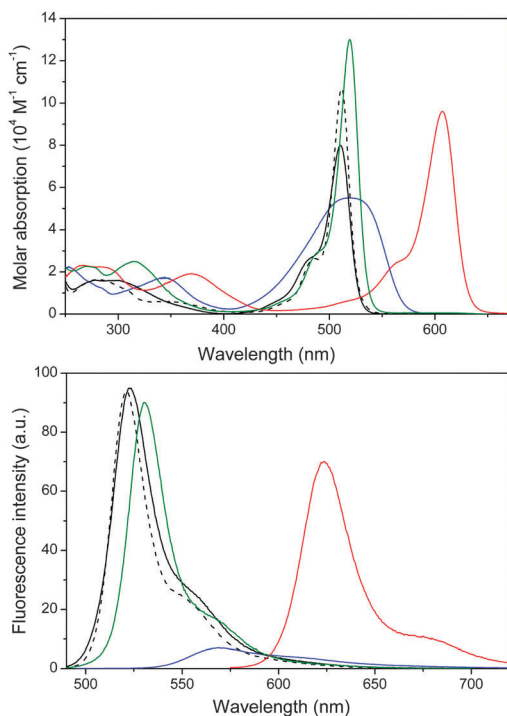


Fig. 6 Absorption (up) and fluorescence (bottom, upon Vis irradiation) spectra of **3** (dashed), **3mA** (black), **3mB** (blue) and **3dA** (green) and **3dB** (red) in ethyl acetate (see ESI† for experimental details).

the Stokes shift is larger, and the fluorescence lifetimes are shorter (*cf.* Fig. 5 and 6; see Table S1 in ESI†) than those recorded for **2mB**, due to the higher electronic interaction provided by the nitrogen linkage.

Switching off the ICT process of **3mB**, by introducing a second unit of aminocoumarin to generate **3dB** (note the suppression of the chlorine electronic effect), boosts the fluorescence efficiency ($\phi = 70\%$; see Fig. 6 and Table S1 in ESI†). Noticeably, a deep red shift of both the absorption and emission spectral bands is now observed, recovering such bands of the typical narrow shape (vibrational resolution) and Stokes shift of parent **3** (*cf.* **3**, **3mB** and **3dB** in Fig. 6, and in Table S1 in ESI†). This spectral shift was properly predicted by the time dependent simulation also (see Table S2 in ESI†). All these data demonstrate the lack of ICT in **3dB**, as well as the existence of an extended conjugation involving coumarins and BODIPY (see Fig. S5 in ESI†). Once again, the UV irradiation of **3dB** was tested to produce the same Vis emission that the obtained by Vis irradiation, showing that this coumarin–BODIPY hybrid could be a promising UV-pumped lasing dye with efficient emission in the orange-edge of the red region (623 nm, see Fig. 6) and, therefore, a promising UV-emitting lasing dye (*ca.* 310 nm) by frequency doubling.

A clear experimental proof of the strong electronic interaction between BODIPY and coumarin moieties in hybrids **3dA** and **3dB** is provided by their electrochemical behavior when compared with the exhibited by parent **3** in the same conditions (see Fig. 7). Thus, the oxidation potential decreases noticeably from 1.70 V for **3** (irreversible process), to 1.18 V and 0.63 V for

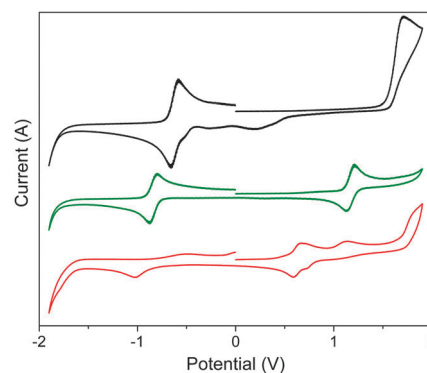


Fig. 7 Cyclic voltammograms of **3** (black), **3dA** (green) and **3dB** (red) in acetonitrile (see ESI† for experimental details).

3dA and **3dB**, respectively (reversible processes; a second oxidation wave at 1.13 V is additionally detected for **3dB**). Moreover, it is observed that the lower the oxidation potential, the closer are the cathodic and anodic peaks (see Fig. 7). These results suggest that the HOMO energy, which is related to the oxidation ability, is significantly higher for the hybrids, as a consequence of the electronic coupling. Therefore, the absorption energy gap, which is related to the separation between the cathodic and anodic peaks, is also significantly lower for the hybrids, in agreement with both the observed absorption red-shifts (see Fig. 6) and the computational predictions (see Table S2 in ESI†).

Regarding hybrids based on **4**, their photophysics are characterized by the marked red-shift of the spectral bands imposed by the *meso* trifluoromethyl group (*cf.* **2**, **3** and **4** in Table S1 in ESI†). Thus, the strong $-I$ inductive effect exerted by the *meso* trifluoromethyl group must stabilize preferentially the LUMO state, since it is characterized by a high electronic density at the *meso* position, and differently to that occurring at the HOMO, where a node is placed at such position (*cf.* the HOMO and LUMO computed for **2** in Fig. S4 in ESI†). This fact must decrease the absorption energy gap, as supported by the conducted theoretical simulations (see Table S2 in ESI†), explaining the observed absorption shifts. However, the same effect should also boost undesired ICT processes from the coumarin to the BODIPY, mainly in the case of mono-aminocoumarin-based **4mB**, but also in mono-hydroxycoumarin-based **4mA**. In fact, **4mB** is observed to be not fluorescent, while **4mA** exhibits less fluorescence ($\phi = 40\%$) and faster lifetime than parent **4** (see Table S1 in ESI†).

Analogous to **3dB**, the double-aminocoumarin substitution of **4dB** enhances the fluorescence ability by decreasing the probability of the fluorescence-quenching ICT process (note the lack of the ICT-promoting chlorine), as well as pushes the spectral bands deeply toward the red region (*cf.* **4mA** and **4dB** in Fig. 8), by the establishment of an extended conjugation (*cf.* the computed energy gaps dated in Table S2 in ESI†). It must be noted that the high fluorescence efficiency ($\phi = 70\%$) of red-emitting (665 nm) **4dB**, joined to the tested viability of both UV or Vis excitation to record the same Vis emission, makes this dye potentially valuable as a red-emitting lasing dye, but also as a UV-emitting one (*ca.* 330 nm) by frequency doubling.

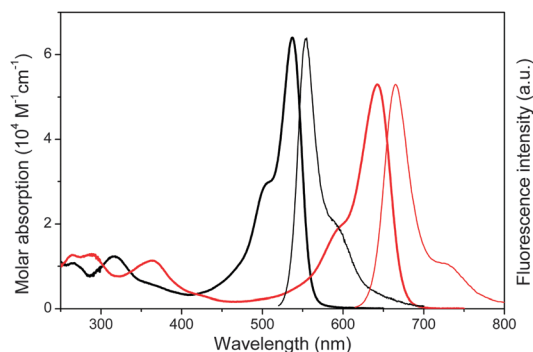


Fig. 8 Absorption (bold) and corresponding normalized fluorescence (thin, upon Vis irradiation) of **4mA** (black) and **4dB** (red) in ethyl acetate (see ESI† for experimental details).

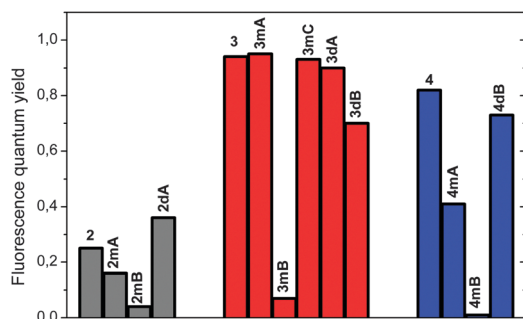


Fig. 9 Fluorescence efficiency of BODIPY-coumarin hybrids and corresponding parent BODIPYs in ethyl acetate (data from Table S1 in ESI†).

The fluorescence efficiency of the studied BODIPY-coumarin hybrids, together with the corresponding parent BODIPYs, is graphically compared in Fig. 9, showing that the most promising hybrids for our purpose (lasing by UV pumping) are **3mA**, **3mC**, **3dA**, **3dB** and **4dB**.

Laser behavior

With the exception of non-fluorescent **4mB** (see Fig. 9), all the obtained coumarin-BODIPY dyes exhibited laser emission either by standard pumping in the UV (355 nm) as in the Vis (532 nm) spectral region. Moreover, coumarin-BODIPY hybridization led to a significant increase in the dye absorption at both pumping wavelengths. This is a key factor from the laser point of view, since it allows reducing significantly the required gain-media concentrations avoiding, consequently, solubility problems, or quenching and/or aggregation processes, all of them with detrimental effects on the laser emission. For instance, hybrid dye **3mB** exhibited molar absorption coefficients of 1.6×10^4 and $5.3 \times 10^4 \text{ M}^{-1} \text{ cm}^{-1}$, at 355 and 532 nm, respectively, which are well above the coefficients exhibited by parent **3** ($0.6 \times 10^4 \text{ M}^{-1} \text{ cm}^{-1}$ at both wavelengths).

Since this work is focused on the development of BODIPY laser dyes able to be UV pumped, we have deeply studied the laser behavior of the obtained coumarin-BODIPY hybrids under laser UV irradiation. To optimize the laser action, we analyzed first the dependence of the laser emission on the dye

concentration, keeping constant the rest of the experimental parameters. Ethyl acetate solutions (1 cm path length) with optical densities within the range 1–35 were studied (see ESI†). Thus, under the experimental conditions (transversal excitation and strong focusing of the incoming pumping radiation), the concentration of the dye must be in the millimolar range to ensure total absorption of the pumping radiation over the first millimeter at most of the sample solution, in order to obtain an emitted beam with near-circular cross section optimizing the lasing efficiency, which is defined as the ratio between the energy of the laser output and the pumping energy incising on the sample surface.

Broad-line-width laser emission, with a pump threshold energy of ~ 0.6 mJ, divergence of 5 mrad and pulse duration of 8 ns full width at half maximum (FWHM), was obtained from all the fluorescent hybrid dyes when placed in a simple plane-plane non-tunable resonator. The lasing properties recorded at the optimal concentration for the studied coumarin-BODIPY hybrids and parent BODIPYs are shown in Table 1, showing good correlation with their photophysical properties: the higher the fluorescence quantum yield, the higher is the lasing efficiency; the longer the fluorescence wavelength, the “redder” is the lasing emission; the lower the non-radiative rate constant, the higher is the lasing photostability.

Hybrid dyes based on 3,5-dicoumarin-substituted BODIPY and involving oxygen linkers (**2dA** and **3dA**) achieved laser efficiencies up to 51%, which are much higher than those reached by the corresponding unsubstituted parent dyes **2** and **3** (see Table 1). In fact, the laser efficiency of **3** was poor under the selected laser conditions (28%), whereas **2** and **4** did not exhibit laser emission, but for different reasons. Thus, while the

Table 1 Lasing properties of coumarin-BODIPY hybrids and parent BODIPY dyes in ethyl acetate solution under transversal UV pumping at 335 nm (see ESI for experimental details)

Dye	$[c]^a/\text{mM}$	Eff. ^b (%)	λ^c/nm	I_n^d (%)	$n/1000^e$
1	12	20	575	0	6
1dA	2	45	565	25	50
2^f	—	—	—	—	—
2mA	1	21	552	20	50
2mB	1	14	610	0	50
2dA	1	35	562	35	50
3	12	22	590	0	50
3mA	2	46	555	40	50
3mB	1	8	615	20	50
3mC	2	45	540	55	50
3dA	2	51	575	55	50
3dB	1	25	645	30	50
4^f	—	—	—	—	—
4mA	1	30	615	35	50
4mB^f	—	—	—	—	—
4dB	1	40	680	55	50

^a Dye concentration optimizing its laser action in ethyl acetate solution.

^b Lasing efficiency, as the ratio between the energy of the laser output and the pump energy incident on the sample surface. ^c Peak wavelength for the laser emission. ^d Intensity decay for the laser-induced fluorescence emission after n pumping pulses at a 10 Hz repetition rate, and measured as $100(I_n/I_0)$ with I_0 being the initial intensity and I_n the after n pulses. ^e Number of pumping pulses. ^f Absence of laser emission under any lasing conditions at 335 nm.

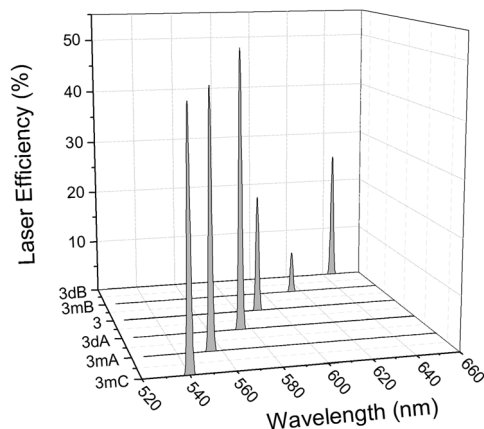


Fig. 10 Lasing emission spectra of BODIPY **3** and their coumarin-BODIPY hybrids **3mA**, **3mB**, **3mC**, **3dA** and **3dB** (data from Table 1).

laser behavior of **2** is due to its low fluorescence yield (see Fig. 9) preventing laser action, the absence of laser emission from **4** is only caused by its low absorption at the selected pumping UV wavelength. Thus, when **4** is pumped in the Vis region at 532 nm, efficient laser emission (68%) centered at 600 nm is recorded.

In the case of coumarin-3 hybrids, the high laser efficiency recorded for the oxygen-linked monocoumarin hybrids **3mA** and **3mC** (*ca.* 45%; see Table 1) must be highlighted, which agrees well with their high fluorescence quantum yields (95% and 93%, respectively, see Fig. 9). More surprising was the peculiar behavior of other monocoumarin hybrids, such as **2mA**, **2mB** and **3mB**, because although they exhibited very low fluorescence quantum yields (4%, 16% and 7%, respectively; see Fig. 9), they not only presented laser emission but also with laser efficiencies as high as 21% (see Table 1). This fact can be explained by the ICT-character of the emitting states of these hybrids (see the Photophysics section), leading to: (a) high Stokes shift (up to 1700 cm^{-1}), which reduces re-absorption/re-emission processes and, thus, their deleterious effect in the laser action; (b) very short fluorescence lifetimes (below to 0.28 ns), which lead to radiative-rate constants similar to those observed for the other hybrid dyes; and (c) high dipole moments allowing the molecular alignment with respect to the polarization of the exciting laser beam to enhance the emission efficiency of the media.²² The combination of all these factors in the same molecule (see Table S1 in ESI[†]) is the origin of the unique lasing properties exhibited by these hybrids.

Depending on the number and position of coumarin units joined to the BODIPY framework as well as on the nature of the linking heteroatom, the wavelength of the laser emission shifts towards the blue or towards the red with respect to the corresponding parent (unsubstituted) BODIPY. For instance, in the case of hybrids based on **3**, hydroxycoumarin hybridization (**3mA**, **3dA** and **3mC**) leads to noticeable hypsochromic shifts, whereas the aminocoumarin hybridization (**3mB** and **3dB**) does the opposite (*i.e.*, towards the red, see Table 1). Noticeably, the dye series based on **3** enables to reach wavelength-tunable laser action within the green-to-red spectral region (520–660 nm; see Fig. 10).

An important parameter for any practical application of the dye lasers is their lasing photostability under repeated pumping. Table 1 collects data on the decrease of the laser-induced fluorescence intensity of the studied coumarin-BODIPY hybrids and their corresponding parent BODIPYs and coumarins, under transversal excitation of capillary containing dye solutions after n pump pulses at 10 Hz repetition rate (see ESI[†]). It is well-known that coumarins are rather unstable dyes under laser irradiation. In fact, the studied coumarins lost their laser emission completely after just 6000 pump pulses under the selected experimental conditions. However, data in Table 1 demonstrate that the new coumarin-BODIPY hybrids became photostable laser dyes, enhancing significantly the photostability recorded for the corresponding parent BODIPYs.

This improvement of the photostability must be related to the excitation energy transfer from the coumarin moieties to the BODIPY core, which allows reducing the rate and extension of the photodegradation processes undergone by coumarins under UV laser irradiation. This behavior is widespread to all the herein developed hybrids, regardless of the acting EET mechanism: *via* FRET if the coumarins are linked to the BODIPY boron, or by electron coupling if they are directly anchored to the BODIPY chromophore. Once again, the dicoumarin-based hybrids involving oxygen as a linking atom became the most photostable, retaining up to 55% of the initial emission after 50 000 pumping pulses. In other words, albeit the photochemically unstable coumarin fragment is directly pumped, the fast transfer of the excitation energy to the BODIPY *via* electronic coupling provides an optimal laser performance over long exposure periods to irradiation.

Conclusions

Unprecedented coumarin-BODIPY hybrids involving push-pull amino or hydroxycoumarins covalently linked to the BODIPY chromophore through to the amino or hydroxyl coumarin heteroatom could be straightforwardly attained from the corresponding coumarins and BODIPYs by nucleophilic halogen-substitution processes involving the boron or the C3/5 BODIPY position, and adjusting conveniently the reaction conditions to promote and control the substitution reactivity, which is especially important in the case of the hybrids based on 3-coumarin or 3,5-dicoumarin-substituted BODIPY involving oxygen as linkage.

The photophysical signatures of the obtained hybrid dyes are controlled by the type and number of coumarin units, as well as by the involved BODIPY linking position and coumarin linking heteroatom (N or O). Thus, boron is demonstrated to be an optimal linking site to promote BODIPY emission by UV irradiation *via* FRET, whereas the direct connection of the coumarin to the conjugated framework of the BODIPY chromophore allows a fine modulation of the spectroscopical properties of the dye. Thus, BODIPY double-substitution with aminocoumarins is recommended to avoid undesired ICT phenomena, and achieve bright emission pushed to the red edge, due to a strong resonant

interaction, whereas hydroxycoumarins are recommended for enhancing the fluorescence performance.

The developed fluorescent coumarin–BODIPY hybrid dyes undergo lasing with good efficiency and high stability, allowing wavelength finely tunable over a wide range (~520–700 nm). Moreover, their laser action is enhanced when compared with the corresponding parent dyes, and correlates well with their photophysics. The highest lasing efficiencies (up to 51% at 355 nm) were recorded from hybrids based on two hydroxycoumarin and 3,5-disubstituted BODIPY. These hybrids also proved to be the most photostable, with laser emission remaining up to 55% of its initial level after 50 000 pump pulses at a 10 Hz repetition rate.

The attainment of these novel hybrid dyes based on BODIPY and coumarin, with strong UV absorption and highly efficient and stable laser emission in the green-red spectral region, concerns one of the greatest challenges in the ongoing development of advanced photonic materials with relevant applications. In fact, these organic dyes are the only ones that allow, by frequency doubling, the generation of tunable UV (~260–350 nm) laser radiation with ultra-short pulses. Radiation with these characteristics is essential to analyze accurately the photochemistry of biological molecules, as important as nucleic acids, trying to understand their stability under solar radiation, since their excited states are known to be involved at the beginning of the complex biological events that culminates in photodamage, including photocarcinogenesis, a growing human health problem.

Acknowledgements

Financial support from Spain (MINECO: MAT2010-20646-C04-01, 02 and -04) and Mexico (DAIP: 2014, and CONACyT: 123732I) is gratefully acknowledged. I. E. thanks Gobierno Vasco for a research contract (IT339-10). G. D.-S. thanks MINECO for a predoctoral FPI grant.

Notes and references

- For example, see: C. E. Crespo-Hernández, B. Cohen, P. M. Hare and B. Kohler, *Chem. Rev.*, 2004, **104**, 1977.
- (a) in *Dye Lasers*, ed. F. P. Schäfer, Springer-Verlag, New York, 3rd edn, 1990; (b) in *Dye Laser Principles*, ed. F. J. Duarte and L. W. Hillman, Academic, New York, 1990; (c) F. López Arbeloa, I. López Arbeloa and T. López Arbeloa, in *Handbook of Advanced Electronic and Photonic Materials and Devices*, ed. H. S. Nalwa, Academic Press, San Diego, 2001, vol. 7; (d) F. J. Duarte, *Tunable Laser Optics*, Elsevier Academic, New York, 2003.
- (a) J. Wang, S. Qian and J. Cui, *J. Org. Chem.*, 2006, **71**, 4308; (b) G. Signore, R. Nifosi, L. Albertazzi, B. Storti and R. Bizzarri, *J. Am. Chem. Soc.*, 2010, **132**, 1276.
- (a) S. Lin and W. S. Struve, *Photochem. Photobiol.*, 1991, **54**, 361; (b) X. Cao, W. Lin, Q. Yu and J. Wang, *Org. Lett.*, 2011, **13**, 6098; (c) Y. Qian, B. Yang, Y. Shen, Q. Du, L. Lin, J. Lin and H. Zhu, *Sens. Actuators, B*, 2013, **182**, 498;
- (d) A. K. Bhoi, S. K. Das, D. Majhi, P. K. Sahu, A. Nijamudheen, N. Anoop, A. Rahaman and M. Sarkar, *J. Phys. Chem. B*, 2014, **118**, 9926; (e) D. Majhi, S. K. Das, P. K. Sahu, S. M. Pratik, A. Kumar and M. Sarkar, *Phys. Chem. Chem. Phys.*, 2014, **16**, 18349.
- (a) B. Wagner, *Molecules*, 2009, **14**, 210; (b) X. Liu, Z. Xu and J. M. Cole, *J. Phys. Chem. C*, 2013, **117**, 16584.
- (a) G. Jones II, W. R. Jackson, C.-Y. Choi and W. R. Bergmark, *J. Phys. Chem.*, 1985, **89**, 294; (b) S. C. Guggenheimer, J. H. Boyer, K. Thangaraj, M. P. Shah, M. L. Soong and T. G. Pavlopoulos, *Appl. Opt.*, 1993, **32**, 3942.
- (a) A. Loudet and K. Burgess, *Chem. Rev.*, 2007, **107**, 4891; (b) G. Ulrich, R. Ziessel and A. Harriman, *Angew. Chem., Int. Ed.*, 2008, **47**, 1184; (c) F. L. Arbeloa, J. Bañuelos, V. Martínez, T. Arbeloa and I. López Arbeloa, *Trends Phys. Chem.*, 2008, **13**, 101; (d) M. Benstead, G. H. Mehl and R. W. Boyle, *Tetrahedron*, 2011, **67**, 3573; (e) N. Boens, V. Leen and W. Dehaen, *Chem. Soc. Rev.*, 2012, **41**, 1130; (f) A. Kamkaew, S. H. Lim, H. B. Lee, L. V. Kiew, L. Y. Chung and K. Burgess, *Chem. Soc. Rev.*, 2013, **42**, 77; (g) A. Bessette and G. S. Hanan, *Chem. Soc. Rev.*, 2014, **43**, 3342; (h) H. Lu, J. Mack, Y. Yang and Z. Shen, *Chem. Soc. Rev.*, 2014, **43**, 4778.
- (a) Y. Xiao, D. Zhang, X. Qian, A. Costela, I. García-Moreno, V. Martín, M. E. Pérez-Ojeda, J. Bañuelos, L. Gartzia and I. López-Arbeloa, *Chem. Commun.*, 2011, **47**, 11513; (b) L. Gartzia-Rivero, H. Yu, J. Bañuelos, I. López-Arbeloa, A. Costela, I. García-Moreno and Y. Xiao, *Chem. – Asian J.*, 2013, **8**, 3133; (c) G. Durán-Sampedro, A. R. Agarrabeitia, L. Cerdán, M. E. Pérez-Ojeda, A. Costela, I. García-Moreno, I. Esnal, J. Bañuelos, I. López Arbeloa and M. J. Ortiz, *Adv. Funct. Mater.*, 2013, **23**, 4195; (d) G. Durán-Sampedro, I. Esnal, A. R. Agarrabeitia, J. Bañuelos, L. Cerdan, I. García-Moreno, A. Costela, I. López Arbeloa and M. J. Ortiz, *Chem. – Eur. J.*, 2014, **20**, 2646.
- (a) R. C. A. Keller, J. R. Silvius and B. De Kruijff, *Biochem. Biophys. Res. Commun.*, 1995, 508; (b) Y. Zhao, Y. Zhang, X. Lu, Y. Liu, M. Chen, P. Wang, J. Liu and W. Guo, *J. Mater. Chem.*, 2011, **21**, 13168.
- (a) A. Y. Bochkov, I. O. Akchurin, O. A. Dyachenko and V. F. Traven, *Chem. Commun.*, 2013, **49**, 11653; (b) Z. Yang, Y. He, J.-H. Lee, N. Park, M. Suh, W.-S. Chae, J. Cao, X. Peng, H. Jung, C. Kang and J. S. Kim, *J. Am. Chem. Soc.*, 2013, **135**, 9181.
- BODIPYs are known to undergo ICT processes with groups at the C3/5 position. For example, see: (a) X. Peng, J. Du, J. Fan, J. Wang, Y. Wu, J. Zhao, S. Sun and T. Xu, *J. Am. Chem. Soc.*, 2007, **129**, 1500; (b) E. Deniz, G. C. Isbasar, Ö. A. Bozdemir, T. L. Yildirim, A. Siemiarczuk and E. U. Akkaya, *Org. Lett.*, 2008, **10**, 3401.
- F. López Arbeloa, J. Bañuelos, V. Martínez, T. Arbeloa and I. López Arbeloa, *Int. Rev. Phys. Chem.*, 2005, **24**, 339.
- (a) C. Tahtaoui, C. Thomas, F. Tohmer, P. Klotz, G. Duportail, Y. Mèly, D. Bonnet and M. Hibert, *J. Org. Chem.*, 2007, **72**, 269; (b) E. M. Sánchez-Carmerero, F. Moreno, B. L. Maroto, A. R. Agarrabeitia, M. J. Ortiz, B. G. Vo, G. Muller and S. de la Moya, *J. Am. Chem. Soc.*, 2014, **136**, 3346.

- 14 (a) T. Rohand, M. Baruah, W. Qin, N. Boens and W. Dehaen, *Chem. Commun.*, 2006, 266; (b) L. Li, B. Nguyen and K. Burgess, *Bioorg. Med. Chem. Lett.*, 2008, **18**, 3112; (c) Y. A. Volkova, B. Brizet, P. D. Harvey, A. D. Averin, C. Goze and F. Denat, *Eur. J. Org. Chem.*, 2013, 4270; (d) E. M. Sánchez-Carnerero, F. Moreno, B. L. Maroto, A. R. Agarrabeitia, J. Bañuelos, T. Arbeloa, I. López-Arbeloa, M. J. Ortiz and S. de la Moya, *Chem. Commun.*, 2013, **49**, 11641.
- 15 T. Sakida, S. Yamaguchi and H. Shinokubo, *Angew. Chem., Int. Ed.*, 2011, **50**, 2280.
- 16 For example see: (a) C. Goze, G. Ulrich and R. Ziessel, *J. Org. Chem.*, 2007, **72**, 313; (b) M. A. H. Alamiry, J. P. Hagon, A. Harriman, T. Bura and R. Ziessel, *Chem. Sci.*, 2012, **3**, 1041; (c) A. Kaloudi-Chantzea, N. Karakostas, F. Pitterl, C. P. Raptopoulou, N. Glezos and G. Pistolis, *Chem. Commun.*, 2012, **48**, 12213; (d) N. Karakostas, I. M. Mavridis, K. Seintis, M. Fakis, E. N. Koini, I. D. Petsalakis and G. Pistolis, *Chem. Commun.*, 2014, **50**, 1362; (e) E. M. Sánchez-Carnerero, L. Gartzia-Rivero, F. Moreno, B. L. Maroto, A. R. Agarrabeitia, M. J. Ortiz, J. Bañuelos, I. López-Arbeloa and S. de la Moya, *Chem. Commun.*, 2014, **50**, 12765.
- 17 (a) T. Förster, *Discuss. Faraday Soc.*, 1959, **27**, 7; (b) J. Fan, M. Hu, P. Zhan and X. Peng, *Chem. Soc. Rev.*, 2013, **114**, 11567.
- 18 A. Harriman, L. J. Mallon, S. Goeb, G. Ulrich and R. Ziessel, *Chem. – Eur. J.*, 2009, **15**, 4553.
- 19 S. Speiser, *Chem. Rev.*, 1996, **96**, 1953.
- 20 (a) J. Iehl, J. F. Nierengarten, A. Harriman, T. Bura and R. Ziessel, *J. Am. Chem. Soc.*, 2012, **134**, 988; (b) D. Bai, A. C. Benniston, J. Hagon, H. Lemmetyinen, N. V. Tkachenko, W. Clegg and R. W. Harrington, *Phys. Chem. Chem. Phys.*, 2012, **14**, 4447.
- 21 G. Duran-Sampedro, A. R. Agarrabeitia, I. García-Moreno, A. Costela, J. Bañuelos, T. Arbeloa, I. López Arbeloa, J. L. Chiara and M. J. Ortiz, *Eur. J. Org. Chem.*, 2012, 6335.
- 22 L. Cerdán, A. Costela, I. García-Moreno, J. Bañuelos and I. López-Arbeloa, *Laser Phys. Lett.*, 2012, **9**, 426.

